

Site Characterization Report for the Basalt Waste Isolation Project

November 1982



**U.S. Department of Energy
Assistant Secretary for Nuclear Energy
Office of Terminal Waste Disposal
and Remedial Action
Under Contract DE-AC06-77RLO1030**

101.8

**DOE/RL 82-3
Volume II**

Document No. WM-10
This document consists of 220 pages
No. 2 of 15 copies, Series

Encl to 11-12-82 ltr
to JG Davis

**Site Characterization Report
for the
Basalt Waste Isolation Project**

November 1982



**Prepared by Rockwell Hanford Operations
Under Contract DE-AC06-77RLO1030**

**Prepared For:
U.S. Department of Energy
Assistant Secretary for Nuclear Energy
Office of Terminal Waste Disposal
and Remedial Action
Washington, D.C. 20545**

VOLUME II

CONTENTS

CHAPTER 6.	GEOCHEMISTRY	6.0-1
6.1	Host Rock Geochemistry.	6.1-1
6.1.1	General Description of Host Rock.	6.1-1
6.1.2	Bulk Chemical Composition of Grande Ronde Basalt. . .	6.1-5
6.1.3	General Mineralogy and Petrography of Grande Ronde Basalt.	6.1-11
6.1.4	Primary Phases in Grande Ronde Basalt	6.1-11
6.1.5	Secondary Phases.	6.1-16
6.1.6	Composition of Interbeds in the Pasco Basin	6.1-24
6.2	Groundwater Geochemistry.	6.2-1
6.2.1	Major Inorganic Content	6.2-1
6.2.2	Trace Elements.	6.2-4
6.2.3	Hydrochemical Field Parameters.	6.2-5
6.2.4	Dissolved Gas	6.2-8
6.3	Chemistry of Waste, Barriers, and Near-Field Environment. . .	6.3-1
6.3.1	Waste Forms	6.3-1
6.3.2	Barrier Materials	6.3-8
6.3.3	Near-Field Environment.	6.3-11
6.4	Geochemical Retardation	6.4-1
6.4.1	Radionuclide Solubilities	6.4-1
6.4.2	Radionuclide Sorption	6.4-5
6.5	Natural Analogs	6.5-1
6.5.1	Waste Form Analogs.	6.5-1
6.5.2	Canister and Overpack Analogs	6.5-10
6.5.3	Backfill Analogs	6.5-11
6.6	Field Tests	6.6-1
6.7	Summary	6.7-1
6.8	Summary of Unresolved Issues.	6.8-1
6.9	References.	6.9-1
CHAPTER 7.	SURFACE HYDROLOGY.	7.1-1
7.1	Hydrologic Description.	7.1-1
7.1.1	Regional.	7.1-1
7.1.2	Pasco Basin	7.1-4
7.1.3	Hanford Site and Reference Repository Location. . . .	7.1-8
7.1.4	Streamflow Characteristics.	7.1-11
7.1.5	Water Control Structures.	7.1-12
7.2	Floods.	7.2-1
7.2.1	Flood History	7.2-1
7.2.2	Flood Potential	7.2-3
7.3	Surface Water Use and Demand for Water Within the Pasco Basin	7.3-1
7.3.1	Surface Water Use	7.3-1
7.3.2	Surface Water Demand.	7.3-2
7.3.3	Surface Water Intakes	7.3-2

7.4	Surface Water Quality	7.4-1
7.4.1	Pasco Basin	7.4-1
7.4.2	Water Quality	7.4-1
7.4.3	Water Quality Associated With Hanford Site Operations.	7.4-13
7.5	Summary of Unresolved Issues.	7.5-1
7.6	References.	7.6-1

CHAPTER 8. CLIMATOLOGY, METEOROLOGY, AND AIR QUALITY. 8.1-1

8.1	Recent Climate and Meteorology.	8.1-1
8.1.1	General Climate of the Region	8.1-1
8.1.2	Sources of Regional and Local Climate Information	8.1-7
8.1.3	Specific Climatic Elements.	8.1-10
8.2	Air Quality	8.2-1
8.2.1	Ambient Air Quality	8.2-1
8.2.2	Emissions	8.2-1
8.2.3	Baseline Concentrations	8.2-2
8.2.4	Basalt Waste Isolation Project Air Quality Impacts.	8.2-4
8.3	Long-Term Climatic Assessment	8.3-1
8.3.1	Paleoclimatology.	8.3-1
8.3.2	Future Climatic Variation	8.3-10
8.4	Meteorological Requirements for the Reference Repository Location	8.4-1
8.4.1	Dispersion Evaluations.	8.4-1
8.4.2	Meteorological Conditions for Design Bases.	8.4-6
8.4.3	Site Paleoclimatic Data	8.4-16
8.5	Summary of Unresolved Issues.	8.5-1
8.6	References.	8.6-1

CHAPTER 9. ENVIRONMENTAL, LAND-USE, AND SOCIOECONOMIC CHARACTERISTICS. 9.1-1

9.1	Environmental Characteristics	9.1-1
9.1.1	Ecology	9.1-1
9.1.2	Climate	9.1-19
9.1.3	Geology	9.1-19
9.1.4	Air Quality	9.1-19
9.1.5	Water Quality and Use	9.1-19
9.1.6	Radiological Background	9.1-19
9.2	Land-Use Characteristics.	9.2-1
9.2.1	Land-Use Categories	9.2-1
9.2.2	Land-Use Change	9.2-5
9.2.3	Ownership	9.2-7
9.2.4	Aesthetics and Recreation	9.2-8
9.2.5	Historic, Archaeological, and Cultural Resources.	9.2-8

9.3	Socioeconomic Characteristics	9.3-1
9.3.1	Demography.	9.3-1
9.3.2	Economy	9.3-1
9.3.3	Service Facilities.	9.3-16
9.3.4	Government and Institutional Organizations.	9.3-22
9.4	Summary of Unresolved Issues.	9.4-1
9.5	References.	9.5-1
CHAPTER 10. REPOSITORY DESIGN		10.0-1
10.1	Conceptual Design Bases	10.1-1
10.1.1	Functions and General Criteria.	10.1-1
10.1.2	Reference Repository Location	10.1-2
10.1.3	Site Arrangement.	10.1-2
10.2	Surface Facilities and Systems.	10.2-1
10.2.1	Surface Facilities.	10.2-1
10.2.2	Waste Handling Systems.	10.2-5
10.2.3	Service Systems	10.2-7
10.3	Access Shafts	10.3-1
10.3.1	Shaft No. 1 - Confinement Air Exhaust Shaft	10.3-1
10.3.2	Shaft No. 2 - Waste Transport Shaft	10.3-1
10.3.3	Shaft No. 3 - Confinement Air Intake Shaft.	10.3-2
10.3.4	Shaft No. 4 - Service Shaft	10.3-2
10.3.5	Shaft No. 5 - Basalt Transport Shaft.	10.3-3
10.3.6	Shaft Pillar.	10.3-4
10.3.7	Shaft Design Options.	10.3-4
10.4	Design of Underground Openings.	10.4-1
10.4.1	Subsurface Facilities	10.4-1
10.4.2	Waste Storage Panels.	10.4-5
10.4.3	Waste Storage Holes	10.4-5
10.5	Strength of Rock Mass	10.5-1
10.5.1	Results of Rock Stress Analysis	10.5-3
10.5.2	Thermomechanical Considerations	10.5-7
10.5.3	Rock Support.	10.5-9
10.5.4	Effects of Stratification on Design	10.5-9
10.5.5	Effects of Other Waste Receipt Ratios on Design	10.5-10
10.6	Construction of Access Shafts and Subsurface Facilities	10.6-1
10.6.1	Access Shafts Construction.	10.6-1
10.6.2	Underground Openings Construction	10.6-1
10.6.3	Construction Contingency Plans.	10.6-3
10.7	Backfill.	10.7-1
10.7.1	Backfill Material	10.7-1
10.7.2	Backfilling Procedure	10.7-1
10.7.3	Effects of Retrievability on Design	10.7-2
10.8	Sealing of Shafts, Boreholes, and Underground Openings.	10.8-1
10.8.1	Seal Design	10.8-5
10.9	Unresolved Repository Issues.	10.9-1
10.10	References.	10.10-1

CHAPTER 11. WASTE PACKAGE	11.0-1
11.1 Waste Forms	11.1-1
11.1.1 Reprocessed High-Level Waste (Borosilicate Glass) . .	11.1-1
11.1.2 Spent Fuel.	11.1-19
11.1.3 Strength and Weaknesses of Reference Waste Forms. . .	11.1-27
11.1.4 Summary of Important Conclusions.	11.1-30
11.2 Design Concepts	11.2-1
11.2.1 Waste Package Description	11.2-1
11.2.2 Functions of a Waste Package for Basalt	11.2-6
11.2.3 Reference Horizontal Borehole Emplacement	11.2-9
11.2.4 Tunnel Emplacement Alternate	11.2-10
11.2.5 Waste Package Component Reliability	11.2-10
11.2.6 Summary of Important Conclusions	11.2-12
11.3 Research and Development	11.3-1
11.3.1 Approach to Research and Development	11.3-1
11.3.2 Status of Research and Development	11.3-2
11.3.3 Summary of Important Conclusions	11.3-37
11.4 Emplacement Conditions	11.4-1
11.4.1 Physicochemical Conditions	11.4-1
11.4.2 Radiological Conditions	11.4-17
11.4.3 Summary of Important Conclusions	11.4-21
11.5 Alternate Waste Package	11.5-1
11.6 Summary	11.6-1
11.7 Summary of Unresolved Issues	11.7-1
11.8 References.	11.8-1
CHAPTER 12. PERFORMANCE ASSESSMENT.	12.0-1
12.1 Long-Term Repository Performance Issues	12.1-1
12.1.1 Groundwater Flow Paths and Travel Times	12.1-1
12.1.2 Repository Release Rates	12.1-2
12.1.3 Releases to the Accessible Environment.	12.1-2
12.1.4 Related Issues	12.1-3
12.2 Approach to Long-Term Repository Performance Analysis	12.2-1
12.2.1 Long-Term Repository Performance Analysis Framework.	12.2-1
12.3 Predictive Models	12.3-1
12.3.1 Mathematical Models	12.3-1
12.3.2 Numerical Models	12.3-5
12.3.3 Code Verification and Benchmarking	12.3-15
12.4 Preliminary Long-Term Repository Performance Analysis	12.4-1
12.4.1 Far-Field Studies to Assess Compliance with U.S. Nuclear Regulatory Commission Proposed Technical Criteria for Groundwater Transit Time . .	12.4-1
12.4.2 Very Near-Field Studies to Assess Compliance with U.S. Nuclear Regulatory Commission Proposed Technical Criteria for Repository Releases.	12.4-24
12.4.3 Near-Field Studies to Assess Compliance with U.S. Environmental Protection Agency Draft Regulations	12.4-28

12.4.4	Summary of Conclusions from Preliminary Long-Term Repository Performance Analysis	12.4-50
12.4.5	Assessment of Uncertainty in Performance Assessment Results	12.4-52
12.5	Summary of Unresolved Issues	12.5-1
12.6	References	12.6-1

FIGURES:

6-1.	Stratigraphy of the Reference Repository Location . . .	6.1-2
6-2.	Typical Intraflow Structures Present in a Grande Ronde Basalt Flow	6.1-4
6-3.	Magnesium Oxide Plotted Versus Titanium Dioxide for Grande Ronde Basalt Chemical Types and Subtypes . . .	6.1-7
6-4.	Magnesium Oxide and Titanium Dioxide Plotted Versus Stratigraphic Depth in Borehole DC-6.	6.1-8
6-5.	Zirconium and Chromium Plotted Versus Stratigraphic Position in Borehole DC-6	6.1-10
6-6.	Compositions of All Clays (mostly smectite) Formed Prior to Deposition of Zeolite or Silica.	6.1-17
6-7.	Compositions of First and Second Generations of Secondary Zeolite	6.1-18
6-8.	Volume Percent, Filled and Unfilled Fractures, Rocky Coulee, McCoy Canyon, and Museum Flows.	6.1-20
6-9.	A Typical Crystallization Sequence for Secondary Minerals.	6.1-23
6-10.	Location of Boreholes Used for Geochemical Studies of Groundwater.	6.2-2
6-11.	Measured Fluid Temperature Versus Depth in Selected Boreholes in the Hanford Site	6.2-6
6-12.	Calculated Pressure Versus Depth in Selected Boreholes in the Hanford Site	6.2-7
6-13.	Solubility of UO_2 in Water as a Function of Temperature; fO_2 in the Experiments Buffered by the Equilibrium Between UO_2 and UO_3 under Oxidizing Conditions.	6.3-2
6-14.	Solution Concentrations of Various Ions from PNL 76-68 Glass as a Function of Time at 300°C, 30 Megapascals in Deionized Water.	6.3-6
6-15.	Comparison of Estimated Solubilities for Actinide Compounds $UO_2(c)$, $UO_2(OH)_2 \cdot H_2O$, $NpO_2(c)$, $PuO_2(c)$, and Am (soil) with the Maximum Permissible Concentrations Under Repository Conditions at 25°C, 0.1 Megapascal, pH 10, and Eh 0.29 Volt (oxidizing) or -0.27 Volt (reducing)	6.4-4
6-16.	Distribution of Activated Kaolin Throughout the Basalt Column after Particulate Flow Experiments. . .	6.4-15
6-17.	Minimum Time Required for Anhydrous Thermal Reconstruction of Natural Glass to a Depth of 10 Microns as a Function of Temperature	6.5-2
6-18.	Time Required for the Hydrothermal Reconstruction of Natural Glass (perlite) to a Depth of 100 Microns as a Function of Temperature	6.5-4

FIGURES (Contd.):

6-19.	Experimental Hydration Rate Curve for Obsidian at 100°C.	6.5-5
6-20.	Logarithm of Hydration Constant as a Function of Inverse Temperature for Natural Rhyolitic Glass Samples	6.5-6
6-21.	Comparison of Relative Toxicities of Various Natural Ores to Nuclear Wastes Using Low-Grade Uranium Ore.	6.5-9
7-1.	Columbia River Drainage Basin	7.1-2
7-2.	Hydrologic Basins Designated for the Columbia Plateau	7.1-3
7-3.	Locations of Principal Dams Within the Columbia Plateau Study Area.	7.1-5
7-4a.	Schematic Representation of the Hydraulic Regime of the Columbia River Showing Major Dams	7.1-6
7-4b.	Schematic Representation of the Hydraulic Regime of the Snake River Showing Major Dams.	7.1-7
7-5.	Schematic of the U.S. Geological Survey Gauging Network for the Pasco Basin	7.1-9
7-6.	Surface Water Bodies Including Ephemeral Creeks on the Hanford Site	7.1-10
7-7.	Yakima River at Kiona, Annual Mean Daily Discharge, Log-Pearson III Distribution.	7.1-13
7-8.	Yakima River at Kiona, Annual Peak Instantaneous Flow, Log-Pearson III Distribution.	7.1-13
7-9.	Yakima River at Kiona, Family of Low-Flow Curves, Log-Pearson III Distribution.	7.1-14
7-10.	Columbia River Below Priest Rapids Dam, Annual Mean Daily Discharge, Log-Pearson III Distribution	7.1-14
7-11.	Columbia River Below Priest Rapids Dam, Annual Peak Instantaneous Flow, Log-Pearson III Distribution.	7.1-15
7-12.	Columbia River Below Priest Rapids Dam, Family of Low-Flow Curves, Log-Pearson III Distribution	7.1-15
7-13.	Schematic Cross Section of the Priest Rapids Dam and Related Facilities.	7.1-18
7-14.	Plan of Ben Franklin Dam.	7.1-19
7-15.	Inundation Along the Hanford Reach of the Columbia River Resulting from Operation of Ben Franklin Dam.	7.1-20
7-16.	Predicted Water Table Resulting from Ben Franklin Dam 122-Meter (400-Foot) Pool	7.1-21
7-17.	Predicted Water Table Rise for Ben Franklin Dam with 122-Meter (400-Foot) Pool	7.1-22
7-18.	Flooded Area During the 1894 Flood.	7.2-2
7-19.	Flooded Area from a 100-Year Flood of the Yakima River in the Vicinity of the Hanford Site	7.2-4
7-20.	Flooded Area for the Probable Maximum Flood	7.2-5
7-21.	Flooded Area Resulting from a 50-Percent Breach of Grand Coulee Dam.	7.2-7
7-22.	Drainage Area Map of the Cold Creek Watershed	7.2-8
7-23.	Projected Demand for Water in the Pasco Basin	7.3-9
7-24.	Surface Water Intakes in the Pasco Basin.	7.3-10
7-25.	Surface Water Monitoring Stations	7.4-4

FIGURES (Contd.):

7-26.	Comparison of 1979 Monthly Mean Temperature Distributions Along the Columbia River Within the Pasco Basin	7.4-11
7-27.	Comparison of 1979 Monthly Mean Temperature Distributions of Columbia River Tributaries Within the Pasco Basin	7.4-12
7-28.	Monthly Sediment Discharge Totals in 1979 for the Yakima River at Kiona, Washington	7.4-14
7-29.	Monthly Mean Specific Conductance in 1979 of the Snake River Near Burbank, Washington.	7.4-15
8-1.	The Hanford Site in Relation to Surrounding Terrain . .	8.1-2
8-2.	Surface-Wind Roses for Various Locations on and Surrounding the Hanford Site, Based on 5-Year Averages, 1952-1956	8.1-4
8-3.	Schematic Flow Pattern Associated with a Surface High Centered East of the Region.	8.1-5
8-4.	Schematic Flow Pattern Typically Associated with High Pressure to the West and Low Pressure to the East of the Region.	8.1-6
8-5.	Return Periods of Rainfall Intensity and Duration Based on the Period 1947-1969 at the Hanford Meteorological Station.	8.1-12
8-6.	Water Balance at Hanford.	8.1-16
8-7.	Monthly Average Wind Roses for the Hanford Meteorological Station Based on 15.2-Meter Level Wind Data, 1955-1970.	8.1-22
8-8.	Seasonal and Diurnal Variation in the 15.2-Meter Level Windspeed (meters per second), 1955-1970. . .	8.1-23
8-9.	Wind Roses as a Function of Stability and for all Stabilities of the Hanford Meteorological Station, Based on Winds at 60 Meters and Air Temperature Stabilities Between 1 and 60 Meters for the Period 1955 through 1970	8.1-24
8-10.	General Trends in Global-Scale Climate for the Past Million Years.	8.3-2
8-11.	Maximum Extent of Glaciation During the Last Ice Age. .	8.3-6
8-12.	Peak Wind-Gust Return-Probability Diagram	8.4-8
8-13.	Lowest Temperatures During Each of the 68 Winters at the Hanford Site Between 1912 and 1980 and Their Probability of Occurrence	8.4-12
8-14.	Highest Temperatures During Each of the 66 Summers at Hanford Between 1912 and 1980 (1943-1944 Missing) and Their Probability of Occurrence.	8.4-14
9-1.	Map of the Hanford Site	9.1-2
9-2.	Major Plant Communities of the Hanford Site	9.1-3
9-3.	General Food Web Diagram for the Hanford Site	9.1-5
9-4.	Map of the 200 Areas Controlled Zone Showing the Reference Repository Location and the Sample Points .	9.1-20
9-5.	Land Use Adjacent to the Reference Repository Location.	9.2-2
9-6.	Utilities and Communications	9.2-6
9-7.	Primary Impact Area	9.3-2

FIGURES (Contd.):

9-8.	U.S. Census Populations for 1980 of Cities Within an 80-Kilometer (50-Mile) Radius of the Hanford Meteorological Station	9.3-3
10-1.	Repository Cutaway.	10.0-2
10-2.	Reference Repository Location Showing Exploratory Shaft-Phase I Site and Principal Borehole (RRL-2) . .	10.1-3
10-3.	Site Arrangement.	10.1-5
10-4.	Surface Facilities Plan--Central Process Area	10.2-3
10-5.	Waste Canister in Horizontal Storage Borehole	10.2-6
10-6.	Shaft-Pillar Ventilation Flow Paths	10.2-9
10-7.	Cooling Water System.	10.2-11
10-8.	Shaft-Pillar Layout	10.3-5
10-9.	Alternate Shaft-Pillar Arrangements	10.4-2
10-10.	Subsurface Facilities Layout (bow-tie arrangement). .	10.4-3
10-11.	Waste Storage Panel Cross Sections.	10.4-6
10-12.	Orientation of Rock Stresses and Excavations.	10.5-4
10-13.	Maximum Theoretical Thermoelastic Rock Stress, Variation with Time (2:1 horizontal to vertical stress ratio; commercial high-level waste).	10.5-6
10-14.	Backfill/Retrievability Decision Flowchart.	10.7-4
10-15.	Role of Various Isolation Components and Their Contribution to the Control of Radionuclide Releases . .	10.8-2
10-16.	Determination of Maximum Permissible Release.	10.8-4
10-17.	Multiple-Zoned Plugs for Tunnels.	10.8-6
10-18.	Detail of Shaft Cut-Off Collar.	10.8-7
11-1.	Centerline Temperatures of a Reference Canister Containing 72-68 Waste Glass (PW-4b type waste), Cooled in Air and Water	11.1-19
11-2.	Typical Light Water Reactor Fuel Assemblies of Recent Design	11.1-21
11-3.	Decay Heat as a Function of Time for Typical Pressurized Water Reactor and Boiling Water Reactor Spent-Fuel Canisters Using Intact Assemblies.	11.1-28
11-4.	Early Waste Package Emplacement Concept	11.2-2
11-5.	Typical Waste Package Emplacement Concept for Basalt. .	11.2-3
11-6.	Waste Canister in Horizontal Storage Borehole	11.2-5
11-7.	Solubility of UO_2 in Water as Function of Temperature; fO_2 in the Experiments Buffered by the Equilibrium Between UO_2 and UO_3 Under Oxidizing Conditions.	11.3-4
11-8.	The Approach to Equilibrium Using a Hydrogen Diffusion Membrane	11.3-5
11-9.	Scanning Electron Micrograph of a Section through the Product of a 4-Week Hydrothermally Treated Sample of a PNL 76-68 Glass Specimen	11.3-11
11-10.	Composition Distance Profile for Leached PNL 76-68 Glass Sphere Shown in Figure 11-9	11.3-12
11-11.	Solution Concentrations of Various Ions from PNL 76-68 Glass as a Function of Time at 300°C, 30 Megapascals in Deionized Water	11.3-14

FIGURES (Contd.):

11-12.	Temperature-Versus-Time Curves for Different Components of a Vertically Emplaced Spent Fuel Waste Package in a Repository Located in Basalt	11.3-17
11-13.	Peak Temperature-Versus-Backfill Conductivity for a Spent Fuel Element Waste Package.	11.3-18
11-14.	Temperature-Versus-Time Curves for Different Components of a Vertically Emplaced Commercial High-Level Waste Package in a Repository Located in Basalt . . .	11.3-19
11-15.	Temperature-Versus-Time Curves for Different Components of a Vertically Emplaced Defense High-Level Waste Package in a Repository Located in Basalt . . .	11.3-19
11-16.	Selected Major Cation Concentrations in Solutions Taken from SPCW 1-1 (SPC-4 + groundwater) Plotted as a Function of Time	11.3-24
11-17.	Selected Major Cation Concentrations in Solutions Taken from BSPW 1-1 (basalt + SPC-4 + groundwater) Plotted as a Function of Time	11.3-25
11-18.	Dehydration of Fracture Mineralization at 0.1 Megapascal.	11.3-29
11-19.	Dehydration of Fracture Mineralization at 30 Megapascals.	11.3-29
11-20.	Schematic Representation of Groundwater Flow Path for Case I.	11.3-33
11-21.	Schematic Representation of Groundwater Flow Path for Case II	11.3-34
11-22.	Summary of Grande Ronde Groundwater Composition . . .	11.4-2
11-23.	Divariant Curve (liquid-vapor) for Water (H ₂ O). . . .	11.4-5
11-24.	Variation Trend of Solution pH as a Function of Time. .	11.4-9
11-25.	Relationship Between Estimated pH Resulting from the Dissociation of Silicic Acid and pH Measured in the Hanford Basalt/Groundwater System Between 100° and 300°C	11.4-10
11-26.	Plot of Ph Versus 1/T for Groundwater in Equilibrium with Umtanum Basalt	11.4-11
11-27.	Cylinder (Canister) Radius Versus Water-to-Fuel Ratio for the Onset of Critical Conditions in Spent-Fuel Waste Packages	11.4-20
11-28.	An Alternate Waste Package Borehole Emplacement Concept	11.5-1
12-1.	Relationship Between Individual Models and Outstanding Long-Term Performance Assessment Issues	12.2-6
12-2.	Relationship of Important Processes Occurring in the Vicinity of a Repository.	12.3-1
12-3.	Typical System Model.	12.3-14
12-4.	Location of Cold Creek Syncline Siting Area, Showing the Reference Repository Location and Borehole DC-3 .	12.4-2
12-5.	Plan View (X-Y) of Two Streamlines Originating at the Repository, Assessment of Effectiveness of Geologic Isolation Systems (AEGIS) Model.	12.4-10

FIGURES (Contd.):

12-6.	East-West Cross-Sectional View (X-Z) of Two Streamlines Originating at the Repository, Assessment of Effectiveness of Geologic Isolation System (AEGIS) Model	12.4-11
12-7.	North-South Cross-Sectional View (X-Z) of Two Streamlines Originating at the Repository, Assessment of Effectiveness of Geologic Isolation System (AEGIS) Model	12.4-11
12-8.	Planar View of Streamlines from Hypothetical Repository to Boundary.	12.4-16
12-9.	Location of Boreholes Used in the Kriging Analysis.	12.4-19
12-10.	Schematic Representation of Groundwater Flow Path for Case I.	12.4-26
12-11.	Schematic Representation of Groundwater Flow Path for Case II	12.4-27
12-12.	Simplified Stratigraphic Section for Columbia River Basalt.	12.4-31
12-13.	Groundwater Pathlines and Travel Times for Middle Sentinel Bluffs Flow: No-Disruption Base Case.	12.4-38
12-14.	Groundwater Pathlines and Travel Times for Umtanum Flow: No-Disruption Base Case.	12.4-39
12-15.	Carbon-14 Concentration Contours at 10,000 Years for Middle Sentinel Bluffs Flow: No-Disruption Base Case.	12.4-41
12-16.	Carbon-14 Concentration Contours at 10,000 Years for Umtanum Flow: No-Disruption Base Case.	12.4-43
12-17.	Groundwater Flow Pathlines for Middle Sentinel Bluffs Flow: Fault Scenario.	12.4-45
12-18.	Groundwater Flow Pathlines for Umtanum Flow: Fault Scenario.	12.4-46
12-19.	Carbon-14 Concentration Contours for Middle Sentinel Bluffs Flow: Fault Scenario.	12.4-48
12-20.	Carbon-14 Concentration Contours for Umtanum Flow: Fault Scenario.	12.4-49

TABLES:

6-1.	Major-Element Composition of Grande Ronde Flows	6.1-6
6-2.	Element Compositions of Grande Ronde Basalt Flows Determined by Instrumental Neutron Activation Analysis.	6.1-9
6-3.	Petrographic Characteristics of Primary Phases in Grande Ronde Basalt	6.1-12
6-4.	Secondary Minerals Identified in Grande Ronde Basalt, Pasco Basin	6.1-13
6-5.	Mean Composition of Hanford Clay and Zeolite with Structural Formulas	6.1-19
6-6.	Relative Proportions of Secondary Minerals in	

TABLES (Contd.):

	Grande Ronde Basalt, Pasco Basin.	6.1-19
6-7.	Summary of Hydrochemical Data Available for Middle Sentinel Bluffs and Umtanum Flow Tops and Bottoms from Boreholes on the Hanford Site.	6.2-3
6-8.	Range and Median Values of Trace Elements for Ground- water Within the Grande Ronde Basalt Beneath the Hanford Site.	6.2-4
6-9.	Median Value and Range in Composition of Dissolved Gas in Grande Ronde Basalt Groundwater.	6.2-8
6-10.	Comparison of the Compositions of Residual Solutions from Experiments Reacting Alternate Waste Forms with Distilled Water at 30 Megapascals.	6.3-4
6-11.	Composition of Supercalcine SPC-4	6.3-7
6-12.	Waste Package Component Functions Versus Repository History for Reference Waste Package Conceptual Design	6.3-9
6-13.	Candidate Backfill Tailoring Agents for Reducing the Mobility of Key Radionuclides in a Repository Constructed in Basalt	6.3-10
6-14.	Analyses of Cesium Remaining in Solution from Hydro- thermally Treated Mixtures of Basalt Phases or Basalts with Cesium Phases	6.3-12
6-15.	SrZrO ₃ Interactions with Basalt or Basalt Phases under Hydrothermal Conditions at 200°C for 2 Months and 300°C for 1 Month	6.3-13
6-16.	Synthetic Groundwater Compositions	6.4-7
6-17.	Groundwater Composition Effects on Radionuclide Distribution Coefficient Values for Umtanum Basalt and Associated Secondary Minerals	6.4-7
6-18.	Temperature Effects on Radionuclide Distribution Coefficient Values for Umtanum Basalt	6.4-9
6-19.	Effect of Eh Conditions on Radionuclide Distribution Coefficient Values for Umtanum Basalt	6.4-10
6-20.	Current Conservative Best Estimates for Radionuclide Distribution Coefficient Values for the Columbia River Basalt Geohydrologic System	6.4-12
6-21.	Sorption Isotherms for Selected Radionuclides on Umtanum Basalt	6.4-13
7-1.	Design Data for Principal Dams and Reservoirs Within the Columbia Plateau	7.1-16
7-2.	Design Statistics for Priest Rapids Dam	7.1-17
7-3.	Benton and Franklin Counties 1975 Water Use Totals and Composition	7.3-1
7-4.	Projected Population of the Pasco Basin, 1980-2080. . .	7.3-3
7-5.	Projected Water Demand From Households, Governments, and Nonagricultural, Nonindustrial Business in the Pasco Basin, 1980-2080	7.3-4
7-6.	Projected Industrial Employment in the Pasco Basin, 1980-2080	7.3-5
7-7.	Projected Industrial Water Demand in the Pasco Basin, 1980-2080	7.3-6

TABLES (Contd.):

7-8.	Projected Agricultural Water Demand in the Pasco Basin, 1980-2080	7.3-7
7-9.	Projected Total Water Demand in the Pasco Basin, 1980-2080	7.3-8
7-10.	Summary of Downstream Surface Water Uses for the Columbia River	7.3-11
7-11.	Comparative Contribution of Pasco Basin Surface Flow Inputs Based on Water Year 1979 Discharge Statistics	7.4-2
7-12.	Washington State Water Quality Standards for the Hanford Reach of the Columbia River	7.4-3
7-13.	Summary of U.S. Geological Survey Surface Water Quality Sampling Activities Within the Pasco Basin	7.4-5
7-14.	Comparison of 1980 "Class A" Quality Parameters Upstream and Downstream from the Hanford Site	7.4-6
7-15.	Radiological Quality of the Columbia River Upstream of the Hanford Site, 1980	7.4-7
7-16.	Radiological Quality of the Columbia River Downstream of the Hanford Site, 1980	7.4-8
7-17.	Comparison of Extreme and Average Surface Water Temperatures Recorded at Various Stations Within the Pasco Basin	7.4-10
7-18.	Extreme Load and Concentration Values and 1979 Total Load of Suspended Sediment Within the Yakima River at Kiona, Washington	7.4-13
7-19.	Summary of U.S. Geological Survey Surface Water Quality Data for Stations on the Columbia River Within the Pasco Basin	7.4-16
7-20.	Summary of U.S. Geological Survey 1979 Surface Water Quality Data for Columbia River Tributaries . .	7.4-20
8-1.	Instrument Height Locations at the Hanford Meteorological Station	8.1-8
8-2.	Averages and Extremes of Precipitation at the Hanford Meteorological Station, 1912-1980	8.1-11
8-3.	Average Return Period and Existing Record for Various Precipitation Amounts and Intensities During Specified Time Periods at Hanford Meteorological Station Based on Extreme-Value Analysis of 1947-1969 Records	8.1-13
8-4.	Thornthwaite-Mather Water Balance for Hanford, Washington, 150-Millimeter Root-Zone Water Capacity	8.1-15
8-5.	Averages and Extremes of Temperature at the Hanford Meteorological Station, 1912-1980	8.1-17
8-6.	Averages and Extremes of Relative Humidity at the Hanford Meteorological Station, 1946-1980	8.1-18
8-7.	Monthly Averages of Psychrometric Data, 1950-1980 . . .	8.1-19
8-8.	Wind Averages and Peak Wind Gusts at the Hanford Meteorological Station, 1945-1980	8.1-21

TABLES (Contd.):

8-9.	Frequency of Wind Direction at the 1,500-Meter Level Over the Hanford Meteorological Station on a Seasonal and Annual Basis	8.1-25
8-10.	Mean Seasonal and Annual Afternoon Mixing Heights for the Spokane Area	8.1-25
8-11.	Tornado and Funnel Cloud History Within 161 Kilometers of the Hanford Meteorological Station	8.1-26
8-12.	Number of Thunderstorm Days at the Hanford Meteorological Station, 1945-1980	8.1-28
8-13.	Distribution of Hailstorm Days by Month, 1947-1970.	8.1-28
8-14.	National Ambient Air Quality Standards	8.1-30
8-15.	Summary of Hanford Duststorm Statistics, 1953-1970	8.1-30
8-16.	Number of Days with Heavy Fog at the Hanford Meteorological Station, 1945-1980	8.1-31
8-17.	Mandatory Class I Areas in the Pacific Northwest	8.2-3
8-18.	Estimates of Glacial Age Surface Temperature Deficits (relative to the present)	8.3-4
8-19.	Characteristics of Existing Ice Sheets and of the Maximum Quaternary Ice Cover	8.3-7
8-20.	Estimates of Minimum and Maximum Temperature Change and Rate of Change from the Present	8.3-11
8-21.	Annual Joint Windspeed, Direction, and Stability Frequencies for Hanford Meteorological Station Based on Hanford Delta-Temperature Stability Groups, 1955-1970	8.4-2
8-22.	Annual Joint Windspeed, Direction, and Stability Figures for Hanford Meteorological Station Based on Pasquill-Gifford Delta-Temperature Stability Groups, 1955-1970	8.4-3
8-23.	Computer Models Available at Hanford for X/Q , D/Q Long-Term Assessment	8.4-5
8-24.	Accident-Case Models Available to Meet U.S. Nuclear Regulatory Commission Guidelines	8.4-7
8-25.	Design Basis Tornado Characteristics	8.4-7
8-26.	Highest Average Monthly Windspeed and Peak Gusts	8.4-9
8-27.	Miscellaneous Snowfall Statistics, 1946 Through 1980.	8.4-10
8-28.	Periods of Extreme Cold Temperature and Persistence	8.4-11
8-29.	Statistics for Two Periods of Extreme High Temperatures	8.4-13
8-30.	Detailed Estimates of the Dust Loadings for the Six Worst Storms, Based on Surface Observations of the Hanford Meteorological Station, 1953-1970	8.4-15
8-31.	Characteristics of Paleoclimate Data Sources	8.4-17
9-1.	Plant Species Known to Occur on the Reference Repository Location	9.1-6
9-2.	Mammal Species Reported to Occur on the Hanford Site.	9.1-11
9-3.	Birds Common to the Hanford Site	9.1-13
9-4.	Reptilian and Amphibian Species Reported to Occur on the Hanford Site	9.1-17
9-5.	Darkling Beetle and Grasshopper Species Known to Occur on the Reference Repository Location	9.1-18

TABLES (Contd.):

9-6.	Summary of Radiological Data from Control Plot No. 2 for 1976 and 1977	9.1-21
9-7.	Median Concentrations of Man-Made Radionuclides in Soil and Vegetation in the Hanford Area Environs . .	9.1-22
9-8.	Summary of 1978 Radiological Data at Seven Sample Sites Along the 200 West Area Fence	9.1-23
9-9.	Summary of 1979 Radiological Data at Seven Sample Sites Along the 200 West Area Fence	9.1-24
9-10.	Washington State Register of Historic Places in Counties Adjacent to the Hanford Site	9.2-9
9-11.	Population Size Based on Census, Current Estimates, and Forecasts for Benton and Franklin Counties and the Primary Impact Area--1970-2000	9.3-4
9-12.	Components of Population Change by County and State . .	9.3-5
9-13.	Population Distribution by Age and Sex	9.3-5
9-14.	Personal Income by Major Sources, Richland- Kennewick-Pasco Standard Metropolitan Statistical Area 1972-1977.	9.3-6
9-15.	Resident Labor Force and Employment, Washington State and Benton-Franklin Counties.	9.3-8
9-16.	Richland-Kennewick-Pasco Standard Metropolitan Statistical Area Employment and Average Annual Worker Needs by Occupational Group, 1976-1985	9.3-10
9-17.	Tri-Cities Total Housing Stock (in units)	9.3-11
9-18.	Benton and Franklin Counties Real Estate Sales	9.3-12
9-19.	Unsold Housing Inventory by Price Range for Tri-Cities Area, 1978 and 1979	9.3-12
9-20.	Local Government Revenues and Expenditures	9.3-13
9-21.	Police Protection in 1978	9.3-16
9-22.	Fire Protection in 1978	9.3-16
9-23.	School Enrollment in Tri-Cities Districts, May 1975 and May 1978	9.3-17
9-24.	Educational Services in Benton and Franklin Counties, Fall 1979	9.3-17
9-25.	Percent Occupancy for Setup and Licensed Beds for the Tri-Cities Area Hospitals, 1972, 1976, and 1978 .	9.3-19
9-26.	Water Resources, Benton and Franklin Counties, 1970 and 1978	9.3-20
9-27.	Sewer Systems and Storm Water, Benton and Franklin Counties, 1978	9.3-21
9-28.	Transportation Facilities	9.3-23
9-29.	Local Government Functions in the Primary Impact Area .	9.3-24
10-1.	Conceptual Design Basis Waste Receipts.	10.1-2
10-2.	Subsurface Ventilation Requirements	10.2-8
10-3.	Key Features of the Most Favorable Alternate Repository Arrangements Considered.	10.4-1
10-4.	Rock-Mass Conceptual Design Assumptions (Umtanum horizon)	10.5-2
10-5.	Thermal and Stress Reference Design Values.	10.5-8
11-1.	Reference High-Level Waste Solids (calcine) Compositions.	11.1-3

TABLES (Contd.):

11-2.	Reference Waste Borosilicate Glass Compositons.	11.1-6
11-3.	Crystalline Phases in Waste-Glass Formulations.	11.1-7
11-4.	Typical Waste Glass Compositions.	11.1-9
11-5.	Chemical Composition of Reference Combined High-Level and Intermediate-Level Liquid Waste in Calcine Form.	11.1-10
11-6.	Chemical Composition of Fission Products and Actinides (plus daughters) at the Time of Reprocessing of Reference Commercially High-Level Waste.	11.1-11
11-7.	General Composition and Physical Properties of Reference Commercial High-Level waste Glass	11.1-12
11-8.	Chemical Composition of Defense Waste Sludge	11.1-14
11-9.	Isotopic Content of Defense Waste Sludge	11.1-15
11-10.	Chemical Composition of Defense Waste Sludge-Based Waste-Glass Form	11.1-16
11-11.	Isotopic Content of Defense Waste Sludge Based on Waste-Glass Form.	11.1-17
11-12.	Physical Properties of Waste-Glass Forms for Defense Waste Sludge	11.1-18
11-13.	Heat-Generation Rates of Simulated PW-4b Waste Glass 72-68	11.1-18
11-14.	Reported Fission Product Phase Chemistry in Spent Fuel.	11.1-26
11-15.	Leachability of Simulated Waste Forms.	11.1-29
11-16.	Waste Package Component Functions Versus Repository History for Reference Waste Package Conceptual Design.	11.2-7
11-17.	Results of Screening Corrosion Tests of Canister/Overpack Materials at 250°C, 5 MPa, and Under Anoxic Conditions	11.2-11
11-18.	Simulated Spent Fuel Fission Products Formulation (burnup of 33,000 MWd/thm).	11.3-6
11-19.	Compositions of Residual Solutions from Experiments Reacting Simulated Spent Fuel with Distilled Water at 30 Megapascals	11.3-7
11-20.	Compositions of Residual Solutions from Experiments Reacting Simulated PNL 76-68 Glass in Distilled Water at 30 Megapascals	11.3-9
11-21.	Assumptions Used for Modeling of Spent Fuel Waste Packages in Basalt.	11.3-16
11-22.	Composition of Supercalcine SPC-4	11.3-22
11-23.	Composition of Simulated Grande Ronde Basalt Groundwater	11.3-26
11-24.	Nuclides Whose Release Rates Must Be Less Than 10^3 per Year to Meet U.S. Environmental Protection Agency Release Draft Limits.	11.3-35
11-25.	Comparison of Estimated Actinide Release Rates from a Repository in Basalt with Release Rates Required to Meet Current U.S. Environmental Protection Agency Draft Limits	11.3-36

TABLES (Contd.):

11-26.	Summary of Repository Equilibrium Conditions.	11.4-17
11-27.	Expected Repository Conditions at the Emplacement Location.	11.6-3
12-1.	Potential Release Inducing Phenomena.	12.2-3
12-2.	Summary of Codes for Repository Performance Analysis. .	12.3-6
12-3.	Hydraulic Conductivities Assumed by Los Alamos Technical Associates, Inc./Intera Environmental Consultants, Inc.	12.4-4
12-4.	Thickness and Porosity of Each Model Layer Assumed by Los Alamos Technical Associates, Inc./ Intera Environmental Consultants, Inc.	12.4-4
12-5.	Major Assumptions in the Assessment of Effectiveness of Geologic Isolation Systems (AEGIS) Basalt Demonstration	12.4-9
12-6.	Effective Hydraulic-Conductivity Values Used in the Initial MAGNUM 3D Pasco Basin Simulation.	12.4-14
12-7.	Hydraulic Conductivity Data Used in the Kriging Analysis.	12.4-20
12-8.	Parameters for Horizontal Streamtubes	12.4-20
12-9.	Parameters for Vertical Streamtubes	12.4-21
12-10.	Groundwater Velocities, Flow Rates, and Travel Times for Horizontal Streamtubes.	12.4-21
12-11.	Groundwater Velocities, Flow Rates, and Travel Times for Vertical Streamtubes.	12.4-22
12-12.	Groundwater Travel Times for Each Scenario.	12.4-22
12-13.	Summary of Pre-Waste-Emplacement Travel Time Estimates	12.4-23
12-14.	Description and Dimensions of Rock Layers for the Geologic Conceptual Model	12.4-32

6. GEOCHEMISTRY

The most credible mechanism for the migration of radionuclides from a repository to the accessible environment is solution transport in groundwater. Hydrothermal interactions controlled by geochemical reactions and reaction kinetics will determine the composition of this transported solution. Evaluation of the importance of geochemical interactions in a repository located in basalt includes characterization of the following processes:

- Groundwater-rock (basalt) alteration reactions
- Reactions among the materials used in the engineered waste package
- Dissolution reactions of proposed waste forms
- Concentration limits imposed on all dissolved radionuclides by solubility constraints
- Radionuclide precipitation and/or sorption reactions in both the near-field and far-field environments.

These chemical reactions are controlled by temperature, pressure, and compositional parameters, which in turn vary over space and time. The coupled feedback between environmental parameters and geochemical reactions leads to a complex variation of geochemical characteristics within the waste isolation system. To understand and eventually model this behavior, geochemical studies must focus on two general areas. The first is the characterization of the prevailing in situ geochemical conditions and reactions within the Hanford repository site. This baseline information also represents a "natural experiment" on the long-term effects of low-temperature hydrothermal alteration between groundwater and basalt. Secondly, literature and laboratory studies, as well as observations of natural systems, must be utilized to identify the perturbations in geochemical parameters and reactions imposed by the emplacement of waste within a repository in basalt. The same studies can be used to extrapolate these perturbing effects to time periods appropriate to U.S. Nuclear Regulatory Commission proposed containment and isolation criteria (NRC, 1981).

Section 6.1 deals with the geochemistry and mineralogy of the basaltic flows beneath the Hanford Site and emphasizes results obtained from studies of the Grande Ronde Basalt. Groundwater chemistry, including pH and Eh values apparently buffered by reaction with basalt, are discussed in Section 6.2. Expected waste-water-rock-engineered barrier interactions in the near-field environment are reviewed in Section 6.3, while far-field geochemical reactions, including sorption, ion exchange, and precipitation are summarized in Section 6.4. Natural analogs of waste package components in other basaltic environments, field tests, and general geochemical stability considerations are described in Sections 6.5 and 6.6, respectively. Section 6.7 summarizes findings to date. Unresolved geochemical issues are addressed in Section 6.8. Section 6.9, containing cited references, concludes the chapter.

6.1 HOST ROCK GEOCHEMISTRY

6.1.1 General Description of Host Rock

The Grande Ronde Basalt flows of the Columbia Plateau are continental flood basalts. The chemical composition of a typical flow (Long and Landon, 1981) which is representative of the most voluminous magma type is as follows (weight percent): SiO_2 , 55.41; TiO_2 , 1.95; Al_2O_3 , 14.82; FeO , 12.12; MnO , 0.21; MgO , 3.43; CaO , 7.20; Na_2O , 2.40; K_2O , 1.96; P_2O_5 , 0.31. Mineralogically, these basalts consist principally of pyroxene-- $(\text{Ca,Mg,Fe})_2\text{Si}_2\text{O}_6$; plagioclase-- $(\text{Ca,Na})(\text{Al,Si})\text{AlSi}_2\text{O}_8$; magnetite-- $(\text{Fe,Ti})_3\text{O}_4$; olivine-- $(\text{Mg,Fe})_2\text{SiO}_4$; and interstitial glass of variable composition. The grain size in these rocks is variable, with an average size of about 0.2 to 0.4 millimeter. Textures vary considerably with typical textures dominated by a lath-shaped plagioclase and pyroxene grains locked together by an interstitial glassy matrix. Proportions of the minerals also are variable (volume percent): pyroxene, 25 to 50 percent; plagioclase, 20 to 40 percent; glassy mesostasis, 15 to 70 percent; magnetite, 0 to 6 percent; and olivine, 0 to 3 percent.

The Columbia Plateau lavas erupted 6 to 16.5 million years ago from linear vent systems up to 150 kilometers in length (Swanson, 1967; Swanson et al., 1975). These vent systems occurred predominantly to the east of the Pasco Basin. Each eruption produced a sheetlike flood of relatively low-viscosity magma that flowed downslope from the fissure and that commonly congealed into a single lava flow that may have covered as many as 75,000 square kilometers. Volumes of individual flows varied greatly, but some are known to exceed 700 cubic kilometers (Swanson and Wright, 1981). Flows with such large volume typically are thick (greater than 40 meters) and are widespread and laterally continuous. The stratigraphy of the reference repository location is presented in Figure 6-1. Preliminary analysis and evaluation (see Chapter 3) have identified two flows within the Grande Ronde Basalt as promising candidate repository horizons. These two flows are the middle Sentinel Bluffs flow and the Umtanum flow. The stratigraphic relationship of these two flows and position with respect to other Grande Ronde Basalt flows across the Hanford Site are illustrated in Figure 6-1. Current plans call for the selection of a single repository horizon based on detailed comparison of these flows. The selection process for the candidate repository horizons will include comparison of data sets of geochemical characteristics significant to a nuclear waste repository in basalt performance. Because of an earlier focus on analysis of the Umtanum flow, the geochemical data base for the Umtanum flow is more extensive than the data base for the middle Sentinel Bluffs flow at this time. Detailed geochemical studies for expanding and bringing into balance these two data sets are in progress.

As each flow was emplaced, it developed a vesicular flow top due to the expulsion of dissolved gases. Subsequent flows buried the earlier flows, creating a sequence of flows each with its own vesicular flow top. The rapid eruption of successive flows within the Grande Ronde Basalt and portions of the Wanapum Basalt prevented extensive weathering and the

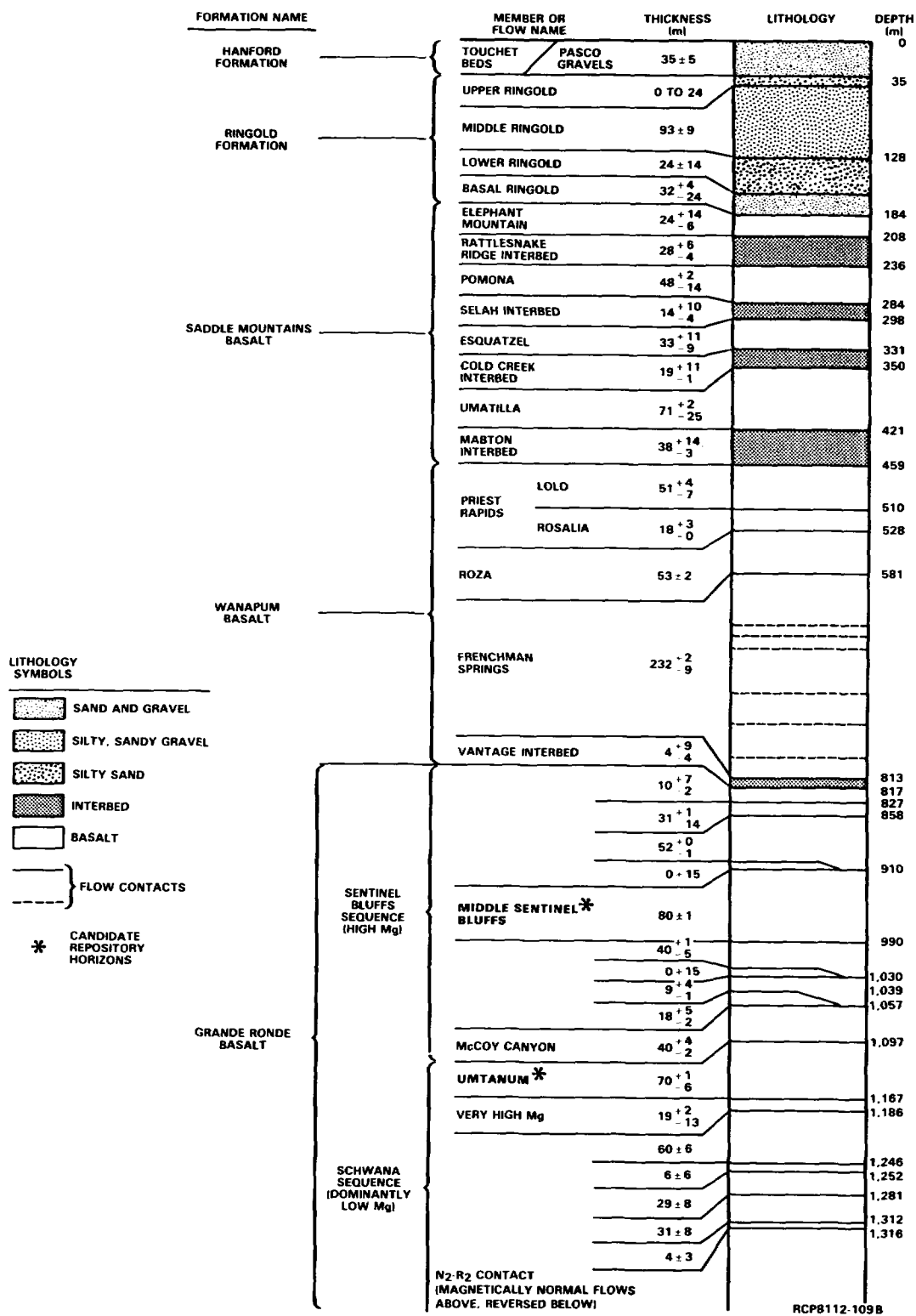


FIGURE 6-1. Stratigraphy of the Reference Repository Location.

development of paleosols (see Chapter 3). Thus, an important discontinuity in these rocks is the contact between flows. The vesicular, porous nature of the flow tops means that they typically have higher permeability than the flow interiors and, consequently, exert a strong influence on groundwater flow. As flows encountered lakes or streams during emplacement, they tended to form what are known as pillowed zones or areas near the base of the flow that consist of rounded masses of glassy basalt. Because the spaces between the masses may not be filled with magma or secondary minerals, pillowed zones may be highly permeable. A schematic diagram of structure within a typical flow is presented in Figure 6-2 (Long and Davidson, 1981).

Cooling of each basalt flow after emplacement resulted in partial crystallization and development of cooling cracks due to thermal contraction. These cooling cracks, also known as cooling joints or columnar joints (Tomkeieff, 1940; Spry, 1962), are the dominant discontinuity in the interior of basalt flows. Cooling joints occur on spacings ranging from approximately 5 to 25 fractures per meter. The major cooling joints in the lower part of the flows are oriented approximately perpendicular to the top and bottom of a flow and so define a columnar structure. Cooling joints in the central part of the flows commonly show less of a preferred orientation.

Subsequent burial and alteration by younger flows resulted eventually in the filling of most fractures by secondary minerals:

- Smectite clay (principally nontronite;
 $(\text{Ca}, \text{Na})_{0.66}(\text{Fe}^{+3}, \text{Fe}^{+2})_{4-6}(\text{Si}, \text{Al})_8\text{O}_{20}(\text{OH})_4 \cdot n\text{H}_2\text{O}$)
- Zeolite (principally clinoptilolite;
 $(\text{Ca}, \text{Na}_2, \text{K}_2)(\text{Al}_{1.5}\text{Si}_{7.5}\text{O}_{18}) \cdot 6\text{H}_2\text{O}$)
- Silica (principally quartz, tridymite, cristobalite, and opal;
 SiO_2).

These secondary minerals are derived from the diagenetic alteration of the basalt by circulation of groundwater at temperatures slightly elevated above surface temperatures (Benson and Teague, 1979). This elevated temperature is imposed by the normal regional geothermal gradient. The width of filled fractures ranges from approximately 0.1 to 4.0 millimeters, with a mean range of 0.2 to 0.4 millimeter.

Tectonic fractures and fault zones have been superimposed on these flows after emplacement, cooling, and burial. Individual fractures are much like cooling joints, except that they tend to occur as closely spaced multiple fractures that cut across cooling joints. They may also transect flow contacts. Examination of surface exposures suggests that tectonic fractures are spaced at intervals ranging from tens to thousands of meters. Mineral fillings of tectonic fractures have not been studied, but presumably are similar to those that fill the cooling joints.

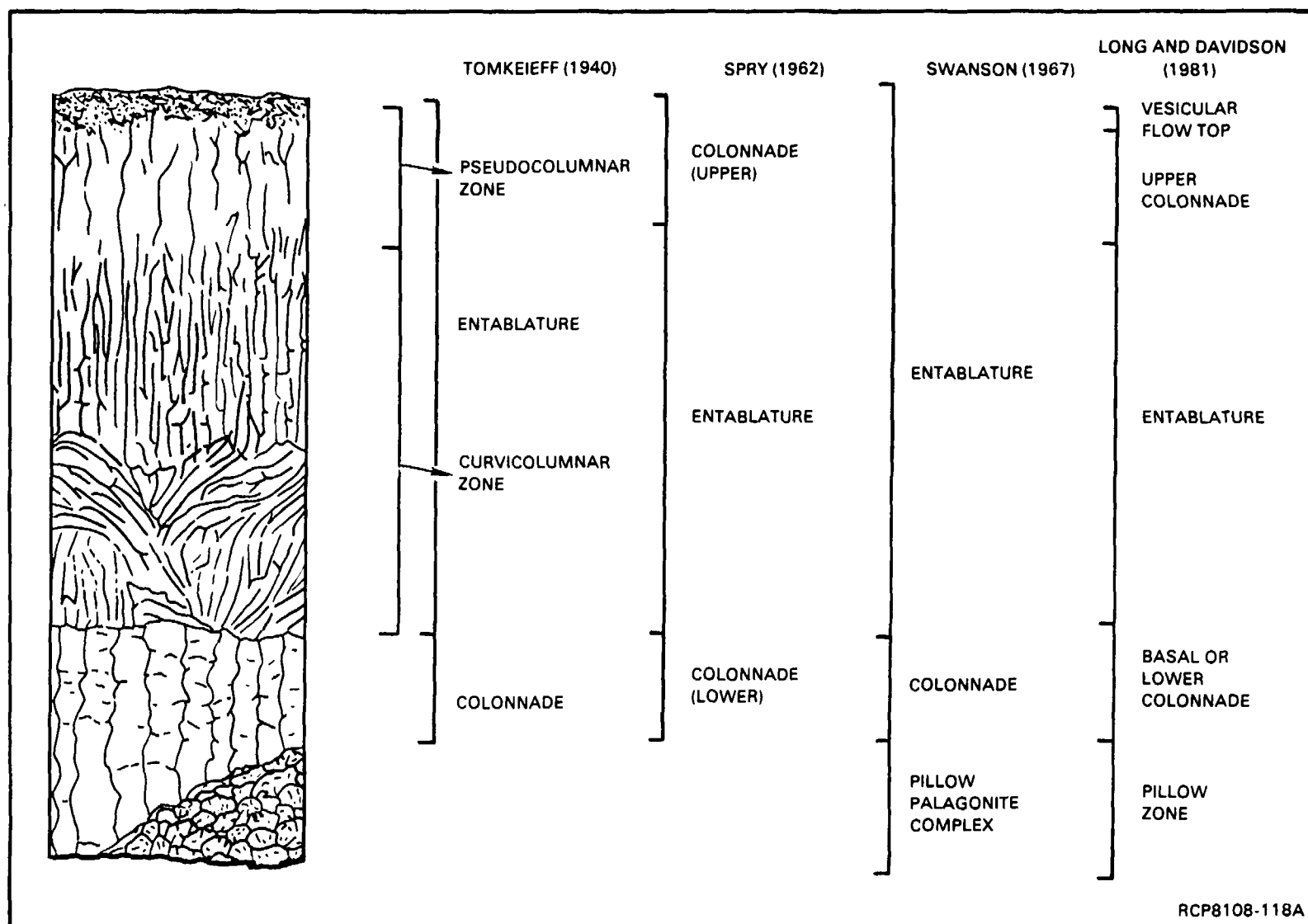


FIGURE 6-2. Typical Intraflow Structures Present in a Grande Ronde Basalt Flow. Nomenclatures used in previous studies are compared (after Long and Davidson, 1981).

Faults represent another structural feature that might create preferential flow pathways to groundwater. Faults that occur in some of these flows range from tectonic joints with slight displacement to major structural features that contain appreciable fault gouge or breccia. Major faults have been specifically avoided in selecting the reference repository location, but lesser faults, with offsets ranging from a few meters to a few centimeters, could occur within the reference repository location. Little is known presently about their likely spacing or the characteristics of the gouges. The underground exploration, which is part of the Exploratory Shaft Program, will provide additional information about these lesser faults. The reference repository location was selected based in part on its minimal structural deformation and it can therefore be expected to contain relatively few tectonic fractures and faults (see Chapter 3).

Cooling joints, tectonic fractures, and vesicular flow tops, thus, are the likely pathways of radionuclide migration through the basalts to the accessible environment. The petrology and mineralogy of these features are described in more detail below. Additional data on the geometry of these features are included in Sections 3.5.4, 3.7.2.2, and 3.7.2.4.

6.1.2 Bulk Chemical Composition of Grande Ronde Basalt

The following section discusses the bulk chemistry of Grande Ronde Basalt in two parts: major-element analyses and trace-element analyses.

6.1.2.1 Major-Element Analyses. More than 2,000 major-element analyses have been performed on Grande Ronde Basalt samples. A complete map of borehole locations for geologic sampling is presented in Section 3.5.4. Typically, two or three samples per flow are analyzed for any given section or borehole. The results are summarized in Table 6-1 and Figure 6-3. The three major Grande Ronde Basalt chemical types are evident in Figure 6-3, based on trends showing a negative correlation between MgO and TiO₂. These major types are the high-magnesium, low-magnesium, and very high-magnesium chemical types. In addition, the low-magnesium and high-magnesium chemical types have subtypes that are referred to as the Umtanum and McCoy Canyon chemical subtypes, respectively. The utility of these chemical features is that they can be related to the physical stratigraphy of Grande Ronde flows in the central part of the Columbia Plateau (Fig. 6-4). For example, the Umtanum flow is distinctly higher in TiO₂ and lower in MgO relative to underlying and overlying flows. Major elements thus provide an important, independent means of stratigraphic correlation, which makes it possible to distinguish groups of flows and, in some cases, individual flows (Reidel and Long, 1980), even in the absence of other physical stratigraphic markers.

6.1.2.2 Trace-Element Analyses. Analyses for 21 selected trace elements have been made on more than 400 Grande Ronde Basalt samples. Selected analyses are summarized in Table 6-2, and an example of the stratigraphic variations of zirconium and chromium within a borehole are illustrated in Figure 6-5. Trace-element analyses have been used to strengthen the

TABLE 6-1. Major-Element Composition of Grande Ronde Basalt Flows (wt%).

Element	N ^a	Mean	Standard deviation	Minimum ^b value	Maximum ^b value	Standard error of mean
High-Mg Flows						
SiO ₂	50	53.61	0.43	52.61	54.45	0.06
Al ₂ O ₃	50	14.88	0.27	14.26	15.51	0.04
FeO ^c	50	12.01	0.52	10.89	12.89	0.07
MgO	50	4.88	0.20	4.38	5.34	0.03
CaO	50	8.75	0.19	8.36	9.20	0.03
Na ₂ O	50	2.60	0.17	2.13	3.17	0.02
K ₂ O	50	0.97	0.15	0.51	1.31	0.02
TiO ₂	50	1.81	0.10	1.62	1.96	0.01
P ₂ O ₅	50	0.28	0.02	0.25	0.38	0.00
MnO	50	0.21	0.01	0.19	0.23	0.00
Middle Sentinel Bluffs Flow						
SiO ₂	55	53.41	0.39	52.43	54.21	0.05
Al ₂ O ₃	55	15.00	0.30	14.26	15.66	0.04
FeO	55	11.73	0.31	11.10	12.50	0.03
MgO	55	4.99	0.22	4.46	5.34	0.03
CaO	55	8.86	0.26	8.16	9.31	0.04
Na ₂ O	55	2.48	0.31	1.44	2.92	0.04
K ₂ O	55	1.03	0.13	0.51	1.40	0.02
TiO ₂	55	1.79	0.08	1.67	2.11	0.01
P ₂ O ₅	55	0.29	0.04	0.24	0.40	0.01
MnO	55	0.21	0.01	0.19	0.23	0.00
Low-Mg Flows						
SiO ₂	13	55.45	0.63	53.82	56.01	0.18
Al ₂ O ₃	13	14.88	0.19	14.44	15.19	0.05
FeO	13	11.95	0.30	11.25	12.40	0.08
MgO	13	3.55	0.12	3.41	3.84	0.03
CaO	13	7.35	0.13	7.11	7.55	0.04
Na ₂ O	13	2.82	0.18	2.45	3.11	0.05
K ₂ O	13	1.63	0.33	1.17	2.47	0.09
TiO ₂	13	1.91	0.03	1.87	1.96	0.01
P ₂ O ₅	13	0.30	0.01	0.28	0.32	0.00
MnO	13	0.20	0.01	0.19	0.21	0.00
Umtanum Flow						
SiO ₂	13	54.90	0.25	54.45	55.45	0.07
Al ₂ O ₃	13	14.34	0.15	14.08	14.59	0.04
FeO	13	13.10	0.21	12.70	13.39	0.06
MgO	13	3.48	0.09	3.38	3.71	0.03
CaO	13	7.30	0.14	7.14	7.64	0.04
Na ₂ O	13	2.66	0.26	1.86	2.95	0.07
K ₂ O	13	1.48	0.24	0.94	1.71	0.07
TiO ₂	13	2.17	0.04	2.12	2.23	0.01
P ₂ O ₅	13	0.35	0.01	0.33	0.36	0.00
MnO	13	0.22	0.00	0.21	0.23	0.00
Very High-Mg Flow						
SiO ₂	10	51.87	0.42	50.82	52.42	0.13
Al ₂ O ₃	10	15.09	0.24	14.79	15.57	0.07
FeO	10	11.89	0.21	11.50	12.16	0.07
MgO	10	5.75	0.15	5.53	6.02	0.05
CaO	10	9.93	0.22	9.68	10.43	0.07
Na ₂ O	10	2.80	0.18	2.50	3.01	0.06
K ₂ O	10	0.53	0.17	0.29	0.76	0.05
TiO ₂	10	1.64	0.07	1.57	1.79	0.02
P ₂ O ₅	10	0.27	0.02	0.25	0.30	0.01
MnO	10	0.22	0.03	0.20	0.30	0.01

^aNumber of samples analyzed.

^bMaximum and minimum values are for individual oxides.

^cTotal Fe given as FeO.

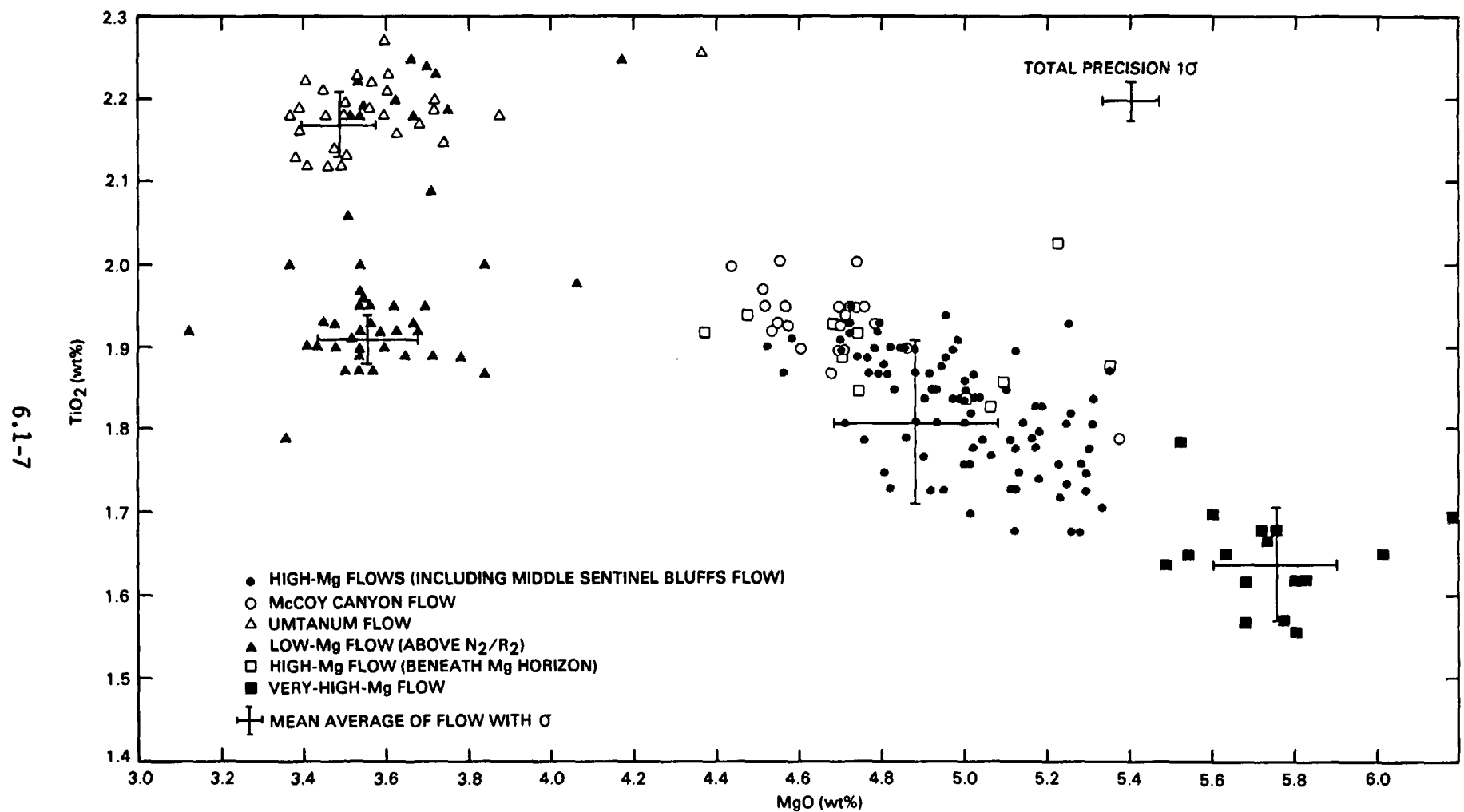
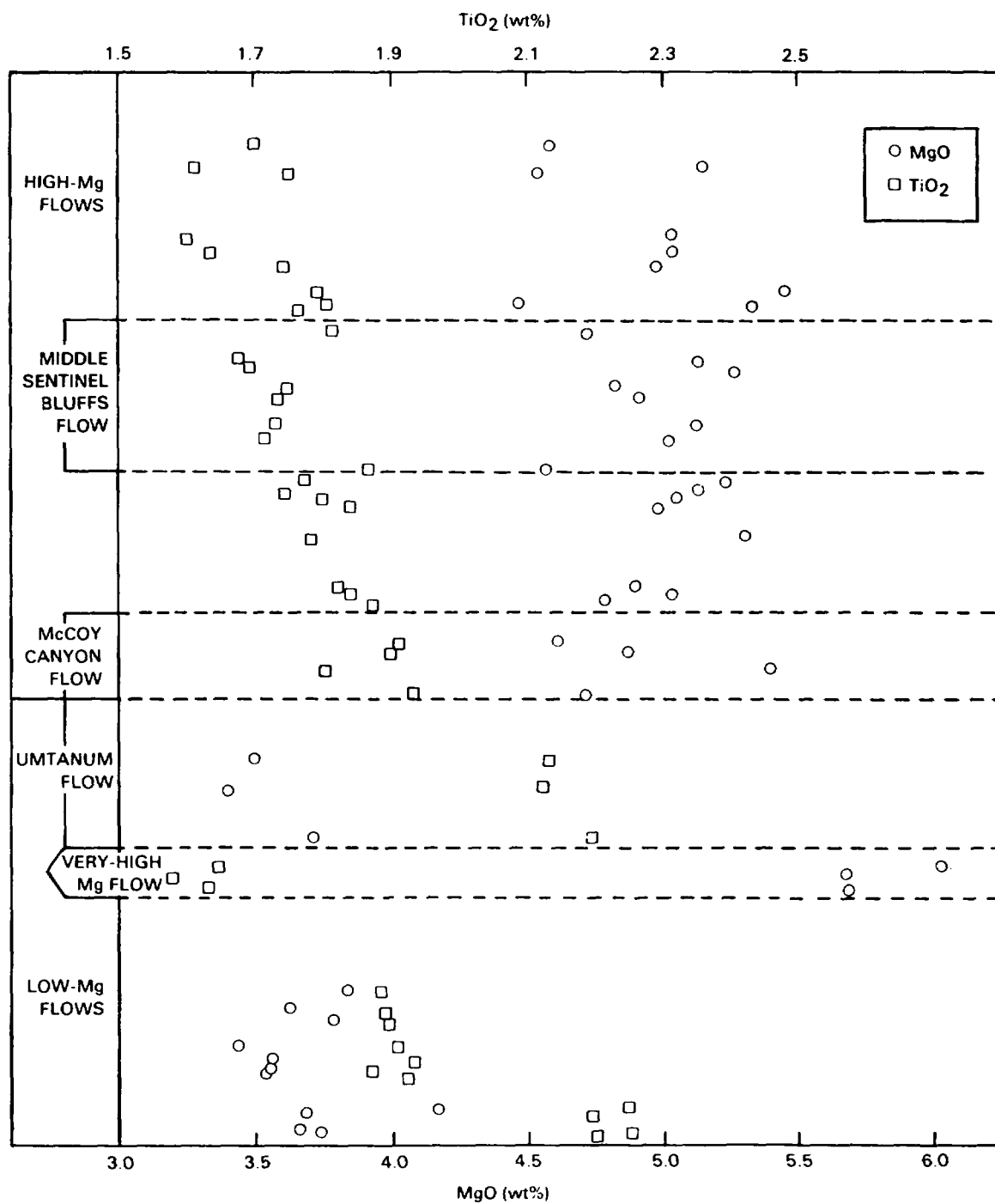


FIGURE 6-3. Magnesium Oxide Plotted Versus Titanium Dioxide for Grande Ronde Basalt Chemical Types and Subtypes.



RCP8108-98B

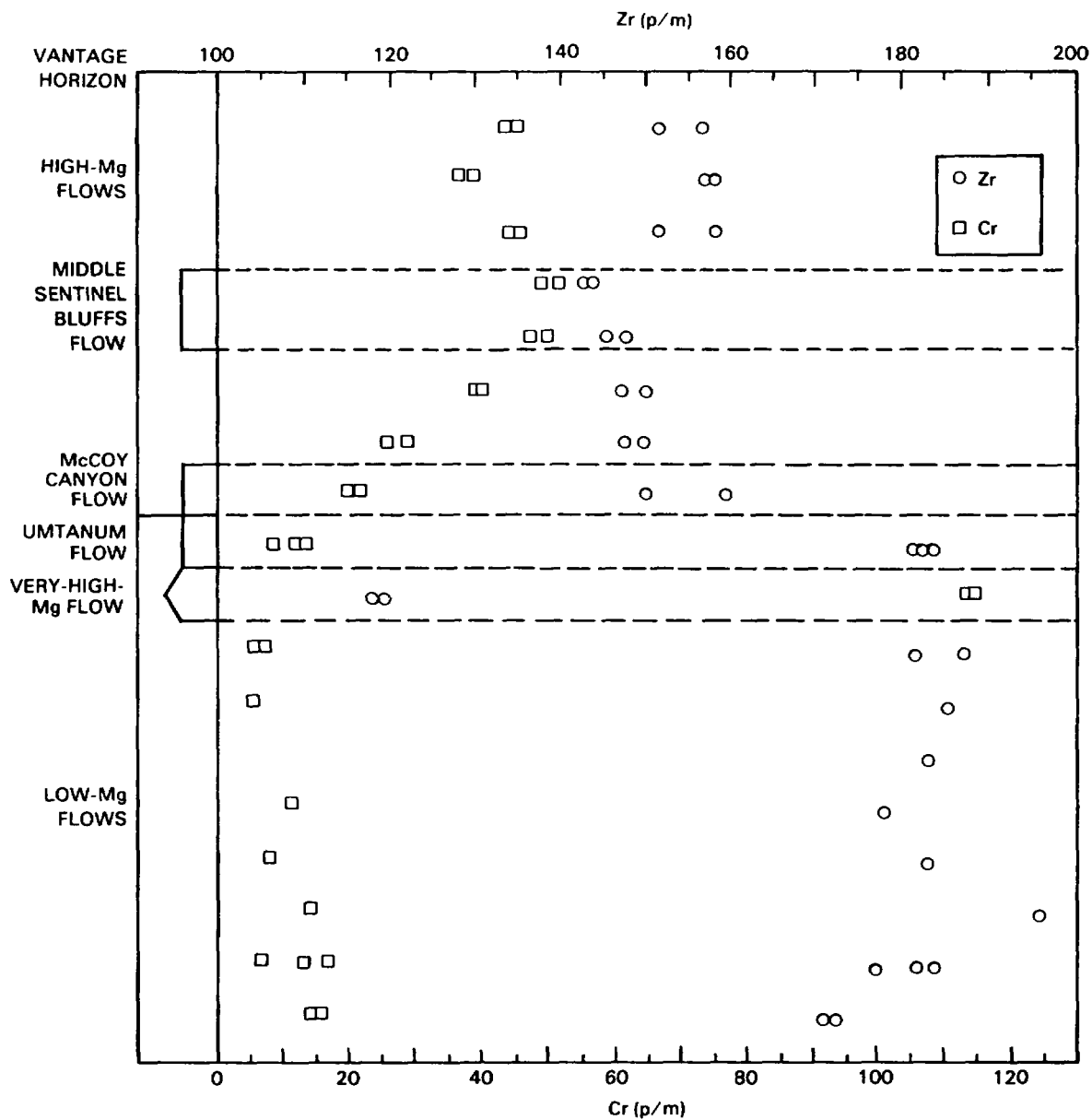
FIGURE 6-4. Magnesium Oxide and Titanium Dioxide Plotted Versus Stratigraphic Depth in Borehole DC-6. (See Section 3.5.4 for location of borehole DC-6.)

TABLE 6-2. Element Compositions of Grande Ronde Basalt Flows Determined by Instrumental Neutron Activation Analysis.

Element	N ^a	Mean	Standard deviation	Minimum value	Maximum value	Standard error of mean
High-Mg Flows (p/m) ^b						
Fe	70	8.83	0.34	8.05	9.54	0.04
Sc	70	36.31	1.45	31.50	39.10	0.17
Cr	70	35.66	9.04	19.60	51.20	1.08
Co	70	41.25	4.56	33.50	57.20	0.54
Zr	66	153.50	5.51	142.50	168.80	0.67
Hf	70	4.09	0.34	3.51	5.24	0.04
Nb	66	13.21	1.66	9.10	17.90	0.20
Ta	65	0.82	0.34	0.41	2.11	0.04
Th	70	3.74	0.46	2.49	4.79	0.05
U	7	1.12	0.32	0.80	1.80	0.12
Na	60	2.17	0.09	1.95	2.35	0.01
Sr	66	308.00	7.00	291.80	323.40	0.90
Ba	64	445.00	58.00	300.00	553.00	7.26
Rb	70	29.20	5.00	15.60	39.60	0.64
Cs	52	0.67	0.21	0.19	1.04	0.02
La	70	17.85	1.21	15.40	20.70	0.14
Ce	69	38.77	2.81	33.60	48.30	0.33
Nd	5	18.02	1.17	16.10	19.00	0.52
Sm	70	5.62	0.32	4.86	6.44	0.03
Eu	70	1.76	0.08	1.60	2.01	0.01
Tb	68	0.88	0.14	0.48	1.14	0.01
Yb	68	3.17	0.31	2.24	3.90	0.03
Lu	66	0.52	0.06	0.30	0.74	0.00
Low-Mg Flows (p/m) ^b						
Fe	28	9.32	0.52	8.52	10.14	0.10
Sc	28	32.79	1.79	29.40	36.10	0.33
Cr	21	7.89	2.33	5.10	13.20	0.51
Co	28	38.01	3.00	35.10	50.00	0.66
Zr	24	185.00	5.00	177.00	201.20	1.12
Hf	28	4.82	0.30	4.22	5.65	0.05
Nb	24	15.55	1.58	11.60	18.10	0.32
Ta	24	0.91	0.27	0.50	1.72	0.05
Th	28	5.99	0.62	4.73	7.27	0.11
U	9	1.45	0.22	1.02	1.70	0.07
Na	28	2.35	0.10	2.02	2.53	0.01
Sr	24	320.00	13.00	304.40	365.00	2.74
Ba	25	636.00	75.00	450.00	850.00	15.15
Rb	28	46.36	9.37	17.60	68.30	1.77
Cs	24	1.33	0.54	0.56	2.43	0.11
La	28	23.30	2.02	15.20	26.70	0.38
Ce	28	49.85	2.53	45.50	57.70	0.47
Nd	4	30.50	6.55	25.00	40.00	3.27
Sm	28	6.69	0.28	6.16	7.26	0.05
Eu	28	1.98	0.11	1.81	2.29	0.02
Tb	25	1.02	0.12	0.75	1.21	0.024
Yb	28	3.53	0.46	2.90	4.59	0.088
Lu	27	0.57	0.07	0.38	0.69	0.014
Very High-Mg Flow (p/m) ^b						
Fe	8	8.69	0.29	8.00	8.91	0.10
Sc	8	40.16	1.30	38.70	41.80	0.46
Cr	8	109.10	11.08	90.00	123.30	3.91
Co	8	43.23	3.69	40.40	50.00	1.30
Zr	7	119.00	5.51	112.10	130.20	2.08
Hf	8	3.39	0.22	3.11	3.75	0.07
Nb	7	13.38	1.98	10.20	15.50	0.75
Ta	7	0.57	0.17	0.36	0.83	0.06
Th	8	2.21	0.14	2.01	2.44	0.05
U	0	-	-	-	-	-
Na	8	2.14	0.09	2.00	2.24	0.03
Sr	7	356.00	17.14	344.70	394.00	6.47
Ba	7	401.00	49.47	340.00	470.00	18.69
Rb	8	13.00	5.58	6.40	24.20	1.97
Cs	5	0.46	0.06	0.37	0.54	0.02
La	8	14.25	0.89	12.90	15.40	0.31
Ce	8	32.35	2.61	28.30	37.50	0.92
Nd	1	19.70	-	19.70	19.70	-
Sm	8	4.89	0.19	4.58	5.17	0.07
Eu	8	1.62	0.11	1.44	1.84	0.04
Tb	8	0.76	0.15	0.49	0.93	0.053
Yb	8	2.81	0.39	2.24	3.30	0.140
Lu	8	0.46	0.045	0.36	0.51	0.016

^aNumber of samples analyzed.

^bExcept values for Fe and Na, which are percent.



RCP8108-99B

FIGURE 6-5. Zirconium and Chromium Plotted Versus Stratigraphic Position in Borehole DC-6. Vertical axis corresponds to flow number in stratigraphic sequence.

statistical significance of the stratigraphic correlations, based on major elements, and to provide a basis for more detailed correlations within the major-element units. Chromium is particularly useful for subdivision of the high-magnesium section, and forms the principal basis, in conjunction with paleomagnetic data, for correlating flows in this otherwise monotonous section.

6.1.3 General Mineralogy and Petrography of Grande Ronde Basalt

Grande Ronde Basalt flows are aphyric to microphyric or very sparsely phyric basalt with hyalo-ophitic, intersertal to intergranular, or slightly ophitic textures. Subequant-to-lath-shaped pyroxene grains (0.05 to 0.2 millimeter) and lath-shaped plagioclase grains (0.07 to 0.3 millimeter) are set in a glassy mesostasis. Equant-to-cruciform or dendritic titaniferous magnetite grains are scattered throughout the rock, but tend to be most common in glassy areas. Orthopyroxene, pigeonite, olivine, and apatite occur as primary phases. Alteration products include clay minerals, principally smectite clays; zeolites, mainly clinoptilolite and mordenite; and silica in a variety of forms ranging from opal to crystalline quartz and including cryptocrystalline chalcedony, cristobalite, and tridymite. Sulfides, notably pyrite, occur mainly as secondary minerals along cooling joints; some occurrences of sulfides as primary phases have been noted (Ames, 1980). Minor amounts of other secondary phases, such as erionite, chabazite, calcite, vermiculite, phillipsite, and gypsum (Benson and Teague, 1979), have been identified in vesicles in Grande Ronde Basalt. Specific phases that buffer the pH and Eh of groundwater are discussed in detail in Sections 6.2.3 and 11.4.1.4.

Primary phases in Grande Ronde Basalt are listed in Table 6-3 and secondary phases in Table 6-4. Each of the principal primary and secondary phases in Grande Ronde Basalt is discussed individually in the following sections. Information on the ferrous/ferric ratio of whole-rock basalt samples and possible redox-controlling phases (e.g., magnetite, glassy mesostasis) is being gathered and will appear in future updates of this document. An extended discussion of this material is presented in Chapter 3.

6.1.4 Primary Phases in Grande Ronde Basalt

6.1.4.1 Plagioclase. Plagioclase is the most abundant phase in Grande Ronde Basalt. It most commonly occurs as euhedral to subhedral laths that range in length from approximately 0.2 to 1 millimeter and in width from approximately 0.05 to 0.5 millimeter. Although plagioclase grains are almost invariably tabular or lath-shaped, the details of crystal outlines, size distribution, and general arrangement create notable differences in rock textures that have been useful in distinguishing separate flow types (see Chapter 3). Samples from the interior of Grande Ronde Basalt flows exhibit no obvious preferred orientation of plagioclase laths, whereas samples from the glassy basal zones and vesicular flow tops do exhibit a strong preferred orientation.

TABLE 6-3. Petrographic Characteristics of Primary Phases in Grande Ronde Basalt.

Characteristic phase	Abundance (vol%)	Compositional range	Compositional zoning	Grain size (mm)	Texture	Special features
Plagioclase	25 - 50	An ₄₅ to An ₆₅	General moderate, normal. Locally reversed and/or oscillatory	0.1 - 1.0, Average ≈0.25	Lath-shaped	Microphenocrysts common; contains glass inclusions and symmetrically arranged pyroxene inclusion
Augite	20 - 45	(Wo ₃₀ En ₃₈ Fs ₃₂) to (Wo ₃₃ En ₄₅ Fs ₂₂)	Moderate, normal, intergrown with pigeonite, some iron-rich rims	0.05 - 0.8, Average ≈0.20	Euhedral to subhedral prismatic grains	
Pigeonite	0 - 10	(Wo ₁₃ En ₅₀ Fs ₃₇) to (Wo ₉ En ₆₄ Fs ₂₉)	Intergrown with augite, occurs as rims on some clinopyroxene or orthopyroxene grains	~0.1	Anhedral, equant	Mode of occurrence and textures suggest limited stability range in certain flows
Orthopyroxene	0 - trace	(Wo ₄ En ₆₁ Fs ₃₅) to (Wo ₆ En ₇₅ Fs ₁₉)	Unzoned to slight normal zoning	~0.2	Subhedral, prismatic, commonly embayed	Resorption textures and reaction rims indicate instability at 0.1 MPa
Titaniferous magnetite	0 - 7	TiO ₂ = 28 to 32 wt%	Unzoned (?)	~0.05 - 0.4	Octahedral, cruciform, or dendritic	Oxidation lamellae occur in colonnade samples
Mesostasis	15 - 70	SiO ₂ = 60 to 74 wt%	Compositional variation apparent adjacent to magnetite and clinopyroxene grains	~0.1 - 0.3	Intersertal interstitial, with or without abundant tachelytic inclusions	Immiscible liquid blebs common. Highly tachelytic in entablature, relatively inclusion-free in colonnade.
Apatite	0 - 2	ND*	ND*	~0.01 - 0.1	Acicular	Occurs both as discrete grains and as minute crystal aggregates within immiscible liquid blebs
Olivine	0 - 3	Fo ₆₇ to Fo ₄₇	Moderate, normal zoning	~0.05	Anhedral to subhedral, equant	Commonly absent from Grande Ronde flows. Occurrence limited to glassy rind of some flows

*Not determined.

TABLE 6-4. Secondary Minerals Identified in Grande Ronde Basalt, Pasco Basin.

Clay Minerals (Smectite)*		
Montmorillonite	$(\text{Ca}, \text{Na})_{0.66}(\text{Al}^{+3}, \text{Mg}^{+2})_{4-6}(\text{Si}, \text{Al})_8\text{O}_{20}(\text{OH})_4 \cdot n\text{H}_2\text{O}$	} dioctahedral
Beidellite	$(\text{Ca}, \text{Na})_{0.66}(\text{Al}^{+3})_{4-5}(\text{Si}, \text{Al})_8\text{O}_{20}(\text{OH})_4 \cdot n\text{H}_2\text{O}$	
Nontronite	$(\text{Ca}, \text{Na})_{0.66}(\text{Fe}^{+3})_{4-6}(\text{Si}, \text{Al})_8\text{O}_{20}(\text{OH})_4 \cdot n\text{H}_2\text{O}$	
Saponite	$(\text{Ca}, \text{Na})_{0.66}\text{Mg}_6(\text{Si}, \text{Al})_8\text{O}_{20}(\text{OH})_4 \cdot n\text{H}_2\text{O}$	} trioctahedral
Zeolites		
Heulandite	$(\text{Ca}, \text{Na}_2)(\text{Al}_2\text{Si}_7\text{O}_{18}) \cdot 6\text{H}_2\text{O}$	
Clinoptilolite*	$(\text{Ca}, \text{Na}_2, \text{K}_2)(\text{Al}_{1.5}\text{Si}_{7.5}\text{O}_{18}) \cdot 6\text{H}_2\text{O}$	
Mordenite	$(\text{Na}_2, \text{K}_2, \text{Ca})(\text{Al}_2\text{Si}_{10}\text{O}_{24}) \cdot 7\text{H}_2\text{O}$	
Phillipsite	$(\text{Ca}, \text{Na}, \text{K})_3(\text{Al}_3\text{Si}_5\text{O}_{16}) \cdot 6\text{H}_2\text{O}$	
Harmotome	$\text{Ba}(\text{Al}_2\text{Si}_6\text{O}_{16}) \cdot 6\text{H}_2\text{O}$	
Chabazite	$\text{Ca}(\text{Al}_2\text{Si}_4\text{O}_{12}) \cdot 6\text{H}_2\text{O}$	
Erionite	$(\text{Na}_2, \text{K}_2, \text{Ca}, \text{Mg})_{4.5}(\text{Al}_9\text{Si}_{27}\text{O}_{72}) \cdot 27\text{H}_2\text{O}$	
Silica Polymorphs*		
Quartz	SiO_2	
Tridymite	SiO_2	
Cristobalite	SiO_2	
Opal	$\text{SiO}_2 \cdot n\text{H}_2\text{O}$	
Miscellaneous Species		
Gypsum	$\text{CaSO}_4 \cdot 2\text{H}_2\text{O}$	
Calcite	CaCO_3	
Pyrite	FeS_2	

*Identifies the dominant secondary minerals.

Microphenocrysts of plagioclase are common, but typically not abundant; they impart a slight bimodal size distribution to the plagioclase grains. Microphenocrysts also exhibit glass or devitrified-glass inclusions that presumably represent melt trapped by the growing crystal. These inclusions commonly occur along twin planes or in association with embayed or corroded crystal interiors. Other inclusions are principally minute pyroxene grains arranged necklace-fashion along major changes in anorthite content.

6.1.4.2 Augite. Augite is the predominant clinopyroxene phase in the Grande Ronde Basalt and is the second most abundant phase overall in this formation. Early-formed augites exhibit typical prismatic forms that are best developed in glassy rinds of pillows or at the base of flows. In the flow interiors, the prismatic morphology is obscured by late growth on early-formed crystals and by the formation of separate, smaller grains. This yields an overall subhedral, slightly ragged shape to the majority of pyroxene grains and imparts a seriate to bimodal size distribution. Seriate textures are most common in the colonnade, whereas a bimodal size distribution is apparent in the entablature samples. Grain sizes range from approximately 0.05 to 0.5 millimeter and average approximately 0.15 millimeter in length. Prismatic grains are commonly about four times as long as they are wide. Slight normal zoning is nearly ubiquitous in augite grains. The molar ratio of magnesium/magnesium + iron commonly spans a range of 55 to 70, with calcium contents ranging from 27 to 34 mole percent Wollastonite. Inclusions are less common in clinopyroxenes than in plagioclases, but both glass and unidentified crystalline inclusions do occur in the larger grains.

6.1.4.3 Pigeonite. Pigeonite, a second, separate clinopyroxene phase found in Grande Ronde Basalt, occurs in moderate to low abundance in almost all of this formation. It commonly occurs as small groundmass grains. Microprobe studies are in progress to determine its abundance and mode of occurrence. Price (1977), however, has reported a value of 9 volume percent for pigeonite abundance in the Grande Ronde Basalt type locality area. These pigeonites contained 19.9 weight percent FeO, 20.1 weight percent MgO, and 4.9 weight percent CaO. The small grain size, low abundance, and apparent lack of pigeonite in some flows suggest that it has a limited stability range.

6.1.4.4 Orthopyroxene. Orthopyroxene occurs rarely in Grande Ronde Basalt flows. It has been reported from widely scattered localities across the Columbia Plateau (Reidel et al., 1978). Its widespread occurrence suggests that, in spite of its low abundance, it may be of petrogenetic significance. Orthopyroxene grains may be prismatic or rounded and are approximately 1 to 2 millimeters in length. Reaction rims and resorption features are ubiquitous. Textural association or even intimate intergrowth with large plagioclase grains is also very common. Zoning is slight to absent, with most grains exhibiting a uniform, inclusion-free interior.

6.1.4.5 Titaniferous Magnetite. Titaniferous magnetite is the dominant iron-titanium oxide phase in Grande Ronde Basalt. It occurs as octahedral, cruciform, or dendritic grains that range in size from approximately 0.2 to 0.05 millimeter. Octahedral or cruciform grains are typically imperfect or incomplete. The compositional range of this material is not well known, but analyzed samples for one flow, the Umtanum, show a nearly constant TiO_2 content, ranging from 28 to 32 weight percent (Noonan et al., 1980). Little other compositional data are currently available from Grande Ronde Basalt samples. Optical examination, however, indicates that partial high-temperature oxidation (Haggerty, 1976) sometimes occurs along grain boundaries of the blocky, octahedral grains. These are most common in the basal and upper colonnades. Titaniferous magnetite typically constitutes from 3 to 7 volume percent of Grande Ronde Basalt samples. Some samples, notably from very hackly entablature and from glassy rinds of pillows, flow bases, or flow tops, exhibit lesser percentages of extremely small magnetite grains.

6.1.4.6 Olivine. Olivine is relatively rare in Grande Ronde Basalt. Abundances range from 0 to as high as 3 volume percent, with the majority of samples containing less than 0.25 volume percent. Compositions typically range from Fo_{67} to Fo_{47} , with moderate, normal zoning. Grains are anhedral, equant, and approximately 0.05 millimeter in diameter, and are most readily observed in glassy pillow rinds. In certain flows, olivine is essentially restricted to the pillow rinds, suggesting that it may have a reaction relationship with the residual liquid (Schiffmann, 1979).

6.1.4.7 Apatite. Apatite abundance ranges from 0 to 2 volume percent of most Grande Ronde Basalt flows. Its most predominant occurrence is as 0.01- to 0.1-millimeter acicular crystals in the mesostasis, but it also occurs as extremely fine grains within immiscible liquid blebs. Preliminary microprobe data suggest that fluorine is present in the apatites at approximately the 1 percent level. It has not yet been demonstrated whether fluorine can be leached from apatites to provide the observed fluoride concentrations in Grande Ronde Basalt groundwater. Other reactive phases, such as glassy mesostasis, have also been suggested as a source for fluorine ions in groundwater from beneath the Hanford Site.

6.1.4.8 Glassy Mesostasis. An interstitial glassy mesostasis (i.e., glassy groundmass) phase occurs abundantly (15 to 70 volume percent) in Grande Ronde Basalt flows. This glass is inherently metastable relative to some assemblages of crystalline phases. It has been experimentally demonstrated that this glass is the most reactive basaltic phase with groundwater at low-temperature (less than 300°C) hydrothermal conditions. Preliminary analysis of in situ hydrochemistry, as well as laboratory tests, confirm that hydrolysis and dissolution of silicate glass minerals act to buffer pH (Barnes and Scheetz, 1979) and Eh (Jacobs and Apted, 1981) for Grande Ronde Basalt groundwaters in contact with basalt. The mechanism for the control of solution compositional parameters through hydrothermal reaction of the glass phase has not been confirmed by direct experimentation. Electron microprobe study of this glassy mesostasis phase, both before and after hydrothermal alteration experiments, will help to resolve this question.

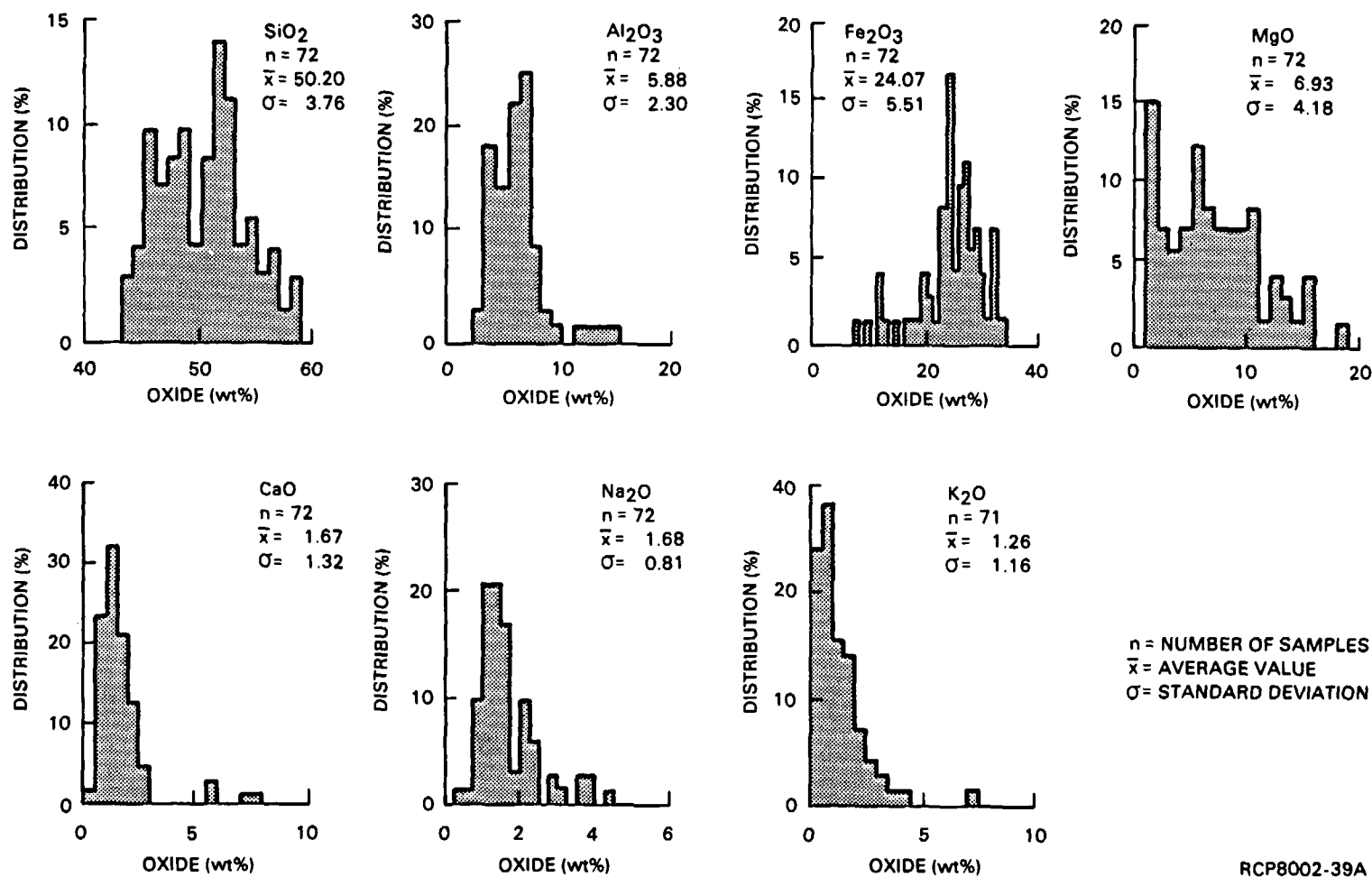
Samples with abundant mesostasis come from the entablature or glassy bases of flows, whereas the samples with the least glass occur in the colonnade. Texture within the mesostasis itself varies considerably with position in the flow. Glass from the colonnade, for example, is relatively inclusion free, whereas glass or mesostasis from the entablature is invariably charged with tiny crystalline inclusions that are dominantly pyroxene, but which also include apatite and magnetite grains. Some of the crystalline inclusions occur as rounded blebs, suggesting that they represent crystallized immiscible liquid. Evidence for liquid immiscibility is also present in colonnade samples, but is absent from glassy pillow rinds and from flow tops. The mesostasis of the flow tops is characterized by felted masses of extremely fine-grained material; presumably, this material is mainly pyroxene.

Compositional data on the mesostasis are sparse. A single study (Noonan et al., 1980) on the Umtanum flow indicates that, at least for that flow, the mesostasis has a highly fractionated bulk composition that is essentially granitic (61 to 73 weight percent SiO_2). Variations in cation abundances exist between the mesostases of entablature and colonnade. The colonnade mesostasis exhibits more K_2O and SiO_2 , but less CaO , Na_2O , FeO , and P_2O_5 than does the entablature mesostasis. It may be that the moderate fluoride concentrations found in Grande Ronde Basalt groundwaters can be attributed to reaction of fluorine-bearing mesostasis.

6.1.5 Secondary Phases

Diagenesis of the Grande Ronde Basalts has produced secondary minerals along fractures, in vugs, and in relatively porous, vesicular rock in flow tops and bottoms. It is observed that the basaltic glass (mesostasis) and groundmass adjacent to vesicles and fractures show a great degree of associated alteration. The principal secondary minerals are predominantly smectite clays and zeolites (clinoptilolite), with lesser amounts of SiO_2 . The data on the minerals reported herein are based on the work of Benson and Teague (1979), Ames (1980), and Teague (1980), as well as on petrographic observations made as part of this study (see Chapter 3). Numerous other secondary minerals have been identified (see Table 6-4), but typically in much lower abundance.

6.1.5.1 Composition and Abundance of Secondary Minerals. The clays and zeolites found in the Pasco Basin basalts have a considerable range in composition, as determined by the electron microprobe studies of Benson and Teague (1979). The average compositions with ranges are illustrated in Figures 6-6 and 6-7. The zeolites and clays are both hydrated silicates; thus the difference between the summations of the average oxides determined and 100 percent is attributed to the presence of water. The average compositions with structural formulas are presented in Table 6-5. The relative abundances of the principal secondary minerals are given in Table 6-6. Note that smectite clays are significantly more abundant in fractures than in vugs.



RCP8002-39A

FIGURE 6-6. Compositions of All Clays (mostly smectite) Formed Prior to Deposition of Zeolite or Silica (after Benson and Teague, 1979).

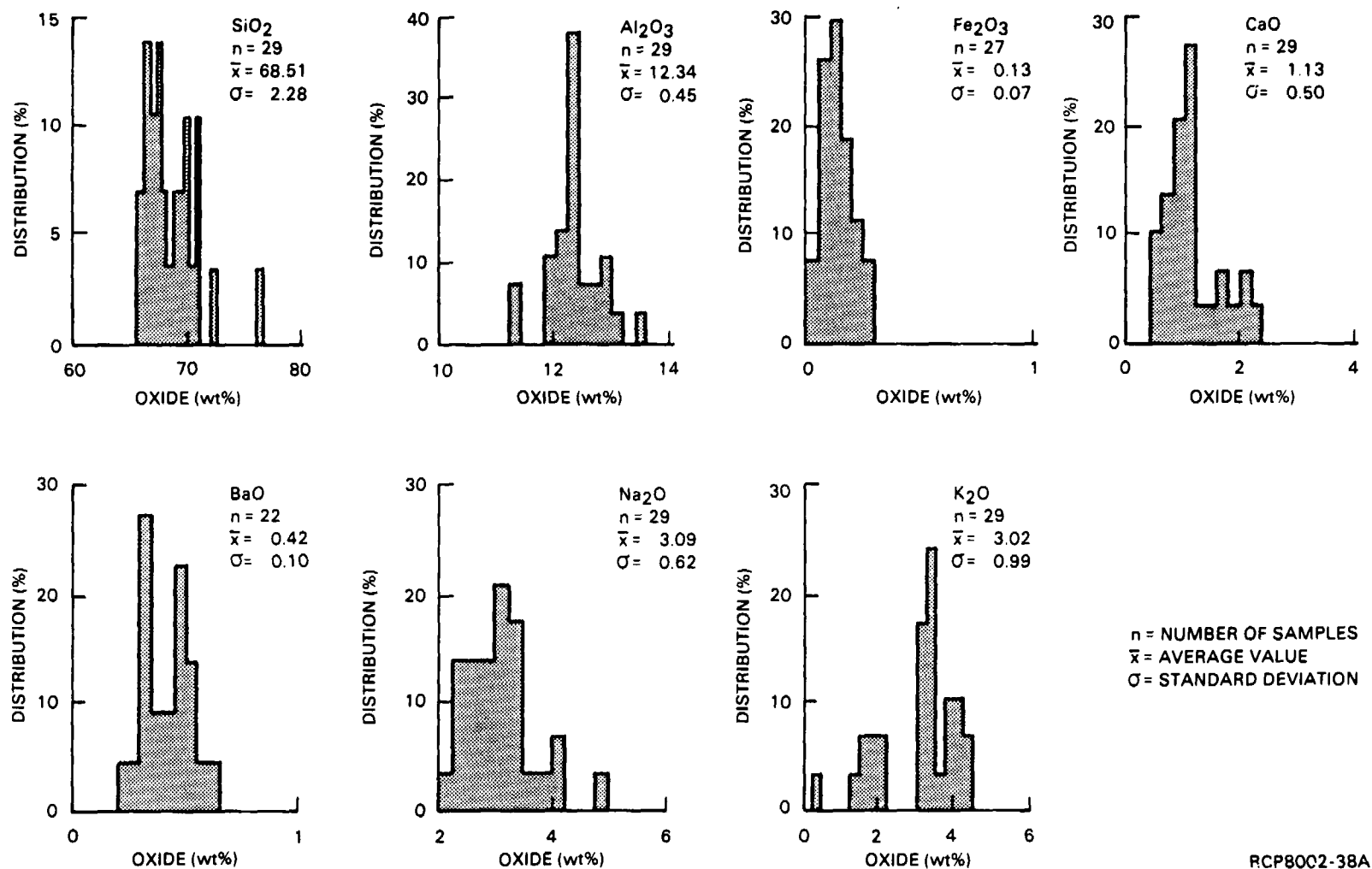


FIGURE 6-7. Compositions of First and Second Generations of Secondary Zeolite (after Benson and Teague, 1979).

TABLE 6-5. Mean Composition of Hanford Clay and Zeolite with Structural Formulas (after Benson and Teague, 1979).

SiO ₂	Al ₂ O ₃	Fe ₂ O ₃	CaO	BaO	Na ₂ O	K ₂ O	MgO	H ₂ O
Smectite								
(Si _{3.64} Al _{0.36}) (Al _{0.23} Fe ⁺³ _{0.72} Fe ⁺² _{0.20} Mg _{1.12}) (Ca _{0.14} Na _{0.46} K _{0.15}) O ₁₀ (OH) ₂								
50.20	5.88	24.07	1.67	0.06	1.68	1.26	6.93	8.25
Clinoptilolite								
(Si _{29.84} Al _{6.34} Fe ⁺³ _{0.04}) (Ca _{0.53} Ba _{0.07} Na _{2.61} K _{1.68} Mg _{0.01}) O ₇₂ 9.44 H ₂ O								
68.51	12.34	0.13	1.13	0.42	3.09	3.02	0.02	11.34

TABLE 6-6. Relative Proportions of Secondary Minerals in Grande Ronde Basalt, Pasco Basin.

Mineral	Vesicles	Fractures
Smectite	~32*	~75
Clinoptilolite	~43	~20
Silica	~25	~5

*Values are in percent by volume of total amount present. For abundance of fracture fillings as a percentage of total rock mass, see Figure 6-8. Data from Benson and Teague (1979).

Fracture measurements have been made by fracture logging of both surface exposures and core samples, with special emphasis on Grande Ronde Basalt flows. The great majority of fractures in drill cores have narrow apertures (less than 0.5 millimeter) and contain multiple generations of secondary minerals (see Section 6.1.5.2). The volume abundance of fractures (both filled and unfilled), relative to the total rock mass, is indicated in Figure 6-8. The total volume percent of all fractures is less than 0.4 percent, but the volume percent of unfilled fractures is even less, ranging from 0.025 to 0.059. The volume percent of vesicle fillings is nil in the interior of the flow, but increases to as much as 20 volume percent in the flow top and vesicular base. Although such data are not yet available specifically for the candidate repository horizons, similar results are expected. These results suggest the volume of unfilled vesicles and fractures, particularly in the dense interior of Grande Ronde Basalt flows, is small and thus the total porosity of this rock is comparably small. In addition, the secondary mineral content and glass-rich texture of such flows are expected to provide sorptive minerals and alteration products to retard radionuclide migration along potential groundwater pathways.

A second significant feature of filled fractures is that clay minerals, when heated above 300°C, may reversibly lose interlayer (sorbed) water and undergo volume reduction (Koster van Groos, 1981). This latter factor could increase permeability and decrease mechanical stability of the rock mass after the emplacement of waste. Alternatively, when the clay-filled fractures are wet by solutions carrying radionuclides, the clay could expand again, thus filling the fractures. At significantly higher temperatures, irreversible dehydration of bound water occurs (Koster van Groos, 1981), causing metamorphic transition of clays to new minerals. Zeolites can also undergo dehydration and associated volume reduction upon heating (Smyth and Caporuscio, 1981). Consequently, the behavior of the fracture-filling materials in the thermal field of the repository may be important in evaluating repository performance. Experimental evidence indicates that pressures at repository depths tend to stabilize the clay minerals (see Section 6.3).

6.1.5.2 Paragenesis of Secondary Minerals. Paragenesis studies of several secondary mineral assemblages by microprobe have been conducted by Benson and Teague (1979). Their general observations are as follows:

- Single generations of clay in vesicles and fractures appear homogeneous, whereas single generations of clinoptilolite are somewhat heterogeneous.
- In vesicles and fractures having multiple generations of clay or clinoptilolite, chemical composition often changes significantly from generation to generation.
- Multiple generations of clay from fractures at the same depth appear to exhibit similar compositional variations.

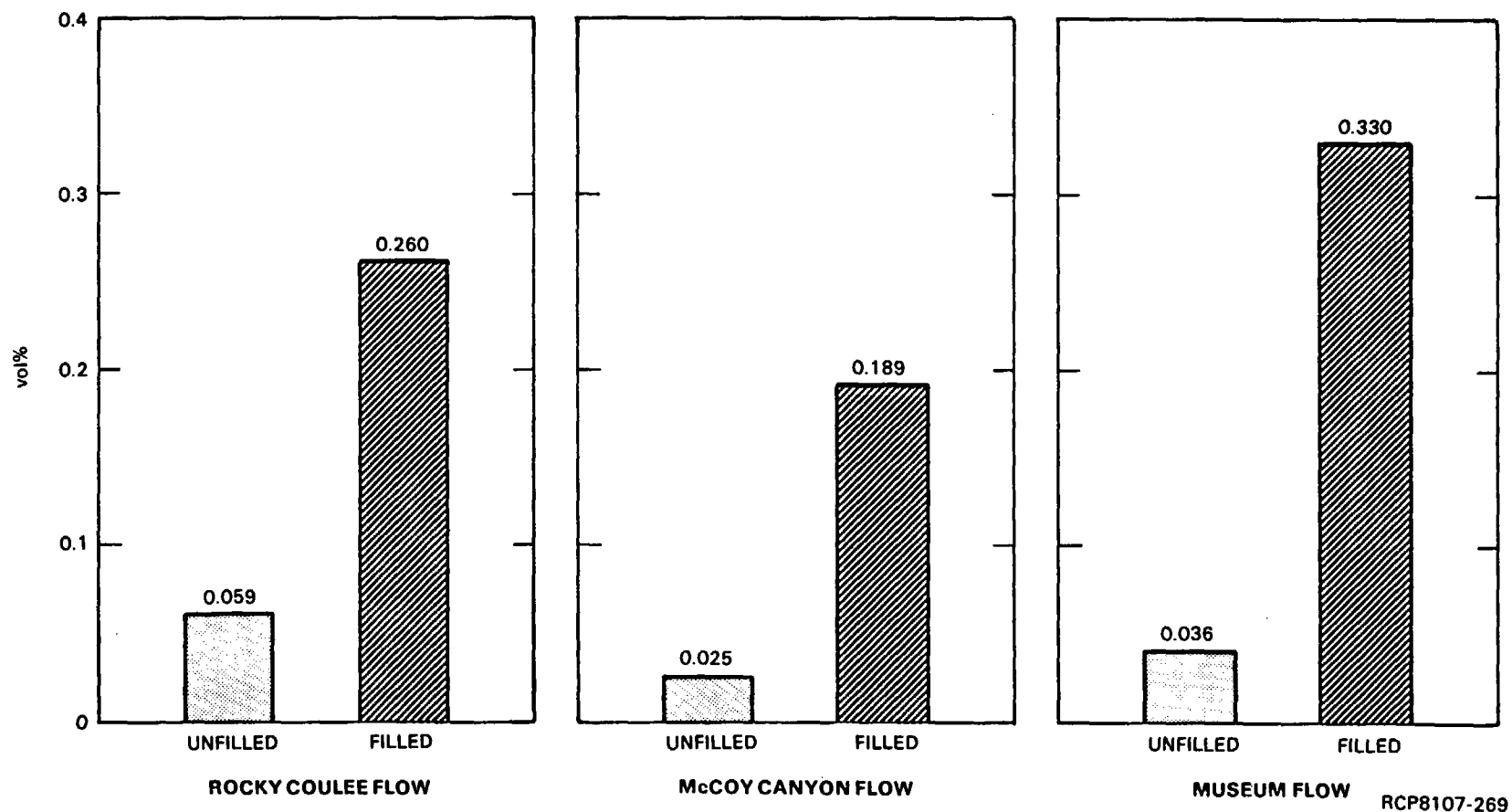


FIGURE 6-8. Volume Percent, Filled and Unfilled Fractures, Rocky Coulee, McCoy Canyon, and Museum Flows. Values presented are calculated by summing fracture widths and dividing by total length of core over which the fractures occur. From these examples, it appears that the maximum fracture volume (filled and unfilled) is less than 0.4 volume percent.

- Multiple generations of clays from vesicles at the same depth also show similar compositional variations from generation to generation.
- There are considerable differences between the compositions of individual generations of clay from either vesicle or fracture samples. No overall systematic trend in composition as a function of distance from vesicle or fracture walls has been found to exist.

It is apparent that the basalt vesicles exhibit a more complex mineralogy than do the fractures. The fractures generally contain clinoptilolite, smectite, and silica with small amounts of illite and pyrite, whereas the vesicles also contain minor amounts of the zeolites (erionite, chabazite, and phillipsite) with vermiculite (chlorite?), gypsum, and calcite. The layered precipitation sequence recognized in both vesicles and fractures, however, seems to be the same. For the assemblages, the sequence is usually clay, clinoptilolite, and silica followed by clay. Benson and Teague (1979) showed that clay is the first mineral to form in 96 percent of the fractures and 94 percent of the vesicles. Clinoptilolite makes up the difference and is the second phase to form in fractures 81 percent of the time and in vesicles 97 percent of the time. For assemblages having additional layers, silica followed by clinoptilolite is in the sequence 100 percent of the time in fractures and 67 percent of the time in vesicles (Fig. 6-9). Clay was again precipitated after zeolite in the remaining 33 percent of the vesicles. It is also recognized that the assemblages are sometimes reversed in no apparent systematic manner. Dissolution followed by reprecipitation of one or more secondary minerals is also recognized as a common occurrence (Smith et al., 1980).

6.1.5.3 Vertical Zonation of Secondary Minerals. The distribution data for secondary minerals as a function of depth have been previously studied (Benson and Teague, 1979; Ames, 1980). These results indicated that, of the clay minerals, smectite seems to occur throughout the sampled section, although it is possibly less abundant below 900 meters; whereas illite occurs unevenly through the section. Quartz occurs throughout all cores. Cristobalite, which occurs as often as quartz throughout the section, is the dominant silica phase in the 600- to 1,000-meter interval. Small amounts of tridymite and opal also occur through the section.

Clinoptilolite occurs in all samples below about 400 meters, but is absent at shallower depths. Dissolution of clinoptilolite is indicated below about 950 meters, the approximate depth at which mordenite first appears. However, both clinoptilolite and mordenite occur in all samples studied below 950 meters. This depth to the initial appearance of mordenite is nearly the same at all wells investigated thus far, and apparently is not deflected by folds in the basalt (Smith et al., 1980). This suggests either that the mordenite was not formed until after folding had occurred or that the dissolution and formation of mordenite were able to keep pace with the rate of folding. There is no textural evidence to

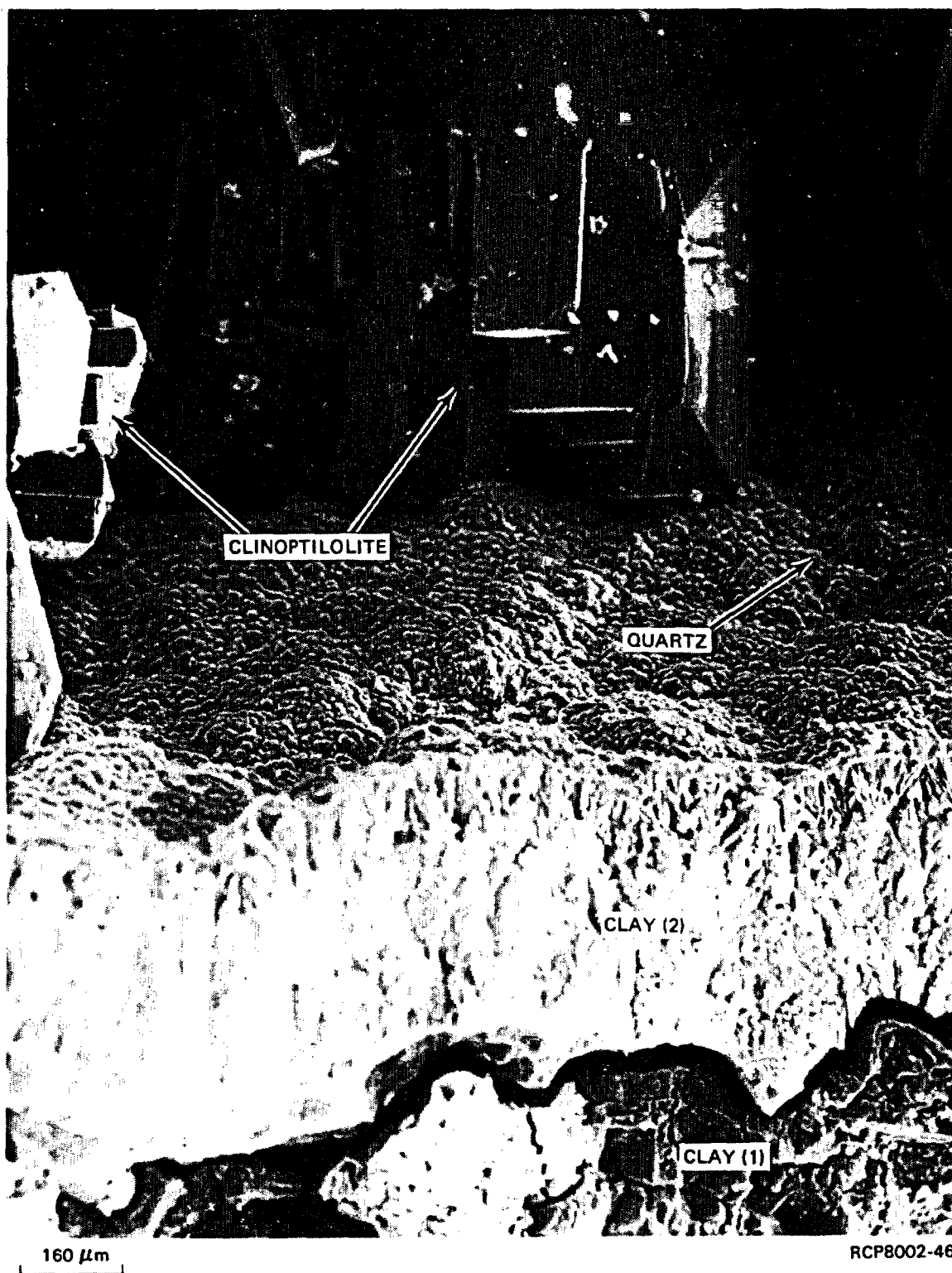


FIGURE 6-9. A Typical Crystallization Sequence for Secondary Minerals. The initial clay, at bottom, shows desiccation cracks and is separating from the second clay layer. The surface of the second clay layer is coated with a layer of quartz followed by large well-developed clinoptilolite crystals (after Benson and Teague, 1979).

support the latter possibility, suggesting that the mordenite distribution was largely established postfolding (i.e., sometime in the last 6 million years). Furthermore, experimental data on the stability of mordenite (Smyth and Caporuscio, 1981) imply that the temperature at the depth at which mordenite first appears should be higher than it actually is. The first appearance of mordenite with depth, then, perhaps represents a fossil geothermal gradient somewhat higher than the one that currently exists.

6.1.5.4 Mineraloids. Chlorophaeite, iddingsite, and mineraloid are terms commonly used to refer to secondary minerals in basalt. Mineraloid is a general term referring to inorganic materials that are amorphous. The only identified alteration phases in these basalts that could be classified as mineraloid are opal and hydrated basaltic glass. In spite of liberal use of the term mineraloid in the literature in reference to secondary minerals in Columbia River basalt, including fracture and vug fillings, the majority of secondary phases are well-defined mineral species.

Chlorophaeite is a "specific" mineraloid similar to chlorite in composition (magnesium, iron, calcium silicate). As with the more general term mineraloid, chlorophaeite is used to refer to vug and fracture fillings, altered interstitial glass, and pseudomorphs after olivine. Chlorophaeite is a useful, general term for field descriptions, but as applied to Columbia River basalt it includes much material that is herein reported as specified mineral species, particularly zeolites and clay minerals.

Iddingsite refers to alteration products of olivine, and is considered to be a mixture of magnesium, calcium, and iron silicates. This term may be applied to olivine-bearing flows but, again, actual mineral species constituting iddingsite are probably specific zeolites and clay minerals.

6.1.6 Composition of Interbeds in the Pasco Basin

Aquifers, both confined and unconfined, represent horizons that might serve as pathways to the release of radionuclides in a disrupted repository. The compositions and structures of these layers are important parameters in the discussion of geochemical interactions with possible radionuclide-bearing groundwaters. In the Pasco Basin, confined aquifers are those permeable interbeds and basalt flow tops occurring between low-permeability basalt flows that act as aquitards. In general, these more permeable units occur in the Wanapum and Saddle Mountains Basalts. The major interbeds occurring throughout the basin are the Vantage in the Wanapum Basalt and the Mabton, Cold Creek, Selah, Rattlesnake Ridge, and Levey in the Saddle Mountains Basalt (see Fig. 6-1 for stratigraphic position). The interbed material is mostly tuffaceous siltstone, although quartzose sands, conglomerates, and well-sorted vitric tuffs also occur.

The Vantage interbed consists of a fine-grained micaceous quartzose sand that marks the contact between the Grande Ronde and Wanapum Basalts in most of the Pasco Basin. The thickness of this marker bed is between 0 and 8 meters, with its greatest thickness in the northwestern portion of the basin. The unit thins to 4 meters in the central part of the basin, where it is composed of black clay, clayey sandstone, and loosely consolidated sand. Locally within the basin the Vantage interbed is absent but is represented by Grande Ronde Basalt sapolite (see Section 3.5.4).

The Mabton interbed is a unit occurring between the Wanapum and Saddle Mountains Basalts and is the most extensive and voluminous interbed within the Pasco Basin. It is a tuffaceous silt characterized by red and purple opal near the top, occurring in thicknesses in excess of 50 meters in the northwestern part of the basin (see Section 3.5.4). Vertical lithologic changes have been recognized within the basin. From top to bottom the unit consists of: (1) a well-indurated lapilli tuffstone, locally baked; (2) a fine-grained tuffaceous, clayey, quartzitic sandstone; and (3) a loosely consolidated, quartzitic or arkosic sand or sandstone with interlayered volcanoclastic sediments.

Saddle Mountains Basalt contains several major interbeds. The lowermost, Cold Creek interbed, occurring between the Asotin and Esquatzel Members, ranges from 0 to 35 meters in thickness and is restricted to the Cold Creek syncline area. The unit is composed of tuffaceous to arkosic sandstone with a middle conglomerate of well-rounded and closely packed basalt cobbles in a black sandstone.

The Selah interbed occurs locally in the Pasco Basin in variable thicknesses, stratigraphically located between the Esquatzel and Pomona Members. It is a clean and well-sorted vitric tuff, locally silty and sandy, with some chert at the Pomona contact. Its distribution also parallels the Cold Creek syncline beneath the Hanford Site, where it is probably at least 20 meters thick.

The Rattlesnake Ridge interbed is a tuffaceous silt and sandstone, thickest along the Cold Creek synclinal axis, but occurring throughout the basin. It occurs between the Pomona and Elephant Mountain Members. Like the Cold Creek interbed, it has a thick cobble-conglomerate facies of mostly basaltic clasts.

The uppermost interbed in the Saddle Mountains Basalt, the Levey interbed, occurs between the Elephant Mountain and Ice Harbor Members. It is generally a tuffaceous siltstone unit from 0 to 6 meters thick, occurring in the eastern part of the Pasco Basin. Minor interbeds within the Saddle Mountains Basalt include a vitric tuff 1 to 2 meters thick, separating two flows of the Esquatzel Member (Gable Mountain interbed) and a thin, 15-centimeter layer separating the Wilbur Creek and Umatilla Members.

6.2 GROUNDWATER GEOCHEMISTRY

At present there are no hydrochemical data available for deep basalt horizons within the reference repository location. Hydrochemical data for a number of groundwater horizons within the Grande Ronde Basalt, however, have been collected from five boreholes (DC-1, -6, -12, -14, and -15) at the Hanford Site (Fig. 6-10). Downhole temperature and pressure data have been compiled from boreholes DC-1, -2, -4, -6, -7, -12, -14, -15, and DB-15 (Fig. 6-10).

Because of the general low permeability of the Grande Ronde Basalt flow interiors, no areal hydrochemical data are currently available for the candidate repository horizons. Data are available, however, for the Umtanum flow top and bottom. Hydrochemical data collected at the five borehole sites listed above are given in Table 6-7. Borehole DC-12 data are also included individually in the table and, because of the proximity of DC-12, may be more representative of the conditions within the candidate repository horizons. This assumption will be tested when data from the boreholes within the reference repository location are completed. A more complete presentation of the material summarized in this section is contained in Chapter 5.

6.2.1 Major Inorganic Content

Examination of Table 6-7 indicates that groundwater in the proposed repository horizons (Fig. 6-1) may be expected to have a total-dissolved-solids content between 600 and 1,200 milligrams per liter, with an ionic strength between 1.7×10^{-2} and 7.4×10^{-3} . Table 6-7 illustrates a similar comparison of the "mean" composition and the range in values for individual chemical species of the middle Sentinel Bluffs and Umtanum flows. However, this table is based upon a limited amount of data and must be considered preliminary in nature. Available hydrochemical data also indicate that the waters are of the sodium-chloride chemical type.

Of particular interest for Grande Ronde Basalt groundwaters are elevated fluoride concentrations that exceed maximum permissible concentrations for drinking water standards (EPA, 1975). The source of fluoride in the groundwater is currently unknown. Fluoride is present as a minor constituent in basalt, primarily occurring in basaltic glass horizons. It is believed to be selectively leached during water-rock interactions (hydrolysis) along interflow contacts. Future studies will include whole-rock analyses for fluoride in basalt flow interiors and interflow contacts and additional investigations to examine geochemical processes that may contribute to the elevated fluoride concentrations.

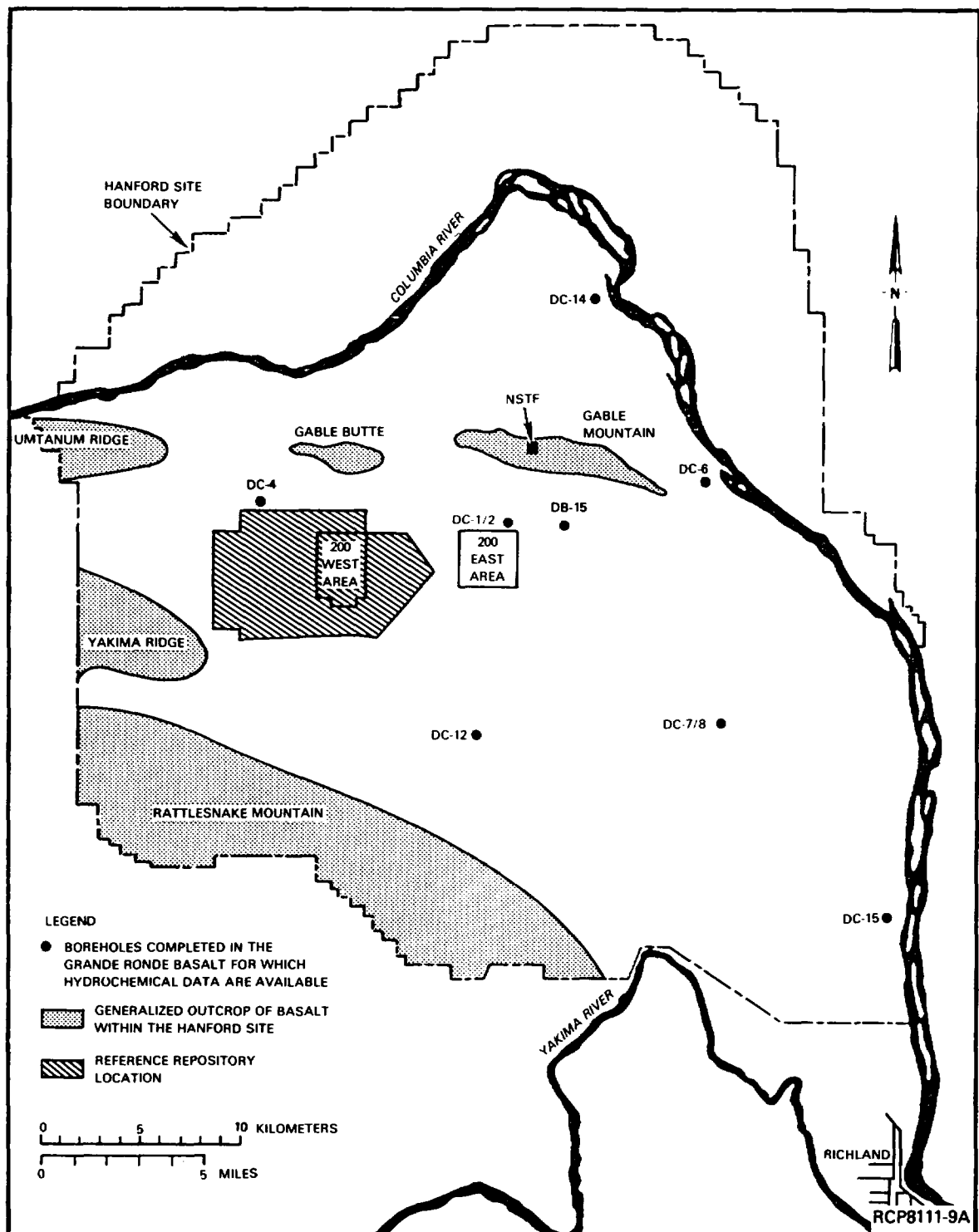


FIGURE 6-10. Location of Boreholes Used for Geochemical Studies of Groundwater.

TABLE 6-7. Summary of Hydrochemical Data Available for
Middle Sentinel Bluffs and Umtanum Flow Tops and
Bottoms from Boreholes on the Hanford Site.

Constituent	Umtanum flow		Middle Sentinel Bluffs flow	
	Range (mg/L)	Mean (mg/L)	Range (mg/L)	Mean (mg/L)
Anions				
HCO_3^-	45 - 102	60	64 - 118	89
CO_3^{2-}	4 - 55	19	8 - 24	18
Cl^-	98 - 289	194	117 - 297	199
SO_4^{2-}	4.2 - 191	121	4 - 197	133
NO_3^-	<0.5	<0.5	<0.5	<0.5
F^-	13 - 42	32	11 - 22	17
H_3SiO_4^-	9.1 - 109	53	23 - 70	44
Cations				
Na^+	161 - 360	274	163 - 350	247
K^+	3.3 - 8.1	5.9	12 - 16	14
Ca^{+2}	0.8 - 4.5	2.4	1.6 - 10	5.5
Mg^{+2}	<0.01 - 0.15	0.04	0.08 - 0.17	0.14
H_4SiO_4	75 - 132	116	107 - 146	124
pH (field)	8.8 - 10.1	9.5	9.3 - 9.6	9.5
Total dissolved solids	626 - 1,071	886	600 - 1,201	857
Ionic strength	1.7 E-02 to 7.4 E-03	1.3 E-02	1.8 E-02 to 7.4 E-03	1.3 E-02

6.2.2 Trace Elements

The range of concentration and the median composition of trace elements within groundwaters of the flow top and flow bottom of the Grande Ronde Basalt are listed in Table 6-8. The elements consistently present in measurable concentrations include aluminum, boron, iron, and molybdenum. The presence of molybdenum in the groundwater samples is probably attributable to minor contamination by molybdenum-based pipe-joint lubricant. Samples from the more productive interflow zones generally do not contain molybdenum in quantities above the detection limit (10 micrograms per liter). Samples are also routinely analyzed for uranium as part of the hydrology isotopic studies. Uranium concentrations in groundwater from zones within the Grande Ronde Basalt are generally below the current detection limits (1 nanogram per liter).

TABLE 6-8. Range and Median Values of Trace Elements for Groundwater Within the Grande Ronde Basalt Beneath the Hanford Site.^a

Trace element	Range (µg/L)	Median (µg/L)
Al	<0 - 180	90
B	<5 - 1,450	980
Ba	<5 - 80	<5
Cd	<5	<5
Co	<5	<5
Cr	<5 - 10	<5
Ca	<5 - 9	<5
Fe	<5 - 2,000 ^b	60
Mn	<10 - 470	<10
Mo	<10 - 990	440
Ni	<5	<5
Zn	<5 - 200	<5

^aIncludes data from boreholes DC-6, -12, -14, and -15.

^bMaximum value is possibly associated with nonrepresentative sample.

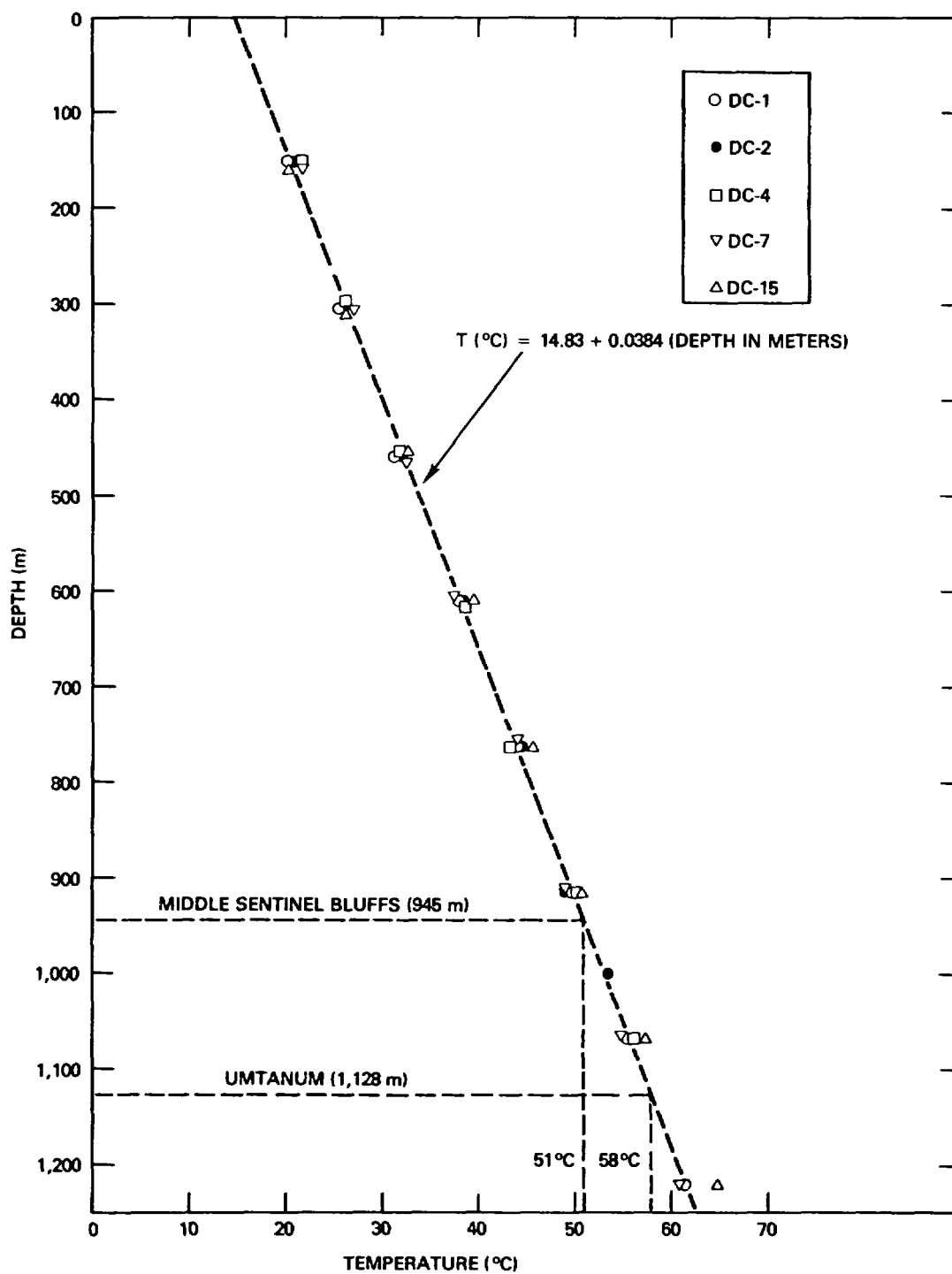
6.2.3 Hydrochemical Field Parameters

6.2.3.1 Temperature. Fluid temperatures within groundwater formations of the Grande Ronde Basalt generally reflect the local geothermal gradient. Fluid temperatures from five representative borehole sites are plotted against depth in Figure 6-11, as well as the linear regression line that was fitted to all of the available borehole data. The average geothermal gradient within the Columbia River Basalt Group at Hanford is calculated to be 38.40°C per kilometer. The depth location of the middle Sentinel Bluffs flow at 945 meters (3,100 feet) and the Umtanum flow at 1,128 meters (3,700 feet) is projected onto the regression line, providing estimated expected temperatures of 51° and 58°C for those respective candidate repository horizons. The downhole temperatures in borehole DC-15 appear slightly higher than the normal geothermal gradient because that hole was logged before downhole temperatures had equilibrated following borehole completion. During site characterization, an additional temperature log of DC-15 will be obtained to provide temperatures, measured under equivalent conditions, between boreholes.

6.2.3.2 Pressure. The profiles of pressure (converted from hydrostatic head data (see Section 5.1.4.2) versus depth from five representative boreholes) are presented in Figure 6-12. These data, as well as all other available borehole hydrostatic head data, have been fitted to a linear regression line, which is also shown in Figure 6-12. The approximate projected pressures for the middle Sentinel Bluffs and Umtanum flows are 9.3 megapascals (1,350 pounds per square inch) and 11.1 megapascals (1,610 pounds per square inch), respectively.

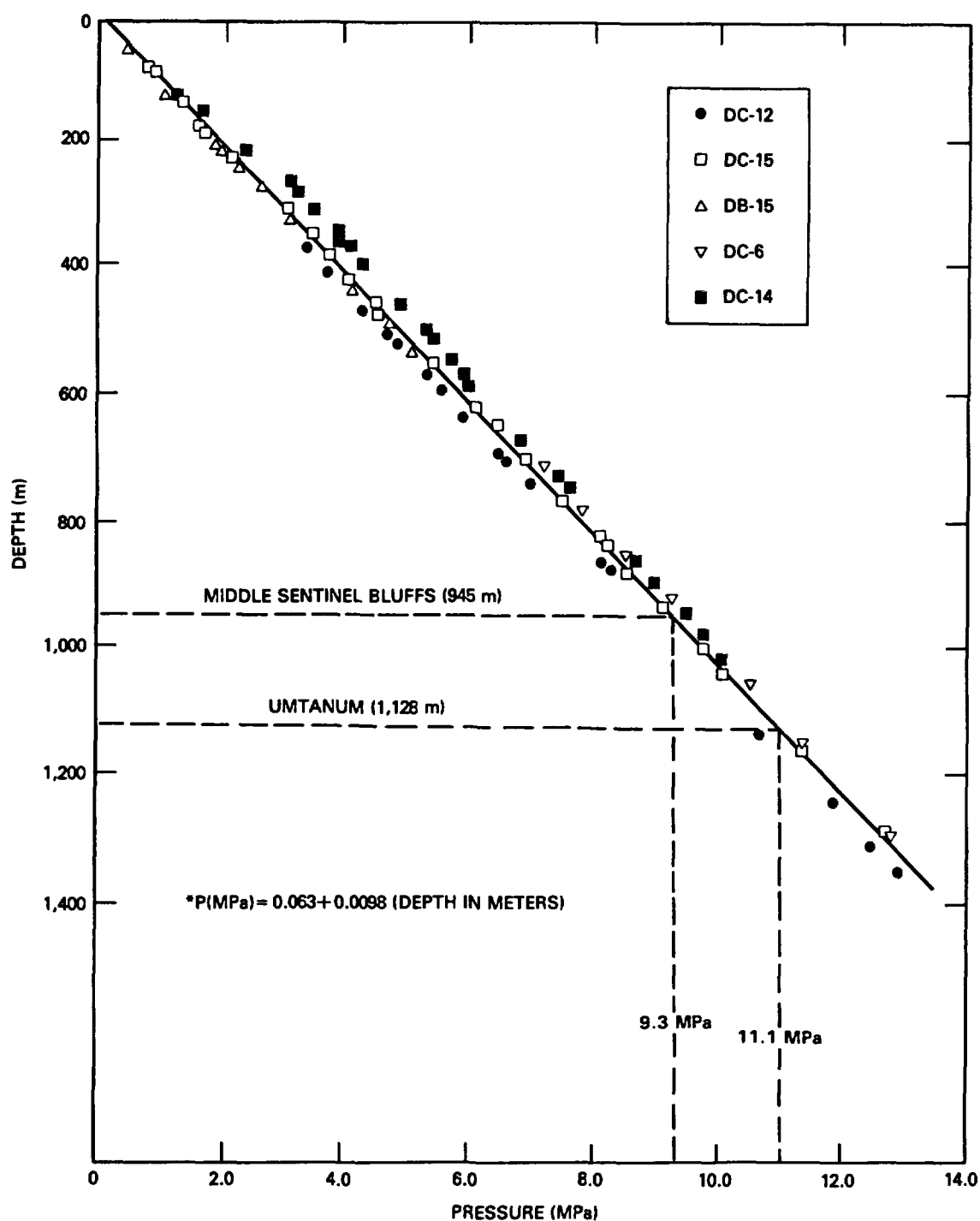
6.2.3.3 pH. The pH of waters in the Umtanum flow top and bottom range from 8.8 to 10.1 at the Hanford Site. These elevated pH values are attributed to hydrolysis of silicate minerals and/or silicate glass (Krauskopf, 1979; Marshall and Warakowski, 1980; Smith et al., 1980). In addition, groundwater within the Umtanum flow top and bottom are highly buffered by the dissolved silica species (see Sections 5.1.5.2.3 and 11.4.1.4). The groundwater pH at borehole DC-12 (Table 6-7) falls within the middle of the range cited for Umtanum flow-top and -bottom waters. Based on borehole DC-12 and available areal data, the pH within groundwaters of the candidate repository horizons in the reference repository location is expected to fall within the middle of the measured pH range (equal to approximately 9.5).

6.2.3.4 Eh. The Eh, a measure of oxidation potential, in the waters of the Columbia River Basalt Group was previously discussed in Section 5.2.3. Surface electrochemical measurements of Eh for groundwaters from the Grande Ronde Basalt at Hanford indicate that the waters are reducing and range from 0 to -0.21 volt. As discussed previously, measurement of this parameter can be qualitative and subject to large measurement errors under the best of conditions (Langmuir, 1971; Stumm and Morgan, 1981). Thermodynamic calculations, based on assemblages of alteration minerals in equilibrium with groundwater at depth and measurement of dissolved redox couples, indicate that Eh may be in the range of -0.45 to -0.55 volt under ambient repository conditions (Smith et al., 1980; Jacobs and Apted, 1981). (See Section 11.4.1.4) Future studies will include downhole potentiometric measurement of Eh and measurement of dissolved redox couples to calculate Eh.



RCP8111-10A

FIGURE 6-11. Measured Fluid Temperature Versus Depth in Selected Boreholes in the Hanford Site. The line represents a linear regression fit to available borehole temperature data.



RCP8111-11A

FIGURE 6-12. Calculated Pressure Versus Depth in Selected Boreholes in the Hanford Site. The line represents a linear regression fit to available borehole hydrostatic head measurements.

6.2.4 Dissolved Gas

Dissolved gas concentrations within groundwaters of the Columbia River basalts have been detected in quantities of 0 to 60 cubic centimeters per liter of water at standard temperature and pressure conditions. Samples containing the greatest amount of dissolved gas are from methane-bearing horizons in the lower Saddle Mountains and upper Wanapum Basalts (see Section 5.1.5).

In contrast with shallow basalt formations, Grande Ronde Basalt groundwaters generally contain only minor amounts of dissolved gas. Gas composition within the Grande Ronde Basalt also differs significantly from that of groundwater zones of overlying basalt formations, being almost entirely nitrogen (Table 6-9). Argon, helium, and methane normally occur in only trace amounts. The variation in gas content (i.e., methane versus nitrogen dominant) and concentration of dissolved gas present within the groundwaters of the Wanapum and Grande Ronde Basalts is consistent with the distinct hydrochemical and isotopic breaks discussed previously (Section 5.1.5), which occur between these two geohydrologic units within the Hanford Site.

As shown in Table 6-9, dissolved oxygen has also been detected in some groundwater samples from the Umtanum flow top and bottom. Eh conditions in the deep basalt zones, however, preclude the presence of detectable quantities of dissolved oxygen in formation groundwaters. The presence of oxygen is, therefore, attributable to contamination by atmospheric oxygen during sample collection.

TABLE 6-9. Median Value and Range in Composition of Dissolved Gas in Grande Ronde Basalt Groundwater.*

Gas type	Range in composition (mole %)	Median composition (mole %)
CO ₂	0.01 - 0.16	0.01
Ar	1.12 - 1.60	1.23
O ₂	0.01 - 0.49	0.01
N ₂	96 - 98	97.6
CO	0.01	0.01
He	0.29 - 0.39	0.32
H ₂	0.01 - 0.36	0.01
CH ₄	0.01 - 1.95	0.48

*Data from boreholes DC-6, -12, -14, and -15.

6.3 CHEMISTRY OF WASTE, BARRIERS, AND NEAR-FIELD ENVIRONMENT

An understanding of the performance of the waste form and engineered waste package components in the near-field environment of a repository in basalt is necessary for the selection of materials and the design of effective site-specific waste packages that meet performance requirements. An extensive testing program has been planned, and work has been initiated to assess these interactions. The purpose of this section is to summarize what is presently known about the interactions among the reference waste forms, candidate barrier materials, and the hydrothermal environment expected in a repository constructed at Hanford. A broader discussion of the subject can be found in Chapter 11.

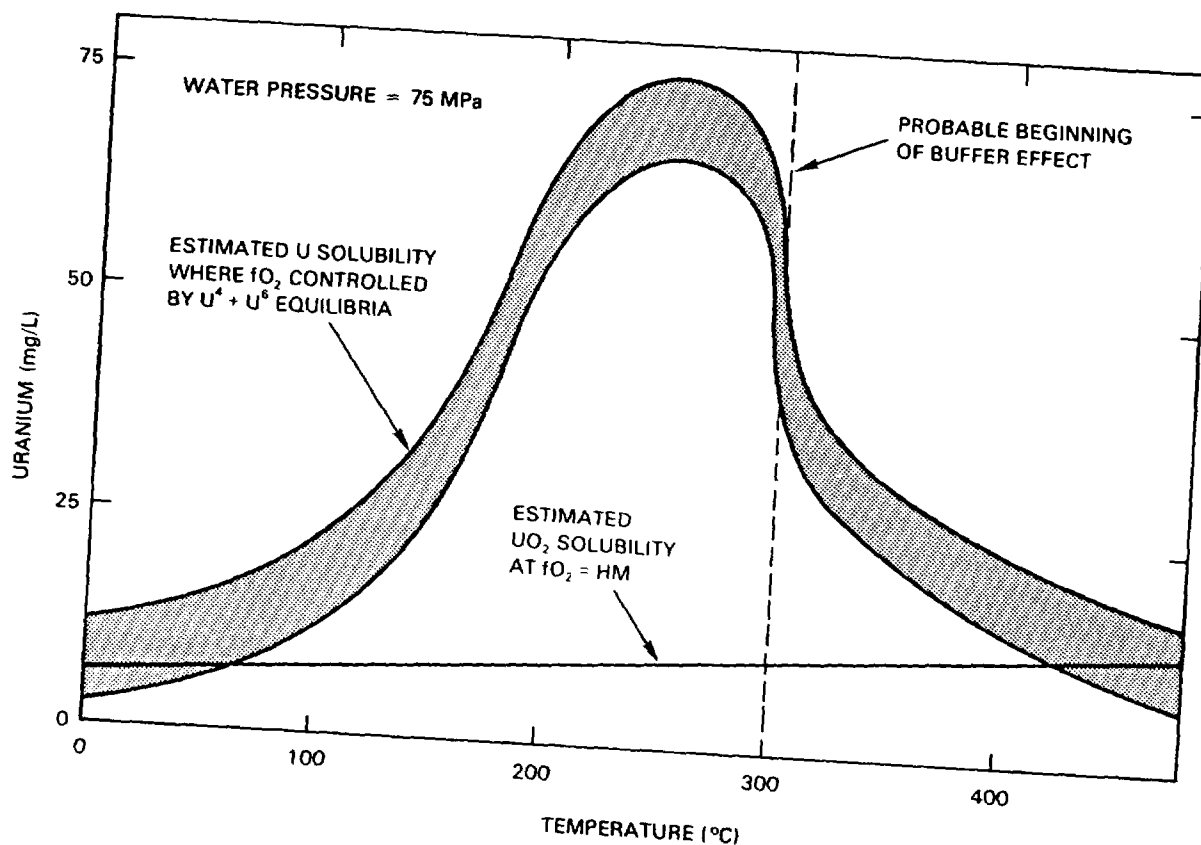
6.3.1 Waste Forms

The National Waste Terminal Storage (NWTs) Program reference waste forms are spent fuel and, for reprocessed commercial high-level waste, borosilicate glass. Tailored ceramic is considered as an alternate waste form. Borosilicate glass is the reference waste form for defense high-level waste. Until recently, supercalcline was also considered an alternate commercial high-level waste form by the NWTs Program. Preliminary studies have been conducted to evaluate the hydrothermal reactions between these waste forms and water.

6.3.1.1 Spent Fuel-Water Interactions. Commercial light water reactor fuel consists of sintered uranium dioxide (UO_2) pellets contained in sealed metal tubes (cladding) that constitute the fuel rods. The fuel rods are mounted in arrays called assemblies. For the Basalt Waste Isolation Project (BWIP) repository conceptual design studies, the reference spent fuel waste form configuration is a close-packed array of the spent-fuel rods that were taken from fuel assemblies and packaged in canisters. Upon discharge from a reactor, a typical light water reactor fuel rod consists essentially of clad but cracked uranium fuel pellets containing rare earth, yttrium, zirconium, and minor amounts of other oxides in solid solution.

The extent of spent fuel dissolution in groundwater will be influenced by the chemical composition of the groundwater in contact with it, particularly its pH. The oxidizing or reducing capacity of the repository environment will also affect dissolution rates, particularly for elements such as uranium, which can exist in either oxidized or reduced form. At present, no experiments have been performed with spent fuel in which direct control of oxidation-reduction potential has been attempted. However, data from other UO_2 dissolution experiments (Lemoine, 1975; Langmuir, 1978) give an indication of the effects that oxidation-reduction may have upon uranium leachability from spent fuel. Lemoine obtained the uranium solubility- (in distilled water) versus-temperature curve shown in Figure 6-13 using a platinum membrane and a hematite-magnetite solid-state buffer (Eugster and Wones, 1962) to fix the oxygen fugacity. The results showed that under a high-oxygen fugacity, typical of that found in the repository immediately following closure, the UO_2 dissolution rate was

higher than when the oxygen fugacity was controlled at a lower value by the hematite-magnetite buffer. This latter oxygen fugacity would be similar to the conditions in the repository following decommissioning, when repository conditions are under control of the basalt and are highly reducing (Jacobs and Apted, 1981).



RCP8107-84

FIGURE 6-13. Solubility of UO_2 in Water as a Function of Temperature; fO_2 in the Experiments Buffered by the Equilibrium Between UO_2 and UO_3 under Oxidizing Conditions (after Lemoine, 1975). Estimated UO_2 solubility at hematite-magnetite (HM) oxygen fugacity (fO_2) plotted as a thin line.

The result of preliminary experiments conducted by The Pennsylvania State University for the BWIP at 100°C to 300°C and under a pressure of 30 megapascals showed that above 100°C, cesium, rubidium, and molybdenum (and by analogy, technetium) are nearly totally leached from simulated spent fuel by distilled water. This behavior tends to be corroborated by the results of analyses of spent fuel storage cooling water (approximately 500°C). In these pools, which are mildly acidic (pH 4.5 to 5.5), about 72 percent of the radionuclides detected in solution are cesium, while strontium accounts for approximately 27 percent (Johnson, 1977). A small amount of ^{131}I has also been detected. Iodine-129, while not detected, should also be present. Ambient-pressure leach tests of actual light water reactor fuel by the Paige method (Katayama, 1976; 1979) have also

indicated that cesium, strontium, plutonium, curium, and uranium are leached from spent fuel at significant rates in deionized water. It should be noted that these latter tests were conducted with atmospheric oxygen content and, therefore, are not directly extendable to probable repository conditions. Also, these radionuclides may be leached at rates 10 to 100 times higher in a repository, due to the presence of sulfate, carbonate, and fluoride in oxygenated groundwater (Rich et al., 1977; Langmuir, 1978).

The observed cesium and strontium solubilities in spent fuel correspond well with the solubility of phases containing these elements in irradiated UO_2 . Cesium has been observed as Cs_2O , CsI , Cs_2MoO_4 , and $\text{Cs}_2\text{U}_2\text{O}_7$ (Cubiaciotti and Sanecki, 1978). These phases are all highly water soluble and tend to concentrate in the outer portions of the fuel pellet. Strontium oxide, which has a solubility of 0.23 gram per milliliter in water at 100°C , has been observed both in the exterior portions of the fuel pellet and in the interior adjacent to the central void (Koizumi et al., 1974). This seems to contradict that volatile materials migrate to the exterior of pellets.

6.3.1.2 Borosilicate Glass. Borosilicate glass is most often produced by the simultaneous melting of a glass frit and the nuclear waste in the form of a calcine. The chemistries of four Pacific Northwest Laboratory (PNL) simulated high-level waste glasses are given in Table 6-10, including the designation numbers and compositions of the glass-making frits required by each particular waste stream. These formulations were developed for several of the high-level waste compositions (calcines) shown in (Table 11-1, Chapter 11), which reflect the composition of the particular fuels reprocessing waste stream from which they evolved. Most of the experimental work performed to measure the leach resistance of borosilicate glass (e.g., Materials Characterization Center, 1981) has been completed using the PNL 76-68 glass (see Table 11-2, Chapter 11) exposed to distilled water and has yielded results of limited use to the site-specific needs and concerns of the BWIP. This work is reviewed in Section 11.3.2.1. Extensive hydrothermal testing of this waste form is presently being conducted by the BWIP.

In prior work, PNL 76-68 borosilicate glass was hydrothermally reacted under oxidizing conditions. The results (Table 6-10) suggest that the glass leaches significantly at 300°C (the worst-case repository condition) and to a lesser extent at 100° and 200°C . The large decrease in dissolved radionuclide concentrations at low temperatures is somewhat misleading because the significant concentrations of dissolved silicon and boron (glass network formers) clearly indicate significant matrix dissolution and degradation of the glass structure. This implies that even at low temperatures the concentrations of dissolved radionuclides will increase with leach duration until solubility (steady-state) dissolution conditions are attained. If this implication is correct, continual glass breakdown at low temperatures will ultimately release amounts of contained waste more accurately predicted by solubility models than by transitory leaching results from the short-term experiments that have been conducted to date.

TABLE 6-10. Comparison of the Compositions of Residual Solutions from Experiments^a Reacting Alternate Waste Forms with Distilled Water at 30 Megapascals.

Element	Supercalcine (SPC-4)		Glass (PNL 76-68)	
	Dissolved concentration (µg/mL)	Relative % dissolved	Dissolved concentration (µg/mL)	Relative % dissolved
Temperature = 300°C				
Rb	25	4.6	3	2
Cs	25	0.6	140	14
Sr	2.3	0.06	ND ^b	--
Mo	370	68	1,050	68
U	--	--	2.6	0.1
Ba	6.1	0.3	1	0.1
Si	340	3.0	610	0.3
Na	230	100	8,500	9.0
B	--	--	15,000	52.0
Others ^c	ND	--	ND	--
Temperature = 200°C				
Rb	30	0.6	ND	--
Cs	10	0.2	10	1.0
Sr	0.5	0.1	ND	--
Mo	83	1.8	405	26
U	--	--	17	0.4
Ba	ND	--	ND	--
Si	110	1.0	590	3.1
Na	27	18	2,000	21.3
B	--	--	1,600	53.8
Others	ND	--	ND	--
Temperature = 100°C				
Rb	ND	--	ND	--
Cs	ND	--	6	0.6
Sr	ND	--	1	0.01
Mo	20	0.1	40	2.4
U	--	--	1.6	0.01
Ba	ND	--	ND	--
Si	11	0.1	330	1.7
Na	ND	--	280	2.9
B	--	--	90	3.0
Others	ND	--	ND	--

^aFour months duration with a water-to-glass ratio of 10 to 1.

^bND = none detected by atomic absorption, atomic emission, or fluorometry.

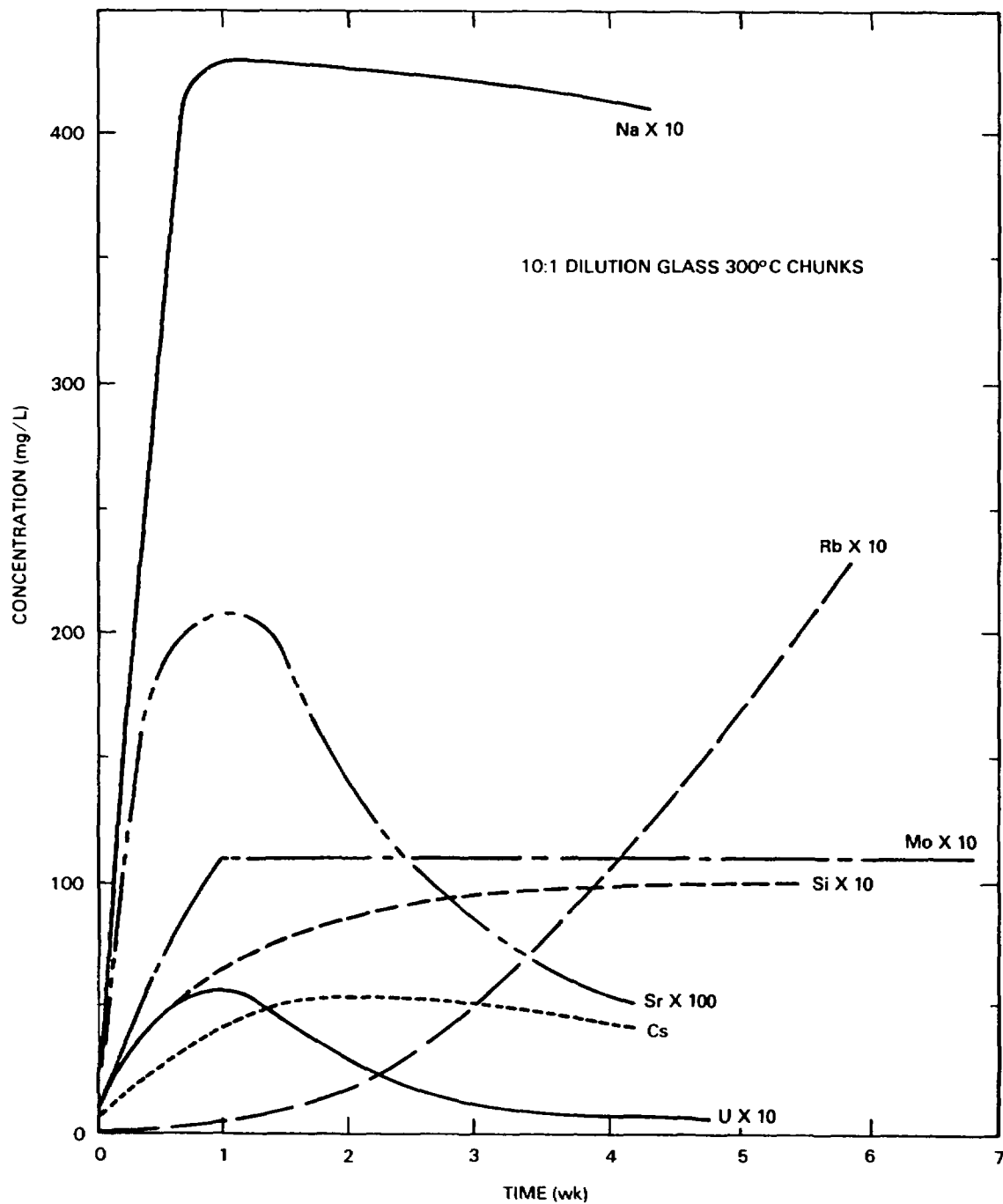
^cLa, Nd, and Zr not detected in solution.

The behavior of various ions leached from PNL 76-68 glass at 300°C, 30 megapascals, and under oxidizing conditions as a function of time is shown in Figure 6-14. The oxides most easily leached are sodium, strontium, molybdenum, uranium, and silicon. The shape of the curves suggests that the early dissolution is followed by precipitation; thus uranium, strontium, and perhaps technetium may be partially immobilized after leaching even under oxidizing conditions. In addition, Wood and Rai (1981) have shown that under reducing conditions (similar to those expected in the repository), uranium and other multivalence-state actinides will be much less soluble than under oxidizing conditions.

6.3.1.3 Tailored Ceramic-Water Interactions. Tailored ceramic (supercalcine) waste forms are synthetic analogs of natural mineral assemblages designed to trap radionuclides in insoluble mineral forms. They are no longer being considered as high-level waste forms, but are important as indicators of geochemically stable crystalline phases related to possible alteration products. Supercalcine is so named because, while sharing common processing steps with ordinary calcines, it provides a more stable product when sintered at high temperatures (McCarthy, 1977a). This waste form was designed to isolate radionuclide ions on an atomic level in crystallographic sites of highly stable crystalline phases. Emphasis in its development was placed on the selection of phases analogous to minerals known to have survived eons of natural weathering in geologic environments.

Data are available on the release of waste ions from prototype supercalcines at several temperatures. The composition of the supercalcine used in these experiments is listed in Table 6-11. The results of hydrothermal leaching tests of supercalcine are shown in Table 6-10, together with glass leaching data under comparable compositions. At 200° and 300°C, solutions in contact with supercalcine contain less than 600 milligrams per liter of fission products. This compares with a total of 1,100 milligrams per liter obtained from identical experiments on borosilicate glass. Cesium and molybdenum concentrations are noticeably lower in the solutions from supercalcine experiments relative to glass leachates, while rubidium and barium show increases beyond glass values.

At 100° to 200°C, the experimental leachate compositions of glass and supercalcine are comparable. This rough equivalence has caused some investigators to conclude that glass and supercalcine will perform equally well at low or moderate repository temperature (Ross et al., 1979). This conclusion must be viewed with caution. The potential long-term degradation of the glass structure, as shown by the concentrations of network formers in the residual solution from the glass-water experiments, indicates that substantial concentrations of radionuclides may be released over the span of repository life. The leachates from experiments with supercalcine do not contain large amounts of network-forming components. This suggests that the long-term resistance of supercalcine to dissolution may be greater than that of glass. However, as discussed in Chapters 11 and 12, the glass from a performance assessment standpoint may be totally acceptable to assure waste isolation.



RCP8107-87

FIGURE 6-14. Solution Concentrations of Various Ions from PNL 76-68 Glass as a Function of Time at 300°C, 30 Megapascals in Deionized Water.

TABLE 6-11. Composition of Supercalcine SPC-4
(after McCarthy, 1977b).

Ion	Molarity	Oxide	Grams of oxide per liter of calcined SPC-2 solution	wt% oxide	
From the Modified PW-7 Waste					
RE ^a	0.204	RE ₂ O ₃	34.07	20.4	(16.0) ^b
Gd	0.153	Gd ₂ O ₃	27.69	16.6	(12.9)
Zr	0.106	ZrO ₂	13.04	7.8	(6.1)
Fe	0.100	Fe ₂ O ₃	8.00	4.8	(3.7)
(PO ₄)	0.100	P ₂ O ₅	7.10	4.3	(3.3)
Mo	0.095	MoO ₃	13.68	8.2	(6.4)
Cs	0.054	Cs ₂ O	7.61	4.6	(3.5)
Ba	0.027	BaO	4.13	2.5	(1.9)
Sr	0.027	SrO	2.81	1.7	(1.3)
Cr	0.012	Cr ₂ O ₃	0.91	0.5	(0.4)
Rb	0.010	Rb ₂ O	0.94	0.6	(0.4)
Na	0.010	Na ₂ O	0.31	0.2	(0.1)
Ru ^c	0.006	RuO ₂	0.80	0.5	(0.4)
Ni	0.005	NiO	0.38	0.2	(0.2)
Cd	0.002	CdO	0.26	0.2	(0.1)
Ag	0.002	Ag ₂ O	<u>0.23</u>	0.1	(0.1)
			121.95		
Supercalcine Additives					
Ca	0.062	CaO	3.47	2.1	(1.6)
Sr	0.041	SrO	4.26	2.6	(2.0)
Al	0.148	Al ₂ O ₃	7.55	4.5	(3.5)
Si	0.489	SiO ₂	<u>29.34</u>	<u>17.6</u>	(13.8)
			166.58	100.0	
		(73.2% waste loading)			
Other High-Level Waste Constituents ^d					
U(Np,Pu)	0.1195	U ₃ O ₈	38.8		(15.7)
Ru ^c	0.053	RuO ₂	7.1		(3.3)
Pd	0.032	PdO	3.9		(1.8)
Te	0.012	TeO ₂	1.9		(0.9)
Rh	0.010	Rh ₂ O ₃	<u>1.3</u>		<u>(0.6)</u>
			214.38		(100.0%)
		(79.2% waste loading)			

^aRE = 0.133 Nd + 0.051 Ce + 0.014 La + 0.003 Pr + 0.002 Sm + 0.002 others; 0.002 RE is a stand-in for Am + Cm.

^bValue in parentheses is the weight percent of the oxide after addition of the appropriate amounts of U, Ru, Pd, Te, Rh.

^cRu concentration in the spray supercalcine SPC-4 was 10% of the actual PW-7 value of 0.59M. The addition of the remaining 0.053M is made after calcination.

^dThese constituents were not included in the large batch of SPC-4 because of their expense or radioactivity. None require fixation additives. The only PW-7 constituent not included above is Tc.

6.3.2 Barrier Materials

6.3.2.1 Canister. Corrosion screening studies have been conducted that employed both oxygenated (oxidizing) and deoxygenated (reducing) seawater and brines to assess the performance of several candidate canister materials (iron-, nickel-, copper-, titanium-, and zirconium-base alloys) in geothermal, seabed, and salt environments. Because of the great chemical disparity between such solutions and average Grande Ronde Basalt groundwater (Table 6-7), these results are of limited utility to BWIP waste package evaluation efforts. Corrosion rates generally ranged from a low of 4×10^{-5} centimeter per year for grade 12 titanium (TiCode 12) to a high of 0.7 centimeter per year for low carbon steel in oxygenated brines and a low of 10^{-4} centimeter per year for Zircaloy-2 to a high of 0.17 centimeter per year for low carbon steel in deoxygenated brines. Values for seawater corrosion generally fell within these ranges.

In more recent corrosion screening studies relevant to the reducing conditions of a repository in basalt (see Section 11.3.2.3; also Anderson, 1981), with simulated Grande Ronde Basalt groundwater sparged with a 0.19 percent H_2 -Ar gas mixture, corrosion rates measured at 250°C ranged from a low of 0.033×10^{-3} centimeter per year for TiCode 12 to a high of 2.7×10^{-3} centimeter per year for cast iron. The corrosion rate for 90-10 cupronickel, a copper-base alloy, was intermediate at 0.094×10^{-3} centimeter per year. Based on these data, a preliminary choice of materials for canisters and overpacks would be 90-10 cupronickel or cast iron (or low carbon steel). Continuing corrosion studies will further evaluate these and alternate materials to define their metallurgical stability and resistance to preferential corrosive attack.

6.3.2.2 Backfill. An optimum backfill component of the waste package is likely to consist of more than one material to effectively meet its functional requirements (Table 6-12). The principal requirements are to retard the intrusion of groundwater to the inner components of the waste package during the first 1,000 years and thereafter to retard or reduce the transport of radionuclides from the canister once it is breached. For the first requirement, the most important properties are the permeability and swelling capacity of the material. For the second, it is the ability of the material to retard radionuclide mobility by sorption, reaction, or diffusional control.

Two materials are presently being evaluated as major backfill components. These are sodium bentonite and crushed basalt. Sodium bentonite is composed primarily of the smectite clay, montmorillonite (approximately 90 to 95 percent), with minor amounts of quartz and feldspar. A significant swelling pressure allows bentonite to penetrate into and seal fissures that may exist in the emplacement hole wall. Pusch (1979) calculated the swelling pressure to be approximately 5 megapascals at a density of 2.1 grams per cubic centimeter. The hydraulic conductivity of 100 percent-saturated bentonite, 2×10^{-14} meter per second, is sufficiently low to impose a negligible groundwater flow rate, thus the transport of radionuclides through bentonite may be diffusion controlled. The results of studies conducted to date to evaluate the sorptive capacity of bentonite are reported in Section 6.4.

TABLE 6-12. Waste Package Component Functions Versus Repository History for Reference Waste Package Conceptual Design.

Barrier	Operating period	Function
Waste form	Preemplacement and repository life	Retard release of radionuclide upon breach of containment
Canister	Preemplacement	Provide physical support and protection of waste form
	Thermal period	Permit retrievability; primary physical barrier to ground-water intrusion and subsequent release of radionuclides
Backfill	Thermal period	Secondary physical barrier (radionuclide diffusion control)
	Geologic control	Primary physical barrier; secondary chemical barrier (supports geology)

The available experimental evidence suggests that montmorillonite will be largely stable below the 300°C temperature limit presently recognized for the waste package. According to Deer et al. (1967), interlayer water is reversibly lost up to 300°C and 0.1 megapascal. However, structural water is not lost until 450° to 500°C. This agrees with the results from differential thermal analysis of samples of secondary minerals (approximately 98 weight percent smectite clay) found in the Pomona basalt at Hanford (Koster van Groos, 1981). Under 0.1-megapascal pressure, interlayer water loss occurred at 126° to 134°C, and structural water loss occurred at 700°C. This suggests that structural alteration does not occur simply from heating below 300°C. On the other hand, Weaver (1979) has compiled studies on natural shale formations and laboratory experiments and has concluded that montmorillonite alteration can begin at temperatures as low as 50°C with the formation of the principal alteration products, illite and, to a lesser extent, chlorite. Major chemical alteration to illite and chlorite will severely reduce the effectiveness of bentonite as a backfill because of reduced chemical reactivity and swelling capacity and increased permeability. For montmorillonite to alter to illite, it is necessary to add potassium to the interlayer space and aluminum must be increased in solution. Therefore, the occurrence and extent of reaction are dependent on the site-specific groundwater composition and temperature (i.e., potassium concentration and possibly the potassium-to-sodium ratio according to work done by Eberl and Hower, 1976). The low potassium content of Grande Ronde Basalt and associated groundwater (approximately 1.5 weight percent and 5.9 milligrams per

liter, respectively) and the smectite-dominated secondary mineralization in the Grande Ronde Basalt fractures (Section 6.1) indicate that this reaction is unlikely to occur in the Hanford basalt environment to a significant degree. Experiments at expected repository temperatures are being conducted to quantify the extent of montmorillonite alteration in the Hanford basalt environment. In particular, an increase of potassium in groundwater reacted with basalt under elevated temperature conditions could lower the thermal stability of montmorillonite.

Crushed basalt must be considered as a candidate major backfill component because of its chemical reactivity, its availability following excavation of the repository, and the need to dispose of excavated basalt. Studies of the chemical retardation properties of basalt are discussed in Section 6.4.

Zeolites are considered as a possible component of the backfill because of their high cation-exchange capacity. Also, minor amounts of zeolites are found in the fracture mineralization in the Grande Ronde Basalts. Zeolites do not, however, possess any swelling properties upon contact with water that would enable zeolite to perform as a diffusion-control barrier to water migration.

There is also a need for a minor backfill component that is specifically tailored for transport retardation (either by sorption or reaction) of key radionuclides that are potentially mobile in the host rock. Attention is being focused on single phases; however, the minor backfill component may be composed of several phases. Candidate tailoring agents being considered are shown in Table 6-13.

TABLE 6-13. Candidate Backfill Tailoring Agents for Reducing the Mobility of Key Radionuclides in a Repository Constructed in Basalt (Smith et al., 1980).

Radionuclide(s)	Potential backfill material
Tc, I, Se	Bornite: Cu_5FeS_4
	Chalcopyrite: CuFeS_2
	Ultramarine: $\text{Na}_8(\text{AlSiO}_4)_6\text{S}_2$
	Graphite: C
	Copper: Cu
Np	Apatite: $\text{Ca}_5(\text{F,Cl,OH})(\text{PO}_4)_3$
	Azurite: $\text{Cu}_3(\text{CO}_3)_2(\text{OH})_2$

6.3.2.3 Buffer. A chemical buffering agent may be added to the backfill component to chemically condition the intruding groundwater by lowering the oxygen content (i.e., lowering the Eh) and buffering the pH at neutral or slightly alkaline values to minimize canister corrosion. Candidate materials for lowering the oxygen content are metallic powders (iron, aluminum, copper), graphite, and powdered basalt. Candidate materials for moderating pH are sodium phosphates. Phosphates tend to moderate both acid and base solutions, generating moderate pH values by phosphoric acid dissociation. Phosphates also have the potential for precipitating transuranics as well as other metal ions. Because the buffer may be an ideal component in which to include the tailoring agents needed to react with key radionuclides, continuing studies will consider a combination backfill-buffer material as a single waste package component.

6.3.3 Near-Field Environment

6.3.3.1 Waste-Basalt-Water Interactions. Komarneni et al. (1980) have investigated the hydrothermal reaction of cesium and strontium phases known to be stable in spent fuel with Hanford basalt and basalt phases. In each case the hydrothermal reaction of the cesium and strontium phases with water was first tested; then each was reacted with water in the presence of basalt or basalt phase. The two basalts used in the investigation were the U.S. Geological Survey's Standard Basalt Columbia River-1 (BCR-1) and a section of core from Hanford borehole DDH-3 (A2120/3320). The basalt phases were plagioclase (An₅₀ to An₇₀), clinopyroxene, iron-titanium oxides, zeolite (heulandite), and basaltic glass.

The results for the cesium and strontium reactions are shown in Tables 6-14 and 6-15, respectively. These preliminary results have determined that cesium phases likely to be stable components of spent fuel (i.e., CsOH, Cs₂MoO₄, Cs₂U₂O₇) have significant hydrothermal solubilities. However, these solubilities are greatly decreased in the presence of basalt and/or basalt phases. In contrast to these results, the strontium phase, SrZrO₃, was found to be extremely insoluble in distilled water and thus its concentration in solution was found to be little affected by the presence of basalt.

Barnes and Scheetz (1979) have reacted powdered Umtanum basalt with synthetic Grande Ronde Basalt groundwater at temperatures ranging from 100° to 300°C and at a pressure of 30 megapascals for run durations of 3 weeks. They found that solution pH values decreased with increasing temperature. Silica concentrations in solution lie between the solubility values for amorphous silica and quartz. Other than a very slight decrease in the sodium concentration, the chemistry of the groundwater did not change significantly. The results are in general agreement with seawater-basalt studies (Bischoff and Dickson, 1976), which show decreasing pH values and sodium concentrations with increasing silica concentrations.

TABLE 6-14. Analyses of Cesium Remaining in Solution from Hydrothermally Treated^a Mixtures of Basalt Phases^b or Basalts with Cesium Phases.^d

Sample	Weight of basalt phase or basalt + Cs phase ^c (mg)	Weight of Cs added ^d (mg)	Cs in solution (%)		
			100°C	200°C	300°C
Basalt Phases or Basalts + Cs ₂ MoO ₄ Mixtures					
Labradorite	123.7	14.8	12.0	0.3	0.3
Diopside (pyroxene)	124.7	15.4	83.4	76.4	57.0
Glass (mineraloid)	125.9	16.2	84.4	74.9	0.6
BCR-1 basalt	124.2	15.1	72.4	2.3	0.4
DDH-3 basalt	123.7	14.8	84.6	21.8	0.5
Basalt Phases or Basalts + CsOH Mixtures					
Labradorite	116.7	14.8	--	1.5	--
Glass (mineraloid)	118.2	16.2	--	0.6	--
BCR-1 Basalt	117.0	15.1	--	0.1	--
DDH-3 basalt	116.7	14.8	--	0.1	--
Basalt Phases or Basalt + β-Cs ₂ U ₂ O ₇ Mixtures					
Labradorite	147.5	14.8	41.3	0.3	0.6
Diopside (pyroxene)	149.4	15.4	30.3	19.1	4.2
Glass (mineraloid)	151.9	16.2	26.8	10.4	1.6
BCR-1 basalt	148.6	15.1	21.0	11.5	2.8
DDH-3 basalt	147.6	14.8	16.0	10.0	3.8

^aAt 100°C for 4 mo, 200°C for 2 mo, and 300°C for 1 mo (30 MPa pressure in all cases).

^b<75 μ m particle size.

^cWeight of basalt phase or basalt is 100 mg in all cases.

^dMolar ratio of Si in basalt phase (or basalt) to Cs added in all cases is 8.

Chemically, the only significant change observed in the basalt mineralogy was a slight increase in the sodium content of the plagioclase, corresponding to a decrease in sodium concentration in the solution. Physically, the minerals of the basalt (clinopyroxenes, plagioclase, and iron-titanium oxides) appeared somewhat etched and pitted and were generally not coated with alteration minerals. This observation is in accord with other studies of mineral dissolution mechanisms (Petrovic, 1976; Holden and Berner, 1979).

TABLE 6-15. SrZrO_3 Interactions with Basalt or Basalt Phases under Hydrothermal Conditions* at 200°C for 2 Months and 300°C for 1 Month.

Sample	Weight of basalt or basalt phase + SrZrO_3	Weight of Sr added (mg)	Weight of Sr in solution (mg)	Sr in solution (%)
Basalt or Basalt Phases + SrZrO_3 Mixtures at 200°C				
BCR-1 basalt	111.8	21.6	0.18	0.9
DDH-3 basalt	92.2	17.8	0.12	0.7
Labradorite	102.0	19.7	0.21	1.0
Diopside	95.8	18.5	0.23	1.2
Ilmenite	95.8	18.5	0.16	0.9
Heulandite	97.9	18.9	0.20	1.1
Basalt or Basalt Phases + SrZrO_3 Mixtures at 300°C				
BCR-1 basalt	95.8	18.5	0.18	1.0
DDH-3 basalt	104.1	20.1	0.15	0.7
Labradorite	99.9	19.3	0.10	0.5
Diopside	106.1	20.5	0.08	0.4
Ilmenite	106.1	20.5	0.16	0.8
Glass	99.9	19.3	0.14	0.7
Heulandite	102.0	19.7	0.04	0.2

*Thirty megapascals pressure in both cases.

The alteration minerals found by Barnes and Scheetz (1979) were located in cracks, microfractures, and on the autoclave walls and included nontronite, illite, mordenite, analcime, and either heulandite or clinoptilolite. These early results suggest that the existing secondary minerals found in the Grande Ronde Basalt (Section 6.1) will be stable under the anticipated repository conditions, apparently even during the early thermal period.

6.4 GEOCHEMICAL RETARDATION

The most likely mechanism for the transport of nongaseous radionuclides to the accessible environment is dissolution of the waste form and transport of the fission products and actinides in groundwater. There are several geochemical processes by which radionuclide transport in groundwater may be retarded in both the near-field and the far-field regimes of a repository in basalt, two of which are recognized as being of major importance. One major process is the precipitation or incorporation of the radionuclides into new mineral phases (solubility constraints). The other major process is the sorption (both physical and chemical) of radionuclides by the host rock and/or engineered barriers materials. Transport of radionuclides in colloidal suspension is possible, but more study is necessary to evaluate the stability of colloids both in radiation fields and at the expected alkaline pH values of the repository. Both radionuclide solubility and sorption behavior (and colloid stability) are highly dependent on the environmental conditions of the repository. Temperature, pH, Eh, and groundwater composition (potential complexing ligands), in particular, are important factors that can control radionuclide solubility and sorption behavior. In addition, the physical and chemical characteristics of the geologic substrate are important factors in evaluating radionuclide retardation behavior. The environmental near- and far-field conditions expected for a repository in basalt are discussed in detail in Section 11.4. Presented in the following sections is a summary of the available solubility and sorption data for key radionuclides (those for which release criteria are most stringent) (Barney and Wood, 1980), which are applicable to a repository located in a basaltic environment.

6.4.1 Radionuclide Solubilities

To predict the maximum concentration of radionuclides in groundwater in contact with basalt, both the solution species and the solubilities of solid phases present in the basalt geologic environment are needed. This includes evaluation of colloid formation and migration of particulates. The types of radionuclide-bearing solid phases that may form in the basalt environment depend on the radionuclide concentrations, the groundwater composition, and the geologic materials present in addition to the waste form itself. The exact nature of such radionuclide-bearing solid phases for the basalt environmental conditions is not well known at this time. Nevertheless, an evaluation of the solubilities of the simple oxides of some of the key radionuclides can be useful in determining the maximum radionuclide concentration in the basalt groundwater.

This approach is reasonable because radionuclide oxides typically occur in spent fuel, and minerals, including radionuclide-bearing solids, will generally undergo continuous change to compositionally related minerals with lower free energy based on thermodynamic principles (Garrels and Christ, 1965, Chapter One; Giggenbach, 1981). Therefore, if the solubilities of the waste form or of the minerals in the waste form were

known, these solubilities would define a time-invariant concentration (assuming no precipitation of new phases) of the radionuclides in groundwaters. If precipitation of new radionuclide-bearing solid phases did occur, this could only lower the concentrations for those radionuclides in solution. Data currently available on the solubilities of actinide-bearing waste forms and key compounds of uranium, neptunium, plutonium, and americium can be extrapolated to permit the estimation of these actinide concentrations in the basalt groundwater under ambient repository conditions. The analysis of the data is discussed in detail in Wood (1980) and Rai et al. (1981). Only a summary of the analyses is presented in this section.

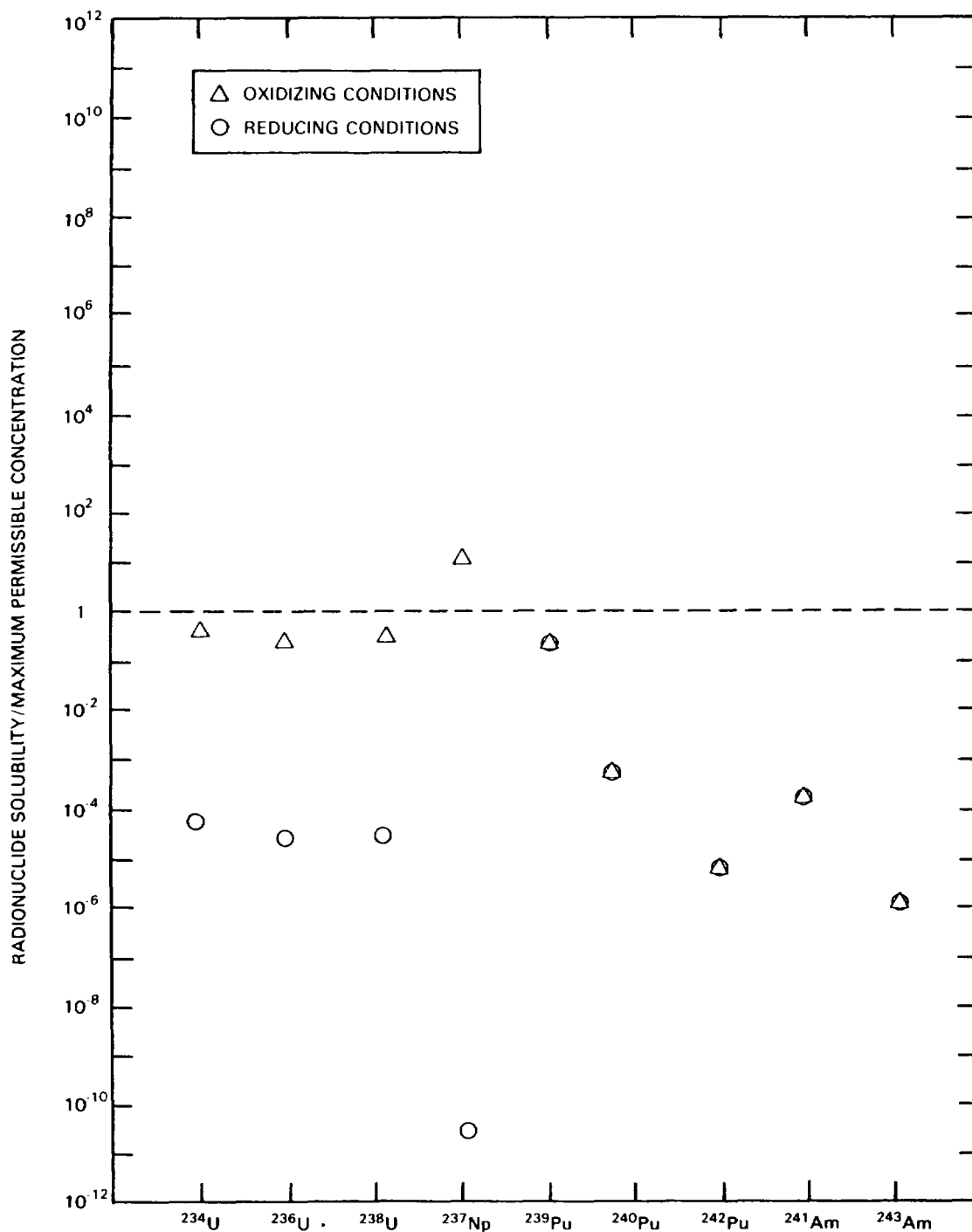
Since UO_2 is the major component of spent fuel, data on uraninite solubility are used to estimate maximum uranium solubilities under reducing repository conditions. At a pH of 10, the maximum solubility of UO_2 under reducing conditions is estimated to be 1×10^{-8} mole per liter. Under oxidizing conditions, schoepite ($\text{UO}_2(\text{OH})_2 \cdot \text{H}_2\text{O}$) rather than UO_2 is the more stable solid phase. Uranium solubility under oxidizing conditions is estimated to be 1×10^{-4} mole per liter. However, the effect of complexing ligands such as CO_3^{2-} on uranium solubility was not considered in these estimates. Uranium may form carbonate complexes in the groundwater of a basaltic environment, which could significantly increase the solubility of uranium under oxidizing conditions. Based on these solubility data, it becomes apparent that reducing conditions expected in the repository basalt environment are a very important and positive contribution to the containment of uranium.

Neptunium also is an important component of spent fuel. Based on available thermodynamic data, NpO_2 is the most stable oxide under all Eh conditions expected for the repository (Rai and Serne, 1978). Data concerning other, more stable neptunium compounds that may form in the repository environment are not available at this time. Under oxidizing conditions, neptunium solubility is estimated to be 2×10^{-7} mole per liter (neptunium(V) is the stable oxidation state). Under reducing conditions, at a pH of 9.5 and temperature of 60°C , neptunium solubility is estimated to be 1×10^{-18} mole per liter. Again, the effect of complexing ligands has not been considered in making these solubility estimates.

Another significant constituent of spent fuel is plutonium. Plutonium dioxide appears to be the most stable of the known plutonium compounds above pH 5 and at all Eh values within the stability field of water (Rai and Serne, 1978). Under oxidizing conditions, PuO_2 solubility is estimated to be 1×10^{-10} mole per liter at pH 10. The solubility of $\text{Pu}(\text{OH})_4$ at this pH is estimated to be 1×10^{-9} mole per liter. Again, this value does not take into consideration the effect of CO_3^{2-} on the plutonium solubility. Plutonium forms soluble plutonyl carbonate complexes, although there are no reliable data on the formation constants of such complexes (Cleveland, 1979). Under reducing conditions, the solubility of plutonium is not estimated to change significantly from that expected under oxidizing conditions.

Americium also is an important constituent of spent fuel. It is probably present in spent fuel as the oxide, AmO_2 , which is the most stable solid phase under alkaline oxidizing conditions. Americium solubility under oxidizing conditions is estimated to be 8×10^{-10} mole per liter at pH 10. Under reducing conditions, the stable americium solid phase is predicted to be $\text{Am}(\text{OH})_3$, although this phase has not yet been identified. Final americium concentrations calculated from apparent sorption coefficients on basalt suggest that the americium solubility under reducing conditions is less than 10^{-9} mole per liter at pH 10.

Groundwater containing uranium, neptunium, plutonium, and americium will have maximum radionuclide concentrations equal to their oxide solubilities, assuming that the oxide phases are the phases that will precipitate under repository conditions. The relative importance of radionuclide solubilities in evaluating radionuclide transport to the accessible environment can be estimated by comparing these radionuclide concentrations to the maximum permissible nuclide concentrations for nuclear discharges established by the NRC (1981). As can be seen in Figure 6-15, uranium concentrations are well below maximum permissible nuclide concentrations under reducing conditions and a pH of approximately 10. Even under oxidizing conditions, the uranium concentration falls slightly below maximum permissible nuclide concentrations. Plutonium concentrations also fall below maximum permissible nuclide concentrations under both oxidizing and reducing conditions. Neptunium concentrations exceed maximum permissible nuclide concentrations under oxidizing conditions and are well below maximum permissible nuclide concentrations under reducing conditions. Americium concentrations, however, are well below maximum permissible nuclide concentrations under both oxidizing and reducing conditions. Based on these solubility estimates, therefore, it appears that at pH 10, under the reducing conditions expected for a repository in basalt, the maximum concentrations of uranium, neptunium, americium, and plutonium in the repository itself will be below maximum permissible nuclide concentrations in the absence of significant concentration increases due to complex or colloid formation. In addition, these concentrations will be considerably lower at the point of discharge to the biosphere, due to radioactive decay, dilution, and sorption. The very low solubilities of these actinides in the expected repository environment indicate that the maximum possible release rates of these radionuclides also will be very low. Assuming a groundwater flow rate of 2×10^6 liters per year through the repository and under reducing conditions, 1×10^{-6} of the total uranium inventory, 4×10^{-13} of the total neptunium inventory, 1×10^{-5} of the total ^{239}Pu inventory, 1×10^{-8} of the total ^{240}Pu and ^{242}Pu inventory, and 1×10^{-9} of the total americium inventory in the repository after 1,000 years will be released in 100,000 years. Based on solubility, the maximum possible release rates for all the radionuclides considered will be below the NRC 10^{-5} proposed release rate criterion (NRC, 1981) and the draft cumulative release criterion (EPA, 1981).



RCP8111-97

FIGURE 6-15. Comparison of Estimated Solubilities for Actinide Compounds $\text{UO}_2(\text{c})$, $\text{UO}_2(\text{OH})_2 \cdot \text{H}_2\text{O}$, $\text{NpO}_2(\text{c})$, $\text{PuO}_2(\text{c})$, and $\text{Am}(\text{soil})$ with the Maximum Permissible Concentrations (NRC, 1981) Under Repository Conditions of 25°C , 0.1 Megapascal, pH 10, and Eh 0.29 Volt (oxidizing) or -0.27 Volt (reducing). Possible complexation of actinides has not been included.

Although the extrapolation of the solubility data (obtained under oxidizing conditions and estimated based on available thermodynamic data) to reducing conditions indicates that uranium, neptunium, americium, and plutonium would be maintained close to or well below the maximum permissible concentration limits (Fig. 6-15), experimental verification is needed. The experimental verification should include solubility measurements for compounds of uranium, neptunium, plutonium, americium, and other key radionuclides under the exact site-specific conditions anticipated to occur in the basalt repositories (low Eh, high temperature, high-radiation field, and complexing ligands). These experiments should extend to the determination of the stable solid phases and solution species under high-temperature reducing conditions and to measurement of the extent to which solid phases would precipitate in a repository. For example, amorphous forms of hydrated actinide oxides may precipitate instead of the crystalline forms. The preliminary analysis presented here indicates that solubility measurements could greatly enlarge the understanding of potential hazards, because solubilities and maximum permissible nuclide concentrations, unlike nuclide velocities, are independent of both the release scenario and the hydrology of the repository and surrounding rock.

6.4.2 Radionuclide Sorption

Radionuclide sorption is also a major mechanism for preventing or retarding the movement of radionuclides in the basalt groundwater. In the basalt environment, sorption of radionuclides can occur on the basalt itself, on the secondary minerals associated with the basalt, on the interbed-interflow materials found between some of the basalt flows, and on the glaciofluvial sediments above the basalts. Secondary minerals are found lining and filling the vesicles, vugs, and fractures found in the Columbia River basalts (see Section 6.1). Because the fractures in the basalt are the most probable pathway for groundwater movement in the basalt, it is likely that these secondary minerals will be a primary sorption medium for the removal of radionuclides from groundwater. In addition, sorption can occur on the waste package materials (e.g., the backfill). A summary of the available sorption data for representative geologic materials comprising a repository in the Columbia River basalts is presented in the following sections. Detailed descriptions and discussions of the sorption data can be found in Ames and McGarrah (1980; 1981a; 1981b), Salter et al. (1981a; 1981b), Barney (1981a; 1981b), and Smith et al. (1980).

6.4.2.1 Radionuclide Distribution Coefficients. One of the most common measures of the ability of geologic material to sorb radionuclides and, therefore, to retard radionuclide migration in groundwater is the radionuclide distribution coefficient. The radionuclide distribution coefficient is defined as the concentration of the solute sorbed on the solid phase ratioed to the equilibrium concentration of the solute in the liquid phase. The distribution coefficient can be used to calculate a

retardation factor for the geologic materials, assuming a linear sorption isotherm and equilibrium sorption. Retardation factors are used in radionuclide transport modeling. The relationship between the retardation factor and sorption isotherms is discussed in more detail in the next section.

The radionuclide distribution coefficient value is an empirical value and, as such, is strongly influenced by many environmental and experimental parameters. Temperature, Eh, pH, and groundwater composition (complexing ligands) are particularly important environmental parameters. Due to the uniqueness of the basalt groundwater geochemistry and the extremely reducing conditions expected for a repository in basalt, much of the available sorption data found in the literature are not useful for predicting radionuclide migration in the Columbia River basalt geohydrologic system. The effects of expected repository temperatures, groundwater composition, pH, and redox conditions on radionuclide distribution coefficient values for basalt and associated secondary minerals are presented in the following four tables. The radionuclide distribution coefficient values were determined using an equilibrium batch technique (Salter et al., 1981a; 1981b).

Two groundwater compositions (Table 6-16) have been used in sorption studies. Groundwater GR-1 simulates the dominant groundwaters in the Saddle Mountains and upper Wanapum Basalts, while GR-2 simulates the dominant groundwaters in the lower Wanapum and Grande Ronde Basalts. The effects of groundwater composition and pH on radionuclide sorption is shown in Table 6-17. Only uranium and radium sorption are significantly affected by groundwater compositions. Groundwater composition effects on the distribution coefficient for plutonium cannot be evaluated at this time because of the large errors associated with the distribution coefficient values. The decrease in the uranium distribution coefficient value in the GR-2 groundwater (pH 10) may be explained by changes in the uranium speciation. As mentioned previously, between pH 6 and 8 the dominant uranium species are $(\text{UO}_2)_3(\text{OH})_5^+$ and UO_2CO_3^0 with the cationic species being the most strongly sorbed. At pH 10 the dominant uranium species are UO_2CO_3^0 and $\text{UO}_2(\text{CO}_3)_2^{2-}$. This anionic species is poorly sorbed by the basalt. The greater uranium sorption on the secondary minerals is the result of both its greater surface area and its pH buffering capacity. Reaction between the secondary minerals and groundwater usually results in a drop in the pH value to around pH 7 to 8. The significant decrease in radium distribution coefficient values in the GR-2 groundwater, with no decrease in strontium distribution coefficient values, is not understood at this time. Strontium and radium should exhibit similar geochemical behavior. If the decrease in the radium distribution coefficient value is the result of increasing competition for sorption sites, due to increased ionic strength of the GR-2 groundwater, there also should have been a decrease in the strontium and cesium distribution coefficient values, since they also should sorb by ion-exchange reaction.

TABLE 6-16. Synthetic Ground-water Compositions.

Constituents	Concentration (mg/L)	
	GR-1	GR-2
Na ⁺	30.7	225
K ⁺	9.0	2.5
Ca ⁺²	6.5	1.06
Mg ⁺²	1.0	0.07
Cl ⁻	14.4	131
CO ₃ ⁻²	0	59
HCO ₃ ⁻	81.5	75
F ⁻	0	29
SO ₄ ⁻²	11.1	72
SiO ₂	25	108
pH	8.0	10.0
Ionic strength	0.002	0.014

TABLE 6-17. Groundwater Composition Effects on Radionuclide Distribution Coefficient Values^a for Umtanum Basalt and Associated Secondary Minerals.

Radionuclide	Distribution coefficient (mL/g) ^b		
	Groundwater	Umtanum basalt	Secondary minerals
233U	GR-1	56 + 11	147 + 70
	GR-2	2.8 ± 0.9	72 ± 2
137Cs	GR-1	1,084 + 140	12,000
	GR-2	1,025 ± 248	9,795 ± 3,976
85Sr	GR-1	158 + 26	451 + 103
	GR-2	133 ± 16	249 ± 49
237Np	GR-1	13 + 1	75 + 38
	GR-2	7 ± 3	157 ± 40
99Tc	GR-1	5.6 + 3.5	0
	GR-2	1.3 ± 0.4	0
79Se	GR-1	3.0 + 0.5	--
	GR-2	2.0 ± 0.9	--
237Pu	GR-1	102 + 97	--
	GR-2	20 ± 3	--
226Ra	GR-1	187 + 24	--
	GR-2	55 ± 5	--

^aOxidizing conditions, 23°C.

^bErrors reported, ±1σ.

It has been found that temperature significantly affects the sorption of only cesium, radium, and uranium on basalt (Table 6-18). Strontium, americium, and selenium distribution coefficient values appear to be affected only by higher temperatures (equal to or greater than 150°C). The decrease in cesium distribution coefficient values with increasing temperature is probably the result of increasing ionic strength (particularly the increase in potassium ion concentration) due to the increased reaction of the groundwater with the basalt at higher temperatures. Cesium is thought to sorb by ion exchange, and increased competition for sorption sites in higher ionic strength solutions will reduce cesium sorption (distribution coefficient value). Radium is also thought to be a simple, uncomplexed ion in groundwater and should sorb by ion exchange. The increase in sorption with temperature may be the result of specific sorption reactions with the surface. Radium concentrations below 10^{-10} mole per liter preclude precipitation of RaSO_4 or RaCO_3 in the groundwater at these temperatures. However, at higher temperatures (150°C), there is considerably greater interaction between the basalt and the groundwater, with a possible increase in sulfate and/or carbonate concentration. In that case, the solubility product may be exceeded for a radium sulfate or carbonate precipitate. There is evidence that precipitation of strontium may also occur at 150°C. The high strontium distribution coefficient value indicates precipitation. Strontium, also a simple divalent cation, behaves similarly to radium and can precipitate as sulfate and carbonate complexes.

Temperature effects on uranium sorption are thought to be the result of changes in uranium speciation with increasing temperature. At 23°C and pH 8, the dominant uranium species in GR-1 groundwater (Table 6-16) are $(\text{UO}_2)_3(\text{OH})_5^+$ and UO_2CO_3 . Only the cationic species, $(\text{UO}_2)_3(\text{OH})_5^+$, is strongly sorbed by geologic substrates. At 60°C, the dominant uranium species at this temperature is $(\text{UO}_2)_3(\text{OH})_5^+$, and the CO_3^{2-} complexes become increasingly unstable with increasing temperature (Langmuir, 1978). Uranium sorption, therefore, should increase with increasing temperature. The extremely high uranium distribution coefficient value at 150°C is probably the result of both sorption and precipitation. For the high-temperature distribution coefficient experiments, the pressure vessels were purged with argon before being sealed, thus removing most of the available oxygen. Under low oxygen, it is possible for conditions to become sufficiently reducing to reduce some of the uranium to uranium(IV) and precipitate UO_2 or USiO_4 at this temperature.

The other isotopes investigated do not exhibit a significant change in distribution coefficient values for temperatures between 23° and 60°C. However, selenium and americium exhibit a considerable increase in distribution coefficient values at 150°C. The increase in the selenium distribution coefficient value may reflect specific sorption onto some of the metallic sulfides present in the basalt or the slow reduction to elemental selenium and precipitation under the slightly reducing conditions present in the pressure vessel. The extremely high americium distribution coefficient value reflects precipitation of americium oxyhydroxides.

TABLE 6-18. Temperature Effects on Radionuclide Distribution Coefficient Values^a for Umtanum Basalt.

Radionuclide	Distribution coefficient (mL/g) ^b		
	23°C	60°C	150°C
⁷⁵ Se	5.4 ± 1.3	0	91 ± 13
⁸⁵ Sr	105 ± 4	122 ± 3	>1,000 ^c
⁹⁹ Tc	26.8 ± 21.9	25.5 ± 5.2	--
¹²⁵ I	6.8 ± 1.3	0	0
¹³⁷ Cs	705 ± 18	463 ± 5	100 ± 3
²²⁶ Ra	187 ± 24	360 ± 69	--
²³⁷ Np	30 ± 13	31.2 ± 4.7	--
²⁴¹ Am	277 ± 103	236 ± 98	>10,000 ^c
²⁴¹ Pu	102 ± 97	353 ± 224	--
²³³ U	56 ± 11	103 ± 12	>2,800 ^c

^aGR-1 groundwater (Table 6-16) used, contact time 55-65 days, oxidizing conditions.

^bErrors reported ±1σ.

^cPossibly due to precipitation.

A comparison of the radionuclide distribution coefficient values for several radionuclides exhibiting more than one stable oxidation state under reducing and oxidizing conditions is shown in Table 6-19. Hydrazine was used in these experiments as an Eh-controlling agent. Except for selenium, all radionuclides investigated show a significant increase in their distribution coefficient values in the presence of hydrazine. Selenium reduction by hydrazine in an alkaline system appears to be a slow reaction at low temperatures; however, at 150°C, under less reducing conditions, there is some evidence that the reduction of selenium(IV) to elemental selenium does occur. Technetium, uranium, and neptunium distribution coefficient values increase at least 1 order of magnitude under the reducing conditions expected for a repository in basalt as a result of the reduction and formation of less soluble species (probably as technetium(IV), uranium(IV), and neptunium(IV) oxides and hydroxides).

TABLE 6-19. Effect of Eh Conditions on Radionuclide Distribution Coefficient Values^a for Umtanum Basalt.

Radionuclide	Eh ^b	Temperature (°C)	Distribution coefficient (mL/g) ^c
²³³ U	R	23	53 \pm 6
	O	23	2.5 \pm 0.9
	R	60	65 \pm 9
	O	60	12 \pm 3
⁷⁹ Se	R	23	3.5 \pm 0.5
	O	23	4.0 \pm 1.0
	R	60	7.2 \pm 3.0
	O	60	2.0 \pm 0.9
⁹⁹ Tc	R	23	29.4 \pm 2.5
	O	23	2.5 \pm 1.7
²³⁷ Pu	R	23	42 \pm 5
	O	23	20 \pm 3
²³⁷ Np	R	25	1,015 \pm 164
	O	25	42 \pm 11

^aGR-2 groundwater used.

^bR = Reducing conditions, -0.3 to -0.4 V (0.1M hydrazine); O = oxidizing conditions, +0.4 to +0.5 V.

^cErrors reported $\pm 1\sigma$.

Plutonium distribution coefficient values increase by only a factor of two under reducing conditions. The small increase probably reflects the fact that a large proportion of the ^{237}Pu tracer used was initially in the +4 state; the small amount of plutonium(V) present initially was probably reduced to plutonium(IV), resulting in a slight increase in the distribution coefficient value.

A summary of the current best estimates for radionuclide distribution coefficient values for the Columbia River basalt geohydrologic system is presented in Table 6-20. These values will be revised as more information concerning the sorptive behavior of the isotopes in the basalt environment is obtained. At present, they represent a conservative estimate of radionuclide sorption on basalt, secondary minerals, and interbed materials that can be used in modeling potential radionuclide transport to the accessible environment.

6.4.2.2 Sorption Isotherms. The sorption of a radionuclide by geologic materials is normally dependent on the concentration of that radionuclide in the groundwater. It becomes independent of radionuclide concentration only when the radionuclide is present at trace levels. One means of describing the dependence of radionuclide sorption on radionuclide concentration is with the use of sorption isotherms. Several such isotherms or equations, some with a theoretical basis and others empirical, have been used to describe solute sorption onto geologic substrates; these are discussed in detail by Salter et al. (1981a). Sorption isotherms have been derived for uranium, selenium, radium, cesium, and strontium and are presented in Table 6-21. These isotherm equations are then used in evaluating the retardation factor used in modeling radionuclide transport. The retardation factor (R) is given as:

$$R = 1 + [\rho/\phi] f'(c) \quad (6.1)$$

where

ρ = substrate density

ϕ = effective porosity.

The term $f'(c)$ is equal to the first derivative of the equation describing sorption as a function of concentration (e.g., an isotherm). If the sorption isotherm is a simple linear equation, $f'(c)$ becomes a constant. This constant is the distribution coefficient. However, as can be seen in Table 6-21, sorption isotherms are often not linear. These equations (Table 6-21) should be used instead of distribution coefficient values when evaluating radionuclide retardation factors.

TABLE 6-20. Current Conservative Best Estimates for Radionuclide Distribution Coefficient Values for the Columbia River Basalt Geohydrologic System.

Radio-nuclide	Distribution coefficient (mL/g)					
	Basalt		Secondary minerals		Interbed materials	
	0a	Ra	0a	Ra	0a	Ra
¹²⁵ I	0 (0-7)	--	0	--	0	--
⁹⁹ Tc	0 (0-1)	29	0	50	0 (0-4)	70 (40-110)
²³⁷ Np	10 (7-42)	200 (150-2,000)	50	200	20	50 (30-100)
⁷⁹ Se	4 (2-9)	8 (3-18)	5 (0-14)	8	0 (0-4)	2
²³³ U	6 (1-15)	40 (17-650)	70	NA ^b	NA ^b	NA ^b
²²⁶ Ra	200 (50-400)	--	100	--	4,000 (2,800-6,200)	--
²³⁷ Pu	22 (20-25)	42	2,000	4,000	300 (200-500)	470 (350-1,000)
²⁴¹ Am	340 (230-600)	NA ^b	1,000	NA ^b	>10,000 ^c	>10,000 ^c
¹³⁷ Cs	500 (200-900)	--	5,000	--	2,200	--
⁸ Sr	170	--	200	--	340	--
Surface area (m ² /g)	10-30		650		50-180	

Values in parentheses are the range of distribution coefficient values measured.

^a0 = Oxidizing conditions, R = reducing conditions.

^bNA = No data available.

^cGreater than 98% removal.

TABLE 6-21. Sorption Isotherms for Selected Radionuclides on Umtanum Basalt.

Radionuclide	Eh ^a	Isotherm type ^b	Equation
233,234,238U	R O	Freundlich Dubinin-Radushkevich	$S = 0.80 C^{1.2}$ $S = 4.6 \exp -0.032 \ln (1 + 1/C)^2$
79Se	R O	Freundlich Freundlich	$S = 0.006 C$ $S = 0.002 C$
226Ra	O	Freundlich	$S = 717.2 C^{1.34}$
135,137Cs	O	Dubinin-Radushkevich	$S = 18.0 \exp -0.024 \ln(1 + 1/C)^2$
90Sr	O	Freundlich	$S = 0.97 C^{0.12}$

^aR = Reducing conditions, O = oxidizing conditions.

^bFreundlich: $S = KC^N$; Dubinin-Radushkevich:

$$S = X_m \exp(-B) RT \ln (1 + 1/C)^2$$

where

S = equilibrium concentration of sorbed ion per gram of solid

C = equilibrium concentration of sorbing ion in bulk solution (moles/liter)

K = constant related to affinity of the ion for the substrate

B, N = constant related to energy of sorption

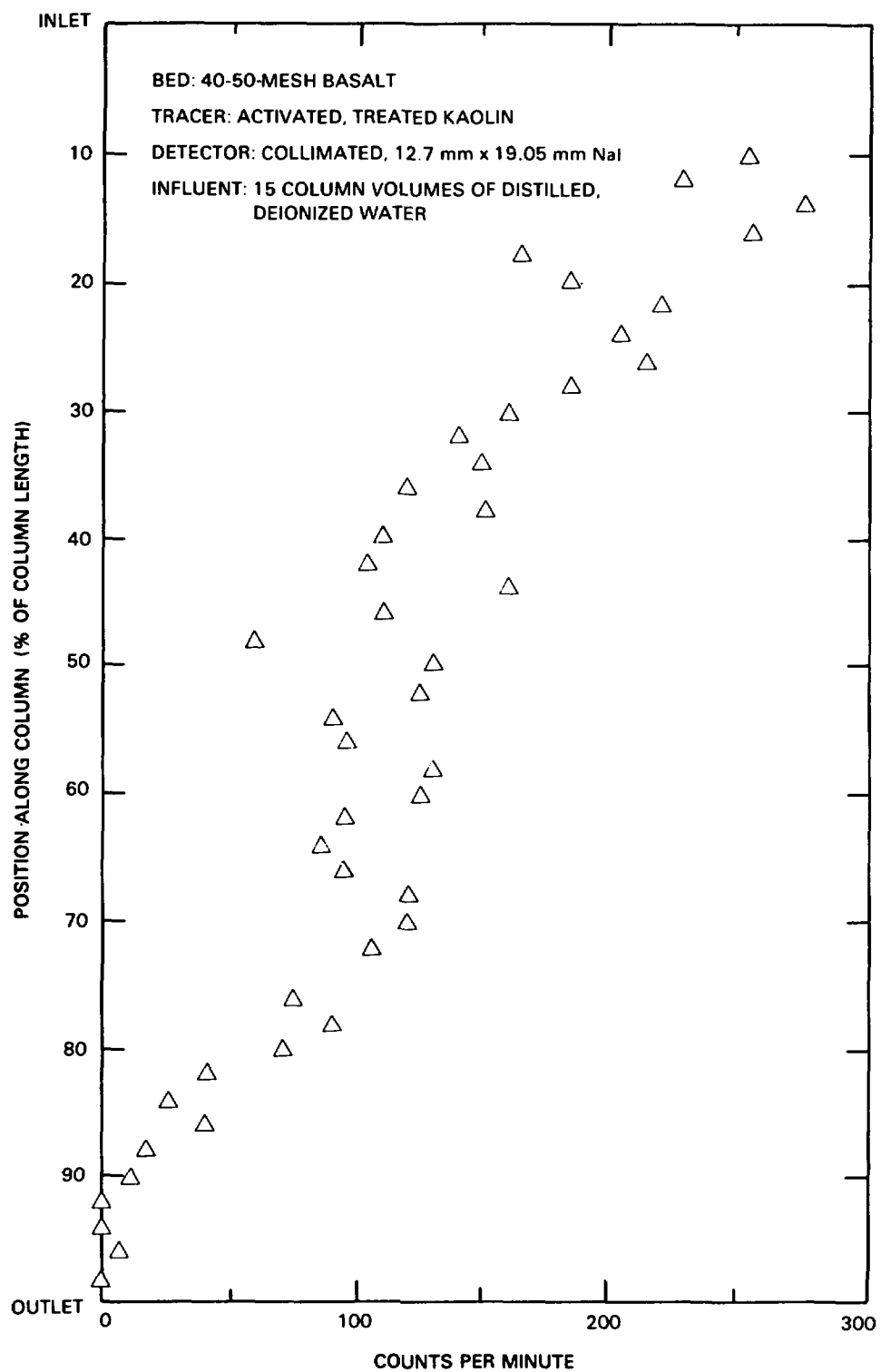
R = 8.314 E-03 kJ deg⁻¹ mole⁻¹

T = temperature, °K (333°K for basalts)

X_m = sorption minimum or capacity of the substrate.

6.4.2.3 Particulate Transport. Another possible mechanism for radionuclide transport from the repository is the sorption of dissolved radionuclides onto suspended colloidal particulates and their subsequent transport through porous, geologic media. The formation of colloidal hydrous oxides of radionuclides by reaction of the waste form with water is also a possibility. Particulates may arise from erosion of host rock material, mobilization of fine clay particles, or surface spalling of waste package materials in the repository (waste matrix, canister overpack, or backfill).

As radioactive particles move through the geologic formation, surrounding rock surfaces will compete for sorbed radionuclides. Also, particles and rock surfaces will interact to control the movement of particles. Eichholz (1979) has reported preliminary studies of these processes. He investigated the movement of labeled kaolin particles through columns of basalt simulating geologic media that might occur near actual repository sites. No significant amounts of kaolin were carried through the crushed rock columns when deionized water was used as the carrier. Less than 0.1 percent of the activity was recovered in a small peak at about one column volume. The activity of the labeled particles was highest at the top of the column and decreased steadily toward the bottom (Fig. 6-16). However, in salt solutions (500 to 1,250 milligrams per liter), more kaolin particles (up to 83 percent of the initial activity after the first pore volume) pass through the column. Particulate transport of radionuclides, therefore, may be a significant factor in some geohydrologic systems; however, more data are needed using basalt groundwater to accurately evaluate the effect of particulate transport on radionuclide transport in the basalt geohydrologic system.



RCP8107-265

FIGURE 6-16. Distribution of Activated Kaolin Throughout the Basalt Column after Particulate Flow Experiments (after Eichholz, 1979).

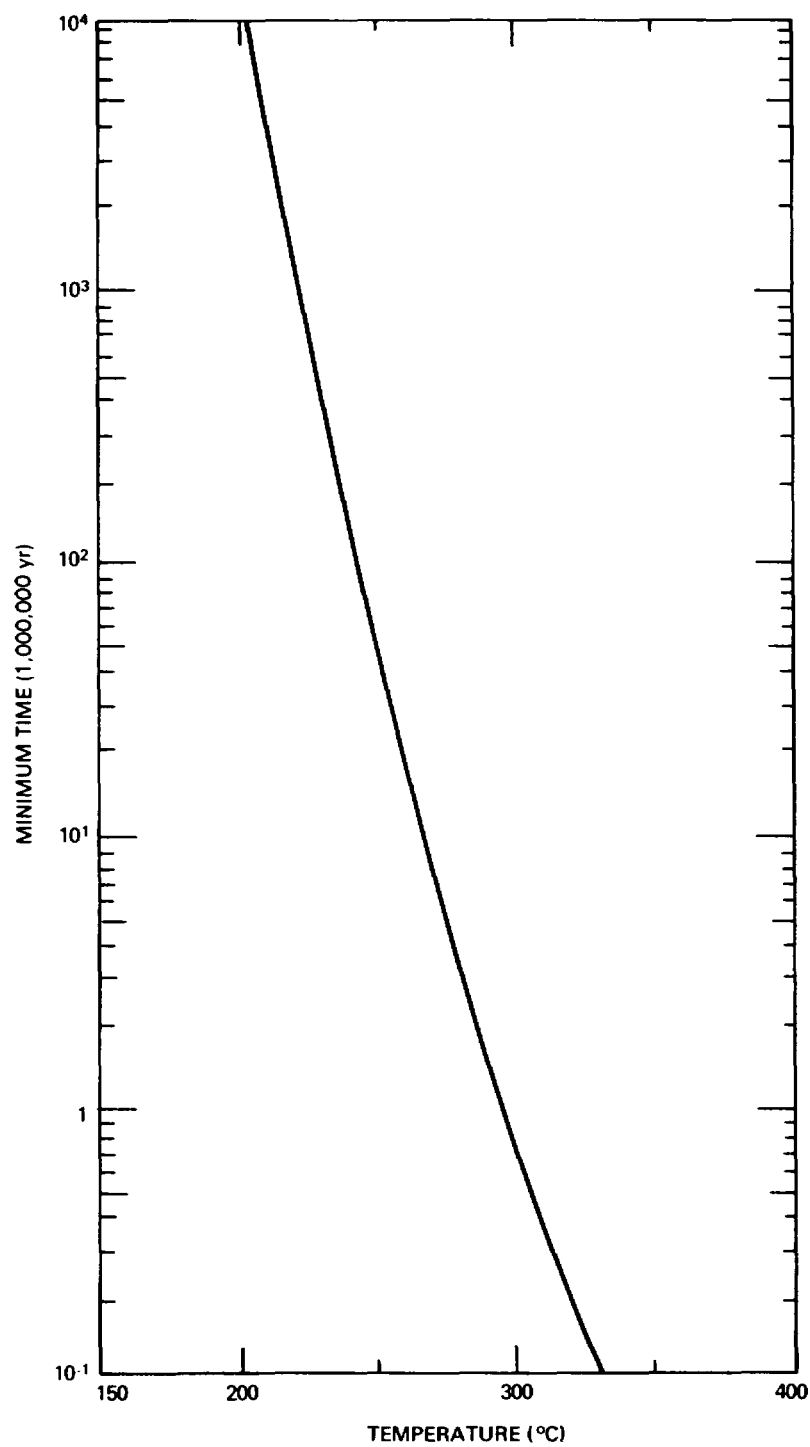
6.5 NATURAL ANALOGS

In evaluating the performance of waste packages for a nuclear waste repository located in basalt, comparison to natural geochemical analogs can be an important consideration. While natural analogs are not available for comparison with the total engineered system, some analogs do exist that can be compared with individual components of the system. The potential toxicity of the spent fuel waste form, for example, may be considered in light of uranium ore bodies, provided that differences in the geochemical conditions between the ore body environment and the repository environment are taken into account. Studies on natural volcanic glasses can yield information pertinent to the analysis of the long-term performance of borosilicate glass. Information from geochemical studies of uranium deposits can aid in establishing radionuclide mobility in hydrothermal solutions. Natural occurrences in basaltic rocks of native metals such as copper and iron (candidate materials for the canister and/or overpack) can provide information concerning the potential stability of these metals under repository conditions. The stability of sodium bentonite deposits in Wyoming and the host rock within which they occur can be useful analogs for an investigation of the stability of the waste package backfill component in Grande Ronde Basalt. The following sections address these analogs as they apply to the waste package and repository at Hanford.

6.5.1 Waste Form Analogs

6.5.1.1 Volcanic Glass as a Natural Analog. Although significantly different in composition from the borosilicate glass waste form, volcanic glass may provide a basis for estimating the long-term persistence of this waste form. Age dating (fission track, potassium/argon methods) of volcanic glasses may yield information on the long-term persistence of borosilicate glass in the repository environment. The greatest age currently available is approximately 40 million years. Most dated samples, however, cluster around 2 million years of age. Thus, although most volcanic glasses do recrystallize in relatively short periods of geologic time, volcanic glass can persist over periods of time much greater than repository performance requirements.

Another important consideration in glass persistence is the rate of devitrification (i.e., recrystallization). Devitrification rates are usually calculated using simple rate theory and experimental data to set an approximate lower limit to the time required for thermal reconstruction as a function of annealing temperature (Marshall, 1961). The times (in millions of years) required to devitrify glass as a function of temperature with no water present are indicated in Figure 6-17, assuming an activation energy for devitrification of 2.1×10^5 joules/mole (Marshall, 1961). Even at 300°C, a temperature not likely to be exceeded within the canister, approximately 1 million years are required for devitrification to a depth of 10 microns.



RCP8107-238

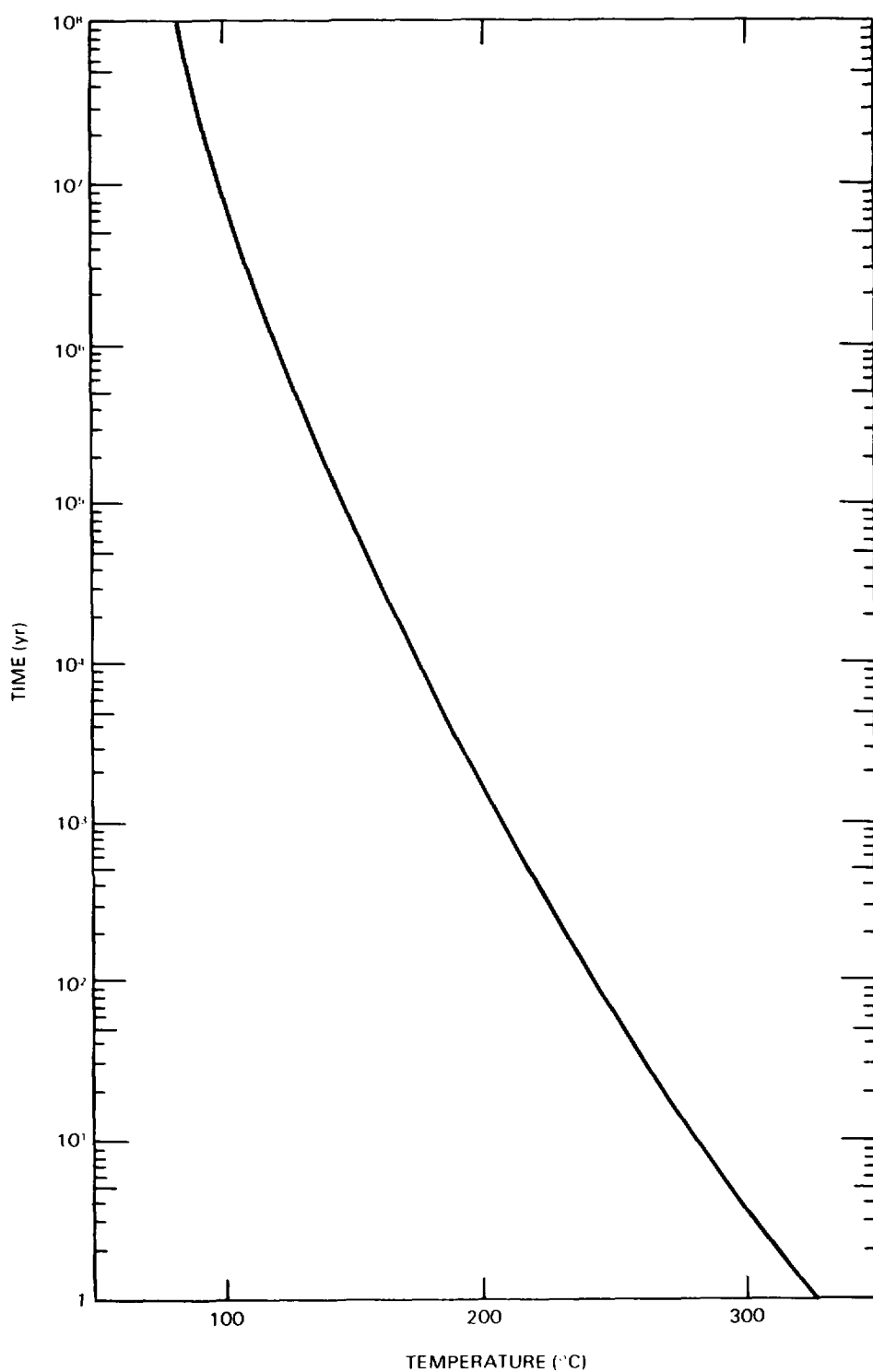
FIGURE 6-17. Minimum Time Required for Anhydrous Thermal Reconstruction of Natural Glass to a Depth of 10 Microns as a Function of Temperature (Marshall, 1961).

However, at 300°C in the presence of water (Fig. 6-18), devitrification of hydrated glass occurs to a depth of 100 microns in only several years. Experimental data (Lofgren, 1970) indicate that devitrification rates are significantly increased (by up to 4 orders of magnitude) if potassium- or sodium-rich solutions are present rather than pure water. This emphasizes the importance of the waste package being able to delay and minimize the influx of water to the waste form.

Another important hydrothermal degradation mechanism for natural glasses, related to and facilitating devitrification, is hydration. Diffusive movement of water through glass is an important mechanism in the ion exchange of cations from glass with hydrothermal solutions (Marshall, 1961). Hydration rates have been experimentally determined to be 4 to 5 orders of magnitude more rapid than devitrification rates (Lofgren, 1970). The experimental hydration rate for obsidian at 100°C performed in a steam atmosphere (Friedman et al., 1966) is shown in Figure 6-19. Figure 6-20 plots the logarithm hydration (or diffusion) rate constants as a function of inverse temperature from natural rhyolitic glass samples that were hydrated under known climatic conditions. The activation energy of hydration can be obtained from the slope of the line plotted in Figure 6-20, and is calculated to be about 80 kilojoules per mole (Friedman et al., 1966). Data on hydration rates and activation energies for hydration of volcanic glasses may be used in evaluating the persistence (i.e., devitrification rate) of radioactive waste glass at any given temperature, because the mechanisms of hydration (diffusion and transport along microfractures) should be similar, and the general bond breaking and atomic rearrangement caused by hydration will promote devitrification (Lofgren, 1970).

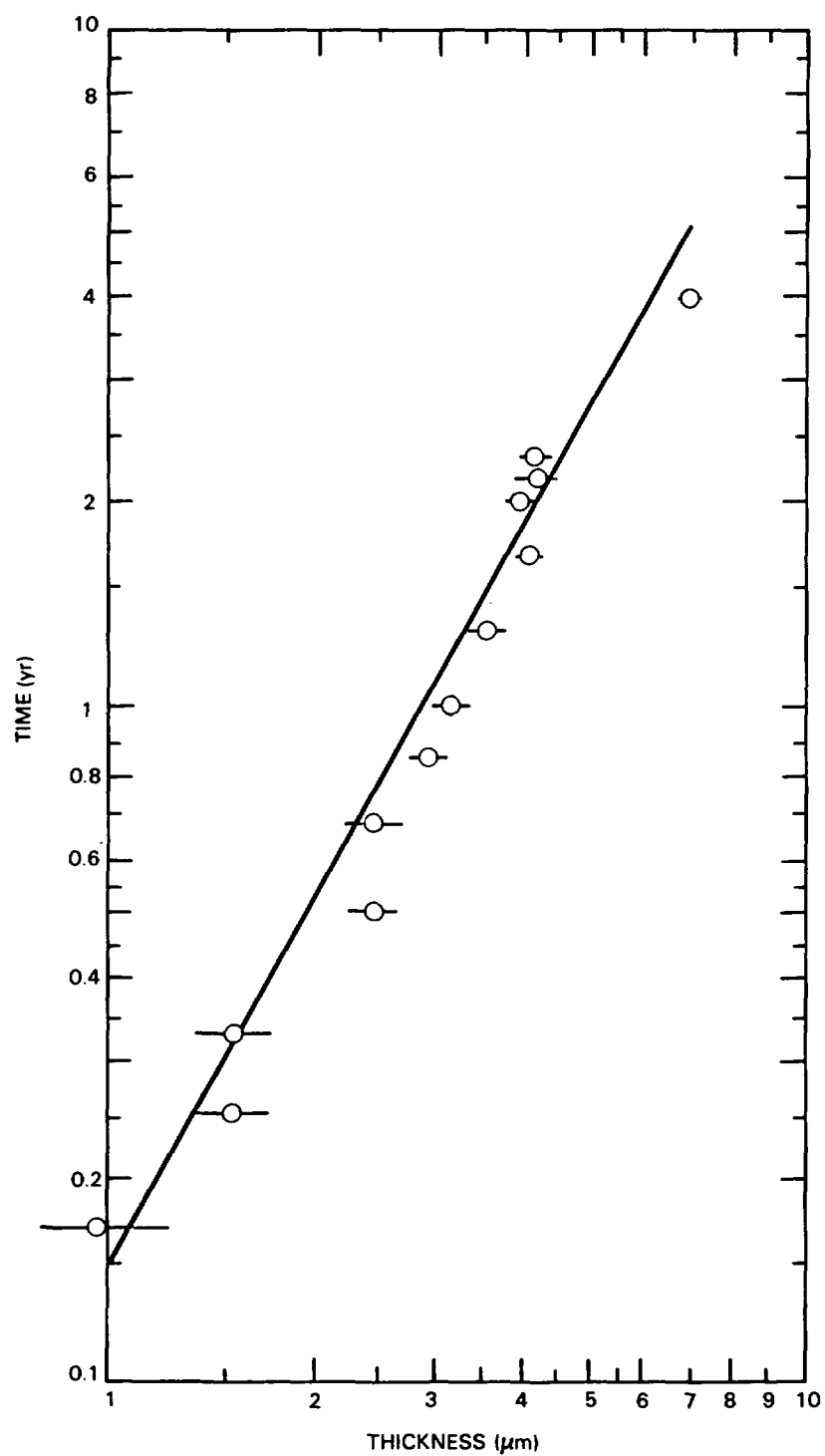
6.5.1.2 Uranium Ore Bodies as Natural Analogs. It is useful to compare a nuclear waste repository to uranium ore deposits to estimate the potential hazards associated with a repository. Comparison of the hazards inherent in deeply buried nuclear waste and those of a "typical" uranium ore body presents a multifaceted problem. There are many methods of evaluating these hazards (Voss, 1979). A few of these methods may be used with confidence, while others are not truly applicable to the problem. Such methods for assessing safety take into account factors such as quantity of radioactive material, decay constants, type and energy of decay, chemical and physical form, toxicity, pathways to man, and comparison of hazards and risks from other materials.

Accurate determination of the hazard presented by a repository or an ore body requires an evaluation of: (1) the solubility (leachability) of the waste package or ore; (2) changes in the environment along the pathway to the biosphere, which may cause sorption or precipitation of phases containing the radionuclide solution; (3) flow rate and volume of water passing through the repository; and (4) path length to the environment. Each of these factors is specific to the repository or ore body in question, making the valid assessment of relative hazards difficult. The relatively uniform dispersion of UO_2 throughout the ore body as part of a permeable rock cannot be readily equated to a mine containing discrete packages of nuclear waste encased in a number of relatively impermeable barriers. This factor further complicates the issue.



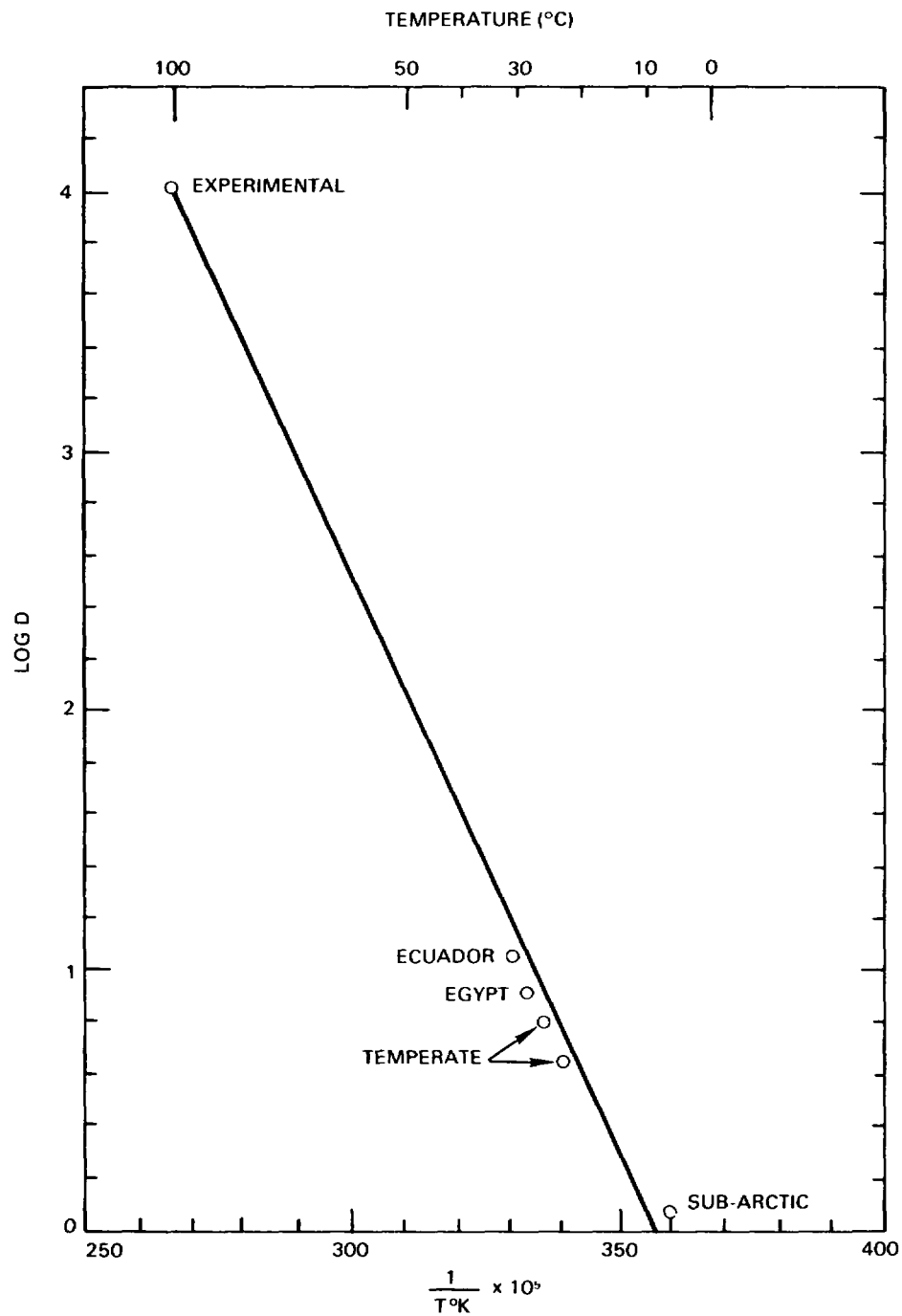
RCP8107-239

FIGURE 6-18. Time Required for the Hydrothermal Reconstruction of Natural Glass (perlite) to a Depth of 100 Microns as a Function of Temperature (Marshall, 1961).



RCP8107-240

FIGURE 6-19. Experimental Hydration Rate Curve for Obsidian at 100°C (Friedman et al., 1966).



RCP8107-241

FIGURE 6-20. Logarithm of Hydration Constant as a Function of Inverse Temperature for Natural Rhyolitic Glass Samples. Activation energy for hydration is equal to the slope of the curve (Friedman et al., 1966).

The overall toxicity of nuclear waste may be determined in several ways. One method assumes that a quantity of nuclear waste, Q , becomes totally dissolved in water. The quantity of water required to dilute the overall radionuclide package to safe levels is determined by the equation (Voss, 1979):

$$\text{Hazard Measure} = \text{HM} = \sum_{i=1}^n \frac{Q_i}{\text{RCG}_i} \quad (6.2)$$

where

Q_i = dissolved quantity of each radionuclide

RCG_i = maximum permissible concentration.

This equation, when plotted as a function of time, gives a measure of relative toxicity of the waste as a function of time.

Because of compositional differences (Cloninger et al., 1980; Smith et al., 1980) between uranium ore bodies, spent fuel, and reprocessed fuel, some method of standardization is required for an accurate comparison of toxicities. This is typically accomplished by (1) comparing equivalent volumes (V) of waste with those of ore or (2) comparing a volume of waste to a volume of ore containing a unit quantity, such as a metric ton, of uranium metal. The approach may be generalized further by comparing a volume of uranium ore containing a given amount of metal with the repository volume containing the spent fuel that originally contained said amount of uranium. In the case of reprocessing wastes, the amount of waste arising from the specified quantity of uranium metal is considered. This toxicity, or hazard index, is defined by the equation (Voss, 1979):

$$\text{Hazard Index} = \text{HI} = \sum_{i=1}^n \frac{Q_i/V}{\text{RCG}_i} \quad (6.3)$$

The hazard index and hazard measure may be converted to a dimensionless number by comparing the relative toxicities of two types of waste or, more typically, waste and a typical uranium ore body. This approach may also be used to compare the toxicity of emplaced nuclear waste to that of other commercially exploitable ores. The relative toxicity index (RTI), is derived from the following equation (Tonnessen and Cohen, 1977):

$$\text{RTI} = \text{HM}_{\text{waste}} / \text{HM}_{\text{comparative base}} \quad (6.4)$$

HM may be replaced by HI throughout this equation.

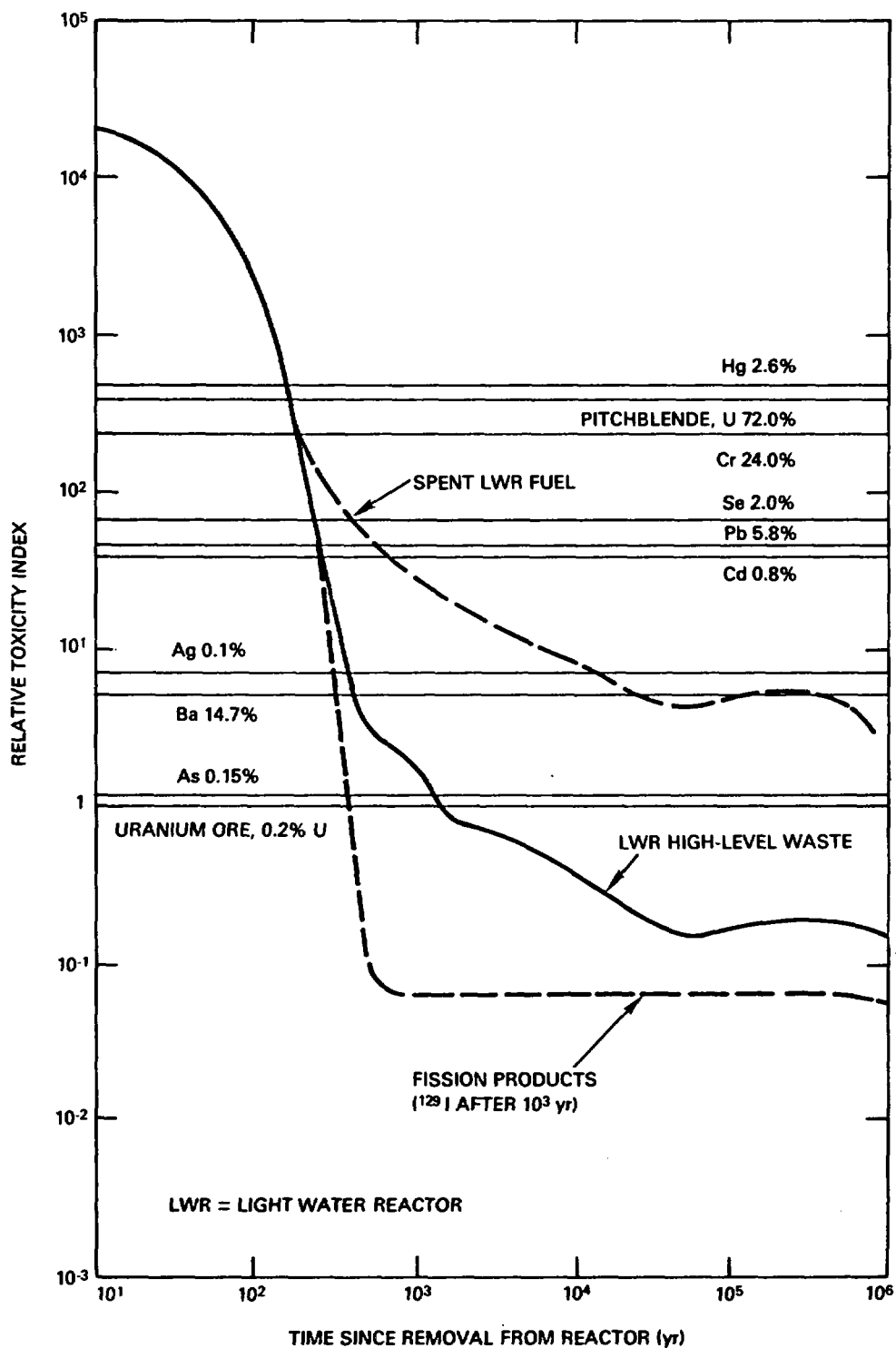
A plot of the relative toxicities of reprocessed nuclear waste, spent fuel, and uranium ore as a function of time is presented in Figure 6-21. This figure is based upon work by Haug (1975; 1976) and Tonnessen and Cohen (1977). Inherent in this figure are the following assumptions:

- Recommended concentration guides for the transuranics were determined by comparison factors for ^{226}Ra .
- The radioactive waste (or spent fuel) is immobilized in a solid matrix of low solubility.
- The waste canisters (20 centimeters in diameter) are placed in individual boreholes 10 meters apart.
- The volume of rock containing the waste canisters is compared to an equal volume of low-grade ^{238}U ore.

Significant differences between high-level waste and spent fuel are immediately apparent. The toxicity of high-level waste dips below that of uranium ore after about 1,000 years. Note that while high-level waste is less toxic than the ore after this time, the origin of hazards from the high-level waste is quite different. The toxicity of this waste is a function of transuranic and ^{129}I content. Spent fuel, on the other hand, is approximately 1 order of magnitude more toxic than the ore at 10^4 years after removal from the reactor and at 10^6 years is still about three times more toxic. In this case, plutonium is the major hazard in the aged waste, along with radium from uranium decay. Again, significant differences in the origin of the waste toxicity compared to that of the ore are apparent. Note also that the toxicity of the nuclear waste decreases to less than that of several important metal-bearing ores in a relatively short time span.

Calculations of this sort are useful to provide a measure of "absolute" toxicity of a section of a nuclear waste repository and equivalent volumes of ore. However, they provide no measure as to the actual hazard that an emplaced repository may pose to a surrounding populace. Factors such as path length to the biosphere, transport time (dependent upon the failure rate, leach rate, groundwater flow, and retardation factors in the migration path), and decay time all must be taken into account.

In assessing realistic potential radiologic hazards of a repository relative to uranium ore bodies, several studies are significant. Wick and Cloninger (1980) modeled granite and salt repositories and found that they are no more hazardous than uranium ore deposits, providing pertinent solubility sorption, leach, and transport data are taken into account. In addition, studies by Bossi (1974), Goodwin (1980), Johnson et al. (1981), Poty et al. (1974), Rich et al. (1977), Walton and Cowan (1975), and Wood and Rai (1981) also suggest that hazards from uranium in repositories should be minimal, based on solubility data and the natural assemblages of minerals found associated with uranium ore deposits.



RCP8107-242

FIGURE 6-21. Comparison of Relative Toxicities of Various Natural Ores to Nuclear Wastes Using Low-Grade Uranium Ore (after Haug, 1975; Tonnessen and Cohen, 1977).

Uranium is soluble when it occurs in the +6 valence state, but is far less soluble in the +4 valence state (Wood and Rai, 1981). (See also Fig. 6-15.) Concentration of uranium into ore deposits probably occurs via the precipitation of uranium(IV) solids from solution of uranium(VI) carbonate complexes, involving a coupled redox process with iron (Poty et al., 1974; Bossi, 1974). Eh conditions for this precipitation process are probably similar to those of either the magnetite-pyrite or magnetite-hematite buffer (see Section 11.4), conditions which correspond to those of the environment of a repository in basalt. Therefore, considering that UO_2 (+4 valence state) will be the likely uranium solid found in waste forms, transport of uranium from the repository should be negligible and not constitute a hazard. A study by Walton and Cowan (1975) on the Oklo deposit supports the above conclusions. The Oklo ore, which contains significant amounts of UO_2 , occurs in organic-rich pelitic sediments, corresponding to relatively reducing Eh conditions. Walton and Cowan (1975) found that many soluble fission products such as cesium, strontium, iodine, and rubidium were mobilized and distributed over a relatively wide areal extent. Uranium, however, being in the insoluble +4 valence state, was not mobilized, but remained concentrated in the ore zone. These observations support the previous conclusions that UO_2 will not be soluble or mobile enough within the repository to represent a significant hazard, because of the reducing Eh conditions that will prevail over most of the life of the repository.

6.5.2 Canister and Overpack Analogs

Most candidate materials under consideration for the canister and overpack are not found in their elemental state in geologic environments. Two exceptions are copper and iron. Existence of these metals in their elemental state provides evidence of their stability in a geologic setting. Other metals, as well, have survived for centuries in natural environments.

6.5.2.1 Native Copper in the Keweenaw Peninsula (Michigan) Basalts. The native copper deposit of the Keweenaw Peninsula, Michigan is a promising natural analog for the evaluation of the long-term stability of copper in a repository located in basalt at the Hanford Site. The Michigan copper deposits occur in tholeiitic flood basalts very similar in general chemical characteristics to those of the Columbia Plateau (Turner and Verhoogen, 1960; Mason and Berry, 1968; Jolly and Smith, 1972; Jolly, 1974). Metallic copper is found in both disseminated and massive form, with little alteration or corrosion readily observable in the interior of the basalt.

Although this natural analog is promising, there are significant differences between the Michigan occurrence and the anticipated repository system. The native copper of Michigan occurs in metamorphosed basalts characterized by the assemblage of chlorite, prehnite, and pumpellyite, whereas the basalts of the Pasco Basin are relatively unaltered and may not become altered even at the temperatures anticipated during the thermal period, because of the much longer geologic time periods required for low-temperature basaltic metamorphism (Winkler, 1979). In addition, the

chemistry of the groundwaters in the two systems is quite different. Waters within the Michigan copper mines have high concentrations of dissolved solids (280 grams per liter of total dissolved species (Lane, 1908)). Grande Ronde Basalt groundwater, on the other hand, has a very low concentration of dissolved solids (744 milligrams per liter total (Gephart et al., 1979)).

Preliminary calculations indicate that copper should be stable with respect to oxidation under the anticipated temperature, pressure, Eh, and pH conditions in a repository at the Hanford Site (see Section 11.4). Planned studies to identify the conditions in the Keweenaw Peninsula basalts that promote copper stability may aid in predicting the long-term performance of copper and its alloys in the Hanford basalt environment.

6.5.2.2 Disko Island Iron Deposit. Because low carbon steel and cast iron are candidate canister and overpack materials, it is useful to evaluate any possible natural analogs of iron that may yield information concerning its stability in basalt. Native iron is commonly found in meteorites, but only rarely occurs in terrestrial rocks. The most notable occurrence is at Disko Island, Greenland (Mason and Berry, 1968).

The iron at Disko Island occurs as large masses and small disseminated grains, both in basalt. Because metallic iron is not often found in basalt, it is obvious that special circumstances resulted in its formation at Disko Island. In this instance, the basalt intruded through coal-bearing sedimentary units. The probable origin of the metallic iron was reduction of iron from the silicate magma by the extremely low Eh conditions, promoted by either coal in the basaltic magma as it cooled or by hydrothermal fluids circulating through the coal and the magma (Brownlow, 1979). Reducing conditions have persisted and the iron remains in its native state. This is significant in evaluating canister and overpack stability in a repository located in basalt at the Hanford Site, where ambient Eh conditions are also expected to be quite reducing (see Section 11.4).

6.5.2.3 Archaeological Objects and Metal Meteorites. A study has been conducted in which several metals have been identified that have survived for centuries in natural environments (Johnson and Francis, 1980). The metals include gold, silver, copper, lead, iron, tin, and mercury occurring as archaeological objects, metal meteorites, and native metals. Archaeological and radiochemical dating have placed the date of fabrication for the oldest metal artifacts at 7000 B.C., while some meteoritic masses have ages estimated to be 5,000 to 20,000 years and have weathered very little.

6.5.3 Backfill Analogs

Bentonite-basalt mixtures, which are candidate backfill materials, are themselves natural analogs. Montmorillonite, a major component of bentonite, is a common alteration product produced by the low-temperature weathering or hydrothermal alteration of basalt (Humphris and Thompson, 1978; Laird, 1980; Seyfried and Bischoff, 1981; Howard and White, 1981; and Section 6.1).

The composition of montmorillonite can vary, due to several cation substitutions (e.g., the exchange of calcium for sodium). Because of the sodium-rich composition of the groundwaters beneath the Hanford Site and the greater swelling capacity of sodium bentonite compared to calcium bentonite, the former has been chosen as a major component of the backfill. Sodium bentonite is found in deposits in Wyoming. A study of the geochemistry of these deposits may be helpful in evaluating the long-term stability of the waste package backfill. Limited experimental data and the observed secondary fracture mineralization indicate that montmorillonite is stable under expected repository conditions (see Sections 6.3 and 11.4). In addition, montmorillonite is found as part of the stable assemblages in metamorphic terranes with estimated temperatures of approximately 300°C (Mueller and Saxena, 1977). Chemical alteration of montmorillonite to nonswelling clays (illite) can proceed from ion exchange between sodic montmorillonite and solutions containing significant amounts of potassium (Hower et al., 1976; Weaver, 1979). The groundwaters in the candidate repository horizons at Hanford are low in potassium and should not lead to significant potassium-sodium exchange; thus the swelling capacity of the bentonite should not be affected.

6.6 FIELD TESTS

Although done primarily for thermomechanical and thermohydrologic reasons, field tests do provide some geochemical data. A significant testing program, and one that may be useful in interpreting expected results from field testing at the Hanford Site, is the test program being conducted at an abandoned iron-ore mine at Stripa in central Sweden. The Stripa mine lies adjacent to a massive body of granite. Near the conclusion of mining operations, an experimental drift was driven far enough into the granite to reveal that the rock mass was suitable for a number of field tests related to the underground disposal of nuclear waste. A cooperative program between the United States and Sweden (Witherspoon and Degerman, 1978) was initiated in late 1977 to assess the effects of nuclear waste emplacement on the stability of a large crystalline rock mass such as this. Over the past 3 years, thermomechanical, fracture hydrology, and geochemical investigations have been conducted in the rock mass at a depth of approximately 340 meters (Witherspoon et al., 1981).

This cooperative program has characterized the rock mass by assembling geologic information of the area, by studying the fracture networks of newly exposed rock surfaces, and by carrying out water injection tests. Measurements are being taken on the effect of pressure and temperature on rock permeability, in particular, the effect of temperature on rock stresses and fracture conditions. Assessments are to be made regarding the temporal variation of subsurface hydrologic conditions. Groundwater samples are also being collected and analyzed.

A second program of tests relevant to field testing in Hanford basalts is the testing being conducted in the Climax Granite at the U.S. Department of Energy's Nevada Test Site. Tests scoped to measure rock response to heat and radiation are being conducted in three parallel drifts at the bottom of a 420-meter shaft drilled to support weapons testing in the 1960s. The technical objectives of the spent fuel storage test are documented by Ramspott et al. (1979).

6.7 SUMMARY

This chapter contains summary geochemical information taken from several separate areas of study: hydrogeology, geology, and waste package. Additionally, other geochemical data are presented in this chapter that do not appear in other chapters. Taken together, this information addresses the determination of initial environmental conditions (temperature, pressure, groundwater composition, basalt mineralogy, Eh, pH) in the reference repository location at the Hanford Site. Expected perturbations in these conditions, arising from emplacement and subsequent hydrothermal geochemical reactions of waste packages in basalt, are also assessed. It is apparent from current knowledge that the synergism between environmental conditions and geochemical reactions of waste-water-rock-engineered barriers will lead to a complex temporal and spatial evolution of chemical conditions in a repository located in basalt (or any other geologic site).

Geologic and hydrologic studies have established the prevailing geochemical conditions of the Grande Ronde Basalt. This has been based on the direct measurement of mineralogic and solution chemistry, as well as evaluation of secondary minerals. The indication is that the solution composition, as well as the pH and Eh, are controlled by reaction of groundwater with basalt (especially the glass portion of the basalt).

Waste package studies have focused on simple hydrothermal reactions between various waste forms and Grande Ronde Basalt groundwater at experimentally maintained repository conditions. Basalt has also been introduced into these tests, and the results confirm the dominant control of groundwater composition and environmental conditions by dissolution of basaltic glass at high temperature. Comparative evaluation of waste form stabilities in a basaltic environment and the stabilities of other waste package components (i.e., backfill, canister, buffer materials) have also been delineated from laboratory testing, investigation of natural occurrences, and literature review.

Several important, competing chemical reactions have been identified as crucial to the modeling of radionuclide release scenarios. Matrix dissolution and leaching (ion exchange) represent the major degradation mechanisms for waste forms. More importantly, hydrothermal studies demonstrate that precipitation of new, less soluble phases from saturated solutions will likely dominate radionuclide concentrations for all meaningful time periods relative to isolation criteria. In addition to these solubility controls, sorption-desorption of radionuclides on a variety of mineral surfaces has shown that this mechanism may be important in retarding the migration of most radionuclides in groundwater. The effect of factors such as colloid formation, anionic complexation of radionuclides, and the effect of radiation fields on solution chemistry are not well known. This is an area of increasing study, particularly with regard to tests utilizing the site-specific environmental conditions of a repository located at Hanford.

Finally, field testing at sites other than Hanford has been discussed regarding expected geochemical data that may be useful in evaluating the Hanford Site. Field investigations of granites located at the Stripa mine in Sweden and granites and tuffs of the Nevada Test Site will provide data that will help the geochemical program at Hanford. It should be emphasized, however, that major chemical differences among these sites, as well as the difficulty in closely controlling and monitoring important environmental parameters in field testing, demand that all direct comparison of results be made cautiously. Note that field studies on salt sites are not relatable to the Hanford Site (and the other silicate rock sites), based simply on the fundamental differences in chemical reactions with water between basalt (silicate) and salt.

6.8 SUMMARY OF UNRESOLVED ISSUES

The previous sections have summarized the current geochemical data obtained by the BWIP. Conceptual geochemical models, guided by observed and postulated geochemical reaction mechanisms, have also been outlined. Several broad areas of unresolved issues remain to be addressed to provide the necessary geochemical understanding for refining design requirements and performance evaluation models. These unresolved issues are identified in Chapter 15 together with plans for their resolution.

6.9 REFERENCES

- Ames, L. L., 1980, Hanford Basalt Flow Mineralogy, PNL-2847, Pacific Northwest Laboratory, Richland, Washington.
- Ames, L. L. and McGarrah, J. E., 1980, Basalt Radionuclide Distribution Coefficient Determinations FY 1979 Annual Report, PNL-3146, Pacific Northwest Laboratory, Richland, Washington.
- Ames, L. L. and McGarrah, J. E., 1981a, Investigation of Basalt-Radionuclide Distribution Coefficients: Fiscal Year 1980 Annual Report, RHO-BWI-C-108/PNL-3462, Pacific Northwest Laboratory for Rockwell Hanford Operations, Richland, Washington.
- Ames, L. L. and McGarrah, J. E., 1981b, High-Temperature Determination of Radionuclide Distribution Coefficients for Columbia River Basalts, RHO-BWI-C-111/PNL-3250, Pacific Northwest Laboratory for Rockwell Hanford Operations, Richland, Washington.
- Anderson, W. J., 1981, Corrosion Tests of Canister and Overpack Materials in Simulated Basalt Groundwater, RHO-BWI-ST-15, Rockwell Hanford Operations, Richland, Washington, May 1981.
- Barnes, M. W. and Scheetz, B. E., 1979, "Laboratory Alteration of a Columbia River Basalt by Hot Groundwater: An Application to Deep Geologic Disposal of Nuclear Waste," Geological Society of America Bulletin, Abstracts, No. 11, p. 384.
- Barney, G. S. and Wood, B. J., 1980, Identification of Key Radionuclides in a Nuclear Waste Repository in Basalt, RHO-BWI-ST-9, Rockwell Hanford Operations, Richland, Washington, May 1980.
- Barney, G. S., 1981a, Radionuclide Reactions with Groundwater and Basalts from Columbia River Basalt Formations, RHO-SA-217, Rockwell Hanford Operations, Richland, Washington.
- Barney, G. S., 1981b, Evaluation of Methods for Measurement of Radionuclide Distribution in Groundwater/Rock Systems, RHO-BWI-LD-47, Rockwell Hanford Operations, Richland, Washington, August 1981.
- Benson, L. V. and Teague, L. S., 1979, A Study of Rock-Water-Nuclear Waste Interactions in the Pasco Basin, Washington, LBL-9677, Lawrence Berkeley Laboratory, Berkeley, California.
- Bischoff, J. L. and Dickson, F. W., 1976, "Seawater-Basalt Interactions at 200°C, 500 Bars, Implication for Origin of Sea-Floor Heavy Metal Deposits and Regulation of Seawater Chemistry," Earth and Planetary Science Letter, Vol. 25, pp. 385-397.
- Bossi, J., 1974, "Use of Fluid Inclusions in the Genetic Study of Vein Deposits," in Proceedings, Symposium on the Formation of Uranium Ore Deposits, International Atomic Energy Agency, Vienna, Austria.

Brownlow, A. H., 1979, Geochemistry, Prentice-Hall, Inc., Englewood Cliffs, New Jersey.

Cleveland, J. M., 1979, "Critical Review of Plutonium Equilibria of Environmental Concern," in Chemical Modeling of Aqueous Systems, Jenne, E. A., ed., American Chemical Society Symposium Series, Vol. 93.

Cloninger, M. O., Cole, C. R., and Washburn, J. F., 1980, An Analysis of the Use of Engineered Barriers for Geologic Isolation of Spent Fuel in a Reference Salt Site Repository, PNL-3356, Pacific Northwest Laboratory, Richland, Washington.

Cubicciotti, D. D. and Sanecki, J. E., 1978, "Characterization of Deposits on Inside Surfaces of LWR Cladding," Journal of Nuclear Materials, Vol. 78, pp. 96-111.

Deer, W. A., Howie, R. A., and Zussman, J., 1967, Rock-Forming Minerals, Longmans, Green and Co., London, England, Vol. 1-5.

Eberl, D. and Hower, J., 1976, "Kinetics of Illite Formation," Geological Society of America Bulletin, Vol. 87, pp. 1326-1330.

Eichholz, G. G., 1979, "Subsurface Migration of Radioactive Waste Materials by Particulate Transport," Annual Progress Report 1978-79, School of Nuclear Engineering, Georgia Institute of Technology, Atlanta, Georgia.

EPA, 1975, Water Programs: National Interim Primary Drinking Water Regulations, U.S. Environmental Protection Agency, Washington, D.C.; also in Federal Register, Vol. 40, No. 248.

EPA, 1981, Working Draft No. 20, Environmental Protection Agency, 40 CFR 191, Environmental Standards and Federal Radiation Protection Guidance for Management and Disposal of Spent Nuclear Fuel, High-Level and Transuranic Radioactive Wastes, U.S. Environmental Protection Agency, Washington, D.C.

Eugster, H. P. and Wones, D. R., 1962, "Stability Relations of the Ferruginous Biotite, Annite," Journal of Petrology, Vol. 3, pp. 82-125.

Friedman, I., Smith, R. L., and Lang, W. D., 1966, "Hydration of Natural Glass Formation of Perlite," Geological Society of America Bulletin, Vol. 77, pp. 323-327.

Garrels, R. M. and Christ, C. L., 1965, Solutions, Minerals, and Equilibria, Freeman, Cooper and Company, San Francisco, California.

Gephart, R. E., Arnett, R. C., Baca, R. G., Leonhart, L. S., and Spane, F. A., Jr., 1979, Hydrologic Studies Within the Columbia Plateau, Washington: An Integration of Current Knowledge, RHO-BWI-ST-5, Rockwell Hanford Operations, Richland, Washington, October 1979.

Giggenbach, W. F., 1981 "Geothermal Mineral Equilibria," Geochimica et Cosmochimica Acta, Vol. 45, pp. 393-410.

Goodwin, B. W., 1980, Maximum Total Uranium Solubility Under Conditions Expected in a Nuclear Waste Vault, TR-29, Atomic Energy of Canada Limited, Pinawa, Manitoba, September 1980.

Haggerty, S. E., 1976, "Oxidation of Opaque Oxides in Basalt," in Oxide Minerals, Short Course Notes, Mineralogical Society of America, Washington, D.C., pp. Hg-1-Hg-100.

Haug, H. O., 1975, Production, Disposal, and Relative Toxicity of Long-Lived Fission Products and Actinides in the Radioactive Wastes from Nuclear Fuel Cycles, KFK-2022, Kernforschungszentrum, Karlsruhe, West Germany.

Haug, H. O., 1976, "Relative Toxicity and Long-Term Problems of Actinide-Bearing Wastes from Fuel Reprocessing," in Proceedings, the Symposium on Waste Management, CONF-761010 University of Arizona, Tucson, Arizona, pp. 262-271.

Holden, G. R. and Berner, R. A., 1979, "Mechanism of Feldspar Weathering I. Experimental Studies," Geochimica et Cosmochimica Acta, Vol. 43, pp. 1161-1171.

Howard, J. and White, W., 1981, "Clay Metamorphism: A Natural Analog for Argillaceous Backfill Behavior," in Proceedings of the 1981 National Waste Terminal Storage Program Information Meeting, U.S. Department of Energy, Columbus, Ohio.

Hower, J., Eslinger, E. V., Hower, M. E., and Perry, E. A., 1976, "Mechanism of Burial Metamorphism of Argillaceous Sediments: 1. Mineralogical and Chemical Evidence," Geological Society of America Bulletin, Vol. 87, pp. 725-737.

Humphris, S. E. and Thompson, G., 1978 "Hydrothermal Alteration of Oceanic Basalts by Seawater," Geochimica et Cosmochimica Acta, Vol. 42, pp. 107-125.

Jacobs, G. K. and Apted, M. J., 1981, "Eh-pH Conditions for Groundwater at the Hanford Site, Washington: Implications for Radionuclide Solubility in a Nuclear Waste Repository Located in Basalt," EOS, Transactions of the American Geophysical Union, Vol. 62, p. 1065.

Johnson, A. B., 1977, Behavior of Spent Nuclear Fuel in Water Pool Storage, BNWL-2256, Battelle, Pacific Northwest Laboratories, Richland, Washington.

Johnson, A. B., Jr. and Francis, B., 1980, Durability of Metals from Archaeological Objects, Metal Meteorites, and Native Metals, PNL-3198, Pacific Northwest Laboratory, Richland, Washington.

Johnson, L. H., Burns, K. I., Joling, H., and Moore, C. J., 1981, The Dissolution of Irradiated UO₂ Fuel Under Hydrothermal Oxidizing Conditions, AECL-TR-128, Whiteshell Nuclear Research Establishment, Atomic Energy of Canada Limited, Pinawa, Manitoba, April 1981.

Jolly, W. T., 1974, "Behavior of Cu, Zr, and Ni During Prehnite--Pumpellyite Rank Metamorphism of the Keweenaw Basalt, Northern Michigan," Economic Geology, Vol. 69, pp. 1118-1125.

Jolly, W. T. and Smith, R. E., 1972, "Degradation and Metamorphic Differentiation of the Keweenaw Tholeiitic Lavas of Northern Michigan, U.S.A.," Journal of Petrology, Vol. 13, p. 2.

Katayama, Y. B., 1976, Leaching of Irradiated LWR Fuel in Deionized and Typical Groundwater, BNWL-2057, Battelle, Pacific Northwest Laboratories, Richland, Washington.

Katayama, Y. B., 1979, Spent LWR Fuel Leach Tests, PNL-2982, Pacific Northwest Laboratory, Richland, Washington.

Koizumi, M., Satoh, M., and Noro, K., 1974, "Phase Study on Solid Fission Products, Ba, Sr, and Zr, in Oxide Fuel," Journal of Nuclear Materials, Vol. 51, pp. 90-94.

Komarneni, S., Scheetz, B. E., McCarthy, G. J., and Coons, W. E., 1980, Hydrothermal Interactions of Cesium and Strontium Phases from Spent Unreprocessed Fuel with Basalt Phases and Basalts, RHO-BWI-C-70, The Pennsylvania State University for Rockwell Hanford Operations, Richland, Washington, March 1980.

Koster van Groos, A. F., 1981, Determination of Dehydration Temperatures of a Secondary Vug-Filling Mineral (Smectite Clay) Using a Differential Thermal Analysis at Various Pressures, RHO-BWI-C-102, University of Illinois for Rockwell Hanford Operations, Richland, Washington, March 1981.

Krauskopf, K. B., 1979, Introduction to Geochemistry, McGraw-Hill Book Company, New York, New York.

Laird, J., 1980, "Phase Equilibria in Mafic Schist from Vermont," Journal of Petrology, Vol 21, pp. 1-37

Lane, A. C., 1908, "Mine Waters," Lake Superior Mining Institute, Proceedings, Vol. 14, pp. 63-151.

Langmuir, D., 1971, "Eh-pH Determination," in Procedures in Sedimentary Petrology, Carver, R. E., ed., Wiley Interscience, New York, New York, pp. 597-635.

Langmuir, D., 1978, "Uranium Solution-Mineral Equilibria at Low Temperatures with Applications to Sedimentary Ore Deposits," Geochimica et Cosmochimica Acta, Vol. 42, pp. 547-569.

Lemoine, A., 1975, Contribution à L'Étude Comportement de UO₂ en Milieu Aquex à Haute Température et Haute Pression, Ph. D. Thesis, Université de Nancy 1, Nancy, France.

Lofgren, G., 1970, "Experimental Devitrification Rate of Rhyolite Glass," Geological Society of America Bulletin, Vol. 81, pp. 553-560.

Long, P. E. and Davidson, N. J., 1981, "Lithology of the Grande Ronde Basalt with Emphasis on the Umtanum and McCoy Canyon Flows," in Myers, C. W. and Price, S. M., eds., Subsurface Geology of the Cold Creek Syncline, RHO-BWI-ST-14, Rockwell Hanford Operations, Richland, Washington, July 1981.

Long, P. E. and Landon, R. D., 1981, "Stratigraphy of Grande Ronde Basalt," in Myers, C. W. and Price, S. M., eds., Subsurface Geology of the Cold Creek Syncline, RHO-BWI-ST-14, Rockwell Hanford Operations, Richland, Washington, July 1981.

Marshall, R. R., 1961, "Devitrification of Natural Glass," Geological Society of America Bulletin, Vol. 72, pp. 1493-1520.

Marshall, W. L. and Warakowski, J. M., 1980, "Amorphous Silica Solubilities-II Effect of Aqueous Salt Solutions at 25°C," Geochimica et Cosmochimica Acta, Vol. 44, pp. 915-924.

Mason, B. and Berry, L. G., 1968, Elements of Mineralogy, W. H. Freeman and Company, San Francisco, California.

Materials Characterization Center, 1981, A State-of-the-Art Review of Materials Properties of Nuclear Waste Forms, PNL-3802, Pacific Northwest Laboratory, Richland, Washington.

McCarthy, G. J., 1977a, "High-Level Waste Ceramics: Materials and Considerations, Process Simulation, and Product Characterization," Nuclear Technology, Vol. 32, pp. 92-105.

McCarthy, G. J., 1977b, Advanced Waste Forms Research and Development, Comprehensive Progress Report, COO-2510-12, The Pennsylvania State University, University Park, Pennsylvania, pp. 14-17.

McElroy, J. L., 1975, Quarterly Progress Report, Research and Development Activities, Waste Fixation Program, January through March 1975, BNWL-1908, Battelle, Pacific Northwest Laboratories, Richland, Washington, p. 34.

Mueller, R. F. and Saxena, S. K., 1977, Chemical Petrology, Springer-Verlag, New York, New York.

Myers, C. W. and Price, S. M., eds., 1981, Subsurface Geology of the Cold Creek Syncline, RHO-BWI-ST-14, Rockwell Hanford Operations, Richland, Washington, July 1981.

Noonan, A. F., Fredrickson, C. K., and Nelen, J., 1980, Phase Chemistry of the Umtanum Basalt: A Reference Repository Host in the Columbia Plateau, RHO-BWI-SA-77, Rockwell Hanford Operations, Richland, Washington, November 1980.

NRC, 1981, "Nuclear Regulatory Commission, 10 CFR 60, Disposal of High-Level Radioactive Wastes in Geologic Repositories," Federal Register, Vol. 46, No. 130, July 8, 1981, Proposed Rules.

Petrovic, R., 1976, "Rate Control in Feldspar Dissolution--II: The Protective Effect of Precipitates," Geochimica et Cosmochimica Acta, Vol. 40, pp. 1509-1521.

Poty, B. P., Leroy, J., and Cuney, M., 1974, "Les Inclusions Fluides dans le Minerais des Gisements d'Uranium Intragránitiques du Limonsin et du Flores (Massif Central, France)," in Proceedings, Symposium on the Formation of Uranium Ore Deposits, International Atomic Energy Agency, Vienna, Austria.

Price, S. M., 1977, An Evaluation of Dike-Flow Correlations Indicated by Geochemistry, Chief Joseph Swarm, Columbia River Basalt, Ph. D. Dissertation, University of Idaho, Moscow, Idaho.

Pusch, R., 1979, "Highly Compacted Sodium Bentonite for Isolating Rock-Deposited Radioactive Waste Products," Nuclear Technology, Vol. 45, pp. 153-157.

Rai, D. and Serne, R. J., 1978, Solid Phases and Solution Species of Different Elements in Geologic Environments, PNL-2651, Pacific Northwest Laboratory, Richland, Washington.

Rai, D., Stuchert, R. G., and Moore, D. A., 1981, Influence of Solid Phases on Americium Concentrations in Solutions, PNL-SA-9106, Pacific Northwest Laboratory, Richland, Washington.

Ramspott, L. D., Ballou, L. B., Carlson, R. C., Montan, D. N., Butkovich, T. R., Duncan, J. E., Patrick, W. C., Wilder, D. G., Brough, W. G., and Mayr, M. C., 1979, Technical Concept for a Test of Geologic Storage of Spent Reactor Fuel in the Climax Granite, Nevada Test Site, UCRL-52796, Lawrence Livermore Laboratory, Livermore, California, June 15, 1979.

Reidel, S. P. and Long, P. E., 1980, Discriminant Analysis as a Method of Flow Identification and Correlation in Layered Basalt Provinces, RHO-BWI-SA-69, Rockwell Hanford Operations, Richland, Washington, November 1980.

Reidel, S. P., Ross, M. E., and Long, P. E., 1978, Orthopyroxene Fractionation in the Grande Ronde Basalt, Columbia River Group, RHO-BWI-SA-5A, Rockwell Hanford Operations, Richland, Washington, December 1978.

Rich, R. A., Holland, H. D., and Petersen, U., 1977, Hydrothermal Uranium Deposits, Elsevier Scientific Publishing Co., Amsterdam, The Netherlands.

Ross, W. A., Bradley, D. J., Bunnel, L. R., Gray, W. J., Katayama, Y. B., Mellinger, G. B., Mendel, J. E., Roberts, F. P., Turcotte, R. P., Wald, J. W., Weber, W. E., and Westsik, J. H., Jr., 1978, Annual Report on the Characterization of High-Level Waste Glasses, PNL-2625, Pacific Northwest Laboratory, Richland, Washington.

Ross, W. A., Turcotte, R. P., Mendel, J. E., and Rusin, J. M., 1979, A Comparison of Glass and Crystalline Waste Materials, PNL-SA-7530, Pacific Northwest Laboratory, Richland, Washington.

Salter, P. F., Ames, L. L., and McGarrah, J. E., 1981a, Sorption of Selected Radionuclides on Secondary Minerals Associated with the Columbia River Basalts, RHO-BWI-LD-43, Rockwell Hanford Operations, Richland, Washington, April 1981.

Salter, P. F., Ames, L. L., and McGarrah, J. E., 1981b, The Sorption Behavior of Selected Radionuclides on Columbia River Basalts, RHO-BWI-LD-48, Rockwell Hanford Operations, Richland, Washington, August 1981.

Schiffmann, P., 1979, "Phase Relations and Cooling Histories of Some Columbia River Pillow Basalts," EOS, Transactions of the American Geophysical Union, Vol. 60, No. 46.

Seyfried, W. E., Jr. and Bischoff, J. L., 1981, "Experimental Seawater-Basalt Interaction at 300°C, 500 Bars, Chemical Exchange, Secondary Mineral Formation and Implication for the Transport of Heavy Metals," Geochimica et Cosmochimica Acta, Vol. 45, pp. 135-147.

Smith, M. J., Anttonen, G. J., Barney, G. S., Coons, W. E., Hodges, F. N., Johnston, R. G., Kaser, J. D., Manabe, R. M., McCarel, S. C., Moore, E. L., Noonan, A. F., O'Rourke, J. E., Schulz, W. W., Taylor, C. L., Wood, B. J., and Wood, M. I., 1980, Engineered Barrier Development for a Nuclear Waste Repository Located in Basalt: An Integration of Current Knowledge, RHO-BWI-ST-7, Rockwell Hanford Operations, Richland, Washington, May 1980.

Smith, M. J., Salter, P. F., and Jacobs, G. K., 1981, Waste Package Performance Requirements for a Repository in Basalt, RHO-BWI-SA-172, Rockwell Hanford Operations, Richland, Washington, November 1981.

Smyth, J. R. and Caporuscio, F. A., 1981, "Zeolite Stability and Radioactive Waste Isolation in Volcanic Rocks," EOS, Transactions of the American Geophysical Union, Vol. 62, No. 17.

Spry, A., 1962, "The Origin of Columnar Jointing Particularly in Basalt Flows," Geological Society of Australia Journal, Vol. 8, pp. 191-216.

Stumm, W. and Morgan, J. J., 1981, Aquatic Chemistry, 2nd ed., John Wiley & Sons, New York, New York.

Swanson, D. A., 1967, "Yakima Basalt of the Tieton River Area, South-Central Washington," Geological Society of America Bulletin, Vol. 78, pp. 1077-1110.

Swanson, D. A. and Wright, T. L., 1981, "Guide to Geologic Field Trip Between Lewiston, Idaho and Kimberly, Oregon, Emphasizing the Columbia River Basalt Group," in Guides to Some Volcanic Terrains in Washington, Idaho, Oregon, and Northern California, D. A. Johnston and Donnelly-Nolen, J., ed., U.S. Geological Survey Circular 838.

Swanson, D. A., Wright, T. L., and Helz, R. T., 1975, "Linear Vent System and Estimated Rate of Magma Production and Eruption for Yakima Basalt on the Columbia Plateau," American Journal of Science, Vol. 275, pp. 877-905.

Teague, L. S., 1980, Secondary Minerals Found in Cores DC2-A1 and DC2-A2 Taken from Grande Ronde Basalt Formation, Pasco Basin, Washington, LBL-10387, Lawrence Berkeley Laboratory, Berkeley, California.

Tomkeieff, S. I., 1940, "Basalt Lavas of the Giants Causeway," Bulletin of Volcanology, Vol. 2, pp. 89-146.

Tonnessen, K. A. and Cohen, J. J., 1977, Survey of Naturally Occurring Hazardous Materials in Deep Geologic Formations: A Perspective on the Relative Hazard of Deep Burial of Nuclear Wastes, UCRL-52100, Lawrence Livermore Laboratory, Livermore, California.

Turner, F. J. and Verhoogen, J., 1960, Igneous and Metamorphic Petrology, 2nd ed., McGraw Hill, New York, New York.

Voss, J. W., 1979, Safety Indices and Their Application to Nuclear Waste Management Safety Assessment, PNL-2727, Pacific Northwest Laboratory, Richland, Washington.

Walton, R. D., Jr. and Cowan, G. A., 1975, "Relevance of Nuclide Migration at Oklo to the Problem of Geologic Storage of Radioactive Waste," in The Oklo Phenomenon, Proceedings from the 1975 Symposium at Libreville, Gabon, IAEA-SM-204/1, International Atomic Energy Agency, Vienna, Austria.

Weaver, C. E., 1979, Geothermal Alteration of Clay Minerals and Shales: Diagenesis, ONWI-21, Office of Nuclear Waste Isolation, Columbus, Ohio.

Wick, O. J. and Cloninger, M. O., 1980, Comparison of Potential Radiological Consequences from a Spent Fuel Repository and Natural Uranium Deposits, PNL-3540, Pacific Northwest Laboratory, Richland, Washington.

Winkler, H. F., 1979, Petrogenesis of Metamorphic Rocks, 5th ed., Springer-Verlag, New York, New York.

Witherspoon, P. A. and Degerman, O., 1978, Swedish-American Cooperative Program on Radioactive Waste Storage in Mined Caverns in Crystalline Rock, LBL-7049, Lawrence Berkeley Laboratory, Berkeley, California, May 1978.

Witherspoon, P. A., Cook, N. G. W., and Gale, F. E., 1981, "Geologic Storage of Radioactive Waste: Field Studies in Sweden," Science, Vol. 211, pp. 894-900, February 27, 1981.

Wood, B. J., 1980, Estimation of Waste Package Performance Requirements for a Nuclear Waste Repository in Basalt, RHO-BWI-ST-10, Rockwell Hanford Operations, Richland, Washington, July 1980.

Wood, B. J. and Rai, D., 1981, Nuclear Waste Isolation: Actinide Containment in Geologic Repositories, RHO-BWI-SA-143/PNL-SA-9549, Rockwell Hanford Operations/Pacific Northwest Laboratory, Richland, Washington, June 1981.

7. SURFACE HYDROLOGY

This chapter examines the regional and site-specific surface water regimes associated with the reference repository location. This examination is presented in terms of the general setting, site screening, and facility design considerations. Because of the organization of data in past reports, this discussion has been segregated in terms of regional (Columbia Plateau), Pasco Basin, and Hanford Site data. The section dealing with the hydrologic setting will be organized according to these headings. The description of surface hydrologic conditions at the reference repository location is covered within the Hanford Site description.

7.1 HYDROLOGIC DESCRIPTION

7.1.1 Regional

The Columbia River, along its 1,954-kilometer (1,214-mile) course, drains portions of seven states and Canada (Fig. 7-1), an area of approximately 670,000 square kilometers (259,000 square miles). From its origin in the Rocky Mountain trench southwest of Calgary, Alberta, the Columbia flows northwest for 240 kilometers (150 miles) before turning south on its course into the United States. The river enters the Columbia Plateau from the Okanogan highlands, where it joins with the Spokane River and immediately begins a westerly course along the Okanogan highlands/Columbia Plateau margin. It turns south again at the foot of the North Cascades near Pateros, Washington and maintains a southerly course for approximately 240 kilometers (150 miles). The area enclosed to the south and east of the river is referred to as the Big Bend Basin of the Columbia Plateau. Along the southerly course, the river cuts through several anticlinal ridge structures, including the Saddle Mountains (at Sentinel Gap), before turning eastward at Umtanum Ridge near the location where it enters the Hanford Site. Upon clearing the easternmost surface expression of the Umtanum Ridge anticline (Gable Mountain), the Columbia River resumes its southerly course, joining with the Yakima River from the west and the Snake River, its principal tributary, from the east below the Hanford Site, in the vicinity of the Tri-Cities (Richland, Kennewick, and Pasco, Washington). Beyond this point it is joined by the Walla Walla River before cutting across the Horse Heaven Hills anticline at Wallula Gap. The Columbia then begins a 480-kilometer (300-mile) westerly course to its mouth at the Pacific Ocean. The average annual discharge of the Columbia River is on the order of 1.73×10^{11} cubic meters (140,000,000 acre-feet) (Gephart et al., 1979).

Hydrologically, the Washington State portion of the Columbia Plateau can be segregated into basins according to the major surface drainage systems present. Such a segregation, made by Leonhart (1979), is shown in Figure 7-2. The Pasco Basin, although shown among other basins, is not hydrologically discrete from the adjacent basins of the region. It is treated separately, however, because it incorporates the Hanford Site and

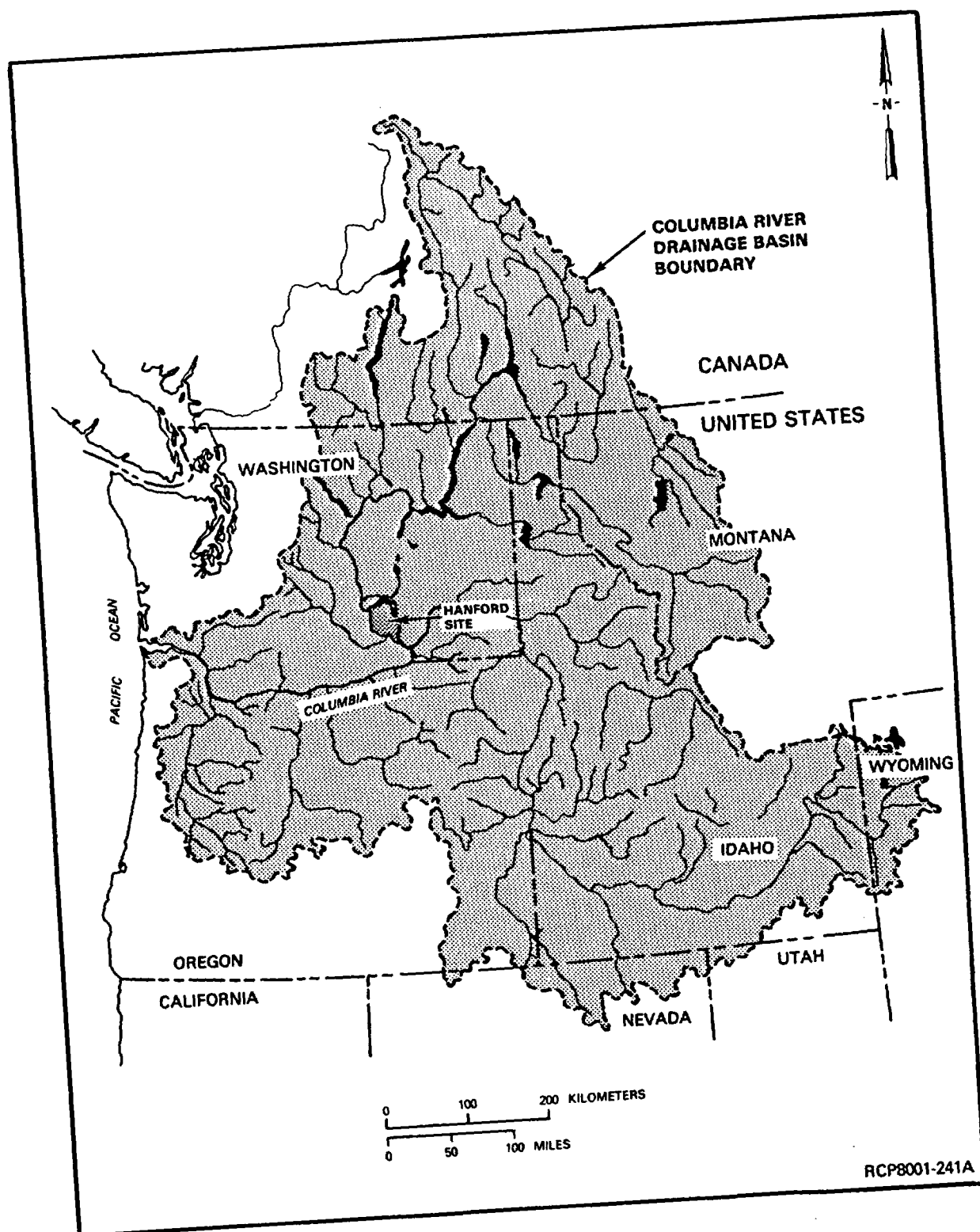
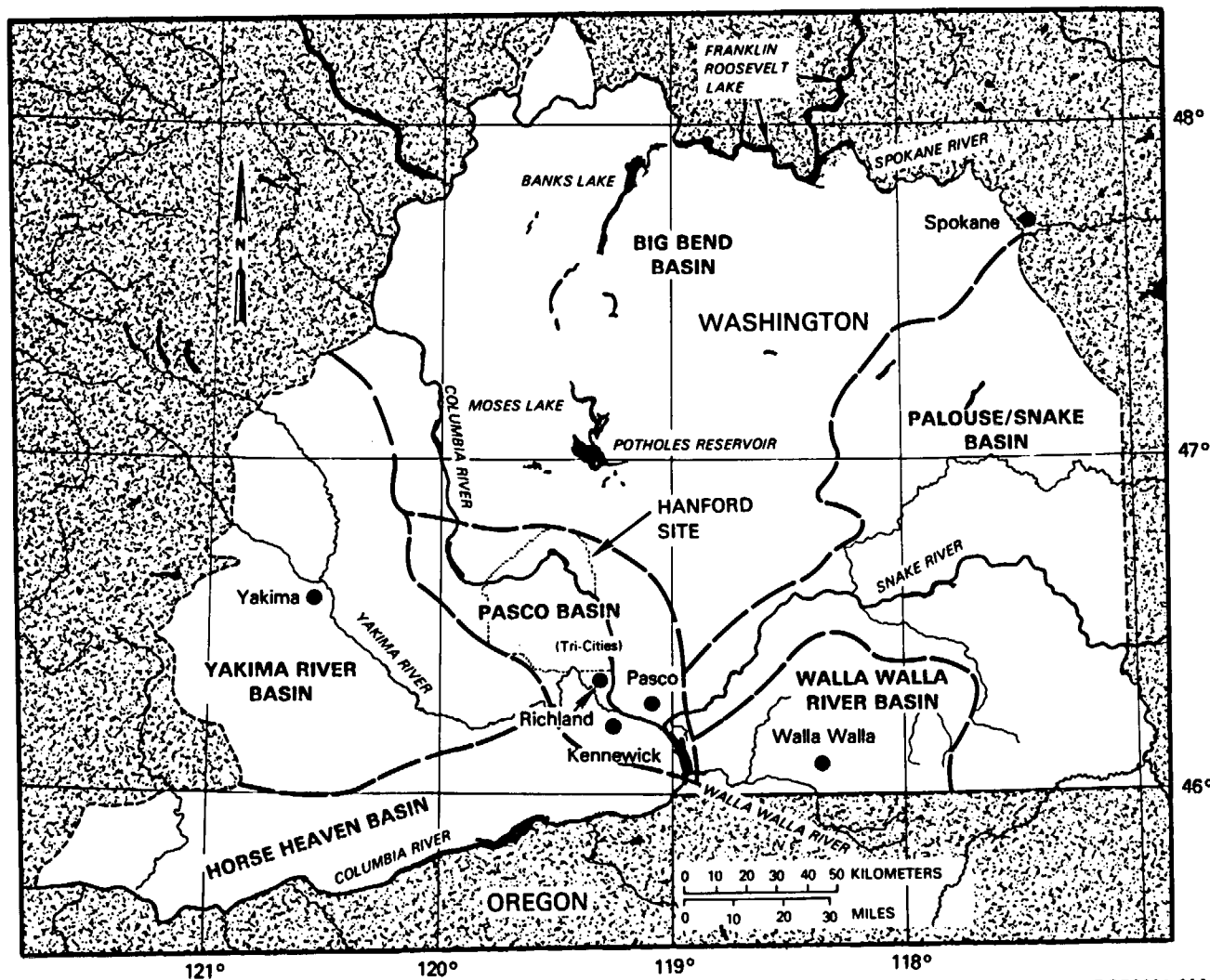


FIGURE 7-1. Columbia River Drainage Basin.



RCP8001-236A

FIGURE 7-2. Hydrologic Basins Designated for the Columbia Plateau (Leonhart, 1979).

because of its relative significance to the Basalt Waste Isolation Project. The other basins interface to some degree with the Pasco Basin. The validity of making such hydrologic segregations for the Columbia Plateau is limited to shallow groundwater and surface water systems.

Of further hydrologic significance is the extensive network of multipurpose water resources projects which have been developed in the region (Fig. 7-3). Most notably, the Grand Coulee Dam backs up to a capacity of 1.2×10^{10} cubic meters (9,402,000 acre-feet) of water. Combined with the 1.9×10^{10} cubic meters (15,500,000 acre-feet) of storage upstream in Canadian reservoirs, a total of 3.1×10^{10} cubic meters (30,000,000 acre-feet) of usable storage are available in the basin above Grand Coulee Dam to regulate the flow of the Columbia River for power and flood control. Additionally, the system has been designed to deliver a full supply of water to 443,130 hectares (1,095,000 acres) of irrigable land within the Columbia Basin Irrigation Project. The Yakima Irrigation Project maintains a storage capacity of about 1.2×10^9 cubic meters (1,000,000 acre-feet) and is designed to deliver irrigation water to 186,800 hectares (461,500 acres). Although no comparably significant irrigation development has occurred along the Snake River, several dams and reservoir projects have been constructed for other multipurpose uses. The current hydraulic regime along the Columbia and Snake Rivers, as they pass through the Columbia Plateau region, is illustrated schematically in Figure 7-4 (a and b, respectively).

7.1.2 Pasco Basin

The Pasco Basin occupies about 4,850 square kilometers (about 1,900 square miles) and is situated within the centermost portion of the Columbia Plateau (Fig. 7-1 and 7-2). Because of its topographically low position within the plateau, surface drainage enters the Pasco Basin from several other basins.

The Columbia River, the primary surface stream, is joined within the basin by major tributaries including the Yakima, Snake, and Walla Walla Rivers. No perennial streams are supported by hydrologic systems operating solely within the Pasco Basin.

Mean annual precipitation within the Pasco Basin ranges from less than 18 centimeters (7 inches) within the Hanford Site to just over 38 centimeters (15 inches) atop Rattlesnake Mountain. Total precipitation over the entire basin is estimated at 9.9×10^8 cubic meters (800,000 acre-feet) annually, averaging less than 20 centimeters (8 inches). Mean annual runoff is very low, generally less than 1.3 centimeters (0.5 inch) for most of the basin. Total annual runoff is less than 3.1×10^7 cubic meters (25,000 acre-feet) per year, and the basin-wide runoff coefficient for all practical purposes is zero.

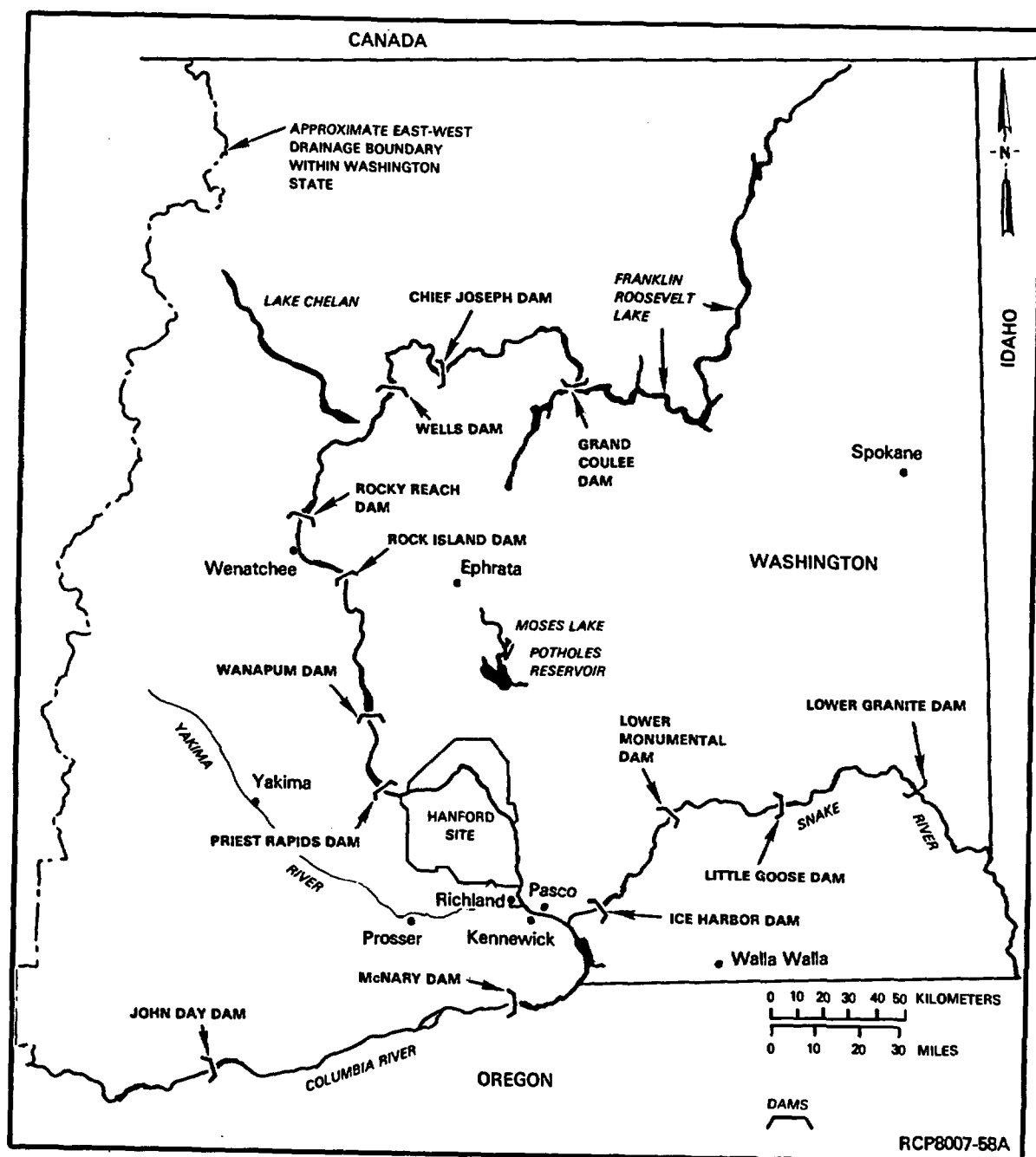


FIGURE 7-3. Locations of Principal Dams Within the Columbia Plateau Study Area (after Leonhart, 1980).

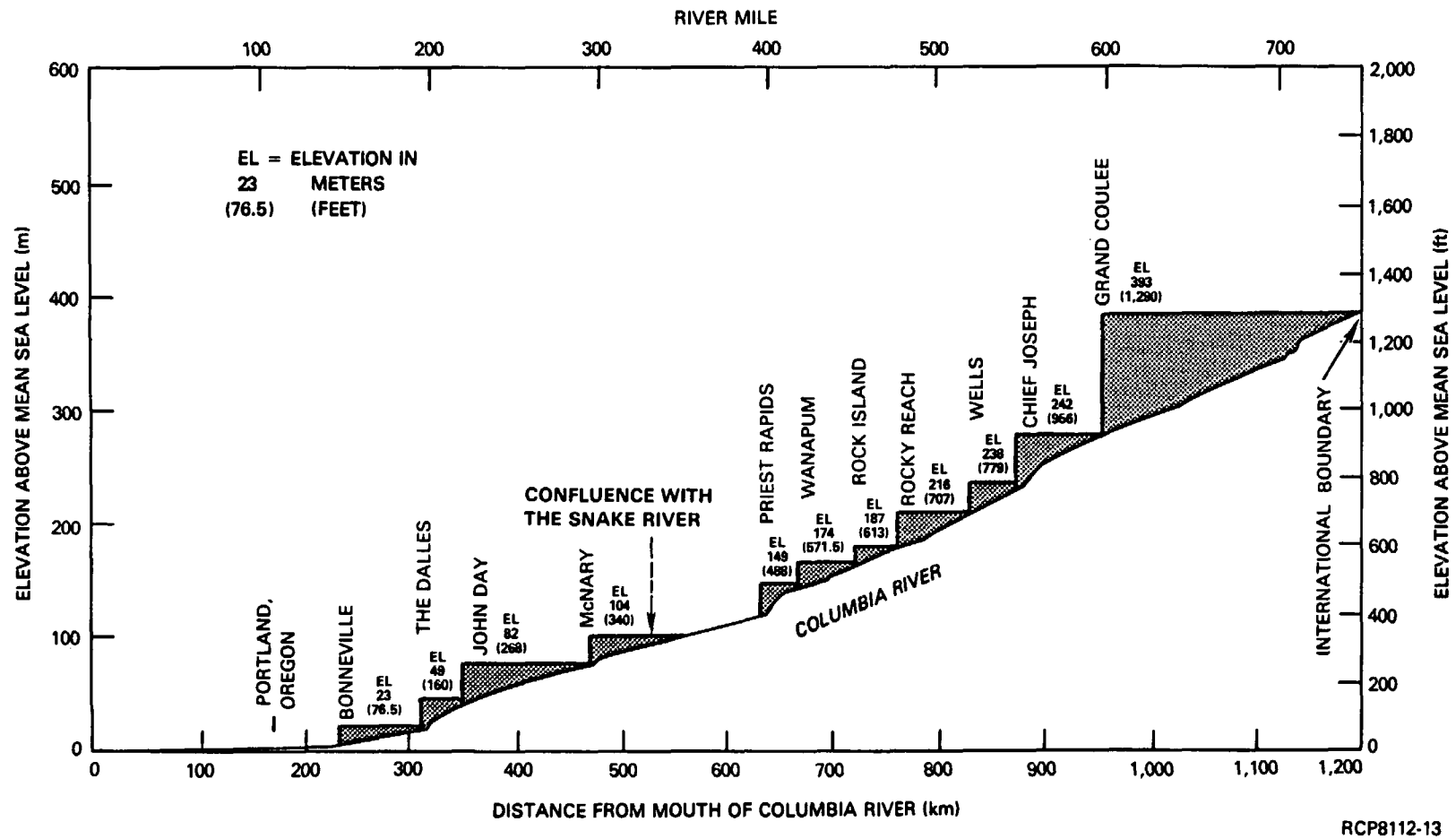


FIGURE 7-4a. Schematic Representation of the Hydraulic Regime of the Columbia River Showing Major Dams (after COE, 1976).

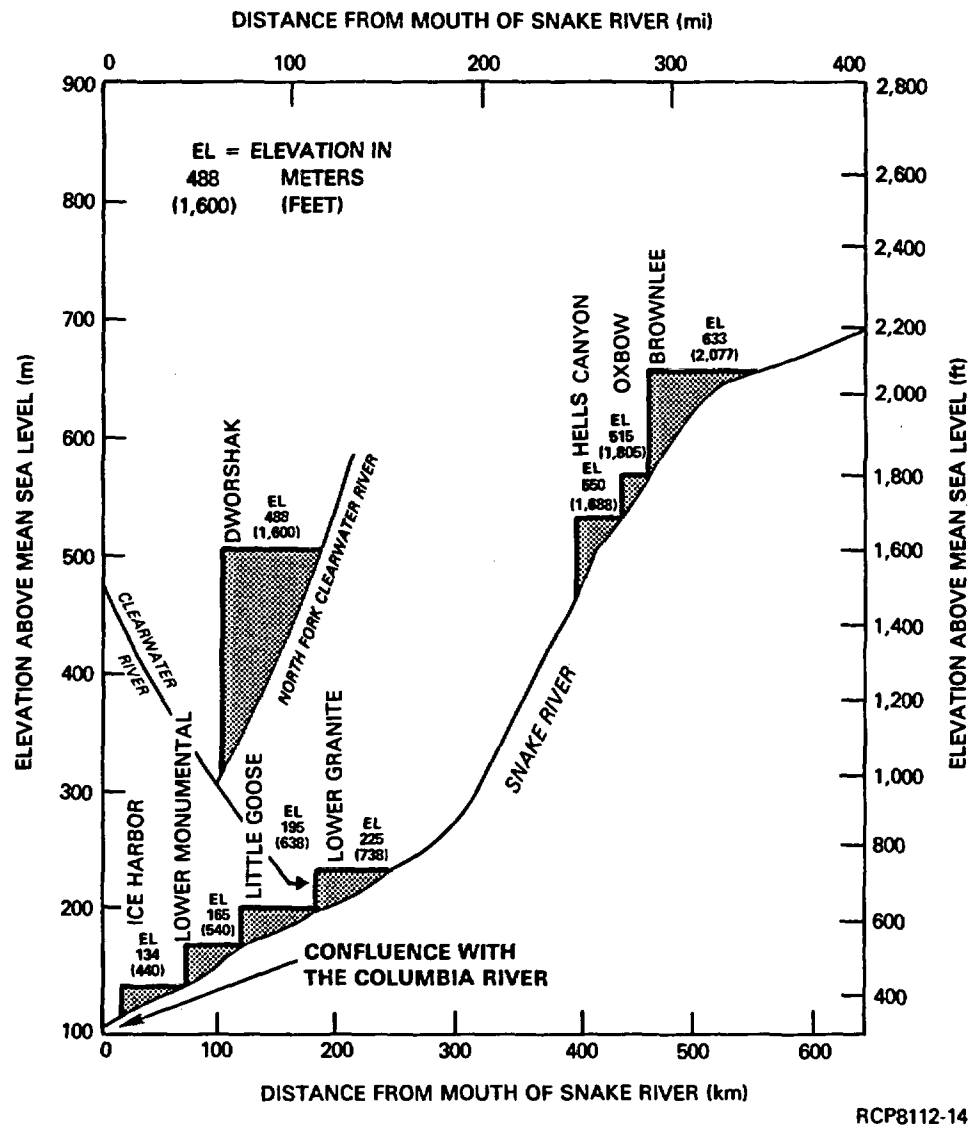


FIGURE 7-4b. Schematic Representation of the Hydraulic Regime of the Snake River Showing Major Dams (after COE, 1976).

Average annual pan evaporation can exceed 152 centimeters (60 inches). Average annual lake evaporation ranges from about 100 to over 105 centimeters (39 to over 42 inches). Actual evapotranspiration for a 15-centimeter (6-inch) water-holding-capacity soil (uncultivated) is about 19 to 22 centimeters (7.5 to 8.5 inches). Based on this estimate, total actual evapotranspiration for the basin would be about 9.9×10^8 cubic meters (800,000 acre-feet) annually.

Streamflow within the Pasco Basin is recorded as inflow at the U.S. Geological Survey gauge below Priest Rapids Dam and outflow at the gauge below McNary Dam. Average annual flow at these stations is 1.1×10^{11} and 1.7×10^{11} cubic meters (87,230,000 and 134,200,000 acre-feet), respectively. A total gauged flow of about 5.5×10^{10} cubic meters (44,830,000 acre-feet) per year enters from tributaries, and an additional 2.8×10^8 cubic meters (225,000 acre-feet) enter as irrigation returns. A schematic of the U.S. Geological Survey gauging network within the Pasco Basin is shown in Figure 7-5.

7.1.3 Hanford Site and Reference Repository Location

The Hanford Site occupies approximately one-third of the land area within the Pasco Basin (about 1,475 square kilometers (about 570 square miles)). Primary surface water features associated with the Hanford Site include the Columbia and Yakima Rivers. Several surface ponds and ditches are present and are generally associated with fuel and waste processing activities (Fig. 7-6).

Approximately two-thirds of the Hanford Site may be considered to drain directly into the Columbia River, although runoff is extremely low. The reference repository location somewhat straddles the divide between the Columbia and Yakima River watersheds. The Columbia River has been inventoried and described in detail in COE (1977) along the Hanford reach, an 84-kilometer (52-mile) stretch from the headwaters of Lake Wallula at river kilometer 555 (river mile 345) to the Priest Rapids Dam at river kilometer 639 (river mile 397). Flow along this reach is controlled by the dam. The western boundary of the Hanford Site intersects the reach at river kilometer 547 (river mile 340). Several drains and intakes are present along the reach. Most notably, these include irrigation seeps and outfalls from the Columbia Basin Project and Hanford Site intakes for the water import system. The former structures occur at various locations throughout the reach, exclusively on the left bank, whereas the latter structures are situated between river kilometer 592 (river mile 368) and river kilometer 618 (river mile 384).

Cold Creek and its tributary, Dry Creek, are ephemeral streams that drain into the Yakima River along the southern boundary of the Hanford Site (Fig. 7-6). Approximately one-third of the Hanford Site is drained by this system. As mentioned above, the reference repository location straddles the watershed boundary between the Columbia and Yakima River systems. The southwestern two-thirds of the reference repository location is situated within the Cold Creek watershed, on the right bank.

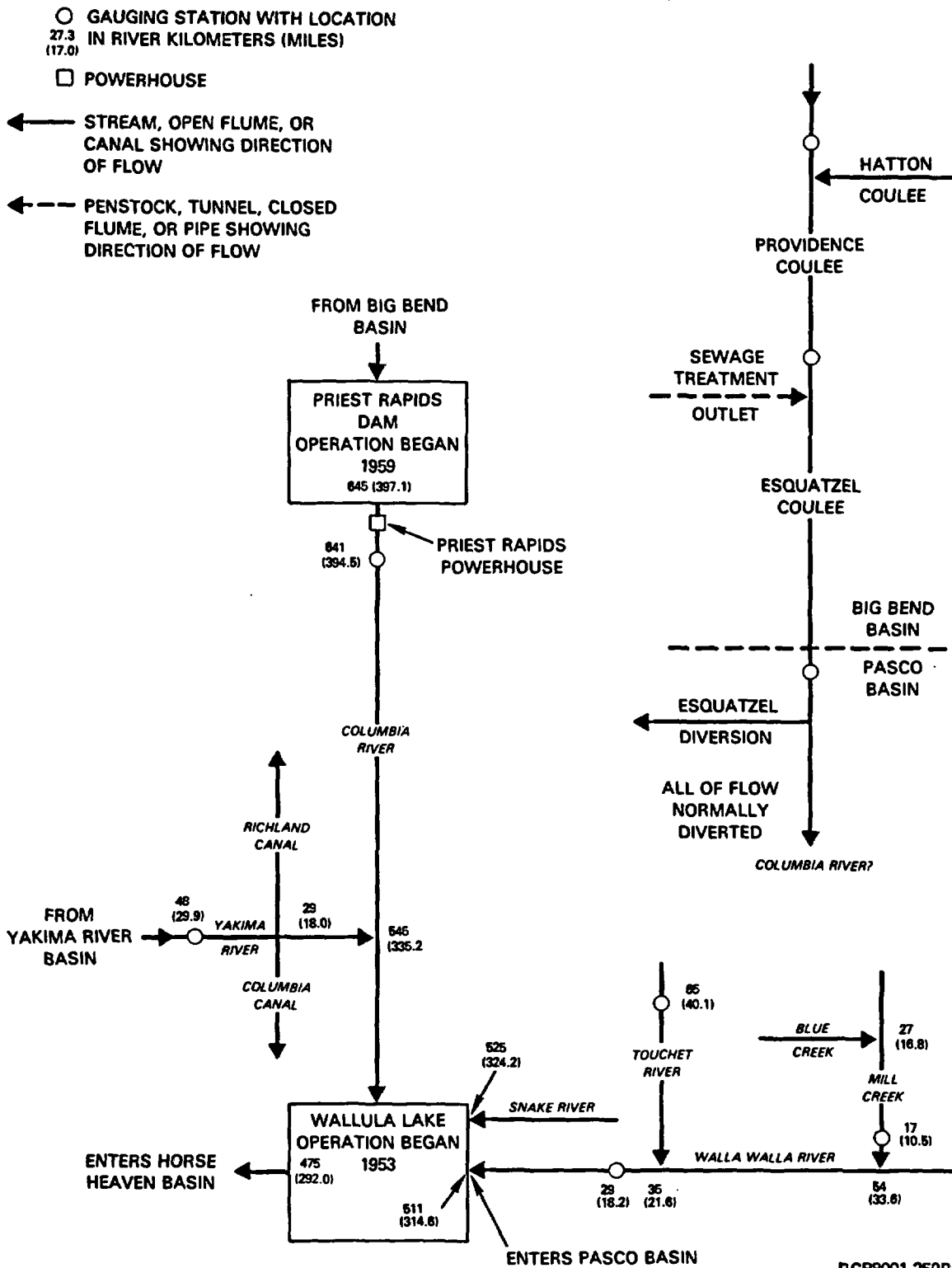


FIGURE 7-5. Schematic of the U.S. Geological Survey Gauging Network for the Pasco Basin.

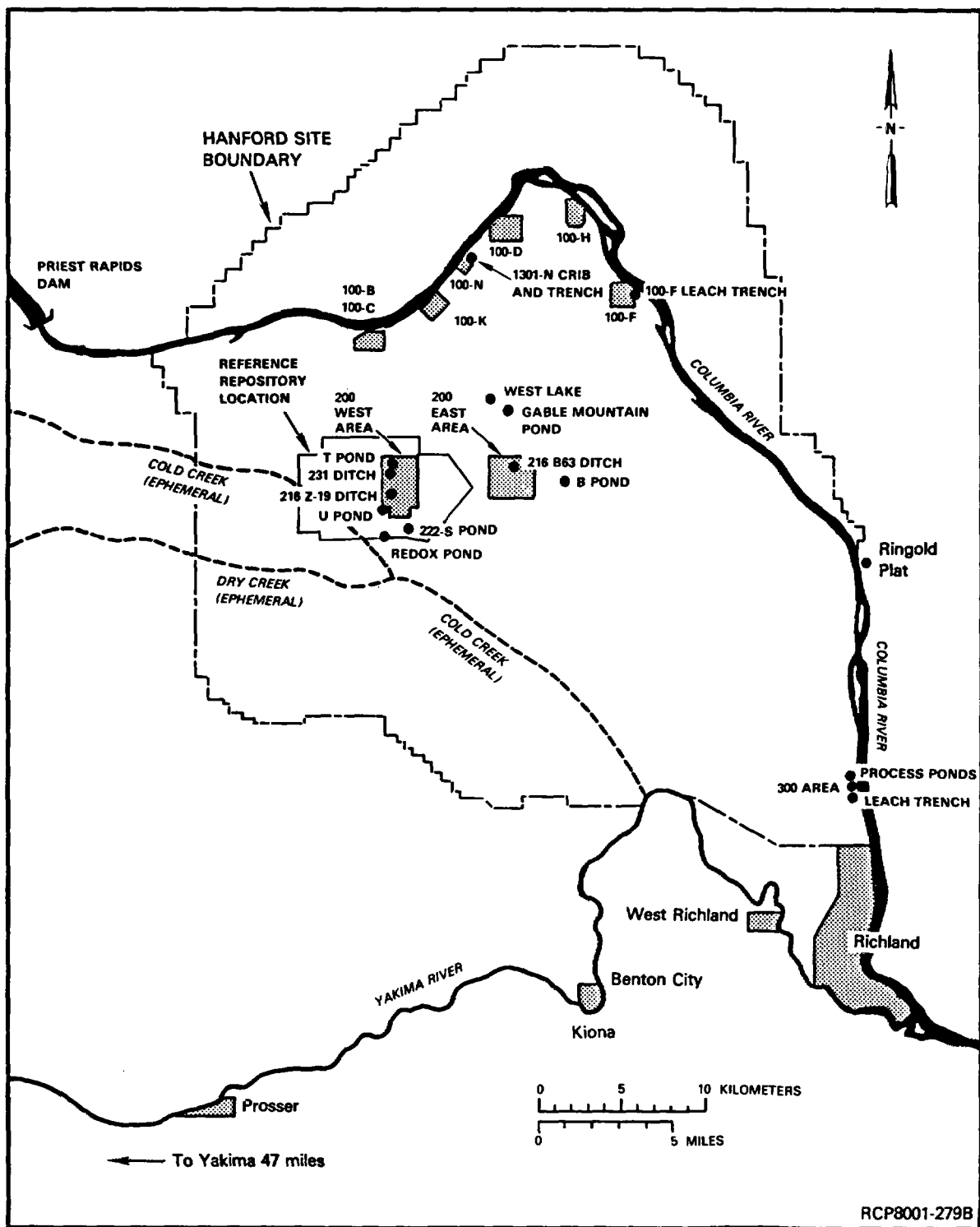


FIGURE 7-6. Surface Water Bodies Including Ephemeral Creeks on the Hanford Site.

The Yakima River has a low annual flow, compared to the Columbia River. Average annual discharge of the Yakima River, measured at Kiona, Washington, is on the order of 3.3×10^9 cubic meters (2,636,000 acre-feet). This water is used extensively along the upstream reaches of the basin, primarily for irrigation purposes.

West Lake, a shallow (less than 1 meter (less than 3 feet)) pond, is the only natural pond within the Hanford Site. Its presence is probably attributable to a combination of factors, but mainly due to a topographic depression (which places it in closer proximity to the water table). Another possible factor might be the potential for increased vertical communication with the uppermost confined aquifers, due to its location along the Gable Mountain anticlinal axis. This latter possibility is somewhat supported by hydrochemical evidence. The lake generally averages about 4 hectares (10 acres) in size. No waste materials are currently being discharged into West Lake. Additionally, a number of man-made ditches and ponds (shown in Fig. 7-6) are used for the disposal of low-level radioactive wastes, certain industrial wastes, other laboratory and sanitary wastes, and discharge of water used for plant cooling (ERDA, 1975; Gephart et al., 1976).

The Hanford Site also incorporates the hydrometeorological extremes found within the Pasco Basin with respect to precipitation and evapotranspiration. The lowest precipitation and highest evapotranspiration values within the basin tend to occur within the lower elevations toward the center of the Hanford Site, whereas the opposite extremes are found atop Rattlesnake Mountain.

7.1.4 Streamflow Characteristics

The U.S. Geological Survey maintains a gauging station on the Columbia River below Priest Rapids Dam at river kilometer 634.9 (river mile 394.5) (Fig. 7-5). This station gauges discharge from approximately 249,000 square kilometers (96,000 square miles). The station has been used continuously since 1917, although not exactly at the same location. The gauge has operated at its present location since 1959. Diversions for the irrigation of about 200,000 hectares (500,000 acres) are made above the station. Flow at this point is regulated by 10 major reservoirs and numerous smaller reservoirs and power plants. On the Yakima River, the U.S. Geological Survey operates a gauging station at Kiona at river kilometer 48.1 (river mile 29.9). This station gauges discharge from approximately 14,543 square kilometers (5,615 square miles). Partial records have been maintained since 1895 and continuous recordings have been made since 1933. Diversions for the irrigation of about 172,000 hectares (424,000 acres) are made above the station. Some regulation of flow is made by various diversions and the operation of five reservoirs situated at the headwaters of the Yakima River and its tributaries. The Kiona canal bypasses the station with a mean flow of approximately 0.7 cubic meter per second (23 cubic feet per second) for the irrigation of about 440 hectares (1,100 acres) below the station. Diversions via the

Kennewick canal, which also bypasses the station, are on the order of 9.9×10^7 cubic meters (80,000 acre-feet) per year (USGS, 1980). Data selected from these tables are graphically shown in Figures 7-7 through 7-12.

7.1.5 Water Control Structures

Dam and reservoir data for the facilities depicted in Figure 7-3 are summarized in Table 7-1. Although there are no known effects upon the Basalt Waste Isolation Project associated with these structures, a description of the Priest Rapids Dam on the Columbia River above the Hanford Site is presented here for informational purposes. A more detailed assessment of possible effects of major dams upon the Basalt Waste Isolation Project was discussed by Leonhart (1980).

Priest Rapids Dam is operated by the Grant County Public Utility District. The dam has a hydraulic capacity of 4,800 cubic meters (170,000 cubic feet) per second, and the operator is required, as a condition of Federal Power Commission licensing, to maintain minimum flows of 1,020 cubic meters (36,000 cubic feet) per second to Hanford, unless inflows are insufficient (COE, 1976). Statistical data for Priest Rapids Dam are summarized in Table 7-2, and a schematic cross section of the facility design is shown in Figure 7-13. Studies are currently being carried out for possible increase in the electrical generating capacity at the Priest Rapids Dam.

Another damsite (Ben Franklin Dam) has been proposed for construction on the Columbia River along the Hanford reach at approximately river kilometer 560 (river mile 348), 16 kilometers (10 miles) upstream from Richland. The Ben Franklin Dam would be a low-head, run-of-the-river dam, having a 15-bay spillway and a navigation lock, all on a straight axis across the river (Fig. 7-14). An assessment of the possible effects of such a facility upon Hanford Site activities was made by Harty (1979). However, the study did not attempt to evaluate the possible effects of the facility upon a deep repository. The inundation of the Columbia River along the Hanford reach, resulting from maintenance of the reservoir at the 122-meter (400-foot) level, is shown in Figure 7-15. Harty's predicted water table elevation and rise, resulting from the impoundment, are shown in Figures 7-16 and 7-17.

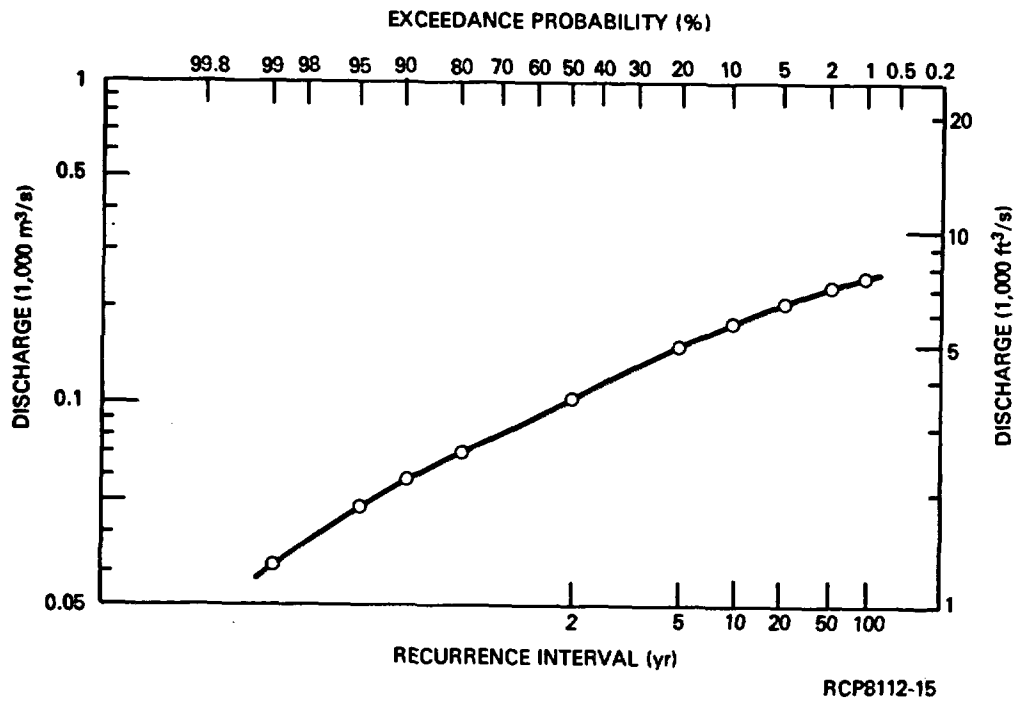


FIGURE 7-7. Yakima River at Kiona, Annual Mean Daily Discharge, Log-Pearson III Distribution.

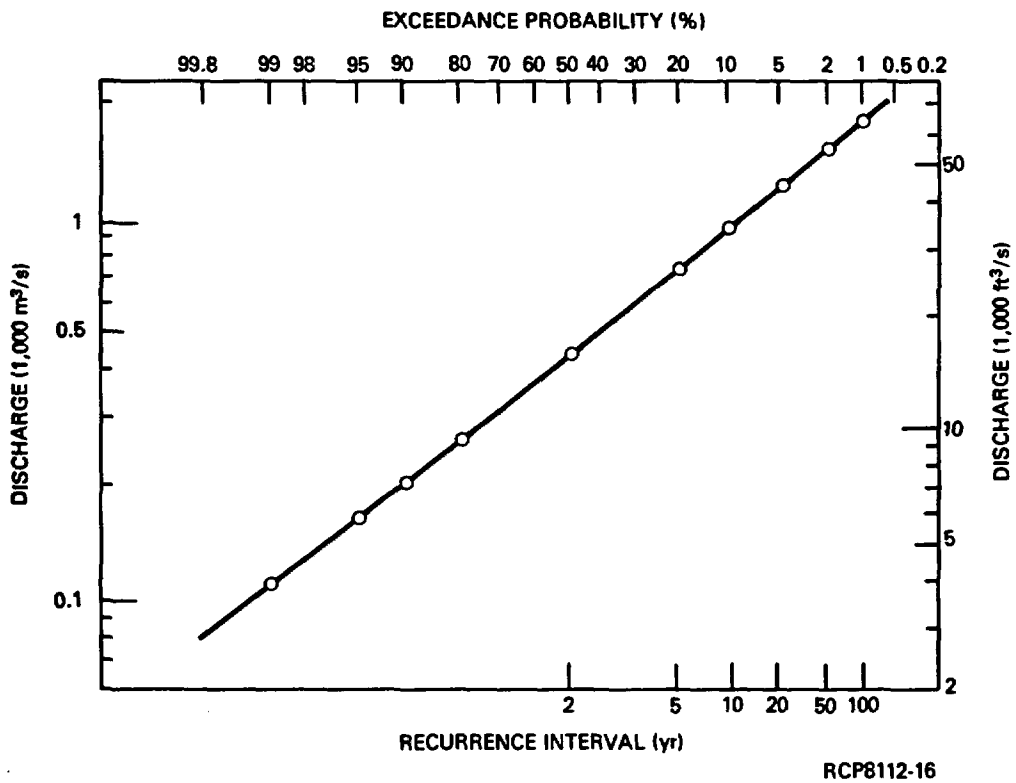


FIGURE 7-8. Yakima River at Kiona, Annual Peak Instantaneous Flow, Log-Pearson III Distribution.

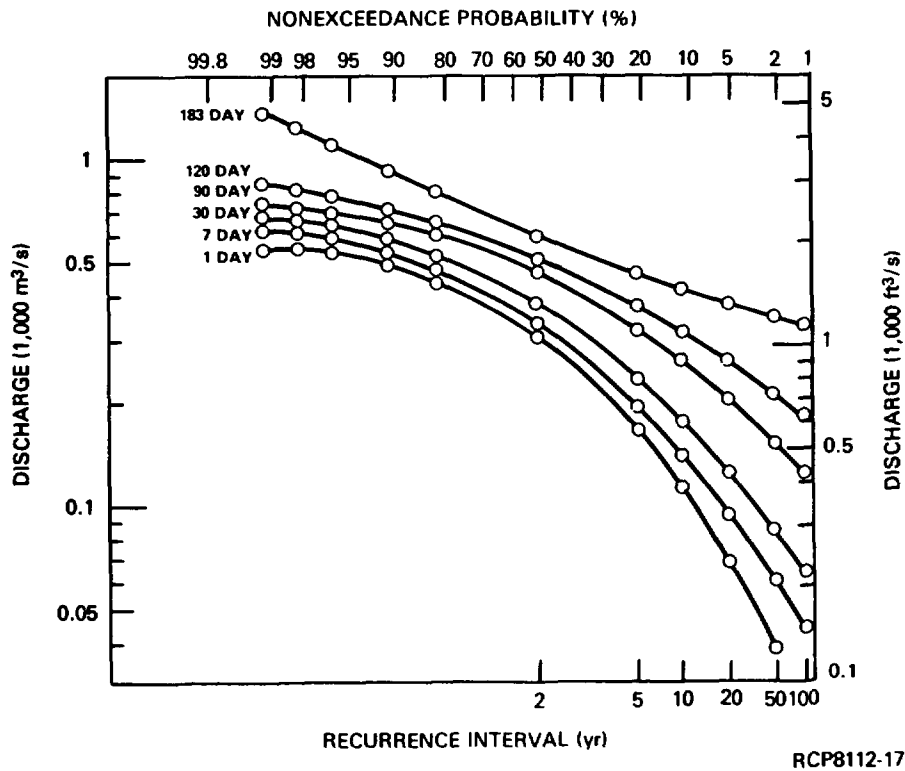


FIGURE 7-9. Yakima River at Kiona, Family of Low-Flow Curves, Log-Pearson III Distribution.

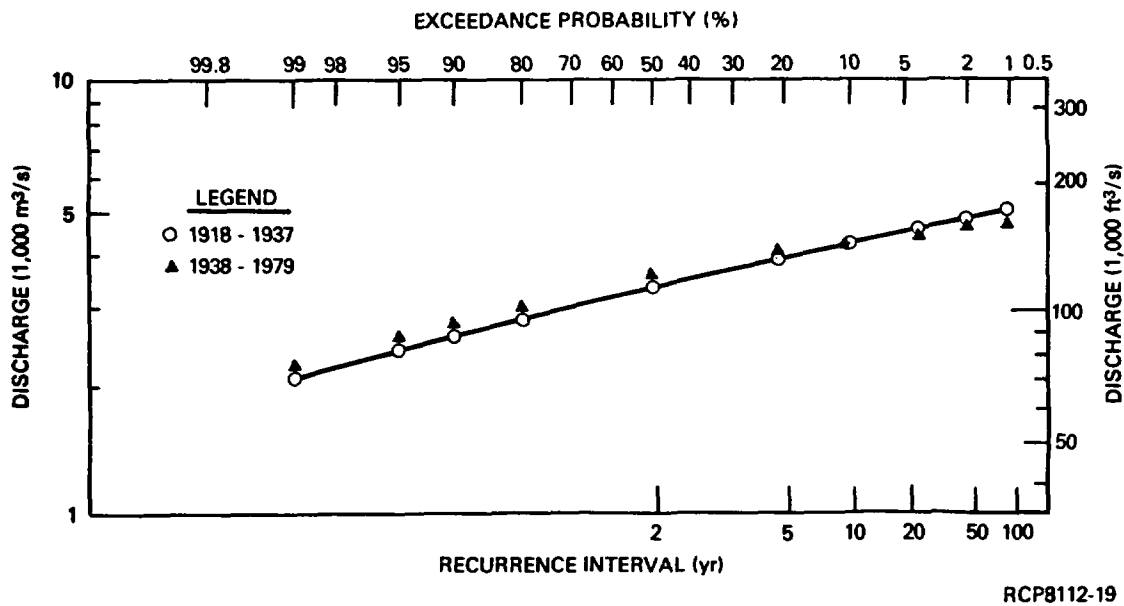
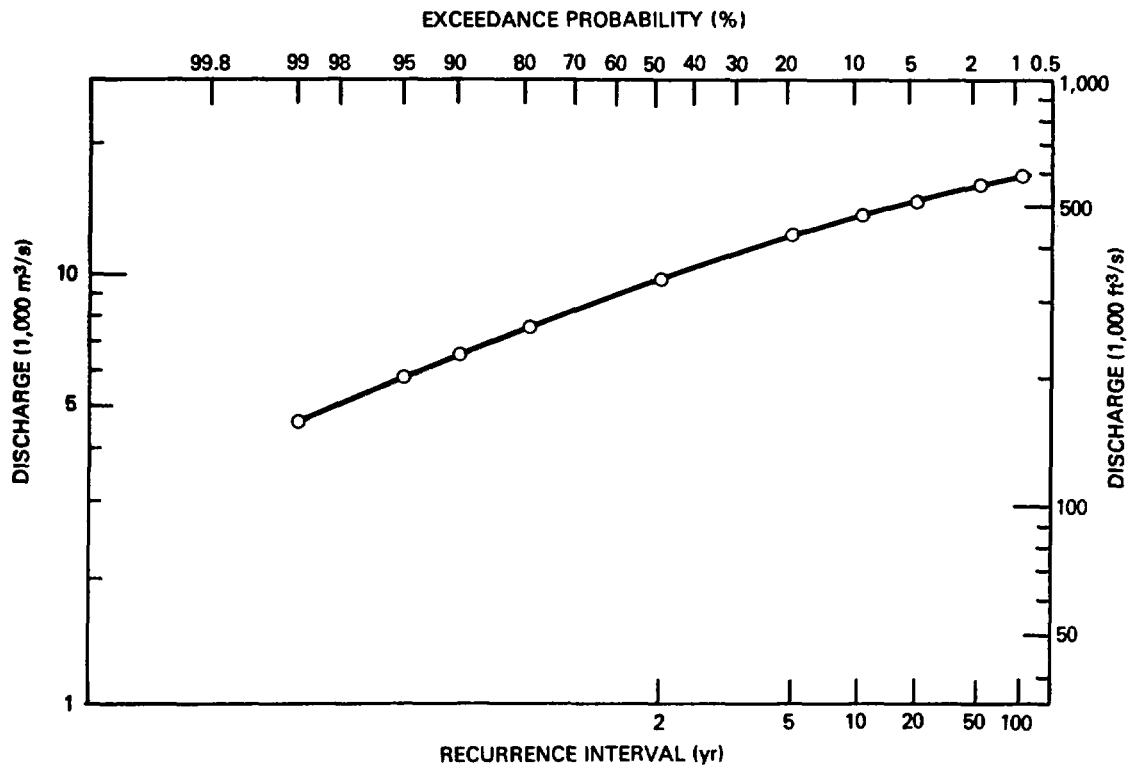
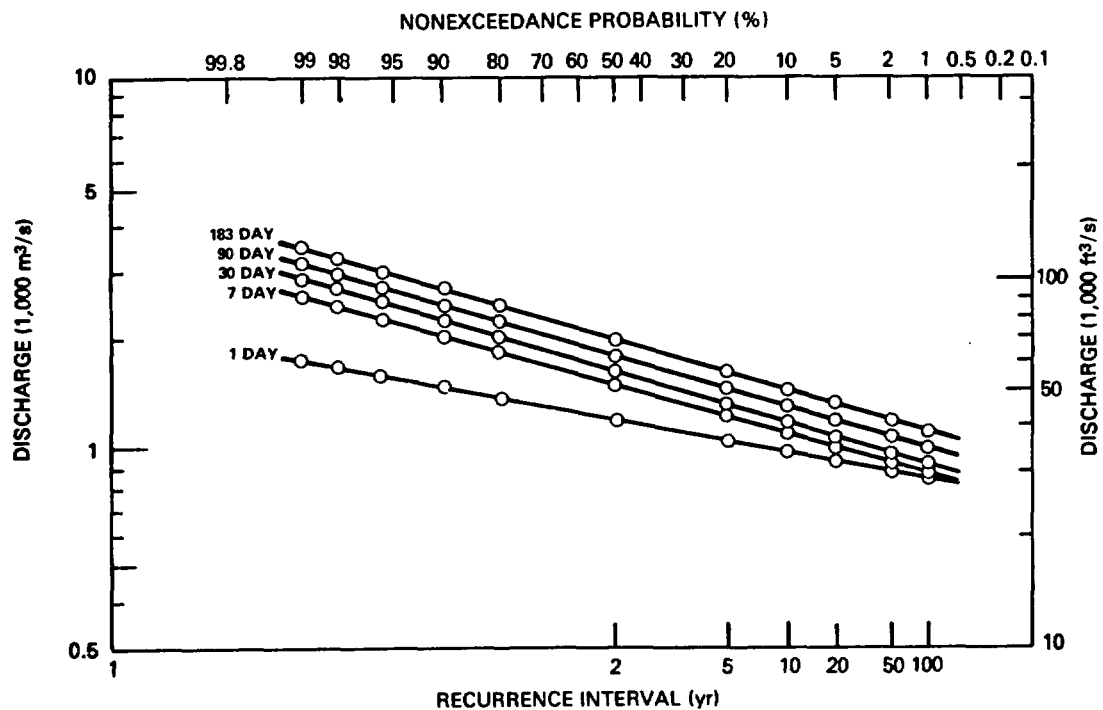


FIGURE 7-10. Columbia River Below Priest Rapids Dam, Annual Mean Daily Discharge, Log-Pearson III Distribution.



RCP8112-20

FIGURE 7-11. Columbia River Below Priest Rapids Dam, Annual Peak Instantaneous Flow, Log-Pearson III Distribution.



RCP8112-22

FIGURE 7-12. Columbia River Below Priest Rapids Dam, Family of Low-Flow Curves, Log-Pearson III Distribution.

TABLE 7-1. Design Data for Principal Dams and Reservoirs Within the Columbia Plateau
(after Leonhart, 1980; data after Wolcott, 1973).

Dam	Use	Location (river), river kilometer (river mile)	Began operation	Elevation above mean sea level		Maximum depth		At capacity average depth		Approximate at spillway level		Approximate surface area of reservoir at spillway level	
				(m)	(ft)	(m)	(ft)	(m)	(ft)	(m ³ E+06)	(acre-ft)	(ha)	(acres)
Upstream from the Hanford Site													
Priest Rapids	P,R	Columbia 639 (397)	1960	148.7	488	26.8	88	8.8	29	280	227,000	3,120	7,700
Wanapum	P,R	Columbia 669 (416)	1963	174.0	571	36.9	121	13.1	43	787	638,000	5,940	14,680
Rock Island	P,R	Columbia 729 (453)	1933	184.4	605	12.8	42	11.6	38	162	131,000	1,400	3,470
Rocky Reach	P,R	Columbia 763 (474)	1961	215.5	707	a	a	6.1	20 ^b	247	200,000 ^b	3,990	9,860
Wells	P,R	Columbia 830 (516)	1967	237.4	779	33.2	109	9.8	32	382	310,000	3,930	9,700
Chief Joseph	P,R	Columbia 877 (545)	1955	288.3	946	57.9	190	20.1	66	636	516,000	3,160	7,800
Grand Coulee	R,I,P, F,C,N	Columbia 961 (597)	1941	392.6	1,288	114.3	375	36.9	121	1,160	9,402,000	31,970	79,000
Downstream from the Hanford Site													
Ice Harbor	P,N,R	Snake 16 (10)	1961	134.1	440	33.2	109	14.9	49	501	406,000	3,390	8,370
Lower Monu- mental	P,N,R	Snake 68 (42)	1967	164.6	540	36.6	120	17.4	57	464	376,000	2,670	6,590
Little Goose	P,N,R	Snake 113 (70)	1962	194.5	638	40.5	133	17.1	56	697	565,000	4,060	10,025
Lower Granite	P,N,R	Snake 174 (108)	1962	224.0	735	41.1	135	15.5	51	566	459,000	3,640	9,000
McNary	N,P,R	Columbia 470 (292)	1953	103.6	340	39.6	130	10.7	35	1,670	1,350,000	15,700	38,800
John Day	P,F,C, N,R	Columbia 348 (216)	1967	80.8	265	44.2	145	14.0	46	2,920	2,370,000	21,000	52,000
The Dalles	P,I,N, R	Columbia 309 (192)	1957	48.8	160	27.4	90	9.1	30	410	332,000	4,530	11,200

Explanation:

C = fishery
F = flood control
I = irrigation

N = navigation
P = power generation
R = recreation

^aNot given.

^bEstimate.

TABLE 7-2. Design Statistics for Priest Rapids Dam
(after Grant, 1980; COE, 1976; USGS, 1980).

<u>Location</u>		
River km (mi)	639.1	(397.1)
<u>Drainage</u>		
Columbia Basin area above dam in approximate km ² (mi ²)	249,000	(96,000)
<u>Proximity to Other Dams</u>		
Upstream: Wanapum Dam, km (mi)	29.0	(18)
Downstream: McNary Dam, km (mi)	169	(105)
<u>Size</u>		
Total overall length, m (ft)	3,360	(11,025)
Reinforced concrete, m (ft)	740	(2,427)
Earth embankments, m (ft)	2,620	(8,598)
Maximum height from deepest point of excavation, m (ft)	54.3	(178)
Rated head, m (ft)	23.8	(78)
<u>Powerhouse</u>		
Length, m (ft)	312	(1,025)
Base width, m (ft)	60.1	(197)
Number of generators	10	
Rated capacity, kw (Provision for up to 6 additional generators)	788,500	
<u>Spillway</u>		
Length, m (ft)	348	(1,142)
Gates - size - 12.2 x 15.2 m (40 x 50 ft)	22	
Hydraulic capacity, m ³ /s (ft ³ /s)	4,800	(170,000)
<u>Fish Facilities</u>		
Number of fish ladders	2	
Spawning channel, 1,844 m (6,050 ft) long	1	
Hatchery, 6.5-million-egg capacity	1	
<u>Reservoir</u>		
Length, km (mi)	29.0	(18)
<u>Schedule</u>		
Construction started	July 1956	
First power generated	October 1959	
Full power production	October 1961	

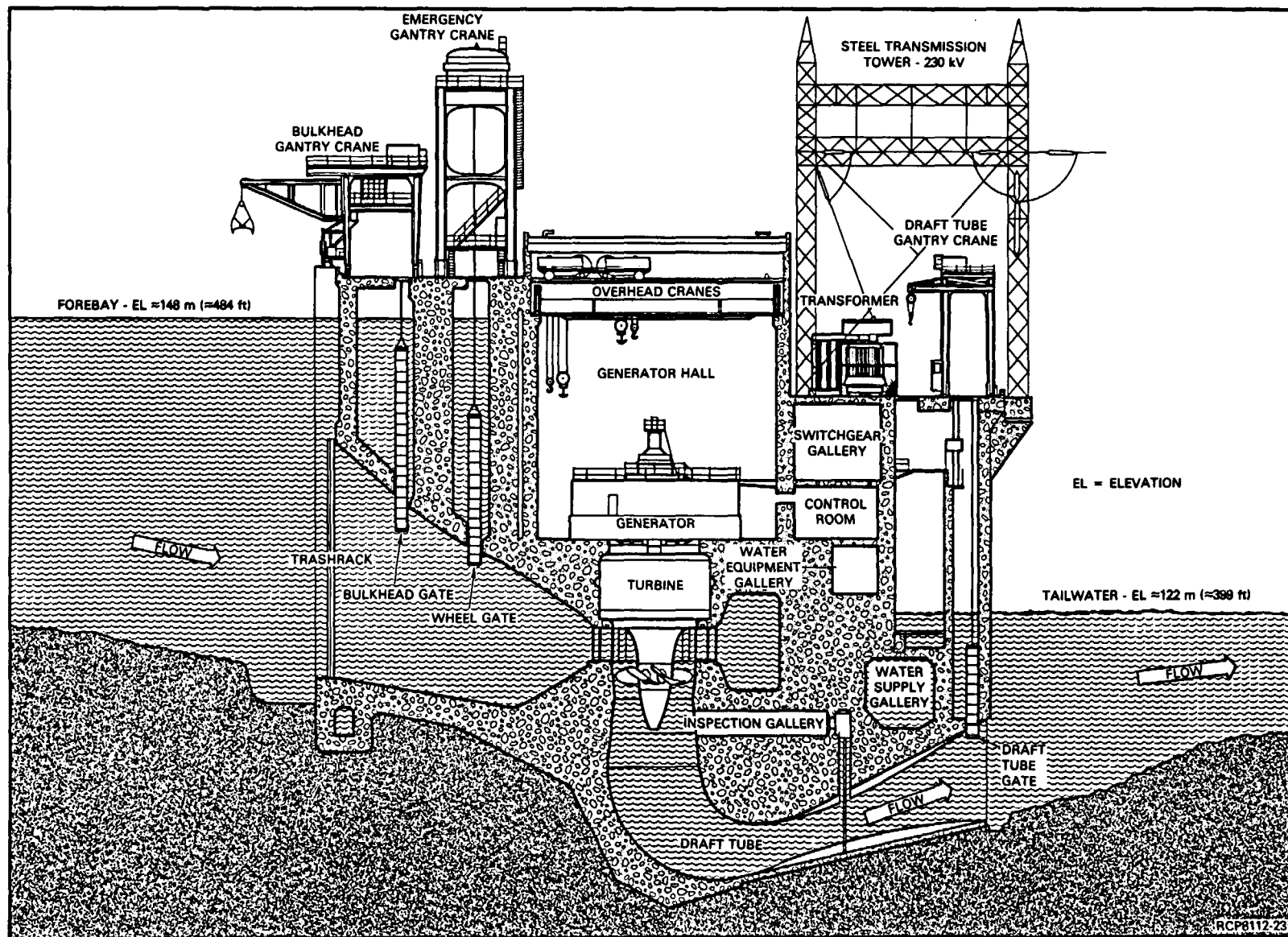


FIGURE 7-13. Schematic Cross Section of the Priest Rapids Dam and Related Facilities (after Grant, 1980).

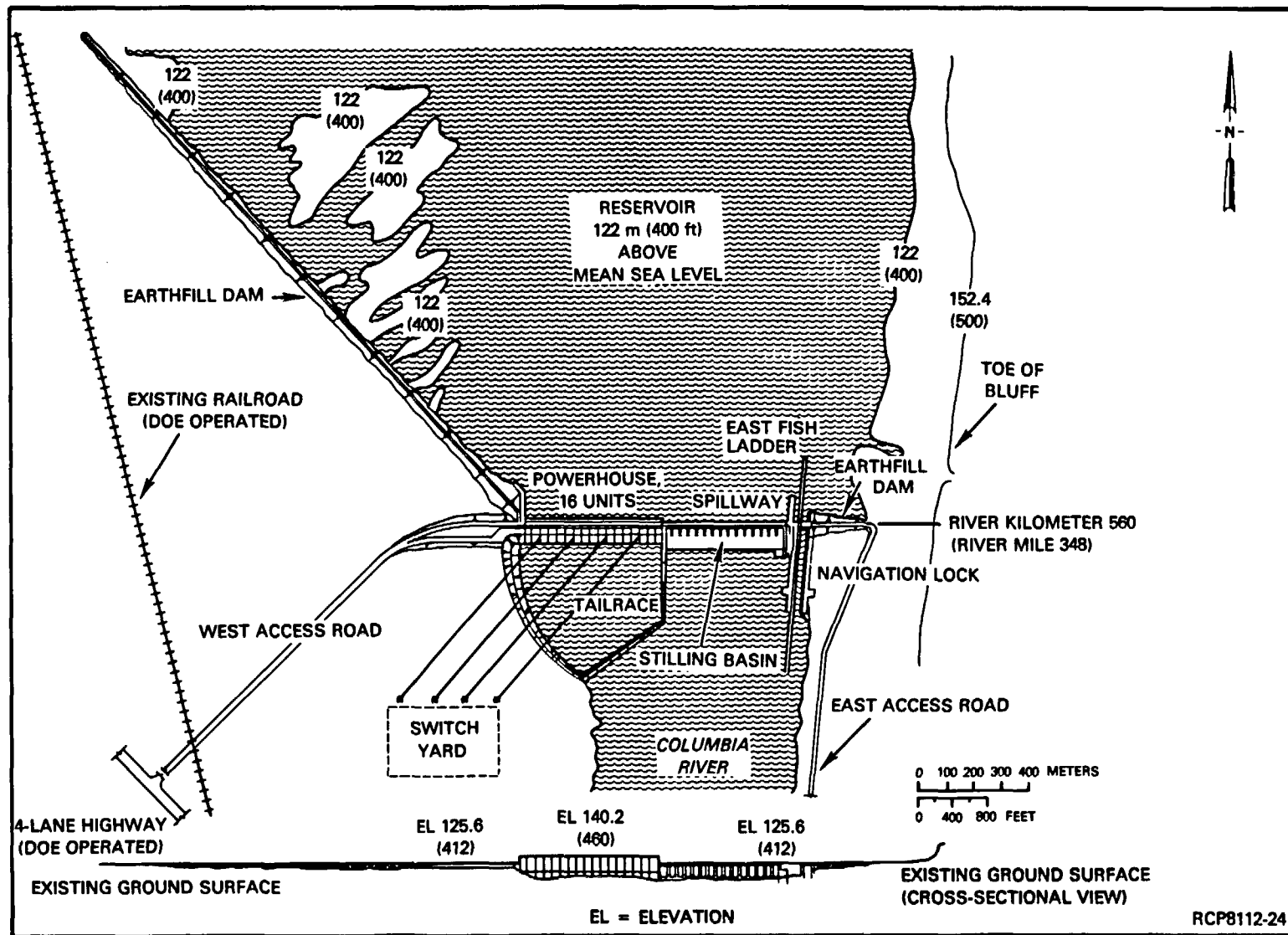


FIGURE 7-14. Plan of Ben Franklin Dam (after Harty, 1979).

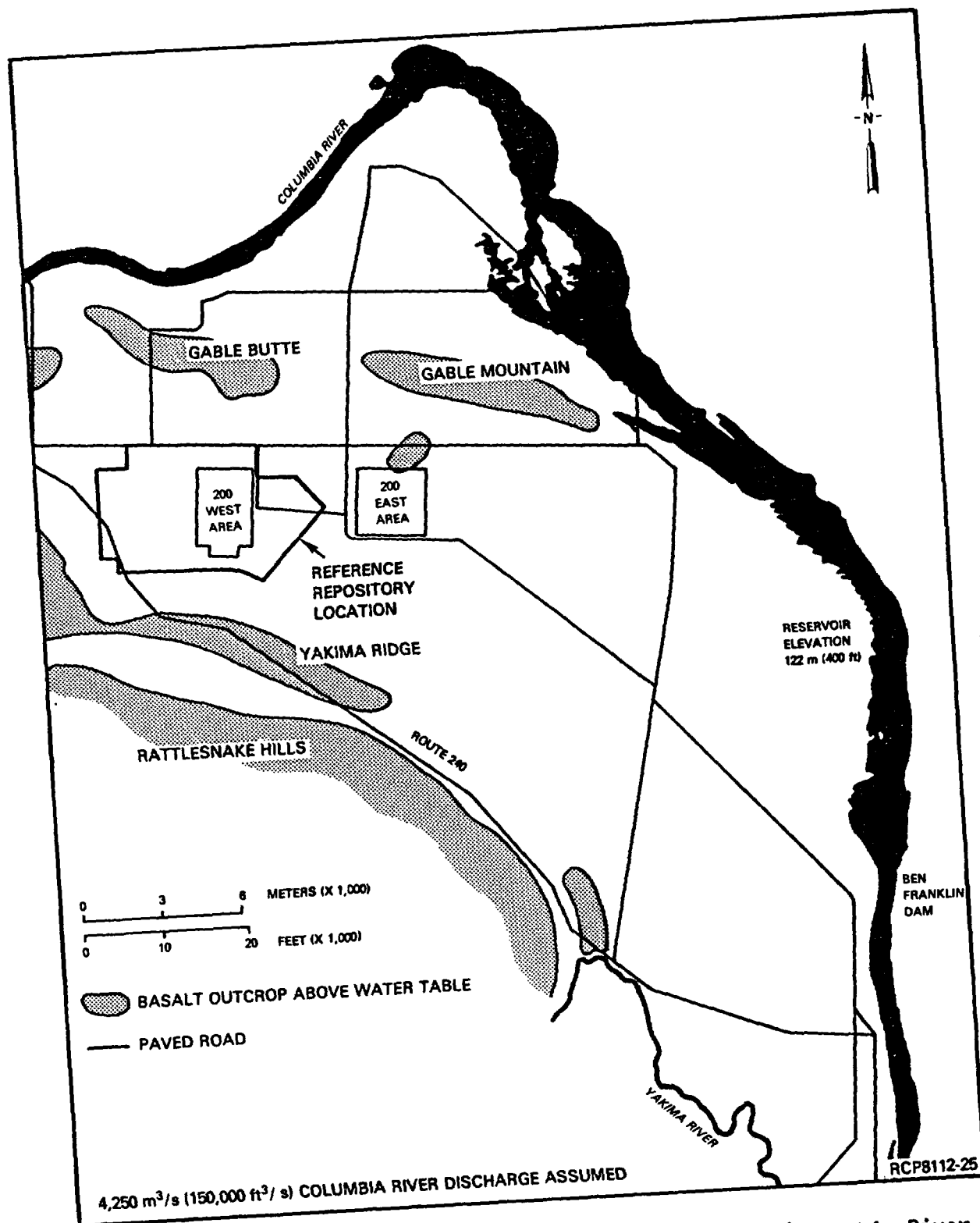


FIGURE 7-15. Inundation Along the Hanford Reach of the Columbia River Resulting from Operation of Ben Franklin Dam (after PNL, 1967).

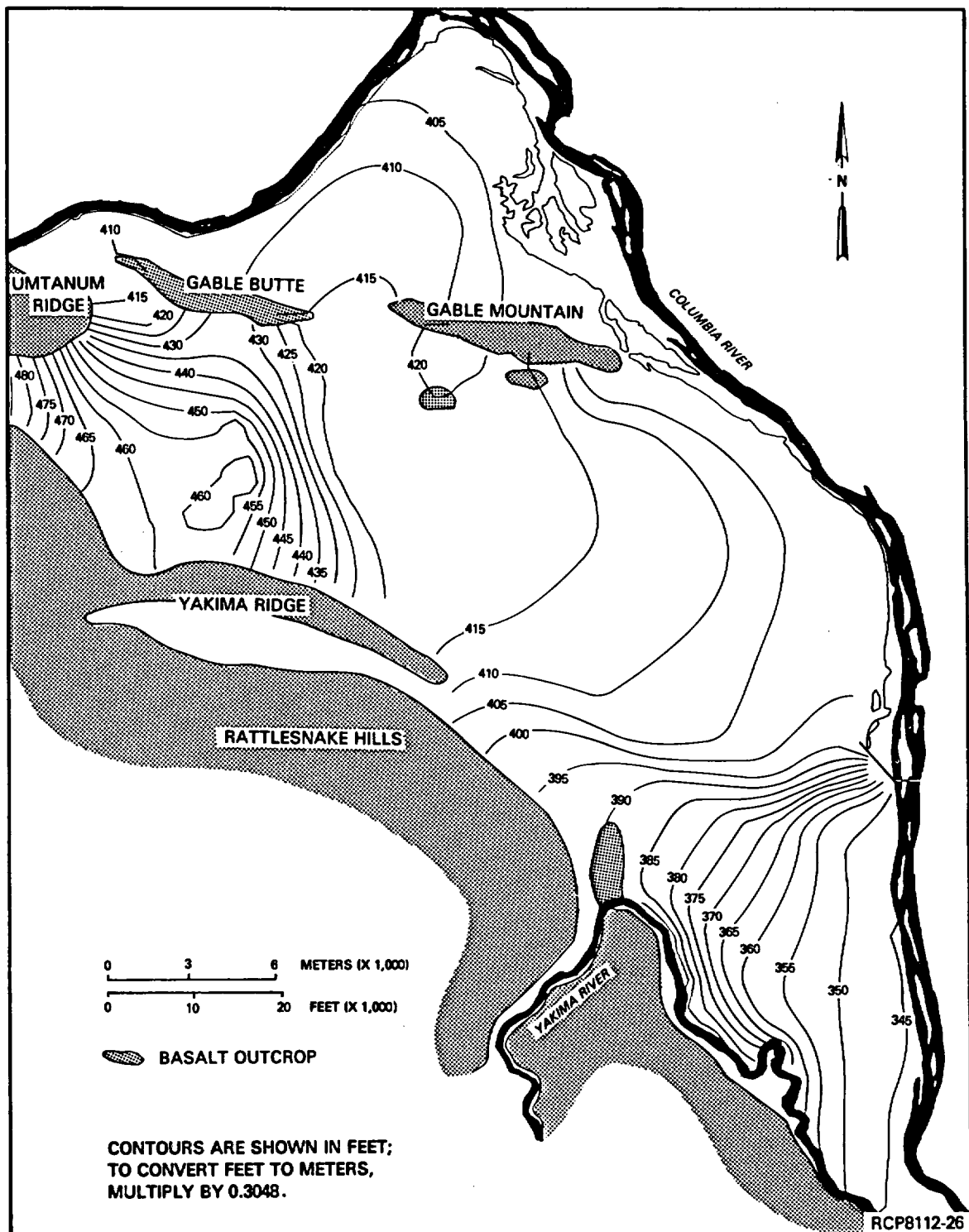


FIGURE 7-16. Predicted Water Table Resulting from Ben Franklin Dam 122-Meter (400-Foot) Pool (after Harty, 1979).

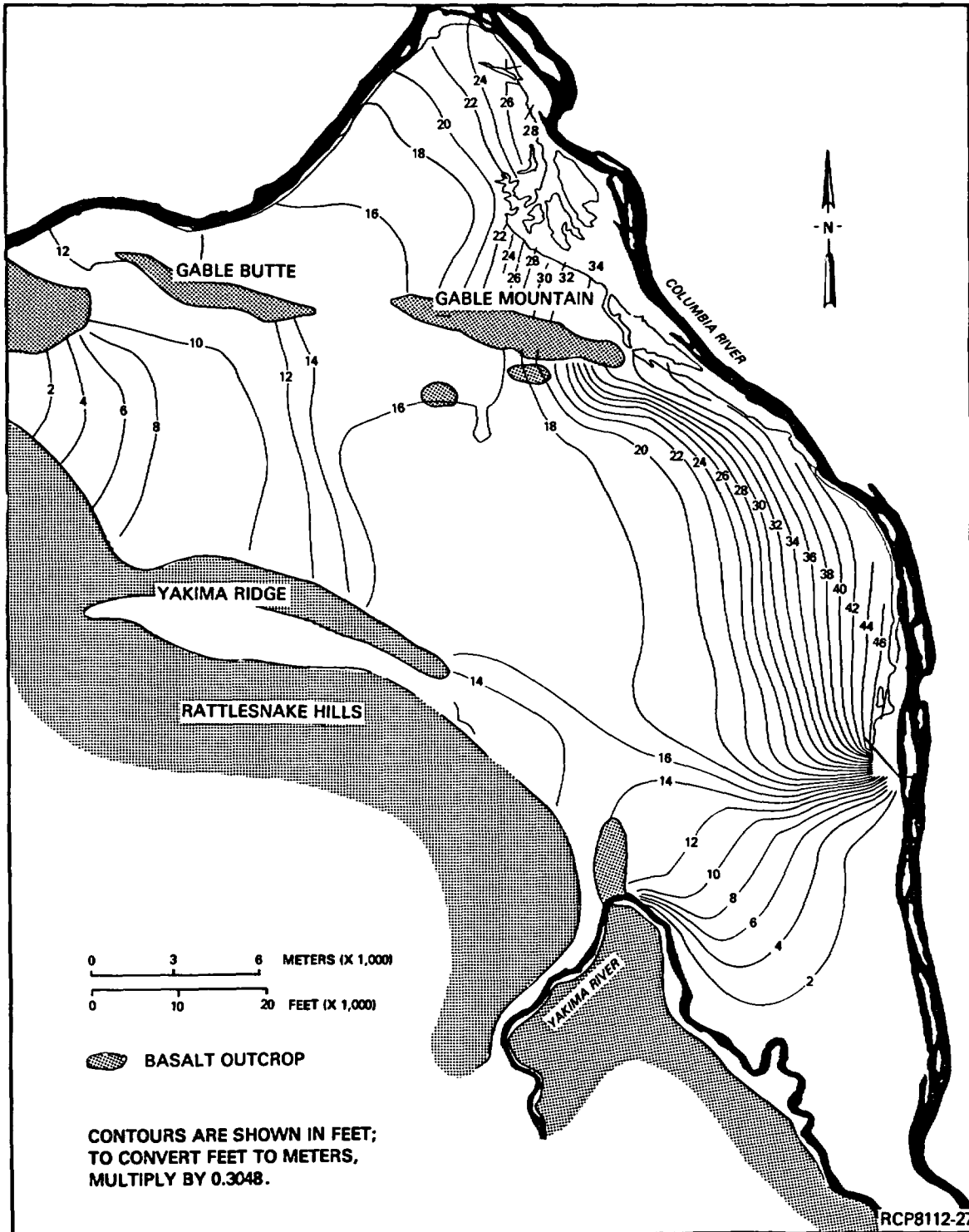


FIGURE 7-17. Predicted Water-Table Rise for Ben Franklin Dam with 122-Meter (400-Foot) Pool (after Harty, 1979).

7.2 FLOODS

Several documents contribute to the understanding and evaluation of flooding within the reference repository location and the Pasco Basin, primarily the COE (1951) report on artificial flooding along the Columbia River, based on failure scenarios of Grand Coulee Dam. Other key reports which focus specifically on the Pasco Basin and/or Hanford Site include ERDA (1976), FEMA (1980), and WPPSS (1981). Cummins et al. (1975) summarized a methodology for determining flooding characteristics of small watersheds, such as the Cold Creek area in eastern Washington. Reports dealing specifically with the probable impacts of flooding upon the Basalt Waste Isolation Project and the reference repository location include Leonhart (1980). Other recent field investigations have been conducted by the Basalt Waste Isolation Project and its subcontractors. Discussions of the nature of catastrophic flooding associated with Pleistocene glaciation are provided in Chapters 3 and 8.

7.2.1 Flood History

7.2.1.1 Columbia River. Major floods on the Columbia River characteristically result from rapid melting of the winter snowpack over a wide area (e.g., as caused by chinook winds) in the spring, augmented by above-normal precipitation. The maximum historical flood on record occurred on June 7, 1894 and was generated by a combination of hydrometeorologic conditions similar to those described above. The peak discharge during the flood at the Hanford reach was 20,950 cubic meters (740,000 cubic feet) per second as estimated from the high-water mark at Wenatchee, Washington. The largest recent flood occurred in 1948 with an observed peak discharge of 19,540 cubic meters (690,000 cubic feet) per second at Hanford. The probability of flooding of the magnitude of the 1894 and 1948 floods has been greatly lowered due to upstream regulation at Priest Rapids Dam. Actual river flows currently range between 1,020 and 4,530 cubic meters (36,000 and 160,000 cubic feet) per second, whereas unregulated flows (prior to Priest Rapids Dam construction) ranged between 1,980 and 10,760 cubic meters (70,000 and 380,000 cubic feet) per second (WPPSS, 1981).

The 1894 flood inundated areas below 122 meters (400 feet) above mean sea level. The floodplain associated with this flood is shown in Figure 7-18. A flood of this magnitude would inundate the 100 F Area and sections of Richland but would have no consequence on the reference repository location. The major four-lane highway on the project would be flooded near the old Hanford townsite. However, access to the reference repository location would be unaffected. The present regulated maximum flow of 4,530 cubic meters (160,000 cubic feet) per second has no effect on any facilities on the Hanford Site.

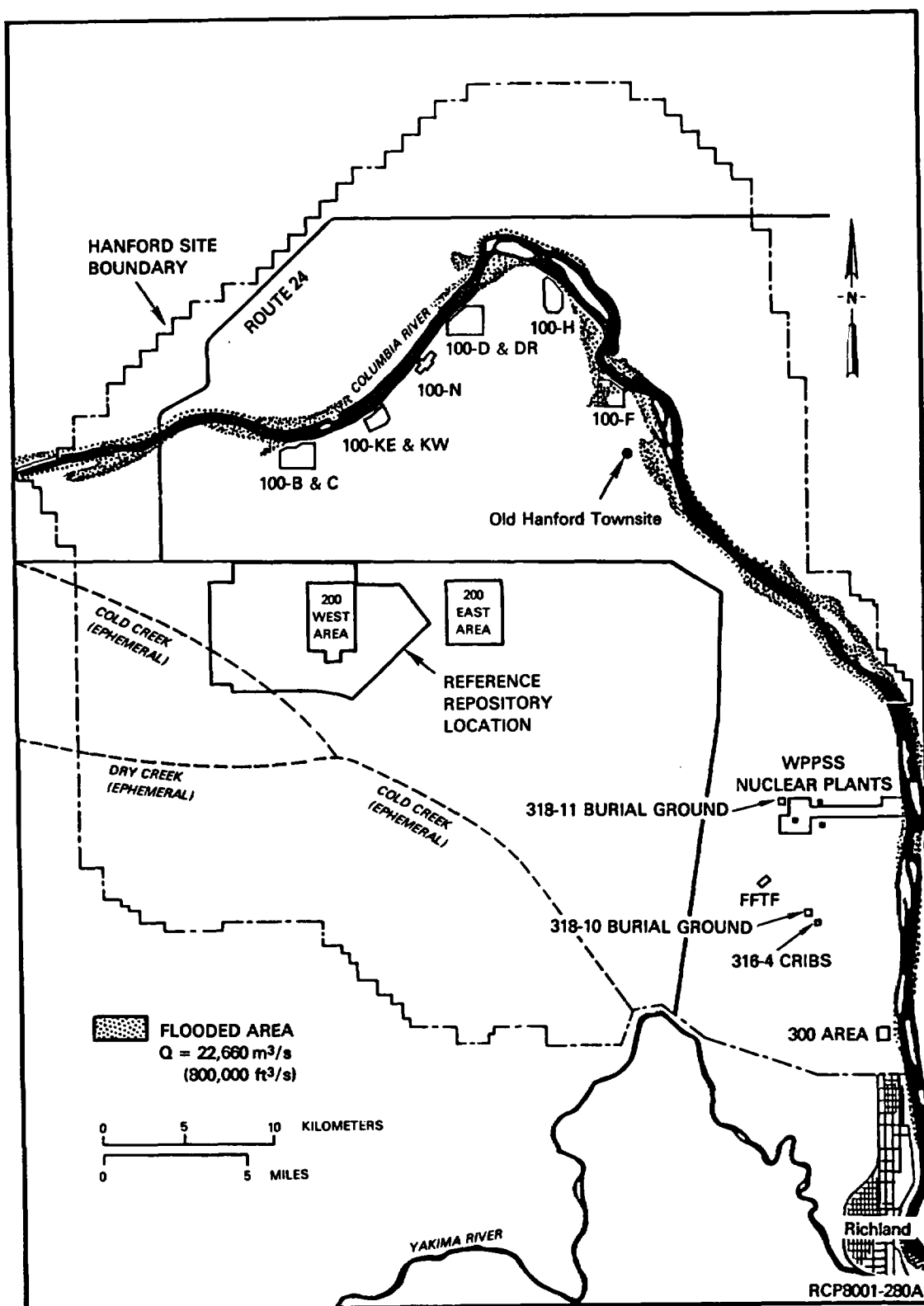


FIGURE 7-18. Flooded Area During the 1894 Flood (after ERDA, 1976).

7.2.1.2 Yakima River. Yakima River floods occur as a result of the same hydrometeorological events which induce Columbia River flood flows. In addition to spring snowmelt and warm rains, ice and debris jams contribute to flooding on the Yakima River. Since 1862, there have been 16 major floods on the Yakima River. The most severe occurred in November 1906, December 1933, and May 1948. The discharge magnitudes of these three floods were 1,870, 1,900, and 1,050 cubic meters (66,000, 67,000, and 37,000 cubic feet) per second, respectively (WPPSS, 1981). The recurrence intervals for the 1933 and 1948 floods are estimated at 170 and 33 years, respectively. The most recent flood occurred in December 1977 with a peak discharge of 820 cubic meters (29,000 cubic feet) per second, corresponding to a recurrence interval of 14 years (FEMA, 1980).

A comparison of flood magnitudes cannot be made on discharge volume alone because the progressive development of six irrigation storage projects has changed the natural flow regime of the Yakima River. The 1906 flood discharge represents natural flow conditions, whereas the 1933 and subsequent discharges were modified by the present system of reservoirs.

Irrigation reservoir development has reduced the flood potential of the Yakima River considerably. For example, the December 1933 flood was reduced from 2,350 to 1,530 cubic meters (83,000 to 54,000 cubic feet) per second (at Yakima) by management of upstream reservoir storage facilities. A December 1959 flood which, if uncontrolled, could have reached a magnitude of 1,560 cubic meters (55,000 cubic feet) per second (at Yakima) was held at 780 cubic meters (27,400 cubic feet) per second by the reservoir system.

Flood susceptible areas resulting from a 100-year flood on the Yakima River are shown in Figure 7-19. Flooded areas in the Horn Rapids area could potentially influence the southern section of the Hanford Site; however, they would not affect the reference repository location. The Yakima River above Horn Rapids is physically separated from the Hanford Site by the Rattlesnake Ridge. This topographic barrier prevents potential flooding on the Yakima River from affecting the reference repository location.

7.2.2 Flood Potential

Associated with evaluating maximum flooding is the concept of the probable maximum flood, which is determined from the upper limit of precipitation falling on a drainage area and other hydrologic factors (such as antecedent moisture conditions, snowmelt, and tributary conditions) that result in maximum runoff. The probable maximum flood for the Columbia River below Priest Rapids Dam has been calculated to be 39,650 cubic meters (1,400,000 cubic feet) per second (COE, 1951; 1969). The floodplain associated with the probable maximum flood is shown in Figure 7-20. The probable maximum flood would inundate the 100 Areas, but the central portion of the Hanford Site would remain unaffected.

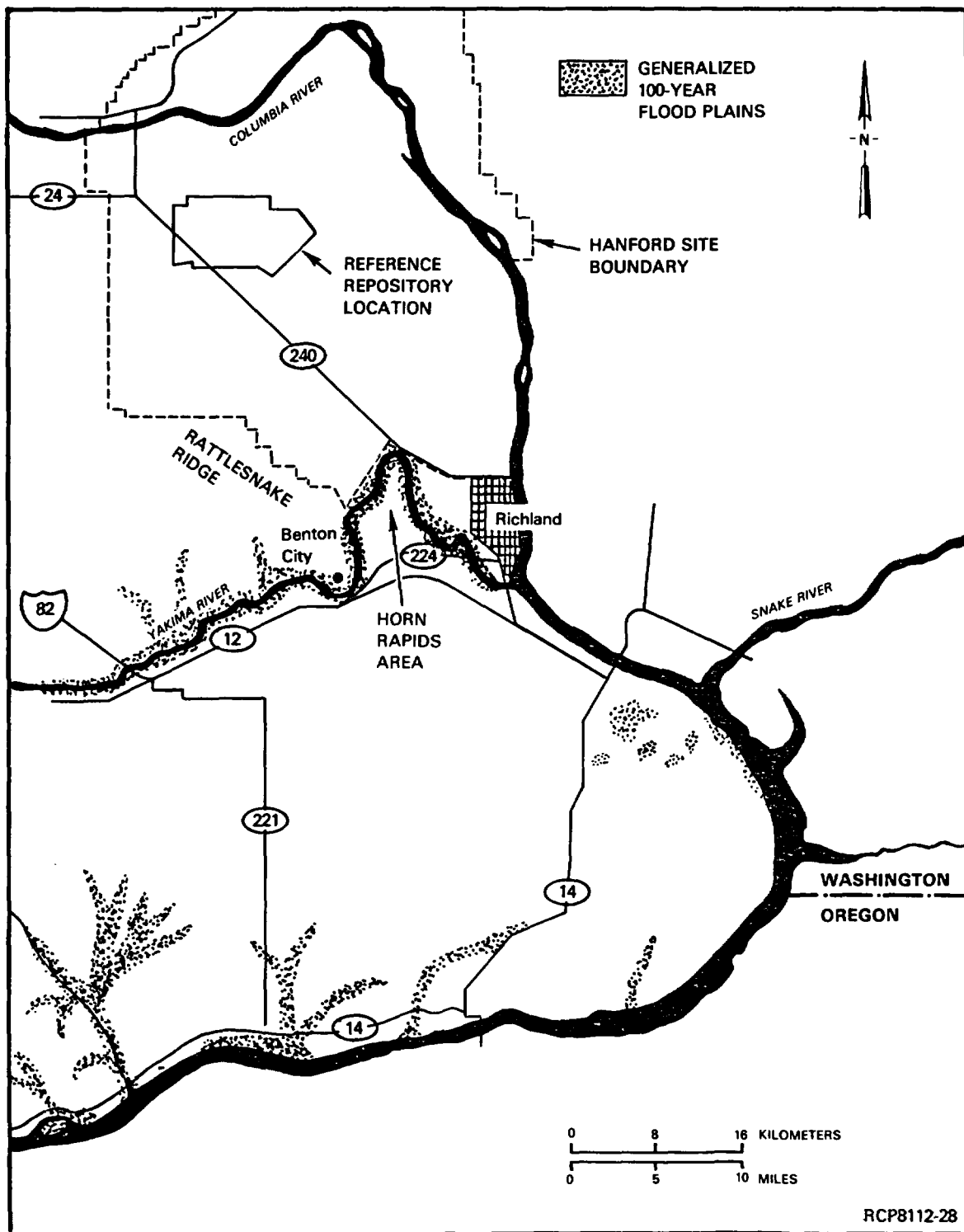


FIGURE 7-19. Flooded Area from a 100-Year Flood of the Yakima River in the Vicinity of the Hanford Site (FEMA, 1980).

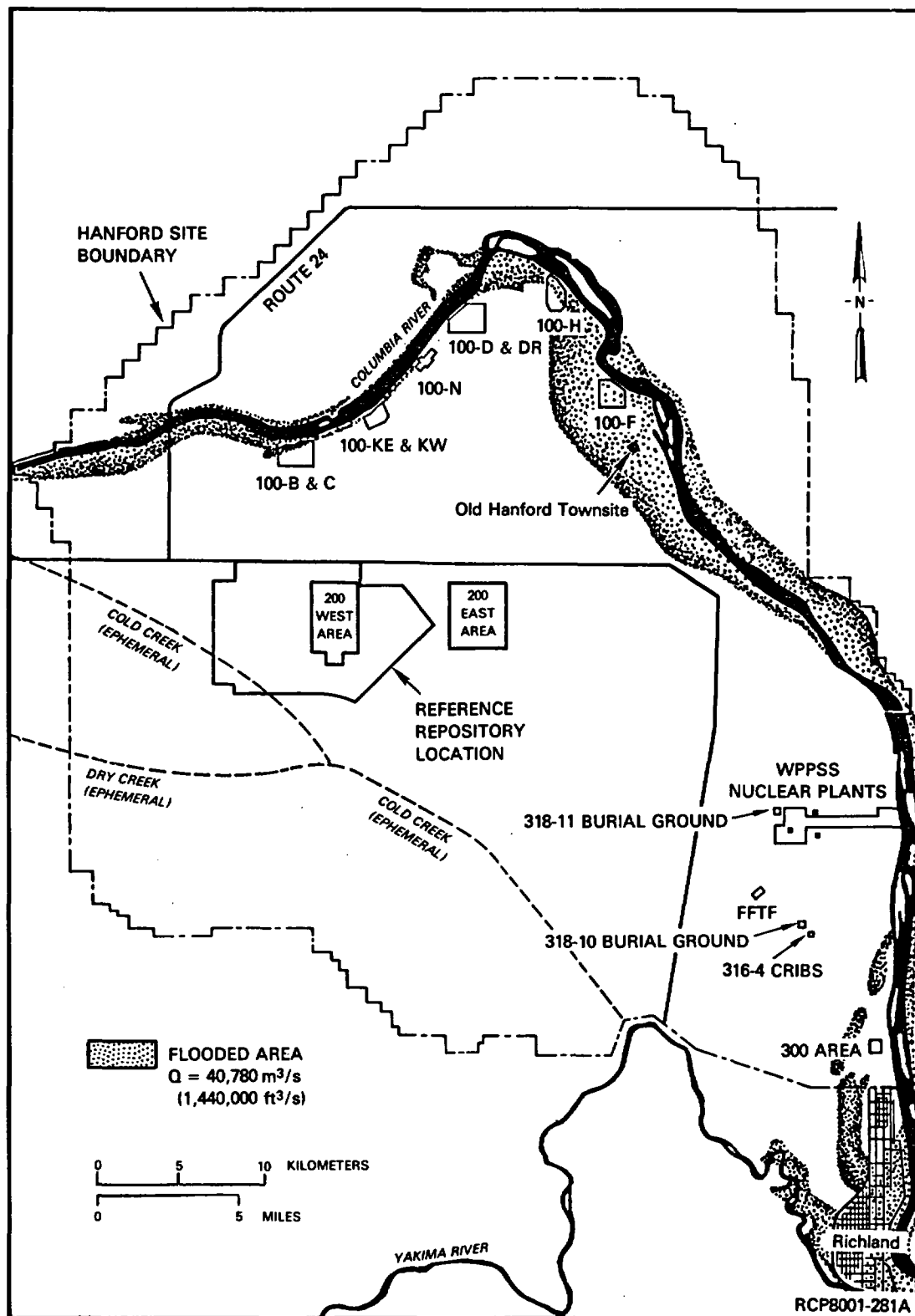


FIGURE 7-20. Flooded Area for the Probable Maximum Flood (after ERDA, 1976).

Potential dam failures on the Columbia River have been extensively evaluated in conjunction with siting a nuclear repository on the Hanford Site. Upstream dam failures may arise from a number of causes; however, the magnitude of the resulting flood depends upon the degree of the breach. The U.S. Army Corps of Engineers (COE, 1951) evaluated a number of scenarios on the effects of failures at Grand Coulee Dam, assuming flow conditions on the order of 11,330 cubic meters (400,000 cubic feet) per second. The resulting discharge at the outfall of the dam was determined to be 595,000 cubic meters (21,000,000 cubic feet) per second. Near N Reactor, this flow would diminish to 227,000 cubic meters (8,000,000 cubic feet) per second, accounting for flow augmentation due to failure of earth portions of downstream dams and the release of their respective storages. The resulting inundations from the 50 percent breach scenario are depicted in Figure 7-21. In addition to the areas inundated by the probable maximum flood, the remainder of the 100 Areas, nearly all of Richland, the 300 Areas, and the Washington Public Power Supply System, Inc. nuclear plants would also be flooded. Although the central portion of the Hanford Site largely remains unaffected, a small arm of flood water inundating the lowlands between Gable Butte and Gable Mountain would affect the highway to the southside of these mountains. No determinations have been made to this point with respect to breaches greater than 50 percent at Grand Coulee Dam or to failures of dams upstream of Grand Coulee Dam and associated resonant failures of dams downstream.

A third catastrophic event which could result in flooding portions of the Hanford Site is river blockage and flooding due to landslides along the Columbia River. One slide area extends along a 75-meter (250-foot) bluff from river kilometer 605 (river mile 376) downstream to river kilometer 571 (river mile 355). This area, commonly referred to as White Bluffs, has recently been undermined by irrigation water and waste ponds near its face. Instability problems have resulted, caused by loss of shear strength in the bluffs due to the addition of water. Calculations indicate that a 0.8-million-cubic-meter (1-million-cubic-yard) landslide concurrent with a flood flow of 17,000 cubic meters (600,000 cubic feet) per second (200-year flood) would result in a flood wave crest elevation of 122 meters (400 feet) above mean sea level (Harty, 1979). In both cases the repository site would be unaffected, although the main roadway from Richland would be inundated in the vicinity of the old Hanford townsite. Areas inundated from such a landslide event would be similar to those shown in Figure 7-20.

7.2.2.1 Cold Creek Watershed/Reference Repository Location Drainage Conditions. The Cold Creek watershed is located along the western boundary of the Pasco Basin along the northwest/southeast orientation. As shown in Figure 7-22, the basin is bordered on the west by the Rattlesnake Hills and Yakima Ridge, on the north side by Umtanum Ridge, and on the east by the central portion of the Hanford Site. The rectangular-shaped, 870-square-kilometer (336-square mile) watershed drains into the Yakima River at about 1.6 kilometers (1 mile) upstream of Horn Rapids Dam. Elevations in the Cold Creek watershed range from about 128 meters (420 feet) above mean sea level at its outlet to over 1,100 meters (3,500 feet) above mean sea level at its headwaters along Yakima Ridge.

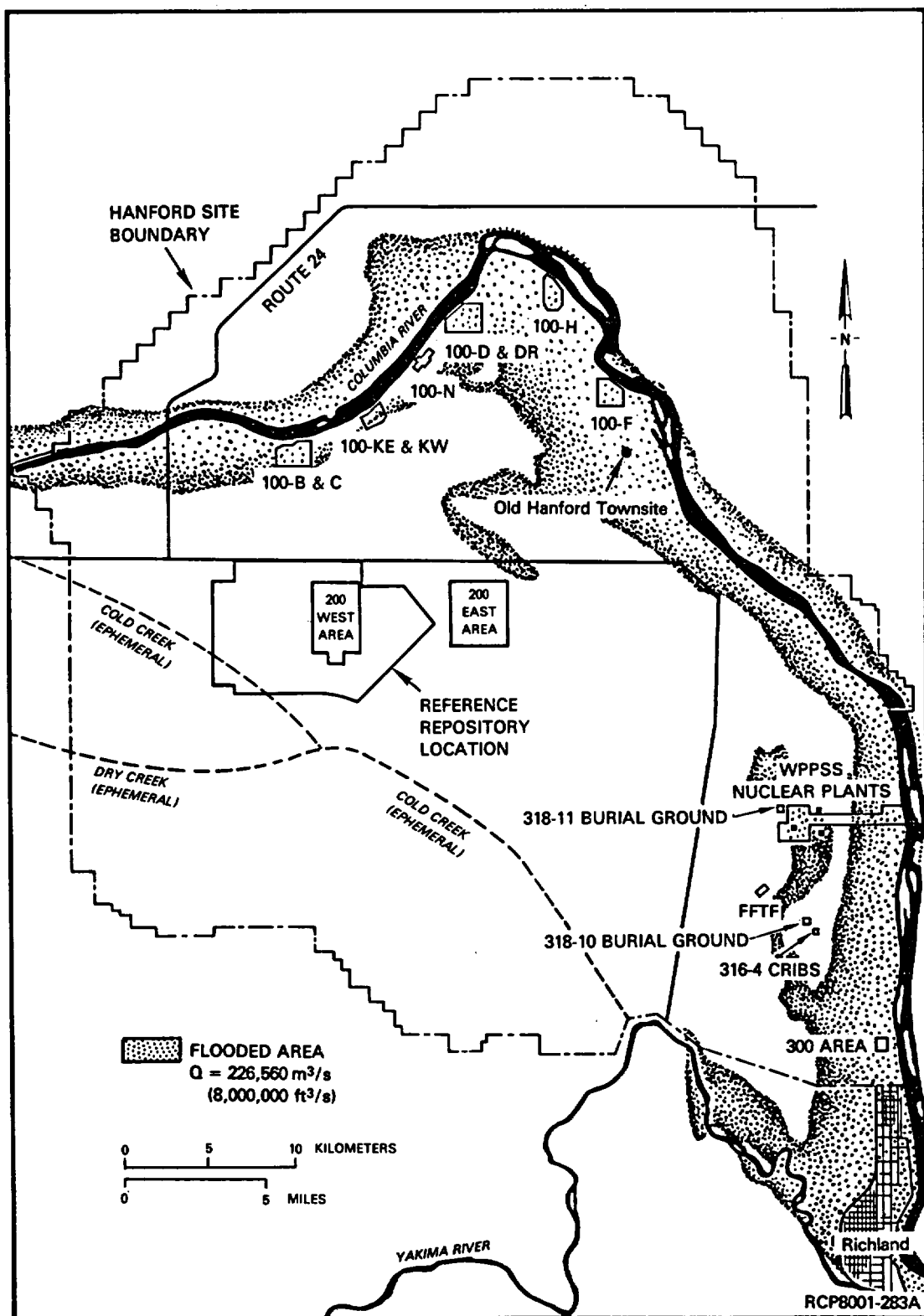


FIGURE 7-21. Flooded Area Resulting from a 50-Percent Breach of Grand Coulee Dam (after ERDA, 1976).

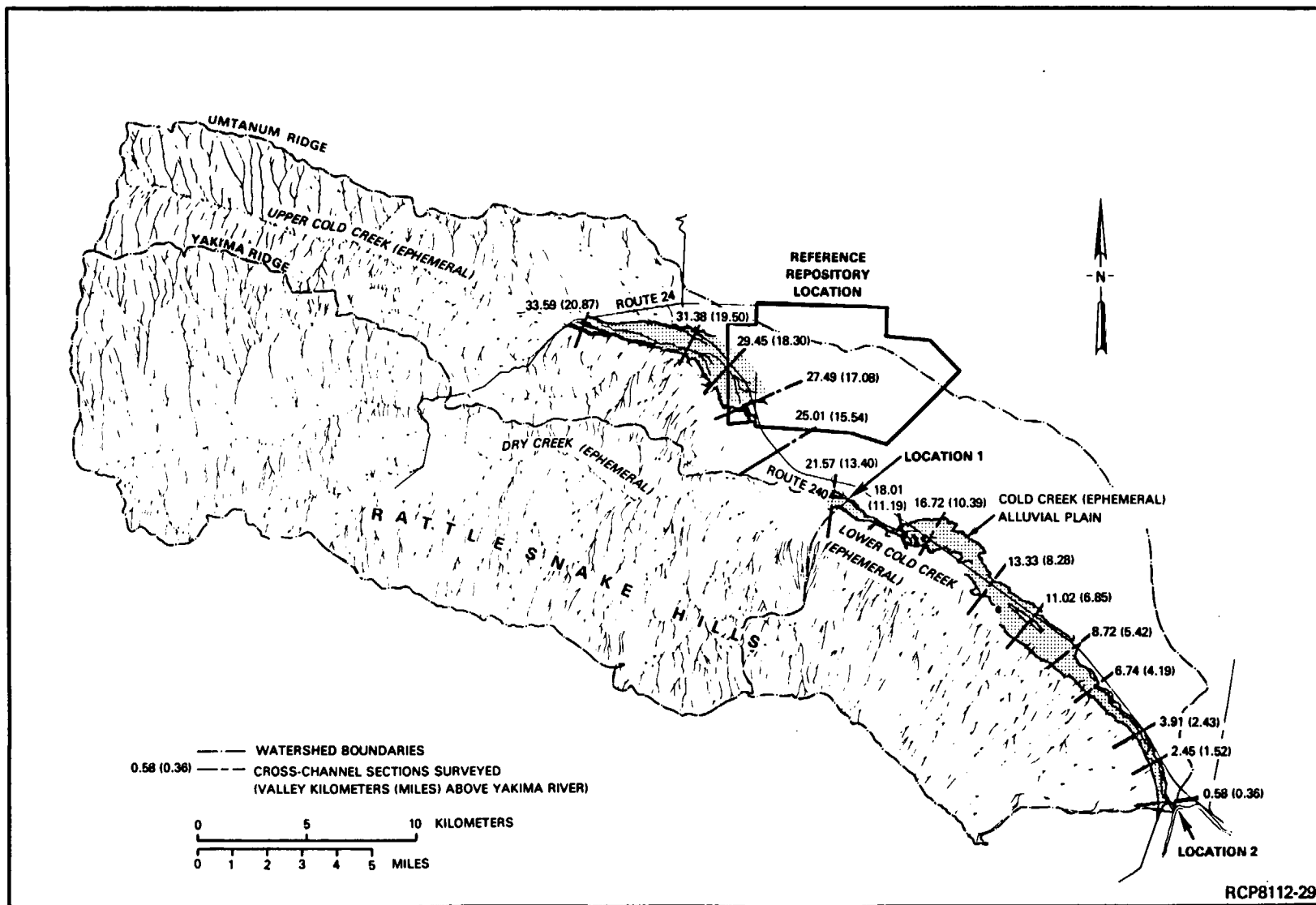


FIGURE 7-22. Drainage Area Map of the Cold Creek Watershed.

The reference repository location lies primarily within the Cold Creek watershed. Elevations across the reference repository location range from about 189 meters (620 feet) above mean sea level in the southwestern corner to over 244 meters (800 feet) above mean sea level in the northwestern portion. Cold Creek, trending northwest-southeast within the southwestern portion of the wash, is the only defined channel within the southeastern portion of the watershed (see Fig. 7-22).

The drainage system within the Cold Creek watershed may be described as ephemeral and discontinuous. This means that the stream flows only in direct response to precipitation events (i.e., it receives no contribution from discharging groundwater or sustained snowmelt runoff). Further, for most runoff events, the water within the channel infiltrates within a given distance of flow. Skaggs and Walters (1981) suggest that the Cold Creek watershed behaves essentially as two distinct drainage systems for most runoff events. The source of the upper drainage system is the area bounded by Umtanum and Yakima Ridges, whereas the lower drainage system occurs just about at the confluence of Cold and Dry Creeks.

The reference repository location is within the lowermost portion of the upper drainage system along a channel segment described by Skaggs and Walters (1981) as resembling the distributary channels that spread out in a fan-shaped network, eventually becoming discontinuous.

As part of their study, Skaggs and Walters (1981) performed cross-channel surveys of Cold Creek. The locations of these surveys are shown on Figure 7-22. In general, they describe the bottom areas of the watershed as consisting of small, ephemeral, low-flow channels, 9 to 15 meters (30 to 50 feet) wide, superimposed on a wide, rectangular-shaped alluvial plan that varies between 225 and 3,660 meters (750 to 12,000 feet) wide.

The areal distribution of Cold Creek Holocene alluvium based on stratigraphic and geomorphic evidence is described in Chapter 3. However, based on currently available geologic field evidence, no firm conclusions can be drawn as to the magnitude or frequency of recent flooding events. It can, however, be said that there is no geologic evidence that would suggest that a continuous flow from headwaters to the Yakima River was ever sustained within Cold Creek during the Holocene.

7.2.2.2 Flood Potential Within the Reference Repository Location. Elevations within the reference repository location generally range between 190 and 230 meters (623 and 757 feet) (mean sea level). This topographic level effectively protects the reference repository location from all conceivable flood scenarios for the Columbia and Yakima Rivers, including both natural flooding and dam-breach or -failure scenarios.

On the other hand, there exists a potential for flash flooding of limited extent within the reference repository location. This phenomenon would primarily occur in "lowlands" along the drainage channel of Cold Creek. While the regulatory criteria do not specifically require analysis of flash flooding, it is possible to analyze the consequences of these events in a similar manner as used for analysis of flooding from large rivers. The glossary in 10 CFR 60 (NRC, 1981) defines a floodplain as, essentially, the area adjacent to a watercourse having a 1 percent or greater chance of being flooded in any given year (i.e., a 100-year return period). For an ephemeral stream such as Cold Creek, a corresponding event would probably be associated with an intense rainfall runoff event.

The analysis required to assess flash flooding potential in the Cold Creek syncline, however, will require detailed resolution of topographic relief within the area to determine whether mitigation measures are appropriate. This work is discussed further in Chapter 13.

7.3 SURFACE WATER USE AND DEMAND FOR WATER WITHIN THE PASCO BASIN

7.3.1 Surface Water Use

Water use within Benton and Franklin Counties may be considered to approximate the total user composition and demand within the Pasco Basin. The one notable exception may be irrigation water use within the Wahluke Slope area, north of the Columbia River and just northwest of the Hanford Site. The only quantitatively significant water use within the Wahluke Slope area is agricultural irrigation. According to estimates from LANDSAT (Wukelic et al., 1981) and U-2 data, as well as survey statistics, approximately 12,000 hectares (30,000 acres) within this area are receiving irrigation. Water use may be approximated by assuming annual irrigation application on the order of 12,800 cubic meters per hectare (4.2 acre-feet per acre). The resulting annual estimate of water use would thus be about 1.51×10^8 cubic meters (40,000 million gallons). Annual water use within Benton and Franklin Counties totals nearly one-fourth of the total demand within the state of Washington, according to 1975 water use statistics (Dion and Lum, 1977). This equals a volume of over 2.3×10^9 cubic meters (600,000 million gallons or about 1.9 million acre-feet). The more significant portions of water demand occur within the industrial and agricultural sectors, which represent 22 and 76 percent, respectively, of the basin water demand. Municipal water use within Benton and Franklin Counties represents less than 2 percent of the total water use within the Pasco Basin.

Primarily, water is supplied from surface water sources. Groundwater withdrawals comprise less than 10 percent of the total Benton and Franklin County demand. The distribution of Benton and Franklin County water demands, as a percentage of the state total, is provided in Table 7-3.

TABLE 7-3. Benton and Franklin Counties 1975 Water Use Totals and Composition (Dion and Lum, 1977).

Type of use	Groundwater (% of state total)	Surface water (% of state total)	Total (% of state total from both sources)
Municipal	3	9	6
Industrial	9	35	31
Irrigation	10	25	25
Total	4	26	24

7.3.2 Surface Water Demand

A preliminary report was prepared on water resource development and potential within the Pasco Basin (Bell and Leonhart, 1980). Later, an economic evaluation of the present and projected Pasco Basin water resource situation was completed (Leaming, 1981). The latter report issued projections to the year 2080. The projections were based largely on the reported 1975 water use statistics by Dion and Lum (1977) described earlier.

The tabular summaries of Leaming's evaluations are presented in Tables 7-4 through 7-9. Population projections (Table 7-4) are also shown because they are used as the basis for several of the projections. The methodologies used to arrive at the projection figures are described in footnotes. The totals of the individual projections for municipally supplied, industrial, and agricultural demands are given in Table 7-9. These projections are shown graphically on Figure 7-23. The figures show that by the year 2080 total annual demand for consumptive water uses at current real costs (i.e., present worth of future value) will increase between 36 and 265 percent over present demand. The "most likely" scenario shows that the increase will be on the order of about 83 percent. Leaming concludes that surface water availability exceeds by orders of magnitude this increased demand, assuming no extra-basin constraints are imposed.

7.3.3 Surface Water Intakes

Known diversions of Columbia River water for various municipal, industrial, and agricultural purposes within the Pasco Basin are shown on Figure 7-24. A listing of the locations and types of these withdrawals is provided in Table 7-10. Water quality of these waters is characterized within Section 7.4.

TABLE 7-4. Projected Population of the Pasco Basin,^a 1980-2080 (Leaming, 1981).

Year	Low ^b	Most likely ^c	High ^d
1950	--	64,933	--
1960	--	85,412	--
1970	--	93,356	--
1980	--	144,469	--
1990	158,700	166,800	195,600
2000	183,300	196,300	246,700
2010	208,000	225,900	297,800
2020	232,600	255,400	348,900
2030	257,300	284,900	400,000
2040	282,000	314,400	451,100
2050	306,600	344,000	502,300
2060	331,300	373,500	553,400
2070	355,900	403,000	578,000
2080	380,600	432,600	629,100

^aThe Pasco Basin population is defined here as equivalent to the population of the Richland-Pasco-Kennewick Metropolitan Area (i.e., Benton and Franklin Counties, Washington).

^bThe low projections assume a continuation of the average growth rate achieved from 1950 to 1980; that is, 24,655 per decade with a linear regression trend value of 35,404 at 1940.

^cThe most likely projection assumes a continuation of the average growth rate achieved from 1960 to 1980; that is, 29,528 per decade with a linear regression trend value of 48,689 at 1950. Most likely amounts listed for 1950, 1960, 1970, and 1980 are actual census counts.

^dThe high projections assume a continuation of the average growth rate achieved from 1970 to 1980 (an increase of 51,113 persons per decade), with a linear trend value of 42,243 at 1960.

TABLE 7-5. Projected Water Demand from Households, Governments, and Nonagricultural, Nonindustrial Business in the Pasco Basin,^a 1980-2080^b (after Leaming, 1981).

Year	Annual water demand at current real costs					
	Low ^c		Most likely ^d		High ^e	
	(m ³ E+06/yr)	(acre-ft/yr)	(m ³ E+06/yr)	(acre-ft/yr)	(m ³ E+06/yr)	(acre-ft/yr)
1980	--	--	58	47,100	--	--
1990	64	51,700	67	54,400	79	63,800
2000	74	59,800	79	64,000	99	80,400
2010	84	67,800	91	73,600	120	97,100
2020	93	75,800	103	83,300	140	113,700
2030	103	83,900	115	92,900	161	130,400
2040	113	91,900	126	102,500	181	147,100
2050	123	100,000	138	112,100	202	163,700
2060	133	108,000	150	121,800	223	180,400
2070	143	116,000	162	131,400	232	188,400
2080	153	124,100	174	141,000	253	205,100

^aThe Pasco Basin is defined here as equivalent to the Richland-Pasco-Kennewick Metropolitan Area (i.e., Benton and Franklin Counties, Washington).

^bIt is assumed that the "real cost" of water will remain constant over this period.

^cThe low projections are based on an average water use of 1,100 liters (291 gallons) per person per day or 398 cubic meters (0.326 acre-feet) per person per year as reported by Dion and Lum (1977) and the "low" population projections shown in Table 7-7.

^dThe most likely projections are based on an average water use of 1,100 liters (291 gallons) per person per day or 398 cubic meters (0.326 acre-feet) per person per year as reported by Dion and Lum (1977) and the "most likely" population projections shown in Table 7-7.

^eThe high projections are based on an average water use of 1,100 liters (291 gallons) per person per day or 398 cubic meters (0.326 acre-feet) per person per year as reported by Dion and Lum (1977) and the "high" population projections shown in Table 7-7.

TABLE 7-6. Projected Industrial Employment in the Pasco Basin,^a 1980-2080 (Leaming, 1981).

Year	Average annual employment in mining, manufacturing, and public utilities		
	Low ^b	Most likely ^c	High ^d
1950		7,700	--
1960	--	6,400	--
1970	--	6,900	--
1980	--	11,700	--
1990	13,000	13,500	16,500
2000	14,400	15,900	21,300
2010	15,700	18,300	26,100
2020	17,000	20,700	30,900
2030	18,400	23,100	35,700
2040	19,700	25,500	40,500
2050	21,000	27,900	45,300
2060	22,400	30,200	50,100
2070	23,700	32,600	54,900
2080	25,000	35,000	59,700

^aThe Pasco Basin is defined here as equivalent to the Richland-Pasco-Kennewick Metropolitan Area (i.e., Benton and Franklin Counties, Washington).

^bThe low projections assume a continuation of the average rate of growth in industrial employment achieved from 1950 to 1980.

^cThe most likely projections assume that industrial employment will remain a relatively consistent proportion of the area's total work force and will average approximately 8 percent of the area's projected population. Most likely amounts listed for 1950, 1960, 1970, and 1980 are actual reported averages.

^dThe high projections assume a continuation of the average rate of growth in industrial employment achieved in the area from 1970 to 1980.

TABLE 7-7. Projected Industrial Water Demand in the Pasco Basin,^a
1980-2080^b (after Leaming, 1981).

Year	Annual industrial water demand at current real costs ^c					
	Low ^d		Most likely ^e		High ^f	
	(m ³ E+06/yr)	(acre-ft/yr)	(m ³ E+06/yr)	(acre-ft/yr)	(m ³ E+06/yr)	(acre-ft/yr)
1980	--	--	690	559,000	--	--
1990	766	621,100	796	645,000	972	788,300
2000	849	688,000	937	759,600	1,255	1,017,600
2010	925	750,100	1,078	874,300	1,538	1,247,000
2020	1,002	812,200	1,220	989,000	1,821	1,476,300
2030	1,084	879,100	1,361	1,103,600	2,104	1,705,600
2040	1,161	941,200	1,503	1,218,300	2,386	1,934,900
2050	1,238	1,003,300	1,644	1,333,000	2,670	2,164,300
2060	1,320	1,070,200	1,780	1,442,800	2,952	2,393,600
2070	1,397	1,132,300	1,921	1,557,500	3,235	2,622,900
2080	1,473	1,194,400	2,063	1,672,200	3,518	2,852,200

^aThe Pasco Basin is defined here as equivalent to the Richland-Pasco-Kennewick Metropolitan Area (i.e., Benton and Franklin Counties, Washington).

^bIt is assumed that the "real cost" of water will remain constant over this period.

^cIndustrial water is defined as water used for mining operations, industrial minerals processing, all manufacturing, and all transportation and public utilities operations exclusive of water used as a transport medium. It includes water used in food processing, paper and paper product manufacturing, chemical processing, and as a coolant in electrical power generation. It does not include falling water used directly in hydroelectric power generation.

^dThe low projections are based on an average industrial water use of 5.89 E+04 cubic meters (47.776 acre-feet) per year per employee and the low employment projections shown in Table 7-11.

^eThe most likely projections are based on an average industrial water use of 5.89 E+04 cubic meters (47.776 acre-feet) per year per employee (as derived from Dion and Lum, 1977) and the most-likely industrial employment projections shown in Table 7-9.

^fThe high projections are based on an average industrial water use of 5.89 E+04 cubic meters (47.776 acre-feet) per employee per year (as derived from Dion and Lum, 1977) and the high industrial employment projections shown in Table 7-9.

TABLE 7-8. Projected Agricultural Water Demand in the Pasco Basin,^a
1980-2080^b (after Leaming, 1981).

Year	Annual agricultural water demand for irrigation at current real costs					
	Low ^c		Most likely ^d		High ^e	
	(m ³ E+06/yr)	(acre-ft/yr)	(m ³ E+06/yr)	(acre-ft/yr)	(m ³ E+06/yr)	(acre-ft/yr)
1980	--	--	1,702	1,380,200	--	--
1990	1,702	1,380,200	1,883	1,526,400	2,049	1,660,800
2000	"	"	2,063	1,672,600	2,395	1,941,400
2010	"	"	2,243	1,818,800	2,741	2,222,000
2020	"	"	"	"	3,087	2,502,600
2030	"	"	"	"	3,433	2,783,100
2040	"	"	"	"	3,779	3,063,700
2050	"	"	"	"	4,125	3,344,300
2060	"	"	"	"	4,471	3,624,900
2070	"	"	"	"	4,817	3,905,500
2080	"	"	"	"	5,163	4,186,100

^aThe Pasco Basin is defined here as equivalent to Benton and Franklin Counties, Washington.

^bIt is assumed that the "real cost" of water will remain constant over this period.

^cThe low estimates are based on an average irrigation water use of 12,800 cubic meters per hectare (4.2 acre-feet per acre) per year (as reported by the Washington State Cooperative Extension Service for minimal water-using crops) and no net change in the amount of land presently under irrigation in the area.

^dThe most likely estimates are based on an average irrigation water use of 13,100 cubic meters per hectare (4.3 acre-feet per acre) per year (as reported by the Washington State Cooperative Extension Service for an average mix of low and high water-using crops) and an increase in the amount of land being irrigated at an average rate of 1,375 hectares (3,400 acres) per year until 2010, after which the amount of land being irrigated would remain constant.

^eThe high estimates are based on an average irrigation water use of 13,700 cubic meters per hectare (4.5 acre-feet per acre) per year (as reported by the Washington State Cooperative Extension Service for high water-using crops) and an average increase in the amount of land being irrigated of 2,510 hectares (6,200 acres) per year until 2080 when all of the land presently in crops in the area would be under irrigation.

TABLE 7-9. Projected Total Water Demand in the Pasco Basin,^a
1980-2080^b (after Leaming, 1981).

Year	Total annual demand for consumptive water uses at current real costs					
	Low ^c		Most likely ^d		High ^e	
	(m ³ E+06/yr)	(acre-ft/yr)	(m ³ E+06/yr)	(acre-ft/yr)	(m ³ E+06/yr)	(acre-ft/yr)
1980	--	--	2,450	1,986,300	--	--
1990	2,532	2,053,000	2,745	2,225,800	3,100	2,512,900
2000	2,625	2,128,000	3,079	2,496,200	3,749	3,039,400
2010	2,711	2,198,100	3,413	2,766,700	4,399	3,566,100
2020	2,798	2,268,200	3,566	2,891,100	5,048	4,092,600
2030	2,890	2,343,200	3,719	3,015,300	5,698	4,619,100
2040	2,977	2,413,300	3,873	3,139,600	6,347	5,145,700
2050	3,063	2,483,500	4,026	3,263,900	6,997	5,672,300
2060	3,156	2,558,400	4,173	3,383,400	7,646	6,198,900
2070	3,242	2,628,500	4,327	3,507,700	8,285	6,716,800
2080	3,329	2,698,700	4,480	3,632,000	8,934	7,243,400

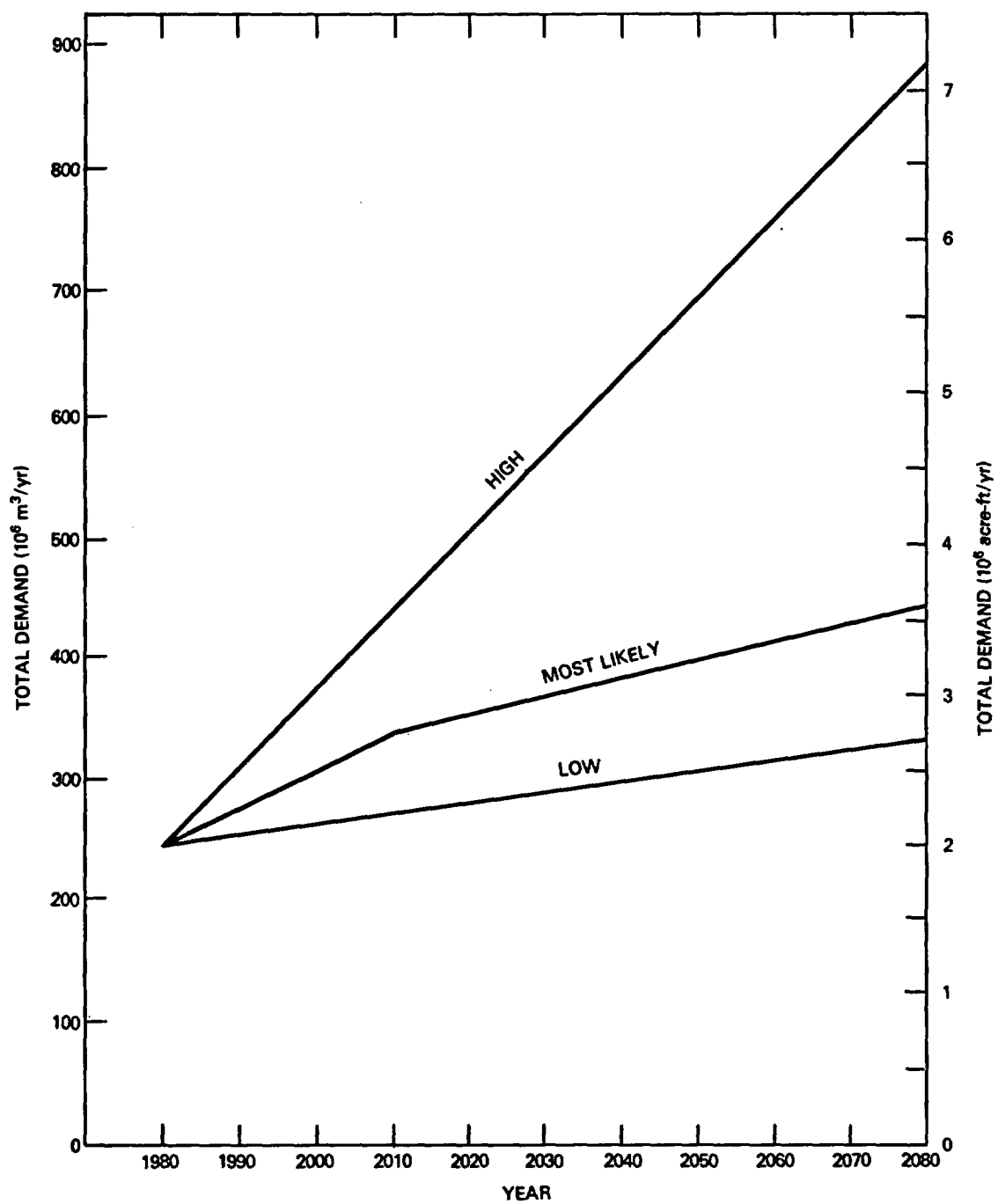
^aThe Pasco Basin is defined here as equivalent to the Richland-Pasco-Kennewick Metropolitan Area (i.e., Benton and Franklin Counties, Washington).

^bIt is assumed that the "real cost" of water will remain constant over this period.

^cThe low projections are the sum of the low estimates for agricultural, industrial, household, government, and all other consumptive-business water uses as presented in Tables 7-8, 7-10, and 7-11.

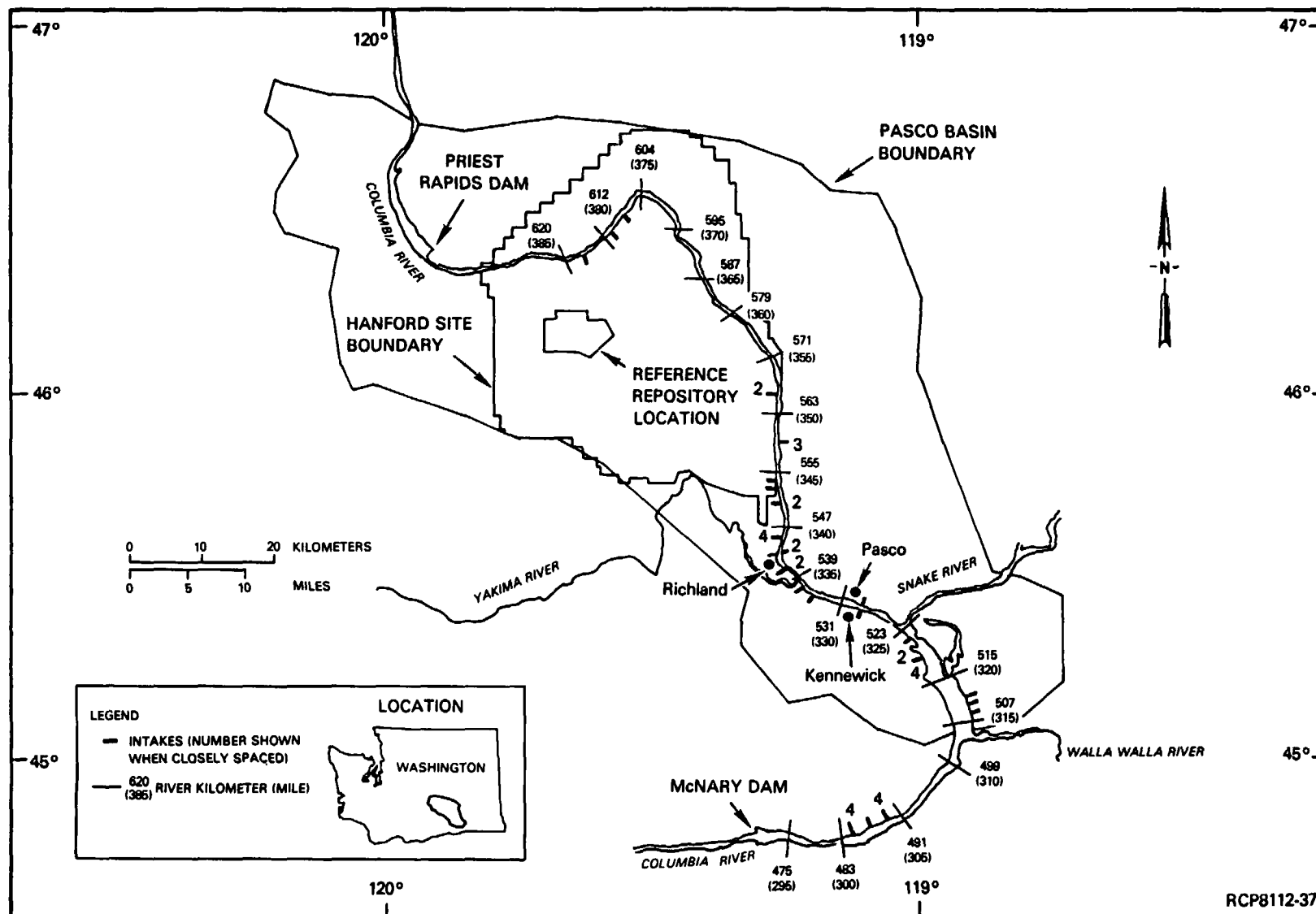
^dThe most likely estimates are the sums of the individual most likely projections for household, government, agricultural, industrial, and all other consumptive-business water uses as presented in Tables 7-8, 7-10, and 7-11.

^eThe high estimates are the sums of the individual projections for consumptive water use by households, governments, agriculture, industry, and all other business as presented in Tables 7-8, 7-10, and 7-11.



RCP8112-36

FIGURE 7-23. Projected Demand for Water in the Pasco Basin.



RCP8112-37

FIGURE 7-24. Surface Water Intakes in the Pasco Basin.

TABLE 7-10. Summary of Downstream Surface Water Uses For the
Columbia River. (Sheet 1 of 2)

User ^a	Location of intake		Bank	Annual quantity withdrawn		Type of use ^b	Population served (if municipal)
	River km	River mi		m ³ E+06	acre-ft		
Hanford (200 E & W)	620	385	Right	c	c	N	--
Hanford (100-K)	615	382	Right	2.54	2,056	N	--
Hanford (100-N)	610	379	Right	568	460,405	N	--
Hanford (200 E & W)	607	377	Right	c	c	N	--
WPPSS	565	351	Right	80.4	65,160	N	--
Peter Kiewit Sons' Co.	565	351	Right	0.89	724	N	--
L. L Bailey	558	347	Left	1.84	1,448	I	--
H. D. Loyd	558	347	Left	0.88	717	I	--
Central Premix Cement	558	347	Left	1.79	1,448	N	--
Hanford (300)	554	344	Right	2.33	1,888	N	--
Battelle Memorial Inst.	552	343	Right	3.93	3,186	I	--
Univ. of Washington	550	342	Right	1.56	1,267	I	--
City of Richland	550	342	Right	0.60	485	M	d
City of Richland	546	339	Right	27.7	22,444	M	d
City of Richland	546	339	Right	20.8	16,833	M	d
City of Richland	546	339	Right	27.7	22,444	M	d
City of Richland	546	339	Right	83.1	67,332	M	d
E. C. Watts	544	338	Right	0.28	224	I	--
H. S. Petty	544	338	Right	0.43	348	I	--
N. H & M. E. Ketchersid	544	388	Left	1.48	1,202	I	--
G. C. Walkley	544	388	Left	2.07	1,680	I	--
R. T. Justesen	541	336	Right	2.27	1,839	I	--
Central Premix Concrete	541	336	Right	0.98	796	N	--
City of Richland	538	334	Right	1.79	1,448	I	--
Benton County	534	332	Right	0.89	724	I	--
City of Kennewick	528	328	Right	49.7	40,327	M	d
City of Pasco	528	328	Left	31.3	25,340	M	d
F. J. Henokel	521	324	Right	0.001	11	I	--
Allied Chemical	521	324	Right	3.17	2,570	N	--

TABLE 7-10. Summary of Downstream Surface Water Uses for the Columbia River. (Sheet 2 of 2)

User ^a	Location of intake		Bank	Annual quantity withdrawn		Type of use ^b	Population served (if municipal)
	River km	River mi		m ³ E+06	acre-ft		
Chevron Chemical	520	323	Right	3.37	2,729	N	--
Chevron Chemical	520	323	Right	35.7	28,960	N	--
Philips Pac. Chemical	520	323	Right	73.2	59,368	N	--
Philips Pac. Chemical	520	323	Right	17.9	14,480	N	--
Boise Cascade Corp.	512	318	Left	21.9	17,738	N	--
L. D. Hoyte	510	317	Left	161	130,175	I	--
D. Howe	509	316	Left	5.72	4,634	I	--
Crawford & Sons	489	304	Right	29.3	23,747	I	--
Barbarosa Farms	489	304	Right	17.9	14,480	I	--
Crawford & Sons	489	304	Right	6.79	5,502	I	--
Rainier Nat. Bank	489	304	Right	8.40	6,806	I	--
Anderson & Coffin	486	302	Right	216	175,208	I	--
Horse Heaven Farms	484	301	Right	73.2	59,368	I	--
Horse Heaven Farms	484	301	Right	491	398,200	I	--
Horse Heaven Farms	484	301	Right	259	209,960	I	--
Anderson & Coffin	484	301	Right	216	175,208	I	--
				Total =	2,554.8		

^aTaken from WPPSS (1981) and ERDA (1975).

^bI = irrigation

M = municipal use

N = industrial use.

^cAnnual water use for Hanford 200 East and 200 West operations withdrawn at river kilometer 620 (river mile 385) and river kilometer 607 (river mile 377) reported as a total figure of 22.4 million m³ (18,166 acre-ft).

^dMunicipal populations served by Richland, Kennewick, and Pasco water supply systems are approximately 34,250, 33,200, and 17,300, respectively.

7.4 SURFACE WATER QUALITY

7.4.1 Pasco Basin

Surface water dynamics of the Columbia River within the Pasco Basin are influenced primarily by the following factors:

- The quality of influent Columbia River waters entering through Sentinel Gap (at the head of the basin)
- The quality of influent tributaries (i.e., Yakima, Snake, and Walla Walla Rivers)
- Discharges associated with Hanford Site operations
- Other industrial discharges
- Municipal discharges
- Agricultural effluents (including return flows, runoff, and seeps)
- Groundwater discharge.

The order of the above list does not imply relative importance.

The relative importance of each of the Columbia River tributaries in influencing the quality of the Columbia River as it flows through the Pasco Basin is partially established by the discharge magnitudes of the tributaries. These discharges are compared on a percentage basis in Table 7-11. The streamflow statistics shown are those for the 1979 water year, which was selected as representative of recent climatic and operational conditions within the system. A small percentage of the annual flow is unaccounted for. This discrepancy is probably attributable to cumulative error due to unmeasured gains or losses (e.g., net groundwater/surface water exchange) and various measurement errors.

7.4.2 Water Quality

The Washington State Department of Ecology has issued a Class A ("excellent") quality designation for the Columbia River along the reach from Grand Coulee Dam through the Pasco Basin (i.e., to McNary Dam). This designation mandates that industrial uses of the river must be compatible with substantially all other uses including sanitary, recreation, and wildlife. A summary of the Class A standards is provided in Table 7-12.

TABLE 7-11. Comparative Contribution of Pasco Basin Surface Flow Inputs
Based on Water Year 1979 Discharge Statistics
(after WAC, 1978).

Station	River	River km	River mi	Flow		Basin outflow(%)
				(m ³ /s)	(ft ³ E+03)	
Priest Rapids Dam	Columbia	634.9	394.5	2,106	74,380	69.6
Kiona	Yakima	48.1	29.9	32	1,135	1.1
Ice Harbor Dam	Snake	15.6	9.7	871	30,770	28.8
Touchet	Walla Walla	29.3	18.2	11	392	0.4
McNary Dam	Columbia	469.9	292.0	3,021	106,677	--
			Total =	6,041	213,354	

TABLE 7-12. Washington State Water Quality Standards for the Hanford Reach of the Columbia River (after Sula and Blumer, 1981).

Parameter	Permissible levels
Fecal coliform organism	(1) ≤ 100 organisms/100 mL (median) (2) $\leq 10\%$ of samples may exceed 200 organisms/100 mL
Dissolved oxygen	> 8 mg/L
Temperature	(1) $\leq 18^{\circ}\text{C}$ (64°F) due to human activities (2) Increases not to exceed $(28/T + 27)$, where T = highest existing temperature in $^{\circ}\text{C}$ outside of mixing zone.
pH	(1) 6.5 to 8.5 range (2) < 0.5 unit of induced variation
Turbidity	≤ 5 NTU* over background turbidity
Toxic, radioactive, or deleterious materials	Concentrations shall be below those of public health significance, or which cause acute or chronic toxic conditions to the aquatic biota, or which may adversely affect any water use.
Aesthetic value	Shall not be impaired by the presence of materials or their effects, excluding those of natural origin which offend the senses of sight, smell, touch, or taste.

*NTU = nephelometric turbidity units--standard candle.

The quality of surface waters within the Pasco Basin is monitored by both the U.S. Geological Survey and Pacific Northwest Laboratory. The U.S. Geological Survey gathers general quality data at six locations significant to the Pasco Basin, including three stations on the Columbia River and one each on the Yakima, Snake, and Walla Walla Rivers. These stations are located in Figure 7-25 and described in Table 7-13. The activities at Pacific Northwest Laboratory are performed in conjunction with the U.S. Department of Energy Environmental Surveillance Program at Hanford. This program is geared to determine whether the U.S. Department of Energy operations at Hanford have an adverse effect upon water quality within the Columbia River. Consequently, Pacific Northwest Laboratory sampling stations are located above, along, and immediately below the Hanford Site boundaries along the Columbia River.

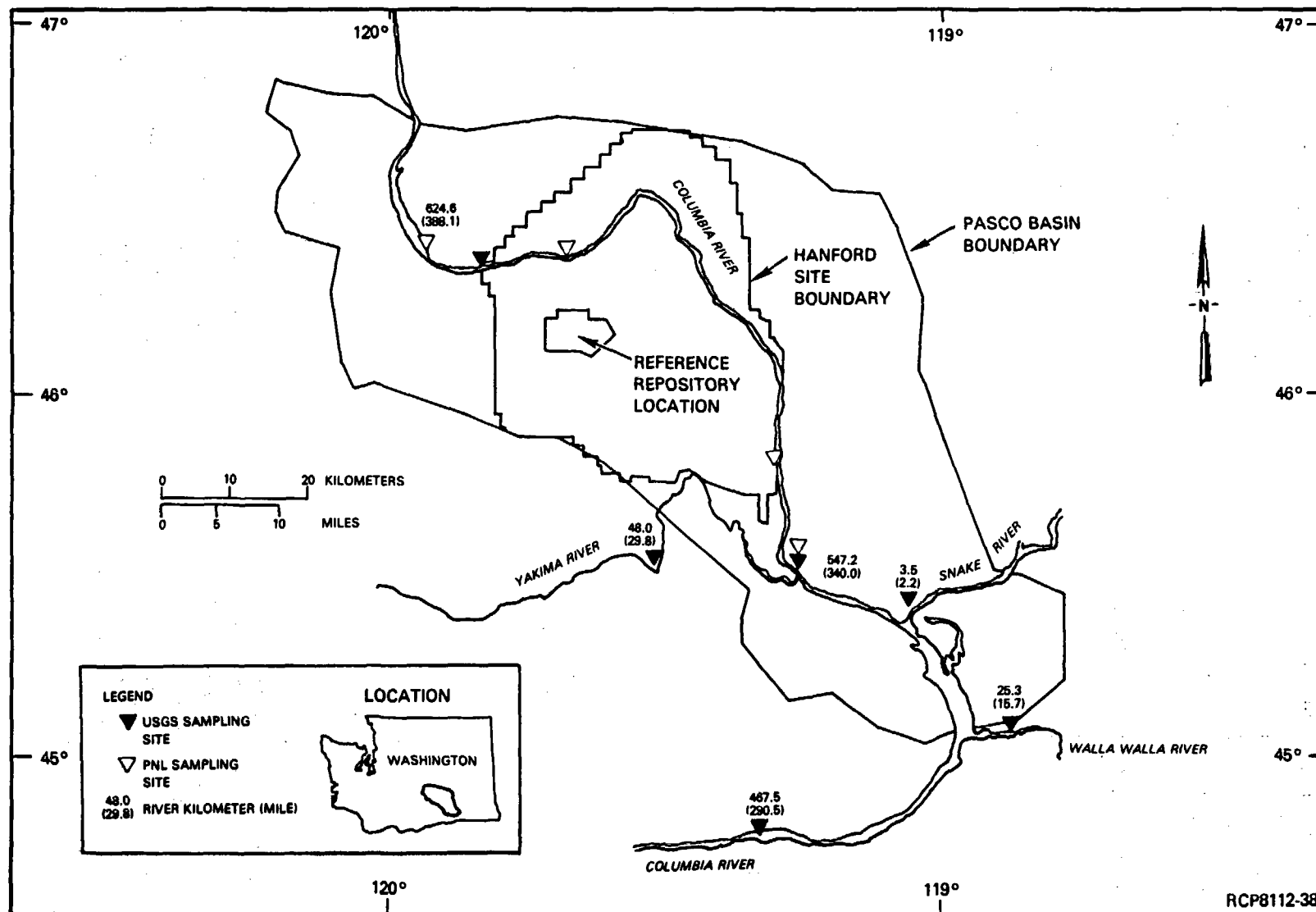


FIGURE 7-25. Surface Water Monitoring Stations.

TABLE 7-13. Summary of U.S. Geological Survey Surface Water Quality Sampling Activities Within the Pasco Basin.

River	River km	River mi	Location	Parameters*	Period(s) of record
Columbia	624.6	388.1	Vernita Bridge	C,T,S,B,M	1962-63, 1972, 1974-present
Columbia	547.2	340.0	Richland	T	1974-present
Yakima	48.0	29.8	Kiona	C,T,S,B,M	1974-present
Snake	3.5	2.2	Burbank	C,T,S,B,M	1960-69, 1972-present
Walla Walla	25.3	15.7	Near Touchet	C	1959-71, 1974-present
Columbia	467.5	290.5	Umatilla	C,T,M	1975-present

*Parameters listed include only those for which regular sampling is made. Other parameters may be sampled at these sites, but at irregular intervals. C = chemical, T = temperature, S = sediment, B = biological, M = microbiological.

A comparison of Class A quality parameters upstream (Vernita) and downstream (Richland) of the Hanford Site is shown in Table 7-14. Similarly, the radiological quality of the Columbia River upstream and downstream of the Hanford Site is given in Tables 7-15 and 7-16, respectively. Data gathered by Pacific Northwest Laboratory as part of the Hanford Environmental Surveillance Program during 1980 (Sula and Blumer, 1981) lead to the conclusion that Hanford operations had a minimal impact upon the quality of Columbia River water. All parameters monitored were well within state or federal limits both upstream and downstream from the Hanford Site (Sula and Blumer, 1981).

7.4.2.1 Biological Composition. As part of a biological survey of the Hanford reach, zooplankton samples were collected from the river from June 1973 through March 1980. Samples were collected at river kilometer 611 (river mile 382) and river kilometer 566 (river mile 354). Crustacean zooplankters dominated most samples collected. The three dominant genera were Bosmina, Diaptomus, and Cyclops. Other types of invertebrates were observed in the samples, including insect larvae, aquatic arachnids, annelids, rotifers, nematodes, tardigrades, and hydras. Drifting insect larvae, especially trichopterans and dipterans, were present in limited numbers (Neitzel et al., 1981). Other bottom-dwelling organisms included limpets (Fisherola nuttali), snails (Physa sp., Lymnaea sp.), sponge (Spongella lucustrus), and crayfish (Pacifasticus leniusculus) (Dauble, 1980). Extensive aquatic ecological studies conducted for the Washington Public Power Supply System, Inc. have provided information on the Hanford reach ecology (Beak, 1980; Gray and Dauble, 1976; Gray and Page, 1977; 1978; 1979a; 1979b; Page et al., 1976).

TABLE 7-14. Comparison of 1980 "Class A" Quality Parameters Upstream and Downstream from the Hanford Site (after Sula and Blumer, 1981).

Analysis	Units	State standard	Vernita				Richland			
			No. of samples	Maximum	Minimum	Annual average ^a	No. of samples	Maximum	Minimum	Annual average ^a
NO ₃	p/m	45	52	0.71	<0.10	0.26 ± 0.15	52	0.64	0.1	0.25 ± 0.14
pH		6.5 to 8.5	45	8.2	6.5	NAB ^b	47	8.2	6.9	NAB ^b
Turbidity	NTUC	5 + Bkgd.	48	12	0.85	2.2 ± 1.7	45	18	0.67	2.4 ± 2.6
Dissolved O ₂	mg/L	8	44	13.4	4.5	10 ± 1.8	43	13.7	5.5	10 ± 1.7
Total coliforms	no./100 mL	None	13	350	11	70 ^d	13	920	33	130 ^d
Fecal coliforms	no./100 mL	100	12	11	<2.0	2.0 ^d	12	49	<2.0	13 ^d
BOD ^e	mg/L	None	14	5.5	0.6	2.3 ± 1.4	14	4.8	<0.5	1.9 ± 1.2

^aAverage ± two standard deviations.

^bNA = not applicable.

^cNephelometric turbidity units.

^dAnnual median.

^eBiochemical oxygen demand.

TABLE 7-15. Radiological Quality of the Columbia River Upstream of the Hanford Site, 1980
(after Sula and Blumer, 1981).^a

Radionuclide	No. of samples ^b	Concentration pCi/L (10 ⁻⁹ µCi/mL)		
		Maximum	Minimum	Annual average
Naturally Occurring				
²²⁶ Ra	4	0.28 + 0.09	0.02 + 0.01	0.10 + 0.25
²²⁸ Ra	4	0.17 + 0.06	0.09 + 0.07	0.13 + 0.10
U-nat	12	0.59 + 0.21	0.30 + 0.10	0.40 + 0.25
Artificially Produced (Worldwide Fallout)				
³ H	12	420 + 150	27 + 120	230 + 310
⁵¹ Cr	17*	0.29 + 0.69	0.02 + 1.0	0.08 + 0.61
⁵⁴ Mn	24*	0.03 + 0.09	0.004 + 0.06	0.007 + 0.06
⁵⁹ Fe	22*	0.09 + 0.20	0.01 + 0.27	0.02 + 0.27
⁶⁰ Co	24*	0.05 + 0.01	0.004 + 0.007	0.01 + 0.05
⁹⁰ Sr	4	0.32 + 0.14	0.14 + 0.26	0.24 + 0.23
⁹⁵ Nb	19*	0.07 + 0.13	0.004 + 0.06	0.01 + 0.08
⁹⁵ Zr	23*	0.05 + 0.14	0.006 + 0.09	0.02 + 0.22
¹²⁵ Sb	24*	0.08 + 0.08	0.009 + 0.51	0.02 + 0.32
¹²⁹ I	4*	7.4 E-06 + 2.1 E-06	4.2 E-06 + 1.3 E-06	5.9 E-06 + 3.2 E-06
¹³¹ I	11*	0.04 + 0.78	0.008 + 0.08	0.02 + 0.31
¹³⁷ Cs	24*	0.09 + 0.01	0.004 + 0.006	0.01 + 0.05
¹⁴⁰ Ba	13*	0.12 + 1.1	0.02 + 0.32	0.05 + 0.63
¹⁴⁰ La	13*	0.07 + 0.04	0.01 + 0.23	0.02 + 0.11
²³⁸ Pu	4*	c	c	<2.7 E-05 ^c
²³⁹ Pu	4*	5.4 E-04 + 1.0 E-04	9.8 E-05 + 2.6 E-05	3.3 E-04 + 3.7 E-04
²⁴⁰ Pu	4*	5.4 E-04 + 1.0 E-04	9.8 E-05 + 2.6 E-05	3.3 E-04 + 3.7 E-04

^aMaximum and minimum concentrations include the 2σ counting error. Average concentrations include an estimate of uncertainty at the 95% confidence level.

^bNumbers marked with * were filter-resin samples of which 24 were taken during 1980. Results of analyses were not included in tabulations if the interval between sampling and analysis exceeded two half-lives. The filter resin samples were composited quarterly for ¹²⁹I and plutonium analysis.

^cAll results reported as "less than" values.

TABLE 7-16. Radiological Quality of the Columbia River Downstream of the Hanford Site, 1980 (after Sula and Blumer, 1981).^a

Radionuclide	No. of samples ^b	Concentration, pCi/L (10 ⁻⁹ µCi/mL)			
		Maximum	Minimum	Annual average	Concentration guide
Naturally Occurring					
²²⁶ Ra	4	0.05 ± 0.02	0.03 ± 0.02	0.04 ± 0.03	30
²²⁸ Ra	4	0.15 ± 0.07	0.05 ± 0.06	0.10 ± 0.11	30
U-nat	12	0.80 ± 0.28	0.38 ± 0.13	0.54 ± 0.34	20,000
Artificially Produced					
³ H ^c	12	490 ± 290	160 ± 76	265 ± 274	3,000,000
⁵¹ Cr	18*	0.28 ± 0.42	0.03 ± 0.53	0.09 ± 0.86	2,000,000
⁵⁴ Mn	24*	0.03 ± 0.04	0.004 ± 0.10	0.008 ± 0.07	100,000
⁵⁹ Fe	21*	0.07 ± 0.10	0.01 ± 0.22	0.03 ± 0.19	50,000
⁶⁰ Co	25*	0.12 ± 0.02	0.007 ± 0.009	0.03 ± 0.06	30,000
⁹⁰ Sr ^c	4	0.22 ± 0.14	0.18 ± 0.14	0.20 ± 0.16	300
⁹⁵ Nb	20*	0.03 ± 0.01	0.004 ± 0.07	0.01 ± 0.08	100,000
⁹⁵ Zr	22*	0.04 ± 0.05	0.007 ± 0.04	0.02 ± 0.19	60,000
¹²⁵ Sb	25*	0.07 ± 0.15	0.01 ± 0.05	0.03 ± 0.22	100,000
¹²⁹ I	4*	9.4 E-05 ± 3.2 E-05	2.9 E-05 ± 6.9 E-06	5.4 E-05 ± 5.8 E-05	60
¹³¹ I	12*	0.13 ± 0.14	0.01 ± 0.01	0.05 ± 0.13	300
¹³⁷ Cs	25*	0.19 ± 0.04	0.005 ± 0.007	0.02 ± 0.10	20,000
¹⁴⁰ Ba	14*	0.16 ± 1.2	0.03 ± 0.51	0.07 ± 0.95	20,000
¹⁴⁰ La	14*	0.07 ± 0.07	0.01 ± 0.13	0.03 ± 0.13	200,000
²³⁸ Pu	4*	\bar{d}	\bar{d}	3.4 E-05 ^d	5,000
²³⁹ Pu	4*	4.8 E-04 ± 6.2 E-05	1.7 E-04 ± 3.6 E-05	3.2 E-04 ± 3.2 E-04	5,000
²⁴⁰ Pu	4*	4.8 E-04 ± 6.2 E-05	1.7 E-04 ± 3.6 E-05	3.2 E-04 ± 3.2 E-04	5,000

^aMaximum and minimum concentrations include the 2σ counting error. Average concentrations include an estimate of uncertainty at the 95% confidence level.

^bNumbers marked with * were filter-resin samples of which 25 samples were taken during 1980. Results of analyses were not included in tabulations if the interval between sampling and analysis exceeded two half-lives. Filter-resin samples were composited quarterly for ¹²⁹I and plutonium analysis.

^cSamples taken at intake to Richland water plant. State drinking water standards for ³H and ⁹⁰Sr are 20,000 pCi/L and 8 pCi/L, respectively.

^dAll results reported as "less than" values.

Gray and Dauble (1976) listed fish species collected in over 30 years of research from the Hanford reach of the Columbia River. Forty-three species of fish representing 13 families have been collected since 1943. Most of the species are residents, but there are also some anadromous forms. During 1973 to 1975, at a collection site several kilometers upstream from N Reactor (between river kilometers 605 and 613 (river miles 376 and 381)), resident redbside shiner (Richardsonius balteatus), northern squawfish (Ptychocheilus oregonensis), large-scale sucker (Catostomus macrocheilus), and the anadromous chinook salmon (Oncorhynchus tshawytscha) were caught in about equal numbers and collectively comprised 90 percent of the total catch. Both species composition and numbers of fish present in any location in the river change dramatically throughout the year, depending on spawning, emergence, and migration.

Further aquatic ecology information and an extensive list of biotic species for the Hanford reach are available in ERDA (1975) and reference literature cited therein. An excellent reference was recently published concerning the biological composition of the associated riparian areas (Rickard et al., 1980).

7.4.2.2 Temperature, Suspended Solids, and Specific Conductance. Based on U.S. Geological Survey data, the monthly mean temperature distribution within the Columbia River does not change significantly as the river flows through the Pasco Basin. The data reveal that temperatures at Umatilla tend to be slightly lower than upstream stations during the period from November through January and about equal to slightly higher during the remaining months. These differences are on the order of about 20C and are statistically insignificant. Mean monthly temperatures of the Snake River at Burbank are also similar to the distribution shown within the Columbia River. This is probably due, in part, to the backwater effect of Lake Wallula. Mean monthly temperatures within the Yakima River are more significantly different, probably due to its significantly lower flow and its distance upstream from the head of Lake Wallula. The mean monthly temperature statistics, as well as the extremes at the various sampling sites within the Pasco Basin, are compared in Table 7-17. A graphic comparison of the 1979 mean monthly temperature distributions within the Columbia River is given in Figure 7-26, while the same distributions for the Yakima and Snake Rivers are given in Figure 7-27.

The only station where continuous measurements of suspended sediment concentrations and load are made is on the Yakima River at Kiona. Extreme values and the 1979 total load are shown within Table 7-18. The 1979 monthly total sediment discharge for this station is shown graphically in Figure 7-28.

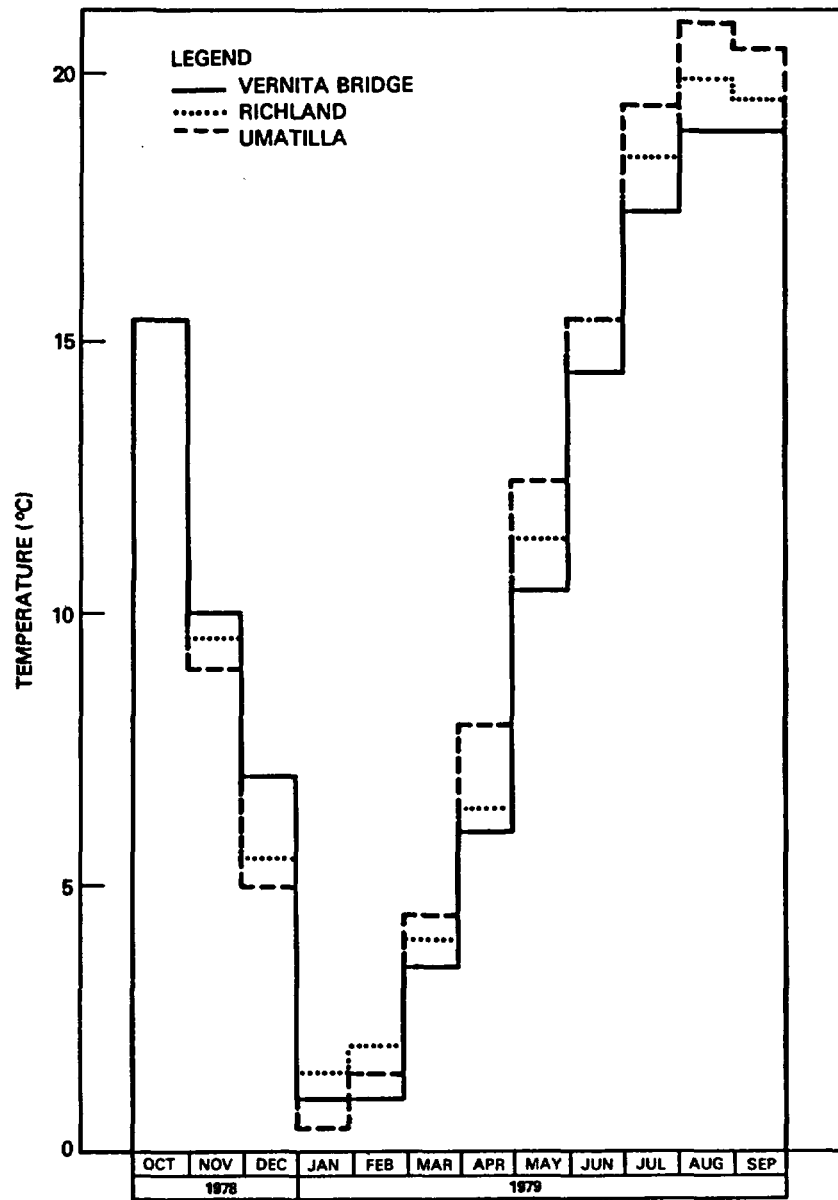
TABLE 7-17. Comparison of Extreme and Average Surface Water Temperatures Recorded at Various Stations Within the Pasco Basin.*

Station	Maximum temperature		Minimum temperature		1979 Mean (°C)
	(°C)	Date	(°C)	Date	
Vernita Bridge	20.5	8/16-21/77	0	2/1-6/79	11.0
Richland	21.5	8/17-20/77	0.5	2/1-4/79	11.0
Yakima River	29.0	7/18/60 7/12/61	0.0	Frequent	14.5
Snake River	24.0	8/3,7,8/73 8/4/74	0	1/26/79 - 2/5/79	11.5
Umatilla	22.5	8/16-17/77	0	1/31/79 - 2/9/79	11.5

*Data after U.S. Geological Survey. Period of record for individual stations may be different (see Table 7-13).

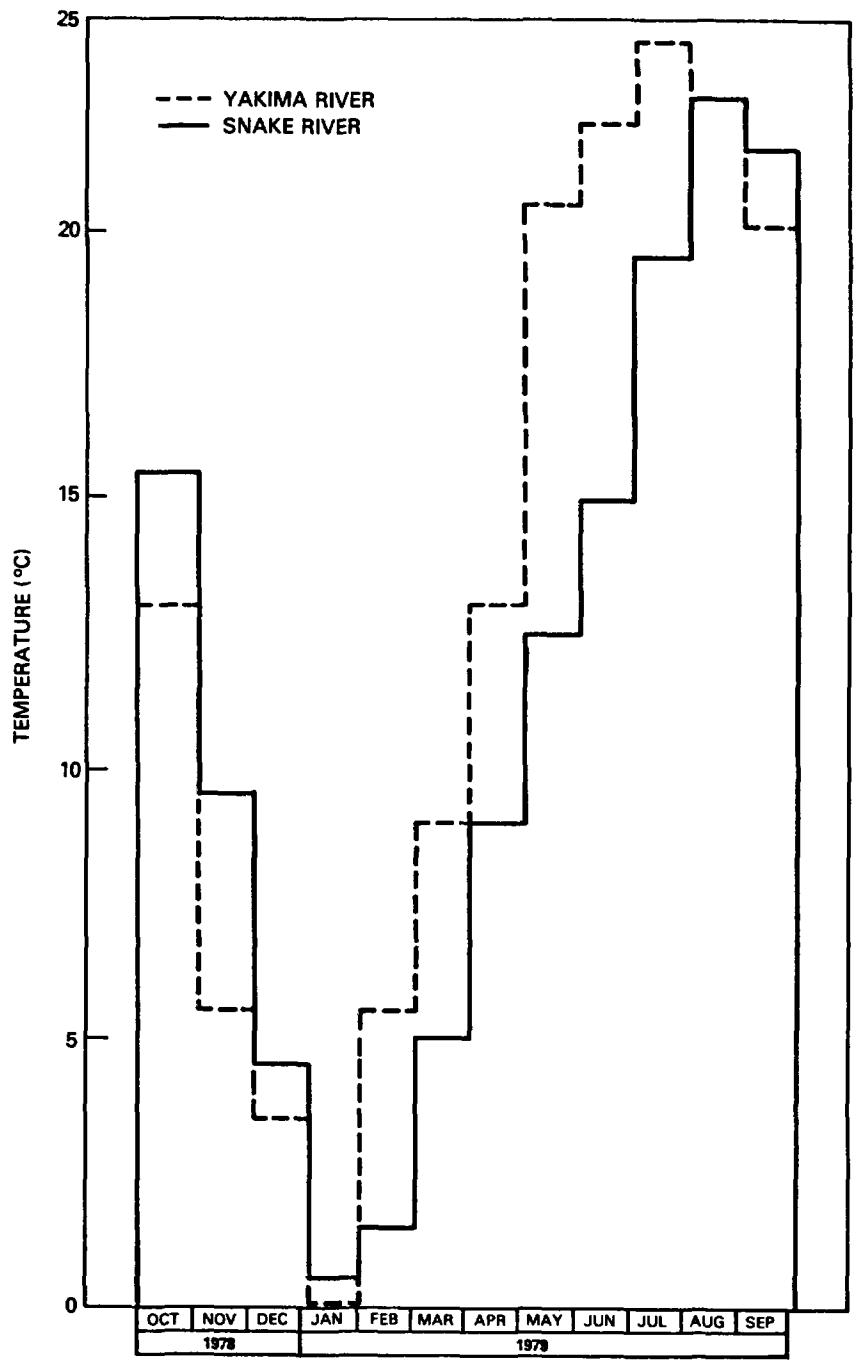
In one study of Columbia River particulate matter (Wildung et al., 1972) the concentration of total suspended matter less than 53 microns in diameter exhibited considerable seasonal variation, ranging from a low of 310 micrograms per liter of river water in November to a high of 34,680 micrograms per liter of water in April. This demonstrated that, relative to other seasons, the concentration of suspended matter increased markedly (over 100-fold) during the spring freshet. This increase was accompanied by a change in particle-size distribution, with the clay-size fraction (less than 2.0 microns) accounting for approximately 63 percent of total solids compared to a range of 14 to 30 percent for other periods of the year. Of the total suspended sediment load in the spring, 24 and 8 percent occurred in the less than 0.5- and less than 0.2-micron fractions, respectively.

Primary minerals inherited from parent rocks (quartz, feldspar, and amphibole) and the layer silicate-mineral species (mica-illite, chlorite, and montmorillonite) were generally present in particulate matter isolated throughout the year. Whereas seasonal changes in the primary mineral composition were not pronounced, the relative concentrations of the layer silicate minerals commonly present in soils increased during spring and summer, corresponding to the periods of spring runoff and the return of irrigation water to the river. Mineral composition also differed between size fractions. Montmorillonite, a layer silicate mineral of comparatively high ion-exchange capacity, increased in relative abundance with decreased particle size.



RCP8112-146

FIGURE 7-26. Comparison of 1979 Monthly Mean Temperature Distributions Along the Columbia River Within the Pasco Basin.



RCP8112-147

FIGURE 7-27. Comparison of 1979 Monthly Mean Temperature Distributions of Columbia River Tributaries Within the Pasco Basin.

TABLE 7-18. Extreme Load and Concentration Values and 1979 Total Load of Suspended Sediment Within the Yakima River at Kiona, Washington.

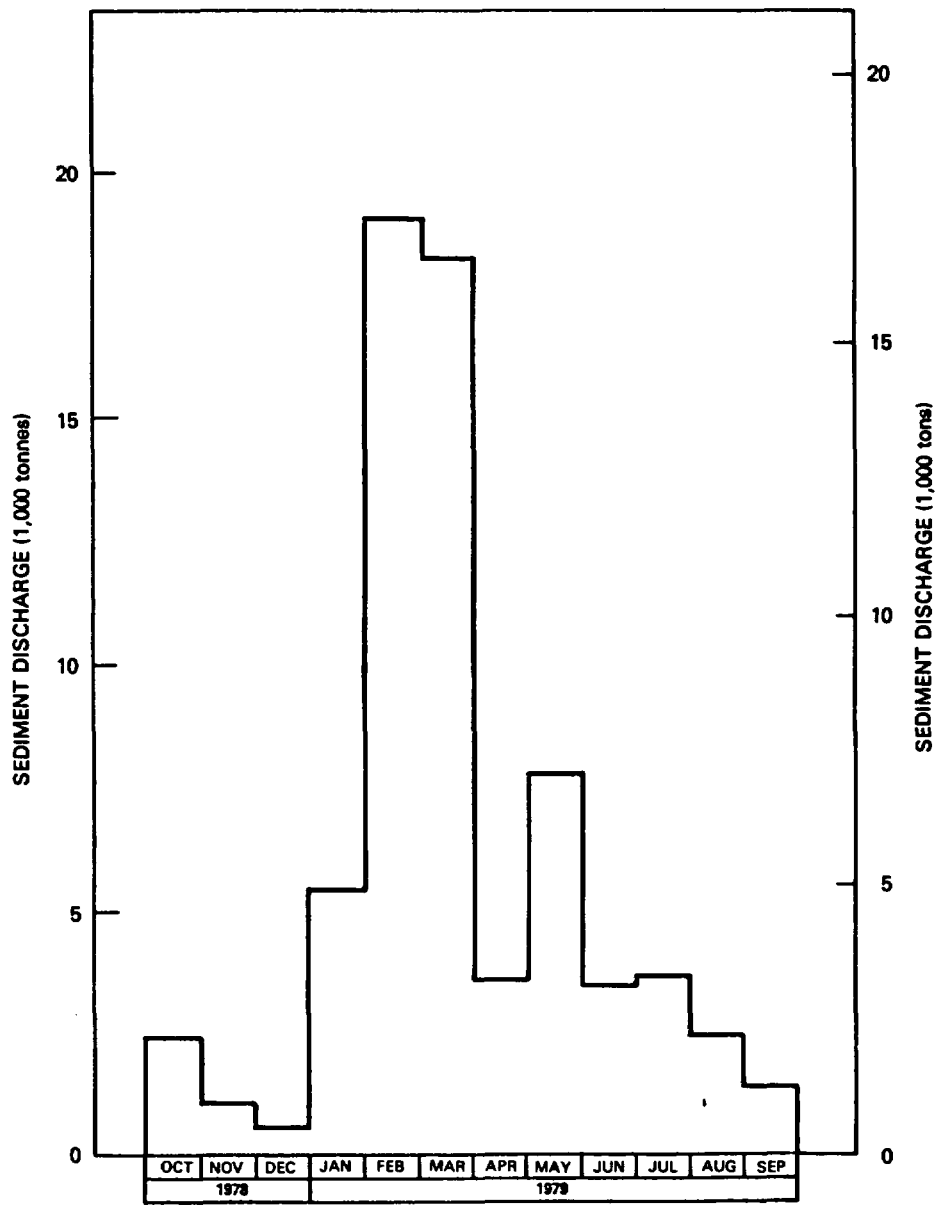
Load	Suspended sediment concentration (daily mean in mg/L)		Suspended sediment load (daily, in tonnes)	
	Concentration	Date	Weight load	Date
Maximum	1,750	12/4/77	99,800	12/4/77
Minimum	1	12/11,14/78	5.6	12/14/78
1979 Total			57,400	

Continuous measurement of specific conductance is taken for the Snake River at Burbank. Over the period of record, a minimum value of 60 micromhos per centimeter was recorded on June 14 and 15, 1978, and a maximum value of 476 micromhos per centimeter occurred on January 7, 1979. The 1979 mean monthly value was 215 micromhos per centimeter. The distribution of 1979 mean monthly specific conductance at this station is shown in Figure 7-29.

Other chemical and biological quality parameters are monitored by the U.S. Geological Survey on a monthly or quarterly basis at the six sites identified in Table 7-13. Data for 1979 at these stations are summarized in Tables 7-19 and 7-20.

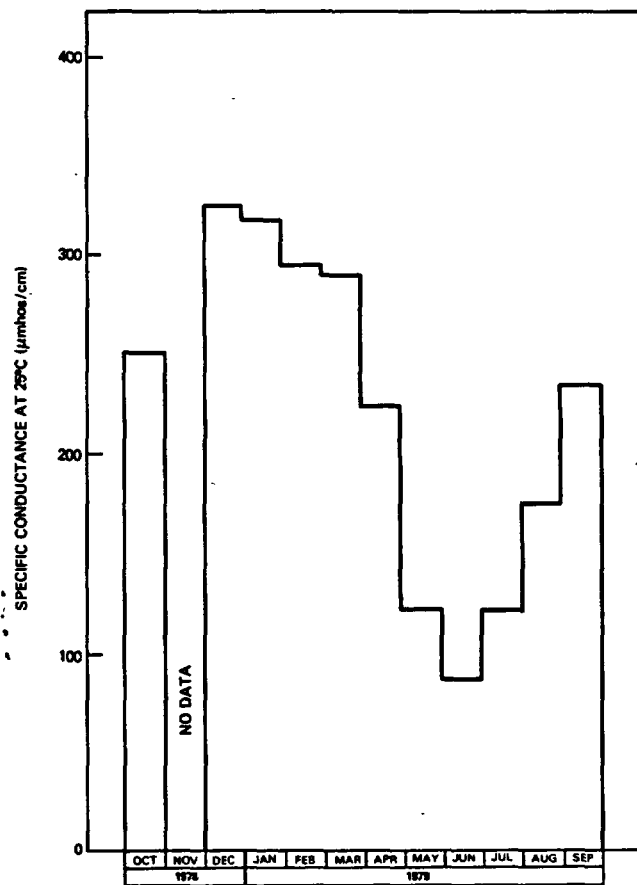
7.4.3 Water Quality Associated With Hanford Site Operations

7.4.3.1 Columbia River. As a result of plutonium production operations at Hanford, low-level radioactive materials were discharged into the Columbia River along the Hanford reach. This discharge began in 1944 upon startup of the first of nine production reactors and lasted into the mid-1960s. Eight of the reactors used river water as a once-through coolant. Upon discharge to the river, the radioactive contaminants were rapidly dispersed and sorbed onto detritus and inorganic particles, incorporated into aquatic biota or, in the case of larger particles of insoluble material, deposited on the riverbed (Cushing et al., 1974; Glenn and Van Atta, 1973; Habbell and Glenn, 1971; Haushild et al., 1971; Nelson and Haushild, 1970; Perkins et al., 1966; Robertson and Fix, 1977; Robertson et al., 1973; Sula, 1980, Toombs, 1966).



RCP8112-148

FIGURE 7-28. Monthly Sediment Discharge Totals in 1979 for the Yakima River at Kiona, Washington.



RCP8112-149

FIGURE 7-29. Monthly Mean Specific Conductance in 1979 of the Snake River near Burbank, Washington.

TABLE 7-19. Summary of U.S. Geological Survey Surface Water Quality Data for Stations on the Columbia River Within the Pasco Basin. (Sheet 1 of 4)

Quality parameter/group	Units	Vernita Bridge				Richland				Umatilla			
		No. of samples	Highest	Lowest	Mean	No. of samples	Highest	Lowest	Mean	No. of samples	Highest	Lowest	Mean
Physical													
Discharge, daily	m ³ /s (ft ³ /s)	Continuous	4,300 (152,000)	1,430 (50,500)	2,900 (102,700)	--	--	--	--	Continuous	8,300 (293,000)	1,650 (58,100)	4,180 (147,700)
Turbidity	NTU	12	4.3	0.4	1.8	4	3.6	0.60	1.8	--	--	--	--
Temperature	°C	Continuous	20.0	0.0	11.0	Continuous	21.0	0.5	11.0	Continuous	21.5	0.0	11.5
Specific conductance	µmhos/cm at 25°C	12	156	109	135	4	150	123	134	11	244	107	175
pH	Units	8	8.8	7.5	8.2	4	8.6	7.7	8.3	10	8.5	7.6	8.1
Gross alpha, dissolved	µg/L as U-Mat	--	--	--	--	--	--	--	--	--	--	--	--
Gross alpha, suspended total	µg/L as U-Mat	--	--	--	--	--	--	--	--	--	--	--	--
Gross alpha, dissolved	pCi/L as U-Mat	--	--	--	--	--	--	--	--	--	--	--	--
Gross beta, dissolved	pCi/L as Cs-137	--	--	--	--	--	--	--	--	--	--	--	--
Gross beta, suspended total	pCi/L as Cs-137	--	--	--	--	--	--	--	--	--	--	--	--
Gross beta, dissolved	pCi/L as Sr/Yt-90	--	--	--	--	--	--	--	--	--	--	--	--
Gross beta, suspended total	pCi/L as Sr/Yt-90	--	--	--	--	--	--	--	--	--	--	--	--
Radium-226, dissolved radon method	pCi/L	--	--	--	--	--	--	--	--	--	--	--	--
Uranium, dissolved, extraction	µg/L	--	--	--	--	--	--	--	--	--	--	--	--
Chemical													
Major Constituents													
Oxygen, dissolved	mg/L	12	15.8	9.2	12.2	4	15.0	9.5	12.3	11	13.8	8.5	11.0
Carbon dioxide, dissolved	mg/L	--	--	--	--	--	--	--	--	2	1.2	0.5	0.9
Solids, residue at 180°C, dissolved	mg/L	12	93	70	80	4	89	70	80	11	139	72	101
Solids, sum of constituents, dissolved	mg/L	12	90	67	78	4	86	67	77	--	--	--	--
Solids, dissolved	tons/acre-ft	12	0.13	0.10	0.11	4	0.12	0.10	0.11	11	0.19	0.10	0.14
Solids, dissolved	tonnes/day (tons/day)	12	29,200 (32,200)	7,530 (8,300)	18,960 (20,900)	--	--	--	--	11	58,600 (64,600)	23,405 (25,800)	37,285 (41,100)
Solids, residue at 105°C, suspended	mg/L	12	9	0	3	4	8	0	4.5	11	80	0	16.9
Hardness	mg/L as CaCO ₃	12	76	59	66	4	76	59	66	--	--	--	--
Hardness, non-carbonate	mg/L as CaCO ₃	12	22	3	13	4	16	7	12	--	--	--	--
Alkalinity	mg/L as CaCO ₃	12	62	43	54	4	60	45	54	3	68	47	59
Silica, dissolved	mg/L as SiO ₂	12	5.2	3.2	4.4	4	4.9	3.0	4.4	11	13	4.0	8
Carbon, organic total	mg/L as C	8	8.6	0.0	2.8	2	3.6	2.4	3.0	10	4.5	1.7	2.7
Carbon, organic dissolved	mg/L as C	4	3.8	1.7	2.9	2	4.4	2.1	3.3	--	--	--	--
Carbon, organic suspended total	mg/L as C	4	0.8	0.1	0.3	2	0.6	0.2	0.4	--	--	--	--
Phosphorus, total	mg/L as P	12	0.050	0.010	0.030	4	0.040	0.010	0.023	11	0.170	0.000	0.044
Phosphorus, dissolved	mg/L as P	12	0.050	0.000	0.020	--	--	--	--	--	--	--	--

TABLE 7-19. Summary of U.S. Geological Survey Surface Water Quality Data for Stations on the Columbia River Within the Pasco Basin. (Sheet 2 of 4)

Quality parameter/group	Units	Vernita Bridge				Richland				Umatilla			
		No. of samples	Highest	Lowest	Mean	No. of samples	Highest	Lowest	Mean	No. of samples	Highest	Lowest	Mean
Major Constituents													
Phosphorus, ortho, dissolved	mg/L as P	4	0.01	0.00	0.01	4	0.01	0.00	0.01	--	--	--	--
Phosphate, ortho, dissolved	mg/L as PO ₄	4	0.03	0.00	0.02	4	0.03	0.00	0.02	--	--	--	--
Nitrogen, nitrate, total	mg/L as N	4	0.12	0.00	0.08	4	0.15	0.01	0.07	--	--	--	--
Nitrogen, nitrite, total	mg/L as N	4	0.02	0.00	0.01	4	0.02	0.00	0.01	--	--	--	--
Nitrogen, NO ₂ + NO ₃ , total	mg/L as N	12	0.28	0.00	0.10	4	0.15	0.03	0.08	11	0.84	0.02	0.24
Nitrogen, ammonia, total	mg/L as N	12	0.02	0.00	0.01	4	0.01	0.00	0.01	10	0.08	0.01	0.04
Nitrogen, organic, total	mg/L as N	12	0.61	0.08	0.23	4	0.61	0.08	0.27	10	0.59	0.13	0.33
Nitrogen, ammonia + organic, total	mg/L as N	12	0.62	0.08	0.24	4	0.61	0.09	0.28	--	--	--	--
Nitrogen, ammonia + organic, suspended, total	mg/L as N	12	0.42	0.02	0.11	--	--	--	--	--	--	--	--
Nitrogen, ammonia + organic, dissolved, total	mg/L as N	12	0.37	0.00	0.13	--	--	--	--	--	--	--	--
Nitrogen, total	mg/L as N	12	0.90	0.10	0.33	4	0.64	0.21	0.36	10	1.3	0.23	0.63
Nitrogen, total	mg/L as NO ₃	12	4.0	0.44	1.47	4	2.8	0.93	1.61	10	5.6	1.0	2.77
Sulfate, dissolved	mg/L as SO ₄	12	16	8.3	13	4	13	10	12	3	15	12	14
Chloride, dissolved	mg/L as Cl	12	2.1	0.9	1.3	4	2.5	1.1	1.8	3	3.9	2.1	3.0
Fluoride, dissolved	mg/L as F	12	0.2	0.1	0.1	4	0.2	0.1	0.1	--	--	--	--
Sodium, dissolved	mg/L as Na	12	2.7	1.8	2.0	4	2.3	2.0	2.2	--	--	--	--
Sodium	Percent	12	10	6	7	4	8	6	7	--	--	--	--
Sodium adsorption ratio	Units	12	0.1	0.1	0.1	4	0.1	0.1	0.1	--	--	--	--
Potassium, dissolved	mg/L as K	12	1.1	0.6	0.8	4	0.9	0.6	0.7	--	--	--	--
Calcium, dissolved	mg/L as Ca	12	23	17	20	4	22	17	19	--	--	--	--
Magnesium, dissolved	mg/L as Mg	12	5.2	1.3	4.1	4	5.2	3.7	4.4	--	--	--	--
Trace Constituents													
Chromium, suspended recoverable	ug/L as Cr	4	0	0	0	--	--	--	--	--	--	--	--
Chromium, dissolved	ug/L as Cr	4	0	0	0	--	--	--	--	--	--	--	--
Chromium, total recoverable	ug/L as Cr	4	0	0	0	4	20	0	5	11	20	0	7
Cobalt, total recoverable	ug/L as Co	4	1	0	0	4	2	0	1	--	--	--	--
Cobalt, suspended recoverable	ug/L as Co	4	0	0	0	--	--	--	--	--	--	--	--
Cobalt, dissolved	ug/L as Co	4	<3	0	--	--	--	--	--	--	--	--	--
Copper, total recoverable	ug/L as Cu	4	12	4	7	4	19	2	10	11	50	1	18
Copper, suspended recoverable	ug/L as Cu	4	12	3	6	--	--	--	--	--	--	--	--
Copper, dissolved	ug/L as Cu	4	1	0	0	--	--	--	--	--	--	--	--
Iron, total recoverable	ug/L as Fe	4	130	80	98	4	180	90	133	10	4,200	140	377
Iron, suspended recoverable	ug/L as Fe	4	100	0	63	--	--	--	--	--	--	--	--
Iron, dissolved	ug/L as Fe	4	100	10	40	--	--	--	--	--	--	--	--
Arsenic, total	ug/L as As	4	1	1	1	4	1	1	1	10	3	1	2
Arsenic, dissolved	ug/L as As	4	1	0	1	4	1	0	1	--	--	--	--
Barium, total recoverable	ug/L as Ba	4	0	0	0	--	--	--	--	--	--	--	--
Barium, suspended recoverable	ug/L as Ba	4	0	0	0	--	--	--	--	--	--	--	--
Barium, dissolved	ug/L as Ba	4	40	0	28	--	--	--	--	--	--	--	--
Cadmium, total recoverable	ug/L as Cd	3	3	1	2	4	7	0	3	10	9	0	3

TABLE 7-19. Summary of U.S. Geological Survey Surface Water Quality Data for Stations on the Columbia River Within the Pasco Basin. (Sheet 3 of 4)

Quality parameter/group	Units	Vernita Bridge				Richland				Umatilla			
		No. of samples	Highest	Lowest	Mean	No. of samples	Highest	Lowest	Mean	No. of samples	Highest	Lowest	Mean
<u>Trace Constituents</u>													
Cadmium, suspended recoverable	ug/L as Cd	3	2	0	1	--	--	--	--	--	--	--	--
Cadmium, dissolved	ug/L as Cd	3	2	<1	--	--	--	--	--	--	--	--	--
Lead, total recoverable	ug/L as Pb	3	73	8	33	4	130	27	75	10	42	3	15
Lead, suspended recoverable	ug/L as Pb	3	61	8	29	--	--	--	--	--	--	--	--
Lead, dissolved	ug/L as Pb	3	12	2	5	--	--	--	--	--	--	--	--
Manganese, total recoverable	ug/L as Mn	4	20	0	13	4	20	10	18	--	--	--	--
Manganese, suspended recoverable	ug/L as Mn	4	20	0	12	--	--	--	--	--	--	--	--
Manganese, dissolved	ug/L as Mn	4	5	0	3	--	--	--	--	--	--	--	--
Mercury, total recoverable	ug/L as Hg	4	0.1	0.0	0.1	4	0.3	0.0	0.1	10	0.5	0.0	0.1
Mercury, suspended recoverable	ug/L as Hg	4	0.1	0.0	0.1	--	--	--	--	--	--	--	--
Mercury, dissolved	ug/L as Hg	4	0.0	0.0	0.0	--	--	--	--	--	--	--	--
Selenium, total	ug/L as Se	4	0	0	0	4	0	0	0	10	0	0	0
Selenium, suspended total	ug/L as Se	4	0	0	0	--	--	--	--	--	--	--	--
Selenium, dissolved	ug/L as Se	4	0	0	0	--	--	--	--	--	--	--	--
Silver, total recoverable	ug/L as Ag	4	0	0	0	--	--	--	--	--	--	--	--
Silver, suspended recoverable	ug/L as Ag	4	0	0	0	--	--	--	--	--	--	--	--
Silver, dissolved	ug/L as Ag	4	0	0	0	--	--	--	--	--	--	--	--
Zinc, total recoverable	ug/L as Zn	4	70	10	38	4	40	20	33	11	170	0	45
Zinc, suspended recoverable	ug/L as Zn	4	50	0	23	--	--	--	--	--	--	--	--
Zinc, dissolved	ug/L as Zn	4	30	4	15	--	--	--	--	--	--	--	--
<u>Organic Compounds</u>													
PCB, total	ug/L	--	--	--	--	--	--	--	--	--	--	--	--
Aldrin, total	ug/L	--	--	--	--	--	--	--	--	--	--	--	--
Chlordane, total	ug/L	--	--	--	--	--	--	--	--	--	--	--	--
DDD, total	ug/L	--	--	--	--	--	--	--	--	--	--	--	--
DDE, total	ug/L	--	--	--	--	--	--	--	--	--	--	--	--
DDT, total	ug/L	--	--	--	--	--	--	--	--	--	--	--	--
Diazinon, total	ug/L	--	--	--	--	--	--	--	--	--	--	--	--
Dieldrin, total	ug/L	--	--	--	--	--	--	--	--	--	--	--	--
Endrin, total	ug/L	--	--	--	--	--	--	--	--	--	--	--	--
Ethion, total	ug/L	--	--	--	--	--	--	--	--	--	--	--	--
Heptachlor, total	ug/L	--	--	--	--	--	--	--	--	--	--	--	--
Heptachlor epoxide, total	ug/L	--	--	--	--	--	--	--	--	--	--	--	--
Lindane, total	ug/L	--	--	--	--	--	--	--	--	--	--	--	--
Malathion, total	ug/L	--	--	--	--	--	--	--	--	--	--	--	--
Methoxychlor, total	ug/L	--	--	--	--	--	--	--	--	--	--	--	--
Methylparathion, total	ug/L	--	--	--	--	--	--	--	--	--	--	--	--
Methyltrithion, total	ug/L	--	--	--	--	--	--	--	--	--	--	--	--
Parathion, total	ug/L	--	--	--	--	--	--	--	--	--	--	--	--
Toxaphene, total	ug/L	--	--	--	--	--	--	--	--	--	--	--	--
Total trithion	ug/L	--	--	--	--	--	--	--	--	--	--	--	--

TABLE 7-19. Summary of U.S. Geological Survey Surface Water Quality Data for Stations on the Columbia River Within the Pasco Basin. (Sheet 4 of 4)

Quality parameter/group	Units	Vernita Bridge				Richland				Umatilla			
		No. of samples	Highest	Lowest	Mean	No. of samples	Highest	Lowest	Mean	No. of samples	Highest	Lowest	Mean
Biological													
Biomass													
Periphyton biomass ash weight	g/m ²	4	8.90	0.000	2.97	--	--	--	--	--	--	--	--
Periphyton biomass total dry weight	g/m ²	4	13.5	0.000	4.24	--	--	--	--	--	--	--	--
Chlor-A periphyton chromographic fluorom	mg/m ²	4	24.5	0.000	6.26	--	--	--	--	--	--	--	--
Chlor-B periphyton chromographic fluorom	mg/m ²	4	7.92	0.000	1.98	--	--	--	--	--	--	--	--
Length of exposure	Days	4	28	21	24	--	--	--	--	--	--	--	--
Phytoplankton													
Total count	cells/mL	4	19,000	1,900	10,000	--	--	--	--	--	--	--	--
Division, diversity	index (d)	4	0.6	0.1	0.3	--	--	--	--	--	--	--	--
Class, diversity	index (d)	4	0.6	0.1	0.3	--	--	--	--	--	--	--	--
Order, diversity	index (d)	4	1.1	0.3	0.8	--	--	--	--	--	--	--	--
Family, diversity	index (d)	4	1.2	0.3	0.9	--	--	--	--	--	--	--	--
Genus, diversity	index (d)	4	1.9	0.3	1.4	--	--	--	--	--	--	--	--
Bacteria													
Coliform, fecal 0.7 UM-MF	colonies/100 mL	12	13	<1	~2	4	10	<1	~3	11	K*19	K2	K6
Streptococci, fecal KF AGAR	colonies/100 mL	12	71	<1	~8	4	16	<1	~9	11	1,100	K1	K112
Sediment													
Sediment, suspended	mg/L	12	7	1	4	4	8	2	5	--	--	--	--
Sediment, discharge suspended	tons/day	12	2,420 (2,670)	187 (206)	907 (1,000)	--	--	--	--	--	--	--	--
Sediment, suspended (fall diameter <0.002 mm)	Percent	↑	↑	↑	↑	--	--	--	--	--	--	--	--
Sediment, suspended (fall diameter <0.004 mm)	Percent	↑	↑	↑	↑	--	--	--	--	--	--	--	--
Sediment, suspended (fall diameter <0.008 mm)	Percent	↑	↑	↑	↑	--	--	--	--	--	--	--	--
Sediment, suspended (fall diameter <0.016 mm)	Percent	↑	↑	↑	↑	--	--	--	--	--	--	--	--
Sediment, suspended (fall diameter <0.031 mm)	Percent	↑	↑	↑	↑	--	--	--	--	--	--	--	--
Sediment, suspended (fall diameter <0.062 mm)	Percent	8	100	49	99	--	--	--	--	--	--	--	--
Sediment, suspended (fall diameter <0.125 mm)	Percent	↑	↑	↑	↑	--	--	--	--	--	--	--	--
Sediment, suspended (fall diameter <0.250 mm)	Percent	↑	↑	↑	↑	--	--	--	--	--	--	--	--
Sediment, suspended (fall diameter <0.500 mm)	Percent	↑	↑	↑	↑	--	--	--	--	--	--	--	--
Sediment, suspended (fall diameter <1.00 mm)	Percent	↑	↑	↑	↑	--	--	--	--	--	--	--	--

* Results based upon colony counts outside the ideal range.

TABLE 7-20. Summary of U.S. Geological Survey 1979 Surface Water Quality Data for Columbia River Tributaries. (Sheet 1 of 4)

Quality parameter/group	Units	Yakima River at Kiona				Snake River at Burbank				Walla Walla River near Touchet			
		No. of samples	Highest	Lowest	Mean	No. of samples	Highest	Lowest	Mean	No. of samples	Highest	Lowest	Mean
Physical													
Discharge, daily average	m ³ /s (ft ³ /s)	Continuous	125 (4,400)	14 (497)	47 (1,675)	Continuous	4,050 (143,000)	76 (2,700)	1,200 (42,510)	Continuous	220 (7,900)	0.02 (0.82)	15 (543)
Turbidity	NTU	12	15	0.60	6.4	12	54	0.7	10.1	11	40	10	24
Temperature	°C	Continuous	28	0.0	14.5	Continuous	23.5	0.0	11.5	11	26.7	2.2	14.0
Specific conductance	µmhos/cm at 25°C	12	362	190	291	Continuous	476	63	215	11	775	180	329
pH	Units	12	8.9	7.8	8.2	9	8.4	7.6	7.9	11	8.5	7.4	7.9
Gross alpha, dissolved	µg/L as U-Nat	--	--	--	--	2	3.6	3.0	3.3	--	--	--	--
Gross alpha, suspended total	µg/L as U-Nat	--	--	--	--	2	<0.4	<0.4	<0.4	--	--	--	--
Gross alpha, dissolved	pCi/L as U-Nat	--	--	--	--	1	2.0	2.0	2.0	--	--	--	--
Gross beta, dissolved	pCi/L as Cs-137	--	--	--	--	1	<0.3	<0.3	<0.3	--	--	--	--
Gross beta, suspended total	pCi/L as Cs-137	--	--	--	--	2	<0.4	<0.4	<0.4	--	--	--	--
Gross beta, dissolved	pCi/L as Sr/Yt-90	--	--	--	--	2	3.3	2.4	2.9	--	--	--	--
Gross beta, suspended total	pCi/L as Sr/Yt-90	--	--	--	--	2	<0.4	<0.4	<0.4	--	--	--	--
Radium-226, dissolved radon method	pCi/L	--	--	--	--	2	0.06	0.03	0.05	--	--	--	--
Uranium, dissolved, extraction	µg/L	--	--	--	--	2	2.1	1.9	2.0	--	--	--	--
Chemical													
Major Constituents													
Oxygen, dissolved	mg/L	12	16.8	8.9	12.18	12	14.2	7.0	10.7	11	13.0	7.0	9.5
Carbon dioxide, dissolved	mg/L	--	--	--	--	--	--	--	--	--	--	--	--
Solids, residue at 180°C, dissolved	mg/L	12	234	119	180	11	211	69	148	--	--	--	--
Solids, sum of constituents, dissolved	mg/L	12	235	120	178	12	213	59	145	--	--	--	--
Solids, dissolved	tons/acre-ft	12	0.32	0.16	0.25	12	0.29	0.09	0.20	--	--	--	--
Solids, dissolved	tonnes/day (tons/day)	12	1,107 (1,220)	435 (480)	797 (878)	12	33,384 (36,800)	2,658 (2,930)	17,835 (19,660)	--	--	--	--
Solids, residue at 105°C, suspended	mg/L	12	57	1	27	12	50	0	13	--	--	--	--
Hardness	mg/L as CaCO ₃	12	160	73	113	12	140	36	82	--	--	--	--
Hardness, non-carbonate	mg/L as CaCO ₃	12	6	0	2	12	25	0	9	--	--	--	--
Alkalinity	mg/L as CaCO ₃	12	150	78	114	12	110	29	74	--	--	--	--
Silica, dissolved	mg/L as SiO ₂	12	29	19	24	12	24	11	16	--	--	--	--
Carbon, organic total	mg/L as C	8	7.1	2.0	3.6	7	5.5	1.9	3	--	--	--	--
Carbon, organic dissolved	mg/L as C	4	7.3	1.8	4.3	4	7.1	2.9	4.8	--	--	--	--
Carbon, organic suspended total	mg/L as C	4	4.3	0.4	1.7	3	0.9	0.2	0.4	--	--	--	--
Phosphorus, total	mg/L as P	12	0.210	0.070	0.119	12	0.130	0.020	0.053	11	0.290	0.070	0.150
Phosphorus, dissolved	mg/L as P	12	0.160	0.030	0.084	12	0.100	0.000	0.037	--	--	--	--
Phosphorus, ortho, dissolved	mg/L as P	--	--	--	--	--	--	--	--	11	0.25	0.01	0.08

TABLE 7-20. Summary of U.S. Geological Survey 1979 Surface Water Quality Data for Columbia River Tributaries. (Sheet 2 of 4)

Quality parameter/group	Units	Yakima River at Kiona				Snake River at Burbank				Walla Walla River Near Touchet			
		No. of samples	Highest	Lowest	Mean	No. of samples	Highest	Lowest	Mean	No. of samples	Highest	Lowest	Mean
Major Constituents													
Phosphate, ortho, dissolved	mg/L as PO ₄	--	--	--	--	--	--	--	--	11	0.77	0.03	0.25
Nitrogen, nitrate, total	mg/L as N	--	--	--	--	--	--	--	--	11	1.8	0.00	0.69
Nitrogen, nitrate, total	mg/L as N	--	--	--	--	--	--	--	--	11	0.04	--	0.02
Nitrogen, NO ₂ + NO ₃ , total	mg/L as N	12	1.5	0.42	0.89	12	1.5	0.08	0.48	11	1.8	0.02	0.70
Nitrogen, ammonia, total	mg/L as N	12	0.13	0.00	0.03	12	0.19	0.01	0.04	11	0.16	0.00	0.05
Nitrogen, organic, total	mg/L as N	12	0.67	0.09	0.40	12	0.70	0.01	0.32	11	1.7	0.17	0.60
Nitrogen, ammonia + organic, total	mg/L as N	12	0.67	0.10	0.43	12	0.71	0.13	0.36	11	1.7	0.19	0.65
Nitrogen, ammonia + organic, suspended total	mg/L as N	11	0.45	0.00	0.14	11	0.63	0.00	0.18	--	--	--	--
Nitrogen, ammonia + organic, dissolved, total	mg/L as N	11	0.54	0.08	0.31	11	0.32	0.00	0.18	--	--	--	--
Nitrogen, total	mg/L as N	12	2.2	0.85	1.3	12	1.8	0.23	0.84	11	2.2	0.57	1.4
Nitrogen, total	mg/L as NO ₃	12	9.6	3.8	5.9	12	8.1	1.0	3.7	11	9.9	2.5	6.0
Sulfate, dissolved	mg/L as SO ₄	12	29	8.9	19	12	40	7.6	25	--	--	--	--
Chloride, dissolved	mg/L as Cl	12	8.8	4.6	7.2	12	21	3.4	11	--	--	--	--
Fluoride, dissolved	mg/L as F	12	0.3	0.1	0.2	12	0.4	0.2	0.3	--	--	--	--
Sodium, dissolved	mg/L as Na	12	25	11	18	12	24	5.8	17	--	--	--	--
Sodium	Percent	12	26	23	25	12	45	26	31	--	--	--	--
Sodium adsorption ratio	Units	12	0.9	0.5	0.7	12	1.0	0.4	0.8	--	--	--	--
Potassium, dissolved	mg/L as K	12	4.3	2.0	3.2	12	3.6	0.7	2.5	--	--	--	--
Calcium, dissolved	mg/L as Ca	12	40	18	28	12	36	9.6	21	--	--	--	--
Magnesium, dissolved	mg/L as Mg	12	14	6.8	10.3	12	11	2.8	7.3	--	--	--	--
Trace Constituents													
Chromium, suspended recoverable	ug/L as Cr	4	10	0	8	4	10	0	5	--	--	--	--
Chromium, dissolved	ug/L as Cr	4	0	0	0	4	0	0	0	--	--	--	--
Chromium, total recoverable	ug/L as Cr	4	10	0	8	4	10	0	5	--	--	--	--
Cobalt, total recoverable	ug/L as Co	4	3	0	1	4	2	0	1	--	--	--	--
Cobalt, suspended recoverable	ug/L as Co	4	0	0	0	4	0	0	0	--	--	--	--
Cobalt, dissolved	ug/L as Co	4	<3	0	<3	4	<3	0	<3	--	--	--	--
Copper, total recoverable	ug/L as Cu	4	14	5	10	4	47	1	16	--	--	--	--
Copper, suspended recoverable	ug/L as Cu	4	13	4	7	4	26	0	9	--	--	--	--
Copper, dissolved	ug/L as Cu	4	6	1	3	4	21	1	7	--	--	--	--
Iron, total recoverable	ug/L as Fe	4	1,300	270	783	4	1,200	50	495	--	--	--	--
Iron, suspended recoverable	ug/L as Fe	4	1,200	110	683	4	1,100	20	430	--	--	--	--
Iron, dissolved	ug/L as Fe	4	200	40	113	4	90	30	58	--	--	--	--
Arsenic, total	ug/L as As	4	2	2	2	4	3	1	2	--	--	--	--
Arsenic, dissolved	ug/L as As	4	2	2	2	4	4	2	2	--	--	--	--
Barium, total recoverable	ug/L as Ba	4	100	0	50	4	100	0	25	--	--	--	--
Barium, suspended recoverable	ug/L as Ba	4	80	0	35	4	70	0	18	--	--	--	--
Barium, dissolved	ug/L as Ba	4	40	0	20	4	30	0	20	--	--	--	--

TABLE 7-20. Summary of U.S. Geological Survey 1979 Surface Water Quality Data for Columbia River Tributaries. (Sheet 3 of 4)

Quality parameter/group	Units	Yakima River at Kiona				Snake River at Burbank				Walla Walla River Near Touchet			
		No. of samples	Highest	Lowest	Mean	No. of samples	Highest	Lowest	Mean	No. of samples	Highest	Lowest	Mean
<u>Trace Constituents</u>													
Cadmium, total recoverable	ug/L as Cd	3	1	0	1	3	280	0	94	--	--	--	--
Cadmium, suspended recoverable	ug/L as Cd	3	0	0	0	3	0	0	0	--	--	--	--
Cadmium, dissolved	ug/L as Cd	3	<1	<1	<1	3	300	<1	100	--	--	--	--
Lead, total recoverable	ug/L as Pb	3	22	9	13	3	310	14	134	--	--	--	--
Lead, suspended recoverable	ug/L as Pb	3	22	7	13	3	220	11	102	--	--	--	--
Lead, dissolved	ug/L as Pb	3	2	0	1	3	95	3	34	--	--	--	--
Manganese, total recoverable	ug/L as Mn	4	130	50	78	4	60	20	33	--	--	--	--
Manganese, suspended recoverable	ug/L as Mn	4	120	20	58	4	30	10	23	--	--	--	--
Manganese, dissolved	ug/L as Mn	4	30	9	20	4	30	0	10	--	--	--	--
Mercury, total recoverable	ug/L as Hg	4	0.1	0.0	0.1	4	0.1	0.0	0.1	--	--	--	--
Mercury, suspended recoverable	ug/L as Hg	4	0.1	0.0	0.0	4	0.1	0.0	0.1	--	--	--	--
Mercury, dissolved	ug/L as Hg	4	0.1	0.0	0.0	4	0	0	0	--	--	--	--
Selenium, total	ug/L as Se	4	0	0	0	4	1	0	0	--	--	--	--
Selenium, suspended total	ug/L as Se	4	0	0	0	4	0	0	0	--	--	--	--
Selenium, dissolved	ug/L as Se	4	0	0	0	4	1	0	0	--	--	--	--
Silver, total recoverable	ug/L as Ag	4	0	0	0	4	0	0	0	--	--	--	--
Silver, suspended recoverable	ug/L as Ag	4	0	0	0	4	0	0	0	--	--	--	--
Silver, dissolved	ug/L as Ag	4	0	0	0	4	0	0	0	--	--	--	--
Zinc, total recoverable	ug/L as Zn	4	50	20	28	4	60	10	33	--	--	--	--
Zinc, suspended recoverable	ug/L as Zn	4	50	0	23	4	30	0	15	--	--	--	--
Zinc, dissolved	ug/L as Zn	4	20	<3	<7	4	50	<3	<17	--	--	--	--
<u>Organic Compounds</u>													
PCB, total	ug/L	4	ND	ND	ND	--	--	--	--	--	--	--	--
Aldrin, total	ug/L	4	ND	ND	ND	--	--	--	--	--	--	--	--
Chlordane, total	ug/L	4	ND	ND	ND	--	--	--	--	--	--	--	--
DDO, total	ug/L	4	ND	ND	ND	--	--	--	--	--	--	--	--
DDE, total	ug/L	4	ND	ND	ND	--	--	--	--	--	--	--	--
DDT, total	ug/L	4	ND	ND	ND	--	--	--	--	--	--	--	--
Diazinon, total	ug/L	4	ND	ND	ND	--	--	--	--	--	--	--	--
Dieldrin, total	ug/L	4	ND	ND	ND	--	--	--	--	--	--	--	--
Endrin, total	ug/L	4	ND	ND	ND	--	--	--	--	--	--	--	--
Ethion, total	ug/L	4	ND	ND	ND	--	--	--	--	--	--	--	--
Heptachlor, total	ug/L	4	ND	ND	ND	--	--	--	--	--	--	--	--
Heptachlor epoxide, total	ug/L	4	ND	ND	ND	--	--	--	--	--	--	--	--
Lindane, total	ug/L	4	ND	ND	ND	--	--	--	--	--	--	--	--
Malathion, total	ug/L	4	ND	ND	ND	--	--	--	--	--	--	--	--
Methoxychlor, total	ug/L	4	ND	ND	ND	--	--	--	--	--	--	--	--
Methylparathion, total	ug/L	4	ND	ND	ND	--	--	--	--	--	--	--	--
Methyltrithion, total	ug/L	4	ND	ND	ND	--	--	--	--	--	--	--	--

TABLE 7-20. Summary of U.S. Geological Survey 1979 Surface Water Quality Data for Columbia River Tributaries. (Sheet 4 of 4)

Quality parameter/group	Units	Yakima River at Kiona				Snake River at Burbank				Walla Walla River Near Touchet			
		No. of samples	Highest	Lowest	Mean	No. of samples	Highest	Lowest	Mean	No. of samples	Highest	Lowest	Mean
Organic Compounds													
Parathion, total	ug/L	4	ND	ND	ND	--	--	--	--	--	--	--	--
Toxaphene, total	ug/L	4	ND	ND	ND	--	--	--	--	--	--	--	--
Total trithion	ug/L	4	ND	ND	ND	--	--	--	--	--	--	--	--
Biological													
Biomass													
Periphyton biomass ash weight	g/m ²	3	3.54	0.080	1.81	4	12.1	0.000	3.13	--	--	--	--
Periphyton biomass total dry weight	g/m ²	3	5.04	0.160	2.57	4	19.7	0.000	5.06	--	--	--	--
Chlor-A periphyton chromographic fluorom	mg/m ²	3	10.8	0.140	5.32	4	96.5	0.000	24.15	--	--	--	--
Chlor-B periphyton chromographic fluorom	mg/m ²	3	3.39	0.000	1.65	4	37.8	0.000	9.45	--	--	--	--
Length of exposure	Days	3	38	24	31	4	36	19	26	--	--	--	--
Phytoplankton													
Total count	cells/mL	8	57,000	1,900	3,850	6	1,800	15	504	--	--	--	--
Division, diversity	index (d)	8	1.6	0.1	1.1	6	1.6	0.0	0.6	--	--	--	--
Class, diversity	index (d)	8	1.6	0.1	1.1	6	1.6	0.0	0.6	--	--	--	--
Order, diversity	index (d)	8	1.8	0.0	1.4	6	2.4	0.0	1.0	--	--	--	--
Family, diversity	index (d)	8	2.5	0.0	1.7	6	3.0	0.0	1.4	--	--	--	--
Genus, diversity	index (d)	8	2.7	0.0	2.1	6	2.6	0.0	1.9	--	--	--	--
Bacteria													
Coliform, fecal 0.7 IM-MF	colonies/100 mL	12	220	17	61	11	K*1,200	<1	K112	--	--	--	--
Streptococci, fecal KE AGAR	colonies/100 mL	12	1,900	3	440	12	79	<1	15	--	--	--	--
Sediment													
Sediment, suspended (instantaneous discharge)	mg/L (ft ³ /s)	2	240 (3,780)	66 (3,660)	153 (3,720)	11	60 (51,800)	2 (71,600)	1,318 (49,200)	--	--	--	--
Sediment, discharge suspended (instantaneous discharge)	tonnes/day (m ³ /s) tons/day (ft ³ /s)	2	2,222 (107) 2,450 (3,780)	591 (104) 652 (3,660)	1,407 (105) 1,551 (3,720)	11	7,611 (46,990) 8,390 (51,800)	41 (238) 45 (8,400)	1,722 (1,393) 1,899 (49,200)	--	--	--	--
Sediment, suspended (fall diameter <0.002 mm)	Percent	2	29	29	29	--	--	--	--	--	--	--	--
Sediment, suspended (fall diameter <0.004 mm)	Percent	2	52	35	44	--	--	--	--	--	--	--	--
Sediment, suspended (fall diameter <0.008 mm)	Percent	2	69	48	59	--	--	--	--	--	--	--	--
Sediment, suspended (fall diameter <0.016 mm)	Percent	2	80	66	73	--	--	--	--	--	--	--	--
Sediment, suspended (fall diameter <0.031 mm)	Percent	2	87	83	85	--	--	--	--	--	--	--	--
Sediment, suspended (fall diameter <0.062 mm)	Percent	2	90	85	88	--	--	--	--	--	--	--	--
Sediment, suspended (fall diameter <0.125 mm)	Percent	2	94	90	92	--	--	--	--	--	--	--	--
Sediment, suspended (fall diameter <0.250 mm)	Percent	2	99	95	97	--	--	--	--	--	--	--	--
Sediment, suspended (fall diameter <0.500 mm)	Percent	2	100	99	100	--	--	--	--	--	--	--	--
Sediment, suspended (fall diameter <1.00 mm)	Percent	2	100	--	100	--	--	--	--	--	--	--	--

* Results based upon colony counts outside the ideal range.

In the years following the deposition of insoluble radioactive material on river sediments, periodic increases in river flow rate, caused by operation of large hydroelectric plants upstream and downstream of the Hanford reach, annual freshets, and occasional floods, have resulted in the resuspension and subsequent deposition of some of the material on river shoreline areas above the current normal river water levels. Following the closure in 1971 of the last once-through cooled reactor, the discharge of radioactive materials into the river from Hanford operations decreased to relatively insignificant levels. Since 1971, the radionuclide burden of the sediments and exposed shoreline areas downstream of the reactor sites has been decreasing, as the radioactive materials deposited in these areas decay.

A recent, extensive radiological survey documents the magnitude and distribution of contamination on the riverbank, broad floodplains, low-lying peninsulas, sloughs, and islands along the Hanford reach and downstream to the confluence of the Columbia and Snake Rivers (Sula, 1980). Contamination on these exposed areas was found to be present in three different distributions:

- A fairly constant, uniformly distributed layer of contamination was observed over the entire study area. The average exposure rate over the area measured 11 ± 3 microroentgens per hour compared to a background exposure rate measured along the shoreline upstream of the Hanford Site of 7 ± 1 microroentgens per hour.
- Ninety-two areas were located in which exposure rate readings exceeded 25 microroentgens per hour. These areas of increased radiation levels are attributed to contaminated sediments that have been concentrated in some places by river action and are referred to as "contamination deposits." The areas ranged in size from a few square meters to several thousand square meters and were usually located in areas of dense vegetation. Areas found to contain the highest levels of river deposited contamination were the White Bluffs slough area, where exposure rates reached 40 microroentgens per hour; the Hanford townsite peninsula, in which an area reading of 45 microroentgens per hour was identified; and Island-344 near the 300 Area, which read 38 microroentgens per hour. The remaining "contamination deposits" were in the 25 to 30 microroentgen-per-hour range and appeared to be evenly distributed over the survey area. Samples of soil and vegetation taken at several sites along the river showed the "contamination deposits" to consist of a mixture of ^{60}Co , ^{137}Cs and ^{152}Eu in approximately equal proportions.
- Discrete particles of contamination containing ^{60}Co were found along the river, usually in flat, rocky areas with little or no vegetation. The particles were observed to be metallic flakes, possibly fragments from cooling system components of the production reactors. Fourteen of the particles were recovered. These particles were found at depths from 0 to 13 centimeters (0 to 5 inches) below the surface and contained from 1.7 to 24 microcuries of ^{60}Co activity.

External dose rates from the uniformly distributed contamination and the "contamination deposit" types of contamination are below applicable external radiation protection dose limits for uncontrolled areas.

A period of high river runoff in the late 1960s resulted in extensive upstream scouring of the river bottom that released predeposited radioactivity from the stretch of free-flowing river between Hanford and Richland, resulting in increased radionuclide levels being transported to the McNary Reservoir downstream. Results of a recent study of these McNary Reservoir sediments have shown that the short- and intermediate-lived radionuclides have now decayed to insignificant levels, and only a few long-lived radionuclides (i.e., ^{54}Mn , ^{55}Fe , ^{60}Co , ^{137}Cs , $^{152-154}\text{Eu}$, ^{238}Pu , $^{239-240}\text{Pu}$, and ^{241}Am) at trace concentrations remain buried in the sediment deposits of the reservoir below the reactor sites (Sula, 1980). The surface sediments contain much lower radionuclide concentrations than deeper sediments because of the buildup of 40 to 80 centimeters (16 to 32 inches) of fresh, relatively uncontaminated new sediments since shutdown of the last once-through-cooled Hanford reactor in 1971. The naturally occurring ^{40}K now accounts for over 48 percent of the total activity of the surface sediments. The ^{137}Cs , ^{238}Pu , $^{239-240}\text{Pu}$, and ^{241}Am concentrations in McNary Reservoir sediments are typical of the fallout "background" levels observed in sediments collected upriver from Hanford.

A large body of literature, abstracted by Becker (1973), has reported the results of radioecological studies of the Columbia River. Many of the studies report the accumulation and loss of radionuclides by biota, with most data concerning the pre-1971 time period. A recent report (Cushing et al., 1980) documents the decline of the body burdens of radionuclides, in the biota of the river ecosystem, after shutdown of the Hanford reactors containing once-through cooling systems. The data showed that the measurable body burdens of fission-produced radionuclides decreased to essentially undetectable levels (at or below "background") within 18 to 24 months after cessation of discharge from the once-through cooling systems in January 1971. This trend was especially evident for the free-flowing Hanford reach of the river.

The unconfined aquifer (Chapter 5) beneath the Hanford Site discharges groundwater into the Columbia River at an estimated flow rate of 2.8 cubic meters (100 cubic feet) per second (Eddy et al., 1978). Some portions of this groundwater flow represent tritium (^3H) contaminated plumes resulting from waste water discharge to the ground by operations on the Site (Eddy and Wilbur, 1980). The leading edges of these plumes reaching the river are contaminated at levels of 30 to 300 picocuries of tritium per milliliter. Tritium discharges from the N Reactor averaging approximately 200 curies per year are also added to the river's flow (Greager, 1980). However, identical analyses performed on samples taken upstream and downstream from the Hanford Site show that there is no apparent, statistically significant difference between upstream and downstream concentrations of tritium. This fact is, no doubt, attributable to the large (1,000 times) dilution of the groundwaters and cooling effluents discharging to the Columbia River, coupled with the extremely low concentrations of tritium present within them.

7.4.3.2 Yakima River. The Yakima River is a small river with annual flow rates between 36.8 and 567 cubic meters (1,300 and 20,000 cubic feet) per second. It is not subject to water withdrawal or disposal from Hanford operations. Its entrance into the Columbia River at Richland diverts the main Columbia flow away from the southern shore between the mouth of the Yakima River and Kennewick. Downstream from Horn Rapids, where it first skirts the Hanford Site, the Yakima River loses water continually through its bed and banks until it joins the Columbia River (ERDA, 1975).

Other than some minimal additions of groundwater carrying nitrate ions at concentrations of 5.1 to 10.0 milligrams per liter via the unconfined aquifer (Eddy and Wilbur, 1980), no contamination resulting from Hanford operations has been found to reach the Yakima River.

7.5 SUMMARY OF UNRESOLVED ISSUES

No items relating to the scope of technical discussion presented within this chapter are considered to be unresolved. The hydrologic data base used in preparation of this chapter is based on ongoing data-gathering programs carried out directly by or with support from federal and state agencies. Preparation of Site Characterization Report revisions will make use of new data as they become available.

7.6 REFERENCES

- Beak, 1980, "Preoperational Environmental Monitoring Studies Near WNP 1, 2, and 4, August 1978 through March 1980," WPPSS Columbia Ecology Studies, Volume 7, Beak Consultants, Incorporated for Washington Public Power Supply System, Inc., Richland, Washington.
- Becker, C. D., 1973, Aquatic Bioenvironmental Studies of the Columbia River at Hanford, 1945-1971: A Bibliography with Abstracts, BNWL-1734 Battelle, Pacific Northwest Laboratories, Richland, Washington.
- Bell, N. M. and Leonhart, L. S., 1980, A Preliminary Evaluation of Water Resource Development and Potential Within the Pasco Basin, RHO-BWI-LD-33, Rockwell Hanford Operations, Richland, Washington, November 1980.
- COE, 1951, Artificial Flood Possibilities on the Columbia River, U.S. Army Corps of Engineers, Washington District, Washington, D.C.
- COE, 1969, Lower Columbia River Standard Project Flood and Probable Maximum Flood, U.S. Army Corps of Engineers, North Pacific Division, Portland, Oregon.
- COE, 1976, Power Pondage Studies, CRT-3Q, U.S. Army Corps of Engineers, North Pacific Division, Portland, Oregon.
- COE, 1977, Reach Inventory, Columbia River Headwater McNary Reservoir to Grand Coulee Dam, CRT-34, U.S. Army Corps of Engineers, North Pacific Division, Portland, Oregon.
- Cummins, J. E., Collings, M. R., and Nassar, E. G., 1975, Magnitude and Frequency of Floods in Washington, Open-File Report 74-336, U.S. Geological Survey, Tacoma, Washington.
- Cushing, C. E., Watson, D. G., Robertson, D. E., and Silker, W. B., 1974, Decline of Radioactivity in the Columbia River - McNary Reservoir Ecosystem Following Shutdown of Hanford Reactors, BNWL-1850, Pt. 2, Battelle, Pacific Northwest Laboratories, Richland, Washington, pp. 84-88.
- Cushing, C. E., Watson, D. G., Scott, A. J., and Gurtisen, J. M., 1980, Decline of Radionuclides in Columbia River Biota, PNL-3269, Pacific Northwest Laboratory, Richland, Washington.
- Dauble, D. D., 1980, Ecology and Use of the Mid-Columbia River, BN-SA-1073, Battelle, Pacific Northwest Laboratories, Richland, Washington.
- Dion, N. P. and Lum, W. E., II, 1977, Municipal, Industrial, and Irrigation Water Use in Washington, 1975, Open-File Report 77-308, U.S. Geological Survey, Tacoma, Washington.

Eddy, P. A., Myer, D. A., and Raymond, J. R., 1978, Vertical Contamination in the Unconfined Ground Water at the Hanford Site, Washington, PNL-2724, Pacific Northwest Laboratory, Richland, Washington.

Eddy, P. A. and Wilbur, J. S., 1980, Radiological Status of the Ground-water Beneath the Hanford Site, January-December 1979, PNL-3346, Pacific Northwest Laboratory, Richland, Washington.

ERDA, 1975, Final Environmental Statement - Waste Management Operations, Hanford Reservation, Richland Washington, ERDA-1538, 2 Volumes, U.S. Energy Research and Development Administration, Washington, D.C., December 1975.

ERDA, 1976, Evaluation of Impact of Potential Flooding Criteria on the Hanford Project, RLO-76-4, Richland Operations Office, U.S. Energy Research and Development Administration, Richland, Washington.

FEMA, 1980, Flood Insurance Study: Benton County, Washington, Federal Emergency Management Agency, Federal Insurance Administration, Washington D.C.

Gephart, R. E., Eddy, P. A., Arnett, R. C., and Robinson, G. A., 1976, Geohydrologic Study of the West Lake Basin, ARH-CD-775, Atlantic Richfield Hanford Company, Richland, Washington, October 1979.

Gephart, R. E., Arnett, R. C., Baca, R. G., Leonhart, L. S., Spane, F. A. Jr., 1979, Hydrologic Studies Within the Columbia Plateau, Washington: An Integration of Current Knowledge, RHO-BWI-ST-5, Rockwell Hanford Operations, Richland, Washington, October 1979.

Glenn, J. L. and Van Atta, R. O., 1973, Relations Among Radionuclide Content and Physical, Chemical and Mineral Characteristics of Columbia River Sediments, Geological Survey Professional Paper 433-M, U.S. Geological Survey, Washington, D.C.

Grant, 1980, Priest Rapids Dam Statistical Data, Grant County Public Utility District, Ephrata, Washington.

Gray, R. H. and Dauble, D. D., 1976, Checklist and Relative Abundance of Fish Species from the Hanford Reach of the Columbia River, BN-SA-536, Battelle, Pacific Northwest Laboratories, Richland, Washington.

Gray, R. H. and Page, T. L., 1977, "Aquatic Ecological Studies Near WNP 1, 2, and 4, September 1975 through March 1976," WPPSS Columbia River Ecology Studies, Volume 3, Battelle, Pacific Northwest Laboratories under contract to United Engineers and Constructors, Inc. for Washington Public Power Supply System, Inc., Richland, Washington.

Gray, R. H. and Page, T. L., 1978, "Aquatic Ecological Studies Near WNP 1, 2, and 4, March through December 1976," WPPSS Columbia River Ecology Studies, Volume 4, Battelle, Pacific Northwest Laboratories under contract to United Engineers and Constructors, Inc. for Washington Public Power Supply System, Inc., Richland, Washington.

Gray, R. H. and Page, T. L., 1979a, "Aquatic Ecological Studies Near WNP 1, 2, and 4, January through December 1977," WPPSS Columbia River Ecology Studies, Volume 5, Battelle, Pacific Northwest Laboratories for Washington Public Power Supply System, Inc., Richland, Washington.

Gray, R. H. and Page, T. L., 1979b, "Aquatic Ecological Studies Near WNP 1, 2, and 4, January through December 1977," WPPSS Columbia River Ecology Studies, Volume 6, Battelle, Pacific Northwest Laboratories for Washington Public Power Supply System, Inc., Richland, Washington.

Gray, R. H., Page, T. L., and Wolf, E. G., 1976, "Aquatic Ecological Studies Near WNP 1, 2, and 4, September 1974 through September 1975," WPPSS Columbia River Ecology Studies, Volume 2, Battelle, Pacific Northwest Laboratories under contract to United Engineers and Constructors, Inc., for Washington Public Power Supply System, Inc., Richland, Washington.

Greager, E. M., 1980, United Nuclear Industries, Inc., Reactor and Fuels Production Facilities, 1979 Effluent Release Report, United Nuclear Industries, Richland, Washington.

Habbell, D. W. and Glenn J. L., 1971, Distribution of Radionuclides in Bottom Sediments of the Columbia River Estuary, Open-File Report (TID-25724), Water Resources Division, U.S. Geological Survey, Portland, Oregon.

Harty, H., 1979, The Effects of the Ben Franklin Dam on the Hanford Site, PNL-2821, Pacific Northwest Laboratory, Richland, Washington.

Haushild, W. L., Stevens, H. H., Jr., Nelson, J. L., and Dempster, G. R., Jr., 1971, Radionuclides in Transport in the Columbia River From Pasco to Vancouver, Washington, Open-File Report (TID-25894), Water Resources Division, U.S. Geological Survey, Portland, Oregon.

Leaming, G. F., 1981, An Evaluation of Water Resource Economics Within the Pasco Basin, RHO-BWI-C-121, Rockwell Hanford Operations, Richland, Washington, September 30, 1981.

Leonhart, L. S., 1979, Surface Hydrologic Investigations of the Columbia Plateau Region, Washington, RHO-BWI-ST-6, Rockwell Hanford Operations, Richland, Washington, July 23, 1979.

Leonhart, L. S., 1980, Assessment of the Effects of Existing Major Dams Upon a Radioactive Waste Repository Within the Hanford Site, RHO-BWI-LD-26, Rockwell Hanford Operations, Richland, Washington, June 1980.

Neitzel, D. A., Page, T. L., and Hanf, R. W., Jr., 1981, Mid Columbia River Zooplankton, BN-SA-1351, Battelle, Pacific Northwest Laboratories, Richland, Washington.

Nelson, J. L. and Haushild, W. L., 1970, "Accumulation of Radionuclides in Bed Sediments of the Columbia River Between the Hanford Reactors and McNary Dam," Water Resources Research, Vol. 6, pp. 130-137.

NRC, 1981, "Nuclear Regulatory Commission, 10 CFR 60, Disposal of High-Level Radioactive Wastes in Geologic Repositories," Federal Register, Vol. 46, No. 130, July 8, 1981, Proposed Rules.

Page, T. L., Gray, R. H., and Wolf, E. G., 1976, "Final Report on Aquatic Ecological Studies Conducted at the Hanford Generating Project, 1973-1974," WPPSS Columbia River Ecology Studies, Volume 1, Battelle, Pacific Northwest Laboratories under contract to United Engineers and Constructors, Inc. for Washington Public Power Supply System, Inc., Richland, Washington.

Perkins, R. W., Nelson, J. L., and Haushild, W. L., 1966, "Behavior and Transport of Radionuclides in the Columbia River Between Hanford and Vancouver, Washington," Limnology and Oceanography, Vol. 11, pp. 235-248.

PNL, 1967, The Effects of Ben Franklin Dam on Hanford, BNWL-412, Battelle, Pacific Northwest Laboratories, Richland, Washington.

Rickard, W. H., Hanson, W. C., and Fitzner, R. E., 1980, The Non-Fisheries Biological Resource of the Hanford Reach of the Columbia River, PNL-SA-8423, Pacific Northwest Laboratory, Richland, Washington.

Robertson, D. E. and Fix, J. J., 1977, Association of Hanford Origin Radionuclides With Columbia River Sediment, BNWL-2305, Battelle, Pacific Northwest Laboratories, Richland, Washington.

Robertson, D. E., Silker, W. B., Langford, J. C., Petersen, M. R., and Perkins, R. W., 1973, "Transport and Depletion of Radionuclides in the Columbia River," in Radioactive Contamination of the Marine Environment -- Proceedings of a Symposium, Seattle, July 10-14, 1972, International Atomic Energy Agency, Vienna, Austria.

Sula, M. J., 1980, Radiological Survey of Exposed Shorelines and Islands of the Columbia River Between Vernita and the Snake River Confluence, PNL-3127, Pacific Northwest Laboratory, Richland, Washington.

Sula, M. J. and Blumer, P. J., 1981, Environmental Surveillance at Hanford for CY-1980, PNL-3728, Pacific Northwest Laboratory, Richland, Washington.

Toombs, G. L., 1966, Lower Columbia River Environmental Survey in Oregon, Division of Sanitation and Engineering, Oregon State Board of Health, Portland, Oregon.

USGS, 1980, Water Resources Data for Washington, Volume 2, Eastern Washington, (Water Year 1979), WA-79-2, U.S. Geological Survey, Tacoma, Washington.

WAC, 1978, "Chapter 173-201, Water Quality Standards for Waters of the State of Washington," Washington Administrative Code, Olympia, Washington.

Wildung, R. E., Routson, R. C., and Schmidt, R. L., 1972, Seasonal Changes in Particle Size Distribution, Composition, and Strontium Exchange Capacity of Particulate Matter Suspended in the Columbia River, BNWL-1638, Battelle, Pacific Northwest Laboratories, Richland, Washington.

Wolcott, E. E., 1973, Lakes of Washington, Volume II, Eastern Washington, Washington State Department of Ecology, Olympia, Washington.

WPPSS, 1981, Final Safety Analysis Report: WPPSS Nuclear Project No. 2, Washington Public Power Supply System, Inc., Richland, Washington.

Wukelic, G. E., Foote, H. P., Blair, S. C., and Begej, C. D., 1981, Monitoring Land and Water-Use Dynamics in the Columbia Plateau Using Remote-Sensing Computer Analysis and Integration Techniques, RHO-BW-CR-122 P/PNL-4047, Pacific Northwest Laboratory for Rockwell Hanford Operations, Richland, Washington.

8. CLIMATOLOGY, METEOROLOGY, AND AIR QUALITY

8.1 RECENT CLIMATE AND METEOROLOGY

8.1.1 General Climate of the Region

The Basalt Waste Isolation Project (BWIP) reference repository location for a nuclear waste repository in basalt is situated in the Pasco Basin in south-central Washington State (Fig. 8-1). Climatologically, the Hanford Site and surrounding region are classified as a midlatitude semiarid desert, with cool, wet winters. Summers are normally sunny, warm, and dry. Winters are mild with occasional fog episodes. In the winter, Pacific storm systems move eastward through the region causing frequent changes in cloudiness, wind, pressure, and precipitation events. Occasionally, an outbreak of cold modified arctic air will result in low temperatures (less than -18°C) in the region.

The Hanford region is influenced by several different types of air masses. Generally, these are maritime polar, continental polar and arctic, continental tropical and, on rare occasions, modified maritime tropical. In all cases these air masses have undergone some modification due to topography and travel over land. In the winter, cold or occluded fronts that pass through or over the region are associated with maritime polar, continental polar, or arctic air masses. Warm fronts often occur in the winter, due to relatively warmer maritime polar air flowing over colder continental polar air entrapped in the lower elevations.

In the warmer months, cold frontal passages are fewer and weaker, since subtropical oceanic high-pressure areas reach their highest latitudes then, thereby diverting cyclonic and frontal storms poleward. On the eastern margin of the Pacific high-pressure area, stable subsiding air brings distinctly drier conditions to the Hanford region. Upper-level cold lows have a tendency to develop during the cool season and cause a variety of weather types for the area. Cold lows situated in Oregon can cause rather wet periods. Persistent upper-level high-pressure ridges often occur over the Hanford region. This synoptic pattern contributes to the aridity of the area and also results in persistent stagnation episodes during the winter months.

The climate of the Hanford region is greatly influenced by the surrounding topography. Directly to the west and south of the reference repository location are the Yakima and Rattlesnake Ridges (Fig. 8-1). To the north are the Saddle Mountains and farther to the west the Cascade Range. These topographic features have a significant effect on precipitation, winds, and temperatures. The Hanford area is in the rain shadow of the Cascade Range, which contributes significantly to the relatively low rainfall (15 to 18 centimeters). The Rocky Mountains and other mountain ranges to the north, northeast, and east in Washington, Idaho, Montana, and British Columbia are effective in protecting the area from

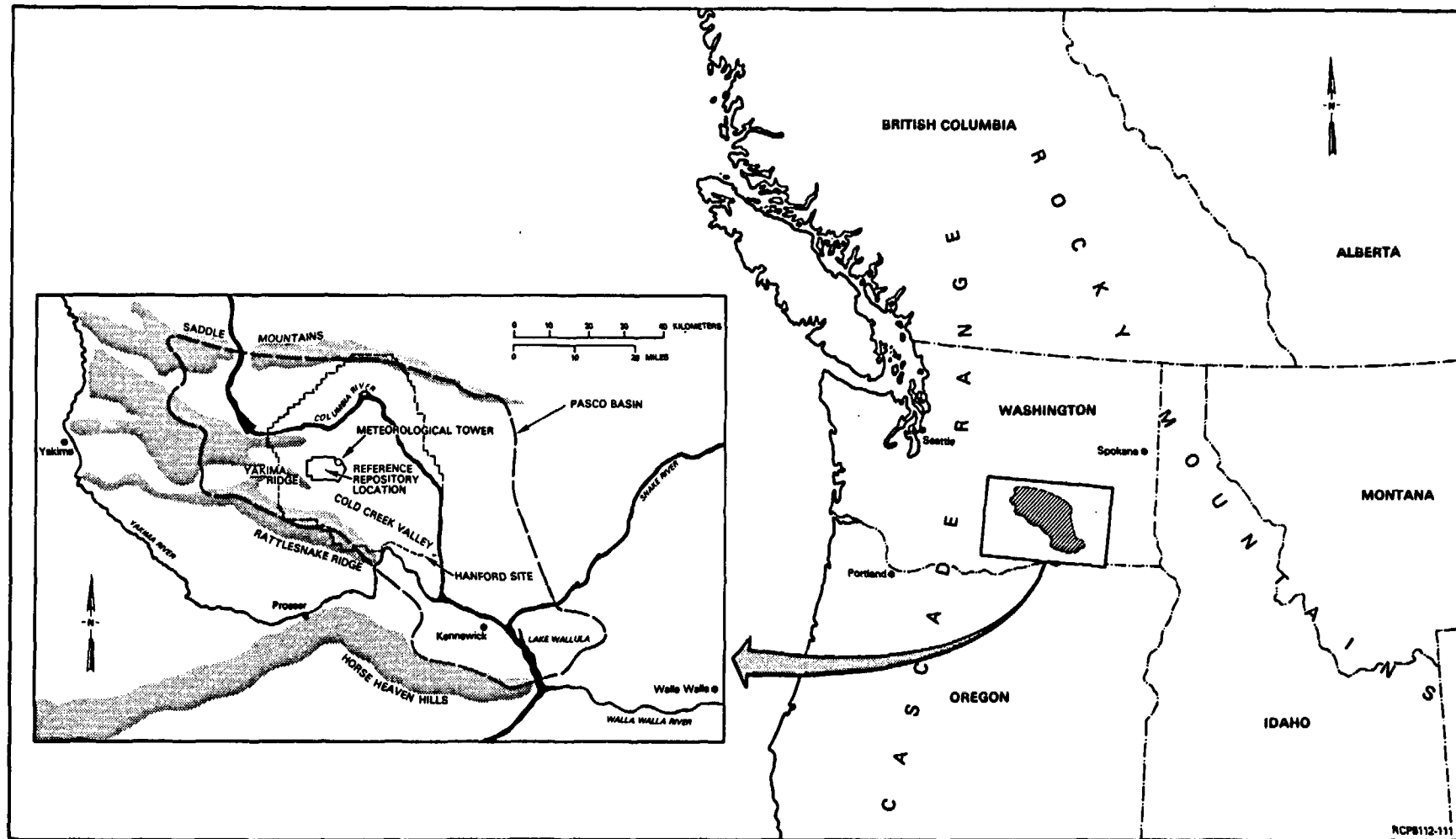


FIGURE 8-1. The Hanford Site in Relation to Surrounding Terrain.

the more severe winter storms and low temperatures associated with the modified arctic air masses that move southward through Canada. Occasionally, an outbreak of cold modified arctic or continental polar air will settle over the area, resulting in subzero temperatures in the winter and damaging spring or fall frosts. The location of the Hanford region with respect to topography results in a continental-type climate, since the Cascades to the west generally block the maritime influence of the ocean except through topographic channeling and during synoptic storms. The continental-type climate not only affects precipitation in the region but also results in wide ranges and variations in temperature.

The general surface airflow patterns surrounding the reference repository location are significantly influenced by the local topography. The prevailing wind near the site is from the northwest to the southwest quadrants, but local topographic features and diurnal wind circulations produce a significant degree of variability in winds at other locations in and near the Hanford region (ERDA, 1975) as seen in Figure 8-2. Two examples of nonfrontal windflow patterns associated with contrasting synoptic pressure features are shown in Figures 8-3 and 8-4, which are cases with high pressure to the east and to the west of the region, respectively. The variation in wind direction over the region can be explained, to a large extent, by topographic diverting and channeling effects (Elliott et al., 1976).

In general, the Hanford region experiences high (greater than 10 meters per second) and gusty winds due to frontal passages, squall lines, thunderstorms, and strong pressure gradients. Extreme high winds vary with location. Gusts as high as 36 meters per second have been observed near the site but speeds of 15 to 30 meters per second are more common. In winter, a chinook (warm and dry) wind from the southwest can result in a sudden large temperature rise (11°C per hour), rapid melting of snow (if present), and strong gusty winds in the Hanford region. During the spring, summer, and fall, strong and gusty winds usually result in periods of dust from suspended soil and sand.

Periods of relatively low windspeed are also part of the Hanford region wind regime. The average frequency of hourly average windspeeds in the 0- to 2-meter-per-second speed class is approximately 38 percent during the winter period and 16 percent for the warmer period. Most fog in the region occurs in conjunction with low windspeeds (73 percent with speeds of 2 meters per second or less).

There is a marked diurnal range of windspeed near the site, especially during the summer months. In July, for example, hourly average windspeeds range from 2.3 meters per second at 9 to 10 a.m. to over 5.8 meters per second at 9 to 10 p.m. In contrast, the corresponding speeds in January are 2.5 and 2.9 meters per second, respectively. These warm-season diurnal winds are apparently the result of an inertial oscillation in the winds, associated with an inland progression of modified marine air, and possibly some drainage winds from the Cascades and surrounding terrain. Although these winds occur regularly in the summer, they are seldom gusty unless reinforced by frontal activity or strong pressure gradients between the coastal region and the Hanford area. In June, the month of highest average speed, there are fewer instances of hourly averages exceeding 14 meters per second than in December, the month of lowest average speed.

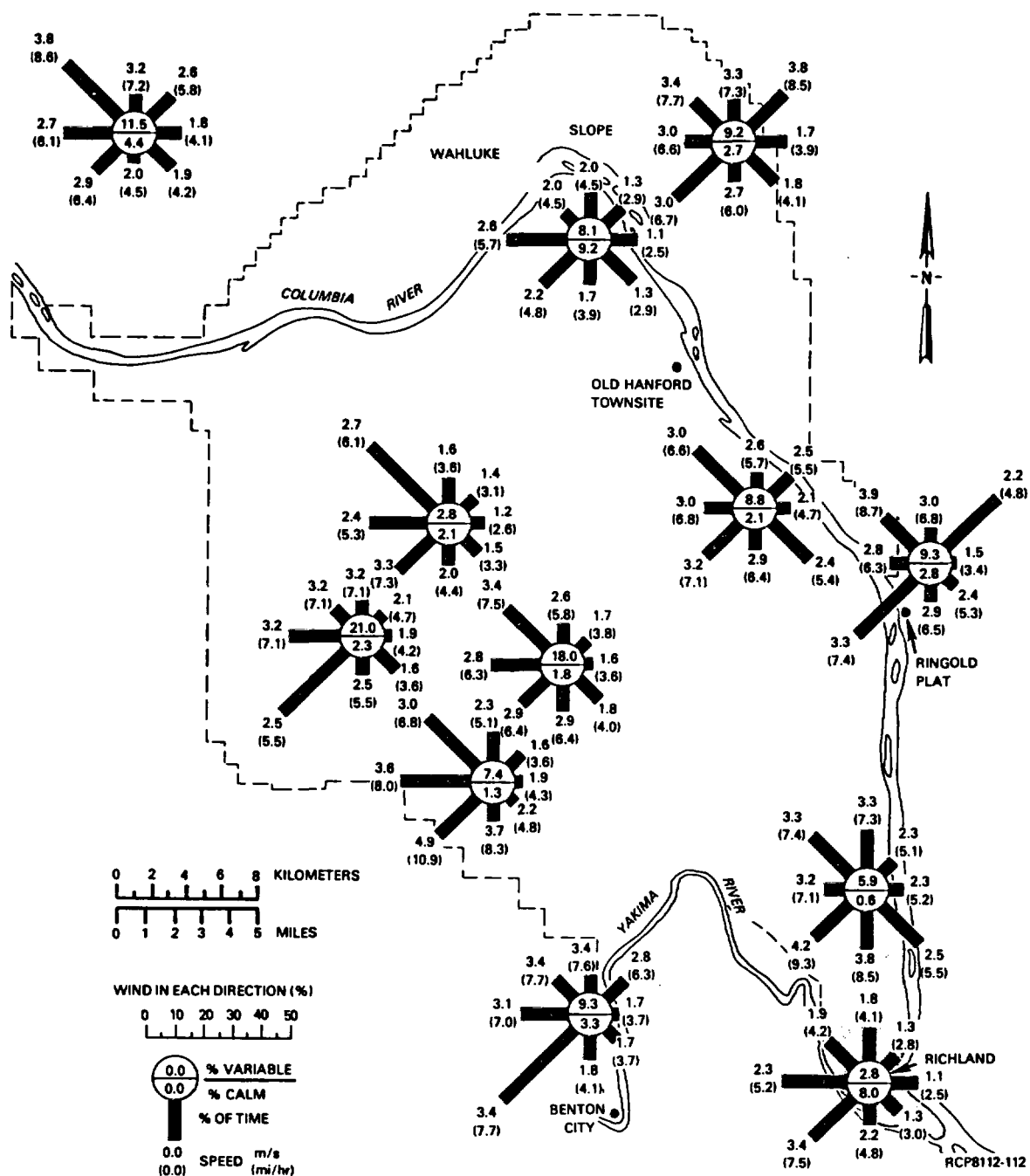


FIGURE 8-2. Surface-Wind Roses for Various Locations on and Surrounding the Hanford Site, Based on 5-Year Averages, 1952-1956. The points of each rose represent the directions from which the winds come.

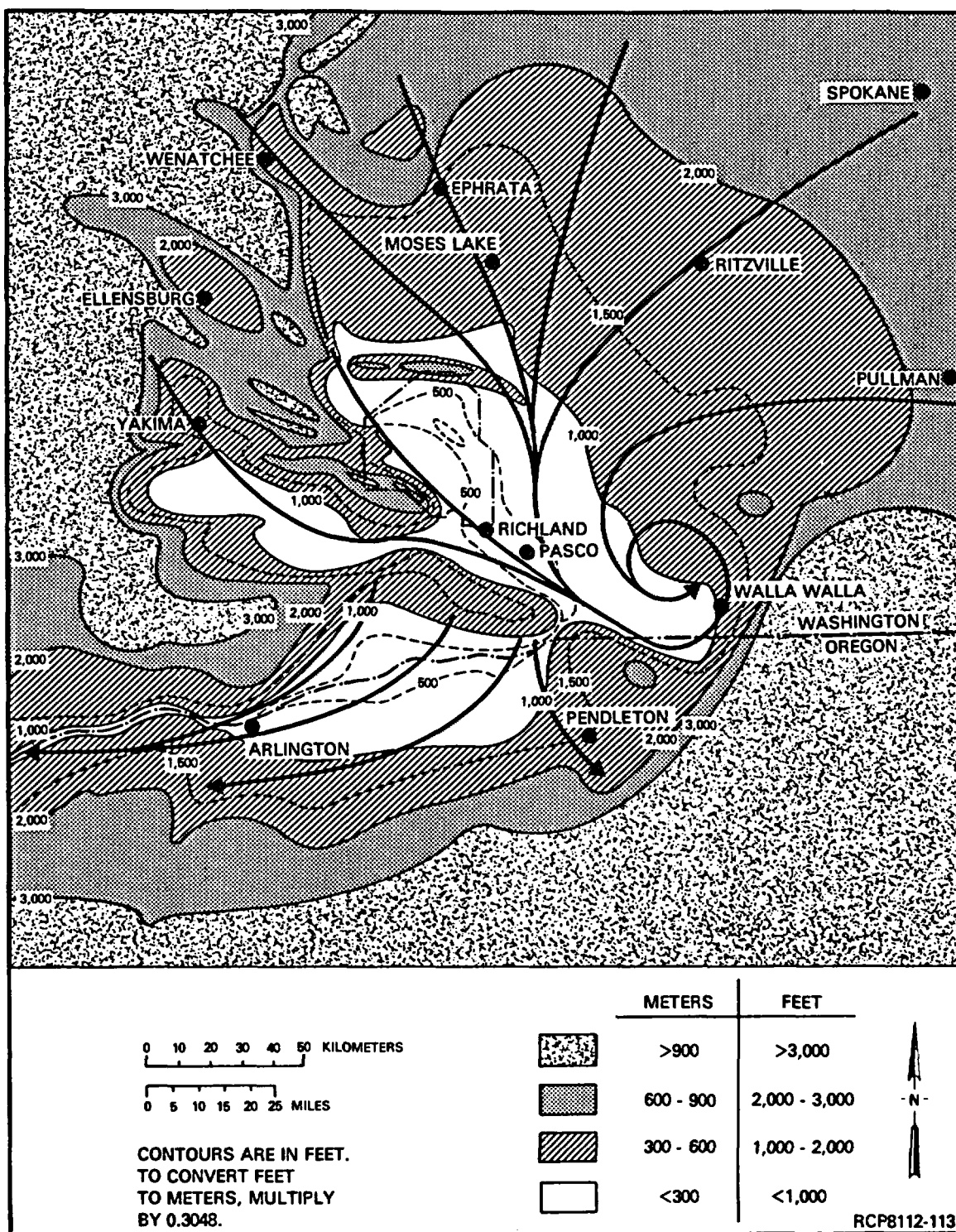


FIGURE 8-3. Schematic Flow Pattern Associated with a Surface High Centered East of the Region.

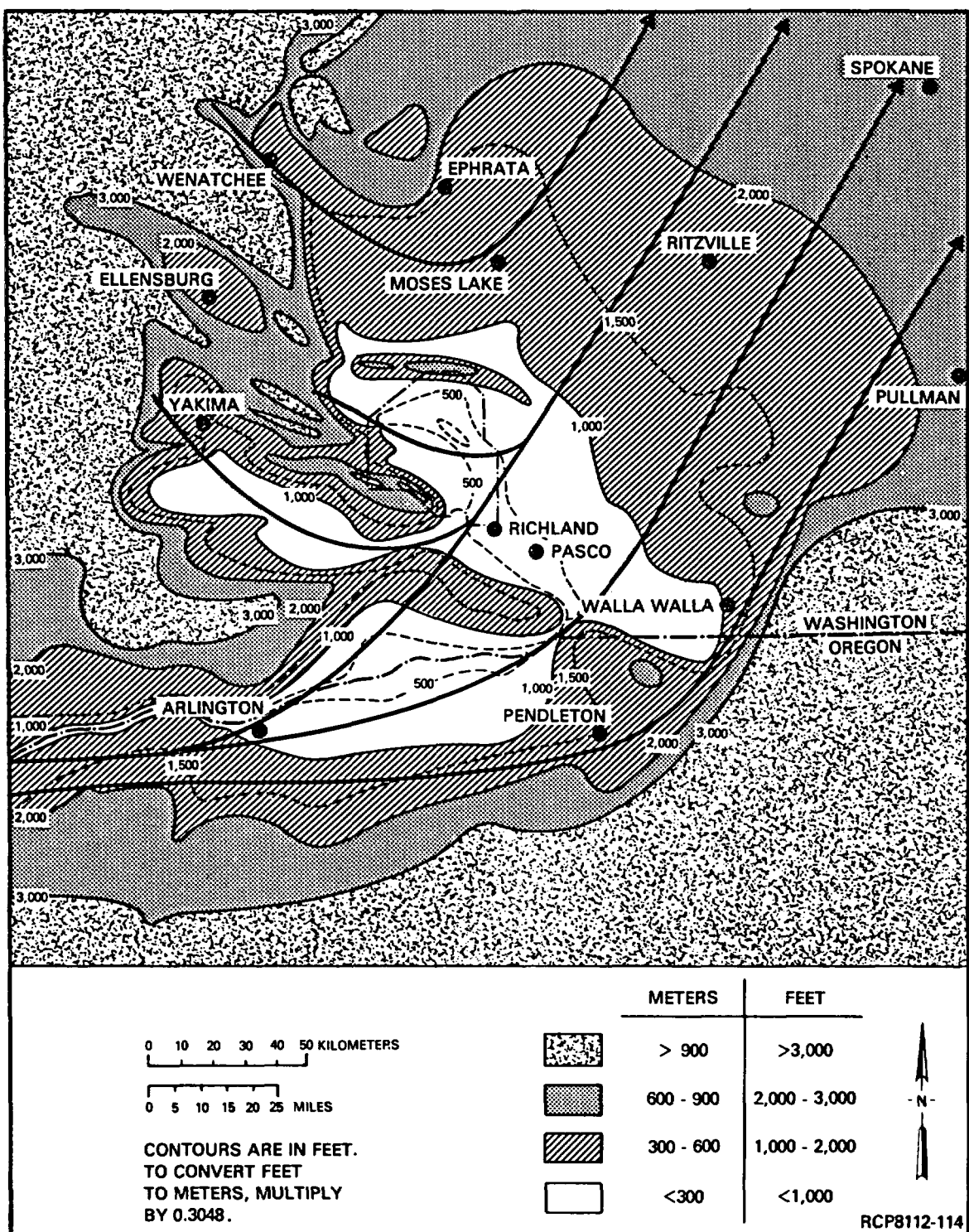


FIGURE 8-4. Schematic Flow Pattern Typically Associated with High Pressure to the West and Low Pressure to the East of the Region.

Further detail on the general climate of the Hanford region is available from the long-term climatic data collected at the Hanford Meteorological Station (Stone et al., 1972). Other important sources of climatic data and analyses include the Hanford Site and the Washington Public Power Supply System, Inc. Nuclear Plant No. 2 Environmental Reports (ERDA, 1975; WPPSS, 1979) and special meteorological studies carried out at the Hanford Site (Elliott et al., 1975; 1976).

8.1.2 Sources of Regional and Local Climate Information

Meteorological data have been collected in the Hanford area since 1912. From 1912 to 1945 data were collected by cooperative observers from the U.S. Weather Bureau near the Hanford Site. This site is 16 kilometers east-northeast of the Hanford Meteorological Station, where data have been routinely collected since 1945. Stone et al. (1972) combined the data from the U.S. Weather Bureau at Hanford, Washington and the Hanford Meteorological Station to develop a single set of data for the period 1912-1970. Most of the climatic information provided in the next section of this chapter is from Stone et al. (1972). This publication is presently being updated to include the last decade, and where available the updated data have been used.

The Hanford Meteorological Station is located within the reference repository location at an elevation of 223 meters above mean sea level. The Hanford Meteorological Station data should be taken as generally representative of the reference repository location unless otherwise indicated in the following sections. Some local variations in climatic elements (e.g., wind directions and speeds) may be expected within the reference repository location, due to local roughness, and topographic effects.

Climatology records from 1945 to 1980 have been evaluated at the Hanford Meteorological Station. The data include standard 24-hour surface observations* as well as other measurements specifically taken to describe the atmospheric-dispersion climatology of the Hanford area (Section 8.4.1). The continuous monitoring program at the Hanford Meteorological Station includes eight levels of wind measurement and ten levels of air-temperature measurement from a 122-meter steel tower. Surface observations of temperature and humidity are taken about 23 meters northwest of the tower. About 450 meters west of the tower is a pyranometer,** a precipitation gauge, and an instrument shelter with maximum and minimum thermometers. Current (1981) sensor height information for the Hanford Meteorological Station is given in Table 8-1. In 1982, all instruments on the Hanford Meteorological Station tower will be replaced by equipment meeting U.S. Nuclear Regulatory Commission (NRC) guidelines (NRC, 1972; 1980).

*Surface observations were only taken for 16 hours per day between July 1971 and June 1974. No observations are available between 1600 and 2400 Pacific standard time.

**An instrument to measure direct-solar and diffuse-sky radiation.

TABLE 8-1. Instrument Height Locations at the Hanford Meteorological Station.

Measurement	Instrument	Surface (m)				Tower levels (m)							
		0.91	2.1	6.1	9.2*	15.2	30.5	47.7	61.0	76.2	91.5	106.7	122.0
Humidity	Dewcel	X											
Windspeed and direction	Aerovane		X		X	X	X	X	X	X	X		X
Air temperature	Thermohm			X	X	X	X	X	X	X	X	X	X

*To be installed in 1982.

At the Hanford Meteorological Station, upper-level wind measurements have been made by the single theodolite pilot-balloon method for over 25 years. Data are presently taken twice daily at 1200 (noon) and 2400 (midnight) Pacific standard time. Some of these observations have been summarized for climatological and case study purposes. No rawinsonde data (temperature, dew point, and winds versus pressure) are taken on a routine basis although a Pacific Northwest Laboratory rawinsonde is available for taking upper-level soundings.

A monostatic acoustic radar has been operating at the Hanford Meteorological Station since 1975 for the purpose of continuously monitoring small-scale temperature and turbulence structure associated with wind shear and convective motion. Mixing-layer depths, breakup and formation of temperature inversions, and characteristics of low-altitude gravity waves are some of the physical phenomena that can be monitored by this instrument system.

The Hanford Meteorological Station and existing climatological record are supported by several supplemental meteorological monitoring systems (ERDA, 1975):

- Hanford Radio-Telemetered Automatic Weather-Station System--A ten station* network of radio-telemetered automatic weather stations operated primarily as a real-time information base for accident-assessment capabilities (1958 to present). Data have been and can be used for spatial analysis of wind fields in the Hanford area.
- Arid Lands Ecology Reserve Climatology System--A network of soil temperature, air temperature, relative humidity, and precipitation stations set up for climatological and ecological purposes (1968 to present).
- N Reactor Meteorological Tower System--A remote station with a 91.4-meter tower containing wind and temperature sensors. Data collection has been sporadic since 1967. A 9.1-meter tower with sensors is part of the Hanford weather station telemetry network (1979 to present). The initial purpose of the 91.4-meter tower was to provide meteorological data for the N Reactor site.
- Washington Public Power Supply System, Inc. Nuclear Plant No. 2 Meteorological System--A remote station with a 73.2-meter tower with wind, temperature, and humidity sensors. Data collection periods were April 1974 to March 1976 and October 1979 to present. Earlier data were taken on a 2-meter tower. The purpose of the meteorological data collection is to meet NRC requirements for the Washington Public Power Supply System, Inc. nuclear plant sites. A 9.1-meter tower with sensors is located near the 73.2-meter tower and is part of the Hanford weather station telemetry network.

*The actual number of stations in operation has varied during the history of the facility.

- Fast Flux Test Facility Meteorological System--In 1969, a remote station was installed with a 3.96-meter mast and wind sensors. Data were collected for 2.5 years from 1969 to 1972. At the present time the station consists of a 9.1-meter tower and is part of the Hanford weather station telemetry network.

8.1.3 Specific Climatic Elements

8.1.3.1 Precipitation. The mean annual precipitation at the Hanford Meteorological Station (Table 8-2) is 161 millimeters. Since 1913 the annual total has varied from 76 to 291 millimeters. The 4-month period of November through February contributes 52 percent of the mean annual precipitation, while the 4-month period of March through June contributes 28 percent. The remaining 4 months, July through October, contribute the remaining 20 percent (see Table 8-2). Note that July is the driest month with 3.8 millimeters, followed by a progressive monthly increase to a maximum in January of 23.4 millimeters, followed by a secondary minimum in March of 9.4 millimeters, and then rising again to a secondary maximum in June of 13.7 millimeters.

Snowfall (including sleet or ice pellets) accounts for about 45 percent of all precipitation during the months of December through February. Total seasonal snowfall has varied from 8 to 1,107 millimeters, and the seasonal normal is 335 millimeters. Snowfall can be expected to accumulate to depths on the ground in excess of 152 millimeters only one winter in eight. The record greatest snow depth was 622 millimeters in February 1916.

Precipitation falls an average of 44.2 hours per month with the average monthly maximum occurring in January with 98.8 hours and the minimum occurring in July with 10.7 hours. The greatest monthly total is 212 hours (January 1969), and the least monthly total is 0 hours (August 1955). Based on observed rainfall rates and durations, extreme value statistics (ERDA, 1975) have been derived to determine the return periods of rainfall duration and intensity shown in Figure 8-5 and Table 8-3.

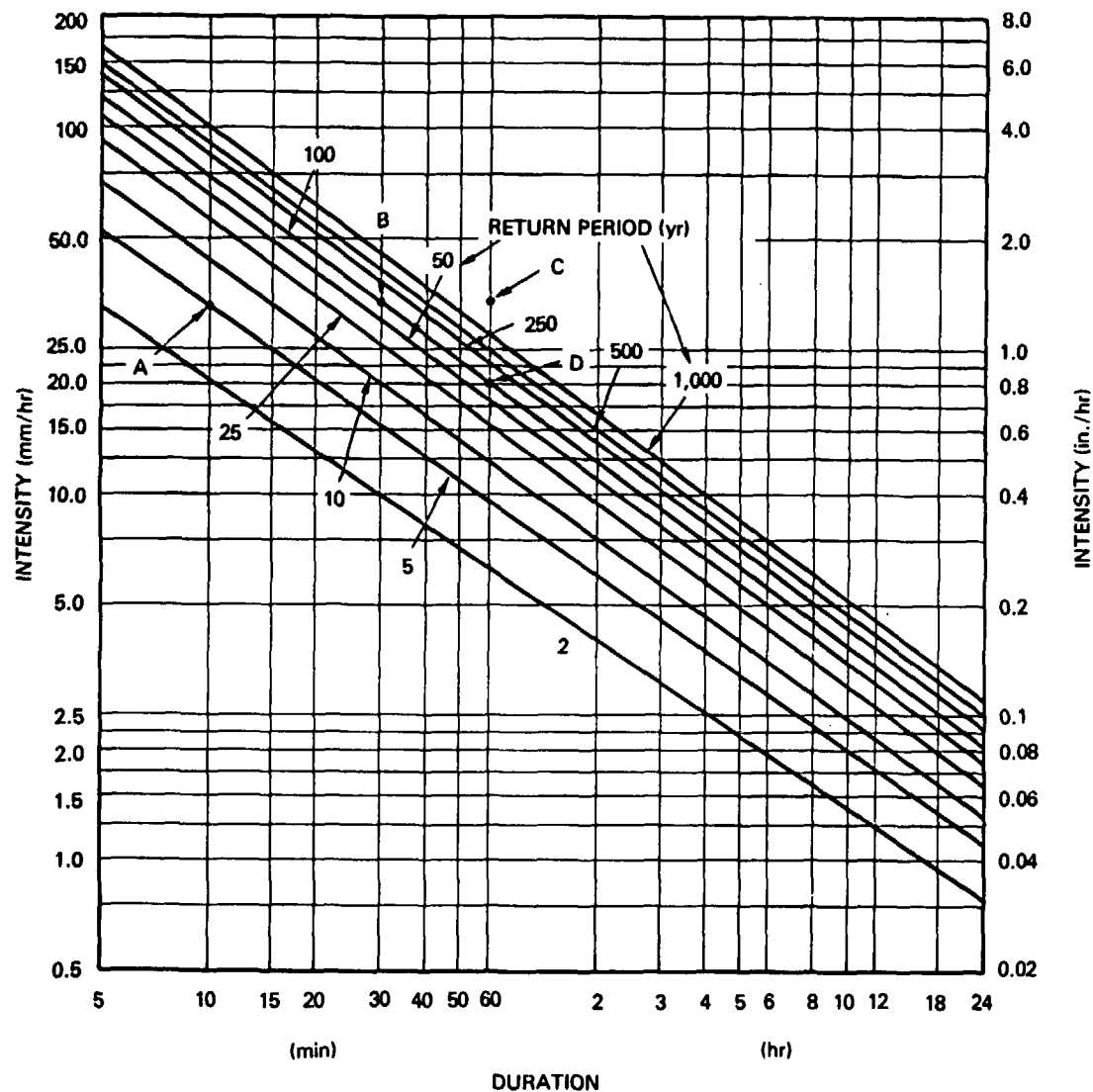
8.1.3.2 Evaporation. Evaporation or evapotranspiration measurements are not made at the Hanford Meteorological Station. The nearest location where routine evaporation measurements are made is the Agricultural Experiment Station at Prosser, Washington, approximately 48 kilometers to the south-southeast (Fig. 8-1). However, a number of special studies have been conducted, and some work is now being done for the Hanford area. Hinds (1975) has made some short-term estimates of evapotranspiration over some of the native grasses, and Pacific Northwest Laboratory (Phillips et al., 1979) has had two weighing lysimeters in operation near the 300 Area since 1979. Routine data on evapotranspiration are not currently available, due to instrument problems.

TABLE 8-2. Averages and Extremes of Precipitation at the Hanford Meteorological Station, 1912-1980.

Month	Precipitation (mm) (in. in parentheses)													
	Mean monthly	Maximum		Maximum		Maximum		Snow, ice pellets (sleet)						
		Monthly	Year	Monthly	Year	In 24 hr	Year	Mean monthly	Maximum		Maximum		Maximum	
									Monthly	Year	In 24 hr	Year	Depth	Year
January	23.4 (0.92)	62.7 (2.47)	1970	2.0 (0.08)	1977	27.4 (1.08)	1948	132 (5.2)	594 (23.4)	1950	180 (7.1)	1954	305 (12.0)	1969
February	15.2 (0.60)	78.2 (3.08)	1940	a	1967	31.5 (1.24)	1916	58 (2.3)	660 (26.0)	1916	457 (18.0)	1916	622 (24.5)	1916
March	9.4 (0.37)	47.2 (1.86)	1957	0	1942 ^b	15.0 (0.59)	1949	8 (0.3)	107 (4.2)	1951	56 (2.2)	1957	58 (2.3)	1957
April	9.9 (0.39)	31.0 (1.22)	1969	0	1933 ^b	14.7 (0.58)	1980	a	a	1968 ^b	a	1968 ^b	0	--
May	12.2 (0.48)	51.6 (2.03)	1972	0	1931	35.3 (1.39)	1972	a	a	1960	a	1960	0	--
June	13.7 (0.54)	74.2 (2.92)	1950	0	1919	38.1 (1.50)	1934	0	0	--	0	--	0	--
July	3.8 (0.15)	20.6 (0.81)	1966	0	1939 ^b	31.7 (1.25)	1942	0	0	--	0	--	0	--
August	6.1 (0.24)	34.5 (1.36)	1977	0	1955 ^b	22.6 (0.89)	1977	0	0	--	0	--	0	--
September	7.9 (0.31)	34.0 (1.34)	1947	a	1976 ^b	20.8 (0.82)	1947	0	0	--	0	--	0	--
October	14.5 (0.57)	69.1 (2.72)	1957	0	1917 ^b	48.5 (1.91)	1957	a	38 (1.5)	1973	38 (1.5)	1973	38 (1.5)	1973
November	21.8 (0.86)	77.5 (3.05)	1926	a	1976 ^b	19.8 (0.78)	1966	36 (1.4)	323 (12.7)	1955	211 (8.3)	1978	231 (9.1)	1978
December	22.9 (0.90)	64.3 (2.53)	1931	2.8 (0.11)	1976 ^b	25.4 (1.00)	1958	102 (4.0)	485.1 (19.1)	1964	137 (5.4)	1965	307 (12.1)	1964
Year	Total annual 160.8 (6.33)	78.2 (3.08)	February 1940	0	August 1955 ^b	48.5 (1.91)	October 1957	Total annual 336 (13.2)	660.4 (26.0)	February 1916	457 (18.0)	February 1916	622 (24.5)	February 1916

^aTrace amount.

^bAlso occurred in an earlier year.



TO USE THIS CHART, SELECT ANY DESIRED RAINFALL INTENSITY AND DURATION AND READ FROM THE DIAGONAL LINES THE EXPECTED FREQUENCY OF SUCH INTENSITY AND DURATION. FOR EXAMPLE, RAINFALL INTENSITY OF 33 mm/hr (1.3 in./hr) FOR 10 MINUTES CAN BE EXPECTED TO OCCUR, ON AVERAGE, ONCE EVERY 5 YEARS (POINT A). HOWEVER, SUCH INTENSITY CAN BE EXPECTED FOR 30 MINUTES DURATION ONLY ABOUT ONCE IN 100 YEARS (POINT B). THE RETURN PERIOD FOR THIS INTENSITY FOR 60 MINUTES DURATION IS GREATER THAN 1,000 YEARS (POINT C).

THERE ARE, OF COURSE, VARIATIONS IN USE OF THE CHART. SUPPOSE, FOR EXAMPLE, IT IS DESIRED TO FIND THE "100-YEAR STORM" FOR 60 MINUTES. THIS IS 20 mm (0.8 in.) (POINT D).

RCP8112-115

FIGURE 8-5. Return Periods of Rainfall Intensity and Duration Based on the Period 1947-1969 at the Hanford Meteorological Station.

TABLE 8-3. Average Return Period and Existing Record for Various Precipitation Amounts and Intensities During Specified Time Periods at Hanford Meteorological Station Based on Extreme-Value Analysis of 1947-1969 Records.

Years	Amount (mm) (in. in parentheses)							Intensity (mm/hr) (in./hr in parentheses)						
	20 min	60 min	2 hr	3 hr	6 hr	12 hr	24 hr	20 min	60 min	2 hr	3 hr	6 hr	12 hr	24 hr
2	4.1 (0.16)	6.6 (0.26)	7.6 (0.30)	9.1 (0.36)	12.2 (0.48)	15.8 (0.62)	18.3 (0.72)	12.4 (0.49)	6.6 (0.26)	3.8 (0.15)	3.0 (0.12)	2.0 (0.08)	1.32 (0.052)	0.76 (0.030)
5	6.1 (0.24)	10.2 (0.40)	12.2 (0.48)	14.0 (0.55)	19.6 (0.77)	24.1 (0.95)	26.9 (1.06)	18.3 (0.72)	10.2 (0.40)	6.1 (0.24)	4.6 (0.18)	3.3 (0.13)	2.01 (0.079)	1.12 (0.044)
10	9.4 (0.37)	12.7 (0.50)	15.0 (0.59)	17.0 (0.67)	24.4 (0.96)	29.7 (1.17)	32.5 (1.28)	27.9 (1.1)	12.7 (0.50)	7.6 (0.30)	5.6 (0.22)	4.1 (0.16)	2.49 (0.098)	1.35 (0.053)
25	11.9 (0.47)	15.8 (0.62)	18.8 (0.74)	21.1 (0.83)	30.7 (1.21)	36.8 (1.45)	39.6 (1.56)	35.6 (1.4)	15.8 (0.62)	9.4 (0.37)	7.1 (0.28)	5.1 (0.20)	3.07 (0.121)	1.65 (0.065)
50	13.5 (0.53)	18.3 (0.72)	21.6 (0.85)	24.4 (0.96)	35.6 (1.40)	42.2 (1.66)	45.0 (1.77)	40.6 (1.6)	18.3 (0.72)	10.7 (0.42)	8.1 (0.32)	5.8 (0.23)	3.51 (0.138)	1.88 (0.074)
100	15.2 (0.60)	20.6 (0.81)	24.4 (0.96)	27.2 (1.07)	40.4 (1.59)	47.5 (1.87)	50.6 (1.99)	45.7 (1.8)	20.6 (0.81)	12.2 (0.48)	9.1 (0.36)	6.9 (0.27)	3.96 (0.156)	2.11 (0.083)
250	17.3 (0.68)	23.6 (0.93)	28.2 (1.11)	31.0 (1.22)	46.2 (1.82)	54.1 (2.13)	57.4 (2.26)	50.8 (2.0)	23.7 (0.93)	14.0 (0.55)	10.4 (0.41)	7.6 (0.30)	4.50 (0.177)	2.39 (0.094)
500	18.5 (0.73)	25.9 (1.02)	31.0 (1.22)	33.8 (1.33)	50.8 (2.00)	59.4 (2.34)	62.7 (2.47)	55.9 (2.2)	25.9 (1.02)	15.5 (0.61)	11.2 (0.44)	8.4 (0.33)	4.95 (0.195)	2.62 (0.103)
1,000	20.3 (0.80)	28.2 (1.11)	33.8 (1.33)	36.8 (1.45)	55.9 (2.20)	64.8 (2.55)	68.1 (2.68)	61.0 (2.4)	28.2 (1.11)	17.0 (0.67)	12.2 (0.48)	9.4 (0.37)	5.38 (0.212)	2.84 (0.112)
Existing record	*	15.0 (0.59)	22.4 (0.88)	27.4 (1.08)	42.7 (1.68)	47.8 (1.88)	48.5 (1.91)	*	15.0 (0.59)	11.2 (0.44)	9.1 (0.36)	7.1 (0.28)	3.99 (0.157)	2.03 (0.080)
Date	--	6/12 1969	10/1 1957	10/1 1957	10/1-2 1957	10/1-2 1957	10/1-2 1957	--	6/12 1969	10/1 1957	10/1 1957	10/1-2 1957	10/1-2 1957	10/1-2 1957

*No records have been kept for time periods of less than 60 minutes. However, the rain gauge chart for 6-12-69 shows that 14.0 mm (0.55 in.) occurred during a 20-minute period from 1835 to 1855 PST. An additional 1.0 mm (0.04 in.) occurred between 1855 and 1910 to account for the record 60-minute amount of 15.0 mm (0.59 in.).

An estimate of monthly values of potential evapotranspiration (i.e., the combined water loss from a surface by evaporation and by transpiration from plants) can be made from empirical relationships and meteorological data. Wallace (1977) has used the Hanford Meteorological Station long-term climatological data to compute and compare estimates of evapotranspiration by three different methods: (1) Penman, (2) Thornthwaite-Mather, and (3) Morton. Potential evapotranspiration, as calculated by all three methods, yielded an annual value 5 to 9 times the mean annual precipitation. Wallace also used the Thornthwaite-Mather method to estimate the water balance using the Hanford Meteorological Station long-term data. These results are shown in Table 8-4 and Figure 8-6. The difference between precipitation and evapotranspiration is also shown in Figure 8-6.

8.1.3.3 Wind Erosion. The principal application of the wind erosion equation is to agricultural field operations (Skidmore, 1974). However, if necessary, the wind erosion equation (or a direct measurement technique developed by Gillette et al. (1972) and a model by Travis (1974)) could provide estimates on wind erosion of soil for the Hanford area (see dust or sand storms in Section 8.1.3.7).

8.1.3.4 Air Temperature, Dew Point, and Humidity. The annual (normal) temperature at the Hanford Meteorological Station site is 11.8°C. From 1912 to 1970 mean annual temperatures have varied from 10.1° to 13.4°C and have indicated an approximately 20-year cycle with warm peaks occurring during the years 1926, 1947, and 1967. The mean monthly temperatures for January and July, the coldest and warmest months of the year, are -1.4° and 24.7°C, respectively. The average daily minimum and maximum temperatures for January are -5.2° and 2.7°C, and for July 16.2° and 33.3°C. The lowest daily minimum temperature recorded was -33°C, while the highest daily maximum temperature was 46°C.

The average number of days free of freezing temperatures is 174, with a range between 134 and 215 days. Further information on the temperature climatology of the Hanford region is given in Table 8-5 and is available in a summary report of the Hanford region climatology (Stone et al., 1972).

The annual mean relative humidity at the Hanford Meteorological Station is 54.3 percent, with the highest relative humidity occurring in December (80.0 percent) and the lowest in July (32.2 percent). The annual mean dew point is 1°C, and the annual mean wet-bulb temperature is 6.6°C. Other humidity information is given in Tables 8-6 and 8-7. Note the 4-year difference in the period of record for the two tables; records in Table 8-6 begin with 1946, while those in Table 8-7 begin with 1950.

TABLE 8-4. Thornthwaite-Mather Water Balance for Hanford, Washington, 150-Millimeter Root-Zone Water Capacity* (after Wallace, 1977).

Property	Water balance (mm)												
	January	February	March	April	May	June	July	August	September	October	November	December	Total for year
Potential evapotranspiration	0	4.8	24.5	51.3	93.6	130.7	163.6	139.1	88.2	41.9	9.4	0	747
Precipitation	23.4	15.2	9.4	9.7	11.9	14.2	3.8	5.1	7.6	14.7	21.8	22.6	159
Difference	23.4	10.4	-15.1	-41.6	-81.7	-116.5	-159.8	-134.0	-80.6	-27.2	12.4	22.6	-588
Storage change	23.4	10.4	2.2	-18.0	-23.0	-17.0	-9.0	-3.0	-1.0	0	12.4	22.6	
Moisture storage	59.4	69.8	72.0	54.0	31.0	14.0	5.0	2.0	1.0	1.0	13.4	36.0	
Actual evapotranspiration	0	4.8	11.6	27.7	34.9	31.2	12.8	8.1	8.6	14.7	9.4	0	164
Moisture deficit	0	0	12.9	23.6	58.7	99.5	150.8	131.0	79.6	27.2	0	0	583
Moisture surplus	0	0	0	0	0	0	0	0	0	0	0	0	0
Runoff	0	0	0	0	0	0	0	0	0	0	0	0	0

*All values in millimeters.

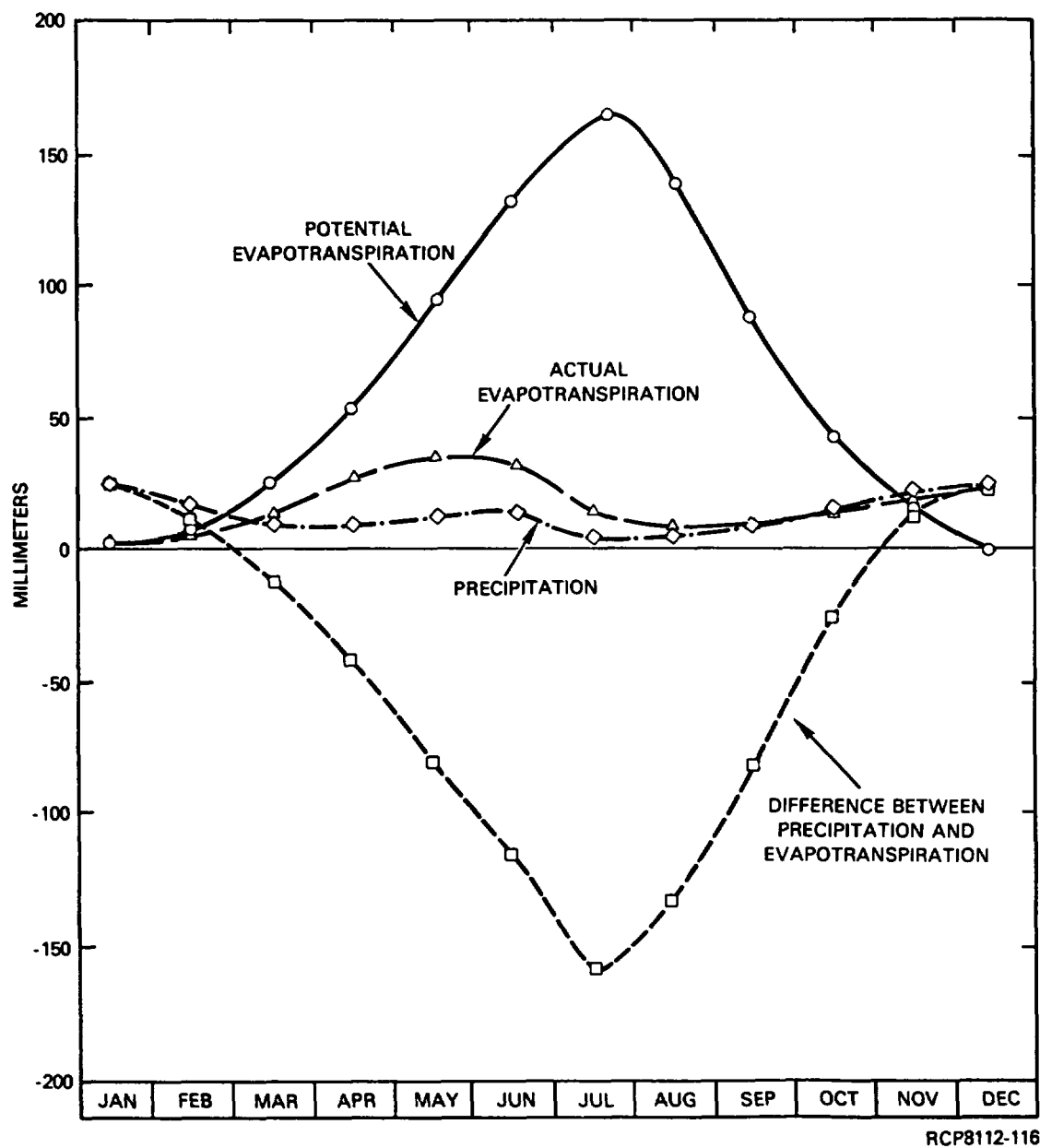


FIGURE 8-6. Water Balance at Hanford.

TABLE 8-5. Averages and Extremes of Temperature at the Hanford
Meteorological Station, 1912-1980.

Month	Temperature (°C) (°F in parentheses)														
	1912-1980 Averages								1912-1980 Extremes						
									Daily maximum				Daily minimum		
	Daily maximum	Daily minimum	Monthly	Highest		Lowest		Recorded	Year	Recorded	Year	Recorded	Year	Recorded	Year
				Monthly	Year	Monthly	Year								
January	2.72 (36.9)	-5.50 (22.1)	-1.39 (29.5)	5.83 (42.5)	1953	-11.06 (12.1)	1950	22.2 (72)	1971	-18.9 (-2)	1950	11.7 (53)	1971	-30.6 (-23)	1934
February	7.67 (45.8)	-2.61 (27.3)	2.56 (36.6)	6.94 (44.5)	1958	-5.89 (21.4)	1929	21.7 (71)	1924	-19.4 (-3)	1950	12.8 (55)	1932	-30.6 (-23)	1950
March	13.50 (56.3)	0.78 (33.4)	7.11 (44.8)	9.89 (49.8)	1926	4.11 (39.4)	1955	28.3 (83)	1960	-4.4 (24)	1960	12.2 (54)	1942	-14.4 (6)	1955
April	18.83 (65.9)	4.22 (39.6)	11.56 (52.8)	15.33 (59.6)	1934	8.61 (47.5)	1955	35.00 (95)	1934	5.0 (41)	1945	15.6 (60)	1956	-11.1 (12)	1935
May	24.22 (75.6)	8.83 (47.9)	16.56 (61.8)	20.44 (68.8)	1947	14.78 (56.6)	1933	39.4 (103)	1936*	9.4 (49)	1918	21.1 (70)	1956	-2.2 (28)	1954
June	28.44 (83.2)	12.94 (55.3)	20.67 (69.2)	24.11 (75.4)	1922	16.22 (63.0)	1953	43.3 (110)	1912	12.8 (55)	1966	27.2 (81)	1924	0.6 (33)	1933
July	33.28 (91.9)	16.17 (61.1)	24.72 (76.5)	27.67 (81.8)	1960	22.44 (72.4)	1963	46.1 (115)	1939	15.0 (59)	1966	27.8 (82)	1925	3.9 (39)	1979
August	31.94 (89.5)	15.22 (59.4)	23.56 (74.4)	27.50 (81.5)	1967	21.00 (69.8)	1964	45.0 (113)	1961	17.2 (63)	1920	27.2 (81)	1961*	4.4 (40)	1918
September	26.61 (79.9)	10.61 (51.1)	18.61 (65.5)	22.06 (71.7)	1967	14.89 (58.8)	1926	38.9 (102)	1976*	11.1 (52)	1934	22.2 (72)	1955	-3.9 (25)	1926
October	18.50 (65.3)	4.78 (40.6)	11.67 (53.0)	15.00 (59.0)	1952	9.33 (48.8)	1930	32.2 (90)	1933	-0.6 (31)	1935	15.6 (60)	1945*	14.4 (6)	1935
November	9.11 (48.4)	-0.33 (31.4)	4.39 (39.9)	7.78 (46.0)	1954	-0.39 (31.3)	1955	23.9 (75)	1975	-10.0 (14)	1955	11.1 (52)	1959*	-18.3 (-1)	1955
December	4.17 (39.5)	-3.28 (26.1)	0.44 (32.8)	3.61 (38.5)	1957	-7.50 (18.5)	1919	20.6 (69)	1980	-19.4 (-3)	1919	13.3 (56)	1975	-32.8 (-27)	1919
Year	18.22 (64.8)	5.17 (41.3)	11.72 (53.1)	27.67 (81.8)	July 1960	-11.06 (12.1)	January 1950	46.1 (115)	July 1939	-19.4 (-3)	February 1950*	27.8 (82)	July 1925	-32.8 (-27)	December 1919

*Also occurred in an earlier year.

TABLE 8-6. Averages and Extremes of Relative Humidity at the Hanford Meteorological Station, 1946-1980.

Month	Relative humidity (%)								
	Mean monthly	1946-1980 Averages				1946-1980 Extremes			
		Highest		Lowest		Highest	Year	Lowest	Year
		Monthly	Year	Monthly	Year				
January	76.4	88.8	1960	60.0	1963	100	1980*	13	1963
February	70.7	86.9	1963	54.0	1967	100	1980*	14	1962
March	55.9	65.9	1950	44.0	1965	100	1979*	12	1965*
April	46.9	64.5	1963	36.9	1966	100	1978*	9	1954
May	43.0	61.9	1948	31.2	1966	100	1978*	7	1953
June	39.7	53.5	1950	30.0	1949	100	1977*	10	1964*
July	32.2	40.5	1955	21.9	1959	99	1972	6	1951
August	35.6	47.8	1976	24.5	1967	100	1972*	7	1951
September	41.6	55.5	1977	33.2	1974	100	1978*	10	1962*
October	56.8	74.2	1962	42.5	1952	100	1980*	10	1952*
November	73.6	88.7	1979	62.8	1976	100	1980*	16	1976*
December	80.0	90.5	1950	69.0	1968	100	1980*	26	1972
Year	Mean annual 54.3	90.5	December 1950	21.9	July 1959	100	December 1980*	6	July 1951

*Also occurred in an earlier year.

TABLE 8-7. Monthly Averages of Psychrometric Data, 1950-1980.

Month	1950-1980 Monthly Averages			
	Measurement ($^{\circ}\text{C}$) ($^{\circ}\text{F}$ in parentheses)			Relative humidity (%)
	Dry bulb	Wet bulb	Dew point	
January	-0.94 (30.3)	-2.28 (27.9)	-4.89 (23.2)	76.0
February	3.06 (37.5)	0.89 (33.6)	-2.56 (27.4)	69.7
March	6.67 (44.0)	2.94 (37.3)	-2.61 (27.3)	55.0
April	11.39 (52.5)	6.00 (42.8)	-0.89 (30.4)	46.4
May	16.56 (61.8)	9.50 (49.1)	2.22 (36.0)	41.8
June	21.06 (69.9)	12.50 (54.5)	5.11 (41.2)	39.4
July	25.28 (77.5)	14.39 (57.9)	5.72 (42.3)	31.5
August	24.06 (75.3)	14.06 (57.3)	6.00 (42.8)	34.9
September	19.44 (67.0)	11.44 (52.6)	4.17 (39.5)	39.9
October	11.78 (53.2)	7.44 (45.4)	2.72 (36.9)	57.7
November	4.50 (40.1)	2.44 (36.4)	-0.50 (31.1)	72.6
December	0.78 (33.4)	-0.44 (31.2)	-2.50 (27.5)	80.8
Year	11.94 (53.5)	6.56 (43.8)	1.00 (33.8)	53.8

8.1.3.5 Wind. The monthly and annual mean prevailing-wind directions and windspeeds at the Hanford Meteorological Station, as well as the peak gust experienced for each month of the year, are given in Table 8-8. The wind data summarized in the table were collected from the height of 12.7 meters aboveground on the 122-meter Hanford Meteorological Station tower during the period 1945 to 1980. Either west-northwest or northwest winds prevail in every month (Fig. 8-7), with June having the highest mean windspeed, 4.1 meters per second, and December having the lowest, 2.7 meters per second. The peak gust in the period of record (36 meters per second) was recorded in January 1972.

The seasonal and diurnal variation of windspeed at the Hanford Meteorological Station is depicted in Figure 8-8. June and July have the largest diurnal range (approximately 3 meters per second) of all the months. The minimum speed occurs around 1000 Pacific standard time and the maximum between 1900 and 2200 Pacific standard time. December has the smallest diurnal variation. Wind roses for each atmospheric-stability class and for all stabilities are shown in Figure 8-9. Joint frequency distributions of atmospheric stability, wind direction, and speed are given in Section 8.4.1. The percent frequency of wind direction at the approximately 1,500-meter level over the Hanford Meteorological Station is shown in Table 8-9. When Table 8-9 is compared with Table 8-8, the turning of wind direction with height can be seen. This turning occurs seasonally as well as annually. The prevailing winds at 12.7 meters are west-northwest, versus southwest at approximately 1,500 meters.

8.1.3.6 Monthly Mixing-Height Data. The mixing height (or depth) is defined as the height above the surface through which relatively vigorous vertical mixing occurs. Mixing heights above the top of the 122-meter tower are not routinely measured at the Hanford Meteorological Station except those measured by the acoustic sounder to 670 meters (1975 to present). Those mixing depths higher than the 122-meter tower would require additional measurements of the vertical distribution of temperature by radiosonde or rawinsonde, measurements not presently taken at the Hanford Meteorological Station. The past data on mixing heights are not totally adequate because (1) the 122-meter tower is not high enough for measuring all mixing heights, (2) the acoustic radar records (1975 to present) extend only to about 670 meters above the ground surface, and (3) the nearest rawinsonde is located near Spokane, Washington (Fig. 8-1). However, seasonal maximum mixing-height data are available for Spokane (Table 8-10) (Holzworth, 1972). These values should be fairly representative of the maximum mixing-height information for the Hanford region, since maximum mixing heights in the Columbia Plateau region should not vary substantially.

8.1.3.7 Severe Weather Phenomena.

Hurricanes. Hurricanes are unknown at the Hanford Site, although moisture and cloudiness from decaying tropical storms can be advected as far north as the Hanford area under unusual circumstances, producing cloudiness, rain, or thunderstorms.

TABLE 8-8. Wind Averages and Peak Wind Gusts at the Hanford Meteorological Station, 1945-1980.

Month	Wind (m/s) (mi/hr in parentheses)								
	1945-1980 Averages						Peak gusts		
	Prevailing direction	Mean monthly speeds	Highest		Lowest		Speed	Direction	Year
			Monthly	Year	Monthly	Year			
January	NW	2.9 (6.4)	4.6 (10.3)	1972	1.4 (3.1)	1955	36 (80)	SW	1972
February	NW	3.2 (7.1)	4.8 (10.8)	1976	2.1 (4.6)	1963	29 (65)	SW	1971
March	WNW	3.8 (8.5)	4.8 (10.7)	1977*	2.6 (5.9)	1958	31 (70)	SW	1956
April	WNW	4.0 (9.0)	5.0 (11.1)	1972*	3.3 (7.4)	1958	33 (73)	SSW	1972
May	WNW	4.0 (8.9)	4.7 (10.5)	1965*	2.6 (5.8)	1957	32 (71)	SSW	1948
June	WNW	4.1 (9.2)	4.8 (10.7)	1949	3.4 (7.7)	1950	32 (72)	SW	1957
July	WNW	3.9 (8.7)	4.3 (9.6)	1963	3.0 (6.8)	1955	31 (69)	WSW	1979
August	WNW	3.6 (8.0)	4.1 (9.1)	1946	2.7 (6.0)	1956	30 (66)	SW	1961
September	WNW	3.4 (7.5)	4.1 (9.2)	1961	2.4 (5.4)	1957	29 (65)	SSW	1953
October	WNW	3.0 (6.6)	4.1 (9.1)	1946	2.0 (4.4)	1952	28 (63)	SSW	1950
November	NW	2.7 (6.1)	3.7 (8.2)	1977	1.3 (2.9)	1956	29 (64)	SSW	1949
December	NW	2.7 (6.1)	3.7 (8.3)	1968	1.3 (3.0)	1963*	32 (71)	SW	1955
Year	WNW	3.4 (7.7)	5.0 (11.1)	April 1972*	1.3 (2.9)	November 1956	36 (80)	SW	January 1972

*Also occurred in an earlier year.

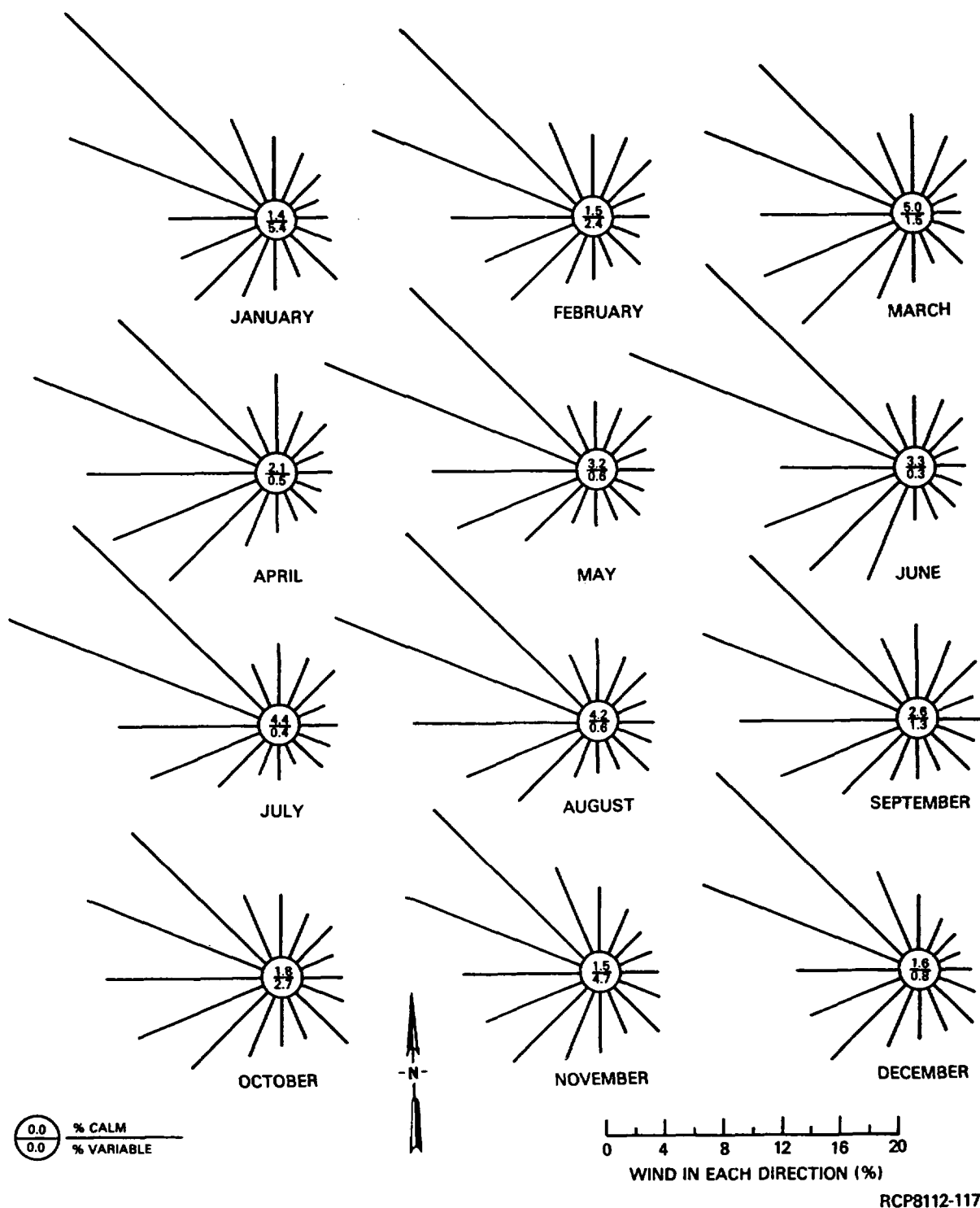


FIGURE 8-7. Monthly Average Wind Roses for the Hanford Meteorological Station Based on 15.2-Meter Level Wind Data, 1955-1970. The points of the rose represent the directions from which the winds come.

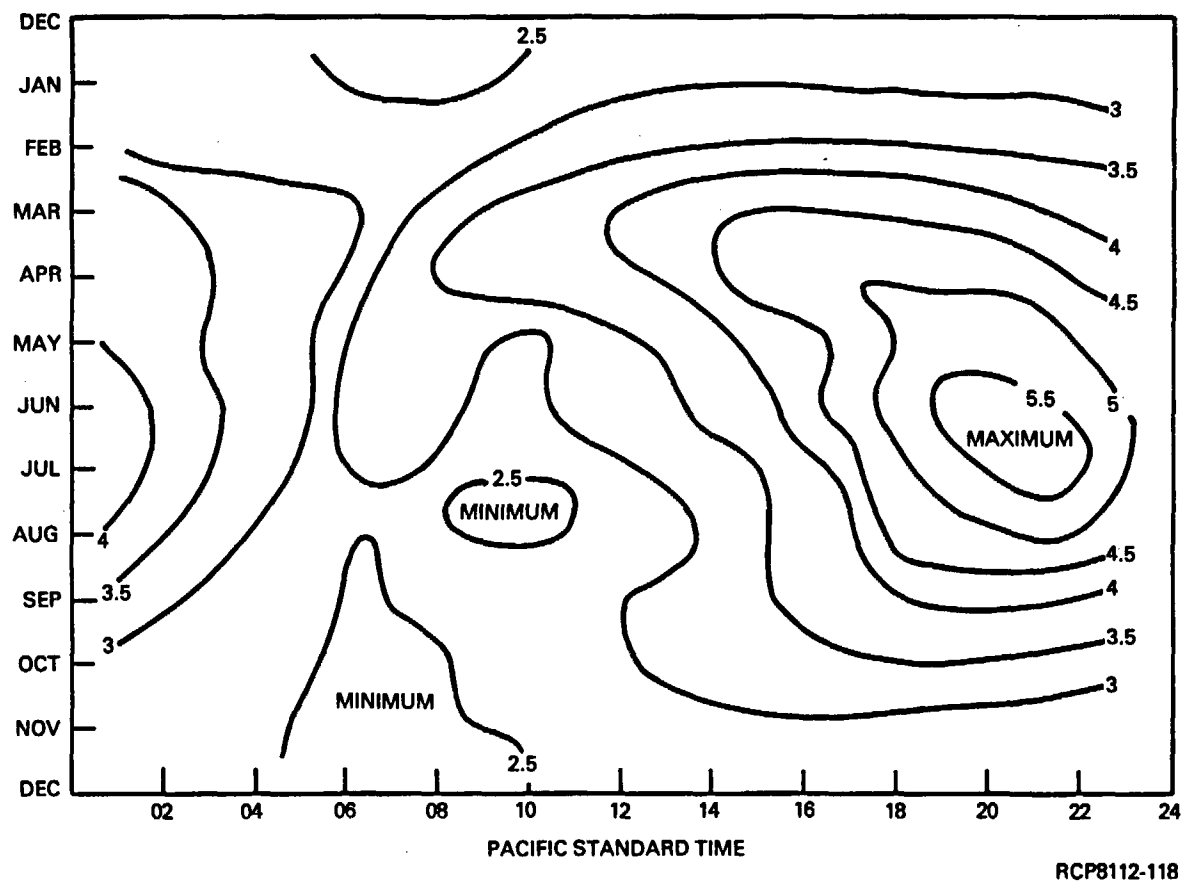
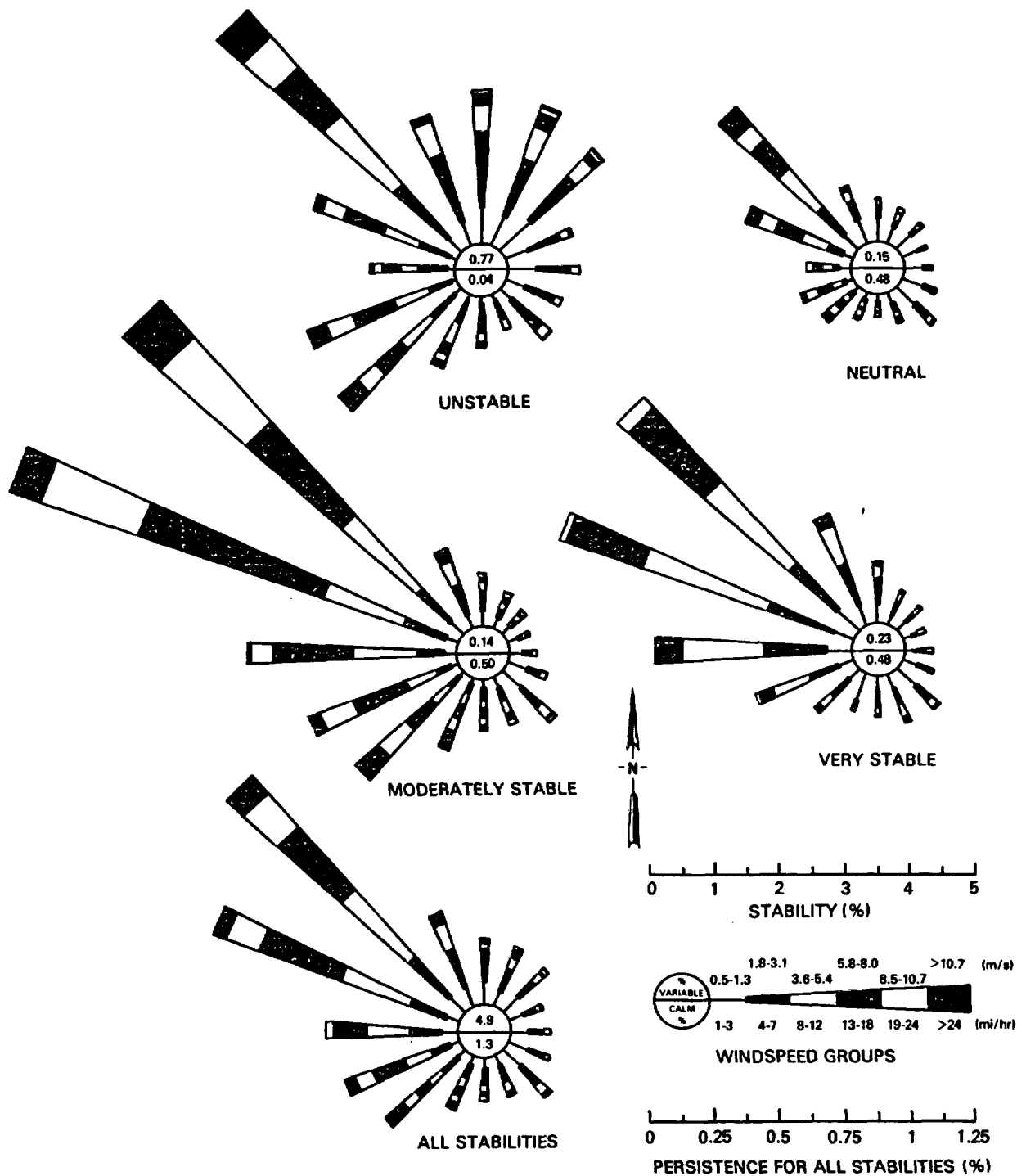


FIGURE 8-8. Seasonal and Diurnal Variation in the 15.2-Meter Level Windspeed (meters per second), 1955-1970.



RCP8112-119

FIGURE 8-9. Wind Roses as a Function of Stability and for all Stabilities of the Hanford Meteorological Station, Based on Winds at 60 Meters and Air Temperature Stabilities Between 1 and 60 Meters for the Period 1955 through 1970. (The points of the rose represent the directions from which the winds come.)

TABLE 8-9. Frequency of Wind Direction at the 1,500-Meter Level Over the Hanford Meteorological Station on a Seasonal and Annual Basis. (Compiled from 5 years of records, 1946-1950.)

Wind direction class interval (deg)	Frequency (%)				Year
	Spring	Summer	Fall	Winter	
345-15	5	5	7	5	6
15-45	5	7	9	4	6
45-75	6	5	6	4	5
75-105	4	4	5	3	4
105-135	3	3	3	2	3
135-165	4	3	2	3	3
165-195	5	7	5	5	6
195-225	10	13	11	11	11
225-255	21	21	19	24	21
255-285	22	20	20	23	21
285-315	10	8	8	12	10
315-345	5	4	5	4	4

TABLE 8-10. Mean Seasonal and Annual Afternoon Mixing Heights for the Spokane Area (m).

Season	NOP ^a	All ^b	%NOPC
Winter	430	523	56.9
Spring	1,861	1,943	72
Summer	2,533	2,559	87.8
Autumn	1,261	1,362	74.7
Annual	1,521	1,597	72.8

^aNo-precipitation cases.

^bPrecipitation and no-precipitation cases.

^cPercent of cases that are no-precipitation.

Tornadoes and Waterspouts. Waterspouts are unknown and tornadoes are rare at the Hanford Site. On the average, the state of Washington experiences less than one tornado each year (Stone et al., 1972). Tornadoes and funnel clouds have been observed three times at the Hanford Site since 1916. During this same time period, seventeen tornadoes or funnel clouds were reported within a 161-kilometer radius of the Hanford Meteorological Station (Table 8-11). The nearest reported tornado damage was at Yakima (April 30, 1957), about 72 kilometers west and at Wallula Junction (June 26, 1958), about 81 kilometers southeast of the Hanford Site. No loss of life or extensive property damage has been reported from any of the tornadoes observed in this region.

TABLE 8-11. Tornado and Funnel Cloud History Within 161 Kilometers of the Hanford Meteorological Station.

Date	Location
June 26, 1916	Walla Walla, Washington
April 15, 1925	Condon, Oregon
September 2, 1936	Walla Walla, Washington
May 20, 1948	Yakima, Washington
May 29, 1948	Yakima, Washington
June 11, 1948	Ephrata, Washington
June 16, 1948	Hanford Site, Washington
May 9, 1956	Kennewick, Washington
April 12, 1957	Ione, Oregon
April 30, 1957	Yakima, Washington
May 6, 1957	Harrington, Washington
April 24, 1958	Walla Walla, Washington
June 26, 1958	Wallula Junction, Washington
March 24, 1961	Hanford Site, Washington
March 14, 1966	Little Goose Dam, Washington
July 15, 1970	Hanford Site, Washington
July 1, 1978	48 km (30 mi) North of Pasco, Washington

Since the tornado history is not extensive around the Hanford region, only a few studies have been conducted on the subject. Fujita (1970) has done a relatively extensive survey of tornadoes in the three northwestern states (Washington, Oregon, and Idaho). Daubek (1970) studied the frequency of tornadoes around the Hanford region and concluded that the probability of a tornado occurring at the Hanford Site is less than 0.00028. Jaech (1970) analyzed the data of Fujita to determine the probability of a tornado striking the Exxon Nuclear Company, Inc. fuel facility, which is about 40 kilometers from the Hanford Meteorological Station. His estimate on the probability of occurrence of a tornado was six chances in 1 million during a given year or about one chance in 4 thousand during a 40-year plant life. Childs and Orgill (1979) investigated the squall line and apparent tornado event of July 1, 1978 that damaged the Bonneville Power Administration power transmission lines east of the Hanford region and near Basin City.

Tornadoes observed in the vicinity of the Hanford Site are weaker than their midwest counterparts. Although capable of creating damage, they are generally of short duration with a short, narrow path. Their maximum rotational windspeeds have been estimated at between 65 and 78 meters per second. Their maximum rotational and translational wind velocities have been estimated at 96 meters per second (Jaech, 1970). Daubek (1970) estimates the maximum translational velocity at around 13 meters per second. The maximum pressure drop in the center of a tornado relative to the environmental pressure is estimated to be up to 10.4 kilopascals (Fujita, 1970).

Thunderstorms. According to the Hanford area climatology (Stone et al., 1972), thunderstorms have occurred during all months of the year except November and January. Ten thunderstorm days per year is the average, although this number has varied from 3 to 23 in individual years. Thunderstorms occur most frequently from April through September (Table 8-12). June and August hold the record for the largest number of thunderstorm days at eight.

Lightning. Although severe thunderstorms* are rare at the Hanford Site (less than one per year), they may be accompanied by lightning, hail, dust, and/or heavy rain. Lightning strikes have occasionally ignited grass fires which have burned thousands of acres. The 122-meter meteorological tower at the Hanford Meteorological Station has been struck several times during its 35-year existence.

*Severe thunderstorms occur when wind gusts exceed 25 meters per second and/or hail equals or exceeds 1.9 centimeters in diameter.

TABLE 8-12. Number of Thunderstorm Days at the Hanford Meteorological Station, 1945-1980.

Month	Mean monthly	Greatest		Least	
		Monthly	Year	Monthly	Year
January	0	0	--	0	--
February	a	1	1972 ^b	0	1980 ^b
March	a	1	1969 ^b	0	1980 ^b
April	1	3	1979 ^b	0	1977 ^b
May	2	7	1956	0	1977 ^b
June	2	8	1972 ^b	0	1963 ^b
July	2	7	1975	0	1973 ^b
August	2	8	1953	0	1974 ^b
September	1	4	1959	0	1976 ^b
October	a	2	1976	0	1980 ^b
November	0	0	--	0	--
December	a	1	1971	0	1980 ^b
Year	Total annual 10	8	June 1972 ^b	0	--

^aLess than 0.5 day.

^bAlso occurred in an earlier year.

Hail. Hail is an unusual phenomenon at the Hanford Meteorological Station, never having fallen more than 2 days during any year of record. Hail was reported on 14 of the 246 thunderstorm days recorded at the Hanford Site from 1947 to 1970. The distribution of hailstorm days by month is given in Table 8-13. Hail was recorded as 5 to 8 millimeters in size, except for two storms for which hail was recorded up to 10 millimeters.

TABLE 8-13. Distribution of Hailstorm Days by Month, 1947-1970.

	J	F	M	A	M	J	J	A	S	O	N	D	Total
Number	0	1	1	4	2	1	2	2	1	0	0	0	14
Total (%)	0	7	7	30	14	7	14	14	7	0	0	0	100

Freezing Rain (Ice Storms). Glaze ice is a coating of ice formed when rain or drizzle freezes on contact with surfaces whose temperature is below freezing. It occurs an average of 7 days per year. Such occurrences have caused serious traffic disruptions in the Hanford area on at least two occasions (Stone et al., 1972). These occurrences have only been between November and March.

Rime ice, formed on objects when supercooled fog droplets freeze, occurs frequently in winter, especially at the higher elevations and, in unusual cases, has been known to break electrical transmission lines (Stone et al., 1972). Statistics on glaze and rime-ice frequencies have not been developed at the Hanford Meteorological Station, although the data are available.

Dust or Sand Storms. Duststorms are a relatively common meteorological phenomenon in the Hanford region. These storms are recorded in the meteorological record when the visibility becomes restricted by dust or blowing dust to 10 kilometers or less. The visibility restriction may be attributed to dust when the visibility impairment is due either to dust carried in from a distant source or to blowing dust when dust is observed to be picked up and blown around locally.

Sources of airborne dust or sand for the Hanford region are local construction activity, the Hanford Site itself, and surrounding agricultural (dryland wheat and irrigated crops) land. One of the greatest sources of airborne dust is from dryland wheat fields in the Horse Heaven Hills south of the Hanford Site. Airborne dust emission from these lands is a major contributor to 24-hour total-suspended-particulate concentrations exceeding the secondary standard of 150 micrograms per cubic meter (Table 8-14) in the three counties of the Horse Heaven Hills (Jenne, 1978).

Duststorms are most frequent during the period of March through May and in September. They are least frequent in August, November, and December (Jenne, 1978). The spring maximum occurs while the soil is disturbed by spring agricultural activity and gusty winds often occur. September duststorms appear to be related to ground breaking for winter wheat in the east-central part of the state north and northeast of the Hanford Site. Duststorms in the Hanford area have been studied by Orgill et al. (1974), Sehmel (1976), and Jenne (1978). Statistics of these duststorms are given in Table 8-15.

Dust is transported and dispersed throughout the Hanford Site by dust devils as well as by windstorms. Dust devils generally occur on sunny days with light winds and can frequently be seen on summer days at the Hanford Site. Characteristics of dust devils and information on their occurrence in the Hanford area can be found in an interim report by Orgill and Schwendiman (1975).

TABLE 8-14. National Ambient Air Quality Standards
(Orgill et al., 1974).

Emission	Standard ($\mu\text{g}/\text{m}^3$)	
	Primary	Secondary
Sulfur oxides ^a		
Annual arithmetic mean	80	--
24-hour maximum ^b	365	--
3-hour maximum ^b		1,300
Suspended particulate matter ^a		
Annual geometric mean	75	60 ^c
24-hour maximum ^b	250	150
Lead ^a		
3-month average	1.5	--
Carbon monoxide ^a		
8-hour maximum ^b	10,000	10,000
1-hour maximum ^b	40,000	40,000
Hydrocarbons ^a		
3-hour (6 to 9 a.m.) maximum ^a	160 ^c	160 ^c
Nitrogen dioxide		
Annual arithmetic mean	100	100
Ozone ^a		
1-hour maximum ^d	235	235

^aCode of Federal Regulations (40 CFR 50.1)
(EPA, 1980a)).

^bNot to be exceeded more than once per year.

^cGuideline.

^dNot to be exceeded on more than 1 day/yr (averaged
over 3 yr).

TABLE 8-15. Summary of Hanford Duststorm
Statistics, 1953-1970.

Total dust hours	476
Total dust days	142
Number of duststorms	150
Average dust (hr/yr)	26.4
Average dust (day/yr)	7.9
Average duststorms per year	8.3
Range in duration of duststorms (hr)	1-18
Average duration of duststorms (hr)	3.2
Average duststorm concentration (mg/m^3)	6.77

High Air-Pollution Potential. High air-pollution potential occurs when low windspeeds and restricted mixing coexist. High pollution concentrations occur when these conditions combine with the emission of large quantities of pollutants. Windspeeds at the Hanford Meteorological Station are lowest in winter (Table 8-8). Vertical mixing is restricted at night and in the fall and winter, when solar radiation is weak and turbulent mixing is weak, due to low wind shear. An especially high air-pollution potential exists when air stagnates in the Pasco Basin in the fall and winter. These stagnation episodes may last for several days and are often accompanied by haze or fog. The available statistics on the frequency of heavy fog at the Hanford Meteorological Station are presented in Table 8-16.

8.1.3.8 48-Hour Probable-Maximum Winter Precipitation. Statistics on 48-hour maximum winter precipitation are not currently available at the Hanford Meteorological Station, but estimates for snow pack have been made from the available data on snowfall (see Section 8.4.2.3).

TABLE 8-16. Number of Days with Heavy Fog^a at the Hanford Meteorological Station, 1945-1980.

Month	Mean monthly	Greatest		Least	
		Monthly	Year	Monthly	Year
January	6	15	1976	0	1949
February	3	11	1963	0	1977
March	1	5	1951	0	1980 ^b
April	c	1	1975 ^b	0	1980 ^b
May	c	1	1958	0	1980 ^b
June	c	1	1971	0	1980 ^b
July	0	0	--	0	--
August	c	1	1959	0	1980 ^b
September	c	1	1977	0	1980 ^b
October	1	7	1980	0	1978 ^b
November	6	13	1965	0	1960
December	8	17	1950	2	1968 ^b
Year	Total annual 25	17	Dec 1950	0	--

^aVisibility 0.4 km (0.25 mi) or less.

^bAlso occurred in an earlier year.

^cLess than 0.5 day.

8.2 AIR QUALITY

Compliance is required with applicable emission and ambient-air-quality standards relative to criteria pollutants (sulfur oxides, total suspended particulates, lead, carbon monoxide, hydrocarbons, nitrogen dioxide, and ozone). These standards are contained in federal, state, and local regulations. Generally, air-quality regulations apply to the routine operation of a facility, as opposed to construction operations. The emissions from the latter are usually short-term and regulated only to the extent that complaints and problems arise.

8.2.1 Ambient Air Quality

National Ambient Air Quality Standards (Table 8-14) should not be exceeded by plant emissions. Significant changes in any of the criteria pollutants caused by routine operations require modeling of impacts in the form of a prevention-of-significant-deterioration emission-permit application. For sulfur oxides and total suspended particulates, the U.S. Environmental Protection Agency has published guidelines on how these computations are to be made (EPA, 1980a). Preliminary guidelines are available for other pollutants, but some pollutants have no guidelines available at present.

The State of Washington has a state implementation plan for enforcing the air quality standards. The Benton-Franklin-Walla Walla Counties Air Pollution Control Authority is the local enforcement agency. Prior to construction of a repository at the Hanford Site, a prevention-of-significant-deterioration review will be undertaken. The permit application is reviewed by local, state, and federal air quality authorities before a decision is made.

Procedures for evaluation of visibility impacts have been outlined by the U.S. Environmental Protection Agency (EPA, 1980b). Maximum prevention-of-significant-deterioration increments are defined for three classes of areas. Most of the Pacific Northwest, including the Hanford region, is Class II. Class I areas, such as wilderness and large national parks, are assigned smaller maximum prevention-of-significant-deterioration increments. The actual available prevention-of-significant-deterioration increments depend on background and current prevention-of-significant-deterioration permits that have been issued. The prevention-of-significant-deterioration increments are concentration changes for the time periods defined by the National Ambient Air Quality Standards. Increment consumptions are computed in terms of the maxima that occur anywhere offsite, as well as the maxima that occur in designated areas with more restrictive requirements. The latter refers to nonattainment areas for pollutants and to Class I areas.

8.2.2 Emissions

Local emissions regulations are specified in general regulation 80-7 of the Benton-Franklin-Walla Walla Counties Air Pollution Control Authority, as of July 1, 1980 (APCA, 1980).

8.2.3 Baseline Concentrations

An air quality evaluation requires both definition of monitored values and the local emission inventory. The data available for the Hanford Site and surrounding areas are contained in a series of recent reports (Jenne, 1980; 1981; Maas, 1981).

With the exception of total-suspended-particulate monitoring, all monitoring stations are at some distance from the reference repository location. Total-suspended-particulate values are obtained through cooperative effort with the local air-pollution control authority at the Hanford Meteorological Station. These data should be fairly representative of total suspended particulates at the reference repository location. All other pollutants would have to be modeled in terms of the nearby sources and background from the distant monitoring stations. A point-source emissions inventory is available for 1979 for Benton, Franklin, and Walla Walla Counties, including sixteen sources related to the Hanford Site operations (Jenne, 1980). This southeastern Washington region has a relatively high potential for air-pollution episodes from a meteorological standpoint. The mean annual mixing depth (Holzworth, 1972) in this area is about 450 meters, and the mixing depth for July is 2,000 meters. This area experiences a significantly high frequency of low-level temperature inversions in winter (Hosler, 1961).

Stagnation is defined as "the persistence of a given volume of air over a region, permitting an abnormal buildup of pollutants from sources within the region" (Huschke, 1968). By considering stagnation to be an uninterrupted period of daily average windspeed of 2.0 meters per second or less and/or a peak gust of 6.0 meters per second or less, a 15-year summary (Jenne, 1963) of stagnation periods covering the months November through February (1947-48 through 1961-62) has been compiled. This shows that although stagnation lasting for 20 days can be expected only one season in 20, a 10-day stagnation period can be expected every other season. Only one season in three will fail to produce a stagnation period of at least 8 days.

The major cause of air pollution in the area is dust occurring during windy periods. The most significant sources are cultivated fields in the surrounding area. Dust or blowing dust occurs on an average of 6 days per year (Stone et al., 1972).

The Hanford Site and surrounding areas are all currently classified as Class II areas. There are no nonattainment areas in the immediate region for any of the criteria pollutants. Total-suspended-particulate values exceed standards, but allowance is made for the nature of the major sources of total suspended particulates in this region (i.e., dryland wheat farms). Although the monitored total-suspended-particulate values at the Hanford Meteorological Station have not been broken down into contributing sources, the major influences leading to high total-suspended-particulate values are duststorms and periods of stagnation. The Class I areas for the Pacific Northwest are shown in Table 8-17 to be sufficiently

TABLE 8-17. Mandatory Class I Areas in the Pacific Northwest.

Area	Total area		Distance (km) ^a
	Hectares	Acres	
Washington			
Mount Rainier National Park	95,198	235,239	135
North Cascades National Park	203,670	503,277	215
Olympia National Park	361,215	892,578	300
Alpine Lakes Wilderness Area	122,826	303,508	155
Glacier Peak Wilderness Area	187,879	464,258	200
Goat Rocks Wilderness Area	33,460	82,680	115
Mount Adams Wilderness Area	13,094	32,356	140
Pasayten Wilderness Area	204,579	505,524	250
Oregon			
Crater Lake National Park	64,867	160,290	430
Diamond Peak Wilderness Area	14,827	36,637	390
Eagle Cap Wilderness Area	118,766	293,476	210
Gearhart Mountain Wilderness Area	7,571	18,709	460
Kalmiopsts Wilderness Area	31,120	76,900	570
Mountain Lakes Wilderness Area	9,337	23,071	510
Mount Hood Wilderness Area	5,730	14,160	190
Mount Jefferson Wilderness Area	40,553	100,208	260
Mount Washington Wilderness Area	18,663	46,116	295
Strawberry Mountain Wilderness Area	13,368	33,033	265
Three Sisters Wilderness Area	80,898	199,902	300
Idaho			
Yellowstone National Park (Idaho Sector)	b		700
Craters of the Moon Wilderness Area	17,500	43,243	600
Hells Canyon Wilderness Area (Oregon)	78,445	193,840	240
Sawtooth Wilderness Area	87,567	216,383	475
Selway-Bitterroot	502,062 ^c	1,240,618 ^c	330
Pacific Northwest Total:	2,313,195	5,716,006	

^aFrom Hanford Meteorological Station.^bTotal park area 898,299 hectares (2,219,737 acres); Idaho portion not given.^cIncludes Montana section.

distant that the criteria pollutants should not have significant impacts in terms of highest and second highest maximum air concentrations. However, the potential exists for a long-range impact on visibility in these Class I areas.

Other areas of local interest in an air-quality analysis are a national park (the Whitman Mission) at Walla Walla and nearby Indian reservations. None of these are under the strict air-quality regulations for a Class I area.

The only prevention-of-significant-deterioration review in this area has been an application by Omega Fuels for an ethyl alcohol plant, to be located about 15 kilometers southeast of Kennewick, Washington on the Lake Wallula section of the Columbia River. This is too distant to have any significant prevention-of-significant-deterioration increment consumption at the reference repository location.

8.2.4 Basalt Waste Isolation Project Air-Quality Impacts

Since little is known at this time about the emissions from the construction and operation of a repository in basalt, the air-quality impact can only be stated in general terms.

Fugitive dust must be dealt with. Depending on the composition and degree of stabilization, storage piles of rock and other debris may be a source of some windblown dust. However, the large size of the basalt fragments should preclude most problems.

The emissions from vents are expected to be very low in total-suspended-particulate concentrations but may contain elevated levels of gases released from the Earth (radon, etc.) as well as from the underground operations.

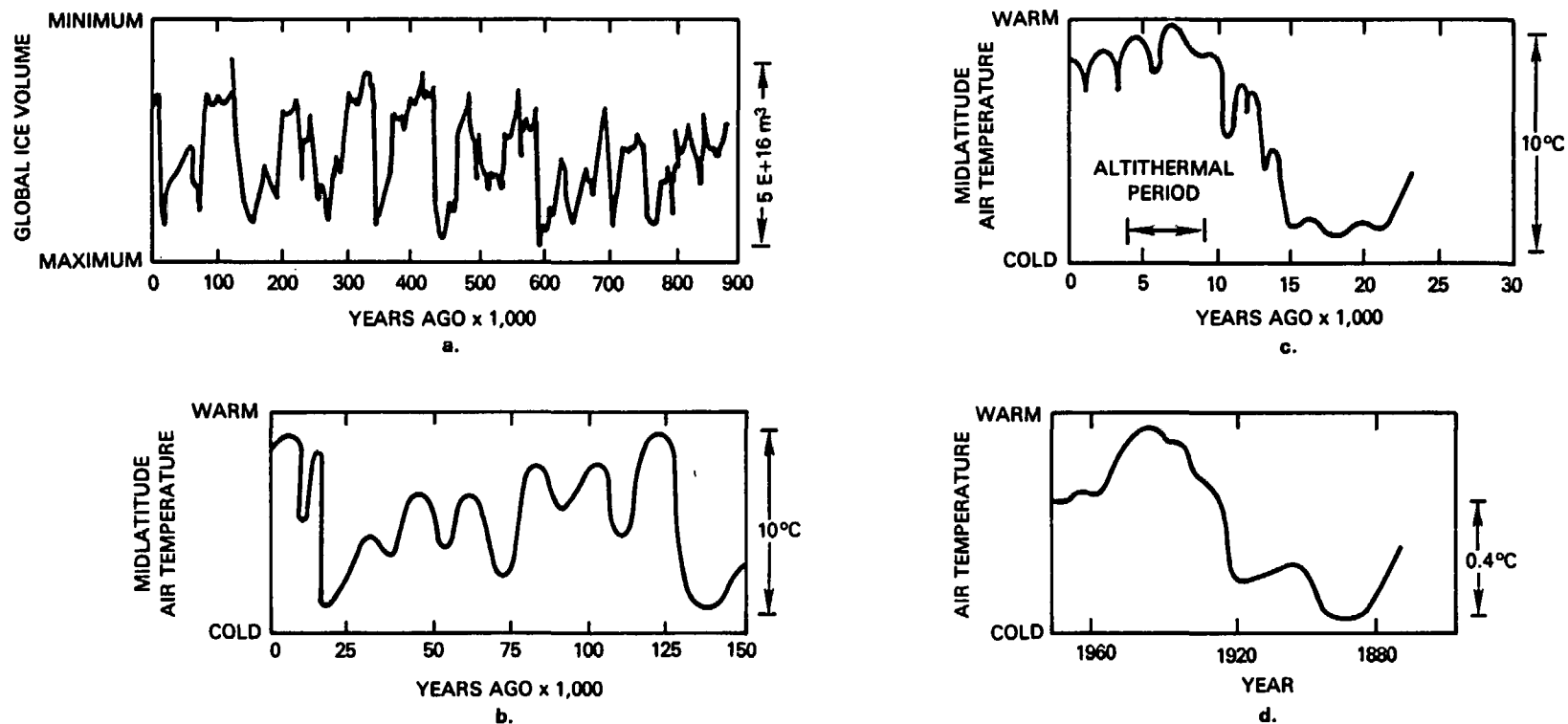
8.3 LONG-TERM CLIMATIC ASSESSMENT

8.3.1 Paleoclimatology

Paleoclimatology, the study of ancient climates, is a relatively new science undergoing rapid change as new paleoclimatic techniques are developed and tested. A coherent hemispherical or continental picture of Quaternary paleoclimate is beginning to emerge from converging evidence from a variety of disciplines, but regional paleoclimatic work for the Pacific Northwest is in the early stage of initial reconnaissance studies. Quaternary paleoclimatic studies of the area have been sparse and, due to the geologic formations and geologic history of the Hanford Site, it seems unlikely that much quantitative information can be developed from onsite investigations. However, palynological work in the forest boundary zones on the periphery of the Columbia Plateau (especially northwest of Spokane) has been conducted. These forest boundary zones are especially suitable for study, since the ecosystems at the boundary are quite sensitive to changes in climate. Therefore, the desired paleoclimatic information required for the project can be developed from these studies.

8.3.1.1 Temperature and Precipitation. The dominant characteristic of the Quaternary in many parts of the world was climatic change. This climatic change resulted in the expansion and recession of glaciers, the appearance and disappearance of desert lakes, and the extinction of various species of plants and animals throughout much of the world. Large ice sheets advanced from the north to within 120 kilometers of the Hanford Site, causing catastrophic floods of unprecedented magnitude in eastern Washington (Baker, 1978) and the extinction of some of the large mammals that grazed in the region only 10,000 years ago (NAS, 1975; Frison, 1975; Knudson, 1980) when early man inhabited the region. The fluctuations in climate are seen in Figure 8-10, where temperature and ice-volume changes are plotted against time for different geologic time periods (NAS, 1977). Such a presentation puts the present climate of the Earth in perspective and forms a basis on which the regional paleoclimatic changes can be evaluated.

Geologic evidence supports the view that average global climate over the past billion years was much warmer (perhaps 10°C warmer) than at present (Mitchell, 1977). During most of this time the Earth was entirely free of polar ice. However, at the beginning of the Cenozoic era, approximately 55 million years ago, a gradual cooling of the Earth began. This cooling culminated 2 million years ago, in the Quaternary period, in the alternation of a series of major ice ages at intervals of approximately 100,000 years (Fig. 8-10 a). During the last 125,000 years mean atmospheric temperature, fluctuating at intervals of about 20,000 years, varied over a 10°C range (Fig. 8-10 b). The coldest part of the last cycle occurred 13,000 to 22,000 years ago (Fig. 8-10 c) and resulted in extensive glaciation on the North American continent. Our present climate is thought to be interglacial. The warmest part of this interglacial



RCP8112-120

FIGURE 8-10. General Trends in Global-Scale Climate for the Past Million Years
 (a. Fluctuations in global ice volume recorded as changes in isotopic composition of fossil plankton in a deep-sea core. b. Generalized Northern Hemisphere air-temperature trends based on midlatitude sea-surface temperature, pollen records, and worldwide sea-level records. c. Generalized Northern Hemisphere air-temperature trends, based on fluctuations in alpine glaciers, changes in tree lines, marginal fluctuations in continental glaciers, and shifts in vegetation patterns recorded in pollen spectra. d. Changes in the 5-year-average surface temperatures over the region 0° to 80° north (WMO, 1975)).

period, termed the altithermal interval, occurred 4,000 to 8,000 years ago, and the midlatitude temperatures have been slowly decreasing since then. Temperature fluctuations on the order of about 0.5°C have occurred on smaller time scales (Fig. 8-10 d). Instrumental data taken since 1880 have shown a clear trend of increasing temperature up to the mid-1940s, followed by a decline to the present.

Over the past 20,000 years temperature changes in the Pasco Basin seem to have closely paralleled the global climate picture described above. Palynological investigations at sites primarily north of the Pasco Basin have concluded from fossil pollen assemblages that the early post-glacial period, lasting from 13,000 to 10,000 years ago, was cooler and moister than today (Mack et al., 1976; 1978c; Nickmann, 1979; Nickmann and Leopold, 1980). Additional evidence for this view has come from studies of rockfall frequencies in caves, from deposition of eolian sediments, from the buildup of organic debris (Fryxell, 1964), and from the rates of accumulation of fanglomerates due to presumably greater runoff (Brown, 1970). During this cool, moist period early man coexisted with many large grazing species including mammoth, bison, and horses on the extensive grasslands of eastern Washington (Brown, 1970). The change to a warm, dry climate about 8,000 years ago has been confirmed by many investigators. The relative aridity has been deduced from changes in plant species (Mack et al., 1976; 1978a; 1978b; 1978c; 1979; Nickmann, 1979; Nickmann and Leopold, 1980; Hansen, 1947), lessened frost activity (Fryxell, 1964), increased wind deposits (ERDA, 1975; Brown, 1970), changes in fauna (Brown, 1970; Frison, 1975; Knudson, 1980), changes in mountain-glacier size and location (Porter, 1977), and changes in patterned ground distribution (Mack et al., 1976).

This warm, dry climate lasted until about 4,000 years ago and saw the extinction or migration of many of the mammal species inhabiting the Columbia Plateau. During this altithermal interval the effective precipitation, which had been enough to support the extensive grassland of the region, was reduced, resulting in many changes in vegetation distribution (Mack et al., 1976; 1978c; Nickmann, 1979). Active sand dunes formed on the Hanford Site and at other locations throughout eastern Washington. Incorporation of Mount Mazama ash beds, from the eruption of 6,700 years ago in southern Oregon (Fryxell, 1965), in some now-stabilized dunes indicates that the dunes themselves formed some 6,000 to 7,000 years ago during this warm, dry period (ERDA, 1975).

A third period of climatic change, to conditions slightly cooler and moister than today, is thought to have occurred roughly between 3,000 or 4,000 years and 1,500 years before present. This change is somewhat controversial, being indicated from palynological data at some sites but absent in data at other sites (Mack et al., 1978c; 1979). The modern climate has prevailed in the region since 1,500 years ago (Mack et al., 1978b).

During the last glacial interval, locations just south of the glacial margins experienced drastic changes in surface air temperatures, which produced far-reaching effects on plant and animal communities, on the rates of change of geological processes, and on the physical environment. Investigators of temperature change in the Pacific Northwest have estimated that seasonal, annual, and monthly average temperatures were 4° to 15°C below present values (Table 8-18).

TABLE 8-18. Estimates of Glacial Age Surface Temperature Deficits (relative to the present).

Temperature deficit (°C)	Location	Averaging time	Reference
6	U.S. latitudes	January	Barry (1973)
5		July	
5 to 6	--	--	Stottlemyre et al. (1981)
4 to 12	Unglaciaded plains	Maximum cooling in Quaternary	Markov (1969)
5.5±1.5	Cascades	Ablation season	Porter (1977)
4.2±1.0	Cascades	Mean annual	Porter (1977)
10 to 15	Northwest U.S. south of glacial margin	July mean	Gates (1976)
5.3	Northern Hemisphere (includes oceans)	July mean	Gates (1976)
4.5	Western Washington	July mean	Heusser (1972)
5	Western Washington	July mean	Heusser (1964; 1965)

The uplift of the Cascades occurred 15 million years ago, establishing land and sea relationships much as they are today. The primary exception to this is the somewhat-reduced sea level during glacial periods. The environmental impact statement for waste management operations at the Hanford Site (ERDA, 1975) states that the Hanford area, separated from the Pacific moisture source by the Cascade Range, has experienced an arid or semiarid climate for nearly 12,000 years. The climate has been responsible for the thin veneer of windblown sediments that covers the area. Geologic data suggest that little runoff has occurred since late Pleistocene or early Holocene times (Brown, 1970).

Based on topographic arguments and geologic information, Kukla (1979) has concluded that the long-term change in mean annual precipitation since the last glacial episode is probably within the range of recent year-to-year variability. The annual precipitation at the Hanford Site has averaged 15.9 centimeters and, since 1913, has varied between 7.6 and 29.1 centimeters (Stone et al., 1972). Thus, mean annual precipitation since about 13,000 years ago is probably within a factor of 2 of the present mean annual precipitation of about 16 centimeters.

Mountain glaciers in the Cascades were greatly expanded relative to their present-day size during the last great ice advance. Porter's investigation (Porter, 1977) of the glaciation thresholds, at the maximum ice advance of the last glacial interval, concludes that the accumulated season's precipitation during the ice advance was probably no more than 30 percent greater than present day values. From palynological evidence in western Washington, Heusser (1964; 1965) indicates that the climate may have been drier during the glacier advance. Sarnthein's work (Sarnthein, 1978), based on the relative frequency of sand dune and desert conditions across the globe, concludes that conditions were dry below the glacial margins.

8.3.1.2 Glaciation. Variations in global ice cover are a prominent feature of the changing climate of the Earth. Over the last 900,000 years (Fig. 8-10 a), the glacial cycles have had a time period of about 100,000 years. These periodic increases in glaciation were accompanied by decreases in sea level throughout the world, as water was removed from the oceanic reservoirs for storage in the ice sheets. During the last glaciation of the Quaternary period, a large continental ice sheet formed in western Canada and advanced southward into northern Washington. This Cordilleran ice sheet had a separate point of origin from the Laurentide ice sheet that advanced into the central and eastern United States and the time of the maximum extent of the ice sheet was quite different. The maximum extent of the Laurentide ice sheet occurred about 18,000 years ago (Clague et al., 1980), while the maximum extent of the Cordilleran ice sheet was about 14,000 years ago in both western and eastern Washington (NAS, 1975; Thorson, 1980). The area covered by the last ice advance in the Northern Hemisphere (Fig. 8-11 and Table 8-19) is estimated to be fully 90 percent of the maximum area covered by ice in the last million years of the Pleistocene epoch (NAS, 1975). The life cycle of the Cordilleran ice sheet has been used as an example of the instability of the Earth's climate, since this ice sheet melted rapidly and had entirely disappeared by 10,000 years ago.

As the ice sheets advanced during the late Pleistocene epoch, grasslands, deserts, and steppes grew at the expense of forested area, and sea levels fell by more than 85 meters (CLIMAP, 1976). The Cordilleran ice sheet advanced to a position 80 kilometers south of Seattle (Thorson, 1980); east of the Cascades, the Okanogan Lobe of the Cordilleran ice sheet advanced southward to within 120 kilometers of the Hanford Site (Richmond et al., 1965; Waite, 1980). The Okanogan lobe and other lobes of the ice sheet advanced southward over tributaries of the Columbia River

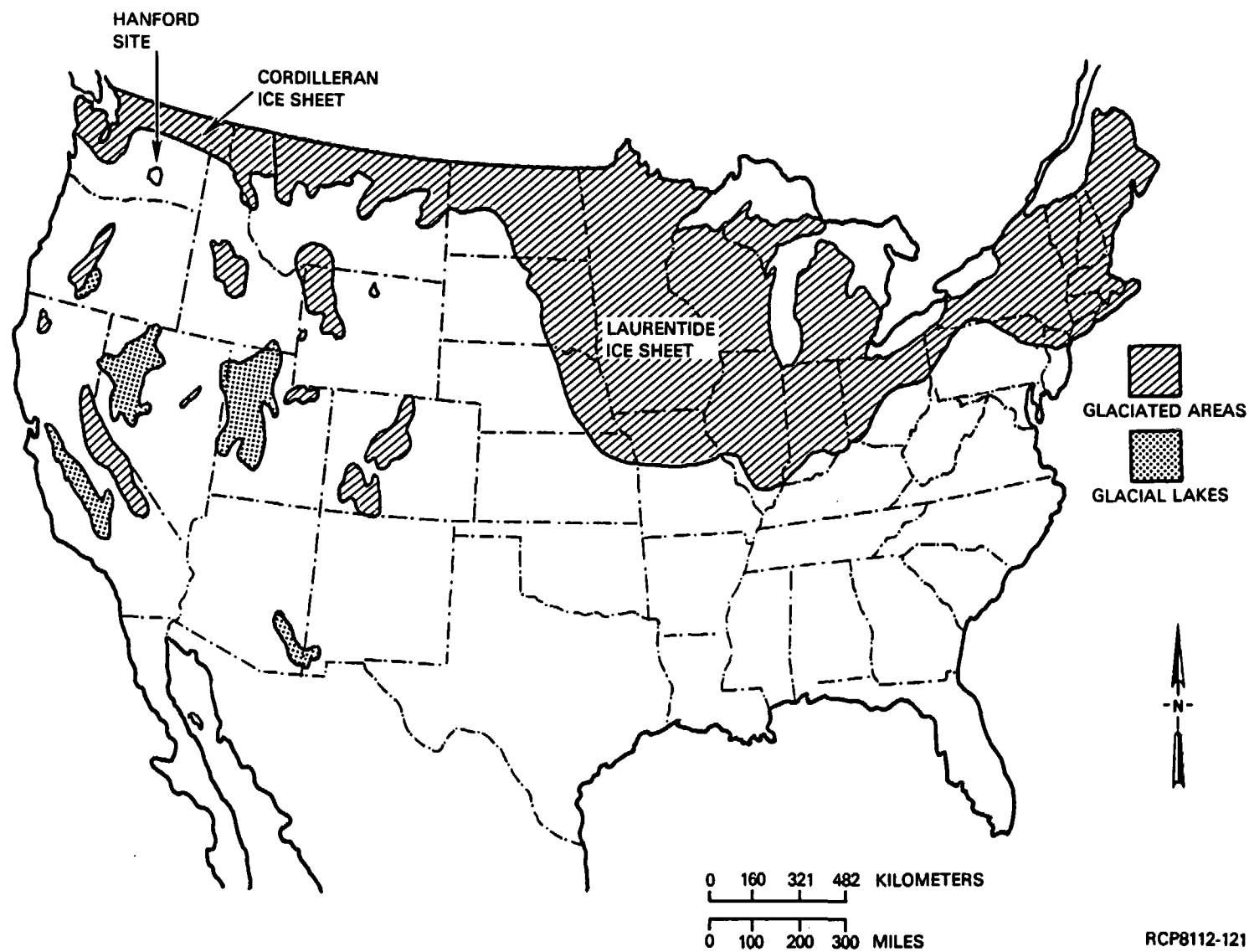


FIGURE 8-11. Maximum Extent of Glaciation During the Last Ice Age (modified after Stottlemire et al., 1981).

TABLE 8-19. Characteristics of Existing Ice Sheets and of the Maximum Quaternary Ice Cover (Flint, 1971).

Glaciation	Area (1 E+12 m ³)
Existing Glaciers	
Greenland	1.80
Spitsbergen and Iceland	0.07
Canadian Archipelago	0.15
North America	0.08
Europe and Asia	0.17
South America	0.03
Antarctica	12.59
Total area	14.99 (3% of Earth's surface)
Total ice volume*	2.5 E+07 km ³
Equivalent sea-level change	70 m
Maximum Quaternary Glaciation	
Greenland	2.30
Spitsbergen and Iceland	0.44
Alaska	1.03
Cordillera	1.58
Laurentide	13.39
Scandinavia	6.67
Europe	0.09
Asia	3.95
South America	0.87
Antarctica	13.81
Other	0.04
Total area	44.17 (9% of Earth's surface)
Total ice volume*	7.5 E+07 km ³
Equivalent sea-level change	210 m

*Based on the present ice thickness of 1,700 meters in Greenland and Antarctica.

and stopped short of the Pasco Basin. Glacial lakes formed where river drainages were blocked by ice, and the sudden release of glacier-dammed lakes caused catastrophic floods of unprecedented magnitude that have produced far-reaching effects on the geology of the region (USGS, 1976). Floods were released not only during glacial retreat but also during the many fluctuations in glacier margins during the ice age.

The two largest floods, one occurring 18,000 to 20,000 years ago and one occurring 13,000 years ago, resulted in floodwaters to elevations of 366 and 274 meters above mean sea level, respectively, in the Pasco Basin. Floodwaters were over 240 meters deep over the lowest areas on the Hanford Site (ERDA, 1975). These floods, and other lesser floods, were responsible for laying down the Pasco gravel beds and the Touchet beds of glaciofluvial deposits on the basalt formations in the basin. The Touchet beds represent the shallow and quiet-water glaciofluvial deposits laid down by floodwaters, while the Pasco gravel beds are the contemporaneous deposits laid down in more rapid water flow (Brown, 1970). The floods are thought to have lasted for periods of 1 day to 2 weeks (Tubbs, 1979). The total number of floods has not been determined. J Harlen Bretz, the geologist who first hypothesized that many geological features in the region were due to catastrophic floods (Bretz, 1923; 1927; 1959), estimated that there had been seven or eight such floods corresponding to nine glacial retreats in northern Montana, Idaho, and eastern Washington (Tubbs, 1979). Brown (1970) states that tentative data show that more than seven floods occurred in the Pasco Basin. Waitt (1980) has recently hypothesized that about 40 such floods must have occurred to form the multiple rhythmites of the Touchet beds. Bjornstad (1980) disagrees with this interpretation, preferring the hypothesis that some of the rhythmites were deposited in multiple flood surges rather than by separate floods.

There is abundant geologic evidence of the catastrophic floods caused by the collapse of ice-dammed lakes in the Columbia River drainage, but there is no evidence that an ice sheet has ever reached as far south as the Hanford Site (Stottlemire et al., 1981). Elevation contours of the surface of the Cordilleran ice sheet at its maximum extent have been reconstructed by Richmond et al. (1965). This ice sheet seems to have been 1,000 to 1,500 meters thick over major valleys in northern Washington, and the vertical accumulation of ice is estimated (Stottlemire et al., 1981) to have occurred at rates from 0.03 to 0.6 meter per year. Little information is available on the rate of ice advance and retreat, but it is generally thought that ice advance occurs at a slower rate than ice retreat. From published estimates of the retreat of the Laurentide ice sheet, Stottlemire et al. (1981) estimate that a reasonable value for the Cordilleran ice sheet retreat is 0.1 to 0.4 kilometer per year.

8.3.1.3 Wind and Circulation Patterns. Paleoclimatic changes in windflow patterns are difficult to reconstruct based on information currently available. The present scarcity of atmospheric-circulation modeling results for the Quaternary period and the lack of full agreement between the models now available will decrease the confidence in conclusions obtained from the literature survey. The largest changes in circulation

patterns near the Hanford area are thought to have occurred between the last glacial maximum and the altithermal interval. Barry (1973) has concluded that the advance of glaciation was accompanied by cooler summers and mild, snowy winters. The circulation changes occurred primarily as a shift in the frequency of certain patterns rather than an abrupt change to a different pattern (Barry et al., 1971). In studying the onset of the full glacial period 60,000 to 70,000 years ago, Lamb and Woodroffe (1970) concluded that a high frequency of meridional flow patterns near the surface of Earth was necessary to carry moisture north to the ice sheets and to allow cold air to flow south off the ice sheets. A meridionally extended upper cold trough was probably also present in the mean upper-air patterns to produce the storms necessary to accumulate the snow over the ice sheet centers. The circulations were probably accompanied by a much-expanded or weakened circumpolar vortex. The moisture source for the Laurentide ice sheet was probably the Gulf of Mexico or the tropical West Atlantic. Lamb and Woodroffe (1970) envisioned little seasonal change in circulation patterns and hypothesized that a radiation deficit was probably necessary to account for the increase in precipitation near 65 degrees north. The wind regime over the ice surfaces must have been anticyclonic (Poser, 1948). If so, cold northerly surface winds may have been prevalent over eastern Washington during the time when the Cordilleran ice sheet was nearby. Nickmann and Leopold (1980) have postulated that the (geologically) sudden change in plant and animal species about 10,000 years ago may be due to the shift in circulation from northerly winds, coming off the anticyclonic circulation over the ice sheet, to southwesterly winds as the ice sheet receded.

Several global circulation models have been used to simulate circulations of the ice age. The basic approach is to determine the boundary conditions that existed for the period of interest (i.e., sea-surface temperatures, topography, distribution of ice, and solar parameters) and, starting with these boundary conditions, to integrate the equations of atmospheric motion long enough for the motions to come into a statistical equilibrium with the boundary conditions. Such an approach depends critically on the accuracy of the boundary conditions. July boundary conditions for the last glacial maximum of the Laurentide ice sheet 18,000 years ago have been determined from paleoclimatic data recently reported by members of the CLIMAP Program, a multi-institutional consortium of scientists studying long-term climatic changes (CLIMAP, 1976). Gates (1976) used these boundary conditions with the RAND Model to find a southward shift and strengthening of the mean Northern Hemisphere westerlies. This resulted from the southward displacement of the zone of maximum meridional temperature gradient caused by the expanded ice sheets. Ice-age evaporation and precipitation in July were reduced 15 percent from the present values. The global circulation model developed at the National Center for Atmospheric Research, running on the same boundary conditions, showed an increase in cloudiness, a precipitation reduction of 50 percent, and no southern displacement of the westerlies. The model developed at the Geophysical Fluid Dynamics Laboratory (Gilchrist, 1978) favored dryness in the ice-age tropics, which agrees qualitatively with the sand dune distribution of Sarnthein (1978). All model integrations agreed that there were lower global temperatures and less rain than at present. The work of Barry (1973) and Williams et al. (1974) preceded the CLIMAP work. They

used the National Center for Atmospheric Research model for July and January conditions at the ice-age maximum. From these simulations they determined that the mean zonal wind strengths in the July ice age in Northern Hemisphere middle latitudes were comparable to present winter conditions. The upper westerlies, surprisingly, were not displaced southward from their present locations. Precipitation in the Northern Hemisphere was slightly less than at present in winter.

Some information is available regarding the variability of major features of atmospheric circulation in the past few centuries (Mitchell, 1977). Major circulation features such as the position of the Inter-tropical Convergence Zone and the centers of high- and low-pressure areas have shifted by two or more degrees of latitude. Midlatitude troughs and ridges have shifted by 10 to 20 degrees of longitude.

8.3.2 Future Climatic Variation

A number of physical mechanisms have been proposed to explain climate change, including variations in the radiation output of the Sun, changes in Earth-Sun geometry, effects of volcanism (Porter, 1981; Stottlemire et al., 1981), effects of carbon dioxide increase or decrease in the troposphere, autovariations in the climate system (Larsen and Barry, 1974; Brown, 1970), and others. Recently, concerns have been expressed regarding the possibility of changes in global climate due to the anthropogenic production of carbon dioxide that results from the consumption of fossil fuels (NAS, 1977). It is generally acknowledged that the climate would warm due to carbon dioxide increases, but it is not known whether particulates being introduced into the atmosphere by man's activities would cause an offsetting cooling effect. Clearly, the prediction of future climatic variation contains numerous assumptions. The best approach to predicting the future climate is to rely primarily on reasonable assumptions and extrapolations based on our present understanding of past changes in climate.

8.3.2.1 Air Temperatures and Precipitation. Midlatitude mean annual air temperatures have varied over a 10°C range in the last 15,000 years (Figure 8-10c). Regional temperatures may have varied over a wider range. Warm interglacial climates, such as the present climate, are typical of only about one-tenth of the climatic record of the last 1 million years (Brown, 1970). Thus, in the absence of significant counteracting atmospheric effects, it seems likely that the largest climate changes will be toward continued cooling. Based on these considerations, on the air-temperature climate record given in Figure 8-10, and on the present climate of the Hanford area, tentative estimates of climatic changes in air temperature are given in Table 8-20. Climatic statistics in the United States are generally calculated over 30-year periods, and the resulting averages are termed "normals." The maximum and minimum rates of temperature change in Table 8-20 should be interpreted as the largest and smallest rates of temperature change between any two 30-year intervals over the time periods stated. Of course, rates of change over smaller averaging times may be outside the ranges given in the table.

TABLE 8-20. Estimates of Minimum and Maximum Temperature Change and Rate of Change from the Present.*

Estimates	Period (yr)		
	0 - 100	100 - 1,000	1,000 - 10,000
Minimum temperature change (°C)	+0.5	+1.0	+3.0
Maximum temperature change (°C)	+2 to -3	+4 to -8	+5 to -15
Minimum rate of temperature change (°C/30 yr)	+0.05	+0.1	+0.2
Maximum rate of temperature change (°C/30 yr)	-1	-2	-3

*The present mean annual temperature as averaged over 58 years is 11.8°C. In individual years the mean annual temperature has ranged from 10.1° to 13.4°C.

Paleoclimate information on regional precipitation is insufficient for future projections. Stottlemire et al. (1981) have stated, however, that it seems unlikely that mean precipitation has varied over a factor of more than 2 from the present values since the last glacial maximum. Thus, mean precipitation has ranged from 8 to 32 centimeters per year.

8.3.2.2 Windflow and Precipitation Patterns. Insufficient information is available to project changes in windflow or precipitation patterns over the next 10,000 years. Some general statements can be made, however. Large circulation changes may occur with the reestablishment of continental ice sheets, should they recur. Cold northerly winds will be a primary circulation feature. The strength and frequency of these winds will depend on the proximity of the ice sheet. Upper-level westerlies will probably increase in strength and move south with the advancing ice sheet.

8.3.2.3 Glaciation and Sea Levels. Global glaciation and sea level are directly related through the hydrologic cycle. Increasing glaciation acts to store water in the solid form, thereby decreasing the storage of water in the oceans and thus the level of the seas.

Past fluctuations in ice volume (Fig. 8-10 a) are assumed to continue into the future. Since the Earth's climate is, at present, thought to be near the end of an interglacial period, there is some concern that a new ice advance may begin in the near geologic future. This has been proposed by several investigators. Morner (1972), comparing the present interglacial with the last interglacial, states that cooling will lead to the first future ice age in 18,800 years. Mitchell (1972) cautions that the

present interglacial is different from the last interglacial in terms of radiation conditions, and that the uncertain effects of increases in carbon dioxide and aerosols make analogies with the last interglacial difficult. Berger (1978) has performed Milankovitch calculations and determined that negative insolation departures will occur at 4,500, 60,000 and 84,000 years in the future, perhaps leading to glacial advances.

Stottlemire et al. (1981) and Petrie et al. (1981) have designed a geologic simulation model that has been applied to the Hanford region. This model uses long-term changes in the Earth-Sun geometry (i.e., the Milankovitch hypothesis) as the climatic forcing function, but also includes a statistical distribution to evaluate the effect of future volcanism on the climate simulations. The model predicts that the glacial ice sheet could reach as far south as the Hanford Site in the future and that glaciation may advance into northern Washington within 10,000 years (Foley et al., 1981). Bull (1979; 1980) estimates that the probability of ice cover at the Hanford Site in the next million years is 50 percent.

The CLIMAP reconstruction of ice-age sea levels determined that sea levels were more than 85 meters below present (CLIMAP, 1976). Bull (1979) states that sea levels 18,000 years ago were between 126 and 165 meters below present. He estimates a drop of as much as 200 meters with extensive glaciation. He has also estimated the rises in sea level that will occur in the present interglacial if the Greenland and West Antarctic ice sheets continue to melt. The probability that the West Antarctic ice sheet will melt during the present interglacial is less than 10 percent; such a melt would cause a sea-level rise of 7 meters. The Greenland ice sheet may also melt (probability less than 5 percent), producing a rise of another 7 meters. There is a 25 percent probability that the entire Antarctic ice sheet may melt in the next million years, increasing sea level by 60 or 70 meters.

8.4 METEOROLOGICAL REQUIREMENTS FOR THE REFERENCE REPOSITORY LOCATION

For preliminary site characterization, Hanford Meteorological Station data have been used. Some local variations in climatic elements may be expected within the reference repository location due to topographic effects.

8.4.1 Dispersion Evaluations

Hanford Meteorological Station tower data have been the historical basis for the evaluation of dispersion for the Hanford Site in the vicinity of the reference repository location. The joint windspeed, direction, and stability-frequency summaries currently used for surface-release dispersion evaluations are contained in Table 8-21. These data, plotted as wind roses, were shown in Figure 8-9. Additional summaries by season and for other measurement heights have been published by Stone et al. (1972). The stability groupings in these summaries are based on delta-temperature stability categories developed for the Hanford area dispersion models. The Hanford Meteorological Station tower data, summarized in a joint-frequency format based on Pasquill-Gifford data-temperature stability categories (NRC, 1972) are presented in Table 8-22.

The joint-frequency distributions are skewed to both poor and good dispersion conditions. Frequent occurrences of low windspeed and stable conditions give a relatively high frequency of poor dispersion conditions. On the other hand, the occurrences of high windspeeds and unstable conditions result in relatively high frequencies of strong dispersion conditions.

Although averages and trends are expected to be similar, some differences between the Hanford Meteorological Station and other areas within the reference repository location may be anticipated based on local topography. The prevailing flow of winds from the northwest will be influenced by a 50-meter hill northwest of the reference repository location. Also, the reference repository location is closer to Rattlesnake Mountain than is the Hanford Meteorological Station and could be expected to be influenced more by the complex air flow over and around Rattlesnake Mountain.

The NRC guidelines allow some latitude as to the specific dispersion models to be used (NRC, 1977; 1979). A number of these computer models are available for the long-term assessments and accident cases. In addition to NRC-developed models, atmospheric dispersion and dose models developed for use at the Hanford Site are summarized in documents by Streng et al. (1976), Napier (1981), and Streng and Peloquin (1981).

The computer code groups available for long-term assessments are summarized in Table 8-23. The use of a model to incorporate the effects of nonuniform horizontal wind fields (MESOI, MESODIF-II) is recommended by the NRC for areas such as the Hanford Site with complex flow patterns.

TABLE 8-21. Annual Joint Windspeed, Direction, and Stability Frequencies for Hanford Meteorological Station Based on Hanford Delta-Temperature Stability Groups, 1955-1970 (wind direction and speed at 61 meters).

Stability class	Windspeed (m/s)	Wind Direction (%)																		Calm	Total
		NNE	NE	ENE	E	ESE	SE	SSE	S	SSW	SW	WSW	W	WNW	NW	NNW	N	VAR			
VS	0-1.5	0.21	0.21	0.15	0.20	0.26	0.38	0.23	0.23	0.20	0.23	0.22	0.40	0.34	0.43	0.37	0.35	0.21	0.48	5.11	
MS		0.17	0.18	0.16	0.21	0.33	0.42	0.20	0.18	0.12	0.12	0.13	0.21	0.22	0.31	0.28	0.29	0.13	0.50	4.15	
N		0.30	0.34	0.27	0.33	0.36	0.44	0.22	0.15	0.13	0.11	0.10	0.18	0.18	0.33	0.41	0.41	0.13	0.48	4.87	
U		0.49	0.64	0.36	0.40	0.31	0.27	0.12	0.17	0.10	0.16	0.10	0.14	0.14	0.27	0.37	0.54	0.46	0.04	5.09	
VS	2.0-3.0	0.21	0.18	0.14	0.17	0.20	0.33	0.28	0.28	0.24	0.35	0.50	0.96	1.08	1.00	0.69	0.39	0.02	0.00	7.02	
MS		0.17	0.15	0.13	0.15	0.22	0.36	0.21	0.17	0.15	0.21	0.24	0.42	0.50	0.68	0.47	0.31	0.02	0.00	4.56	
N		0.12	0.13	0.10	0.12	0.19	0.26	0.14	0.10	0.07	0.10	0.11	0.16	0.27	0.55	0.33	0.18	0.01	0.00	2.94	
U		0.94	0.90	0.55	0.58	0.53	0.62	0.37	0.45	0.45	0.51	0.37	0.38	0.48	1.13	1.11	1.18	0.30	0.00	10.84	
VS	3.5-5.5	0.13	0.11	0.08	0.07	0.07	0.13	0.21	0.11	0.12	0.24	0.59	1.23	2.00	1.74	0.60	0.20	0.00	0.00	7.65	
MS		0.11	0.08	0.03	0.06	0.10	0.21	0.19	0.13	0.20	0.34	0.50	0.96	1.47	1.53	0.38	0.14	0.00	0.00	6.43	
N		0.06	0.04	0.03	0.03	0.04	0.09	0.07	0.04	0.06	0.09	0.14	0.14	0.42	0.78	0.15	0.06	0.00	0.00	2.26	
U		0.48	0.33	0.12	0.09	0.09	0.15	0.11	0.14	0.34	0.59	0.56	0.33	0.59	1.42	0.52	0.45	0.00	0.00	6.31	
VS	6.0-8.0	0.05	0.03	0.02	0.02	0.00	0.04	0.10	0.03	0.03	0.09	0.25	0.43	1.25	1.53	0.17	0.05	0.00	0.00	4.10	
MS		0.10	0.05	0.02	0.02	0.02	0.07	0.13	0.15	0.25	0.54	0.87	1.24	3.04	2.23	0.18	0.10	0.00	0.00	9.03	
N		0.05	0.01	0.01	0.01	0.00	0.03	0.04	0.05	0.07	0.14	0.24	0.16	0.44	0.58	0.06	0.04	0.00	0.00	1.94	
U		0.26	0.13	0.03	0.01	0.01	0.03	0.04	0.05	0.18	0.54	0.68	0.26	0.64	0.98	0.09	0.14	0.00	0.00	4.07	
VS	8.5-10.5	0.00	0.00	0.00	0.00	0.00	0.00	0.01	0.01	0.01	0.02	0.04	0.02	0.06	0.18	0.00	0.00	0.00	0.00	0.37	
MS		0.04	0.03	0.01	0.00	0.00	0.02	0.06	0.11	0.21	0.53	0.50	0.33	1.55	1.45	0.03	0.02	0.00	0.00	4.91	
N		0.02	0.02	0.00	0.00	0.00	0.01	0.01	0.03	0.08	0.15	0.17	0.05	0.25	0.34	0.01	0.02	0.00	0.00	1.17	
U		0.06	0.05	0.01	0.00	0.00	0.00	0.01	0.02	0.11	0.34	0.41	0.12	0.32	0.63	0.01	0.03	0.00	0.00	2.13	
VS	over 10.5	0.00	0.00	0.00	0.00	0.00	0.00	0.00	0.00	0.01	0.01	0.00	0.00	0.00	0.00	0.00	0.00	0.00	0.00	0.04	
MS		0.01	0.01	0.00	0.00	0.00	0.01	0.02	0.08	0.30	0.47	0.22	0.06	0.55	0.76	0.00	0.01	0.00	0.00	2.50	
N		0.01	0.01	0.00	0.00	0.00	0.00	0.01	0.02	0.08	0.17	0.09	0.03	0.21	0.30	0.00	0.01	0.00	0.00	0.93	
U		0.02	0.03	0.01	0.00	0.00	0.00	0.00	0.01	0.09	0.40	0.31	0.08	0.17	0.46	0.01	0.00	0.00	0.00	1.57	
VS	Totals	0.60	0.54	0.39	0.47	0.53	0.88	0.83	0.67	0.61	0.95	1.61	3.05	4.73	4.89	1.83	1.00	0.23	0.48	24.29	
MS		0.60	0.50	0.36	0.45	0.67	1.08	0.82	0.83	1.22	2.21	2.46	3.23	7.33	6.96	1.34	0.87	0.14	0.50	31.57	
N		0.56	0.55	0.42	0.49	0.60	0.82	0.49	0.40	0.48	0.76	0.85	0.72	1.78	2.88	0.95	0.72	0.15	0.48	14.11	
U		2.25	2.08	1.08	1.09	0.94	1.07	0.65	0.84	1.27	2.53	2.43	1.30	2.35	4.90	2.11	2.34	0.77	0.04	30.03	

*VS - very stable, MS - moderately stable, N - neutral, U - unstable.

TABLE 8-22. Annual Joint Windspeed, Direction, and Stability Figures for Hanford Meteorological Station Based on Pasquill-Gifford Delta-Temperature Stability Groups, 1955-1970 (wind direction and speed at 61 meters). (Sheet 1 of 2)

Stability class	Windspeed (m/s)	Wind Direction (%)																		
		N	NNE	NE	ENE	E	ESE	SE	SSE	S	SSW	SW	WSW	W	WNW	NW	NNW	VAR	Calm	Total
Extremely unstable	Calm	0.00	0.00	0.00	0.10	0.00	0.00	0.00	0.00	0.00	0.00	0.00	0.00	0.00	0.00	0.00	0.00	0.00	0.01	0.01
	0.5-1.5	0.15	0.19	0.19	0.09	0.10	0.08	0.09	0.04	0.04	0.02	0.04	0.03	0.03	0.03	0.07	0.09	0.15	0.00	1.43
	2.0-3.0	0.47	0.47	0.40	0.24	0.23	0.21	0.24	0.15	0.18	0.16	0.17	0.11	0.11	0.14	0.35	0.38	0.14	0.00	4.15
	3.5-5.5	0.18	0.22	0.16	0.05	0.03	0.03	0.05	0.04	0.05	0.10	0.19	0.14	0.07	0.17	0.43	0.17	0.00	0.00	2.08
	6.0-8.0	0.06	0.12	0.07	0.01	0.01	0.00	0.00	0.01	0.01	0.04	0.17	0.18	0.07	0.21	0.35	0.04	0.00	0.00	1.36
	8.5-10.5	0.01	0.03	0.02	0.01	0.00	0.00	0.00	0.00	0.00	0.03	0.10	0.12	0.04	0.13	0.30	0.01	0.00	0.00	0.80
	11.0-up	0.00	0.00	0.01	0.00	0.00	0.00	0.00	0.00	0.00	0.02	0.12	0.10	0.03	0.08	0.22	0.00	0.00	0.00	0.59
	Total	0.87	1.03	0.84	0.40	0.37	0.32	0.39	0.24	0.29	0.37	0.79	0.68	0.36	0.76	1.72	0.69	0.29	0.01	10.42
Moderately unstable	Calm	0.00	0.00	0.00	0.00	0.00	0.00	0.00	0.00	0.00	0.00	0.00	0.00	0.00	0.00	0.00	0.00	0.00	0.00	0.00
	0.5-1.5	0.05	0.06	0.08	0.03	0.05	0.04	0.05	0.02	0.02	0.02	0.02	0.01	0.01	0.01	0.03	0.03	0.05	0.00	0.58
	2.0-3.0	0.12	0.09	0.11	0.08	0.07	0.07	0.08	0.04	0.06	0.05	0.07	0.04	0.05	0.05	0.12	0.11	0.03	0.00	1.24
	3.5-5.5	0.06	0.08	0.04	0.02	0.02	0.01	0.03	0.01	0.02	0.04	0.06	0.07	0.04	0.06	0.15	0.06	0.00	0.00	0.76
	6.0-8.0	0.01	0.03	0.02	0.01	0.00	0.00	0.00	0.01	0.01	0.02	0.07	0.08	0.03	0.08	0.12	0.01	0.00	0.00	0.51
	8.5-10.5	0.00	0.01	0.01	0.00	0.00	0.00	0.00	0.00	0.00	0.02	0.04	0.05	0.01	0.05	0.10	0.00	0.00	0.00	0.30
	11.0-up	0.00	0.01	0.00	0.00	0.00	0.00	0.00	0.00	0.00	0.01	0.05	0.04	0.01	0.02	0.07	0.00	0.00	0.00	0.22
	Total	0.24	0.28	0.26	0.14	0.14	0.13	0.16	0.09	0.10	0.16	0.29	0.29	0.16	0.28	0.59	0.22	0.08	0.00	3.61
Slightly unstable	Calm	0.00	0.00	0.00	0.00	0.00	0.00	0.00	0.00	0.00	0.00	0.00	0.00	0.00	0.00	0.00	0.00	0.00	0.01	0.01
	0.5-1.5	0.07	0.05	0.08	0.05	0.07	0.05	0.05	0.02	0.02	0.02	0.02	0.02	0.02	0.02	0.03	0.03	0.05	0.00	0.68
	2.0-3.0	0.12	0.11	0.10	0.06	0.08	0.07	0.09	0.05	0.05	0.06	0.06	0.05	0.05	0.06	0.11	0.13	0.03	0.00	1.26
	3.5-5.5	0.06	0.05	0.05	0.02	0.02	0.01	0.02	0.02	0.02	0.05	0.08	0.08	0.05	0.07	0.17	0.06	0.00	0.00	0.83
	6.0-8.0	0.02	0.03	0.01	0.00	0.00	0.00	0.00	0.01	0.01	0.03	0.07	0.10	0.04	0.10	0.13	0.01	0.00	0.00	0.59
	8.5-10.5	0.00	0.01	0.01	0.00	0.00	0.00	0.00	0.00	0.00	0.02	0.05	0.06	0.01	0.05	0.08	0.00	0.00	0.00	0.29
	11.0-up	0.00	0.00	0.01	0.00	0.00	0.00	0.00	0.00	0.00	0.02	0.07	0.05	0.01	0.03	0.08	0.00	0.00	0.00	0.29
	Total	0.28	0.25	0.24	0.14	0.16	0.14	0.17	0.11	0.10	0.20	0.35	0.36	0.19	0.33	0.61	0.24	0.08	0.01	3.96
Neutral	Calm	0.00	0.00	0.00	0.00	0.00	0.00	0.00	0.00	0.00	0.00	0.00	0.00	0.00	0.00	0.00	0.00	0.00	0.66	0.66
	0.5-1.5	0.71	0.49	0.65	0.46	0.55	0.60	0.60	0.28	0.26	0.19	0.21	0.16	0.29	0.31	0.52	0.64	0.34	0.00	7.25
	2.0-3.0	0.67	0.43	0.47	0.30	0.37	0.42	0.56	0.31	0.30	0.27	0.36	0.31	0.41	0.60	1.14	0.82	0.10	0.00	7.82
	3.5-5.5	0.24	0.24	0.16	0.08	0.08	0.10	0.16	0.14	0.14	0.27	0.45	0.49	0.48	0.88	1.48	0.40	0.00	0.00	5.77
	6.0-8.0	0.12	0.17	0.07	0.02	0.01	0.01	0.05	0.07	0.12	0.25	0.53	0.71	0.52	1.06	1.12	0.11	0.00	0.00	4.95
	8.5-10.5	0.04	0.05	0.05	0.01	0.00	0.00	0.01	0.03	0.07	0.20	0.47	0.49	0.21	0.79	0.81	0.02	0.00	0.00	3.26
	11.0-up	0.01	0.02	0.02	0.00	0.00	0.00	0.00	0.01	0.06	0.24	0.54	0.30	0.08	0.52	0.76	0.00	0.00	0.00	2.56
	Total	1.79	1.40	1.41	0.89	1.02	1.13	1.38	0.83	0.95	1.42	2.56	2.45	1.98	4.15	5.83	2.00	0.44	0.66	32.28

TABLE 8-22. Annual Joint Windspeed, Direction, and Stability Figures for Hanford Meteorological Station Based on Pasquill-Gifford Delta-Temperature Stability Groups, 1955-1970
(wind direction and speed at 61 meters). (Sheet 2 of 2)

Stability class	Windspeed (m/s)	Wind Direction (%)																		Calm	Total
		N	NNE	NE	ENE	E	ESE	SE	SSE	S	SSW	SW	WSW	W	WNW	NW	NNW	VAR			
Slightly stable	Calm	0.00	0.00	0.00	0.00	0.00	0.00	0.00	0.00	0.00	0.00	0.00	0.00	0.00	0.00	0.00	0.00	0.00	0.55	0.55	
	0.5-1.5	0.36	0.23	0.24	0.20	0.25	0.33	0.43	0.25	0.23	0.16	0.19	0.18	0.32	0.31	0.43	0.36	0.18	0.00	4.67	
	2.0-3.0	0.44	0.23	0.18	0.15	0.18	0.25	0.38	0.25	0.23	0.21	0.28	0.38	0.73	0.85	0.98	0.68	0.00	0.00	6.40	
	3.5-5.5	0.23	0.15	0.13	0.09	0.10	0.12	0.21	0.22	0.13	0.18	0.33	0.65	1.24	2.18	1.74	0.49	0.00	0.00	8.19	
	6.0-8.0	0.10	0.09	0.05	0.02	0.04	0.02	0.07	0.12	0.10	0.17	0.42	0.73	1.06	2.89	1.85	0.18	0.00	0.00	7.91	
	8.5-10.5	0.01	0.02	0.02	0.01	0.00	0.00	0.01	0.04	0.07	0.13	0.35	0.36	0.20	1.07	1.03	0.02	0.00	0.00	3.37	
	11.0-up	0.00	0.00	0.00	0.00	0.00	0.00	0.00	0.01	0.05	0.18	0.26	0.13	0.04	0.28	0.38	0.00	0.00	0.00	1.33	
Total	1.14	0.73	0.63	0.48	0.56	0.72	1.10	0.90	0.81	1.03	1.83	2.44	3.58	7.58	6.41	1.72	0.21	0.55	32.42		
Moderately stable	Calm	0.00	0.00	0.00	0.00	0.00	0.00	0.00	0.00	0.00	0.00	0.00	0.00	0.00	0.00	0.00	0.00	0.00	0.20	0.20	
	0.5-1.5	0.20	0.10	0.10	0.08	0.09	0.13	0.21	0.11	0.12	0.10	0.11	0.10	0.17	0.16	0.20	0.19	0.11	0.00	2.28	
	2.0-3.0	0.18	0.09	0.07	0.06	0.06	0.09	0.18	0.14	0.14	0.13	0.17	0.22	0.44	0.51	0.54	0.38	0.00	0.00	3.39	
	3.5-5.5	0.07	0.04	0.03	0.01	0.01	0.02	0.09	0.11	0.06	0.06	0.11	0.30	0.62	0.93	1.17	0.34	0.00	0.00	3.95	
	6.0-8.0	0.02	0.03	0.01	0.01	0.01	0.00	0.04	0.08	0.02	0.02	0.05	0.20	0.32	0.86	1.25	0.11	0.00	0.00	3.03	
	8.5-10.5	0.00	0.00	0.00	0.00	0.00	0.00	0.01	0.01	0.01	0.01	0.01	0.04	0.03	0.09	0.21	0.00	0.00	0.00	0.44	
	11.0-up	0.00	0.00	0.00	0.00	0.00	0.00	0.00	0.01	0.01	0.01	0.01	0.01	0.00	0.00	0.01	0.00	0.00	0.00	0.05	
Total	0.47	0.26	0.21	0.15	0.17	0.24	0.52	0.46	0.36	0.32	0.47	0.86	1.59	2.55	3.38	1.02	0.12	0.20	13.35		
Extremely stable	Calm	0.00	0.00	0.00	0.00	0.00	0.00	0.00	0.00	0.00	0.00	0.00	0.00	0.00	0.00	0.00	0.00	0.00	0.06	0.06	
	0.5-1.5	0.09	0.06	0.11	0.03	0.07	0.07	0.12	0.07	0.08	0.07	0.07	0.07	0.10	0.05	0.11	0.13	0.11	0.00	0.41	
	2.0-3.0	0.11	0.07	0.07	0.05	0.06	0.05	0.08	0.09	0.10	0.06	0.08	0.12	0.18	0.16	0.16	0.18	0.03	0.00	1.64	
	3.5-5.5	0.02	0.01	0.01	0.01	0.01	0.01	0.03	0.04	0.03	0.04	0.04	0.07	0.13	0.16	0.31	0.19	0.00	0.00	1.10	
	6.0-8.0	0.00	0.00	0.00	0.00	0.00	0.00	0.01	0.01	0.02	0.02	0.01	0.03	0.07	0.14	0.32	0.05	0.00	0.00	0.67	
	8.5-10.5	0.00	0.00	0.00	0.00	0.00	0.00	0.00	0.01	0.01	0.01	0.01	0.00	0.01	0.01	0.03	0.00	0.00	0.00	0.08	
	11.0-up	0.00	0.00	0.00	0.00	0.00	0.00	0.00	0.00	0.00	0.00	0.00	0.00	0.00	0.00	0.00	0.00	0.00	0.00	0.01	
Total	0.22	0.14	0.19	0.09	0.14	0.13	0.25	0.21	0.24	0.20	0.22	0.29	0.50	0.52	0.92	0.54	0.14	0.08	4.99		

TABLE 8-23. Computer Models Available at Hanford for X/Q , D/Q
Long-Term Assessment.

Computer model	Type	Description	Use	Input	Output
MESOI (Ramsdell and Athey, 1981)	Variable puff	LaGrangian-Gaussian puff model, can be multisource at different release heights	Average X/Q , D/Q plus it can be used operation- ally in case of accidental releases	Hanford wind fields from telemetry data, stability from tower data, and acoustic sounder information	Trajectory and X/Q and D/Q fields
HANFORD (Slade, 1968; Napier, 1981)*	Straight line	Gaussian - <ul style="list-style-type: none"> • Plume rise • Building wake effects 	Average X/Q and D/Q (with real- time data hourly and annually)	Joint frequen- cies of wind speed and direc- tion as a func- tion of Hanford stability classes	X/Q and D/Q fields
XOQDOQ (Sagendorf and Goll, 1977)	Straight line	Gaussian--has options for the following: <ul style="list-style-type: none"> • Plume rise • Ground-level or elevated- release heights • Building or terrain wake effects • Wind speeds can be extrapolated vertically • Topography • Radioactive decay • Plume depletion by dry deposition • Local air recirculation stagnation 	Average X/Q and D/Q	Joint frequen- cies of wind speed and direc- tion versus MRC Pasquill sta- bility class	X/Q and D/Q fields
MESODIF-II (Powell et al., 1979)	Variable plume	LaGrangian-Gaussian plume model has options for the following: <ul style="list-style-type: none"> • Plume rise • Two release heights • Topography effects • Horizontal diffusion • Plume deposition and decay • Fixed sampling grid plus special sampling points 	Average X/Q , and D/Q	Gridded wind fields, and stability	X/Q , and D/Q , fields

*Hanford dispersion coefficients are given in Slade (1968). These are implemented in Hanford dispersion/dose models summarized by Napier (1981).

The accident-case-dispersion computer models appropriate for the reference repository location are summarized in Table 8-24. The NRC model is a fairly simple approach that provides consistent estimates. An estimate of accident-dispersion conditions based on statistical analyses is provided by HANFORD-STAT. A procedure for using a standard set of meteorological conditions that have been incorporated in the Hanford Site dose models is called HANFORD-STAN.

8.4.2 Meteorological Conditions for Design Bases

Severe and extreme meteorological phenomena that should be considered for design and operating bases of the reference repository location are tornadoes, high winds (gusts), weight of snow and ice, extreme temperatures, thunderstorms and lightning, severe duststorms, and blowing and drifting snow.

8.4.2.1 Tornado Parameters. The probability of a tornado occurring in the Hanford region, expected translational and rotational speeds of a severe tornado, and maximum pressure differentials have been examined for the Hanford area (Section 8.1.3.7). These values are equal to or less than those tornado parameters listed for a Class III region as indicated in Table 8-25. Structures will be designed in accordance with Class III.

8.4.2.2 Fastest Mile of Wind. The fastest mile of wind is generally defined as either the fastest speed associated with 1 mile of passing wind or fastest observed 1-minute windspeed. The annual extreme fastest mile of windspeed for a given region has been commonly used as the best available measure of wind for design purposes (ERDA, 1975). Standard reference speed height is normally chosen at the 9.1-meter elevation, and windspeed is assumed to vary with the one-seventh power of height.

The structures at the reference repository location will be designed to withstand a basic wind (fastest mile) velocity, including gusts, of 36 meters per second (80 miles per hour) at a height of 9.1 meters above the site grade (ANSI, 1972). This design speed value is appropriate since the 100-year-return-period peak gust, as shown in Figure 8-12, at the Hanford Meteorological Station is 38.4 meters per second (86 miles per hour) at an elevation of 15.2 meters. Also, at that level, peak gusts have not exceeded 36 meters per second (80 miles per hour) during the period 1945 to present, as shown in Table 8-26. The 100-year-return-period fastest mile of wind would be less than 38.4 meters per second, since by definition gust velocity divided by an appropriate gust factor provides the velocity of the fastest mile of wind. Although not recorded in historical records, the 100-year fastest mile of wind can be expected to be in the range of 30 to 35 meters per second. These values are based on the application of gust factors of 1.3 and 1.1 for gusts of 1- and 10-second durations, respectively, to the estimated historical value of 38.4 meters per second (ERDA, 1975).

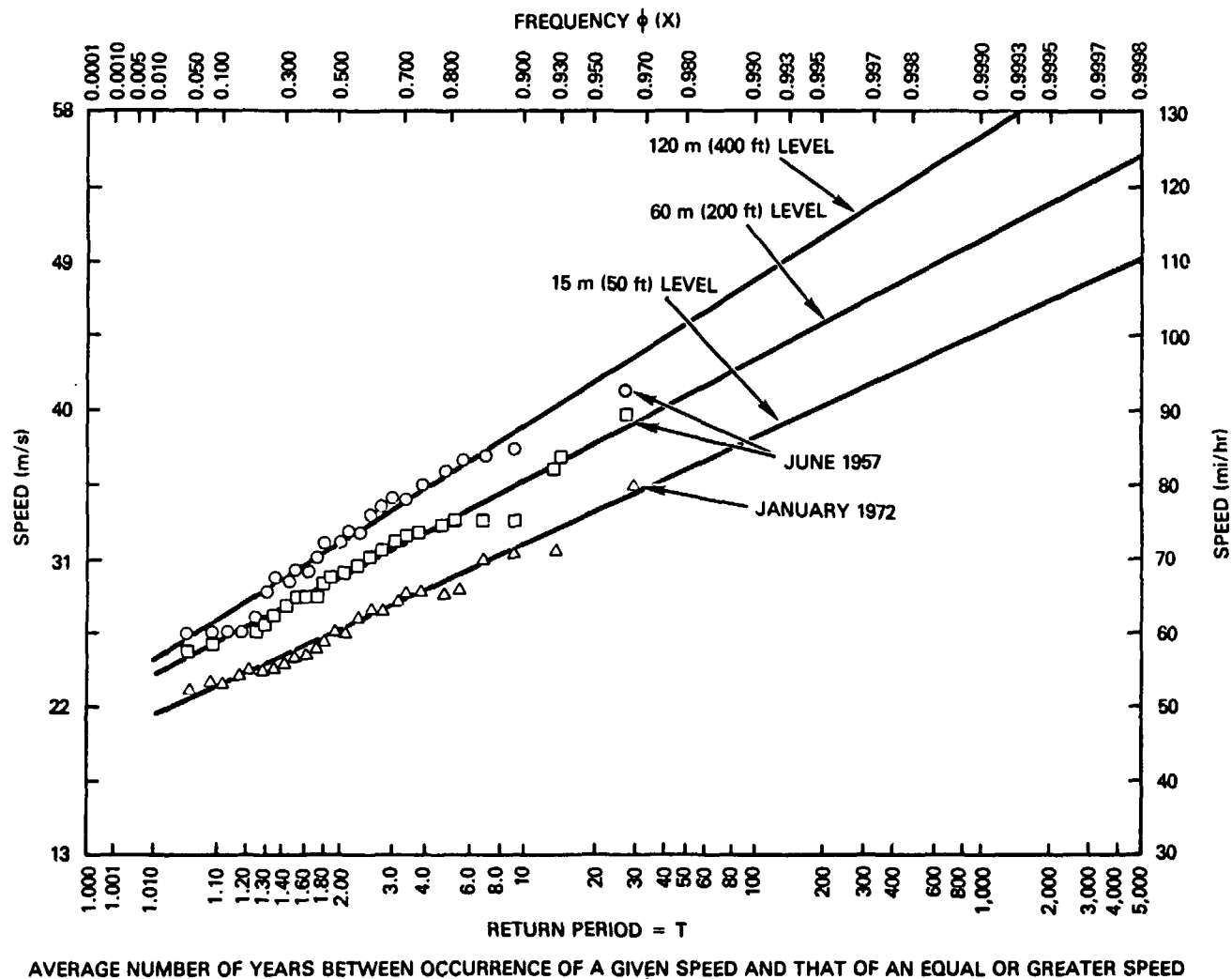
TABLE 8-24. Accident-Case Models Available to Meet
U.S. Nuclear Regulatory Commission Guidelines.

Model	Type	Description	Use	Input	Output
NRC-GUIDE (NRC, 1974a; 1974b)	Procedure	Gaussian straight line, NRC Pasquill dispersion coefficients	Preliminary site evaluations	Distance to receptor	Maximum X/Q estimates
HANFORD-STAN (Streng and Peloquin, 1981)	Procedure	Gaussian straight line, Hanford dis- persion formulation	Preliminary site evaluations	Distance to receptor	Maximum X/Q estimates
NRC (Markee and Levine, 1977)	Computer code	Gaussian straight line, NRC Pasquill dispersion coefficients	Site evaluations with onsite data	Windspeed, direction, and stability- frequency tables	Maximum X/Q estimates
HANFORD- STAT*	Computer code	Gaussian straight line, Hanford dispersion formulation	Site evaluations with onsite data	Hourly X/Q values	Maximum X/Q estimates for 95 and 50 percentiles

*HANFORD-STAT is a model developed at the Hanford Site to provide a statistical estimate of worst-case conditions. It has been applied in several cases. Formal documentation of code would be required for application at the reference repository location.

TABLE 8-25. Design-Basis-Tornado
Characteristics (WPPSS, 1979).

Property	Class III	
Maximum windspeed, m/s (mi/hr)	110	(240)
Rotational speed, m/s (mi/hr)	85	(190)
Translational speed		
Maximum, m/s (mi/hr)	22	(50)
Minimum, m/s (mi/hr)	2	(5)
Radius of maximum rotational speed, m (ft)	46	(150)
Pressure drop, kPa (lb/in ²)	10	(1.5)
Rate of pressure drop, kPa/s (lb/in ² /s)	4.1	(0.6)



RCP8201-71

FIGURE 8-12. Peak Wind-Gust Return-Probability Diagram (ERDA, 1975).

TABLE 8-26. Highest Average Monthly Windspeed and Peak Gusts (ERDA, 1975).

Month	Highest average windspeed (m/s)		Peak gusts (m/s)		
	Monthly	Year	Speed	Direction	Year
January	4.6	1972	36	S	1972
February	4.2	1961	28	SW	1965
March	4.8	1964	31	SW	1956
April	5.0	1959	27	WSW	1969
May	4.7	1965*	32	SSW	1948
June	4.8	1949	32	SW	1957
July	4.3	1963	25	WSW	1968
August	4.1	1946	30	SW	1961
September	4.1	1961	29	SSW	1953
October	4.1	1946	28	SSW	1950
November	3.5	1945	29	SSW	1949
December	3.7	1968	32	SW	1955
Year	3.7	1968*	36	SW	1972

*Also occurred in an earlier year.

8.4.2.3 Weight of Snow and Ice. The American National Standards Institute (ANSI, 1972) provides weights of 100-year-return-period ground-level snow packs for the Hanford region. If the ANSI (1972) value of 98 kilograms per square meter is used as the design snow (and ice) load for BWIP structures and a snow density of 0.10 gram per cubic centimeter (specific gravity of 0.1) is assumed, then the denser snow load would correspond to a snow depth of 0.98 meter. The above snow load is conservative for the site, as snow depth seldom exceeds 15 centimeters, and the greatest depth of 53.3 centimeters was recorded in February 1916. The weight of the 48-hour probable maximum winter precipitation can be estimated from the data in Table 8-27. Since the greatest snowfall in 24 hours was 21.1 centimeters (November 1978), and a record depth of approximately 30.5 centimeters lasted 4 days (December 1964), these depths would correspond to snow loads of 21.1 and 30.5 kilograms per square meter, respectively.

TABLE 8-27. Miscellaneous Snowfall Statistics, 1946 Through 1980.^a

		October	November	December	January	February	March	Season
0400 Pacific Standard Time, Number of Days								
Average number of days, depth								
cm	(in.)							
2.5	(1) or more	0	1	5	9	4	b	19
7.5	(3) or more	0	1	2	5	3	0	11
15	(6) or more	0	b	b	2	1	0	3
30	(12) or more	0	0	b	b	0	0	6
Record greatest number of days and year, depth								
cm	(in.)							
2.5	(1) or more	0	1978 ^c 12	1972 18	1969 31	1950 17	1950 3	1955-56 54
7.5	(3) or more	0	1978 12	1955 14	1969 23	1950 16	0	1978-79 ^d 40
15	(6) or more	0	1978 6	1964 12	1965 23	1969 ^d 8	0	1964-65 35
30	(12) or more	0	0	1964 4	1969 1	0	0	1964-65 4
Year and Depth (cm)								
Record greatest depth		1973 3.8	1978 23	1964 30.7	1969 30.5	1969 25.4	1957 5.8	December 1964 30.7
Greatest in 24 hours		1973 3.8	1978 21	1965 14	1954 18	1975 14	1957 ^d 5.6	November 1978 21
Average (%)								
Water equivalent of all precipitation		4	19	41	45	28	14	25

^aTaken, in part, from Stone et al. (1972).^bLess than 1/2 day.^cYear of occurrence.^dAlso occurred in an earlier year.

8.4.2.4 Extreme Maximum and Minimum Temperatures. The periods of December 1 to 17, 1919 (18 days duration), January 24 to February 5, 1950 (13 days duration), and January 12 to February 3, 1957 (23 days duration) were record-breaking cold periods. These three periods accounted for 7 of the 10 days of record with a daily maximum temperature of not more than -18°C and for 9 of the 16 days of record with a minimum temperature of not more than -29°C .

Other periods of cold temperatures are identified in Table 8-28. These periods, together with those of 1919, 1950, and 1957, account for all 16 days of record with a minimum temperature of not more than -29°C . The lowest temperatures in each of the 68 winters at the Hanford Meteorological Station and their probabilities of occurrence are plotted in Figure 8-13.

Two of the most unseasonable periods of above normal temperatures occurred in 1958 and 1971. Statistics for these periods are given in Table 8-29. The highest temperatures during each of 66 summers at the Hanford Site and their probability of occurrence are shown in Figure 8-14.

TABLE 8-28. Periods of Extreme Cold Temperature and Persistence (Stone et al., 1972).

Period	Total	Number of Days			Extreme low	
		Maximum 0°C (32°F) or below	Minimum -18°C (0°F) or below	Minimum -29°C (-20°F) or below	$^{\circ}\text{C}$	$^{\circ}\text{F}$
December 30, 1915 to January 20, 1916	22	20	11	2	-31	-23
January 6, 1930 to January 31, 1930	26	25	13	3	-30	-22
January 5, 1937 to February 2, 1937	29	29	12	2	-31	-23

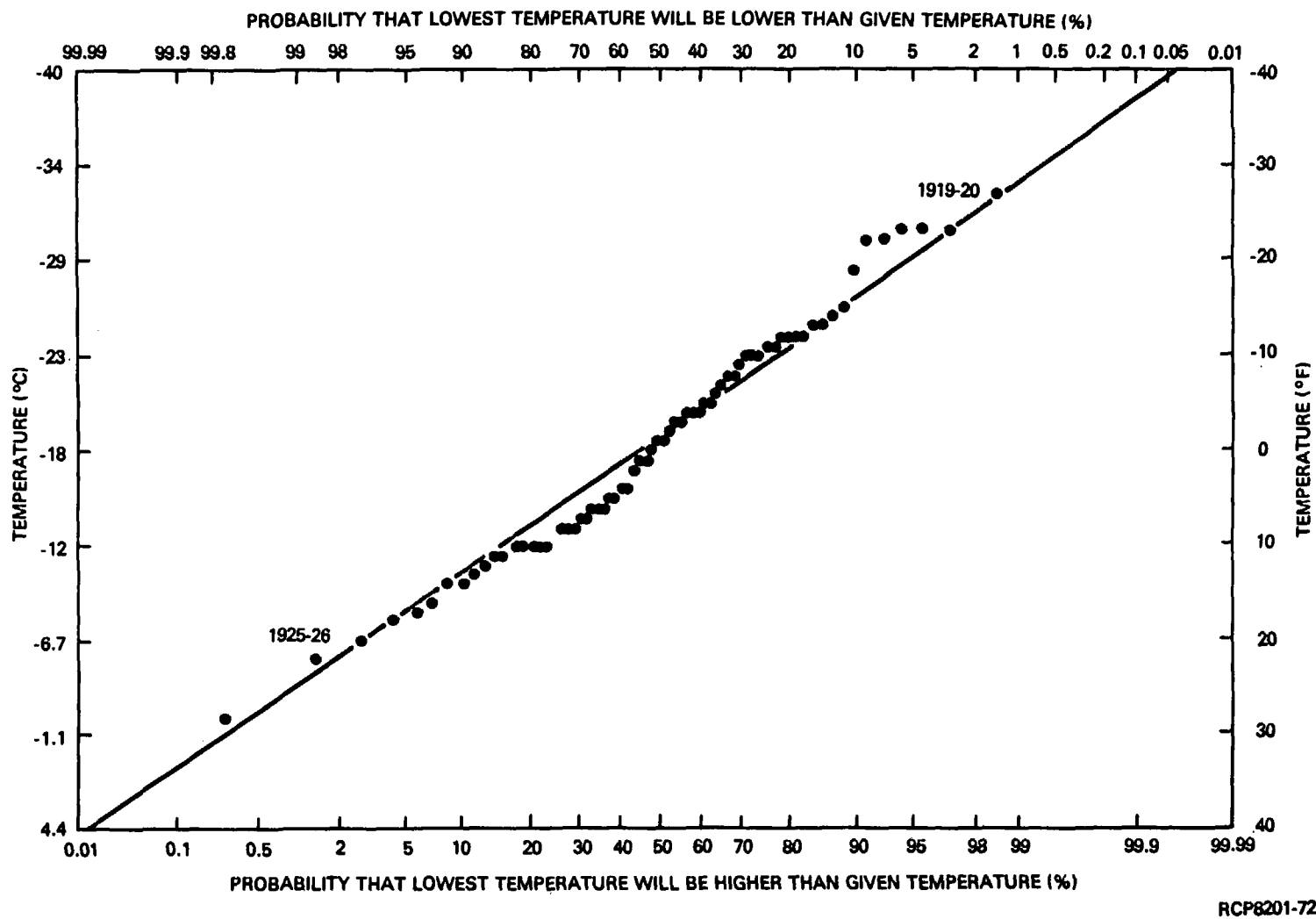


FIGURE 8-13. Lowest Temperatures During Each of the 68 Winters at the Hanford Site Between 1912 and 1980 and Their Probability of Occurrence (taken in part from Stone et al., 1972).

TABLE 8-29. Statistics for Two Periods of Extreme High Temperatures (Stone et al., 1972).

Total count	July 5 to August 26, 1958 (53 days)		July 13 to August 21, 1971 (40 days)	
Number of days with maximum 32°C (90°F) or above	50		39	
Number of days with maximum 38°C (100°F) or above	21		27	
Number of nights with minimum 21°C (70°F) or above	13		16	
Number of nights with minimum 16°C (60°F) or above	7		5	
Temperature	°C	°F	°C	°F
Average daily maximum	36.6	97.9	39.6	103.2
Average daily minimum	18.8	65.8	20.7	69.3
Mean temperature	27.7	81.8	30.1	86.2
Extreme high	42 (July 28)	107	44 (August 9)	112
Extreme low	13 (August 5)	55	13 (July 13- August 15)	56

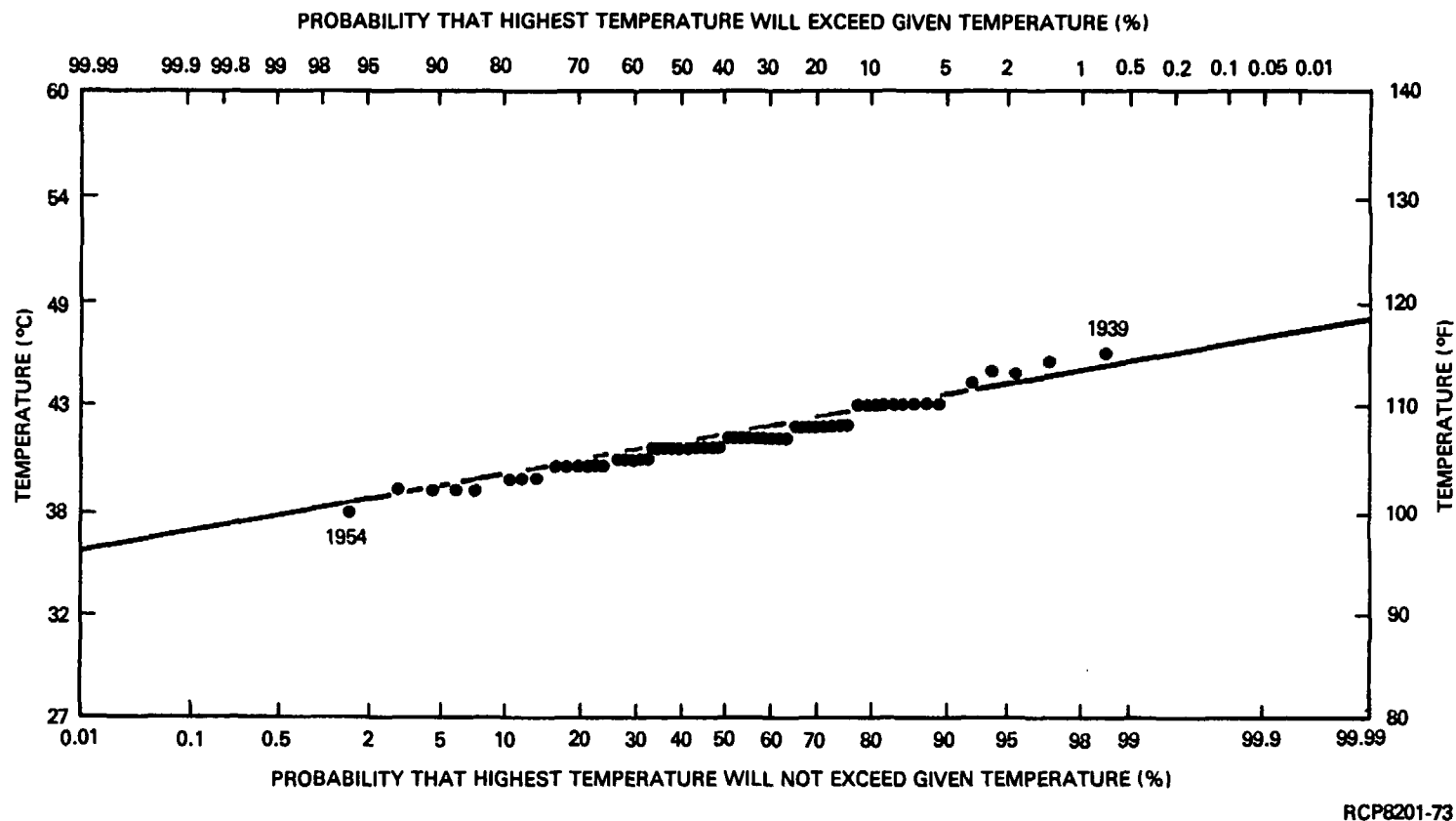


FIGURE 8-14. Highest Temperatures During Each of the 66 Summers at Hanford Between 1912 and 1980 (1943-1944 missing) and Their Probability of Occurrence (taken, in part, from Stone et al., 1972).

8.4.2.5 Thunderstorms and Lightning. A thunderstorm day is one in which thunder is heard. Thunderstorms may occur during any month of the year in the Hanford Site area. However, the thunderstorm season essentially includes only the months of April through September. Although the average in the Hanford Site area is 11 thunderstorm days per year, the number has varied from 3 to 23 (Stone et al., 1972).

Lightning-strike frequency can be estimated by the commonly observed climatological statistics of thunderstorm days (Cianos and Pierce, 1972). An estimate was made for the 122-meter Hanford Meteorological Station tower, which gave an annual lightning-strike frequency of 0.225, or one strike every 4.44 years (ERDA, 1975). The "reasonableness" of this technique can be shown by the observation that the tower has had three or more confirmed strikes during its 30-year existence; however, not all strikes may have been observed.

8.4.2.6 Severe Duststorms. The climatological study of duststorms at the Hanford Site for 1953 to 1970 (Orgill et al., 1974) was examined for the purpose of establishing the "worst-case" duststorm which may have occurred during that period. The worst-case duststorm (i.e., that storm which had the largest calculated time-integrated dust loading (milligrams per hour per cubic meter)) may be used in assessing the design and operation of the BWIP plant filters. Dust loadings for the worst-case duststorms are shown in Table 8-30. These loadings should apply for a height of 1.5 to 1.8 meters above the ground.

TABLE 8-30. Detailed Estimates of the Dust Loadings for the Six Worst Storms, Based on Surface Observations of the Hanford Meteorological Station, 1953-1970 (WPPSS, 1979).

Storm number	Total dust loading (mg-hr/m ³)	Actual duration (hr)	Average dust loading (mg/m ³)	Average wind-speed at 15.2 m (m/s)
1	40*	0.67	60	27
2	100	1.0	100	18
3	160	18	8.9	8
4	44	2.6	17	14
5	90	3.1	29	15
6	80	7	11	8

*Value is less than actual dust loading as a result of less than 1-hour duration.

8.4.2.7 Blowing and Drifting Snow. Blowing and drifting snow, like dust-storms, may be of importance in assessing the design and operation of BWIP plant filters. The prerequisites for the phenomena are a certain depth (2.54 centimeters or more) of dry, powdery snow on the ground, subfreezing temperatures, and sufficient wind to suspend the snow. This combination of meteorological events is seldom experienced in the Hanford region.

One significant storm event occurred during February 4-5, 1948. The storm reached its peak on the 5th when blowing snow reduced visibility to 3 kilometers. The storm was augmented with dust and the snow was piled into dirty drifts about 1 meter deep.

8.4.3 Site Paleoclimatic Data

Due to the physiography, climate, and geological history of the reference repository location, good paleoclimatic data sources are unavailable at the site or from the surrounding area. Paleoclimatic data have historically been obtained from a number of natural paleoclimatic indicators (Table 8-31). These indicators are, potentially, any biological, chemical, or physical characteristics that respond to climate. The most useful data sources have a stratigraphic character; i.e., the ambient values of a climatologically sensitive parameter are preserved within the layers of a slowly accumulating natural deposit or material (NAS, 1975). Natural paleoclimatic indicators thus include sediments left by melting glaciers; sediments developed in peat bogs, on lake bottoms, and on ocean floors; layers in soil and in the polar ice caps; and annual layers of wood formed in growing trees. The absence of fossils in the basalt layers and in the glaciofluvial deposits that rest upon them and the episodic nature of the glaciofluvial deposits have produced little useful paleoclimatically sensitive stratigraphic material in the Hanford region. Glaciers did not reach the site during the last ice age; peat bogs, stable lake sites, and ocean floors are not present near the site; and woody Artemisia growing near the site can extend the climate record back only to the 19th century (Hinds and Thorp, 1970).

Nearly all of the palynological work in the region has been conducted on the periphery of the Columbia Plateau (especially northwest of Spokane, Washington) on the steppes or forest boundaries where bogs and lakes are plentiful and fossil pollen techniques can be utilized. The forest boundary zones are especially suitable for study since the ecosystems at the boundary are quite sensitive to changes in climate. For this reason the aforementioned studies in the region may be good indicators of climate changes at the reference repository location (Section 8.3.1).

TABLE 8-31. Characteristics of Paleoclimate Data Sources (NAS, 1975).

Proxy data source	Variable measured	Continuity of evidence	Potential geographical coverage	Period open to study (yr before present)	Minimum sampling interval (yr)	Usual dating accuracy	Climatic inference
Layered ice cores	Oxygen isotope concentration, thickness (short cores)	Continuous	Antarctica, Greenland	10,000	1-10	$\pm 1-100$ yr	Temperature, accumulation
	Oxygen isotope concentration (long cores)	Continuous	Antarctica, Greenland	>100,000	Variable	Variable	Temperature
Tree rings	Ring-width anomaly, density, isotopic composition	Continuous	Midlatitude and high-latitude continents	1,000 (common) 8,000 (rare)	1	± 1 yr	Temperature, runoff, precipitation, soil moisture
Fossil pollen	Pollen-type concentration (varved core)	Continuous	Midlatitude continents	12,000	1-10	± 10 yr	Temperature, precipitation, soil moisture
	Pollen-type concentration (normal core)	Continuous	50°S to 70°N	12,000 (common) 200,000 (rare)	200	$\pm 5\%$	Temperature, precipitation, soil moisture
Mountain glaciers	Terminal positions	Episodic	45°S to 70°N	40,000	--	$\pm 5\%$	Extent of mountain glaciers
Ice sheets	Terminal positions	Episodic	Midlatitude to high latitudes	25,000 (common) 1,000,000 (rare)	--	Variable	Area of ice sheets
Ancient soils	Soil type	Episodic	Lower and mid-latitudes	1,000,000	200	$\pm 5\%$	Temperature, precipitation, drainage
Closed-basin lakes	Lake level	Episodic	Midlatitudes	50,000	1-100 (variable)	$\pm 5\%$ ± 1 yr	Evaporation, runoff, precipitation, temperature
Lake sediments	Varve thickness	Continuous	Midlatitudes	5,000	1	$\pm 5\%$	Temperature, precipitation
Ocean sediments (common deep-sea cores, 2-5 cm/1,000 yr)	Ash and sand accumulation rates	Continuous	Global ocean (outside red clay areas)	200,000	>500		Wind direction
	Fossil plankton composition	Continuous	Global ocean (outside red clay areas)	200,000	>500	$\pm 5\%$	Sea-surface temperature, surface salinity, sea-ice extent
	Isotopic composition of planktonic fossils; benthic fossils; mineralogic composition	Continuous	Global ocean (above CaCO_3 compensation level)	200,000	>500+	$\pm 5\%$	Surface temperature, global ice volume; bottom temperature and bottom-water flux; bottom-water chemistry
(rare cores >10 cm/1,000 yr)	As above	Continuous	Along continental margins	>10,000	20	$\pm 5\%$	As above
(cores, <2 cm/1,000 yr)	As above	Continuous	Global ocean	>1,000,000	>1,000	$\pm 5\%$	As above
Marine shorelines	Coastal features, reef growth	Episodic	Stable coasts, oceanic islands	400,000	--	$\pm 5\%$	Sea level, ice volume

8.5 SUMMARY OF UNRESOLVED ISSUES

No significant issues or problems have been defined or discovered. Climatological data at the reference repository location will continue to be gathered to comply with NRC requirements. Paleoclimatic information discussed in the preceding section will be used to construct scenarios to assess the performance of the repository. Plans to accomplish this work are discussed in Chapter 13.

8.6 REFERENCES

- ANSI, 1972, Building Code Requirements for Minimum Design Loads in Buildings and Other Structures, ANSI A58, 1-1972, American National Standards Institute, New York, New York.
- APCA, 1980, General Regulation 80-7 of the Benton-Franklin-Walla Walla Counties Air Pollution Control Authority, Board of Directors of the Benton-Franklin-Walla Walla Counties Air Pollution Control Authority, Richland, Washington, published May 6, 1980, effective July 1, 1980.
- Baker, V. R., 1978, "The Spokane Flood Controversy and the Martial Outflow Channels," Science, Vol. 202, pp. 1249-1256.
- Barry, R. G., 1973, "Conditions Favoring Glacierization and Deglaciation in North America From a Climatological Viewpoint," Arctic and Alpine Research, Vol. 5, No. 3, Part 1, pp. 171-184
- Barry, R. G., Ives, J. D., and Andrews, J. T., 1971, "A Discussion of Atmospheric Circulation During the Last Ice Age," Quaternary Research, Vol. 1, pp. 415-418.
- Berger, A. L., 1978, "Long-Term Variations of Daily Insolation and Quaternary Climatic Changes," Journal of Applied Meteorology, Vol. 35, pp. 2362-2367.
- Bjornstad, B. N., 1980, Sedimentology and Depositional Environment of the Touchet Beds, Walla Walla River Basin, Washington, RHO-BWI-SA-44, Rockwell Hanford Operations, Richland, Washington, June 1980.
- Bretz, J H., 1923, "The Channeled Scablands of the Columbia Plateau," Journal of Geology, Vol. 31, pp. 617-649.
- Bretz, J H., 1927, "Channeled Scabland and the Spokane Flood," Washington Academy of Science Journal, Vol. 17, pp. 200-211.
- Bretz, J H., 1959, "Washington's Channeled Scabland," Washington Division of Mines Geological Bulletin, No. 45, Olympia, Washington.
- Brown, R. E., 1970, Interrelationships of Geologic Formations and Processes Affecting Ecology as Exposed at Rattlesnake Springs, Hanford Project, BNWL-B-29, Battelle, Pacific Northwest Laboratories, Richland, Washington.
- Bull, C., 1979, "Glaciological Parameters of Disruptive Event Analysis," in A Summary of FY-1978 Consultant Input for Scenario Methodology Development, Scott, B. L., Benson, G. L., Craig, R. A., and Harwell, M. A., eds., PNL-2851, Pacific Northwest Laboratory, Richland, Washington.
- Bull, C., 1980, Glaciological Parameters of Disruptive Event Analysis, PNL-2863, Pacific Northwest Laboratory, Richland, Washington.

Childs, J. T. and Orgill, M. M., 1979, "Case Study of a Severe Convective Storm in the Pacific Northwest," PNL-SA-7998 presented at 26th Pacific Northwest Regional Meeting of the American Geophysical Union, September 17-18, 1979, Pacific Northwest Laboratory, Richland, Washington.

Cianos, N., and Pierce, E. T., 1972, A Ground-Lightning Environment for Engineering Usage, Technical Report Number 1, Stanford Research Institute, Menlo Park, California.

Clague, J. J., Armstrong, J. E., and Mathews, W. H., 1980, "Advance of the Late Wisconsin Cordilleran Ice Sheet in Southern British Columbia Since 22,000 Years B.P.," Quaternary Research, Vol. 13, pp. 322-326.

CLIMAP, 1976, "The Surface of the Ice-Age Earth," CLIMAP Project Members, Science, Vol. 191, No. 4232, pp. 1131-1144, March 19, 1976.

Daubek, H. G., 1970, Tornado History and a Discussion of the Tornado Warning System, BNW/JN 19-20, Battelle, Pacific Northwest Laboratories, report to Jersey Nuclear Company, Richland, Washington.

Elliott, D. C., Sandusky, W. F., and Woodruff, R. K., 1975, "An Investigation of Regional Flow Patterns for Improving Estimates of Effluent Transport and Diffusion," BNWL-B-459, presented at The Annual Meeting of the Pacific Northwest International Section - Air Pollution Control Association, Vancouver, British Columbia, November 19-21, 1975, Battelle, Pacific Northwest Laboratories, Richland, Washington.

Elliott, D. C., Sandusky, W. F., and Woodruff, R. K., 1976, "An Investigation of Regional Flow Patterns over an Area of Complex Terrain," Pacific Northwest Laboratory, Annual Report for 1975, Part 3, Atmospheric Sciences, BNWL-2000PT3, Battelle, Pacific Northwest Laboratories, Richland, Washington, pp. 246-252.

EPA, 1980a, National Primary and Secondary Ambient Air Quality Standards: Definitions, Title 40, Code of Federal Regulations, Part 50.1, U.S. Environmental Protection Agency, Washington, D.C.

EPA, 1980b, Workbook for Estimating Visibility Impairment, EPA-450/4-80-031, Office of Air Quality Planning and Standards, U.S. Environmental Protection Agency, Research Triangle Park, North Carolina.

ERDA, 1975, Final Environment Statement - Waste Management Operations, Hanford Reservation, Richland, Washington, ERDA-1538, 2 Volumes, U.S. Energy Research and Development Administration, Washington, D.C., December 1975.

Flint, R. F., 1971, Glacial and Quaternary Geology, John Wiley & Sons, New York, New York.

Foley, M. G., Petrie, G. M., and Craig, R. G., 1981, Geological Simulation Model for a Hypothetical Site in the Columbia Plateau: Results, PNL-3542-2, Pacific Northwest Laboratory, Richland, Washington.

Frison, G. C., 1975, "Man's Interaction with Holocene Environments on the Plains," Quaternary Research, Vol. 5, pp. 289-300.

Fryxell, R., 1964, "Regional Patterns of Sedimentation Recorded by Cave and Rock-Shelter Stratigraphy in the Columbia Plateau, Washington," abstract in Geological Society of America Special Paper 76, p. 273.

Fryxell, R., 1965, "Mazama and Glacier Peak Volcanic Ash Layers: Relative Ages," Science, Vol. 147, pp. 1288-1290.

Fujita, T., 1970, Estimate of Maximum Windspeed of Tornadoes in Three Northwestern States, SMRP Research Paper No. 92, COM-71-00731, University of Chicago, Chicago, Illinois, December 1970.

Gates, W. L., 1976, "Modeling the Ice-Age Climate," Science, Vol. 191, pp. 1138-1144.

Gilchrist, A., 1978, "Numerical Simulation of Climate and Climate Change," Nature, Vol. 276, pp. 341-345.

Gillette, D. A., Blifford, I. H., Jr., and Fenster, C. R., 1972, "Measurements of Aerosol Size Distributions and Vertical Fluxes of Aerosols on Land Subject to Wind Erosion," Journal of Applied Meteorology, Vol. 11, No. 6, pp. 977-987.

Hansen, H. P., 1947, "Postglacial Forest Succession, Climate, and Chronology in the Pacific Northwest," Transactions, American Philosophical Society, Vol. 37, Part 1.

Heusser, C. J., 1964, "Palynology of Four Bog Sections From the Western Olympic Peninsula, Washington," Ecology, Vol. 45, pp. 23-40.

Heusser, C. J., 1965, "A Pleistocene Phytogeographical Sketch of the Pacific Northwest and Alaska," in The Quaternary of the United States, Wright, H. E. and Frey, D. G., ed., Princeton University Press, Princeton, New Jersey, pp. 469-483.

Heusser, C. J., 1972, "Palynology and Phytogeographical Significance of a Late-Pleistocene Refugium Near Kalaloch, Washington," Quaternary Research, Vol. 2, pp. 189-201.

Hinds, W. T., 1975, "Energy and Carbon Balances in Cheatgrass, an Essay in Autecology," Ecological Monographs, Vol. 45, No. 4, pp. 367-388.

Hinds, W. T. and Thorp, J. M., 1970, "Prerecorded Climatology of the Hanford Region," Pacific Northwest Laboratory Annual Report for 1979, Part 1, BNWL-1307 PT 1, Battelle, Pacific Northwest Laboratories, Richland, Washington, pp. 132-133.

Hosler, C. R., 1961, "Low Level Inversion Frequency in the Contiguous United States," Monthly Weather Review, Vol. 89, pp. 319-339.

Holzworth, G. C., 1972, Mixing Heights, Windspeeds, and Potential for Urban Air Pollution Throughout the Contiguous United States, OAPP No. AP-101, Office of Air Programs, U.S. Environmental Protection Agency, Research Triangle Park, North Carolina.

Huschke, R. E., ed., 1968, Glossary of Terms Frequently Used in Air Pollution, American Meteorological Society, Boston, Massachusetts.

Jaech, J. L., 1970, Statistical Analysis of Tornado Data for the Three Northwestern States, Jersey Nuclear Company, Richland, Washington.

Jenne, D. E., 1963, Frequency Analysis of Some Climatological Extremes at Hanford, HW-75445, General Electric Hanford Atomic Products Operations, Richland, Washington.

Jenne, D. E., 1978, Airborne Dust and Its Impact on Hi-Vol Sampling Results at Richland, Washington, Benton-Franklin-Walla Walla Counties Air Pollution Control Authority, Richland, Washington.

Jenne, D. E., 1980, Annual Report, Tri-County Air Pollution Control Authority, 1979, Benton-Franklin-Walla Walla Counties Air Pollution Control Authority, Richland, Washington.

Jenne, D. E., 1981, Annual Report, Tri-County Air Pollution Control Authority, 1980, Benton-Franklin-Walla Walla Counties Air Pollution Control Authority, Richland, Washington.

Knudson, R., 1980, "Ancient Peoples of the Columbia Plateau," Journal of Forestry, Vol. 78, No. 8, pp. 477-479.

Kukla, G. K., 1979, "Probability of Expected Climate Stresses in North America in the Next One Million Years," A Summary of FY-1978 Consultant Input for Scenario Methodology Development, Scott, B. L., ed., PNL-2851, Pacific Northwest Laboratory, Richland, Washington.

Lamb, H. H. and Woodroffe, A., 1970, "Atmospheric Circulation During the Last Ice Age," Quaternary Research, Vol. 1, pp. 29-58.

Larsen, J. A. and Barry, R. G., 1974, "Paleoclimatology," in Arctic and Alpine Environments, Ives, J. D. and Barry, R. G., eds., Methuen and Company, Limited, London, England.

Maas, L. J., 1981, Chemical and Biological Pollution Surveillance of the Hanford Environs: Quarterly Report January 1 to March 31, 1981, Hanford Environmental Health Foundation, Richland, Washington.

Mack, R. N., Bryant, V. M., Jr., and Fryxell, R., 1976, "Pollen Sequence From the Columbia Basin, Washington: Reappraisal of Postglacial Vegetation," The American Midland Naturalist, Vol. 95, No. 2, pp. 390-397.

Mack, R. N., Rutter, N. W., Bryant, V. M., Jr., and Valastro, S., 1978a, "Late Quaternary Pollen Record From Big Meadow, Pend Oreille County, Washington," Ecology, Vol. 59, No. 5, pp. 956-966.

Mack, R. N., Rutter, N. W., Bryant, V. M., Jr., and Valastro, S., 1978b, "Reexamination of Postglacial Vegetation History in Northern Idaho: Hager Pond, Bonner County," Quaternary Research, Vol. 10, pp. 241-255.

Mack, R. N., Rutter, N. W., Valastro, S., and Bryant, V. M., Jr., 1978c, "Late Quaternary Vegetation History at Waits Lake, Colville River Valley, Washington," Botanical Gazette, Vol. 139, No. 4, pp. 499-506.

Mack, R. N., Rutter, N. W., and Valastro, S., 1979, "Holocene Vegetation History of the Okanogan Valley, Washington," Quaternary Research, Vol. 12, pp. 212-225.

Markov, K. K., 1969, "Geographical Regions and Zones and Their Quaternary Development," pp. 3-5 in Quaternary Geology and Climate, Wright, H. E., Jr., ed., National Academy of Sciences, Washington, D.C.

Markee, E. H., Jr. and Levine, J. R., 1977, "Probabilistic Evaluations of Atmospheric Diffusion Conditions for Nuclear Facility Design and Siting," 5th Conference on Probability and Statistics in Atmospheric Sciences, preprint, Las Vegas, Nevada, November 15-18, 1977.

Mitchell, J. M., Jr., 1972, "The Natural Breakdown of the Present Interglacial and Its Possible Intervention by Human Activities," Quaternary Research, Vol. 2, pp. 436-445.

Mitchell, J. M., Jr., 1977, "The Changing Climate," Energy and Climate, National Academy of Sciences, Washington, D.C.

Morner, N. A., 1972, "When Will the Present Interglacial End?" Quaternary Research, Vol. 2, pp. 341-349.

Napier, B. A., 1981, Standardized Input for Hanford Environmental Impact Statements - Part 1, PNL-3509 PT1, Pacific Northwest Laboratory, Richland, Washington.

NAS, 1975, Understanding Climate Change - A Program for Action, National Academy of Sciences, Washington, D.C.

NAS, 1977, Energy and Climate, Studies in Geophysics, National Academy of Sciences, Washington, D.C.

Nickmann, R. J., 1979, The Palynology of Williams Lake Fen, Spokane County, Washington, M. S. Thesis, Eastern Washington University, Cheney, Washington.

Nickmann, R. J. and Leopold, E., 1980, A Postglacial Pollen Record From Goose Lake, Okanogan County, Washington: Evidence for an Early Holocene Cooling, Contribution 82-2, Quaternary Research Center, University of Washington, Seattle, Washington.

NRC, 1972, Onsite Meteorological Programs, Regulatory Guide 1.23, U.S. Nuclear Regulatory Commission, Washington, D.C.

NRC, 1974a, Assumptions Used for Evaluating the Potential Radiological Consequences of a Loss of Coolant Accident for Boiling Water Reactors, Regulatory Guide 1.3, U.S. Nuclear Regulatory Commission, Washington, D.C.

NRC, 1974b, Assumptions Used for Evaluating the Potential Radiological Consequences of a Loss of Coolant Accident for Pressurized Water Reactors, Regulatory Guide 1.4, U.S. Nuclear Regulatory Commission, Washington, D.C.

NRC, 1977, Methods for Estimating Atmospheric Transport in Routine Releases from Light-Water-Cooled Reactors, Regulatory Guide 1.111, U.S. Nuclear Regulatory Commission, Washington, D.C.

NRC, 1979, Atmospheric Dispersion Models for Potential Accident Consequence Assessments at Nuclear Power Plants, Regulatory Guide 1.145, U.S. Nuclear Regulatory Commission, Washington, D.C.

NRC, 1980, Proposed Revision to Regulatory Guide 1.23-Meteorological Programs in Support of Nuclear Power Plants, U.S. Nuclear Regulatory Commission, Washington, D.C.

Orgill, M. M., Sehmel, G. A., and Bander, T. J., 1974, "Regional Wind Resuspension of Dust," Pacific Northwest Laboratory Annual Report for 1973, Part 3, Atmospheric Sciences, BNWL-1850 PT3, Battelle, Pacific Northwest Laboratories, Richland, Washington, pp. 214-219.

Orgill, M. M. and Schwendiman, L. C., 1975, Nature and Significance of Convective Vortices (Dust Devils) in the Hanford Project, BNWL-2079, Battelle, Pacific Northwest Laboratories for Atlantic Richfield Hanford Company, Richland, Washington.

Petrie, G. M., Zellmer, J. T., Lindberg, J. W., and Foley, M. G., 1981, Geological Simulation Model for a Hypothetical Site in the Columbia Plateau, PNL-3542, Pacific Northwest Laboratory, Richland, Washington.

Phillips, S. J., Campbell, A. C., Campbell, M. D., Gee, G. W., Hooper, H. H., and Schwarzmiller, K. O., 1979, A Field Test Facility for Monitoring Water/Radionuclide Transport Through Partially Saturated Geologic Media: Design, Construction, and Preliminary Description, PNL-3226, Pacific Northwest Laboratory, Richland, Washington.

Porter, S. C., 1977, "Present and Past Glaciation Threshold in the Cascade Range, Washington, U.S.A.: Topographic and Climatic Controls, and Paleoclimatic Implications," Journal of Glaciology, Vol. 18, No. 78, pp. 101-116.

Porter, S. C., 1981, "Recent Glacier Variations and Volcanic Eruptions," Nature, Vol. 291, pp. 139-142.

Poser, H., 1948, "Boden-und Klima-Verhältnisse in Mittel-und West-Europe während der Würmeiszeit," Erdkunde, Vol. 2, pp. 53-68.

Powell, D. C., Wegley, H. L., and Fox, T. D., 1979, MESODIF-II: A Variable Trajectory Plume Segment Model to Assess Ground-Level Air Concentrations and Deposition of Effluent Releases from Nuclear Power Facilities, NUREG/CR-0523 and PNL-2419, Pacific Northwest Laboratory, Richland, Washington.

Ramsdell, J. V. and Athey, G. F., 1981, MESOI: Interactive LaGrangian Trajectory Puff Diffusion Model, PNL-3998, Pacific Northwest Laboratory, Richland, Washington.

Richmond, G. M., Fryxell, R., Neff, G. E., and Weis, P. L., 1965, "The Cordilleran Ice Sheet of the Northern Rocky Mountains, and Related Quaternary History of the Columbia Plateau," The Quaternary of the United States, Wright, H. E., Jr. and Frey, D. G., eds., Princeton University Press, Princeton, New Jersey, pp. 231-242.

Sagendorf, J. F. and Goll, J. T., 1977, XOQ DOQ Program for the Meteorological Evaluation of Routine Effluent Releases at Nuclear Power Stations, NUREG-0324, U.S. Nuclear Regulatory Commission, Washington, D.C.

Sarnthein, M., 1978, "Sand Deserts During Glacial Maximum and Climatic Optimum," Nature, Vol. 272, pp. 43-46.

Sehmel, G. A., 1976, "The Influence of Soil Insertion on Atmospheric Particle Size Distribution," Pacific Northwest Laboratory Annual Report for 1975, Part 3, Atmospheric Sciences, BNWL-2000PT3, Pacific Northwest Laboratory, Richland, Washington, pp. 99-101.

Skidmore, E. L., 1974, "A Wind Erosion Equation: Development, Application, and Limitations," ERDA Symposium Series 38 CONF-740921, Atmosphere-Surface Exchange of Particulate and Gaseous Pollutants, U.S. Energy Research and Development Administration, Washington, D.C., pp. 452-465.

Slade, D. H., ed., 1968, Meteorology and Atomic Energy, U.S. Atomic Energy Commission, Division of Technical Information Extension, Oak Ridge, Tennessee. Available as TID 24190 from the U.S. Government Printing Office, Washington, D.C.

Stone, W. A., Jenne, D. E., and Thorp, J. M., 1972, Climatography of the Hanford Area, BNWL-1605, Battelle, Pacific Northwest Laboratories, Richland, Washington.

Stottlemire, J. A., Petrie, G. M., Benson, G. L., and Zellmer, J. T., 1981, A Conceptual Model for Release Scenario Analysis of a Hypothetical Site in Columbia Plateau Basalts, PNL-2892, Pacific Northwest Laboratory, Richland, Washington.

Streng, D. L. and Peloquin, R. A., 1981, HADOC - A Computer Code for Calculation of External and Inhalation Doses from Acute Radionuclide Releases, PNL-3503, Pacific Northwest Laboratory, Richland, Washington.

Streng, D. L., Watson, E. C., and Droppo, J. G., 1976, Review of Calculational Models and Computer Codes for Environmental Dose Assessment of Radioactive Releases, BNWL-B-454, Battelle, Pacific Northwest Laboratories, Richland, Washington.

Thorson, R. M., 1980, "Ice-Sheet Glaciation on the Puget Lowland, Washington, During the Vashon Stade (Late Pleistocene)," Quaternary Research, Vol. 13, pp. 303-321.

Travis, J. R., 1974, "A Model for Predicting the Redistribution of Particulate Contaminants From Soil Surfaces," ERDA Symposium Series 38, CONF-740921, Atmosphere-Surface Exchange of Particulate and Gaseous Pollutants, U.S. Energy Research and Development Administration, Washington, D.C., pp. 906-944.

Tubbs, D. W., 1979, "Pacific Northwest Geomorphology and Hydrology: Rates and Probabilities of Selected Processes and Events," A Summary of FY-1978 Consultant Input for Scenario Methodology Development, Scott, B. L., Benson, G. L., Craig, R. A., and Harwell, M. A., eds., PNL-2851, Pacific Northwest Laboratory, Richland, Washington.

USGS, 1976, The Channeled Scablands of Eastern Washington - The Geologic Story of the Spokane Flood, U.S. Geological Survey, U.S. Government Printing Office, Washington, D.C.

Waite, R. B., Jr., 1980, "About Forty Last-Glacial Lake Missoula Jökulhlaups Through Southern Washington," Journal of Geology, Vol. 88, pp. 653-679.

Wallace, R. W., 1977, A Comparison of Evapotranspiration Estimates Using ERDA Hanford Climatological Data, PNL-2698, Pacific Northwest Laboratory, Richland, Washington.

Williams, J., Barry, R. G., and Washington, W. M., 1974, "Simulation of the Atmospheric Circulation Using the NCAR Global Circulation Model With Ice Age Boundary Conditions," Journal of Applied Meteorology, Vol. 13, No. 3, pp. 305-317.

WMO, 1975, "The Physical Basis of Climate and Climate Modeling," Report of the International Study Conference in Stockholm, July 29-August 10, 1974, GARP Publication Series No. 16, World Meteorological Organization, International Council of Scientific Unions, Geneva, Switzerland.

WPPSS, 1979, "Meteorology," WPPSS - Nuclear Project No. 2 Final Safety Analysis Report (FSAR), Chapter 2.3 of Vol. 2, Amendment No. 7, Washington Public Power Supply System, Richland, Washington.

9. ENVIRONMENTAL, LAND-USE, AND SOCIOECONOMIC CHARACTERISTICS

9.1 ENVIRONMENTAL CHARACTERISTICS

This section describes the existing environmental characteristics and parameters of the Hanford Site as they relate to the reference repository location. The information presented is to provide a general knowledge of the environment of the Hanford area and should not be construed as documentation for compliance with the National Environmental Policy Act (CEQ, 1978). The U.S. Department of Energy (DOE) has developed a National Environmental Policy Act implementation plan (DOE, 1982a) that is integrated with the overall DOE planning and decision-making framework for the deep geologic disposal of radioactive waste (DOE, 1982a). As part of this implementation plan, an environmental assessment has been made for the Basalt Waste Isolation Project exploratory shaft construction (DOE, 1982b) and a finding of no significant impact has been issued (DOE, 1982c).

9.1.1 Ecology

For clarification, the following terms and definitions are provided. The Hanford Site boundaries are as seen in Figure 9-1. The reference repository location is that area surrounding the 200 West Area and delineated in Figure 9-2. The majority of the ecological information presented here refers to the Hanford Site in general, except in those limited instances where information is available specific to the reference repository location.

The Hanford Site was established in 1943 as a national security area for plutonium production and was subsequently designated as a National Environmental Research Park by the U.S. Energy Research and Development Administration in 1977. Dominant topographical features at the Hanford Site include the Columbia River, unstabilized sand dunes, and basaltic ridges. Soils are mostly Rupert sand and Burbank sandy loam with a pH range of 7.4 to 8.5. The Hanford Site has been characterized as a shrub-steppe grassland (Daubenmire, 1970) made up of a variety of plant communities. The sagebrush/cheatgrass community currently dominates the majority of the reference repository location. It gives food, cover, and shelter to many species of wildlife. The most important big-game mammal is the mule deer. Coyotes are the principal predators. The Great Basin pocket mouse is the most abundant small mammal occurring in the Hanford region environs, although cottontail rabbits may be found in some areas. The most common upland game birds are chukar partridge and California quail, with ring-necked pheasants being found in limited numbers. Raptors such as Swainson's hawks, red-tailed hawks, golden eagles, American kestrels and burrowing owls utilize many areas of the Hanford region as nesting sites. Reptiles and amphibians are relatively scarce, with the bull (gopher) snake and side-blotched lizard being the most common.

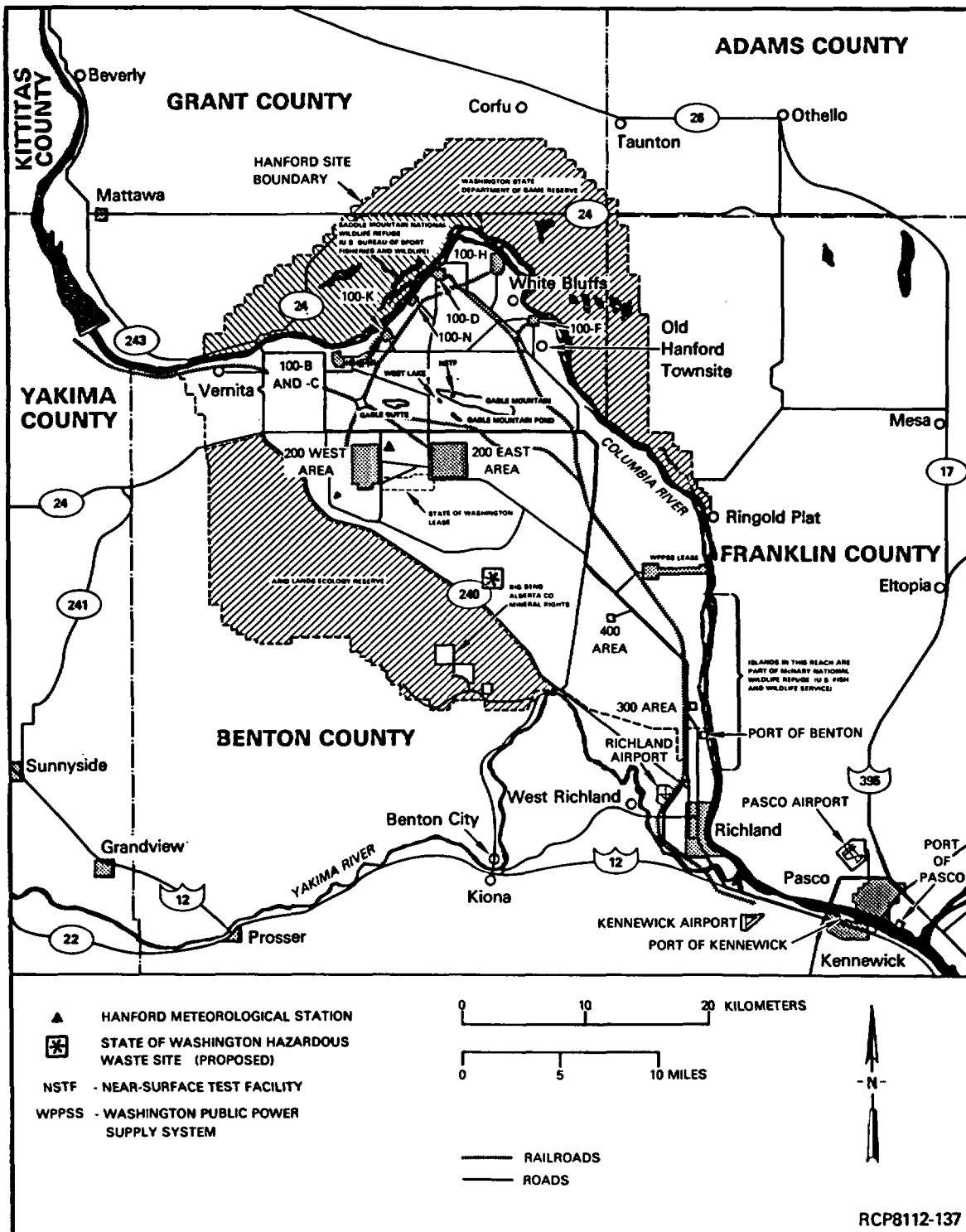


FIGURE 9-1. Map of the Hanford Site.

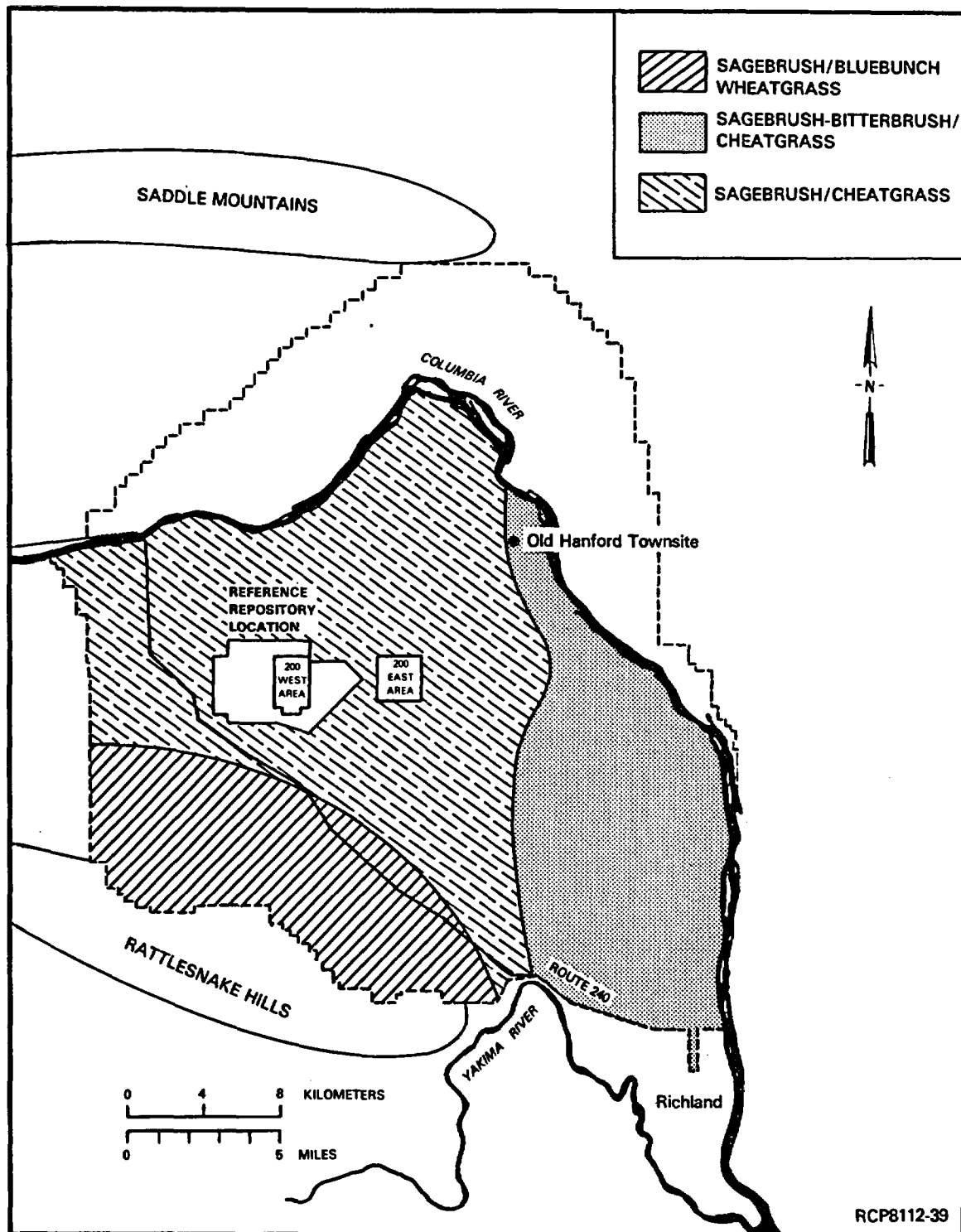


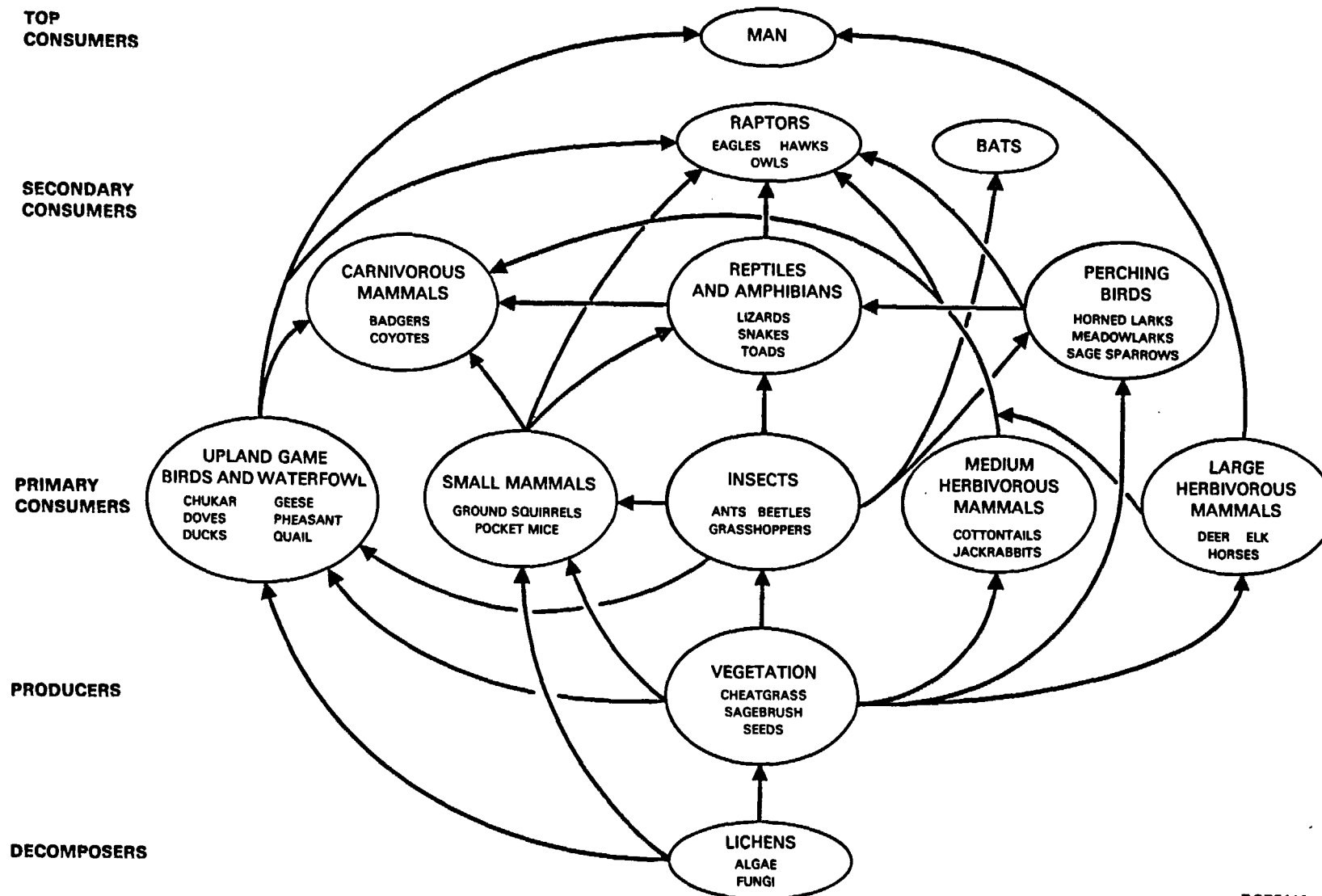
FIGURE 9-2. Major Plant Communities of the Hanford Site.

In 1968, the U.S. Atomic Energy Commission designated 311 square kilometers, south and west of Route 240, as an Arid Lands Ecology Reserve (Fig. 9-1). During the 1970s, an area of about 130 square kilometers north of the Columbia River was leased to the U.S. Fish and Wildlife Service for the Saddle Mountain National Wildlife Refuge and an area of about 220 square kilometers north of the river was leased to the Washington State Department of Game to be used for outdoor recreation.

The Hanford Site is bounded on the north by the Saddle Mountains, on the east by the Columbia River, and on the south and west by the Yakima River and Rattlesnake Hills, respectively. The dominant topographical features of the Hanford Site include the Rattlesnake Hills (elevation 1,090 meters), the Columbia River (and associated aquatic habitats which act as an attraction and a migration corridor for those species associated with water and wetlands), unstabilized sand dunes located near the Columbia River, and the basaltic ridges, which interrupt the rolling landscape of the site and whose ledges provide nest sites for birds of prey.

9.1.1.1 Vegetation. The Hanford Site has been classified as a shrub-steppe grassland (Daubenmire, 1970) and is comprised of nine plant communities: sagebrush/bluebunch wheatgrass, sagebrush-bitterbrush/cheatgrass-Sandberg's bluegrass, sagebrush/cheatgrass-Sandberg's bluegrass, cheatgrass, riparian (streamside) habitats, greasewood, spiny hopsage, winterfat, and thyme buckwheat. Some of these plant communities are extremely limited in distribution. These nine plant communities have been combined into three major vegetation types: (1) sagebrush/bluebunch wheatgrass, (2) sagebrush-bitterbrush/cheatgrass, and (3) sagebrush/cheatgrass (Fig. 9-2). The sagebrush/cheatgrass community currently dominates the majority of the proposed reference repository location, with other small tracts of different vegetation types interspersed throughout. Some of these other vegetation types are found at World War II army bunker sites dominated by locust trees and Siberian wheatgrass, an undisturbed area consisting of spiny hopsage, and several disturbed areas dominated by tumbleweeds and cheatgrass. These plant communities not only stabilize the soil but provide food, cover, and shelter for many terrestrial animals. The sagebrush/cheatgrass community is susceptible to brush fires during the hot summer months. For example, two range fires occurred within the vicinity of the reference repository location during the summer of 1980.

A general food web for the Hanford Site, based on vegetation and decomposers, is presented in Figure 9-3, which shows the existing relationships between various plant and animal species that are common on the site. A partial list of the common plant species that are known to occur in the area surrounding the 200 Areas and, as such, are representative of the species expected to occur within the reference repository location is given in Table 9-1.



RCP8112-40

FIGURE 9-3. General Food Web Diagram for the Hanford Site.

TABLE 9-1. Plant Species Known to Occur on the Reference Repository Location. (Sheet 1 of 4)

Scientific name	Common name
Cyperaceae	Sedge Family
<u>Scirpus americanus</u>	Three-square bulrush
<u>Scirpus validus</u>	Tule, softstem bulrush
<u>Scirpus maritimus</u>	Seacoast bulrush
<u>Scirpus acutus</u>	Hardstem bulrush
Gramineae	Grass Family
<u>Agropyron dasytachyum</u>	Thickspike wheatgrass
<u>Agropyron spicatum</u>	Bluebunch wheatgrass
<u>Bromus tectorum</u>	Cheatgrass
<u>Panicum capillare</u>	Common witchgrass
<u>Echinochloa crusgalli</u>	Large barnyard-grass
<u>Festuca octoflora</u>	Six-weeks fescue
<u>Oryzopsis hymenoides</u>	Indian ricegrass
<u>Poa sandbergii</u>	Sandberg's bluegrass
<u>Sporobolus cryptandrus</u>	Sand dropseed
<u>Sitanion hystrix</u>	Bottlebrush squirreltail
<u>Stipa comata</u>	Needle and thread grass
<u>Poa ampla</u>	Alkali bluegrass
<u>Poa canbyi</u>	Pine bluegrass
<u>Setaria viridis</u>	Green bristlegrass
<u>Muhlenbergia asperifolia</u>	Alkali muhly
<u>Phalaris arundinacea</u>	Reed canarygrass
Typhaceae	Cattail Family
<u>Typha latifolia</u>	Cattail
Liliaceae	Lily Family
<u>Brodiaea douglasii</u>	Douglas' brodiaea
<u>Brodiaea howellii</u>	Howell's brodiaea
<u>Calochortus macrocarpus</u>	Sego lily
<u>Asparagus officinalis</u>	Asparagus
Orobanchaceae	Broomrape Family
<u>Orobanche corymbosa</u>	Broomrape
Salicaceae	Willow Family
<u>Populus deltoides</u>	Necklace poplar
<u>Salix amygdaloides</u>	Peach-leaf willow
<u>Salix exigua</u>	Sandbar willow
Urticaeae	Nettle Family
<u>Urtica dioica</u>	Stinging nettle

TABLE 9-1. Plant Species Known to Occur on the Reference
Repository Location. (Sheet 2 of 4)

Scientific name	Common name
Santalaceae	Sandalwood Family
<u>Comandra umbellata</u> var. <u>pallida</u>	Bastard toad-flax
Polygonaceae	Buckwheat Family
<u>Eriogonum heracleoides</u>	Parsnip-flowered eriogonum
<u>Eriogonum microthecum</u>	Slenderbush buckwheat
<u>Eriogonum niveum</u>	Snow buckwheat
<u>Eriogonum sphaerocephalum</u>	Round-headed eriogonum
<u>Eriogonum strictum</u> var.	
<u>Eriogonum strictum</u> var.	
<u>Eriogonum thymoides</u>	Thyme-leaved eriogonum
<u>Rumex crispus</u>	Sour dock
<u>Rumex venosus</u>	Veiny dock
<u>Polygonum persicaria</u>	Heartweed, smartweed
<u>Eriogonum vimineum</u> var. <u>vimineum</u>	Broom buckwheat
Chenopodiaceae	Goosefoot Family
<u>Bassia hyssopifolia</u>	Slimleaf Bassia goosefoot
<u>Chenopodium leptophyllum</u>	Spiny hopsage
(Atriplex) <u>Grayia spinosa</u>	Russian thistle
<u>Salsola kali</u>	
Cruciferae	Mustard Family
<u>Descurainia pinnata</u>	Western tansymustard
<u>Draba verna</u>	Spring whitlow-grass
<u>Erysimum asperum</u>	Rough wallflower
<u>Rorippa nasturtium-aquaticum</u>	Watercress
<u>Sisymbrium altissimum</u>	Jim Hill mustard
<u>Thelypodium laciniatum</u>	Thick-leaved thelypody
Leguminosae	Pea Family
<u>Astragalus leibergii</u>	Leiberg's milkvetch
<u>Astragalus purshii</u>	Woolly-pod milkvetch
<u>Astragalus sclerocarpus</u>	Stalked-pod milkvetch
<u>Melilotus alba</u>	White sweet-clover
<u>Psoralea lanceolata</u>	Lance-leaf scurf pea
<u>Swainsona salsula</u>	Swainsona
Geraniaceae	Geranium Family
<u>Erodium cicutarium</u>	Stork's-bill
Malvaceae	Mallow Family
<u>Sphaeralcea munroana</u>	Munro's globe-mallow

TABLE 9-1. Plant Species Known to Occur on the Reference
Repository Location. (Sheet 3 of 4)

Scientific name	Common name
Loasaceae	Blazing-Star Family
<u>Mentzelia albicaulis</u>	White-stemmed mentzelia
Polypodiaceae	Common Fern Family
<u>Pteridium aquilinum</u>	Bracken fern
Onagraceae	Evening-Primrose Family
<u>Epilobium suffruticosum</u>	Shrubby willow-herb
<u>Oenothera andina</u>	Obscure evening-primrose
<u>Oenothera pallida</u>	Pale primrose
Umbelliferae	Parsley Family
<u>Cymopterus terebinthinus</u>	Turpentine cymopterus
<u>Lomatium canbyi</u>	Canby's lomatium
<u>Lomatium dissectum</u>	Fern-leaved lomatium
<u>Lomatium farinosum</u>	Coeur d'Alene lomatium
<u>Lomatium grayi</u>	Gray's lomatium
<u>Lomatium macrocarpum</u>	Large-flowered lomatium
<u>Lomatium triternatum</u>	Nine-leaf lomatium
Apocynaceae	Dogbane Family
<u>Apocynum sibiricum</u>	Clasping-leaved dogbane
<u>Apocynum androsaemifolium</u>	Spreading dogbane
Polemoniaceae	Phlox Family
<u>Microsteris gracilis</u>	Pink microsteris
<u>Phlox longifolia</u>	Long-leaf phlox
<u>Gilia leptomeria</u>	Gilia
<u>Polemonium micranthum</u>	Annual polemonium
Hydrophyllaceae	Waterleaf Family
<u>Phacelia linearis</u>	Threadleaf phacelia
Boraginaceae	Borage Family
<u>Amsinckia lycopsoides</u>	Tarweed fiddleneck
<u>Amsinckia tessellata</u>	Tessellate fiddleneck
<u>Cryptantha circumscissa</u>	Matted cryptantha
<u>Cryptantha pterocarya</u>	Winged cryptantha
<u>Lappula redowskii</u>	Stickseed
Scrophulariaceae	Figwort Family
<u>Penstemon acuminatus</u>	Sand-dune penstemon
<u>Verbascum thapsus</u>	Common mullein
<u>Veronica anagallis-aquatica</u>	Water speedwell

TABLE 9-1. Plant Species Known to Occur on the Reference Repository Location. (Sheet 4 of 4)

Scientific name	Common name
Plantaginaceae	Plantain Family
<u>Plantago patagonica</u>	Indian wheat
Valerianaceae	Valerian Family
<u>Plectritis macrocera</u>	Long-horn plectritis
Compositae	Composite Family
<u>Achillea millefolium</u> var. <u>lanulosa</u>	Yarrow
<u>Erigeron pumilus</u>	Shaggy fleabone
<u>Bidens frondosa</u>	Leafy beggar-tick
<u>Centaurea repens</u>	Russian knapweed
<u>Artemisia tridentata</u>	Big sagebrush
<u>Machaeranthera canescens</u>	Hoary aster
<u>Balsamorhiza careyana</u>	Carey's balsamroot
<u>Chaenactis douglasii</u>	Hoary chaenactis
<u>Chrysothamnus nauseosus</u>	Common rabbitbrush (gray)
<u>Chrysothamnus viscidiflorus</u>	Green rabbitbrush
<u>Cirsium brevifolium</u>	Palouse thistle
<u>Conyza canadensis</u>	Horseweed
<u>Crepis atrabarba</u>	Hawksbeard
<u>Erigeron filifolius</u>	Thread-leaf fleabane
<u>Ambrosia acanthicarpa</u>	Burrageed (bursage)
<u>Gnaphalium chilense</u>	Cotton-batting plant (cudweed)
<u>Lactuca serriola</u>	Prickly lettuce
<u>Layia glandulosa</u>	White daisy tidy-tips
<u>Microseris troximoides</u>	False-agoseris
<u>Solidago occidentalis</u>	Western goldenrod
<u>Taraxacum officinale</u>	Dandelion
<u>Townsendia florifer</u>	Showy townsendia
Equisetaceae	Horsetail Family
<u>Equisetum laevigatum</u>	Smooth scouring-rush
<u>Equisetum hyemale</u>	Dutch rush
Nyctaginaceae	Four-o'clock Family
<u>Abronia mellifera</u>	White sandverbena
Ranunculaceae	Buttercup Family
<u>Delphinium huttalliaum</u>	Larkspur

9.1.1.2 Mammals. A total of 27 mammal species (excluding bats) are known to occupy the Hanford Site (Rogers and Rickard, 1977) (Table 9-2). Big-game species include elk and mule deer. Only the mule deer is found with any regularity on the reference repository location, although the small elk herd is becoming more frequent to the reference repository location since the range fires during the summer of 1980. The small herd of wild horses on the Hanford Site has not been documented within the reference repository location. Medium-sized mammals which inhabit the Hanford Site include porcupines, coyotes, skunks, badgers, raccoons, black-tailed jackrabbits and cottontail rabbits. Coyotes are the principal predators. They consume such prey as rodents, insects, rabbits, birds, snakes, and lizards. Of the five species of small mammals that occur at the Hanford Site, pocket mice, deer mice, and Townsend's ground squirrels are probably the most common species inhabiting the reference repository location. Pocket mice and Townsend's ground squirrels are excellent burrowers and serve as a prey base for the larger carnivores. Bats probably play a minor role in the ecosystem at the reference repository location.

9.1.1.3 Birds. Although the prevailing desert-like conditions dictate that the diversity of avian species is low, there are several species that are known to regularly occur at the Hanford Site (Table 9-3). The majority of these species could possibly be found within, or proximal to, the reference repository location. The most common upland game birds found within the reference repository location include the ring-necked pheasant and chukar partridge; however, California quail and Hungarian partridge may also be found in limited numbers. The only native game bird expected to be common to the reference repository location is the mourning dove, which migrates south each fall. Common raptorial birds include Swainson's hawks, rough-legged hawks, red-tailed hawks, American kestrels, and burrowing owls. Other less common raptorial species include an occasional snowy owl, prairie falcon, merlin bald eagle, golden eagle, and ferruginous hawk. Swainson's hawks, kestrels, and red-tailed hawks are known to nest in the reference repository location.

Some of the aquatic sites proximal to the reference repository location attract numerous species of waterfowl and shorebirds. These areas are an important stopover point for migrating species and home to numerous residents such as Canada geese, mallards, canvasbacks, buffleheads, scaups, and coots. Long-billed curlews could be expected to nest at the reference repository location. Common song and perching birds known to nest within the study site include sage sparrows, lark sparrows, Western kingbirds, blackbirds, Say's phoebes, magpies, crows, ravens, Loggerhead shrikes, horned larks, and meadowlarks. Many of these birds migrate south during the winter, returning to the Hanford region to nest in the spring.

TABLE 9-2. Mammal Species Reported to Occur on the Hanford Site. (Sheet 1 of 2)

Family	Common name	Scientific name	Occurrence
Soricidae	Vagrant shrew	<u>Sorex vagrans</u>	*
Vespertilionidae	Little brown myotis	<u>Myotis lucifugus</u>	*
	Fringed myotis	<u>Myotis thysandoes</u>	
	California myotis	<u>Myotis californicus</u>	
	Small-footed myotis	<u>Myotis leibii</u>	
	Long-legged myotis	<u>Myotis volans</u>	
	Long-eared myotis	<u>Myotis evotis</u>	
	Hoary bat	<u>Lasiurus cinereus</u>	*
	Silver-haired bat	<u>Lasionycteris noctivagans</u>	*
	Big brown bat	<u>Eptesicus fuscus</u>	
	Western pipistrelle	<u>Pipistrellus hesperus</u>	
	Townsend's big-eared bat	<u>Plecotus townsendii</u>	
	Pallid bat	<u>Antrozous pallidus</u>	
Mustelidae	Mink	<u>Mustela vison</u>	*
	Longtail weasel	<u>Mustela frenata</u>	*
	Badger	<u>Taxidea taxus</u>	*
	Striped skunk	<u>Mephitis mephitis</u>	*
Procyonidae	Raccoon	<u>Procyon lotor</u>	*
Canidae	Coyote	<u>Canis latrans</u>	*
Felidae	Bobcat	<u>Lynx rufus</u>	*
Sciuridae	Townsend's ground squirrel	<u>Spermophilus townsendii</u>	*
Castoridae	Beaver	<u>Castor canadensis</u>	*
Geomyidae	Northern pocket gopher	<u>Thomomys talpoides</u>	*
Heteromyidae	Great Basin pocket mouse	<u>Perognathus parvus</u>	*

TABLE 9-2. Mammal Species Reported to Occur on the Hanford Site. (Sheet 2 of 2)

Family	Common name	Scientific name	Occurrence
Cricetidae	Western harvest mouse	<u>Reithrodontomys megalotis</u>	*
	Deer mouse	<u>Peromyscus maniculatus</u>	*
	Northern grasshopper mouse	<u>Onychomys leucogaster</u>	*
	Bushy-tailed woodrat	<u>Neotoma cinerea</u>	*
	Montane vole	<u>Microtus montanus</u>	*
	Sagebrush vole	<u>Lagurus curtatus</u>	*
	Muskrat	<u>Ondatra zibethicus</u>	*
Muridae	Norway rat	<u>Rattus norvegicus</u>	*
	House mouse	<u>Mus musculus</u>	*
Erethizontidae	Porcupine	<u>Erethizon dorsatum</u>	*
Leporidae	Black-tailed jackrabbit	<u>Lepus californicus</u>	*
	White-tailed jackrabbit	<u>Lepus townsendii</u>	*
	Nuttall's cottontail	<u>Sylvilagus nuttallii</u>	*
Cervidae	Mule deer	<u>Odocoileus hemionus</u>	*
	Elk	<u>Cervus canadensis</u>	*

*Documented sightings at the reference repository location.

TABLE 9-3. Birds Common to the Hanford Site.
(Sheet 1 of 3)

Family	Common name	Scientific name
Ardeidae	Great blue heron	<u>Ardea herodias</u>
Accipitridae	Sharp-shinned hawk	<u>Accipiter striatus</u>
	Red-tailed hawk	<u>Buteo jamaicensis</u>
	Swainson's hawk	<u>Buteo swainsoni</u>
	Marsh hawk	<u>Circus cyaneus</u>
	Rough-legged hawk	<u>Buteo lagopus</u>
Falconidae	American kestrel	<u>Falco sparverius</u>
Phasianidae	California quail	<u>Lophortyx californicus</u>
	Ring-necked pheasant	<u>Phasianus colchicus</u>
	Chukar	<u>Alectoris chukar</u>
Charadriidae	Killdeer	<u>Charadrius vociferus</u>
Scolopacidae	Long-billed curlew	<u>Numenius americanus</u>
Recurvirostridae	American avocet	<u>Recurvirostra americana</u>
Laridae	California gull	<u>Larus californicus</u>
	Ring-billed gull	<u>Larus delawarensis</u>
Columbidae	Rock dove	<u>Columba livia</u>
	Mourning dove	<u>Zenaida macroura</u>
Strigidae	Great horned owl	<u>Bubo virginianus</u>
	Burrowing owl	<u>Athene cunicularia</u>
Caprimulgidae	Common nighthawk	<u>Chordeiles minor</u>
Picidae	Common flicker	<u>Colaptes auratus</u>
Tyrannidae	Western kingbird	<u>Tyrannus verticalis</u>
	Say's phoebe	<u>Sayornis saya</u>
Alaudidae	Horned lark	<u>Eremophila alpestris</u>

TABLE 9-3. Birds Common to the Hanford Site.
(Sheet 2 of 3)

Family	Common name	Scientific name
Hirundinidae	Barn swallow	<u>Hirundo rustica</u>
	Cliff swallow	<u>Petrochelidon pyrrhonota</u>
Corvidae	Black-billed magpie	<u>Pica pica</u>
	Common raven	<u>Corvus corax</u>
	Common crow	<u>Corvus brachyrhynchos</u>
Troglodytidae	Long-billed marsh wren	<u>Cistothorus palustris</u>
Mimidae	Sage thrasher	<u>Orescoptes montanus</u>
Turdidae	American robin	<u>Turdus migratorius</u>
Laniidae	Loggerhead shrike	<u>Lanius ludovicianus</u>
	Northern shrike	<u>Lanius excubitor</u>
Sturnidae	Starling	<u>Sturnus vulgaris</u>
Parulidae	Yellow warbler	<u>Dendroica petechia</u>
	Yellow-rumped warbler	<u>Dendrocia auduboni</u>
Ploceidae	House sparrow	<u>Passer domesticus</u>
Icteridae	Western meadowlark	<u>Sturnella neglecta</u>
	Yellow-headed blackbird	<u>Xanthocephalus xanthocephalus</u>
	Red-winged blackbird	<u>Agelaius phoeniceus</u>
	Northern oriole	<u>Icterus galbula</u>
	Brewer's blackbird	<u>Euphagus cyanocephalus</u>
	Brown-headed cowbird	<u>Molothrus ater</u>
Fringillidae	House finch	<u>Carpodacus mexicanus</u>
	Sage sparrow	<u>Amphispiza belli</u>
	White-crowned sparrow	<u>Zonotrichia leucophrys</u>
	Song sparrow	<u>Melospiza melodia</u>
	Lark sparrow	<u>Chondestes grammacus</u>
	Dark-eyed junco	<u>Junco hyemalis</u>

TABLE 9-3. Birds Common to the Hanford Site.
(Sheet 3 of 3)

Family	Common name	Scientific name
Anatidae	Whistling swan	<u>Olor columbianus</u>
	Canada goose	<u>Branta canadensis</u>
	Mallard	<u>Anas platyrhynchos</u>
	Gadwall	<u>Anas strepera</u>
	Pintail	<u>Anas acuta</u>
	Green-winged teal	<u>Anas crecca</u>
	Blue-winged teal	<u>Anas discors</u>
	Cinnamon teal	<u>Anas cyanoptera</u>
	American wigeon	<u>Mareca americana</u>
	Northern shoveler	<u>Anas clypeata</u>
	Redhead	<u>Aythya americana</u>
	Ring-necked duck	<u>Aythya collaris</u>
	Canvasback	<u>Aythya valisineria</u>
	Lesser scaup	<u>Aythya affinis</u>
	Common goldeneye	<u>Bucephala clangula</u>
	Barrow's goldeneye	<u>Bucephala islandica</u>
	Bufflehead	<u>Bucephala albeola</u>
	Ruddy duck	<u>Oxyura jamaicensis</u>
	Common merganser	<u>Mergus merganser</u>
Podicipedidae	Horned grebe	<u>Podiceps auritus</u>
	Eared grebe	<u>Podiceps nigricollis</u>
	Western grebe	<u>Aechmophorus occidentalis</u>
	Pied-billed grebe	<u>Podilymbus podiceps</u>
Rallidae	American coot	<u>Fulica americana</u>

9.1.1.4 Reptiles and Amphibians. Reptile and amphibian species are relatively scarce at the Hanford Site (Table 9-4). Since amphibians require moisture and standing water in which to propagate, they probably play only a minor role in the ecosystem of the reference repository location. Reptiles are more abundant than amphibians, because of their physiological adaptations to the semiarid desert environment. Snakes that are probably common to the reference repository location include the gopher snake, Northern Pacific rattlesnake, and Western yellow-bellied racer. The most common lizard is the side-blotched lizard. Lizards depend primarily upon insects as food items, and snakes prey upon a variety of small mammals. Both lizards and snakes are common prey items of mammalian and avian carnivores.

9.1.1.5 Insects. Although insects are not usually addressed to a great extent in environmental studies, they do play a significant role and are a major component of the Hanford region ecosystem. Major fluctuations or outbreaks in local insect populations can affect the total ecosystem. Insects impact the surrounding plant community as well as serving as the prey base for many species of birds, reptiles, and mammals. The major insect groups that have been studied within the reference repository location are several genera of grasshoppers and darkling beetles, both of which consume sagebrush, which is the dominant shrub on the Hanford Site (Table 9-5). Other major groups of insects include bees, butterflies, ants, and scarab beetles.

9.1.1.6 Special and Unique Habitats. The Hanford Site, with the exception of White Bluffs, is one of the few large areas of land in the region that has not been developed for agricultural use. The Hanford Site is also unique, in that use of the area is restricted and limited to projects directly associated with the nuclear industry. Outdoor recreational activities, such as fishing and hunting, are not allowed on the Hanford Site.

Terrestrial habitats that contribute unique qualities to the Hanford Site are the Rattlesnake Hills, which provide the site's only mountainous environment; the unstabilized sand dunes near the Columbia River, which rise 3 to 5 meters above ground level and create sandy habitats ranging from less than one to several hundred hectares in size; basaltic ridges such as Gable Butte and Gable Mountain; and streamside habitats along the Columbia River as well as the ponds and ditches of the Hanford Site area.

Aquatic habitats exist on the Hanford Site in the area limited to the Columbia River system; one natural pond, West Lake; and several man-made ditches and ponds that are unique to the Hanford Site area, since they were created as a result of man's activities. These man-made systems attract many animal species which would not otherwise be found in these normally arid locations. The total aquatic habitat aside from that provided by the Columbia River system is approximately 57 hectares.

TABLE 9-4. Reptilian and Amphibian Species Reported to Occur on the Hanford Site.

Family	Common name	Scientific name	Occurrence
Reptiles			
Iguanidae	Sagebrush lizard	<u>Sceloporus graciosus</u>	*
	Side-blotched lizard	<u>Uta stansburiana</u>	*
	Pygmy short-horned lizard	<u>Phrynosoma douglassi</u>	*
	Western fence lizard	<u>Sceloporus occidentalis</u>	*
Colubridae	Striped whipsnake	<u>Masticophis taeniatus</u>	*
	Western yellow-bellied racer	<u>Coluber constrictor</u>	*
	Gopher snake	<u>Pituophis melanoleucus</u>	*
	Desert night snake	<u>Hypsiglena torquata</u>	*
	Common garter snake	<u>Thamnophis sirtalis</u>	
	Western terrestrial garter snake	<u>Thamnophis elegans</u>	
Viperidae	Northern Pacific rattlesnake	<u>Crotalus viridus</u>	*
Testudinidae	Painted turtle	<u>Chrysemys picta</u>	*
Scincidae	Western skink	<u>Eumeces skiltonianus</u>	
Amphibians			
Bufonidae	Western toad	<u>Bufo boreas</u>	*
	Woodhouse's toad	<u>Bufo woodhousei</u>	*
Ranidae	Leopard frog	<u>Rana pipiens</u>	
	Bullfrog	<u>Rana catesbeiana</u>	
Ambystomidae	Long-toed salamander	<u>Ambystoma macrodactylum</u>	
	Tiger salamander	<u>Ambystoma tigrinum</u>	
Pelobatidae	Great Basin spadefoot	<u>Scaphiopus intermontanus</u>	*
Hylidae	Pacific treefrog	<u>Hyla regilla</u>	

*Documented sightings at the reference repository location.

TABLE 9-5. Darkling Beetle and Grasshopper Species Known to Occur on the Reference Repository Location.

Darkling beetles	Grasshopper
<u>Anemia californica</u>	<u>Ageneotettix deorum</u>
<u>Blapstinus species</u>	<u>Amphitornus coloradus</u>
<u>Coniontis lanei</u>	<u>Apote notabilis</u>
<u>Coniontis ovalis</u>	<u>Arphia pseudonietana</u>
<u>Coniontis setosa</u>	<u>Aulocara ellioti</u>
<u>Conisattus nelsoni</u>	<u>Conozoa wallula</u>
<u>Eleodes granulata</u>	<u>Hesperotettix viridis</u>
<u>Eleodes hispilabris</u>	<u>Melanoplus cinereus</u>
<u>Eleodes humeralis</u>	<u>Melanoplus sanguinipes</u>
<u>Eleodes nigrina</u>	<u>Melanoplus yarrowii</u>
<u>Eleodes novoverrucula</u>	<u>Oedaleonotus enigma</u>
<u>Elodes obscura</u>	<u>Paropomala pallida</u>
<u>Eusattua muricatus</u>	<u>Steiroxys species</u>
<u>Oxygonodera hispidula</u>	<u>Trimerotropis balobata</u>
<u>Philolithus densicollis</u>	<u>Trimerotropis caeruleipennis</u>
<u>Stenomorphia puncticollis</u>	<u>Trimerotropis pallidipennis</u>
	<u>Xanthippus lateritus</u>

9.1.1.7 Threatened and Endangered Species.

Plants. Currently there are no federally recognized threatened or endangered plant species known to occur on the reference repository location. However, the U.S. Fish and Wildlife Service is reviewing the status of four species, Allium robinsonii, Astragalus columbianus, Erigeron piperanus, and Balsamorhiza rosea, for future consideration as threatened or endangered species (FWS, 1980a). These four species are known to occur on the Hanford Site, but it is not known if they are found in the reference repository location. Eriogonum thymoides, indicated as endangered (ERDA, 1975), is no longer considered as such (FWS, 1980b).

Animals. At this time, no threatened or endangered mammal species are known to inhabit the Hanford Site. Two threatened and endangered bird species, the bald eagle, Haliaeetus leucocephalus, and the peregrine falcon, Falco peregrinis, (FWS, 1980a) are known to occur as winter migrants on the Hanford Site. The peregrine falcon is considered a rare visitor (Fitzner et al., 1980). Bald eagles, which have only threatened status in the state of Washington, are fairly common along the Columbia River from November through February. Additionally, their numbers have increased since 1975 to an average of 15 to 20 eagles sighted annually (Allen, 1979). Although not common within the 200 Areas these birds have been sighted infrequently within the boundaries of the reference repository location, as noted during recent studies when bald eagles were observed foraging within the reference repository location.

9.1.2 Climate

See Chapter 8.

9.1.3 Geology

See Chapter 3.

9.1.4 Air Quality

See Section 8.2 of Chapter 8.

9.1.5 Water Quality and Use

See Chapters 5 and 7.

9.1.6 Radiological Background

There are a number of radiological monitoring and surveillance locations in the general vicinity of the reference repository location (Fig. 9-4). The monitoring and surveillance systems consist of the following:

- A monitoring station with a thermoluminescent dosimeter and an air sampler positioned near the west perimeter fence on the 200 West Area boundary
- Seven sample stations located 150 meters (500 feet) west of the western fenceline of the 200 West Area and spaced about 610 meters (2,000 feet) apart (north-south direction)
- A control plot located within the reference repository location
- A sample plot located southwest of the 200 West Area
- An air-sample station at the Yakima Barricade, approximately 1.5 kilometers upwind (northwest) of the reference repository location
- Air-sample stations within the 200 West Area.

Data on the environmental status of the Hanford Site for the years 1971 through 1978 indicate that the monitoring station and the sample plot (located southwest of the 200 West Area) show increases in concentrations for radionuclides in air, soil, and vegetation when compared with values from the Yakima Barricade station located upwind. Additionally, dose rate, measured by thermoluminescent dosimeters from the monitoring station, is consistently higher than the rates at the seven sample stations and almost double the values for the Yakima Barricade air-sample station (i.e., 130 versus 72 millirem (Houston and Blumer, 1978)).

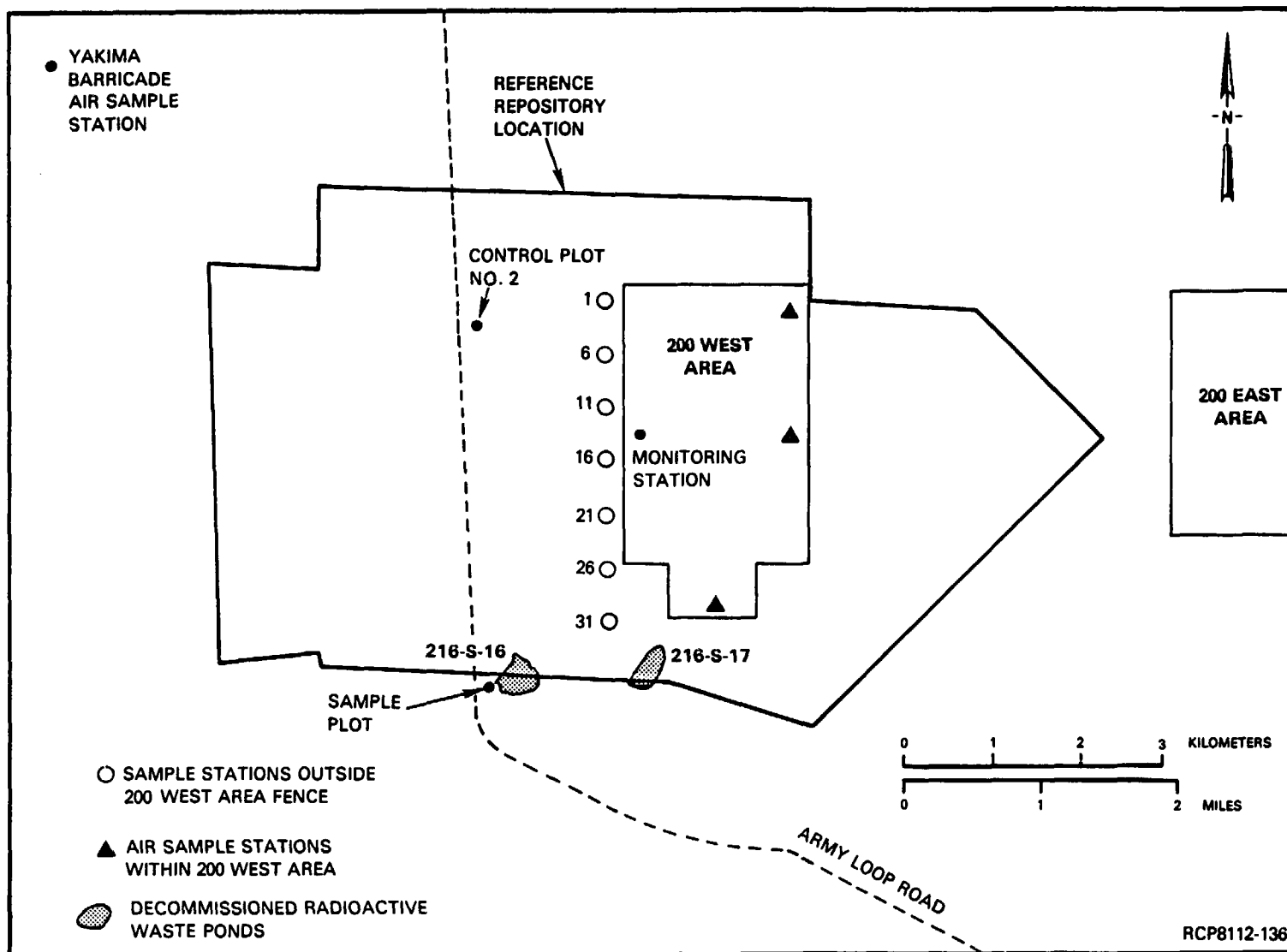


FIGURE 9-4. Map of the 200 Areas Controlled Zone Showing the Reference Repository Location and the Sample Point.

Data collected from the proposed project area show an increase in values for radionuclides incorporated in biological systems. Data from samples collected in 1976 and 1977 at Control Plot No. 2, located within the reference repository location, are given in Table 9-6. The values obtained for ^{137}Cs and ^{90}Sr at that sample site were up to 100 times the median concentrations for the Hanford area environs (Table 9-7).

TABLE 9-6. Summary of Radiological Data from Control Plot No. 2 for 1976 and 1977.

Species/component	Year	Dry weight (pCi/g)		
		^{137}Cs	^{141}Ce	^{90}Sr
Cheatgrass	1976	255.0	a	a
Russian thistle	1976	53.0	a	a
Big sagebrush	1976	9.0	a	a
Sandberg's bluegrass	1976	379.0	a	a
Soil	1977	0.8	b	177.0
Rabbit pellets	1977	14.5	b	16.1
Russian thistle	1977	15.7	8.8	3.9
Big sagebrush	1977	97.9	9.1	3.1
Cheatgrass	1977	86.0	b	5.4

^aSample not taken.

^bGenerally less than detectable.

Information derived from the seven sample stations along the 200 West Area fence (Fig. 9-4) is presented in Tables 9-8 and 9-9. These values are generally within the Hanford area median concentrations, but the values tend to increase toward the southerly sample stations (notably Sample Stations 26 and 31). An elevation of values above background levels can be noted with regard to rabbit fecal samples. It would appear that the animals either have access to radioactive sources outside the fenceline or are entering the 200 West Area under the fence and ingesting contaminated material. In either case, material with higher radioactive concentration is being deposited and spread within the reference repository location boundaries.

TABLE 9-7. Median Concentrations of Man-Made Radionuclides in Soil and Vegetation in the Hanford Area Environs (Miller et al., 1977).

Radionuclide	Soil, median concentration (pCi/g) ^a	Vegetation, median concentration (pCi/g) ^a
⁵⁴ Mn	0.014	b
⁵⁸ Co	0.016	0.0001
⁶⁰ Co	0.022	0.024
⁶⁵ Zn	0.07	0.45
⁹⁰ Sr	0.13	0.68
⁹⁵ Zr-Nb	b	0.6
¹⁰⁶ Ru	0.36	0.41
¹³¹ I	c	0.25
¹³⁴ Cs	0.03	b
¹³⁷ Cs	0.6	0.37
¹⁴⁰ Ba-La	b	11.0
¹⁴¹ Ce	0.074	b
¹⁴⁴ Ce-Pr	0.6	1.8
¹⁴⁴ Ce	0.25	b
²³⁸ Pu	0.0013	7.5 E-04
²³⁹ Pu	0.01	1.7 E-03
²⁴⁰ Pu	0.01	1.7 E-03

^aDry weight.

^bGenerally less than detectable.

^cNot routinely analyzed.

TABLE 9-8. Summary of 1978 Radiological Data at Seven Sample Sites Along the 200 West Area Fence.

Radionuclide parameters	Sample site, dry weight (pCi/g)						
	1	6	11	16	21	26	31
Soil							
^{137}Cs	0.9	0.8	0.3	0.7	0.7	1.6	0.0
^{90}Sr	0.06	0.03	0.01	0.3	0.1	0.4	0.2
$^{238,240}\text{Pu}$	0.05	a	0.01	0.03	0.02	0.06	0.16
Vegetation							
^{137}Cs	0.54	b	b	b	b	b	b
^{90}Sr	0.16	b	b	b	b	b	b
$^{239,240}\text{Pu}$	0.02	b	b	b	b	b	b
Feces (rabbit)							
^{137}Cs	2.37	1.41	1.08	1.07	3.08	2.28	8.45
mR/yr							
Dose rate (TLD's ^c)	74	70	66	74	73	71	65

^aLess than detection limits.

^bSample not taken.

^cThermoluminescent dosimeters.

TABLE 9-9. Summary of 1979 Radiological Data at Seven Sample Sites Along the 200 West Area Fence (Wheeler and Law, 1980).

Radionuclide parameters	Sample site, dry weight (pCi/g)						
	1	6	11	16	21	26	31
Soil							
^{137}Cs	0.57	0.22	0.39	0.29	0.31	1.30	0.72
^{90}Sr	0.64	0.17	0.22	0.14	0.13	0.14	0.24
$^{239,240}\text{Pu}$	0.04	0.034	0.022	0.061	0.012	0.010	0.079
Vegetation							
^{137}Cs	a	0.09	0.14	a	a	0.30	0.16
^{90}Sr	0.14	0.22	0.17	0.18	0.20	0.17	0.13
$^{239,240}\text{Pu}$	3.61	0.035	0.075	0.051	0.074	0.012	0.017
Feces (rabbit)							
^{137}Cs	2.0	0.96	2.27	1.56	2.76	2.53	14.5
^{90}Sr	3.9	1.36	0.85	0.84	5.41	9.88	23.0
$^{239,240}\text{Pu}$	a	0.08	a	0.02	0.07	0.06	0.10
mR/yr							
Dose rate (TLD's ^b)	78	71	65	77	73	81	72

^aLess than detection limits.

^bThermoluminescent dosimeters.

It should be noted that at Sample Station 1 there was an increase of 2 orders of magnitude in the level of $^{239, 240}\text{Pu}$ contained in vegetation. The source term has not yet been located.

In the vicinity of the reference repository location, there are two decommissioned radioactive waste ponds comprising an area of approximately 20 hectares (see Fig. 9-4). Radiological studies at pond 216-S-17 (Paine et al., 1979) have documented contamination in all major ecological compartments, including small mammals (Landeem and Mitchell, 1981), soils, and vegetation. Surface soil samples collected from mammal burrows have contained up to 4,600 picocuries per gram of ^{137}Cs and 300 picocuries per gram of ^{90}Sr . Small mammals collected at the pond have contained maximum values of 83 picocuries per gram of ^{137}Cs and 658 picocuries per gram of ^{90}Sr . Radiological data collected for the shallow-rooted Siberian wheatgrass have indicated values up to 66 picocuries per gram of ^{137}Cs and 446 picocuries per gram of ^{90}Sr . Tumbleweeds and other deep-rooted plants at the pond have levels of radionuclides orders of magnitude above the values indicated for Siberian wheatgrass. Recent radiological surveys at pond 216-S-16 have identified only limited areas of surface soil contamination.

Surveys conducted over the past 10 years at a shallow underground radioactive-liquid-waste disposal site (the B-C cribs) in the vicinity of the reference repository location indicate that radionuclides are present in all major ecologic compartments associated with the 835 hectares of this designated Controlled Area. Results from monthly environmental surveillance programs for the past 3 years show surface contamination ranging from 5,000 to 10,000 counts per minute and vegetation samples (mostly tumbleweed) ranging from 6.0 to 23,000 picocuries per gram of ^{137}Cs . Radioactive particles from weathered jackrabbit pellets have been spread over several square kilometers in the general area of the Cold Creek syncline (O'Farrell et al., 1973).

9.2 LAND-USE CHARACTERISTICS

Land use is directly related to the direction and management of growth in an area.

9.2.1 Land-Use Categories

Land use in the Columbia Plateau region and in the vicinity of the Hanford Site is divided into the following categories.

9.2.1.1 Commercial, Industrial, and Residential Sites. Urban areas which contain the majority of commercial, industrial, and residential sites can be seen in Wukelic et al. (1981, Fig. 4). Most of these sites in the vicinity of the Hanford Site are located in and around the Tri-Cities area. Section 9.3 further describes distribution of commercial, industrial, and residential sites.

The DOE's Hanford Site occupies approximately 1,480 square kilometers in southeastern Washington State. Existing facilities and operational areas on the Hanford Site are identified by area numbers. Each area is a controlled or limited access area enclosed by a fence. The major areas are:

- The 100 Areas, bordering directly on the southern bank of the Columbia River in the northern portion of the Hanford Site, are the sites of nine plutonium production reactors. Only the dual-purpose N Reactor is in operation.
- The 200 Areas, located on a plateau about 11 kilometers from the Columbia River, are the site of fuel reprocessing, waste processing, and waste management activities.
- The 300 Area is closest to the city of Richland. Nuclear research and development laboratories and the fuel fabrication facility for the N Reactor are located here.
- The 400 Area is about 11 kilometers north of the 300 Area and is the site of the Fast Flux Test Facility used in the testing of breeder reactor systems.

Remaining government-controlled areas on the Hanford Site include the Near-Surface Test Facility (an in situ laboratory where thermomechanical properties of the Columbia River basalts are being tested), the Arid Lands Ecology Reserve, and the game reserves north of the Columbia River. Operational areas for the overall Hanford Site are depicted in Figure 9-1. Land use in the immediate vicinity of the reference repository location is detailed in Figure 9-5.

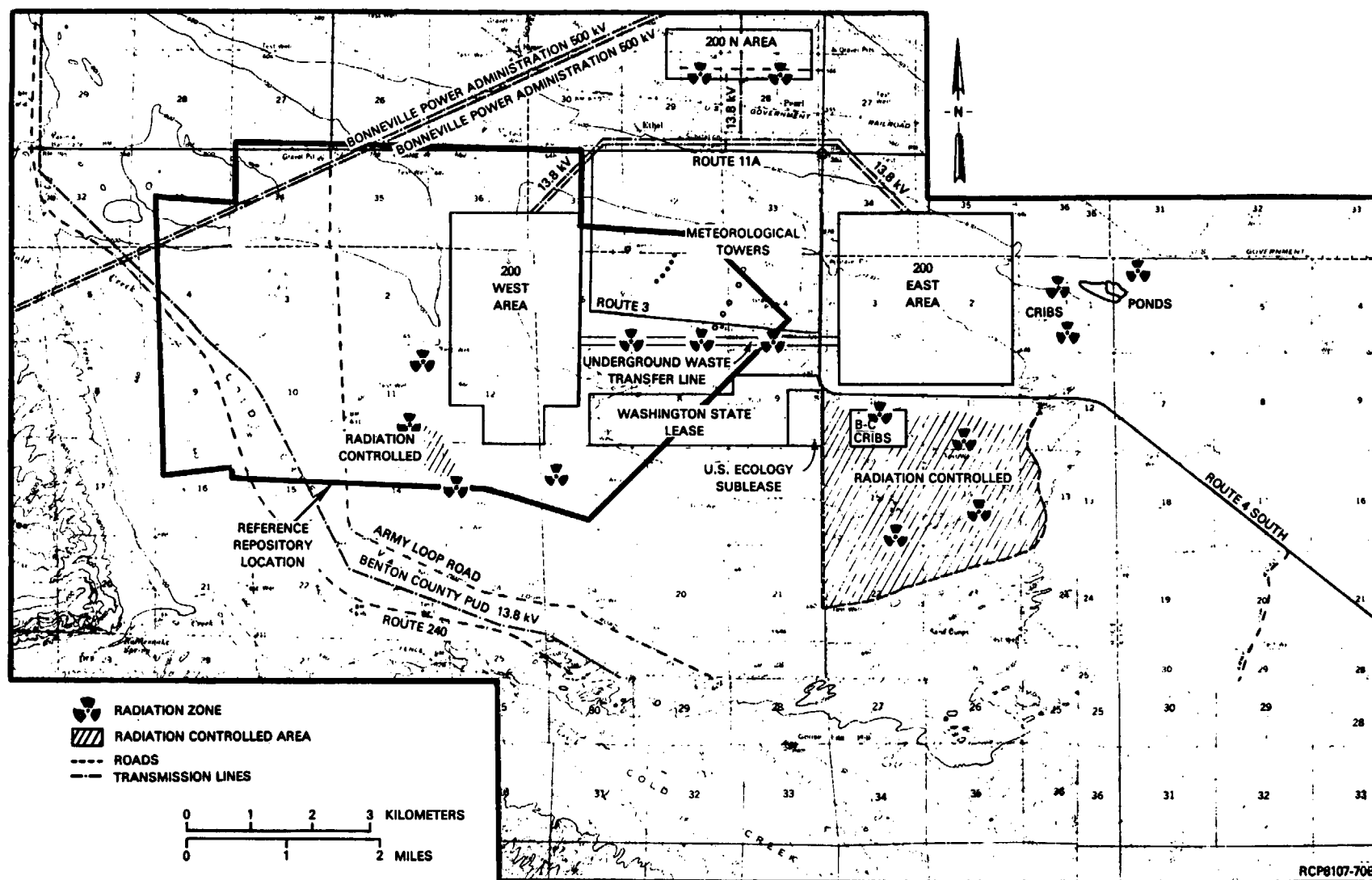


FIGURE 9-5. Land Use Adjacent to the Reference Repository Location.

Privately owned facilities located within the Hanford Site (see Fig. 9-1) include the Washington Public Power Supply System, Inc. generating station adjacent to the N Reactor, the Washington Public Power Supply System, Inc. nuclear reactor sites, and a low-level radioactive waste burial site. A nuclear fuel fabrication facility operated by the Exxon Nuclear Company, Inc. is located immediately adjacent to the southern boundary of the Hanford Site.

9.2.1.2 Hydrologic Features. The hydrology of the Hanford area is dominated by the Columbia River, which flows through the northern portion of the site and forms its eastern boundary. Other significant hydrologic features in the vicinity include the Yakima River to the south and west and the Snake River to the east. Two ephemeral streams, Cold and Dry Creeks on the Hanford Site, flow for a short time after heavy rainfall or snowmelt. Surface water bodies located within the Hanford Site include one natural pond, West Lake, of about 4 hectares in size and several man-made ditches and ponds that are used for the disposal of low-level radioactive liquid waste, some industrial wastes, and cooling water from various processes. Several ponding areas maintained by Water and Power Resources Service at the terminus of irrigation wasteways are located north of the Columbia River on the Hanford Site. These naturally occurring ponds are supplemented by irrigation runoff waters from outside the Hanford Site to provide wildlife habitat. Section 7.1 provides a more detailed hydrologic description of the site.

9.2.1.3 Agricultural Areas. Both dryland farming and irrigated agriculture supplied by surface water diversion and groundwater are important industries in areas surrounding the Hanford Site. Growth of irrigated agriculture has been spurred by the development of a series of dams as part of the Yakima and Columbia Basin projects. Principal agricultural products include wheat, potatoes, sugar beets, hay, corn, peas, apples, soft fruits, hops, mint, grapes, and vegetables. The distribution of irrigated agriculture in eastern Washington is shown in Wukelic et al. (1981, Fig. 4), while nonirrigated farmland areas are shown in Stephan et al. (1979, Fig. 18).

9.2.1.4 Grazing Areas. Cattle grazing in the vicinity of the Hanford Site is conducted on both irrigated and open rangeland. Rangeland in eastern Washington, dominated by sage and grass vegetation, is depicted in Stephan et al. (1979, Fig. 16). While the areas shown as grass-covered rangeland are not necessarily in use as grazing areas, their distribution indicates potential areas for expansion of grazing operations.

9.2.1.5 Forest Lands and Timber Production. There are no forested lands or timber production near the Hanford Site.

9.2.1.6 Mineral Extraction. There are presently no commercial operations producing crude oil, natural gas, coal, geothermal energy, peat, or metallic minerals within 100 kilometers of the Hanford Site. Natural gas was once produced for commercial purposes at the Rattlesnake Hills gas field on the Hanford Site. The gas field was first discovered in 1911 on the north slope of Rattlesnake Mountain and was in commercial operation from 1929 to 1941, yielding 37 million cubic meters of high-methane gas. It was depleted and closed down in 1941.

At the present time, two types of industrial minerals are found and exploited in commercial quantities within 100 kilometers of the Hanford Site. The most important is sand, gravel, and crushed stone, used primarily in concrete aggregate. Nearly all of the sand and gravel deposits being worked commercially in the area are adjacent to major streams and are in or near urbanized areas. Most of the crushed stone quarries utilize basalt. Diatomaceous earth is being produced from several deposits in Grant County and is processed at a plant near Quincy. The active mining operations are in surface mines, where minerals are extracted from relatively shallow depths.

Pumice and pumicite have been commercially produced in areas on or near the Hanford Site, but there are no deposits which are currently being commercially exploited. Pumice has been mined at two sites north of Ephrata in Grant County and at Zillah in eastern Yakima County. Commercial production has occurred in pumicite deposits near Beverly in southeastern Grant County, at Roza in southeastern Kittitas County, and on the Hanford Site northwest of Benton City.

See Section 3.9 for a more detailed discussion of mineral resources of the Columbia Plateau region.

9.2.1.7 Wildlife Preserves. Hanford Site lands north and east of the Columbia River are managed by the U.S. Bureau of Sport Fisheries and Wildlife and the Washington State Department of Game. Of this area, 13,000 hectares are designated as the Saddle Mountain National Wildlife Refuge and the remaining 22,000 hectares are managed by the state of Washington. Seven islands within the Hanford reach of the Columbia River are part of the McNary Wildlife Refuge, administered by the U.S. Fish and Wildlife Service. These islands serve as an important winter habitat for migratory waterfowl. The Arid Lands Ecology Reserve on the Hanford Site is a 310-square-kilometer tract set aside exclusively for the protection and study of native plant and animal ecosystems. The Arid Lands Ecology Reserve is managed by the DOE. The distribution of wildlife preserves is shown in Figure 9-1.

9.2.1.8 Parks and Recreation. County, state, and federal agencies maintain numerous park facilities near the Hanford Site. Most of these are adjacent to the Columbia and Snake Rivers, providing camping, boating, and other water-related recreational activities. Municipalities in the area provide park facilities which support outdoor sports and picnic facilities. A discussion of major recreational activities is provided in Section 9.3.3.4.

9.2.1.9 Scenic Views and Vistas. See Section 9.2.4.

9.2.1.10 Archaeological and Historic Areas. See Section 9.2.5.

9.2.1.11 Major Transportation Facilities. Major transportation facilities are located in the Tri-Cities area, comprised of the cities of Richland, Kennewick, and Pasco, which serves as a regional transportation and distribution center. The Tri-Cities Regional Airport, located in Pasco, provides connections to other major cities. The Richland Airport

has facilities for commuter and private air traffic, while the Kennewick Airport is limited to serving private aircraft. Commercial rail service is centered in Pasco, including a passenger train station and a major switching yard for freight traffic. Rail service within the Hanford Site is controlled and maintained by the DOE. Port facilities for barge traffic on the Columbia River are available at each of the three cities. Primary roads in the area include Routes 12, 395, 260, and 17 and Interstate-82, which is presently under construction. Routes 240 and 24, which traverse the Hanford Site, are maintained by the state of Washington while other secondary roads within the site are maintained by the DOE. Bridges across the Columbia River currently exist at Vernita in the northwest corner of the Hanford Site and at two locations connecting Kennewick and Pasco. Currently, a new bridge is being constructed across the Columbia River which will connect Richland to West Pasco.

Major transportation facilities in areas within and surrounding the Hanford Site are shown in Figure 9-1.

9.2.1.12 Utility Transportation Lines. Existing utility lines on the Hanford Site are shown in Figure 9-6.

9.2.1.13 Communication Facilities. Communication facilities on the Hanford Site are shown in Figure 9-6.

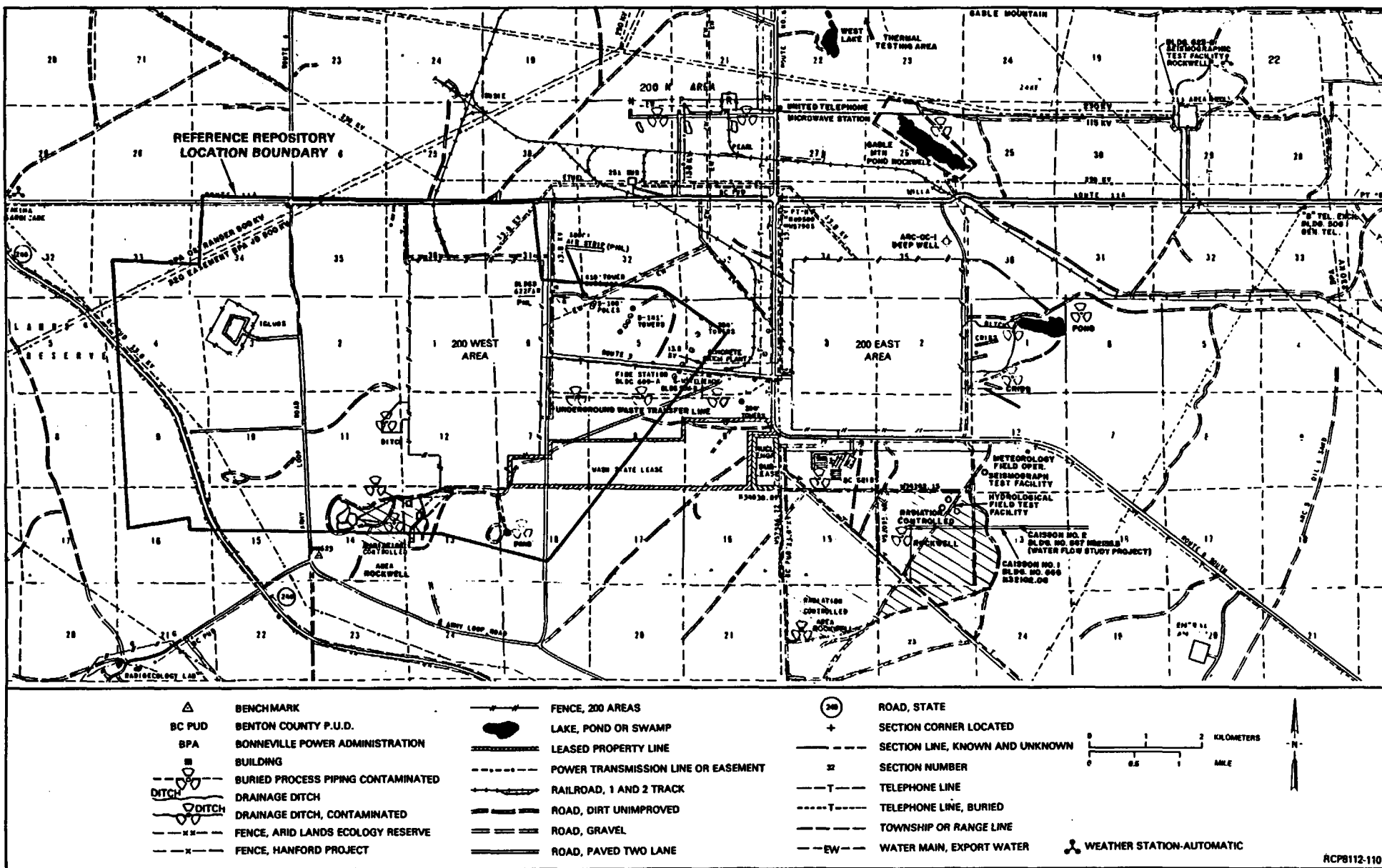
9.2.1.14 Community Service Facilities. See Section 9.3.3.

9.2.2 Land-Use Change

Growth in the population of the Tri-Cities metropolitan area is resulting in increasing urban land uses. Between 1970 and 1980, population in Benton and Franklin Counties grew by 62 and 36 percent, respectively, as compared to the state-wide average of 21 percent. Continued population growth and attendant urbanization are largely dependent on the future of the DOE energy-related projects at Hanford and the continued diversification of the local economy.

Irrigated agriculture in areas adjacent to the Hanford Site has also undergone substantial growth. Between 1975 and 1979, irrigated cropland acreage in the Columbia Plateau region increased by 20 percent (Wukelic et al., 1981, Fig. 4). Agricultural growth will likely continue in the Pasco Basin. However, continued demand and competition for increasingly scarce water resources, particularly on Yakima Basin project lands, may tend to constrain potential agricultural growth.

Potential land-use changes on the Hanford Site, other than the construction of a repository, include possible expansion of existing facilities and new construction projects. Preliminary feasibility studies sponsored by the Puget Sound Power and Light Company are currently under way at several locations to evaluate potential sites for a nuclear power reactor.



RCP8112-110

FIGURE 9-6. Utilities and Communications.

9.2.3 Ownership

Lands within the reference repository location and the remainder of the Hanford Site have been within the jurisdiction of the Federal Government since 1943. The Hanford Site is presently managed by the DOE. Hanford Site land north of the Columbia River is managed for the DOE by the U.S. Bureau of Sport Fisheries and Wildlife and the Washington State Department of Game. The lands designated for the repository consist of acquired lands plus Section 10, Township 12 North, Range 25 East of the Willamette Meridian, which is public domain. That Section 10 has been withdrawn from all forms of appropriation under the public land laws including the mining and mineral leasing-laws, and reserved for use by the U.S. Atomic Energy Commission in connection with its Hanford Operations. The applicable language in the applicable Public Land Order 1273 (BLM, 1956) is as follows:

"Subject to valid existing rights, the following-described public lands in Washington are hereby withdrawn from all forms of appropriation under the public-land laws, including the mining and the mineral-leasing laws, and reserved for use of the Atomic Energy Commission in connection with its Hanford Operations."

All functions of the Atomic Energy Commission with respect to the Hanford Site and certain other locations have been transferred to the Secretary of Energy. As a result, Section 10, Township 12 North, Range 25 East of Willamette Meridian, under the jurisdiction of the DOE which holds that land pursuant to the above-described provisions of Public Land Order 1273 (BLM, 1956).

Two parcels of land within the Hanford Site are leased to the State of Washington and the Washington Public Power Supply System, Inc. The state subleases a portion of its leased land to U.S. Ecology, Inc. for disposal of low-level radioactive wastes. The Washington Public Power Supply System, Inc. lease land serves as a site for the construction of three nuclear power reactors. The state also retains fee title to a section of land for use as a proposed hazardous waste disposal site. In addition, the Big Bend Alberta Company owns the mineral rights for several parcels of land within the Arid Lands Ecology Reserve. The status of land ownership and control within the Hanford Site is shown in Figure 9-1.

Lands adjacent to the Hanford Site are privately owned, with the exception of those areas controlled by the State of Washington and county and city governments. The state exercises control over state and federal highways and special-use areas such as parks and wildlife reserves. County and city governments have jurisdiction over publicly owned facilities and establish land-use controls within their respective borders.

The closest Indian reservation is owned by the Yakima Nation and is located approximately 25 kilometers (16 miles) west of the Hanford Site. The U.S. Army Yakima Firing Center is located about 10 kilometers (6 miles) west of the Hanford Site.

9.2.4 Aesthetics and Recreation

The National Registry of Natural Landmarks lists two sites which are within 80 kilometers of the Hanford Site (NPS, 1980). These are:

- Ginkgo Petrified Forest, located in Kittitas County, 47 kilometers east of Ellensburg
- Grand Coulee, located in Grant County between the towns of Grand Coulee and Soap Lake.

Other natural features in the area, which are not of national significance, include Sentinel Gap and the Saddle Mountains to the north of the Hanford Site. The Columbia River is the most notable natural feature of this area. The Hanford reach of the Columbia River is the last free-flowing stretch of this river in the United States. The White Bluffs, rising 60 to 90 meters above the eastern shoreline of the river, provide another natural landmark. The southwestern edge of the Site is marked by the Rattlesnake Hills and Rattlesnake Mountain (elevation 1,100 meters), the highest peak in the vicinity of the Hanford Site. Another notable scenic feature is Wallula Gap, on the Columbia River south of the Hanford Site.

See Section 9.3.3.4 for a discussion of local recreation activities.

9.2.5 Historic, Archaeological, and Cultural Resources

The Columbia River was one of the most densely inhabited regions of aboriginal North America. With the exception of sites located on the Hanford reach of the Columbia River, evidence of aboriginal culture has been virtually erased. Controlled access to the Hanford Site has provided protection to these remaining sites from destruction by relic collectors.

At present, nine archaeological properties on the Hanford Site are listed in the National Register of Historic Places (State of Washington, 1981c).

The known archaeological sites closest to the reference repository location are some of the Rattlesnake Springs sites, which are within 2.5 kilometers of the reference repository location boundary.

Historic properties and archaeological sites in counties adjacent to the Hanford Site which are listed in the National Register and Washington State Register of Historic Places (State of Washington, 1981c) are shown in Table 9-10.

A number of other archaeological sites, which are not of national significance, have been identified on the Hanford Site (Rice, 1968a; 1968b). Areas along the Columbia River shoreline are particularly rich in Indian artifacts. Some of the traditional winter campsites and fishing grounds were occupied as late as 1943, when the Hanford Site was created.

**TABLE 9-10. Washington State Register of Historic Places
in Counties Adjacent to the Hanford Site
(State of Washington, 1981c).**

Adams County
Dr. Frank R. Burroughs House, Ritzville* Stephen Devenish Ranch, Ritzville vicinity Nelson H. Greene House, Ritzville* Othello Museum and Arts Center, Othello Seivers Brothers Ranchhouse and Barn, Lind vicinity* Strap Iron Corral, Hooper vicinity* Zion Congregational Church, Ritzville
Benton County
Benton County Courthouse, Prosser* Columbia Park (Bateman) Island, Kennewick vicinity Coyote Rapids Archaeological District, Richland vicinity Gable Mountain Archaeological Site, Richland vicinity Glade Creek Site, Prosser vicinity* Hanford Island Archaeological Site, Richland vicinity* Hanford North Archaeological District, Richland vicinity* Locke Island Archaeological District, Richland vicinity* Rattlesnake Springs Sites, Richland vicinity* Ryegrass Archaeological District, Richland vicinity* Snively Canyon Archaeological District, Ringold vicinity* Telegraph Island Petroglyphs, Paterson vicinity* Wahluke Archaeological District, Richland vicinity Wooded Island Archaeological District, Richland vicinity* Charles Conway House, Kennewick
Franklin County
Ainsworth, Pasco vicinity Allen Rockshelter, Pasco vicinity* Burr Cave, Walker vicinity* Franklin County Courthouse, Pasco* Marmes Rockshelter, Lyons Ferry vicinity* James Moore House, Pasco* Palouse Canyon Archaeological District, Lower Palouse River vicinity Pasco Carnegie Library, Pasco Savage Island Archaeological District, Ringold vicinity* Strawberry Island Village, Pasco vicinity* Tri-Cities Archaeological District, Pasco vicinity Windust Caves Archaeological District, Ice Harbor Reservoir, Snake River
Grant County
Grant County Courthouse, Ephrata* Lind Coulee Archaeological Site, Warden vicinity* Mesa 36, Soap Lake vicinity* Paris Archaeological Site, Vernita vicinity* Wilson Creek State Bank, Wilson Creek*

*Also listed in the National Register of Historic Places (State of Washington, 1981c).

9.3 SOCIOECONOMIC CHARACTERISTICS

The geographic area likely to be impacted by a repository is defined in terms of a local, primary impact area and the larger region that contains and interacts with the local area. The primary impact area boundaries were identified based on the actual extent of impacts associated with other large construction projects on the Hanford Site. The primary area likely to experience any potential socioeconomic impacts associated with locating a repository at the Hanford Site is shown in Figure 9-7.

9.3.1 Demography

Understanding demographic patterns in the vicinity of a proposed repository site at the Hanford Site is an important part of socioeconomic impact analyses. The 1980 census data on the population of incorporated cities and counties within 80 kilometers of the Hanford Meteorological Station are shown in Figure 9-8. Current and projected population statistics for Benton and Franklin Counties and the primary socioeconomic impact area are given in Table 9-11. Cities and towns outside the impact area have absorbed only a small amount of growth from the larger area. Unincorporated portions of the bicounty area, however, received a significant percentage (41.7 percent) of the growth between 1970 and 1980. Since the rate of a city's population growth tends to decrease as it matures, the distributional pattern of growth in the bicounty and primary impact areas will almost certainly be different than in the past. Growth patterns will also be affected by future construction of bridges across the Columbia River and the growth or decline of various economic sectors.

As can be seen in Table 9-12, most of the growth during the past decade in Benton County can be attributed to the large number of people (78.3 percent) moving into the area (migration) rather than to natural increase (birthrate). In Franklin County less than half of the growth in population can be attributed to migration.

High levels of net immigration tend to be selective of the age group between 20 and 65. This is illustrated by the data presented in Table 9-13. The bicounty area is forecasted to have increasingly higher proportions of its population concentrated in this age group.

9.3.2 Economy

The economy in the vicinity of the reference repository location is primarily based on the energy-related projects at the Hanford Site and agriculture. The relative contribution of the various economic sectors is shown in Table 9-14. Agricultural employment is expected to remain relatively stable over the next two decades. Federally funded, energy-related activities on the Hanford Site, however, account for the major share of the current economic prosperity and projected growth of the area. In 1978, the Hanford Site payroll exceeded \$400 million, much of which continued to be recycled throughout the local economy. This economic prosperity has attracted new economic growth to the area, helping

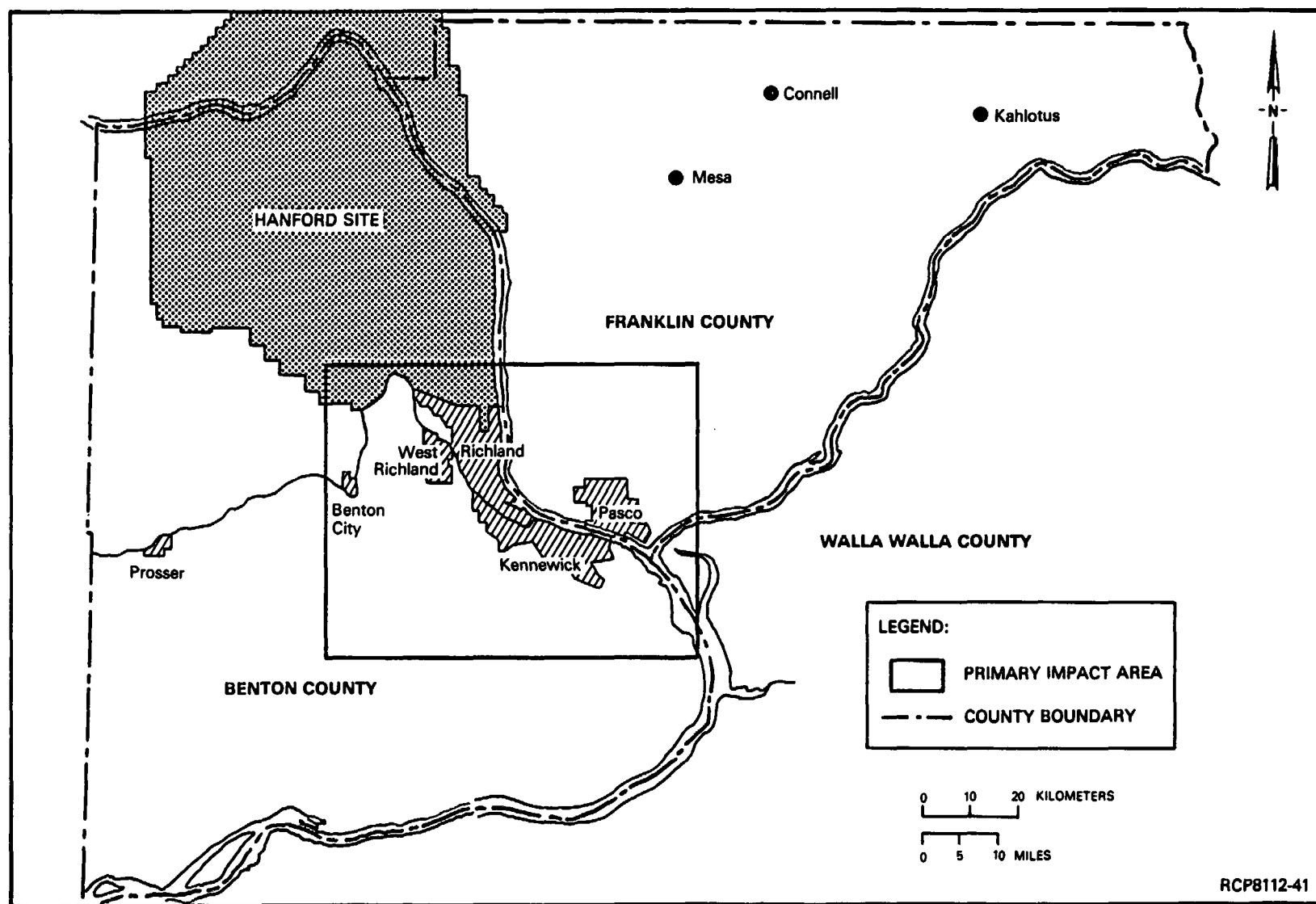


FIGURE 9-7. Primary Impact Area.

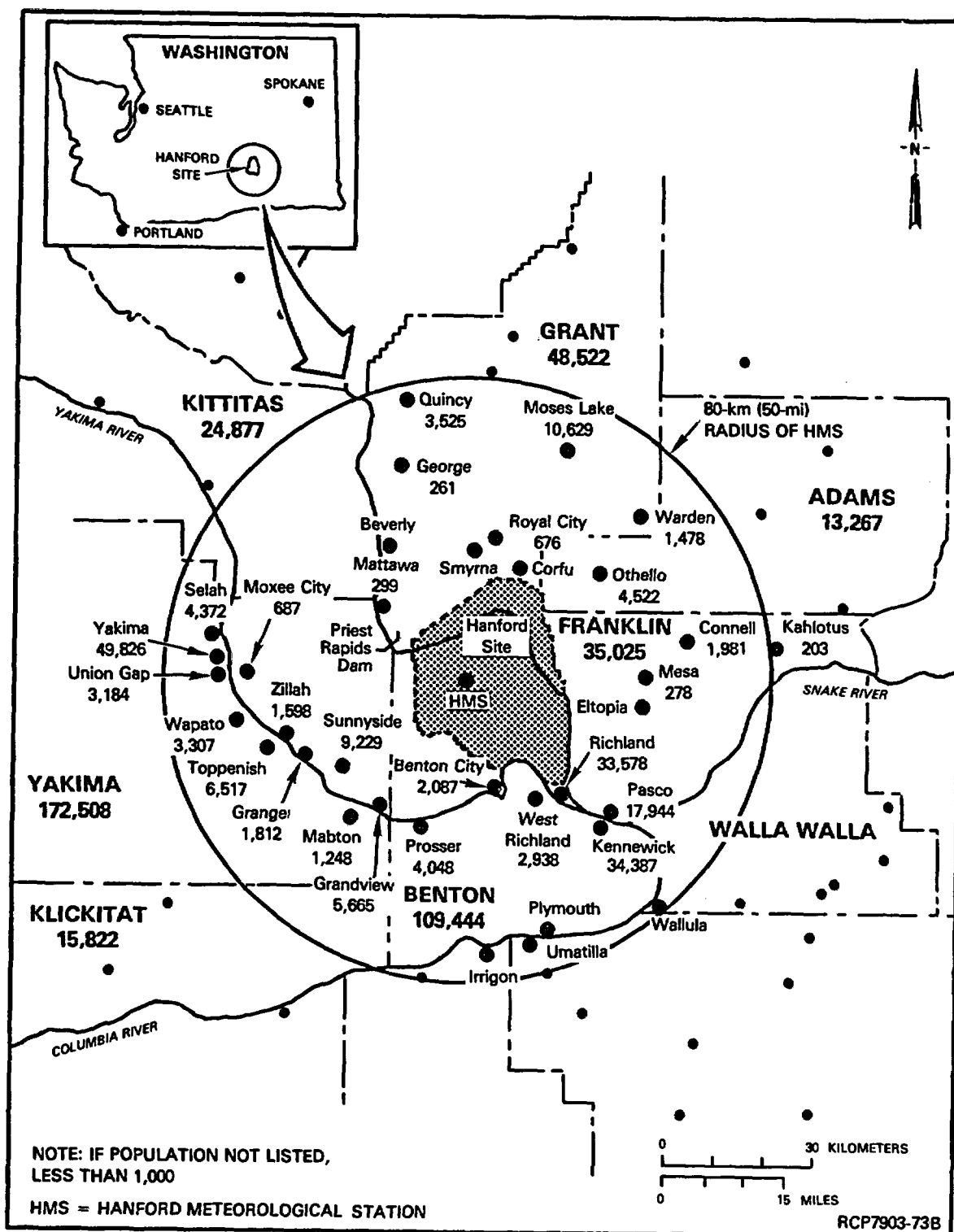


FIGURE 9-8. U.S. Census Populations for 1980 of Cities Within an 80-Kilometer (50-Mile) Radius of the Hanford Meteorological Station.

TABLE 9-11. Population Size Based on Census, Current Estimates, and Forecasts for Benton and Franklin Counties and the Primary Impact Area--1970-2000.

Municipality by county	Census and current estimates			Change (%) 1975-1980	Forecasts	
	1970 ^{a,b}	1975 ^a	1980 ^{b,c}		1990	2000
Benton	67,540	73,300	109,444	49.3	140,239 ^d 111,321 ^e	162,138 ^d 120,162 ^e
Benton City	1,070	1,315 ^b	1,980	50.6		
Kennewick	15,212	18,253 ^b	34,397	88.4		
Richland	26,290	28,600 ^b	33,578	17.4		
West Richland	1,107	1,477 ^b	2,938	98.9		
Balance of county	23,861	23,655 ^b	36,551	54.5		
Franklin	25,816	26,700	35,025	31.2	47,656 ^d 43,016 ^e	57,307 ^d 50,566 ^e
Pasco	13,920	14,450	17,944	24.2		
Balance of county	11,896	12,250	17,081	39.4		
Bicounty total	93,356	100,000	144,469	44.5	187,895 ^d 154,337 ^e	219,445 ^d 170,728 ^e
Primary impact area ^f	57,599	64,095	90,837	41.7	118,374 ^g 97,232 ^g	138,250 ^g 107,559 ^g
State total	3,413,244	3,504,727	4,130,163	17.8		

^aState of Washington (1979a, Table 1).

^bActual census count.

^cBOC (1981).

^dState of Washington (1981a).

^eState of Washington (1978).

^fThe five incorporated cities listed above comprise the primary impact area as defined for this study. Although this area (see Fig. 9-7) includes some people living in unincorporated places, that component cannot be accurately measured with currently available data (see text).

^gForecasts for the primary impact area are based on a projected 63 percent share of the respective bicounty forecasts.

TABLE 9-12. Components of Population Change by County and State.

Area	Population size ^a		Population change 1970-1980		Change (%) 1970-1979 ^b due to:	
	1970	1980	Number	Percent	Natural increase	Net migration
Benton County	67,540	109,444	41,904	62.0	21.7	78.3
Franklin County	25,816	35,025	9,209	35.7	59.3	40.7
Washington State	3,413,244	4,130,163	716,919	21.0	42.3	57.7

^aBOC (1981).^bState of Washington (1979a), Table 14. Comparable data were not yet available for 1980.

TABLE 9-13. Population Distribution by Age and Sex.*

Area	Age category	1970		1980		1990	
		Population Distribution (%)					
		Male	Female	Male	Female	Male	Female
Benton County	0-19	42.9	40.7	36.4	34.2	33.4	32.0
	20-64	51.0	52.5	57.0	58.1	59.8	59.9
	65+	6.1	6.8	6.6	7.7	6.8	8.1
Franklin County	0-19	43.1	41.4	36.8	35.4	34.1	32.8
	20-64	51.0	51.3	56.8	56.5	59.4	58.6
	65+	5.8	7.3	6.3	8.1	6.6	8.6
Washington State	0-19	38.9	36.7	32.4	30.8	30.2	28.9
	20-64	53.0	52.7	58.9	57.6	60.8	58.7
	65+	8.2	10.6	8.7	11.6	9.0	12.4

*State of Washington (1981a).

TABLE 9-14. Personal Income by Major Sources, Richland-Kennewick-Pasco Standard Metropolitan Statistical Area 1972-1977.^a (Sheet 1 of 2)

Total labor and proprietors income by place of work ^b	Annual income in thousands of dollars		Average annual income change over period (%)		Richland-Kennewick-Pasco area as % of state income		Income category as % of total earnings	
	1972 ^c	1977 ^d	1972-1976	1976-1977	1972	1977	1972	1977
By type								
Wage and salary disbursements	275,588	675,135	16.6	23.2	2.8	3.8		
Other labor income	13,216	41,889	22.3	26.1	2.5	3.2		
Proprietors income ^e	53,459	56,273	9.5	-33.0	3.8	2.6		
Farm	27,057	5,312	5.9	-186.5	6.8	1.4		
Nonfarm ^e	26,402	50,961	12.8	14.8	2.6	2.9		
By industry								
Farm	38,003	33,124	12.2	-62.4	7.4	5.2	11.1	4.3
Nonfarm	304,260	740,173	16.3	23.6	2.7	3.6	88.9	95.7
Private	255,861	655,764	17.1	25.7	2.5	4.1	74.8	84.8
Agriculture service, forestry, fisheries, and others ^f	1,720	4,370	21.1	8.9	2.4	2.6	0.5	0.6
Mining	935	958	-16.9	69.9	4.2	2.1	0.3	0.1
Construction	35,739	168,386	26.8	47.8	4.8	10.5	10.4	21.8
Manufacturing	59,232	136,308	16.3	18.0	2.3	3.0	17.3	17.6
Nondurable goods	53,246	119,907	15.3	20.0	7.1	9.2	15.6	15.5
Durable goods	5,986	16,401	24.1	4.5	0.3	0.5	1.7	2.1

TABLE 9-14. Personal Income by Major Sources, Richland-Kennewick-Pasco Standard Metropolitan Statistical Area 1972-1977.^a (Sheet 2 of 2)

Total labor and proprietors income by place of work ^b	Annual income in thousands of dollars		Average annual income change over period (%)		Richland-Kennewick-Pasco area as % of state income		Income category as % of total earnings	
	1972 ^c	1977 ^d	1972-1976	1976-1977	1972	1977	1972	1977
Transportation and public utilities	19,810	37,843	11.4	19.1	2.2	2.6	5.8	4.9
Wholesale trade	8,752	23,036	21.2	12.0	1.2	1.6	2.6	3.0
Retail trade	34,252	66,027	12.3	16.5	2.5	2.9	10.0	8.5
Finance, insurance, and real estate	8,089	17,010	11.5	28.3	1.3	1.6	2.4	2.2
Services	87,332	201,826	15.7	20.9	5.1	6.1	25.5	26.1
Government and government enterprises	48,399	84,409	11.7	8.8	1.8	2.0	14.1	10.9
Federal, civilian	10,699	18,629	12.1	7.2	1.7	2.8	3.1	2.4
Federal, military	1,944	2,540	5.6	4.5	0.5	0.5	0.6	0.3
State and local	35,756	63,240	11.9	9.5	2.2	2.4	10.4	8.2

^aState of Washington (1979b).

^bConsists of wage and salary disbursements, other labor income, and proprietors income.

^cEstimates based on 1967 Standard Industry Code.

^dEstimates based on 1972 Standard Industry Code.

^eIncludes the capital consumption adjustment for nonfarm proprietors.

^fIncludes wage and salaries of United States residents working for international organizations.

to strengthen and diversify the area's economy. Continued growth in the local economy will be dependent on federal support for research and waste management programs and utility company construction of nuclear power plants at the Hanford Site. In the past year, decline in support for some energy programs at Hanford, and construction cutbacks at the Washington Public Power Supply System, Inc., have led to extensive job losses in the area.

Employment in the bicounty area has been estimated at 72,940 for the spring of 1981, compared with 1,755,800 for the state (Table 9-15). The unemployment rate for the two counties increased slightly from 6.4 percent of the labor force in May 1980 to an estimated 6.7 percent in May 1981, slightly lower than the state average. The unemployment rate for August 1982 was 15.3 percent.

TABLE 9-15. Resident Labor Force and Employment,
Washington State and Benton-Franklin Counties.^a

Employment	Benton-Franklin Counties	State total
May 1980 Preliminary ^b		
Labor force	78,200	1,920,300
Employment	72,940	1,755,800
Unemployment	5,260	164,500
Unemployment rate %	6.7	8.6
May 1980 Revised		
Labor force	75,810	1,926,600
Employment	70,950	1,789,900
Unemployment	4,860	136,700
Unemployment rate (%)	6.4	7.1

^aState of Washington (1981b).

^bEstimates for the state labor market areas are not strictly comparable with those for prior years because the methodology used to develop current year estimates differs from that used in developing final prior year estimates.

The major occupational categories for workers in 1976 are illustrated and projected to 1985 in Table 9-16. These figures were calculated assuming the greatest proportional growth in clerical and service workers, reflecting the strength of secondary employment effects induced by the primary energy developments that had taken place and were projected for the next decade. As a proportion of all occupations, white-collar service positions were expected to increase relatively more than blue collar and farm workers. Farm employment is expected to remain unchanged over the next 5 years, largely because industrial development is competing with farming for scarce land and resources. Because of recent cutbacks in the Washington Public Power Supply System, Inc. and in Hanford energy programs these figures need to be reassessed.

Per capita income data for the primary impact area in 1978 are as follows:

Standard Metropolitan Statistical Area
(State of Washington, 1980).

Tri-Cities	- \$8,789
Benton County	- \$8,989
Franklin County	- \$8,168

Available 1979 per capita income data for the Tri-Cities Standard Metropolitan Statistical Area show an increase to \$9,705 (DOC, 1981).

As indicated in Table 9-17, total housing stock grew significantly between May 1975 and May 1980. Mobile homes and apartment units experienced particularly expansive growth. In terms of total units, Kennewick has experienced the greatest growth, with almost 44 percent of the current housing stock having been added since May 1975. The corresponding percentages for Richland and Pasco are 29.0 and 30.6 percent, respectively.

Corresponding with the general growth in size of the housing stock, prices have increased dramatically, with real estate sales totaling almost \$400 million in 1978 for Benton and Franklin Counties combined. According to these figures, the average real estate transaction in 1965 was \$10,866, while in 1978 the average amount had increased to \$38,551 (Table 9-18).

Most unsold housing in the Tri-Cities area in 1978 and 1979 had sales prices in excess of \$40,000 (Table 9-19). In early 1981, 14 percent of unsold new housing was priced below \$55,000 as was 26 percent of unsold previously occupied dwellings. Data on Table 9-19 also indicate that there are fewer new homes under construction and on the market than previously occupied homes, a reflection of the tightening of the housing market and the steep increase in construction costs.

TABLE 9-16. Richland-Kennewick-Pasco Standard Metropolitan Statistical Area Employment and Average Annual Worker Needs by Occupational Group, 1976-1985.*

Occupations	Employment 1976	Employment 1985	Change (%) 1976-1985	Average annual worker needs 1976-1985		
				Total openings	Openings due to growth	Openings due to replacement
Total listed occupations	49,050	71,800	46.4	4,430	2,520	1,910
White collar workers	23,939	36,500	52.5	2,300	1,390	910
Professional, technical, kindred	8,962	13,100	46.2	720	460	260
Managers and officials	5,498	8,200	49.1	540	300	240
Sales workers	2,605	3,900	49.7	260	140	120
Clerical workers	6,874	11,300	64.4	780	490	290
Blue collar workers	14,904	21,500	44.3	1,740	1,030	710
Craft and kindred workers	7,395	11,100	50.1	670	410	260
Operatives	5,045	7,000	38.8	360	220	140
Laborers, except farm	2,464	3,400	38.0	710	400	310
Service workers	5,703	9,300	63.1	170	100	70
Farmers and farm workers	4,504	4,500	-0.1	220	5	220

*State of Washington (1979c), Table 6.

TABLE 9-17. Tri-Cities Total Housing Stock (in units).^a

Area	Total units	Single-family residences	Mobile homes	Apartment units ^b
Area Total				
May 1975	30,465	24,751	2,271	3,443
May 1976	34,253	26,347	2,685	5,221
Nov. 1977	39,328	26,056	3,820	9,452
Dec. 1978	43,386	27,781	4,893	10,712
Oct. 1979	46,027	28,467	5,223	12,337
May 1980	47,598	29,660	5,729	12,209
Kennewick				
May 1975	11,807	9,473	966	1,368
May 1976	13,663	9,812	1,398	2,453
Nov. 1977	16,267	10,804	1,805	3,658
Dec. 1978	18,642	11,567	2,405	4,670
Oct. 1979	20,008	12,054	2,362	5,592
May 1980	21,059	12,699	2,736	5,624
Richland				
May 1975	10,969	9,301	517	1,151
May 1976	11,835	10,370	96	1,369
Nov. 1977	13,561	9,054	712	3,795
Dec. 1978	14,636	9,523	883	4,230
Oct. 1979	15,139	9,727	1,072	4,340
May 1980	15,458	10,156	933	4,369
Pasco				
May 1975	7,689	5,977	788	924
May 1976	8,755	6,165	1,191	1,399
Nov. 1977	9,500	6,198	1,303	1,999
Dec. 1978	10,108	6,691	1,605	1,812
Oct. 1979	10,880	6,686	1,789	2,405
May 1980	11,081	6,805	2,060	2,216

^aRRERC (1981).^bIncludes condominium units.

TABLE 9-18. Benton and Franklin Counties Real Estate Sales.^a

Year	Total		Benton County		Franklin County	
	Number	Amount ^b	Number	Amount ^b	Number	Amount ^b
1960	--	--	NA	NA	633	6,467
1965	3,260	35,424	2,100	24,606	1,160	10,818
1970	3,838	42,972	2,672	29,260	1,166	13,712
1975	6,967	160,054	5,215	121,096	1,752	38,958
1976	7,460	210,773	5,338	163,423	2,122	47,350
1977	8,241	260,781	6,282	211,704	1,959	49,077
1978	9,779	376,994	7,510	308,685	2,269	68,309

^aRERC (1979) p. 16.

^bIn thousands of dollars.

TABLE 9-19. Unsold Housing Inventory by Price Range for Tri-Cities Area, 1978 and 1979.*

Year	Total units	Sales price				
		Under \$40,000	\$40,000 to 49,999	\$50,000 to 59,999	\$60,000 to 74,999	Over \$75,000
Completed New Homes						
1978	472	2	49	76	229	116
1979	712	8	19	44	415	226
Under Construction						
1978	346	4	34	69	130	107
1979	501	59	21	34	219	168
Previously Occupied Homes						
1978	697	144	214	126	112	101
1979	1,032	101	166	184	345	236

*RERC (1979) pp. 22-24.

The growth, development, and increasing complexity of the Tri-Cities area has put ever-increasing demands on local government revenues. All three cities are experiencing budget constraints and are implementing austerity programs to cope with revenue constrictions. Economic development plans, tax base diversification, and increased sales tax dollars are only a few of the solutions being promoted to keep pace with increasing costs. The 1981 estimated revenues and budgeted expenditures for Kennewick, Richland, and Pasco are summarized in Table 9-20.

TABLE 9-20. Local Government Revenues and Expenditures. (Sheet 1 of 3)

City of Kennewick--1981 Estimated Revenues and Budgeted Expenditures ^a	
Revenues	
Cash	\$ 5,226,513
Charges for services	1,910,063
State and federal shared revenue	1,710,467
Taxes	5,377,500
Interest income	661,800
Licenses and permits	405,650
Miscellaneous	498,550
Utilities	3,560,000
State and federal grants	1,098,844
Interfund transfers	1,253,570
Net revenues	<u>\$21,702,957</u>
Expenditures	
Personal services	\$ 6,771,428
Capital outlay	4,409,318
Debt service	2,231,532
Reserves	1,842,845
Suppliers	757,165
Other services and charges	4,437,099
Interfund transfers	1,253,570
Net expenditures	<u>\$21,702,957</u>

TABLE 9-20. Local Government Revenues
and Expenditures. (Sheet 2 of 3)

City of Richland--1981 Estimated Revenues and Budgeted Expenditures ^b	
Beginning fund balance	\$ 2,876,510
Revenue	
General property tax	1,536,167
Retail sales and use tax	800,000
Other taxes	2,006,999
Licenses and permits	316,400
Charges and services	418,300
Fines and forfeitures	132,953
Intergovernmental revenue	3,247,665
Miscellaneous revenue	360,301
Nonrevenue receipts	24,000
Total revenue	<u>\$11,719,295</u>
Transfers from general fund	610,939
Net revenue	<u>\$12,330,234</u>
Expenditures	
Personal services	\$ 6,964,908
Supplies	359,190
Charges and services	1,956,457
Capital outlay	151,506
Debt service and reserves	83,622
Ending fund balance	2,203,612
Transfer from general fund	610,939
Net expenditures	<u>\$12,330,234</u>

TABLE 9-20. Local Government Revenues
and Expenditures. (Sheet 3 of 3)

City of Pasco--1981 Estimated Revenues and Budgeted Expenditures ^c	
Revenues	
Taxes	\$ 2,819,300
Licenses and permits	197,180
Grants	414,930
State shared revenue	693,360
Charges for services	1,518,000
Fines and forfeitures	137,500
Federal shared revenue	328,400
Miscellaneous	978,950
Resources forward	373,520
Intra-government service funds	1,011,740
Project funds	2,276,820
Trust funds	657,600
Net revenue	<u>\$11,407,300</u>
Expenditures	
General fund	\$ 4,424,540
City street	532,570
Arterial street	15,000
Cooperative Education and Training Act	115,580
Neighborhood facility	17,900
Cemetery	73,480
Boat basin	11,270
Debt service - government bonds	300,370
Golf	187,200
Water/sewer	1,508,370
Debt service - revenue bonds	274,860
Equipment rental	583,900
Administrative service	427,840
Washington Public Power Supply	95,500
Stadium/convention center	10,350
Golf Course Redevelopment	1,132,970
Intercity bridge	38,000
Old bridge demolition	1,000,000
Demolition and repair	1,200
Federal revenue sharing	328,400
Firemen's pension	40,000
Community development block grant fund	288,000
Net expenditures	<u>\$11,407,300</u>

^aCity of Kennewick (1981).

^bCity of Richland (1981).

^cCity of Pasco (1981).

9.3.3 Service Facilities

9.3.3.1 Police and Fire Prevention. Police and fire protection facilities in Richland, Pasco, and Kennewick in 1978 are summarized in Tables 9-21 and 9-22, respectively.

TABLE 9-21. Police Protection in 1978.

City	Personnel	Officers per 100 residents	Equipment
Pasco ^a	38	2.4	8 patrol radio cars
Richland ^b	51	1.6	13 sedans, 1 jeep, boat
Kennewick ^c	35	1.3	10 autos, 2 radar units

^aState of Washington (1976).

^bState of Washington (1977a).

^cState of Washington (1977b).

TABLE 9-22. Fire Protection in 1978.

City	Personnel	Equipment
Pasco ^a	26	4 pump trucks, 1 rescue truck, 2 ambulances, ladder truck
Richland ^b	38	2 pumpers, 1 aerial pumper, salvage hose truck, 2 ambulances (1 in reserve), 3 staff cars, 1 pick-up tanker truck
Kennewick ^c	30 full-time 14 volunteer	5 pumpers, 3 cruisers 2 ambulances, 1 rescue truck

^aState of Washington (1977b).

^bState of Washington (1976).

^cState of Washington (1977a).

9.3.3.2 Education. In 1978 there were over 26,000 students enrolled in the six school districts of the immediate Tri-Cities area (Table 9-23). The educational services available in Benton and Franklin Counties are listed in Table 9-24. In addition to these, the area is also served by a 2-year community college in Pasco and a Joint Center for Graduate Study in Richland sponsored by several universities. Other 4-year degree programs are available through extension programs offered by Central Washington University and Eastern Washington University.

The teacher-to-student ratio of elementary through high school education is approximately 1 to 23 in Pasco, 1 to 21 in Kennewick, and 1 to 22 in Richland. The districts are experiencing fewer facility strains than they did in the mid-1970s, although some have used portable classrooms to accommodate temporary expansion needs. In the past 3 years, the area has seen the construction of two new high schools, four new elementary schools, and the expansion of existing buildings to add classrooms.

TABLE 9-23. School Enrollment in Tri-Cities Districts, May 1975 and May 1978.*

School district	May 1975	May 1978	Change (%)
Columbia	473	767	62.2
Finley	579	724	25.0
Kennewick	7,831	9,500	21.3
Kiona-Benton	745	1,030	38.3
Pasco	5,034	5,371	6.7
Richland	7,870	8,470	11.9

*CDS (1979)

TABLE 9-24. Educational Services in Benton and Franklin Counties, Fall 1979.*

Type	Number
School districts (public)	12
Preschool/day care	30
Private schools	9
Developmental/special needs	3
Community/continuing education	7
Vocational schools	8

*Benton-Franklin (1979).

9.3.3.3 Medical Facilities. Four hospitals currently serve the Tri-Cities region. Statistics on the number of licensed hospital beds, their percent occupancy, and the ratio of beds to city residents are presented in Table 9-25. Currently available hospital facilities are considered sufficient to meet projected needs through 1985 (Arthur Young and Co., 1977).

There are seven nursing homes in the area, with 411 available beds. These beds are also used by the developmentally disabled and other populations requiring custodial care, but the practice is being discouraged. The Benton-Franklin County Public Health Department is staffed by one doctor and 16 nurses in two health centers.

The Mid-Columbia Mental Health Center is the major provider of mental health services in the Tri-Cities area and currently provides direct service to 3 percent of the population. At present, there is approximately one practicing psychiatrist or psychologist for each 10,000 residents. Services include both in-patient and out-patient programs and treatment for drugs and other special problems, including crisis intervention, family-planning programs, and some services for the developmentally disabled. Maximum in-patient capacity for the center will be reached with a population of 140,000. Out-patient services are more flexible and are influenced primarily by revenue availability and demand for services.

9.3.3.4 Parks and Recreation. There are 67 federal-, state-, county-, and city-maintained park facilities totaling almost 5,000 hectares in the Tri-Cities area. Most of the federal, state, and county parks are located on the Columbia and Snake Rivers, providing camping, boating, swimming, and picnic facilities. City-managed parks generally provide facilities for outdoor sports activities.

Both fishing and hunting are important outdoor recreational activities in the area. Other recreational activities include sailing, water-skiing, flying, boating, bicycling, parachuting, and hang gliding.

9.3.3.5 Water and Sewer Services. Existing water and sewer services in 1978 are summarized in Tables 9-26 and 9-27 for the Tri-Cities. None of the peak demands have exceeded the capacities, but in several cases the figures have been very close. In Richland and Kennewick, for example, peak demand for water in 1978 was only 2×10^3 cubic meters per day (0.5 million gallons per day) less than the pumping capacities of the systems. According to the Franklin County Comprehensive Plan, low-pressure problems are currently experienced in Pasco during peak demand, although capacity is projected to be adequate until 1985 (Franklin County Planning Commission, 1979). Filtration capacity will be a limiting factor to adequate delivery of peak water demands. Service in east Pasco is also limited by the need for additional distribution mains and storage facilities. In Kennewick, a \$6.3-million water-filtration plant will soon be under construction, supplementing the city's water supply with Columbia River water.

TABLE 9-25. Percent Occupancy for Setup and Licensed Beds for the Tri-Cities Area Hospitals, 1972, 1976, and 1978.^{a,b}

Hospital	Licensed beds ^c		Total setup beds					
	Number of beds	Occupancy (%)	Number of beds		Occupancy (%)		Beds per 1,000 residents	
	1978	1978	1972	1978	1972 (approx.)	1976	1978	1976
Kadlec	136	67.6	135	135	63	68	68.1	4.50
Kennewick General	61	58.2	60	60	55	59	59.2	2.82
Our Lady of Lourdes	80	58.1	80	81	69	67	57.4	5.47
Prosser Memorial ^d	59	10.4	45	41	49	--	15.1	--

^aArthur Young and Co.(1977).

^bCDS (1976).

^cLicensed beds are the number authorized through licensing or certificate of need, but may not necessarily physically exist.

^dFigures for 1978 do not include nursing home beds.

TABLE 9-26. Water Resources, Benton and Franklin Counties, 1970 and 1978.

Resource	Franklin County			Benton County	
	Pasco ^a	West Pasco	Connell	Richland ^b	Kennewick ^c
Water source 1970	Columbia River	Wells	Wells	Wells and Columbia River	Columbia River
1978	Columbia River, treated by filtration	2 storage tanks, well water	Well water	Wells and Columbia River	Columbia River
Pumping capacity 1970			Maximum 0.54 m ³ /s (3.5 Mgal/d) reservoir capacity 1.14 x 10 ⁴ m ³ (3 x 10 ⁶ gal)		
1978	2.76 m ³ /s (18+ Mgal/d)			5.44 m ³ /s (35.5 Mgal/d)	2.07 m ³ /s (13.5 Mgal/d)
Average demand 1978	0.84 m ³ /s (5.5 Mgal/d)			2.3 m ³ /s (15 Mgal/d)	0.9 m ³ /s (6 Mgal/d)
Peak demand 1978	2.35 m ³ /s (15.3 Mgal/d)			5.37 m ³ /s (35 Mgal/d)	1.99 m ³ /s (13 Mgal/d)
Planned expansion	New reservoir to be built				

^aState of Washington (1976).^bState of Washington (1977a).^cState of Washington (1977b).

TABLE 9-27. Sewer Systems and Storm Water,
Benton and Franklin Counties, 1978.

Sewer system	Franklin County	Benton County	
	Pasco	Richland	Kennewick
Design capacity	0.18 m ³ /s (4.2 Mgal/d) 114 m ³ /d (30,000 gal/d) (for storm water system)	0.26 m ³ /s (6 Mgal/d) (secondary treatment)	0.38 m ³ /s (8.7 Mgal/d) (secondary treatment)
Average demand	0.09 m ³ /s (2 Mgal/d)	0.22 m ³ /s (5 Mgal/d)	0.22 m ³ /s (5 Mgal/d)
Peak demand	Not available	0.24 m ³ /s (5.5 Mgal/d)	0.28 m ³ /s (6.5 Mgal/d)

In Richland and Pasco, the peak demands on the sewage systems have been approaching each system's capacity. However, Pasco's storm water system is reported to be adequate until 1990. In Kennewick, the city has completed a new \$2.1-million sewer main to serve the Columbia Center area.

Existing sewage-treatment facilities in Richland are 30 years old and are not expected to last more than five additional years, despite recent pump modifications. Severe odor problems plague the existing facilities. A new sewage treatment plant, expected to be on line in 1987, is in the final design phase. The present system serves a population of approximately 33,000 while the new system is sized for 65,000 residents.

9.3.3.6 Solid Waste. The incorporated areas of West Richland, Prosser, Kennewick, and Benton City, and the unincorporated portions of Benton County contract with private carriers to handle collection and disposal of solid waste. The city of Richland is the only jurisdiction in the bicounty area which operates its own garbage collection and disposal as a municipal utility. The Richland landfill site is located near the western city limits adjacent to Route 240. Franklin County is served by a private carrier which maintains a landfill site northeast of Pasco. This site also serves portions of Benton County.

9.3.3.7 Transportation. In the Tri-Cities, traffic problems are recognized as one of the major consequences of the rapid growth in the area. Heavy rush-hour traffic flows are particularly evident between cities. Because of the topography of the area, there are inevitable bottlenecks created by bridges, by the elongated nature of the settlement pattern, and by the location of the Hanford Site in relation to the population center. Some of this congestion will be alleviated by the construction of the Interstate-82 bridge.

A public transportation system was put into service in May 1982. This system serves the Tri-Cities and surrounding area. Also, the DOE (through Rockwell Hanford Operations) operates a shuttle bus system from Richland to the Hanford Site.

Transportation facilities in the area are shown in Table 9-28. See Section 9.2.1.11 for further detail.

9.3.4 Government and Institutional Organizations

Major local government agencies in the primary impact area include Benton and Franklin Counties and the cities of Richland, Kennewick, Pasco, West Richland, and Benton City. Some of the major functions of these government agencies are listed in Table 9-29. The combined Tri-Cities (together with the remainder of Benton and Franklin Counties) have been designated a Standard Metropolitan Statistical Area by the Bureau of the Census.

The three cities, nevertheless, guard their independence and autonomy. There are three police departments, three fire departments, three hospitals, and three ports. The residents of one community generally see their own place of residence as being quite distinct from the other two cities.

TABLE 9-28. Transportation Facilities.

Area	Rail	Truck	Air	Water	Bus	Regional roadways
Franklin County						
Pasco ^a	Burlington Northern, Union Pacific	Served by major lines and several independents	Tri-Cities Regional Airport	Barge service between Pasco and lower Columbia River	Greyhound	Routes 12, 395, I-82, I-182 (to be completed)
Benton County						
Richland ^b	Burlington Northern, Union Pacific	Served by major lines	Richland Airport (private and commuter flights)	Barge traffic on Columbia River	Greyhound	Routes 12, 240
Kennewick ^c	Burlington Northern, Union Pacific	Served by major lines	Kennewick Airport (private and business planes)	Barge traffic on Columbia River	Greyhound	Routes 12, ways 14, I-82

^aState of Washington (1976).^bState of Washington (1977a).^cState of Washington (1977b).

**TABLE 9-29. Local Government Functions in the
Primary Impact Area. (Sheet 1 of 2)**

Benton County	
Assessor	Mosquito Control District
Auditor	Parks and Recreation
Building and Fire Prevention	Planning Department
Cooperative Extension Agent	Prosecuting Attorney
County Engineer	Road Department
District Courts	Rural Fire Protection
Emergency Services	Sheriff's Department
Health Department	Superior Court
Horticultural Inspection	Treasurer
Juvenile Department	
Franklin County	
Assessor	Fire Marshall
Auditor	Golf Course
Building Inspector	Health Department
Cooperative Extension	Juvenile Department
Coroner	Planning Department
District Court	Prosecutor
Emergency Services	Sheriff's Department
Engineering	Superior Court
City of Richland	
Ambulance	Policy
Fire Department	Recreation
Landfill	Senior Citizen's Center
Library	Utilities

TABLE 9-29. Local Government Functions in the
Primary Impact Area. (Sheet 2 of 2)

City of Kennewick	
Ambulance	Parks and Recreation
Fire Department	Police Department
Library	Senior Citizen's Center
City of Pasco	
Building Inspection	Library
Community Development	Parks and Recreation
Engineering	Planning Department
Fire Department	Police Department
Golf Course	Public Works
West Richland	
Fire Department	Maintenance Department
Golf Course	Police Department
Library	
Benton City	
Ambulance	Police Department
Fire Department	

9.4 SUMMARY OF UNRESOLVED ISSUES

The previous sections have presented the ecologic, socioeconomic, and land-use information which is currently available. Further socioeconomic studies will be conducted when a definition of the size of the proposed repository and associated work force is available. Also, baseline ecological and radiological conditions at the reference repository location will be determined. Based on these determinations, the impacts of the construction, operation, and decommissioning of a repository on the environment will be assessed. The plans addressing this ongoing work are discussed in Section 13.3.2. No items within this chapter are considered to be unresolved.

9.5 REFERENCES

Allen, H. L., 1979, An Inventory of Bald Eagle Habitat on BLM Land in Washington, Washington State Department of Game, Olympia, Washington.

Arthur Young and Co., 1977, Tri-Cities Joint Hospital Planning Project, Final Report, Portland, Oregon, September 1977.

Benton-Franklin, 1979, Educational Services Directory for Benton-Franklin Counties, Benton-Franklin Governmental Conference, Richland, Washington, Fall 1979.

BOC, 1981, 1980 Census of Population and Housing, Washington, PHC80-V-49, Advance Reports, Bureau of the Census, U.S. Department of Commerce, Washington, D.C., March 1981.

BLM, 1956, "Department of Interior, Bureau of Land Management, Public Land Order 1273," Federal Register, Vol. 21, p. 1719.

CDS, 1976, Socioeconomic Impact Study, WNP 1 & 4, Vol. 1: First Progress Report, 4 Volumes, Community Development Services, Inc. Seattle, Washington, for Washington Public Power Supply System, Inc., Richland, Washington, October 1976.

CDS, 1979, Socioeconomic Impact Study, WNP 1 & 4, Final Report, Community Development Services, Inc. Seattle, Washington, for Washington Public Power Supply System, Inc., Richland, Washington, May 1979.

CEQ, 1978, Regulations for Implementing the Procedural Provisions of the National Environmental Policy Act, Title 40, Code of Federal Regulations, Parts 15-1508/Council on Environmental Quality, Washington, D.C.; also in Federal Register, Vol. 43, pp. 55978.

City of Kennewick, 1981, Budget 1981, Kennewick, Washington.

City of Pasco, 1981, Budget 1981, Pasco Washington.

City of Richland, 1981, Budget 1981, Richland, Washington.

Daubenmire, R., 1970, Steppe Vegetation of Washington, Technical Bulletin 62, Washington State Agricultural Experiment Station, Pullman, Washington.

DOC, 1981, Newsletter, Bureau of Economic Analysis, U.S. Department of Commerce, May 20, 1981.

DOE, 1982a, Public Draft, National Plan for Siting High-Level Radioactive Waste Repositories and Environmental Assessment, DOE/NWTS-4, DOE/EA-151, National Waste Terminal Storage Program, U.S. Department of Energy, Washington, D.C., February 1982.

DOE, 1982b, Environmental Assessment for the Basalt Waste Isolation Project Exploratory Shaft Construction, DOE/EA-0188, U.S. Department of Energy, Washington, D.C., August 13, 1982.

DOE, 1982c, "Department of Energy, Finding of No Significant Impact and Notice of Availability of Environmental Assessment for the Conduct of Detailed Site Through the Construction of an Exploratory Shaft on the Hanford Site," Federal Register, Vol. 47, No. 180, pp. 40820-40821.

ERDA, 1975, Final Environmental Statement - Waste Management Operations, Hanford Reservation, Richland, Washington, ERDA-1538, 2 Volumes, U.S. Energy Research and Development Administration, Washington, D.C., December 1975.

Fitzner, R. E., Rickard, W. H., Cadwell, L. L., and Rogers, L. E., 1980, Raptors of the Hanford Site, PNL-3212, Pacific Northwest Laboratory, Richland, Washington.

Franklin County Planning Commission, 1979, Comprehensive Plan, Franklin County, Washington, Final Draft, Franklin County Planning Commission, Pasco, Washington, August 1979.

FWS, 1980a, "Endangered and Threatened Wildlife and Plants: Review of Plant Taxa for Listing an Endangered or Threatened Species, U.S. Fish and Wildlife Service," Federal Register, Vol. 45, No.242, pp. 82480-82569.

FWS, 1980b, "Endangered and Threatened Wildlife, U.S. Fish and Wildlife Service," Federal Register, Vol. 45, No. 99, pp. 33768-33781.

Houston, J. R. and Blumer, P. J., 1978, Environmental Surveillance at Hanford for CY-1977, PNL-2614, Pacific Northwest Laboratory, Richland, Washington.

Landeen, D. and Mitchell, R. M., 1981, Intrusion of Radioactive Waste Burial Sites by the Great Basin Pocket Mouse (Perognathus parvus), RHO-SA-211, Rockwell Hanford Operations, Richland, Washington.

Miller, M. L., Fix, J. J., and Bramson, P. E., 1977, Radiochemical Analyses of Soil and Vegetation Samples Taken From the Hanford Environs, 1971-1976, BNWL-2249, Battelle, Pacific Northwest Laboratories, Richland, Washington.

NPS, 1980, "National Registry of Natural Landmarks, U.S. National Park Service," Federal Register, Vol. 45, No.232, p. 79721.

O'Farrell, T. P., Fitzner, R. E., and Gilbert, R. D., 1973, Distribution of Radioactive Jackrabbit Pellets in the Vicinity of the B-C Cribs, 200 East Area, USAEC, Hanford Reservation, BNWL-1794, Battelle, Pacific Northwest Laboratories, Richland, Washington.

Paine, D., Price, K. R., and Mitchell, R. M., 1979, Evaluation of a Decommissioned Radwaste Pond, RHO-SA-99, Rockwell Hanford Operations, Richland, Washington.

RERC, 1979, Tri-Cities Real Estate Research Report, Tri-Cities Real Estate Research Committee, Kennewick, Washington, Autumn 1979.

RERC, 1981, Tri-Cities Real Estate Research Report, Tri-Cities Real Estate Research Committee, Kennewick, Washington, Spring 1981, p. 28.

Rice, D. G., 1968a, Archaeological Reconnaissance-Ben Franklin Reservoir Area, 1968, Laboratory of Anthropology, Washington State University, Pullman, Washington.

Rice, D. G., 1968b, Archaeological Reconnaissance-Hanford Atomic Works, Washington State University, Pullman, Washington.

Rogers, L. E. and Rickard, W. H., 1977, Ecology of the 200 Area Plateau Waste Management Environs: A Status Report: PNL-2253, Pacific Northwest Laboratory, Richland, Washington.

State of Washington, 1976, A Standard Community Industrial Survey: Pasco, Washington, Washington State Department of Commerce and Economic Development, Olympia, Washington, March 1976.

State of Washington, 1977a, corrected copy, A Standard Community Industrial Survey: Richland, Washington, Washington State Department of Commerce and Economic Development, Olympia, Washington.

State of Washington, 1977b, A Standard Community Industrial Survey: Kennewick Washington, Washington State Department of Commerce and Economic Development, Olympia, Washington, March 1977.

State of Washington, 1978, Washington State County Population Forecasts by Age and Sex: 1970-2005, Population, Enrollment, and Economic Studies Division, Washington State Office of Financial Management, Olympia, Washington, June 1978.

State of Washington, 1979a, State of Washington Population Trends, 1979, Population, Enrollment, and Economic Studies Division, Washington State Office of Financial Management, Olympia, Washington, August 1979.

State of Washington, 1979b, Revised Personal Income Estimates for Washington State: State, County, and SMSA Data, 1969-1977, Division of Research and Information, Washington State Department of Revenue, Olympia, Washington, May 1979.

State of Washington, 1979c, Annual Planning Report: Richland-Pasco-Kennewick SMSA, Research and Statistics Branch, Washington State Employment Security Department, Olympia, Washington, July 1979.

State of Washington, 1980, Revised Personal Income Estimates for Washington State-State, County and SMSA Data 1959-1978, Washington State Department of Revenue, Olympia, Washington, June 1980.

State of Washington, 1981a, Forecasts of the State and County Populations by Age and Sex: 1985-2000, With Estimates for 1980, Special Report No. 36, Forecasting and Support Division, Washington State Office of Financial Management, Olympia, Washington, May 1981.

State of Washington, 1981b, Labor Area Summary: Washington State, Research and Statistics Branch, Washington State Employment Security Department, Olympia, Washington, June 29, 1981.

State of Washington, 1981c, Washington State Register of Historic Places, Washington State Office of Archaeology and Historic Preservation, Olympia, Washington.

Stephan, J., Foote, H., and Coburn, V., 1979, Well Location and Land-Use Mapping in the Columbia Plateau Area, RHO-BWI-C-61/PNL-3295, Pacific Northwest Laboratory for Rockwell Hanford Operations, Richland, Washington.

WCC, 1975, Socioeconomic Study: WPPSS Nuclear Projects 1 and 4 and Supplement, Woodward-Clyde Consultants, San Francisco, California, for Washington Public Power Supply System, Inc., Richland, Washington, April 1975.

Wheeler, R. E. and Law, A. G., 1980, Rockwell Hanford Operations Environmental Surveillance Report for Calendar Year 1979, RHO-LD-132, Rockwell Hanford Operations, Richland, Washington.

Wukelic, G. E., Foote, H. P., Blair, S. C., and Begej, C. D., 1981, Monitoring Land and Water-Use Dynamics in the Columbia Plateau Using Remote-Sensing Computer Analysis and Integration Techniques, RHO-BW-CR-122 P/PNL-4047, Pacific Northwest Laboratory for Rockwell Hanford Operations, Richland, Washington, September 1981.

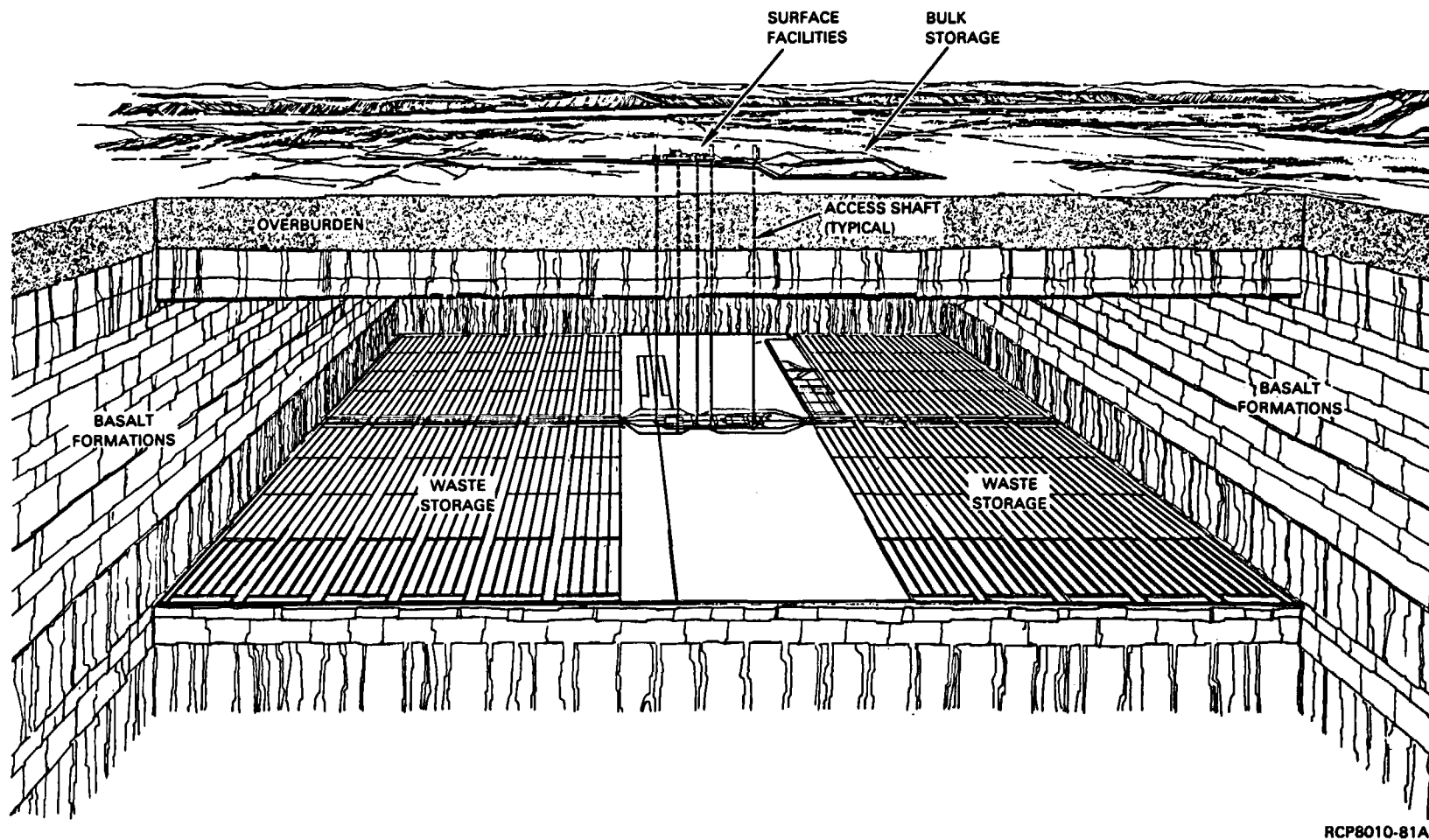
10. REPOSITORY DESIGN

A nuclear waste repository in basalt can handle and isolate commercial high-level waste, commercial spent fuel (if declared as waste), and commercial low-level transuranic waste, and can also accommodate defense high-level waste. The design description presented in this chapter is based on completed design studies (KE/PB, 1982) and the conceptual design (currently in design review). Figure 10-1 shows a repository cutaway that represents the conceptual design, including surface facilities, five access shafts, a central shaft pillar, and underground waste storage areas.

The reference stratigraphy used in the conceptual design is that which underlies the Hanford Site, as discussed in Chapter 3. There are currently two candidate repository horizons (basalt flows) being considered for the nuclear waste repository in basalt: the Umtanum flow and the middle Sentinel Bluffs flow. The Umtanum flow is the uppermost flow in the Schwana sequence at a depth of approximately 1,100 meters (3,700 feet) to the flow top and is estimated to be 70 meters (230 feet) thick, with an interior thickness of about 25 meters (82 feet). The middle Sentinel Bluffs flow, located some 190 meters (620 feet) higher, is estimated to be 80 meters (260 feet) thick with an interior thickness of about 78 meters (255 feet). The horizontal-to-vertical stress ratio of 2:1 is considered representative of both flows. In the conceptual design, the deeper and more widely investigated Umtanum flow has been used as a reference repository horizon, and data obtained from this flow have been used for design calculations. Using the deeper of the candidate flows as the reference horizon resulted in a conservative design; i.e., a comparable repository located in an upper horizon is expected to provide cost reduction, schedule improvement, and less technologic risk.

This chapter emphasizes repository isolation and constructibility considerations of the conceptual design and is organized as follows:

- Section 10.1 identifies the conceptual design bases regarding the waste receipts and the site.
- Section 10.2 addresses repository systems such as surface facilities, waste handling systems, and service systems.
- Section 10.3 provides a design description of the five access shafts shown in the conceptual design.
- Section 10.4 provides a design description of the subsurface facilities, including the waste storage panel, placement rooms, and storage holes.
- Section 10.5 defines the rock-mass parameters and resulting stresses and temperatures used in the conceptual design.



RCP8010-81A

FIGURE 10-1. Repository Cutaway.

- Section 10.6 describes the construction techniques proposed for the access shafts and subsurface facilities.
- Section 10.7 provides a design description of the proposed repository backfill procedure.
- Section 10.8 identifies the sealing system for shafts, boreholes, and underground openings.

Many of the conceptual design approaches discussed will require in-depth trade-off studies before an optimum design can be established. These trade-off studies will consider alternate methods for construction, waste package storage, engineered barriers, repository operation, retrieval option, and final decommissioning, and will be evaluated from a total systems standpoint prior to the selection of a final design for a nuclear waste repository in basalt.

10.1 CONCEPTUAL DESIGN BASES

Functional design criteria governing the conceptual design are contained in BWIP and KE/PB (1982).

10.1.1 Functions and General Criteria

The function of the repository is to provide long-term containment and isolation following a waste retrievability period of up to 50 years. The retrievability period provides a span of time when repository performance can be confirmed and ensures that the option to retrieve the waste is preserved in accordance with the U.S. Nuclear Regulatory Commission proposed technical criteria (NRC, 1981). Repository operating functions include receiving precontainerized nuclear waste, inspecting and preparing the containerized waste for underground storage, developing subsurface storage facilities, transporting and storing the nuclear waste in the underground storage facility, monitoring the nuclear waste during the 50-year retrievability period, and subsequently sealing the repository. Nuclear waste forms considered in the conceptual design for disposal are discussed in Chapter 11 and include the following:

- Canisters containing reprocessed commercial high-level waste
- Canisters containing fuel rods from disassembled spent fuel assemblies from commercial boiling water reactors and pressurized water reactors
- Drums of solidified commercial low-level transuranic waste.

Both commercial high-level waste and spent fuel are assumed to have been removed from the reactor core a minimum of 10 years before shipment to the repository. The design basis receiving and emplacement period is 20 years and is on a 50/50 split (metric tons of heavy metal basis) between commercial high-level waste and spent fuel as shown in Table 10-1.

The design basis receipt rate for commercial low-level transuranic waste is 1,600 contact-handled drums (nominally 208 liters (55 gallons)) per year for 20 years, for a total of 32,000 drums.

A system of multiple barriers, natural and man-made (engineered), shall be provided to protect the biosphere from unacceptable radiologic effects of stored nuclear waste. The natural barriers will be provided by the geologic formation in which the repository is constructed. The following engineered barriers shall be provided:

- Waste form
- Waste package
- Storage room backfill
- Access and shaft seals.

TABLE 10-1. Conceptual Design Basis Waste Receipts.

	BWR	PWR	BWR+PWR	CHLW	Total
Metric tons of heavy metal/canister	1.32	1.38	--	2.28*	--
Decay heat (kW)/canister	1.33	1.65	--	2.21	--
Canisters/year	370	505	875	520	1,395
Metric tons of heavy metal/year	488	697	1,185	1,185	2,370
Canisters/20 years	7,400	10,100	17,500	10,400	27,900
Metric tons of heavy heavy metal/20 Years	9,760	13,940	23,700	23,700	47,400

BWR = Boiling water reactor.

CHLW = Commercial high-level waste.

PWR = Pressurized water reactor.

*Equivalent metric tons.

10.1.2 Reference Repository Location

The Basalt Waste Isolation Project siting work leading to identification of a reference repository location is presented in Chapter 2. The reference repository location shown in Figure 10-2 was identified as site A-H (Chapter 2). Also shown in Figure 10-2 are the proposed location of the exploratory shaft and the principal borehole (RRL-2).

10.1.3 Site Arrangement

The conceptual design is based on a hypothetical location within the reference repository location. Areal requirements for the repository are indicated graphically on Figure 10-2. Surface facilities are within an 80-hectare (200-acre) central process area located over and contained within the surface projection of the 600-hectare (1,500-acre) subsurface facilities. Surrounding the projection of the subsurface facilities to the surface is a 2-kilometer (6,560-foot) control zone with an area of approximately 3,840 hectares (9,500 acres). The total area enclosed by the outside boundary of the control zone is approximately 4,240 hectares (10,500 acres).

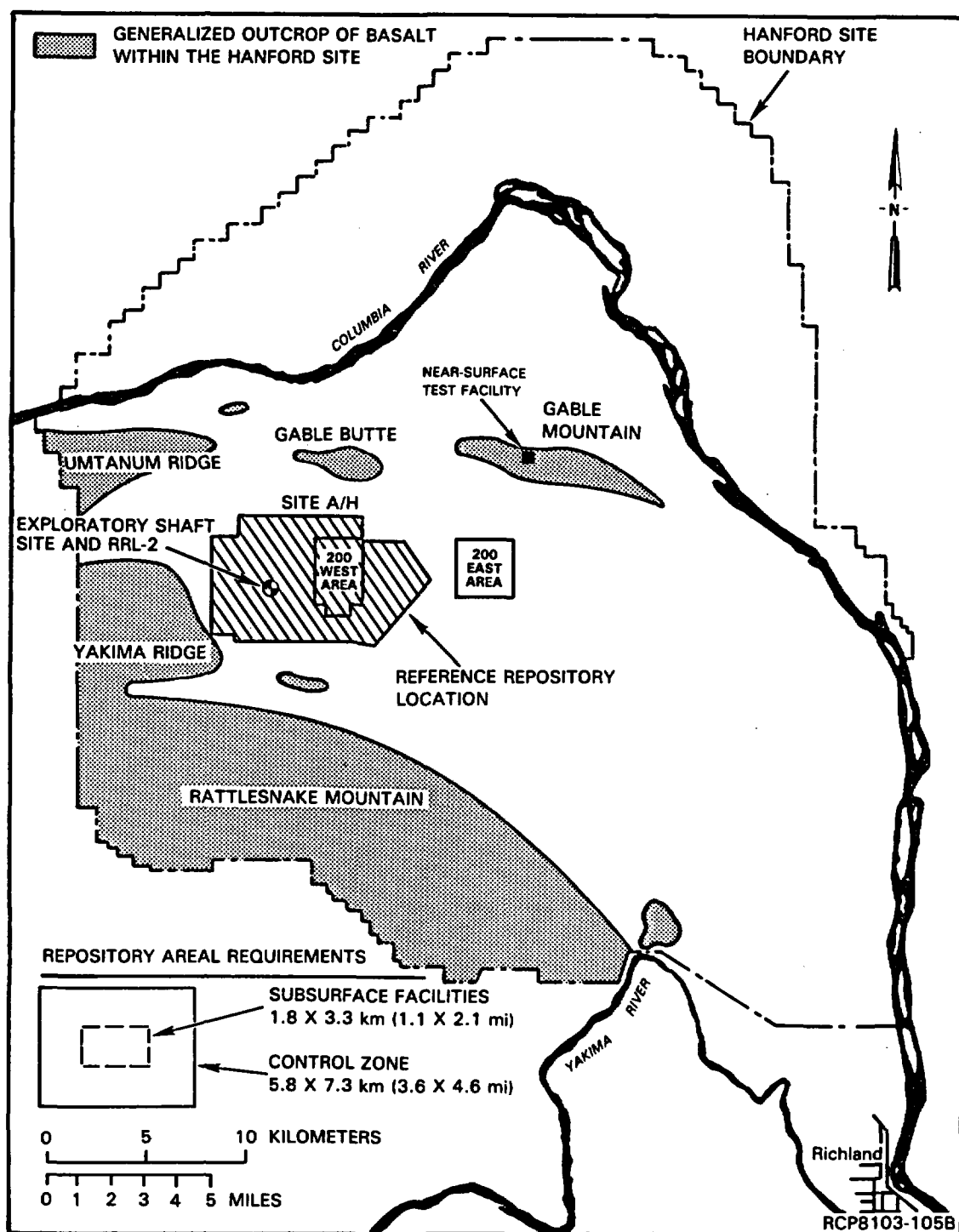
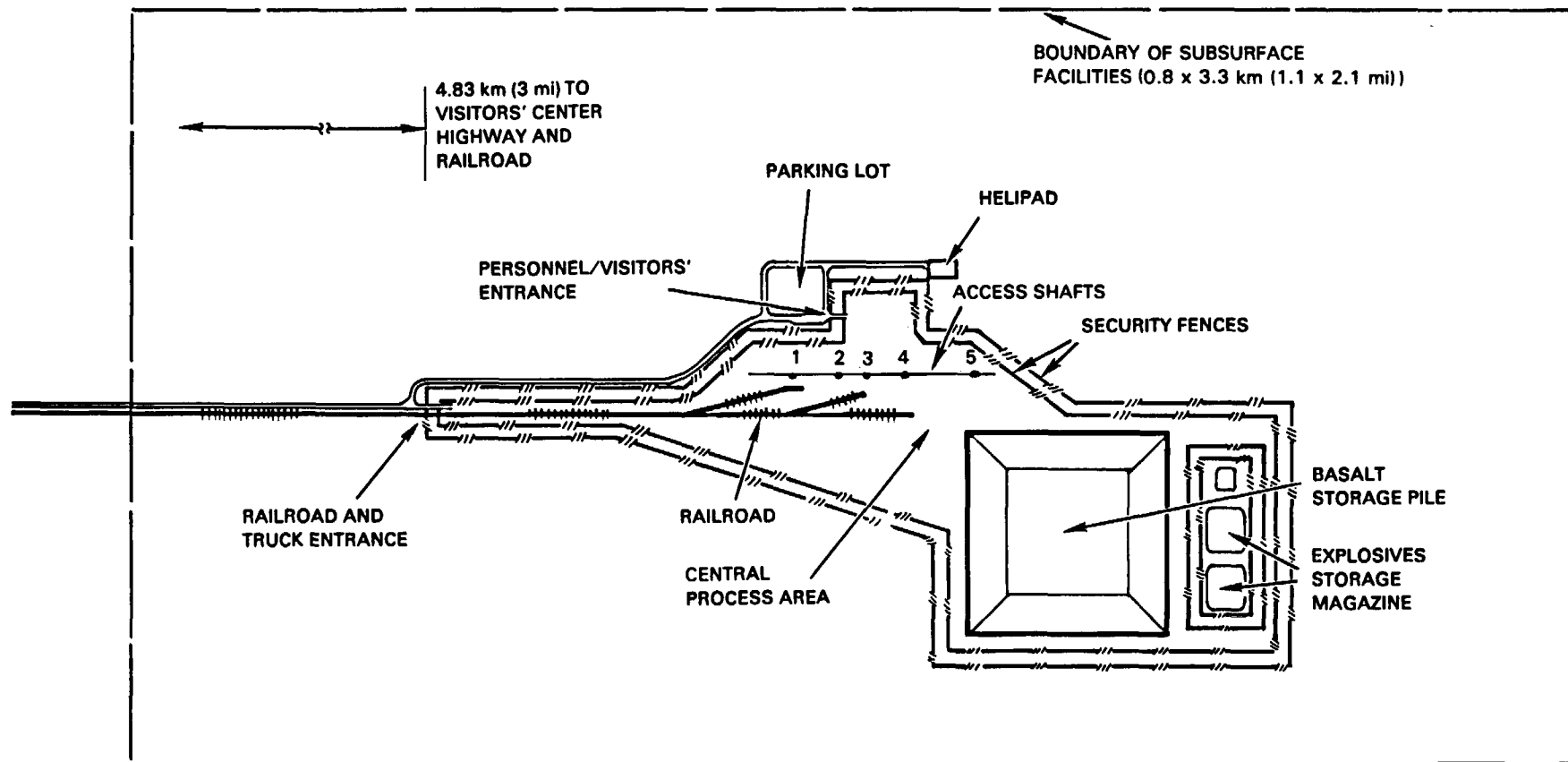


FIGURE 10-2. Reference Repository Location Showing Exploratory Shaft-Phase I Site and Principal Borehole (RRL-2).

The conceptual design assumes that a waste packaging plant is not necessarily colocated at the repository. It further assumes that canisters are shipped to the repository by truck or rail in shipping casks. There is considerable latitude for arranging facilities to conform to the features of an actual site. The repository will be oriented on a specific site by considering the geohydrologic and structural geologic characteristics of the surface and subsurface of the site. Future detailed design of the surface and subsurface facilities will also consider factors such as the seismic response of the site to the maximum credible earthquake.

A conceptual site arrangement in Figure 10-3 shows the central process area within the boundary of the subsurface facilities. Prominent features include the basalt storage pile, explosives storage magazine, and five repository access shafts.



RCP8010-97D

FIGURE 10-3. Site Arrangement.

10.2 SURFACE FACILITIES AND SYSTEMS

10.2.1 Surface Facilities

The surface facilities include offsite development, central process area, land improvements, waste handling building and supporting buildings, and surface storage facilities.

10.2.1.1 Foundation Design of Surface Facilities. The overburden materials at the reference site are sand, gravel, cobbles, and boulders of the Hanford and Ringold Formations. Minor amounts of silt are present. These sediments are approximately 152 meters (500 feet) thick; therefore, all surface structure foundations are in these sediments and not on bedrock.

A conservative bearing value was used, ranging from 0.16 megapascal (3,500 pounds per square foot) at ground surface to 0.38 megapascal (8,000 pounds per square foot) at a depth of 2.4 meters (8 feet). Since these sediments give an excellent foundation condition and groundwater does not exist within the range of surface foundations, foundation problems are not expected.

10.2.1.2 Offsite Development. Offsite development consists of transportation, utilities, offsite monitoring stations, and the visitors' center.

Transportation to the site is provided by connections to the existing Hanford Site road and railroad networks. Rail traffic originates at the Burlington-Northern yard in Pasco, Washington and is transferred at the site boundary to Hanford locomotives. A helicopter landing (helipad) pad is provided at the repository.

Incoming utilities consist of water, electric power, and telephone. Raw water is supplied from the Columbia River by the existing 100 K Area river pump station, which is to be modified by the addition of new pumps and other facilities. A new buried pipeline connects these new pumps to the repository. Two new 138-kilovolt transmission lines, routed over separate parallel rights-of-way, connect the repository to the Hanford Site power system. A new overhead telephone line connects the repository to the Hanford Site telephone network.

Offsite monitoring stations, which are not a part of the repository project, record any repository effluents migrating to surrounding areas. Signals from these monitors are displayed and recorded at the repository control console.

A visitors' center, located at the intersection of the access road with an existing Hanford Site road, provides facilities for informing the public of the mission and nature of the nuclear waste repository in basalt through use of audiovisual presentations.

10.2.1.3 Central Process Area. The central process area (shown in Fig. 10-4) is arranged around the line of five repository shafts, 0.4 kilometer (0.25 mile) in length. Located over these five shafts, arranged west to east, are the confinement exhaust ventilation building, waste handling building, confinement air intake building, personnel and material access facility, and basalt headframe and materials handling building. North of these five core area buildings is the administrative area, consisting of the administration building, Gatehouse No. 1, fire station, security headquarters, industrial safety building, and training center. The maintenance building is located between the administrative area and the five core area buildings. The utility facilities are south of the core area buildings, and include the substations, standby generator building, sewage treatment area, and water storage, treatment, and pumping facilities. The waste receiving facilities are centrally located between the core area and the utility area to the south. The drill core storage building, warehouse, subsurface water retention ponds, and process waste evaporation ponds are also south of the core area. The basalt storage pile occupies the southeastern portion of the central process area. The entire central process area is surrounded by a double security fence. The parking lot, helicopter landing pad, and mine water percolation pond are located outside this fence.

10.2.1.4 Land Improvements. Land improvements consist of site preparation, roads, walkways, storm drainage, landscaping, and rail system. The site is prepared by clearing and stripping prior to construction of culverts, drainage structures, and larger diameter sewers. Excavation and embankment operations are then performed to bring the area to designated elevations and grades.

Asphalt roads and concrete walkways within the repository site are provided for movement of vehicles and personnel. The parking lot and some portions of the administrative area have curbs. The basalt haul road is not paved, but consists of stabilized base course only.

Graded areas are sloped to open ditches for storm drainage. Curbs and gutters in heavy traffic areas, such as the administrative area, are sloped to storm water inlets. Buried storm sewers connect these inlets to the open ditches. Roof drains discharge to the nearest ditch or storm sewer. Discharge points for storm drainage from the repository are monitored for radioactivity.

The administrative area of the repository and the visitors' center are landscaped with shrubs, trees, and lawns.

Wastes are received in the shipping cask by both rail and truck. The waste receiving system consists of a classification yard, inspection pits, cask storage yards, distribution tracks and roads, and docks for unloading full and returning empty shipping casks.

1. PERSONNEL/VISITORS' ROAD
2. TRUCK ROAD
3. SECURITY FENCES
4. PARKING LOT
5. GATEHOUSE NO. 1
6. HELIPAD
7. ADMINISTRATION BUILDING
8. LUNCHROOM
9. SUBSTATION
10. INDUSTRIAL SAFETY CENTER
11. TRAINING CENTER
12. GATEHOUSE AND SECURITY BUILDING
13. FIRE STATION
14. CONFINEMENT EXHAUST BUILDING
15. STACK
16. SHAFT NO. 1--CONFINEMENT EXHAUST
17. COOLING TOWERS
18. STACK
19. SHAFT NO. 2--WASTE TRANSPORT
20. WASTE HANDLING BUILDING
21. CASK CAR STORAGE YARD
22. REFRIGERATION BUILDING
23. SHAFT NO. 3--CONFINEMENT INTAKE
24. CONFINEMENT AIR INTAKE BUILDING
25. PERSONNEL AND MATERIAL ACCESS FACILITY
26. SHAFT NO. 4--SERVICE AND REPOSITORY DEVELOPMENT VENTILATION INTAKE
27. REPOSITORY AIR INTAKE
28. MAINTENANCE
29. SHAFT NO. 5--BASALT HOISTING AND REPOSITORY DEVELOPMENT VENTILATION EXHAUST
30. REPOSITORY EXHAUST STACK
31. REPOSITORY EXHAUST BUILDING
32. BASALT AND MATERIALS HANDLING BUILDING
33. PATROL ROAD
34. BASALT CRUSHER BUILDING
35. REPOSITORY CORE STORAGE AND LABORATORY BUILDING
36. SLEEVE AND PLUG STORAGE YARD
37. SUSPECT RAIL CAR AND TRUCK STORAGE AREA
38. STANDBY GENERATOR BUILDING
39. REPOSITORY WATER RETENTION PONDS
40. RECEIVING SUBSTATION
41. WAREHOUSE
42. SANITARY SEWAGE TREATMENT PLANT
43. PROCESS WASTE EVAPORATION PONDS
44. OVERHEAD POWERLINES
45. REPOSITORY WATER PERCOLATION POND
46. BASALT HAUL POND
47. BASALT STORAGE PILE

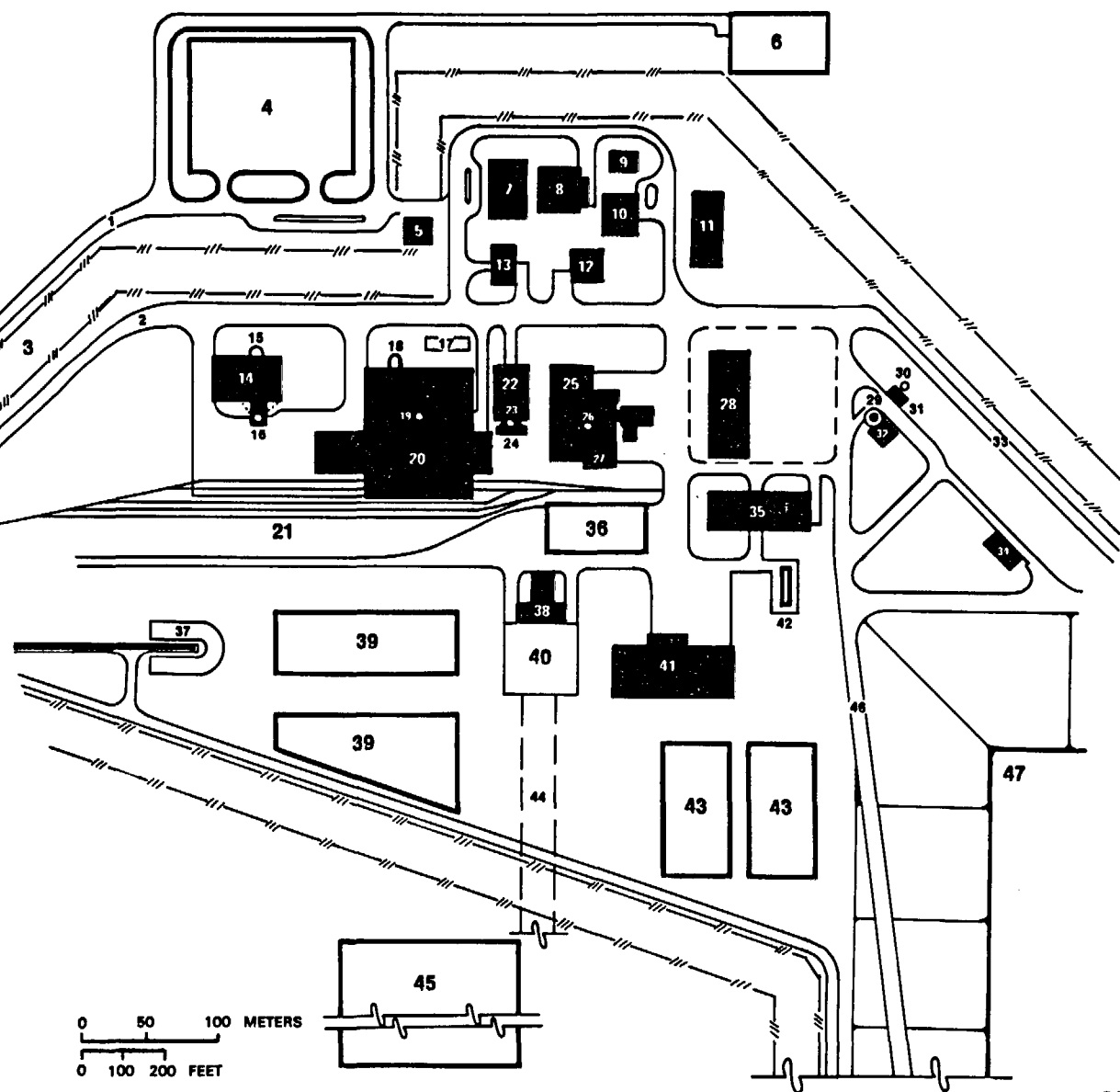


FIGURE 10-4. Surface Facilities Plan--Central Process Area.

10.2.1.5 Waste Handling Building and Other Buildings Important to Safety. The waste handling building receives and processes both remote- and contact-handled waste, and transfers them to the headframe area of the waste transport shaft for lowering to the subsurface facilities. This headframe is an integral part of the waste handling building, which is a sealed, multi-story, monolithic, concrete structure that provides confinement for the waste handling process; i.e., separates potential sources of contamination from the public and from the operating personnel.

The core of the building is the second floor where the primary (receiving) hot cell and secondary (transfer) hot cell are located. These are flanked by the operating and service galleries. On the ground floor, beneath the hot cells, the shipping cask unloading area provides a space in which the cask is upended and connected to the shielding sleeve from the hot cell, thus providing a shielded route for transfer of canisters from the cask to the primary hot cell.

A contact waste handling area is located in the west side of the building. Waste containers are unloaded in a receiving area and are transferred by air pallet to the drum unloading area. The drums are removed from the containers, inspected, decontaminated, palletized, and moved by forklift through the commercial low-level transuranic waste transfer room to the headframe area for loading into the waste transport cage.

The building support areas include radioactive waste treatment facilities, ventilation fan and filter rooms, mechanical and electrical rooms, service areas, and administrative areas.

Two separate ventilating systems are furnished in the building: the confinement system for the waste handling areas and a standard ventilating system for support and administrative areas. The confinement system supplies fresh air to the waste handling areas and exhausts it through high-efficiency particulate air filters to the stack.

Buildings important to nuclear safety are constructed to quality assurance Level I standards. These buildings are the waste handling building, headframe portion of the personnel and material access facility, standby generator building, security headquarters, mine exhaust building, confinement exhaust ventilation building, headframe portion of the basalt headframe and materials handling building, and confinement air intake building. These are all sealed, monolithic, concrete buildings. The remainder of the buildings shown in Figure 10-4 are of conventional, not confinement, construction.

10.2.1.6 Storage Facilities. A warehouse and adjoining yard provide storage for operational supplies and parts. Underground tanks with pumps provide gasoline and diesel fuel storage; magazines on the southeast side of the basalt storage pile provide storage for explosives used in excavating the subsurface facilities.

10.2.2 Waste Handling Systems

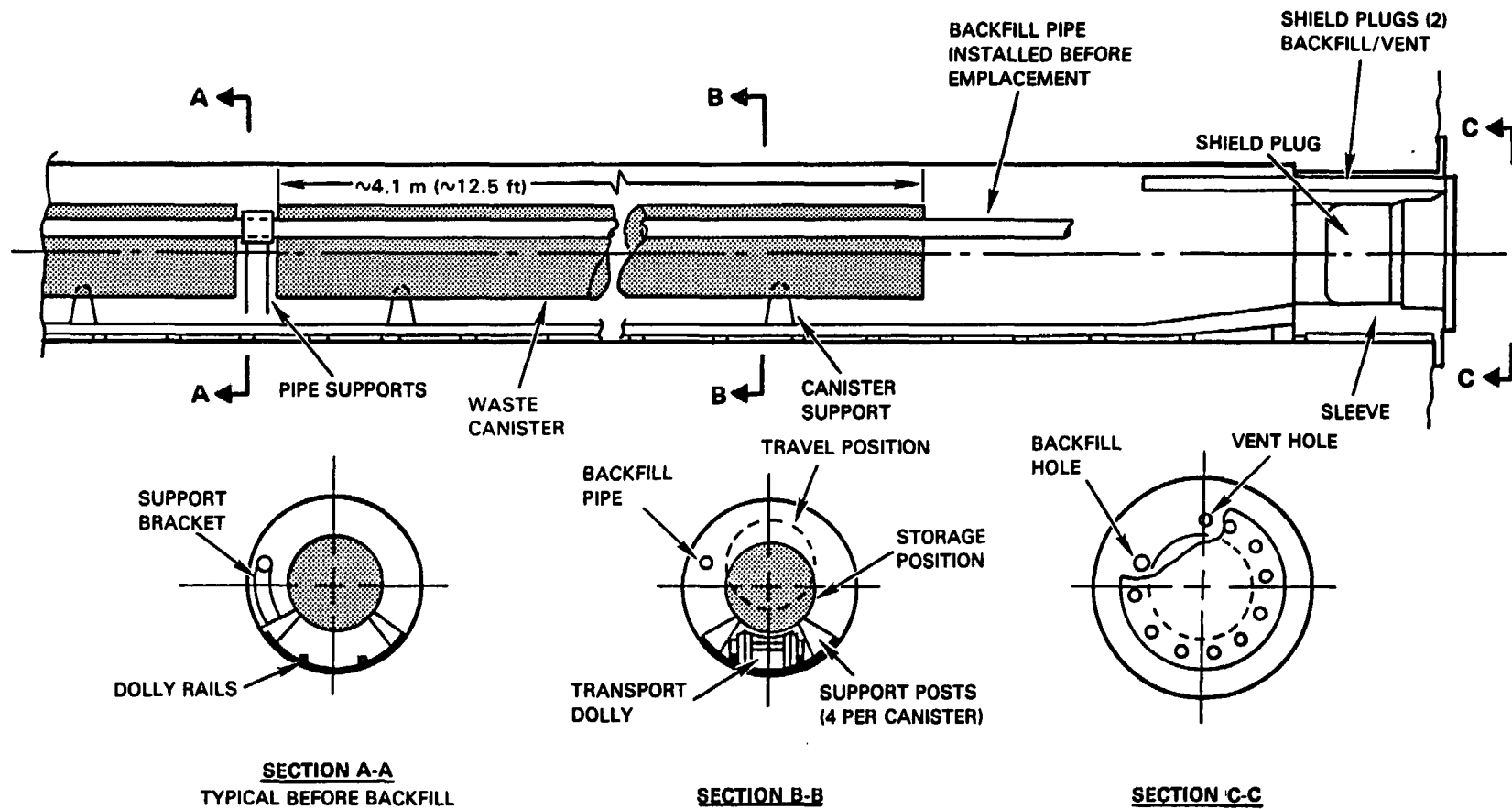
Waste is received at the waste handling building, located above the waste transport shaft. Most shipments are expected by rail car, but provisions for truck shipments are also provided.

The shipping cask for waste canisters of commercial high-level waste or spent fuel is held in a near-horizontal position during shipment. In the receiving area beneath the hot cell of the waste handling building, the cask is tilted to the vertical position for unloading and is mated with a shielding collar lowered from the hot cell. After removal of the shielding plugs for the hot cell and the cask, each waste canister is raised up into the primary hot cell, checked at the automated smear test station, and stored temporarily in the lag storage pit (minimum capacity 20 canisters). From there it is transferred to one of two process tanks, which have the capability of welding a carbon steel overpack for a commercial high-level waste canister, inspecting spent fuel or overpacked commercial high-level waste canisters (both helium-leak and ultrasonically tested for structural soundness), decontaminating if necessary, and transferring the waste canister from the possibly contaminated primary hot cell to the secondary (and clean) hot cell.

From here, the completed and clean waste canister is lowered from the secondary hot cell into a transfer cask, which reduces radiation levels to 10 mrem/hour at a distance of 1 meter (3 feet) from the cask surface. This transfer cask shields the waste canister during its journey from the hot cell to the waste transport shaft conveyance, down the shaft, and out to its final disposal location.

Waste canisters are emplaced by a diesel-powered, rubber-tired transporter that receives a transfer cask at the base of the waste transport shaft, carries it to the placement location in a horizontal position, and then mates the cask with the shielded door assembly that has been previously attached to the horizontal storage borehole. Both borehole and transfer cask doors are then opened, and the 381-millimeter (15-inch) diameter waste canister is hydraulically ejected from the cask and onto skidrails inside the storage borehole. From there, a transport dolly lifts the waste canister and carries it farther into the borehole to its designated placement location (Fig. 10-5). At that point, the dolly lowers the waste canister onto a supporting structure and returns to the borehole entrance, ready for the next package. After the borehole is filled with packages, the dolly is retrieved into the transfer cask, a permanent shielding plug is installed, and the borehole shield door assembly is transferred to the next borehole.

Between the emplaced waste canisters and their borehole is 152 millimeters (6 inches) of radial clearance available for future pneumatic backfilling through a 76-millimeter (3-inch) pipe that was installed during construction.



RCP8205-44

FIGURE 10-5. Waste Canister in Horizontal Storage Borehole.

The commercial low-level transuranic waste will be concreted into drums and shipped inside cargo carriers to the repository. After preliminary inspection and washdown, the drums will be removed from the carriers, inspected closely for radiation and surface contamination levels, decontaminated if necessary, palletized, transferred to the placement level in the same waste cage that handles the transfer casks, and stored in the contact waste chamber. Damaged drums may be overpacked.

Commercial high-level waste, spent fuel, and commercial low-level transuranic waste will be retrievable for up to 50 years after emplacement of the first waste.

All waste handling and storage operations will be designed to meet radiation and other applicable requirements of 10 CFR 20 (NRC, 1979).

10.2.3 Service Systems

Service systems comprise bulk handling; material transfer; subsurface ventilation; electric power; communications; instrumentation, control, and alarm; water supply; fire protection; decontamination; radioactive waste management; nonradioactive material disposal; physical security; and miscellaneous.

10.2.3.1 Bulk Handling. The bulk handling systems are those for handling basalt; aggregate; cement, additives, and bentonite; and shotcrete, concrete, and room backfill.

Broken basalt from mining operations is discharged from the basalt hoisting skips to a surface surge bin adjacent to the basalt hoisting headframe. Two off-road mine haulers carry the broken basalt to the basalt storage pile where it is spread by a bulldozer. The same haulers return the basalt as feed to the aggregate crushing and screening facilities in the basalt headframe and materials handling building. A train of crushers, screens, conveyors, and a bucket elevator sort the broken basalt into coarse and fine aggregate and store the products in bins and storage piles at the materials handling building.

Cement and bentonite are received by truck and rail and stored in bins east of the materials handling building. Bentonite storage and handling are provided at the time of backfilling. These materials are recovered from the bins and transferred to batching and mixing machinery in the materials handling building by pneumatic piping systems.

Shotcrete, concrete, and backfill mix are produced in the materials handling building by an arrangement of vibrating feeders, screw conveyors, pneumatic piping, a weigh hopper, and a concrete mixer. Dry shotcrete mix is transferred to the service shaft headframe by narrow-gauge mine cars that are lowered to the subsurface in the service shaft hoist. Wet concrete mix is transferred to the subsurface by the same method and route.

Backfill mix, consisting of bentonite, bentonite prills, and aggregate, is proportioned by the same machinery used for shotcrete and concrete, and is then dumped into the basalt skips for transfer to the repository horizon. This operation takes place after all underground excavation is completed and the skips are no longer required for hoisting basalt.

10.2.3.2 Material Transfer. Material transfer throughout the surface facilities, other than bulk materials handling described above, is by motor vehicle on the plant roads.

10.2.3.3 Subsurface Ventilation. There are two separate subsurface ventilation systems: one for mining development ventilation and the other for confinement ventilation. Supply and exhaust flow paths are shown in Figure 10-6 and flow rates are given in Table 10-2.

TABLE 10-2. Subsurface Ventilation Requirements.

Designation	Shafts		Air quantity, m ³ /min (ft ³ /min)
	Description	Size, m (ft)	
1	Confinement air exhaust shaft	3.4 (11)	6,853 (242,000)
2	Waste transport shaft	3.7 (12)	710 (25,000)
3	Confinement air intake shaft	3.7 (12)	6,260 (221,000)
4	Service and repository development ventilation intake shaft	4.9 (16)	6,287 (222,000)
5	Basalt hoisting and repository development ventilation exhaust shaft	4.3 (14)	6,061 (214,000)

The mining development ventilation system provides ventilation for initial shaft pillar, main entry, and panel development. Ventilation air quantities have been minimized by the use of electrically driven equipment, instead of diesel, in mining operations. The mining air system uses multiple fans for reliability; push-pull main supply and exhaust air fans are located at the surface. Air from the mining intake fans is delivered

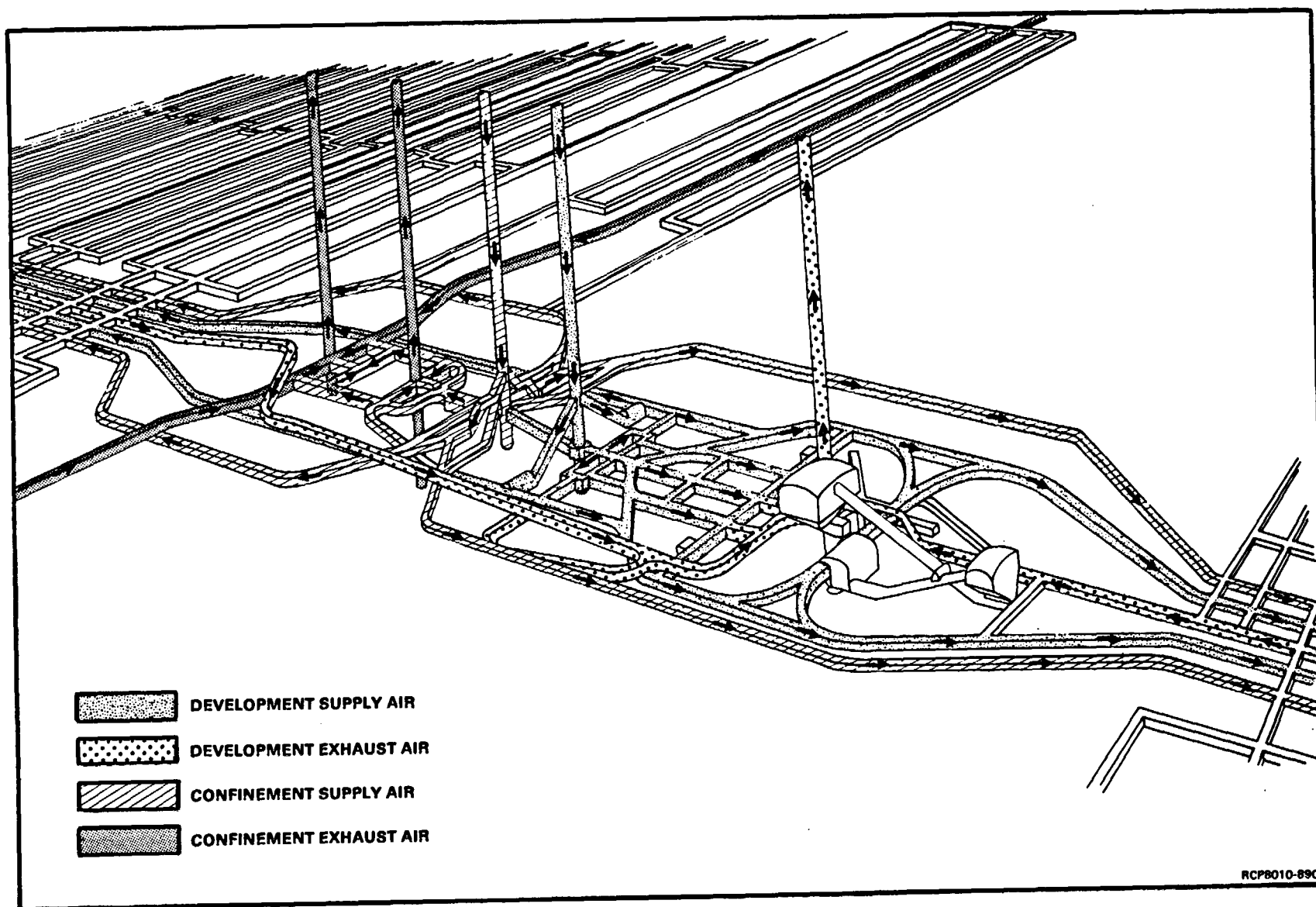


FIGURE 10-6. Shaft-Pillar Ventilation Flow Paths.

down the service shaft. From the base of the shaft the supply air is distributed to the maintenance and placement areas and to the mine intake airways. A system of stoppings, air lock doors, and regulators control the flow of supply air to the work places.

Because of the relatively high basalt temperature and the heat added by the waste package, cooling of the repository is required for personnel safety (ACGIH, 1980) in both the development and the confinement areas. A simplified flow diagram of the cooling water system is shown in Figure 10-7. Chilled water supply and return lines in the confinement intake shaft (Fig. 10-7) circulate water through heat exchangers at the storage level. The heat exchangers isolate the secondary chilled water system in the repository from the 11-megapascal (1,600-pound-per-square-inch) hydrostatic pressure at the bottom of the primary systems. The total repository cooling load is 3,800 tonnes (3,700 tons).

Exhaust air is collected at the work places; booster fans and ducts deliver this air to the mining return airway. The main mining exhaust air fans located at the surface provide the negative pressure (suction) required to draw the exhaust air through the mining return airways and up the basalt transport shaft to the surface.

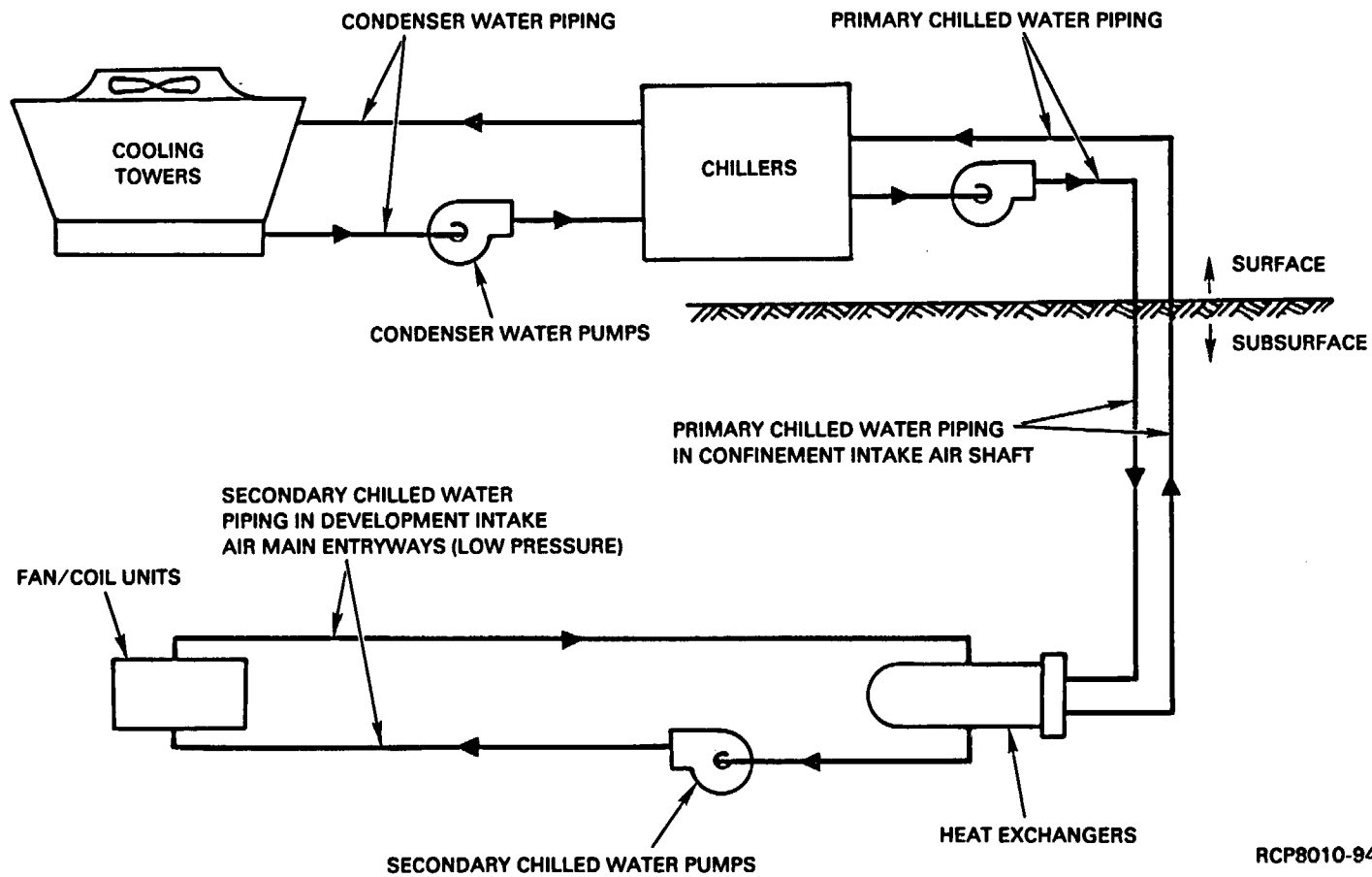
The confinement air system provides the ventilation to support all activities related to waste handling operations, including transport, emplacement, and retrieval operations. The system minimizes the potential of air leakage between the confinement areas. During early stages, before waste is placed, this air system will also service development work.

The confinement ventilation system is a push-pull system. Air from the supply fans is delivered down the confinement air intake shaft. Mobile air handling units, with chilled water cooling units, control the temperature of the air required for precooling and ventilating the entries, rooms, or room segments.

Ventilation air delivered to the point of the waste emplacement activity continues to travel the length of the placement room to the confinement return airway at the perimeter of the repository. The exhaust air is drawn through the confinement return airway and up the confinement exhaust shaft by the confinement exhaust fans, and bypasses the high-efficiency particulate air filters unless the system detects radioactivity. If radioactivity is detected in the ventilation exhaust, the high-efficiency particulate air filters prevent release of radioactive material to the atmosphere.

After a room has received its full complement of emplaced waste, it is sealed off and full ventilation to that room ceases; only a small air stream is bled off to permit monitoring of the room air.

The confinement ventilation system provides ventilation for all underground activities in connection with mass retrieval of the previously emplaced nuclear waste. The system is sized for a backfill rate of one panel per year.



RCP8010-94A

FIGURE 10-7. Cooling Water System.

10.2.3.4 Electric Power. There are three electric power systems: normal, standby, and uninterruptible. Dual incoming transmission lines from the Hanford Site power supply system provides normal power to the receiving substation. The maximum demand for the repository is 29,000 kilowatts. Each half of the substation supplies one-half of the dual radial distribution system that supplies the repository. Each dual feeder supplies one of two standby switchgear buses, each of which is also fed from a 12,000-kilovolt-amp standby diesel generator. Upon failure of normal power to either bus, the corresponding standby generator starts automatically and feeds selected loads connected to the standby bus. A normally open automatic intertie between the standby buses closes upon failure of one of the generators, so that the bus may be supplied by the opposite standby generator.

Uninterruptible power units, which include a rectifier, battery bank, and inverter, are located near the many facilities that require uninterruptible power.

10.2.3.5 Communications. The communication facilities consist of telephone, radio, intercom/paging, and microwave. All communication systems are supplied with both normal and uninterruptible power. A private automatic branch exchange telephone system installed in the administration building is connected to the Hanford Site telephone network by a new trunk line. A very high-frequency mobile radio system provides two-way voice communication to mobile patrol units, to plant maintenance and operational vehicles, to Hanford security headquarters, and to outside law enforcement agencies. The microwave system provides voice communication and data transmission between the repository and U.S. Department of Energy offices in Richland, Washington.

10.2.3.6 Instrumentation, Control, and Alarm. This system provides for radiation monitoring, process control, subsurface air quality monitoring, subsurface geomechanical sensors, and security sensors. It is based on distributed control, in which local, solid-state, modular microprocessor-based units receive digital and analog input from local sensors, then provide local control, indication, and alarm functions by means of a preprogrammed routine in the microprocessor memory. Simultaneously with local indication and control, signals are transmitted via multiplex units and two redundant coaxial data highways to the central control console at the waste handling building control room for cathode ray tube display, visual and recorded monitoring, and alarm.

10.2.3.7 Water Supply. Raw water is withdrawn from the Columbia River at the existing, but currently inactive, 100 K Area river pump station. New vertical pumps discharge water through a 11.3-kilometer (7-mile) pipeline to the repository water treatment plant. Filtered and chlorinated water is then stored in a surface storage tank that supplies a looped distribution system to meet the combined potable, process, and fire protection water demands of the surface and subsurface facilities. Normal supply is met by pumps for potable and process water. Two fire pumps (one electric and one diesel-driven standby) supply water upon sensing falling pressure

when fire supply valves are opened. The system is capable of supplying peak fire demand of 7,570 liters per minute (2,000 gallons per minute) simultaneously with the peak potable and process flow of 5,680 liters per minute (1,500 gallons per minute).

10.2.3.8 Fire Protection. Fires are extinguished by fixed systems for water sprinkling, small hose, Halon gas, and dry powder, as appropriate to the particular facility hazard. Yard fire hydrants are provided throughout the surface facility. Hydrants and sprinkler systems are supplied from the combined water distribution system.

Fire detection equipment includes smoke detectors and manual alarm pull boxes, as well as local flow alarms at all sprinkler and standpipe risers, and at Halon and dry powder systems.

10.2.3.9 Radioactive Waste Management. Radioactive waste disposal is subdivided into solid, liquid, and gaseous radioactive waste systems.

Solids that become contaminated are decontaminated, if possible. If they cannot be decontaminated or burned, they are packaged and solidified in 208-liter (55-gallon) drums and stored in the subsurface commercial low-level transuranic waste storage area. If such solids are combustible, they are transferred to the radioactive waste incinerator and burned. The incinerator uses the sodium carbonate, fluidized bed process, producing an ash that is then mixed with concrete, and placed in drums for permanent placement in the subsurface facility. The gaseous incineration product is filtered, cooled, and treated in the gaseous radioactive waste system.

The liquid radioactive waste system collects the liquid in an underground tank, then purifies it by ion exchangers.

Radioactive gases are collected and passed through a cooler, moisture-entrainment separator, caustic scrubber, heater, prefilter, and high-efficiency particulate air filter. The discharge from the high-efficiency particulate air filter is routed to the primary confinement ventilation system, then to the stack.

10.2.3.10 Nonradioactive Material Disposal. Nonradioactive material systems dispose of nonradioactive solids and process liquids, subsurface drainage water, and sanitary sewage. Solid wastes are collected, compacted, and deposited by cut-and-cover methods onsite. Process liquids are disposed of in one of two evaporation ponds onsite; one pond being available for evaporation while sludge is being removed from the other.

Subsurface drainage water is discharged to one of two surface retention ponds. If the water is found to be nonradioactive, it is then discharged to the percolation pond. If radioactive, the water is held in the retention pond and decontaminated with a portable deionizer.

Sanitary sewage is collected through underground sewer pipes that drain by gravity to a lift station. Pumps at the lift station discharge the sewage to an aerobic digestion unit from which purified effluent flows to surface percolation in a tile drain field. The sludge is hauled to existing Hanford Site sludge disposal beds.

10.2.3.11 Physical Security. Security for the nuclear waste repository in basalt is provided for the prevention of radiological sabotage. All surface facilities are in a protected area surrounded by a perimeter barrier, penetrated only at two points of controlled access. The perimeter barrier and the access points are provided with special security measures and instrumentation to exclude unauthorized entry. Certain facilities in the protected area are designated as vital areas and are also provided with procedures, barriers, and instrumentation to exclude unauthorized entry. All security sensors read out at manned central security consoles.

10.2.3.12 Miscellaneous. Compressed air is piped from compressors in the waste handling building to meet air demands in that building. Demands in other buildings are supplied by local compressors. Subsurface compressed air is provided from a compressor in the shaft-pillar area. Cooling water is supplied to the refrigeration building chillers from a grade-level cooling tower. The heating, ventilating, and air conditioning cooling water for the waste handling building is supplied from a tower on the roof of the building.

Diesel fuel and gasoline are stored in buried tanks at a surface refueling station near the maintenance building. Buried tanks near the standby generator building and the water pumphouse provide fuel for the generators and the engine-driven fire pump. Nitrogen is stored in cylinders above ground near the waste handling building. Oxygen and acetylene are similarly stored near the maintenance building.

10.3 ACCESS SHAFTS

In the conceptual design, there are five vertical access shafts located on a line parallel to the long axis of the repository (see Fig. 10-3 and 10-6).

This central arrangement of five shafts is similar to prior design studies for repositories in basalt (Staff, 1980) as well as other geologic media (KE, 1978). Studies are continuing on the number, size, location, construction method, and sinking sequence of the shafts. As criteria are finalized, the design described herein may change.

10.3.1 Shaft No. 1 - Confinement Air Exhaust Shaft

The confinement exhaust shaft, an upcast shaft, is located on the west edge of the shaft pillar. The shaft is used to remove the spent ventilation air from the confinement, retrieval, or backfill operations in the repository. A fan system, equipped with high-efficiency particulate air filters, moves the ventilation air. The high-efficiency particulate air filters are used only when radioactive contamination in the exhaust air is detected. A shaft station is located 1,120 meters (3,680 feet) below the surface. There is no headframe and no equipment in the shaft, except for a rack-and-pinion shaft inspection hoist. Pertinent shaft data are as follows:

- Diameter: 3.4 meters (11 feet) inside diameter
- Depth: 1,140 meters (3,750 feet)
- Equipment:
 - Rack-and-pinion shaft inspection hoist (two-man)
 - Sump pump
- Airflow: 6,853 cubic meters per minute (242,000 cubic feet per minute).

10.3.2 Shaft No. 2 - Waste Transport Shaft

The waste transport shaft provides the route for moving the waste canister transfer casks and commercial low-level transuranic waste drums between the waste handling building and the repository horizon. The shaft station for transferring canisters is 1,130 meters (3,700 feet) below the surface. Areas for transporter maintenance and decontamination are adjacent to the station. An emergency shock absorber in the sump prevents breaching of the transfer cask should there be a free-fall of the cage and its contents. There is a waste transport hoist for the shaft, and a two-person inspection hoist attached to the shaft wall. A small amount of air

(710 cubic meters per minute (25,000 cubic feet per minute)) is pulled up the shaft and into the fan house of the waste handling building. Pertinent shaft data are as follows:

- Diameter: 3.7 meters (12 feet) inside diameter
- Depth: 1,180 meters (3,880 feet)
- Equipment:
 - Waste transport cage with counterweight
 - Shaft inspection hoist
 - Impact-absorbing material installed on the shaft bottom
 - Sump pump
- Airflow: 710 cubic meters per minute (25,000 cubic feet per minute).

10.3.3 Shaft No. 3 - Confinement Air Intake Shaft

The confinement air intake shaft provides fresh air for the confinement side of the repository. All of the ventilation air used in the confinement area is brought down this intake shaft, which is isolated by regulators and air lock doors. There is no headframe or any equipment in the shaft except for a rack-and-pinion shaft inspection hoist. Pertinent shaft data are as follows:

- Diameter: 3.7 meters (12 feet) inside diameter
- Depth: 1,140 meters (3,750 feet)
- Equipment:
 - Shaft inspection hoist
 - High-pressure chilled water pipelines
 - Sump pump
- Airflow: 6,260 cubic meters per minute (221,000 cubic feet per minute).

10.3.4 Shaft No. 4 - Service Shaft

The service shaft supplies and removes the personnel, material, and equipment necessary to support the underground mining and waste disposal activities. During mining and final backfilling, this shaft also provides the mining intake ventilation. The station is approximately 1,130 meters (3,700 feet) below the surface, and here the incoming ventilation is forced into the mine intake airways. The airflow into nearby operations areas is limited or blocked by air lock doors and regulators. The shaft

contains a cage for personnel and materials, its counterweight, a ladder-way, a sump, and waterlines. The operations near the shaft are maintenance and stores, operations control, service station, explosives magazines, and switchgear. Pertinent shaft data are as follows:

- Diameter: 4.9 meters (16 feet) inside diameter
- Depth: 1,155 meters (3,790 feet)
- Equipment:
 - 2.4- by 3.7-meter (8- by 12-foot) cage for personnel, equipment, and material
 - Sump pump
- Airflow: 6,287 cubic meters per minute (222,000 cubic feet per minute).

10.3.5 Shaft No. 5 - Basalt Transport Shaft

The basalt transport shaft is equipped to hoist mined rock to the surface and return it for backfill. The shaft also provides for the exhaust of spent air from mining development to the surface. The mine return air is in the central airway; when the air returns to the shaft pillar, it enters an incline and joins the shaft 13 meters (43 feet) above the basalt loading station. The basalt transport shaft, which is the final shaft in the shaft pillar, is located 189 meters (620 feet) east of the service shaft. The shaft station is approximately 1,130 meters (3,700 feet) below the surface, while at the bottom of the shaft is a system to load/unload basalt for hoisting to the surface (or return to the repository). There are pump stations at depths of 1,070 and 550 meters (3,510 and 1,800 feet). Pertinent shaft data are as follows:

- Diameter: 4.27 meters (14 feet) inside diameter
- Depth: 1,170 meters (3,830 feet)
- Equipment:
 - Two 9.1-tonne (10-ton) basalt hoisting skips
 - Inspection cage
 - Lines for utilities and water disposal
 - Dewatering pumps
- Airflow: 6,061 cubic meters per minute (214,000 cubic feet per minute).

10.3.6 Shaft Pillar

The conceptual design places the five access shafts (that connect the surface and subsurface facilities) on a line parallel to the long axis of the repository in a shaft pillar located between four waste storage areas. This arrangement was selected primarily to concentrate the surface facilities, utilities, and transportation within an area that can be adequately secured and controlled. In addition, it minimizes the number of shafts required and enables the ventilation system to be fully operable prior to the construction of the storage areas.

The space between the shaft pillar and the underground storage areas is designated to provide thermal and rock stress separation between the two areas. The lengths of the entries are sized to provide thermal isolation from the placement rooms and to provide adequate length for the seals to be installed prior to repository closure. The separation distance between shaft pillar and storage areas and the length of the entries preclude significant shaft, shaft-pillar, and entry temperature increases resulting from the heat generated by the radioactive waste in the storage areas.

The shaft pillar includes areas for waste transfer, bulk materials handling, maintenance, stores, service equipment, and personnel and administrative functions at the repository depth. The complexity and extent of the shaft pillar are increased by the need to isolate the confinement and development areas from each other. The conceptual design layout of the pillar, shown in Figure 10-8, identifies the shafts and the many operational functions that are provided in the shaft-pillar area.

10.3.7 Shaft Design Options

In addition to considerations of access for construction and waste storage operations, subsurface ventilation and cooling are other major considerations in establishing the size and number of repository shafts. The conceptual design is based on cooling subsurface facilities located in the Umtanum flow, which has an in situ temperature of about 58°C. Location of the repository in an upper, cooler horizon such as the middle Sentinel Bluffs flow could allow the use of smaller, shorter shafts.

The exploratory shaft will allow access to the selected candidate horizon for in situ testing. Based on site-specific information obtained from this testing and planned repository design optimization studies, the size and arrangement of repository shafts will be finalized.

FIGURE 10-8. Shaft-Pillar Layout.

RCP8010-B8A

10.4 DESIGN OF UNDERGROUND OPENINGS

10.4.1 Subsurface Facilities

The subsurface facilities include the shaft pillar, main access ways, waste storage panels (for commercial high-level waste and spent fuel), experimental panel, and contact waste storage panel (for commercial low-level transuranic waste). These are engineered excavations in the repository horizon and are developed from the shaft stations.

To optimize the subsurface facilities layout, eleven alternate arrangements (KE/PB, 1982) shown in Figure 10-9 were analyzed. Based on an areal thermal loading from nuclear waste of 139 kilowatts per hectare (56 kilowatts per acre), each arrangement provides a storage area of 310 hectares (766 acres), consisting of 20 panels of 15.5 hectares (38.3 acres) each. In addition, the subsurface facilities will require areas for panel separation, accessways, shaft pillars, and a shaft-pillar buffer zone. Among the eleven alternates studied, the bow-tie, panhandle, and sash-window arrangements had the most favorable features; these are compared in Table 10-3. The bow-tie arrangement was selected for the conceptual design, based on the minimum haulage distance and ventilation air-travel distance. When site-specific underground information concerning the relative desirability of using specific underground regions for a repository becomes available, that information may favor an alternate arrangement to the bow-tie and the orientation of the selected arrangement.

TABLE 10-3. Key Features of the Most Favorable Alternate Repository Arrangements Considered.

Design	Subsurface area, ha (acres)	Air travel, m (ft)	Entries/returns, m (ft)	Haulage, m (ft)
Bow-tie	600 (1,500)	4,800 (16,000)	25,000 (82,000)	4,700 (15,000)
Panhandle	750 (1,850)	7,200 (24,000)	21,000 (69,000)	7,100 (23,000)
Sash-window	650 (1,600)	8,000 (26,000)	30,000 (98,000)	8,400 (28,000)

The layout of the bow-tie arrangement of subsurface facilities is shown in Figure 10-10. The shaft pillar is near the center of the repository with the contact waste storage panel and an experimental panel nearby. The remainder of the subsurface facilities are divided into 20 waste package storage panels with room for an additional panel if required.

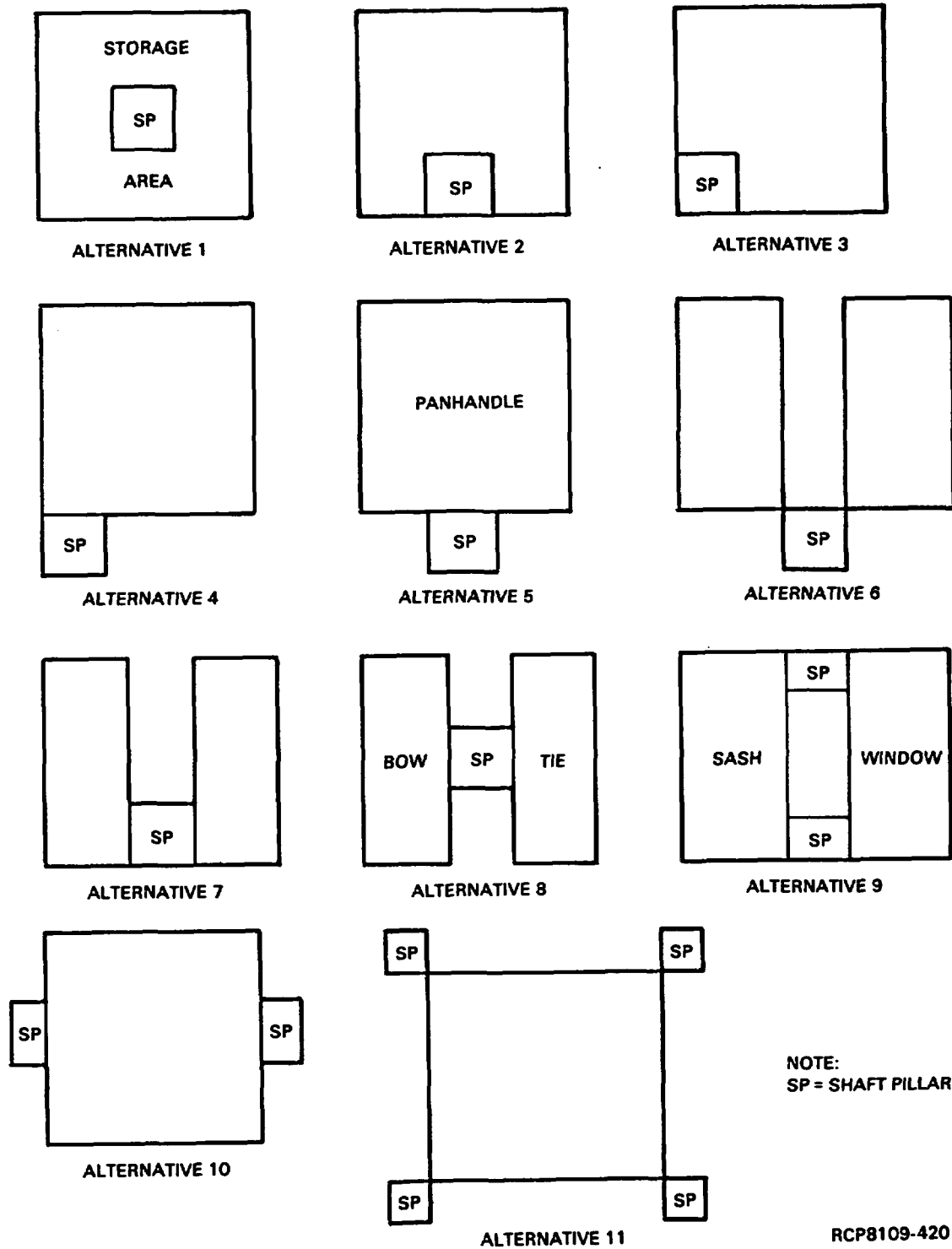
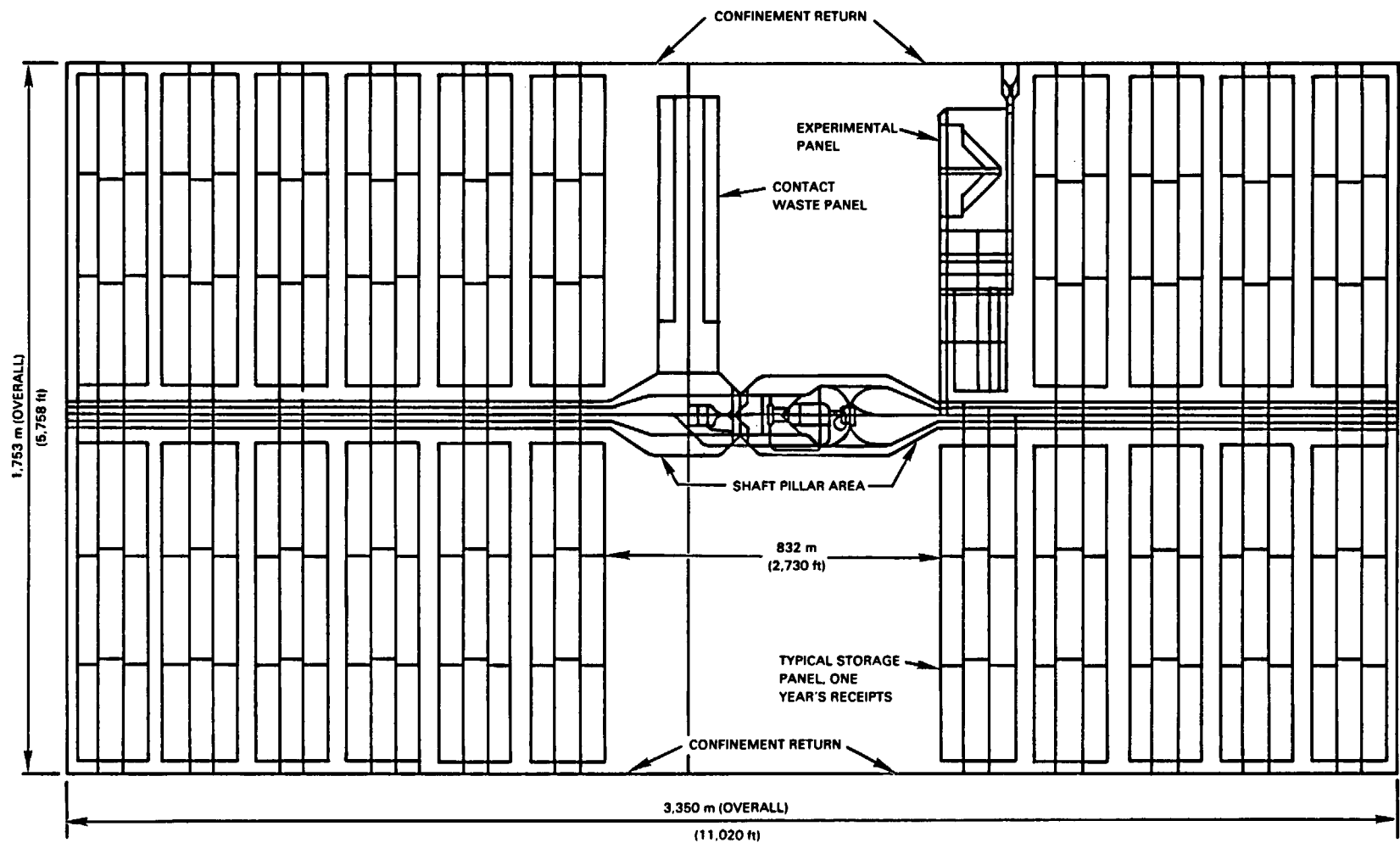


FIGURE 10-9. Alternate Shaft-Pillar Arrangements.



RCP8010-90E

FIGURE 10-10. Subsurface Facilities Layout (bow-tie arrangement).

Main access ways connect the various subsurface areas and provide for the following:

- Personnel and materials required for waste handling, mining, and support operations
- Waste transport
- Basalt and bulk material transport system
- Backfill operations
- Ventilation, including accommodations for the two air circuits (one air system for mining and a separate confinement air system for locations containing radioactive waste)
- Service systems.

Space is also developed along the main access ways for electrical distribution systems and facilities for dewatering and temporary maintenance. Main access ways leading to panel areas are separated from waste panels by a zone of pillar rock. The layout and spacing of the main access ways allow the total separation of the two air circuits. Main access ways will remain operational throughout the retrieval period and until repository closure.

An experimental panel is provided near the shaft area for the following:

- Testing experimental mining systems
- Testing alternative configurations for waste disposal
- Developing repository seals
- Developing monitoring and calibrating systems
- Testing backfill and retrieval procedures.

This panel will be operational at repository start-up and will remain operational throughout the retrieval period. Exploratory shaft underground test areas could possibly provide the nucleus from which the experimental panel is developed.

The commercial low-level transuranic waste delivered over the life of the repository is placed in a contact waste storage panel located close to the shaft pillar. This panel is also operational throughout the retrieval period of the repository.

10.4.2 Waste Storage Panels

A waste storage panel is a discrete area providing space for 1-year receipt of nuclear waste in the form of 520 commercial high-level waste canisters and 875 spent fuel canisters. There are 20 waste panels plus one contingency panel.

The panel shape and size are determined by mining constraints and the placement density of waste packages. In the conceptual design, each panel includes two placement rooms and two reaming access drifts that run the full length of the panel with crosscuts at intermediate locations for escape and ventilation purposes. Each panel, including end crosscuts, will occupy an area of 771 by 201 meters (2,528 by 660 feet) or 15.5 hectares (38.3 acres). The disposal area--20 panels total--thus occupies 357 hectares (882 acres), including a 30.5-meter (100-foot) space between panels, but not including the space between panels and main accesses. A waste storage panel cross section, showing the emplacement tunnels, access tunnels, and horizontal storage holes, is illustrated in Figure 10-11.

Space for 1-year receipts is developed each year. Two independent ventilation systems are provided: a confinement air circuit to serve areas of the facility where nuclear waste is handled or placed and a mining air circuit to serve development and support activities.

Thirty-meter (100-foot) rock pillars separate adjacent panels. Each panel is served by two entries that connect directly into the two central placement rooms.

10.4.3 Waste Storage Holes

Waste is stored in multiple horizontal emplacement holes that are perpendicular to horizontal emplacement rooms. The longest multiple horizontal hole compatible with constructibility and waste emplacement considerations was chosen. Storage holes for waste packages extend 61 meters (200 feet) horizontally at midheight between adjacent panel rooms, as shown in Figure 10-11. Optimization studies during conceptual design led to the following pitches (center-to-center spacings) between storage holes:

<u>Waste form</u>	<u>Pitch, m (ft)</u>	<u>Waste packages per storage hole</u>
Commercial high-level waste	32.6 (107)	17
Spent fuel (pressurized water reactor)	18.3 (60)	13

Storage holes are backreamed to a finish diameter of 686 millimeters (27 inches). Spacers maintain a 152-millimeter (6-inch) radial clearance between the outer diameter of the waste package and the storage hole. There is a 152-millimeter (6-inch) (end-to-end) space between emplaced

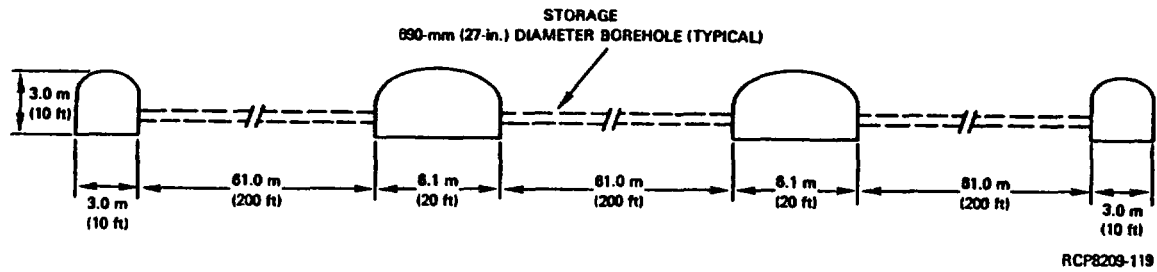


FIGURE 10-11. Waste Storage Panel Cross Sections.

waste packages. The storage hole length not occupied by waste packages and their end-to-end 152-millimeter (6-inch) space is left as an unoccupied buffer, equally divided between both ends of each storage hole. The spaces around and between the waste packages are to be filled by backfill some time after placement (deferred backfill).

The storage holes are displaced one-half pitch on opposite sides of a placement room. Therefore, the overall placement pattern is termed "asymmetrical, horizontal long-hole placement."

10.5 STRENGTH OF ROCK MASS

The conceptual design developed a waste emplacement configuration that complies with the temperature criteria and the chosen maximum basalt design stress of 186 megapascals (27,000 pounds per square inch) for a 2:1 horizontal-to-vertical stress ratio. Current test data indicate the basalt has a compressive strength of 200 to 220 megapascals (29,000 to 32,000 pounds per square inch). The waste package component, basalt maximum temperatures, and maximum basalt stresses are a function of the center-to-center distance (pitch) between the multiple horizontal storage holes. The maximum temperature and stresses decrease as the pitch increases. The conceptual design emplacement pitches were chosen to satisfy the 186-megapascal (27,000-pound-per square-inch) basalt design stress. At the chosen pitches, the maximum temperatures are lower than those required by the temperature criteria. The conceptual design is based upon 10-year-old waste; older waste would allow smaller pitches for the 186-megapascal (27,000-pound-per-square-inch) design stress for storage.

When more precise basalt stress and stress ratio data are developed, primarily from exploratory shaft testing, the basalt design stress will be redefined and the emplacement pitches will be correspondingly adjusted. The established feasibility of the design concept will not be altered by changing the emplacement pitches. Any cost increase resulting from a redefined design stress that increases the emplacement pitches can be offset by detailed design considerations of the waste age; much of the waste may be older than that assumed for the conceptual design.

Principal rock-mass conceptual design assumptions used are given in Table 10-4. As the design progresses, each iterative phase will be based on the latest available site-specific data. The geoenvironmental background is presented in Chapter 4.

Information to date indicates some change of the temperature-dependent properties over the predicted range of near-field temperatures. Additional data on temperature-dependent near-field media properties are sought from the exploratory shaft program. As appropriate for a conceptual design, some stress calculations used only the limiting temperature-dependent values appropriate for the near-field temperatures.

Time-dependent near-field phenomena, such as the resaturation times in the near field of storage rooms, are being studied to identify the time-dependent phenomena to be included in future and more detailed stress analyses. Time-dependent strength (usually less than short-term strength) and the effect of high temperature on strength will be considered in the design as data become available.

TABLE 10-4. Rock-Mass Conceptual Design Assumptions
(Umtanum horizon).

Conditions at Repository Depth
Repository horizon depth: 1,100 m (3,700 ft)
Basalt flow thickness: 62 to 87 m (203 to 285 ft)
Ratio between horizontal and vertical in situ stresses: 2:1
Initial in situ rock temperature: 57°C
Rock Properties
Density: 2.8 g/cm ³ (175 lb/ft ³)
Uniaxial compressive strength: 200 MPa (29,000 lb/in ²)
Tensile strength: 14 MPa (2,030 lb/in ²)
Young's modulus: 67,800 MPa (9,830,000 lb/in ²)
Poisson's ratio: 0.26
Thermal expansion coefficient: 7.45 E-06/°C
Specific heat: 0.95 kJ/kg°C
Thermal conductivity: 2.3 W/m°K
Diffusivity: 6.5 E-07 m ² /s
Joints are tight: 3 to 10/m
Maximum Temperature Permitted
Waste: 500°C for commercial high-level waste and cladding 380°C for spent fuel
Canister and overpack: 430°C
Basalt: 500°C

10.5.1 Results of Rock Stress Analysis

10.5.1.1 Conceptual Design with 2:1 Stress Ratio. The conceptual design is based upon an assumed maximum horizontal-to-vertical in situ stress ratio of 2:1 at the repository horizon. Information on the consequence of having a greater in situ stress ratio are included for comparison (see Section 10.5.1.2). The ratio of maximum-to-minimum horizontal stresses for the conceptual design is assumed to be 1.5:1.

The maximum allowed rock stress calculated by thermoelastic analyses is assumed to be 200 to 220 megapascals (29,000 to 32,000 pounds per square inch). The maximum basalt design stress was taken as 186 megapascals (27,000 pounds per square inch).

The vertical in situ rock stress is assumed to be 30 megapascals (4,370 pounds per square inch) at the repository horizon. When the horizontal-to-vertical in situ stress ratio is 2:1, the maximum horizontal stress will be 60 megapascals (8,740 pounds per square inch) at the repository horizon. For the analyses, a horizontal stress of 42 megapascals (6,120 pounds per square inch) is assumed, oriented perpendicular to the 60-megapascal (8,740-pound-per-square-inch) stress. The actual directions of the 60- and 42-megapascal (8,740- and 6,120-pound-per-square-inch) horizontal stresses are assumed to be known.

For the 2:1 stress ratio, the repository arrangement is oriented to take advantage of the directional horizontal stress values. As shown in Figure 10-12, the storage holes are parallel to the 60-megapascal (8,740-pound-per-square-inch) stress direction and perpendicular to the 42-megapascal (6,120-pound-per-square-inch) stress direction. The rooms are parallel to the 42-megapascal (6,120-pound-per-square-inch) stress direction and perpendicular to the 60-megapascal (8,740-pound-per-square-inch) stress direction. Using the chosen orientation, the maximum stress occurring at the crown in the placement room is 92 megapascals (13,330 pounds per square inch) and the placement hole stress is 96 megapascals (13,980 pounds per square inch) before any decay heat from emplaced waste is released into the rock. The shape of the placement room was chosen so that the stresses on the room's surfaces would be approximately uniform before any decay heat is released.

Using the orientation described for the 2:1 stress ratio, the following theoretical maximum stresses are obtained:

<u>Waste form</u>	<u>Placement room crown maximum stress, MPa (psi)</u>	<u>Storage hole maximum stress, MPa (psi)</u>
Commercial high-level waste	167 (24,200)	186 (27,000)
Spent fuel (pressurized water reactor)	156 (22,600)	186 (27,000)

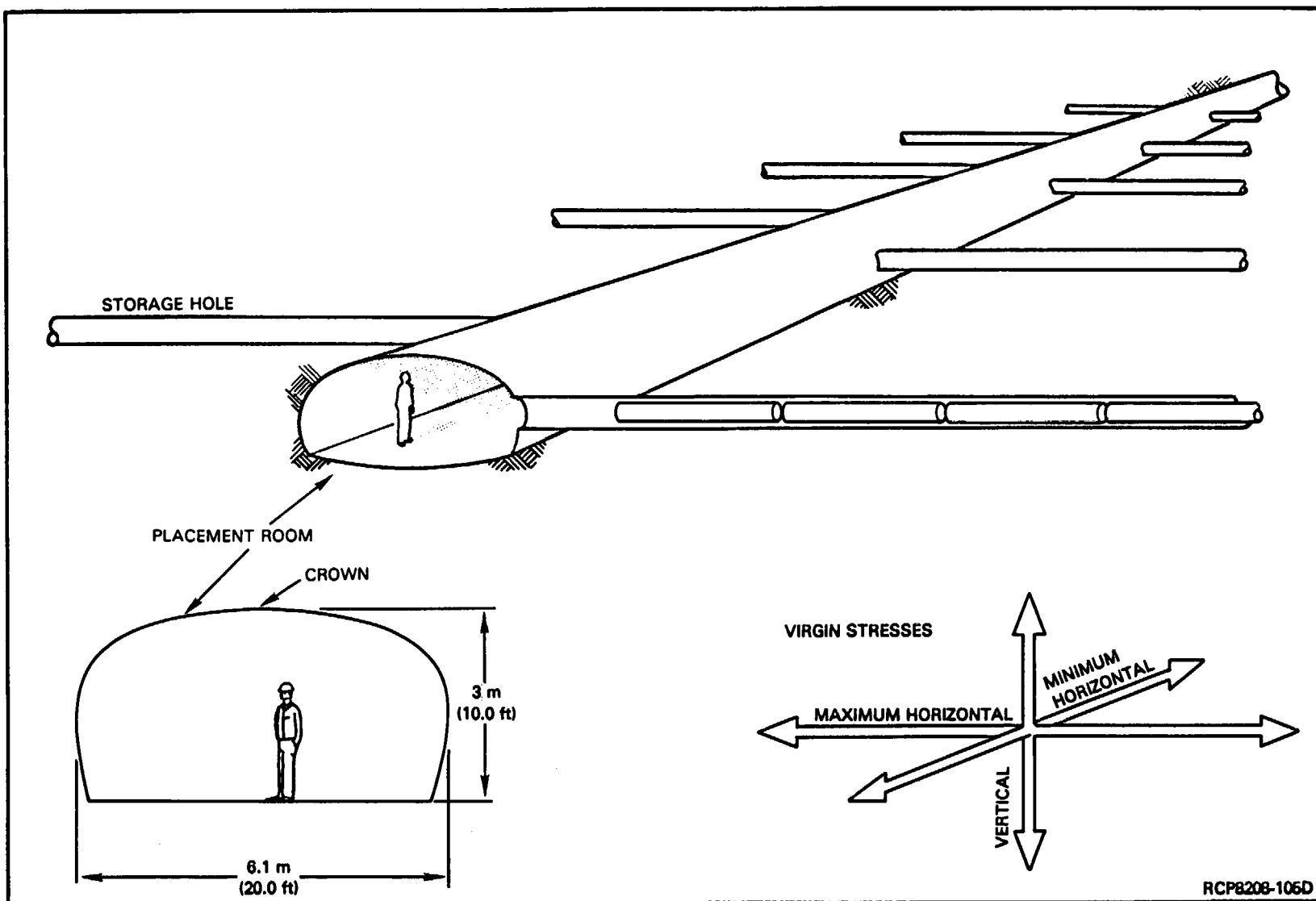


FIGURE 10-12. Orientation of Rock Stresses and Excavations.

As an illustration of theoretical rock stress increase with time, Figure 10-13 shows the time-dependent stress variation for commercial high-level waste. The analytical models used to calculate the rock stress accommodate near-field temperature-dependent properties. However, these temperature-dependent properties do not change appreciably over the calculated temperature range. Investigations are under way to quantify time-dependent near-field phenomena, such as the near-field resaturation rate, that can affect the stress calculations.

10.5.1.2 Alternative Stress Ratio. For a 3:1 stress ratio, the principal horizontal stress at the repository horizon is 90 megapascals (13,100 pounds per square inch) and the horizontal stress perpendicular to the principal stress line is 63 megapascals (9,170 pounds per square inch). Again, the storage holes will be oriented parallel to the principal horizontal stress. Nevertheless, the pitches required to achieve a maximum 186-megapascal (27,000-pound-per-square-inch) stress in the storage hole are appreciably greater for a 3:1 stress ratio than for a 2:1 stress ratio. Further, the placement room cross-sectional shape would have to be changed to a width/height ratio of approximately 3, so that the stresses on the room's surfaces would be approximately uniform before any decay heat is released.

Using the orientation described for the 3:1 stress ratio and the same placement room used for the 2:1 stress ratio, the following maximum stresses are obtained:

<u>Waste form</u>	<u>Pitch, m (ft)</u>	<u>Placement room crown maximum stress, MPa (psi)</u>		<u>Storage hole maximum stress, MPa (psi)</u>	
		MPa	(psi)	MPa	(psi)
Commercial high-level waste	218 (715)	186	(27,000)	166	(24,000)
Spent fuel (pressurized water reactor)	76 (250)	166	(24,000)	172	(25,000)

Using a room with an increased aspect ratio would result in reducing the above pitches for a 3:1 stress ratio.

The change of stress ratio does not directly affect the temperatures. Regardless of stress ratio, the maximum temperatures will be less than those calculated for the conceptual design if the placement pitches are greater than those selected for the conceptual design.

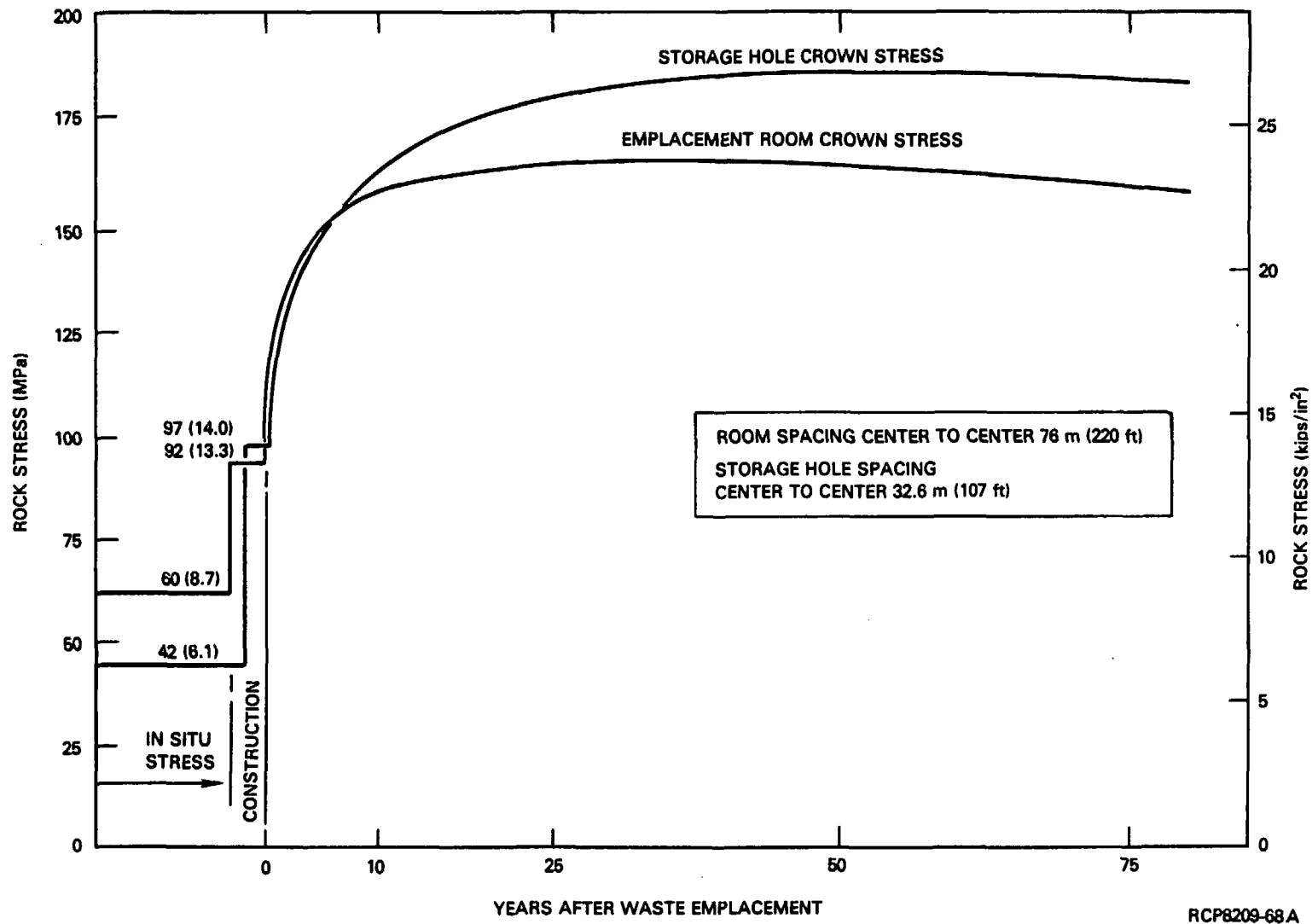


FIGURE 10-13. Maximum Theoretical Thermoelastic Rock Stresses, Variations with Time (2:1 horizontal to vertical stress ratio; commercial high-level waste).

10.5.2 Thermomechanical Considerations

Thermomechanical analyses are required to accomplish the following:

- Ascertain rock support requirements for excavation
- Ensure that temperatures do not exceed prescribed limits
- Evaluate requirements for, and the effects of, ventilation cooling
- Predict stresses and strains around openings that may affect safety or change the permeability of the host rock and assure that stresses do not exceed prescribed limits
- Assess the risk that tensile stresses at a distance may open paths for water ingress or egress
- Assess the risk of rock bursts or induced seismicity that may alter permeabilities
- Determine probable or potential paths of escape for radionuclides and probable radionuclide travel times.

Spacings and positions of waste packages, spacings and layouts of rooms and panels, and shapes and configurations of rooms and other openings are designed and selected to yield temperature and stress conditions that will:

- Inhibit degradation of engineered components, including components of the waste package and construction materials.
- Inhibit degradation of natural materials, including the basalt rock and infillings in joints.
- Not adversely affect the stability of rooms and other openings.

Because of the 57°C ambient rock temperature at the below-ground repository horizon, intake air requires cooling for personnel safety. This cooling is provided, where personnel are working, via fan/coil units served by a chilled water system. This cooling water system is described in Section 10.2.3.3

Each waste storage panel contains the annual commercial high-level waste and spent fuel package receipts shown in Table 10-1. For modeling purposes, the spent fuel package spacing, resulting temperatures, and stresses are based upon the pressurized water reactor waste package.

Table 10-5 shows the maximum temperatures that occur with the selected placement arrangement. If there is no backfill around the commercial high-level waste package, the commercial high-level waste reaches its maximum temperature of 303°C 2.5 years after emplacement.

TABLE 10-5. Thermal and Stress Reference Design Values.

	Commercial high-level waste			Spent fuel		Maximum allowable (BWIP and KE/PB, 1982)
	No backfill	Immediate backfill	Backfill delayed (10 yr)	No backfill	Immediate backfill	
Temperature (°C)						
Center of waste	303	373	348	187	220	500 for commercial high-level waste, 380 for spent fuel
Stainless steel waste can	253	322	308	--	--	430
Carbon steel overpack	240	311	299	186	219	430
Backfill	--	310	298	186	219	300
Basalt at storage hole	224	224	223	174	174	300
Basalt at emplacement room	131	131	131	131	131	300
Basalt at entries	60	60	60	60	60	None given
Stresses, MPa (lb/in ²)						
Storage hole ^a	186 (27,000)			186 (27,000)		186 (27,000) ^b
Crown of room ^a	167 (24,000)			156 (22,600)		186 (27,000) ^b

^a2:1 horizontal-to-vertical stress ratio.^bDeveloped during conceptual design.

Table 10-5 shows also that backfill cannot be placed around the commercial high-level waste package prior to the tenth year of placement without exceeding the backfill temperature limit of 300°C set forth in the functional design criteria (BWIP and KE/PB, 1982).

All operating temperatures for the conceptual design are less than the limits set by the conceptual design criteria, provided 10 years pass before backfilling around the commercial high-level waste package. The thermal characteristics and interactions between the waste package and the repository are identified in Chapter 11.

10.5.3 Rock Support

Theoretical analyses of rock stresses, as well as empirical evidence from other tunnels, suggest that rock support may be needed for stability. It is recognized, however, that the applicability of the theoretical analyses is not well proven and that there is no experience in the construction and support of tunnels in basalt at the depths considered.

Supports are required for purposes other than initial stability. In spite of adequate rock stress, there will be areas of nominal overstress due to variability of the rock strength. The consequence of nominal overstress will be a redistribution of stresses associated with minor motions along rock joints. It is necessary to minimize such motions to preserve the integrity and low permeability of the rock mass. A rock support and reinforcement system will minimize motions along rock joints, both in the initial construction phase and in the subsequent thermal phase.

The proposed rock support scheme includes rock bolts grouted in a regular pattern and the use of shotcrete; these will provide redundancy in the support system, partly overlapping in function and partly acting separately to minimize different types of minor potential rock motion. The differential thermal expansion between shotcrete and the host rock will be evaluated by testing prior to preliminary design.

The location and the methods of installation, nondestructive post-installation testing, and removal of the rock support reinforcement system will be required as input to the detailed design of the repository. The effects of these rock supports on repository sealing and waste isolation will also be evaluated.

10.5.4 Effects of Stratification on Design

The repository would be located within a Grande Ronde Basalt flow. The strength of the rock and its Young's modulus are lower by nearly an order or magnitude near the top of the flow and in the interflow region. This significantly reduces the capability of the rock to transfer shear strains from a flow to the next flow above or below it. Based on analyses assuming a homogeneous rock mass, horizontal compressive stresses induced by waste heat tend to stay within the host flow and not be redistributed

into adjacent flows, thereby increasing the horizontal thermal stresses within the flow beyond what they would be in a homogeneous mass. On the other hand, the horizontal compressive stresses induced in the host flow make it less probable that tensile cracks, which could be deleterious to long-term sealing, would be created some distance above the repository. Also, the thermal gradient in the rock decreases rapidly, and propagation of cracks in the far field is unlikely.

Analyses using tensile crack information to predict far-field migration of radionuclides are in preliminary stages. Refined far-field calculations, based on data obtained from the exploratory shaft program, will resolve present uncertainties.

10.5.5 Effects of Other Waste Receipt Ratios on Design

The rock stresses resulting from the storage of commercial high-level waste approximately equal those resulting from the storage of spent fuel because both have approximately the same kilowatt-per-square-meter initial thermal loading; analogously, the maximum repository temperatures outside the room area are approximately equivalent for storing either high-level or spent fuel waste packages.

Consequently, if the repository is sized to annually store canisters containing a given equivalent metric tons of heavy metal, the repository can also handle any desired mixture of spent fuel and high-level waste canisters. Impacts resulting from simultaneously handling both spent fuel and high-level waste include the biological-shielding differences required for the two waste forms, separately dedicated storage holes for each, and modification of the handling mechanisms to accommodate the differences in waste package dimensions.

10.6 CONSTRUCTION OF ACCESS SHAFTS AND SUBSURFACE FACILITIES

The construction techniques for the shafts and underground openings are described in the following paragraphs.

10.6.1 Access Shafts Construction

A choice of technologies is available for sinking, lining, and sealing large-diameter shafts in basalt. Such technological options include conventional drilling and blasting methods with grouting or freezing in advance of shaft sinking to control groundwater; blind boring; and a selective combination of conventional methods with blind boring in areas prone to heavy groundwater flow. The feasibility of boring large-diameter shafts in basalt is as yet unproven, and will require the development of larger drill rigs and new shaft liner designs. However, blind boring has such overriding potential advantages (e.g., groundwater control, construction safety, isolation enhancement, cost/schedule improvements) over other methods that development is highly desirable.

In Phase I of the exploratory shaft program, a 1.83-meter (6-foot) finished diameter shaft will be sunk by blind boring. The conceptual design for a nuclear waste repository in basalt (currently in design review) is based on sinking five repository shafts, ranging from 3.4 to 4.9 meters (11 to 16 feet) using the combined method; i.e., blind boring through the upper strata and conventionally sinking through the deeper basalt flows.

The final decision on the sinking method for repository shafts has not been reached and will be dependent on: the shaft diameters finally selected for the repository, the depth of the repository horizon, the site-specific geotechnical and hydrological conditions, the results of the exploratory shaft-sinking demonstration, and the developments in the technology for blind boring that could occur over the next several-year period.

10.6.2 Underground Openings Construction

Following completion of the shafts and shaft stations, the geologic repository is developed by excavating outward from the underground shaft stations. The shaft stations open into rooms, haulageways, and airways, within an approximately 195- by 832-meter (640- by 2,730-foot) area, designated as the shaft pillar.

The underground openings will be excavated by either the conventional drilling and blasting techniques or tunnel boring machines. Although the conventional drilling and blasting techniques are standard for the hard-rock mining industry, damage to the tunnel walls has the potential for increasing permeability of the host rock. Controlled-blasting techniques will reduce this effect and the use of tunnel boring machines may be useful to keep the disturbed rock zone to a minimum. Hydraulic fracturing

tests indicate horizontal-to-vertical stress ratios on the order of 2:1, which could affect the mining techniques being considered, influence the size and configuration of tunnels and placement rooms, or change the type of support system being contemplated for the repository.

In the conceptual design, excavation is accomplished by a series of steps: drilling, blasting, mucking, haulage, and ground support. Horizontal storage holes are blind bored and back reamed. Work is carried out utilizing proven technology and equipment.

Drilling in preparation for blasting is done with electric-powered, jumbo-mounted, hydraulic drills. Drill jumbos are phased in as needed to maintain the required rate of advance. Controlled blasting techniques are used to reduce overbreak and minimize deleterious effects to the structural competency of the rock.

Headings are ventilated to remove dust and fumes after blasting, and the broken basalt is watered down to control dust during mucking. The back, ribs, and face are scaled and tested before, during, and after the mucking operation.

Electric-powered, gathering-arm-type loaders are used to load the broken basalt into rubber-tired shuttle cars. The battery/trolley-type, electric-powered shuttle cars transport the basalt to a loading point at a main access way and transfer it into rail haulage cars. An electric-powered, trolley-type locomotive pulls a train of loaded haulage cars to the basalt shaft pocket.

After a heading has been mucked, the back and ribs are again tested, and roof bolts are installed immediately if necessary; otherwise, bolting follows a short distance behind the face advance. As roof bolts are installed, wire mesh is placed to cover the back and rib areas, if required. When the face has advanced a suitable distance, shotcrete is placed to cover the wire mesh to form a smooth lining in the drift. The shotcrete lining aids airflow for ventilation and enhances rock stability in the drift.

Following completion of excavation, roof bolting, and shotcrete lining of a panel (61 meters (200 feet) long), large-diameter holes are bored horizontally between adjacent chambers within the panel. Packages of waste will be stored in these horizontal holes. The horizontal attitude of the waste storage boreholes requires consideration of concepts that are relatively new in large-diameter hole boring, primarily removal of cuttings from the hole. In downward vertical hole boring, cuttings are generally removed by drilling fluids moving in normal or reverse circulation; in upward vertical hole boring (raise boring), cuttings are removed by gravity. Neither method is easily adaptable to horizontal boring. Review and evaluation of recent developments in the art of boring indicate that the most plausible method is to blind bore a relatively small-diameter pilot hole and backream an annulus to the required finished diameter. The smaller diameter pilot hole is expected to produce greater accuracy in drilling than blind boring a full-diameter placement hole. Cuttings from

the pilot hole are removed by compressed air. Cuttings from backreaming are removed by one of three conceptual methods: a swivel and slusher/scrapper arrangement, a sectional auger arrangement, or a vacuum hose arrangement. Each requires that the backreaming bit be fitted with helical blades to push cuttings rearward, away from the cutters, to prevent excessive regrinding and clogging of the bit. Each concept will be evaluated, and the one proven to be most suitable will be developed.

When a panel is completed, the rooms are closed pending their use for waste placement.

10.6.3 Construction Contingency Plans

It is recognized that assumptions concerning geology and other underground parameters contain a measure of uncertainty: in some areas the selected repository horizon may dip, thin, infiltrate water, or otherwise vary in an anomalous manner that precludes development of the symmetrical layout shown in the conceptual design.

The design and construction planning will contain contingency plans for these occurrences. Exploratory drifts and pilot holes in advance of repository excavation are planned to provide early warning of anomalies. It is anticipated that changes to the current design will be required.

10.7 BACKFILL

Backfilling of underground openings and shafts is an integral part of the repository sealing system (discussed in Section 10.8). As such, the performance requirements for backfill material will be determined by seal system performance requirements and seal location. Consideration may also require that some backfill material have certain structural characteristics, that require specific development and testing.

Tailored backfill used as a component of the waste package is discussed in Chapter 11.

10.7.1 Backfill Material

In the conceptual design, reclaimed basalt is conveyed to a crusher for reduction to 6.35 centimeters (2.5 inches); it is then conveyed to surge storage at the materials handling building. Bentonite powder, brought to the site by rail and unloaded into storage at the materials handling building, is batch mixed with bentonite pellets and the 6.35-centimeter (2.5-inch) basalt into a weight hopper that discharges into skip-loading hoppers. Suitable dust control equipment is provided. The room backfill material is lowered down the basalt transport shaft and is discharged to a surge bin that supplies the underground train. The mine rail system will be utilized to haul backfill and the basalt transport shaft will be utilized to lower backfill from the surface.

Backfill materials will be tested under laboratory and in situ conditions to determine mechanical properties, radionuclide sorption and retardation characteristics, compatibility and performance with the host rock and selected seal material, and long-term performance under in situ conditions.

10.7.2 Backfilling Procedure

10.7.2.1 Backfill Preparation and Transport. Backfill material is loaded into skips for transport down the basalt hoisting shaft to the shaft station. The backfill material is discharged from the skip into a pocket and conveyed horizontally to a surge bin located above the mining level.

Backfill will be loaded into mine cars and hauled to the work places via the rail haulage system installed for muck removal. The train moves through air lock doors from the repository exhaust to the repository intake airways. The train then moves to the backfill unloading point in the panel being backfilled where the backfill will be transferred to rubber-tired shuttle cars.

The first step in backfilling a room is to construct a fill fence, or bulkhead, of aluminum on the confinement return side so that fill can be placed against it and not slump over into the return airway. The fence is built up in stages as the room is vertically filled, so that through-ventilation exists for the longest possible time.

Fill is hauled into the room, dumped, and spread by a bulldozer in 0.2-meter (8-inch) lifts. To achieve maximum compaction, each 0.2-meter (8-inch) lift is dampened and compacted mechanically before the next lift is started. This sequence continues, using large equipment, until the fill reaches half the height of the room. Low-profile equipment will then be used to complete the lift to within 1.8 meters (6 feet) of the roof. The final 1.8 meters (6 feet) of space remaining in the room are backfilled, utilizing a yet-to-be-developed piece of equipment. As presently conceived, this equipment is a traveling shield with hydraulic cylinders for jacking against the walls of the room and a hydraulic ram for compacting the fill.

After the fill fence has been built up to the roof, a shield is put in place near the fence, the distance to be derived through operating practice. Backfill, together with a small amount of water, is introduced through a hole in the top of the shield. Dampening of the backfill is needed to prevent the fill from slumping. When the space behind the shield is full, the hydraulic ram on the shield pushes forward to compact the fill. The shield is then retracted and the process is repeated. The work area is ventilated by ducts and portable fans during the final fill phase, since the room is closed off from central ventilation.

The two entry ways into the panels from the main entry passages are backfilled using bucket elevators and hand tools.

The confinement ventilation system provides ventilation for all underground activities related to backfilling. Ventilation air is delivered to the repository through the service shaft by the repository intake supply fans. The repository intake airways will be utilized to carry the supply air to the panel where the backfilling is in progress. Exhaust air is collected through the confinement return airways and exhausted (through high-efficiency particulate air filters) by the confinement exhaust fans. Backfilling of the perimeter confinement return airways is facilitated by utilizing the panel and crosscut adjacent to the confinement return airway as a parallel path for exhaust air.

10.7.3 Effects of Retrievability on Design

The provisions for retrievability presented in the conceptual design are consistent with the following National Waste Terminal Storage Program position (DOE, 1982).

The geologic repository operations area shall be designed, constructed, and operated in a manner that incorporates, as a planned contingency, the ability to retrieve the inventory of wastes. Since the capability to retrieve waste does in fact exist as long as access to the underground facility is maintained, retrievability shall be maintained until a license amendment is granted authorizing full decommissioning and sealing of the repository. This will occur subsequent to the performance confirmation program for the repository, as defined in the license review process and by 10 CFR 60 (NRC, 1981), being satisfactorily completed.

Retrieval shall be initiated in the event of failure of the system for geologic disposal to meet established public health and safety performance objectives. A reasonable schedule for retrieval is one that takes about the same overall period of time as was devoted to the construction of the geologic repository operations area and to the emplacement of wastes, although slower-paced retrieval consistent with public health and safety may be entirely acceptable.

Results from the performance confirmation program of the repository govern retrieval requirements. In particular, results from approximately the first 5 years of repository operation (initial verification period) will be used to decide whether or not to shift from a readily retrievable emplacement configuration to a backfilled (yet still retrievable) configuration. This decision, made at the end of the initial verification period of the performance confirmation program, will be based on results obtained from monitoring of emplacement areas, from dedicated experimental areas, and from geologic mapping of open areas, and on a consideration of the degree of confidence in the necessity for future retrieval.

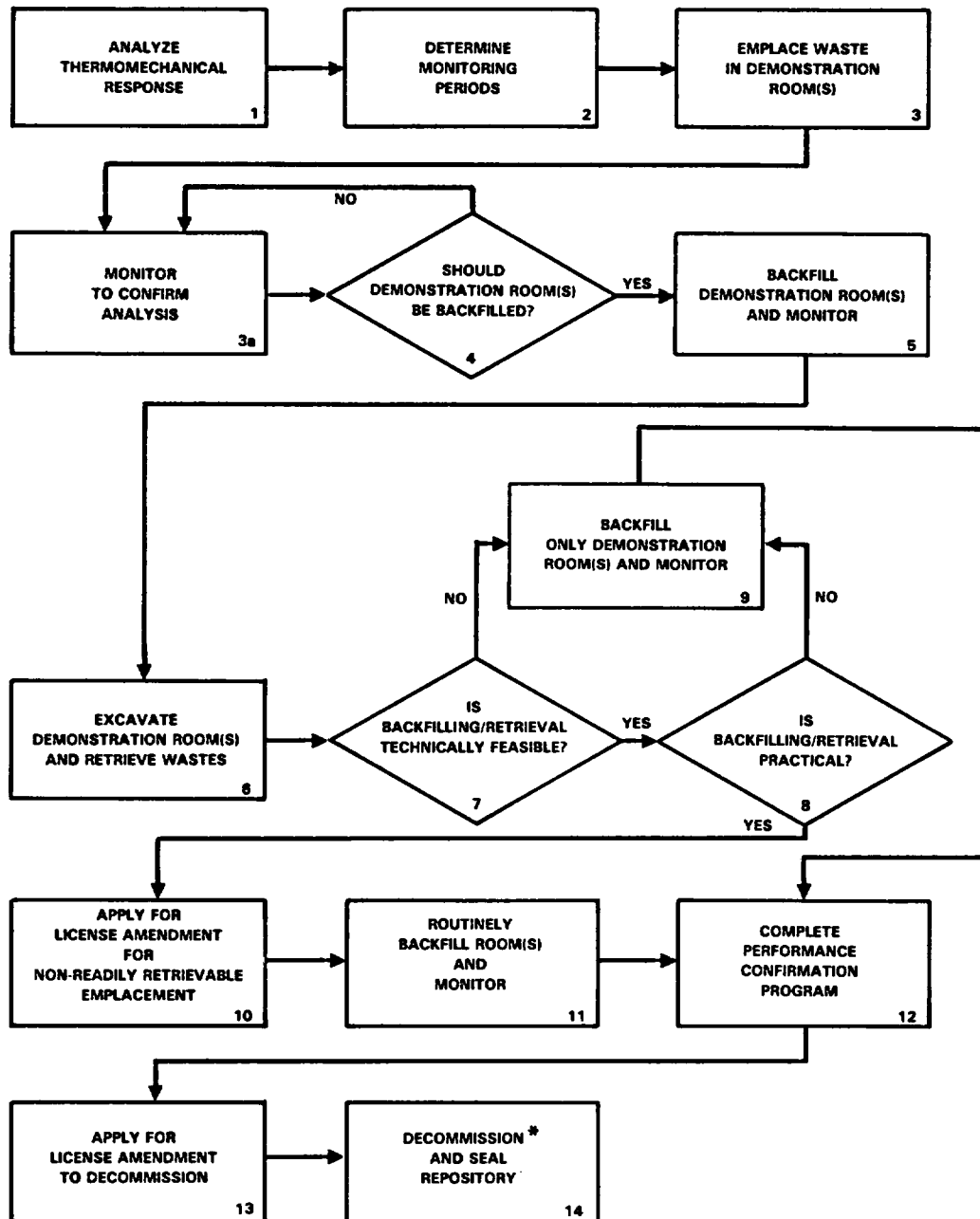
The approach that will be followed to resolve questions regarding backfilling and retrievability is shown in the decision flowchart (Fig. 10-14).

The requirement for the proposed 10 CFR 60 (NRC, 1981) 50-year retrievability period (beginning with emplacement of the first waste package) has an impact when backfill will be placed.

The conceptual design assumed "deferred backfilling." Each waste storage panel is bulkheaded off after it is filled and "trickle" ventilation is maintained through the rooms to remove excess humidity and preclude buildup of potentially dangerous gases. Backfilling would start at the end of the 50-year retrievability period. If backfilling did start at an earlier date, it would still be feasible to retrieve waste. The backfill would have to be cooled, removed, and replaced at a later date.

The temperature rises expected are shown in Table 10-5. Results of tests conducted in basalt at the Near-Surface Test Facility revealed that deformation or instability of emplacement holes at elevated temperatures (approximately 400°C) was insignificant. Additional tests to determine room stability are planned during Phase II of the exploratory shaft program. Stability of underground openings is of prime concern from a safety standpoint and will be thoroughly evaluated when actual in situ stress measurements are available.

Prior to retrieval (if required) or backfilling, precooling of emplacement rooms that have been closed off for 50 years will be accomplished by placing movable cooling air handling units near the emplacement entrance and lowering the air temperatures to approximately 27°C. Wall temperatures will be reduced to approximately 52°C during this period of retrieval or backfilling. It is estimated that it will take 90 days to cool the hottest room before personnel can enter.



* STEP 14 WOULD INCLUDE BACKFILLING OF EMPLACEMENT ROOMS IF THIS WERE NOT DONE ROUTINELY DURING EMPLACEMENT OPERATIONS (STEP 11).

RCP8209-163

FIGURE 10-14. Backfill/Retrievability Decision Flowchart.

Only one waste storage panel will be retrieved (if necessary) or backfilled at a time and the ventilation system is designed to accommodate that requirement. It is estimated that 5,140 cubic meters per minute (182,000 cubic feet per minute) of ventilation air will be required for waste retrieval. Of this, 708 cubic meters per minute (2,500 cubic feet per minute) are used for ventilating the waste handling area, 3,840 cubic meters per minute (136,000 cubic feet per minute) are required to precool a room prior to retrieval (90 days), and the remainder is used to maintain ventilation for operating the transporter during retrieval.

10.8 SEALING OF SHAFTS, BOREHOLES, AND UNDERGROUND OPENINGS

The isolation of nuclear wastes in deep, mined repositories will require the sealing of all penetrations, such as shafts, tunnels, repository rooms or boreholes, into and nearby the repository. A research and development program is on-going to develop and demonstrate required technology for sealing penetrations related to a repository excavated in basalt.

Current efforts have concentrated on establishing performance requirements and design criteria for a seal system. To accomplish this objective, the repository seal system is considered as one component of the multiple barriers concept for waste isolation. Previous studies have shown the site (geologic setting) to be the most dominant barrier for isolation of nuclear waste. Figure 10-15 illustrates how various isolation components (engineered and geologic) contribute to the control of radionuclide releases.

It is important to consider the performance of the site in establishing the minimum performance required of the seal system. Additionally, the required performance of the seal system depends on the performance of the waste package. During the waste package containment period, requirements on the seal system for the isolation of radionuclides are minimal as long as the waste package maintains its integrity. During the postcontainment period, while the waste package functions to provide the slow release of radionuclides, the required performance of the seal system is dependent on the release rate from the waste package and the contribution of the site to provide isolation of the radionuclides.

In assessing the required performance of the repository seal system, the following expression can be written:

$$\begin{array}{l} \text{Required performance of} \\ \text{seal system} \end{array} = \begin{array}{l} \text{Function of regulatory criteria,} \\ \text{site, and waste package performance} \end{array} \quad (10-1)$$

Application of Equation 10-1 to the derivation of seal system performance requirements implies that the regulatory criteria be applicable to the overall isolation system. In U.S. Environmental Protection Agency draft regulations (EPA, 1981), acceptable releases to the accessible environment may be met by a combination of site and engineered barrier performance. The U.S. Nuclear Regulatory Commission proposed technical criteria (NRC, 1981) have a similar flexibility for the underground facility engineered barriers (e.g., room and tunnel backfill barriers), but not for the criteria applicable to the shaft and borehole seals. For the sake of demonstration, the repository seal system is treated as one component

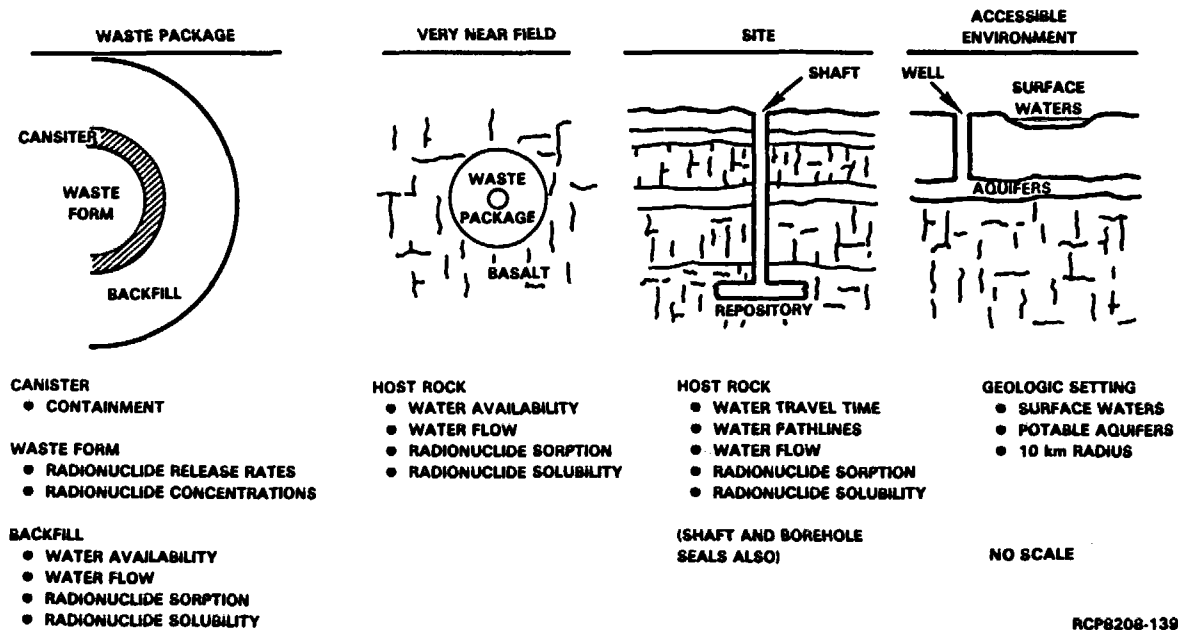


FIGURE 10-15. Role of Various Isolation Components and Their Contribution to the Control of Radionuclide Releases.

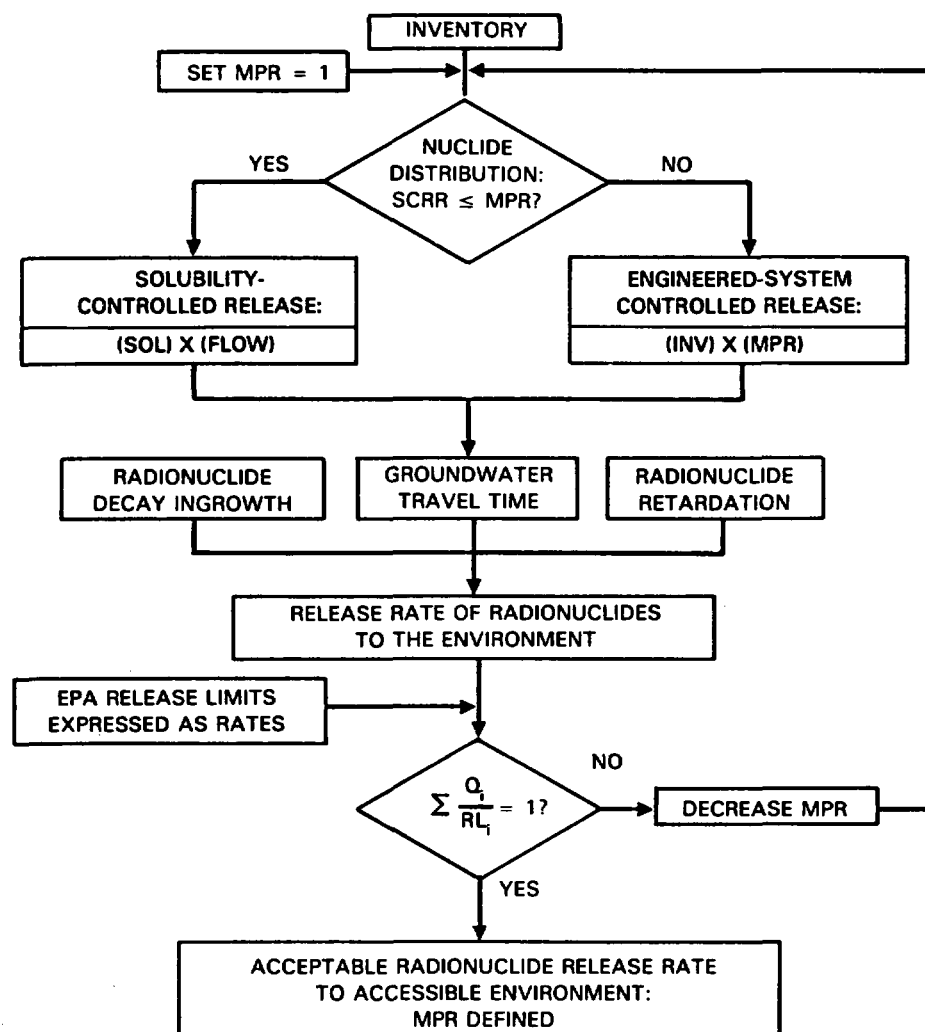
of the overall isolation system. In this manner, performance requirements for the seal system may be derived based on Equation 10-1 and used for two purposes:

- (1) To establish preliminary design criteria
- (2) To provide a useful comparison of the required performance for the seal system with the current U.S. Nuclear Regulatory Commission proposed technical criteria for the seal system.

Establishing performance requirements for the seal system requires defining releases to the accessible environment based on the performance parameters listed in Figure 10-16. The cumulative release can be defined by considering the two controls on radionuclide releases from the engineered system (near-field solubility controls and waste package release rates) and the decay and in-growth of these initial releases. Radionuclide releases to the accessible environment can then be calculated for these initial releases as a function of water flow rate through the repository, water travel time to the accessible environment, and containment time.

Figure 10-16 also illustrates the calculation process that has been developed. A computer program, RAFSCATT (Release Rate as a Function of Solubility, Containment, and Radionuclide Travel Time) has been prepared to calculate maximum permissible release rate. In this manner, the maximum permissible release rate from the waste package can be calculated for a given combination of containment time, water travel time to the accessible environment, and water flow rate through the repository. A more detailed evaluation of this relationship is being studied to develop a basis for both waste package and repository seal performance requirements. As an example, although the U.S. Nuclear Regulatory Commission proposed technical criteria (NRC, 1981) are not finalized, by assuming that the waste package will meet the proposed release rate criteria, a series of acceptable flow rate and travel time combinations can be defined for the site and repository seal system. By apportioning performance between the site and the seal system, maximum flow rates and minimum travel times through the seal system can be determined.

Generic seal studies conducted by the National Waste Terminal Storage Program have also revealed (Kelsall et al., 1982) that areas around underground openings and shafts are disturbed by excavation and stress relieving. The disturbed rock zone may provide a preferential pathway for groundwater flow and radionuclide migration. The effect of the disturbed rock zone on repository seal performance will be initially assessed by sensitivity analysis. The results of these studies may determine that a preferred method should be used in underground opening and shaft construction, or that sealing areas affected by disturbance is required.



LEGEND:

EPA = U.S ENVIRONMENTAL
PROTECTION AGENCY
INV = INVENTORY
MPR = MAXIMUM PERMISSIBLE
RELEASE RATE
SCRR = SOLUBILITY-CONTROLLED
RELEASE RATE
SOL = SOLUBILITY

$$\sum \frac{Q_i}{RL_i} \leq 1$$

WHERE

Q_i = CUMULATIVE RELEASE
OF RADIONUCLIDE i

RL_i = EPA RELEASE LIMIT
FOR RADIONUCLIDE i

RCP8208-141A

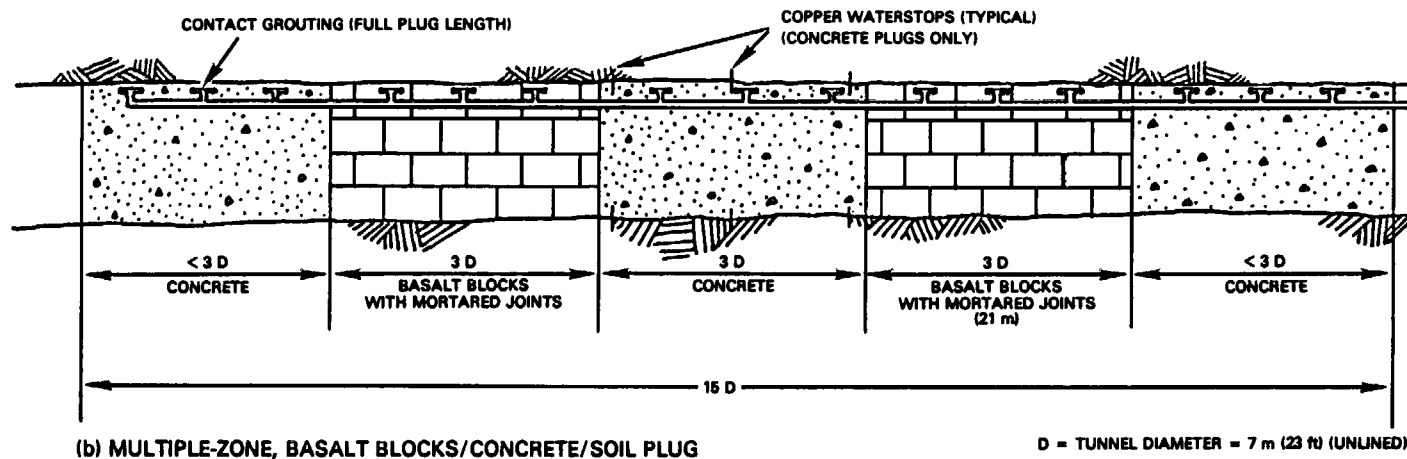
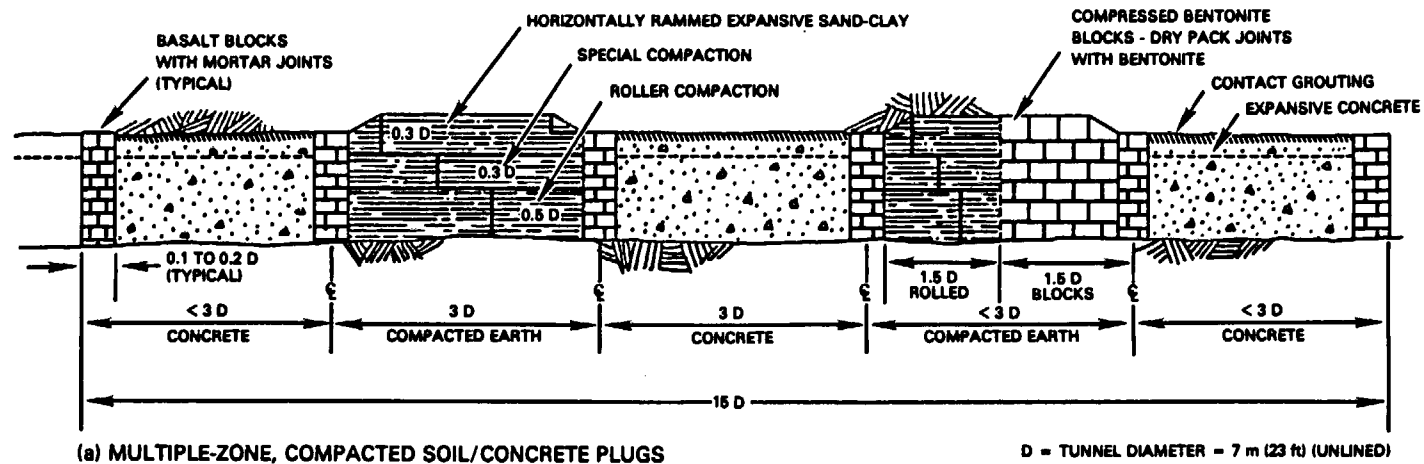
FIGURE 10-16. Determination of Maximum Permissible Release.

10.8.1 Seal Design

A number of schematic designs (Smith et al., 1980) for sealing shafts and underground openings have been generated by the generic National Waste Terminal Storage Seal Program. These designs (Fig. 10-17 and 10-18) will be evaluated and conceptual designs prepared for specific seals (tunnel, shaft, and boreholes). Seal materials will also be developed and screened for site-specific conditions and long-term compatibility with the basalt host rock. These materials will be tested under laboratory conditions simulating the in situ conditions anticipated at the repository horizon. Emplacement techniques will also be developed and demonstrated in large-scale field tests as needed.

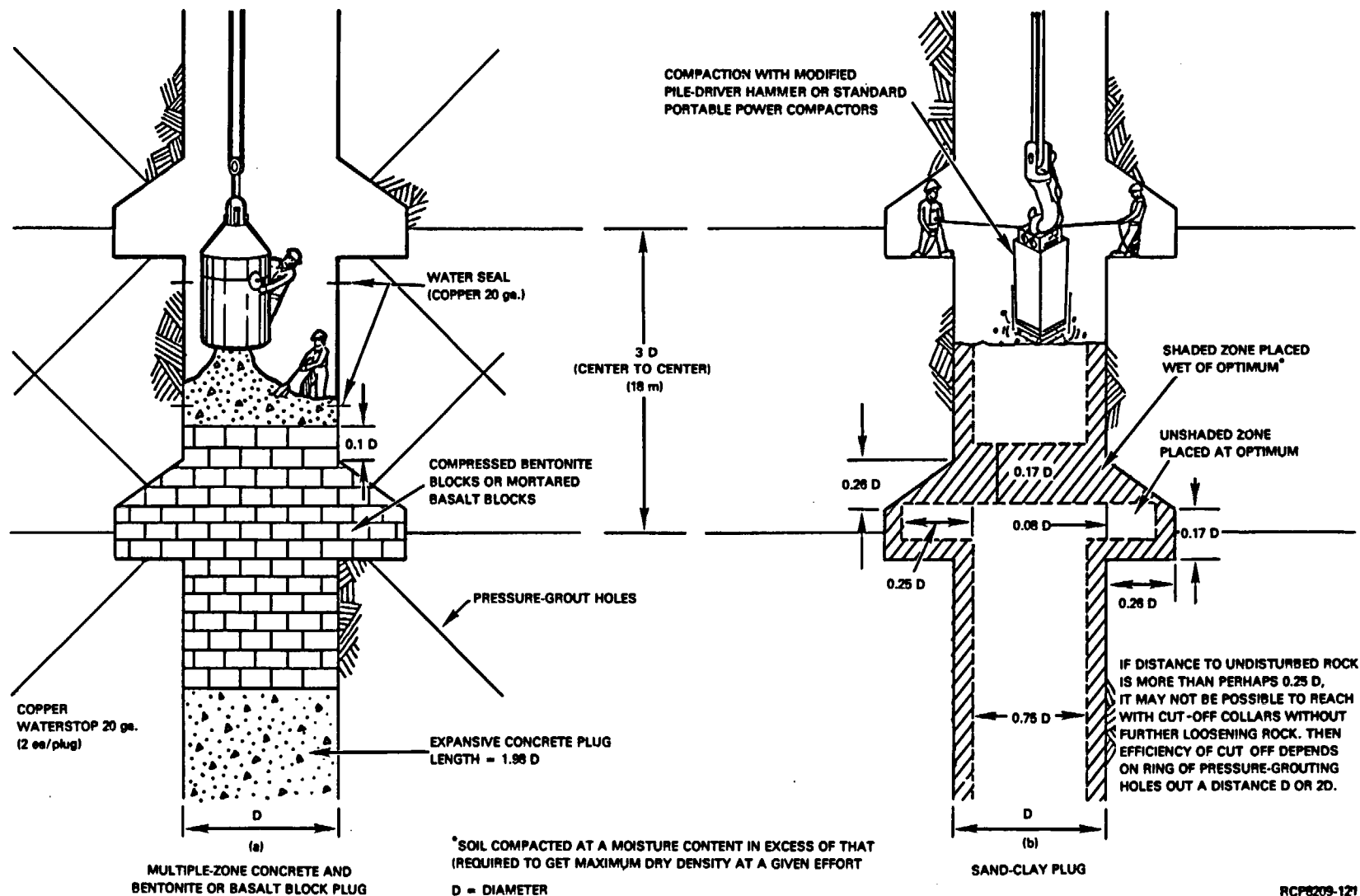
At the time of decommissioning, seals will be installed in optimized locations throughout the repository and in shafts above the repository. Certain structural details such as shaft cut-off collars (as shown in Fig. 10-18) may be necessary as groundwater and structural barriers during decommissioning when sections of the shaft liners are removed. They may also be required to reduce the area of disturbed rock zone if analysis shows that a pathway for radionuclide migration exists.

Any small-diameter boreholes in the vicinity of the repository will also be sealed prior to or at decommissioning.



RCP8208-120

FIGURE 10-17. Multiple-Zoned Plugs for Tunnels.



RCP8209-121

FIGURE 10-14b. Detail of Shaft Cut-Off Collar.

10.9 UNRESOLVED REPOSITORY ISSUES

A comprehensive review of the repository design activity has identified several issues that need resolution to complete the development of a nuclear waste repository in basalt. These issues and the plans for their resolution are presented in Chapter 14.

10.10 REFERENCES

ACGIH, 1980, Threshold Limit Values for Chemical Substances in Working Air, adopted by the American Conference of Government Industrial Hygienists, p. 59, Table 1.

BWIP and KE/PB, 1982, Nuclear Waste Repository in Basalt, Project B-301, Functional Design Criteria, RHO-BW-DC-1 P, Staff, Basalt Waste Isolation Project and KE/PB, A Joint Venture of Kaiser Engineers, Inc. and Parsons Brinckerhoff Quade & Douglas, Inc. for Rockwell Hanford Operations, Richland, Washington, March 1982.

DOE, 1982, NWTS Baseline Document, NWTS Program Position on Retrievability, OWI/NB-5, Office of Waste Isolation, National Waste Terminal Storage Program, U.S. Department of Energy, Washington, D.C., May 1982.

EPA, 1981, Working Draft No. 20, Environmental Protection Agency, 40 CFR 191, Environmental Standards and Federal Radiation Protection Guidance for Management and Disposal of Spent Nuclear Fuel, High-Level and Transuranic Radioactive Wastes, U.S. Environmental Protection Agency, Washington, D.C.

KE, 1978, Conceptual Design Report, A National Waste Terminal Storage Repository in a Bedded Salt Formation for Spent Unreprocessed Fuel, Volume II, 78-57-RE, Kaiser Engineers, Oakland, California, December 1978.

KE/PB, 1982, Engineering Study, Nuclear Waste Repository in Basalt, Project B-301, RHO-BWI-C-116, Volumes I and II, A Joint Venture of Kaiser Engineers, Inc. and Parsons Brinckerhoff Quade & Douglas, Inc. for Rockwell Hanford Operations, Richland, Washington, March 1982.

Kelsall, P. C., Case, J. B., and Chabannes, C. R., 1982, Topical Report, A Preliminary Evaluation of the Rock Mass Disturbance Resulting from Shaft, Tunnel, or Borehole Excavation, D'Appolonia Consulting Engineers, Inc. for Battelle Memorial Institute, Project Management Division, Office of Nuclear Waste Isolation, Columbus, Ohio, July 22, 1982.

NRC, 1979, Standards for Protection Against Radiation, Title 10, Code of Federal Regulations-Energy, Part 20, U.S. Nuclear Regulatory Commission, Washington, D.C., June 15, 1979.

NRC, 1981, "Nuclear Regulatory Commission, 10 CFR 60, Disposal of High-Level Radioactive Wastes in Geologic Repositories," Federal Register, Vol. 46, No. 130, July 8, 1981, Proposed Rules.

Smith, M. J., Anttonen, G. J., Barney, G. S., Coons, W. E., Hodges, F. N., Johnston, R. G., Kaser, J. D., Manabe, R. M., McCarel, S. C., Moore, E. L., Noonan, A. F., O'Rourke, J. E., Schulz, W. W., Taylor, C. L., Wood, B. J., and Wood, M. I., 1980, Engineered Barrier Development for a Nuclear Waste Repository Located in Basalt: An Integration of Current Knowledge, RHO-BWI-ST-7, Rockwell Hanford Operations, Richland, Washington, May 1980.

Staff, 1980, Nuclear Waste Repository in Basalt, Project B-301, Preconceptual Design Report, RHO-BWI-CD-35, Rockwell Hanford Operations, Richland, Washington, February 1980.

11. WASTE PACKAGE

The original philosophy behind geologic disposal of high-level nuclear waste placed great emphasis on the host rock acting as the primary barrier for the containment of radionuclides. Recognizing the complexity of fully predicting the long-term performance of geologic formations as barriers to radionuclide migration, the United States has (since 1977) adopted a multiple-barrier waste package approach to high-level waste disposal. This approach involves the concept of multiple engineered barriers (i.e., waste form, canister, buffer, overpack, backfill, etc.), "as a defense in depth," acting in concert with the natural barriers (geologic strata, distance to biosphere, etc.) to prevent the unacceptable release of radionuclides and hazardous nonradioactive materials to the biosphere. The U.S. Department of Energy (DOE) approach to multiple barriers has been clearly stated in the Interagency Review Group report (IRG, 1979) and the DOE position statement in the U.S. Nuclear Regulatory Commission (NRC) confidence rulemaking (DOE, 1980d). Proposed criteria for waste package design and performance are described in NRC (1981), U.S. Environmental Protection Agency (EPA) (1981), and NWTs (1981b).

Before the satisfactory performance of a nuclear waste repository can be assured, the geochemical processes affecting that performance must be thoroughly understood. The performance assessment must be based on the ability of the waste package and geologic medium to provide initial containment and subsequent retardation of radionuclide transport (NRC, 1981). The present NRC proposed performance requirements (see Chapter 15 for specific wording of these criteria) mandate that waste be contained within the engineered system for 1,000 years and that release thereafter be constrained to 1 part in 100,000 of the maximum amount of each radionuclide calculated to be present in the underground facility. Because of this there is a need for better site-specific geochemical knowledge concerning the interaction of the waste package (including the waste form) with the repository environment. It is, therefore, important that effective waste packages for emplacement in basalt be designed taking geochemistry, particularly the hydrothermal chemistry in the near field, into consideration. Waste package design must be concerned with heat-transfer characteristics of the geologic medium and waste package components as well as the structural behavior and corrosion characteristics of package materials, which are affected by the geochemical and geophysical characteristics of the site. This position has received strong support from several sources (NAS, 1979; NRC, 1981; DOE, 1980a; 1980b; DOE/USGS, 1980; NWTs, 1981a; 1981b), among which a clear case is made for pursuing media-specific geochemical studies. A strong program to obtain information required for waste package design has been described by the Office of NWTs Integration (NWTs, 1981c). The U.S. Geological Survey (Smedes, 1980) has stated that:

"Inasmuch as the most probable medium for transporting the waste to the biosphere is water, the prime criterion for isolation becomes a hydrologic one. Specifically, the net effect of (1) the rate of entry of

"groundwater into the repository site, (2) the rate of corrosion of the canister, (3) the rate of dissolution of the contained radionuclides by groundwater, and (4) the rate of flow of those nuclides in the groundwater must be sufficiently slow and the flow path sufficiently long so that those nuclides will not reach the biosphere until they have diminished to safe levels. This prime criterion is the same regardless of the specific host rock. However, fundamental differences in the physical and chemical conditions and properties of various rock types and the regional terrains in which they occur affect the above rates in widely and media-specific different ways."

The U.S. Geological Survey approach to waste isolation focuses on waste package design and performance as well as engineered barrier issues. These include:

- Designing a corrosion-resistant canister
- Providing a waste form that is insoluble in the repository environment
- Defining backfills and borehole plugs that create a tight hydraulic seal
- Developing a waste package backfill and buffer that is highly sorptive of specific nuclides in the waste
- Assuring predictable interaction of waste form, barriers, and water-saturated host rock (hydrothermal testing).

The Basalt Waste Isolation Project (BWIP) has initiated a waste package program that is strongly based on hydrothermal testing. The program encompasses the issues defined by Smedes (1980) with the exception of the second bullet. The BWIP in concert with the remainder of the National Waste Terminal Storage (NWTs) Program is developing site-specific waste packages for spent fuel and candidate commercial and defense high-level waste forms.

The approach that the BWIP is taking to develop the data and information necessary for the preparation of site-specific waste package designs is described in Sections 11.3 and 15.4. The program relies heavily on close, frequent communication between experienced modelers, design engineers, geochemists, and materials scientists to incorporate laboratory and engineering data into the design and performance models. In this approach, the main driving forces behind the waste package program are scheduling requirements and the need for design and predictive modeling in waste package development, as described in Chapter 12. The modeling is based on laboratory and field test data and is used to give assurances of effective, long-term performance by the repository system. This approach ultimately results in a highly directed program geared toward providing the information necessary to qualify a waste disposal system constructed in basalt for licensing in a timely manner.

The physical and chemical properties of the reference waste forms, spent fuel (if declared as waste) and reprocessed high-level waste, together with their strengths and weaknesses, are reviewed in Section 11.1. The BWIP waste package design concepts and status of the research and development program are reviewed in Sections 11.2 and 11.3, respectively. The repository conceptual design (Chapter 10, Section 10.1) is based on storing a limited number of drums of solidified commercial low-level transuranic waste. The requirement for inclusion of transuranic wastes in a nuclear waste repository in basalt is under DOE-Headquarters review at this time. To date, the basalt project has done no specific research and development work on transuranic wastes. The environmental conditions expected in a repository in basalt that affect the design and performance of waste packages are discussed in Section 11.4. The remaining sections include a review of alternate waste packages (Section 11.5), the summary and conclusions to Chapter 11 (Section 11.6), a summary of unresolved issues (Section 11.7), and references (Section 11.8). The geochemistry of the waste package and near field of the repository has also been reviewed in Chapter 6. Plans for the resolution of unresolved waste package issues are described in Chapter 15.

11.1 WASTE FORMS

The physical and chemical properties of the waste form, the other components of the waste package (e.g., canister, backfill, etc.), and of the repository rock will basically determine the design of the waste packages required to prevent release of unacceptable amounts of radionuclides to the accessible environment. Accurate, detailed characterization of the waste forms and their interactions with other package components and with the natural geologic materials of the repository are necessary for the design and development of effective waste packages for emplacement in basalt.

High-level waste forms are typically defined as solids in which the radioactive by-products of power generation, both fission products and irradiated material, are immobilized. The current reference candidate for commercial high-level waste forms for use in waste package design is a borosilicate glass. An alternate candidate waste form is the spent fuel pins themselves if declared waste. Pacific Northwest Laboratory (PNL) has been assigned by the DOE the responsibility of optimizing the composition of the borosilicate glass proposed as a waste form for commercial high-level waste. This program is scheduled to begin in fiscal year 1983. The current reference waste form for defense high-level waste is a borosilicate glass, for which Savannah River Laboratory, Aiken, South Carolina has the lead responsibility.

In this section, the physical and chemical properties of the reference candidate high-level waste forms for commercial and defense high-level waste and spent fuel are discussed. The discussion is focused on those properties and characteristics of waste forms that are considered most relevant to design and performance questions pertaining to waste disposal in a repository in basalt.

11.1.1 Reprocessed High-Level Waste (Borosilicate Glass)

Over the last 20 years, glass has probably received more study as a potential form for high-level waste immobilization than all other waste forms combined (Mendel, 1978). The concept has attracted much attention, due to its relative engineering simplicity, low cost, and acceptable performance. Among the positive attributes of glass as a waste form are its ability to incorporate a wide variety of elements in the glass-forming network, its monolithic form when poured and cast, and its physical strength and resistance to leaching in most of the expected repository environments, including basalt (Mendel, 1978). A glass waste form is also likely to be insensitive to many of the fluctuations in waste stream composition that will occur in a reprocessing plant. In addition, the stability of glass is not greatly affected by radiation damage as are some crystal structures.

Radwaste glass-melting operations are perceived as either a two-step or a one-step operation. For the two-step operation, the liquid waste from spent fuel reprocessing is further processed to produce a product (powder or granules), called calcine, either by spray or by fluidized bed calcination (evaporation) techniques to drive off water and nitrates. The calcine is blended with a glass-forming material (frit) and is melted. The melter may be either an in-can type, in which the canister itself is the melt container, or a continuous melter whose contents are periodically emptied into a canister. For the one-step operation, the properly mixed liquid waste stream may also be added directly to some melters. Drying, denitration, and glass-melt formation occur simultaneously in such a device. Another waste form configuration option is to produce small glass spheres by methods such as dropping beads of molten glass into a marble-making machine.

11.1.1.1 High-Level Waste Streams. The waste stream materials resulting from the reprocessing of commercial nuclear reactor fuel pins are a key component of the feedstock used in producing a solid waste form for use in geologic disposal. The composition of the specific waste stream significantly influences the recipe for additives and waste-form-matrix materials that are needed to produce the final waste form (e.g., a waste-loaded borosilicate glass).

Prototypic waste processing methods have been designed to use the calcined waste stream material in the processes to produce waste forms like glass (McCarthy, 1977a; Mendel, 1978). Most of this development work on waste-glass forms has been focused on waste stream calcine compositions from among six calcine compositions (PW-4b, -7, -7a, -7c, -8a, -9) that have been documented for a PUREX-type process (Cleveland, 1970) when used in spent fuel reprocessing. The compositions of these waste streams are listed in Table 11-1.

The PW-4b high-level waste formulation corresponds to waste from an optimized reprocessing plant operation, in which little uranium or plutonium is lost to the waste stream (Mendel et al., 1977). It is also low in inerts or reprocessing chemicals. Waste PW-4b is a low-sodium waste (McCarthy, 1977a). Researchers at PNL (Mendel et al., 1977) consider this waste stream representative of that proposed for General Electric Company's Midwest Fuel Recycle Plant and a suitable substitute for high-level waste that may be generated by a fuels reprocessing plant, such as that proposed by Exxon Corporation. At present, there is no commercial reprocessing of power reactor fuels under way in the United States.

The PW-7a waste is similar to that which was planned for the Allied General Nuclear Service plant in Barnwell, South Carolina. This waste is a combination of high-level waste with added intermediate-level waste, which is responsible for the high sodium and phosphorus content. Excess gadolinium has been added to this waste stream as a neutron absorber for criticality control. The uranium and plutonium contents of this waste are higher than those in PW-4b, due to lower projected separation efficiencies (99.0 versus 99.9 percent). The PW-7 composition is a low-sodium version of PW-7a.

TABLE 11-1. Reference High-Level Waste Solids (Calcine)
Compositions (after McElroy, 1975; Ross et al., 1978).

Waste composition	wt% oxides					
	PW-4b	PW-7	PW-7a	PW-7c	PW-8a	PW-9
Inerts						
Na ₂ O	--	0.18	9.06	9.50	15.08	10.12
Fe ₂ O ₃	3.70	4.62	3.98	3.63	29.21	2.61
Cr ₂ O ₃	0.84	0.53	0.45	0.05	1.24	0.60
NiO	0.35	0.22	0.19	0.02	0.61	0.24
P ₂ O ₅	1.65	4.10	8.36	7.03	1.44	1.16
MnO ₂	--	--	--	0.32	--	--
Gd ₂ O ₃	--	15.83	13.65	30.71	--	--
ZrII Fine (ZrO ₂)	--	--	--	0.40	--	--
Fission Products						
Rb ₂ O	0.87	0.54	0.47	0.33	0.38	0.73
SrO	2.59	1.62	1.40	0.86	1.14	2.10
Y ₂ O ₃	1.46	0.91	0.79	0.52	0.64	1.18
ZrO ₂	12.11	7.55	6.52	4.50	5.31	9.66
MoO ₃	12.67	7.91	6.82	4.69	5.55	10.34
Tc ₂ O ₇	3.16	1.97	1.70	1.24	1.39	2.31
RuO ₂	7.28	4.54	3.92	2.57	3.19	6.43
Rh ₂ O ₃	1.17	0.73	0.63	0.48	0.52	0.91
PdO	3.63	2.27	1.95	1.47	1.59	3.44
Ag ₂ O	0.22	0.13	0.12	0.07	0.09	0.14
CdO	0.24	0.15	0.13	0.08	0.10	0.24
TeO ₂	1.78	1.11	0.96	0.65	0.78	1.46
Cs ₂ O	7.05	4.40	3.80	2.37	3.09	5.80
BaO	3.84	2.39	2.07	1.64	1.68	3.31
La ₂ O ₃	3.62	2.26	1.95	1.34	1.59	3.09
CeO ₂	8.14	5.08	4.38	2.73	3.57	6.97
Pr ₆ O ₁₁	3.63	2.26	1.95	1.30	1.59	3.12
Nd ₂ O ₃	11.07	6.91	5.96	4.31	4.85	9.45
Pm ₂ O ₃	0.30	0.19	0.16	0.03	0.13	0.26
Sm ₂ O ₃	2.26	1.41	1.22	0.98	0.99	1.94
Eu ₂ O ₃	0.49	0.31	0.26	0.17	0.21	0.42
Gd ₂ O ₃	0.34	0.21	0.18	0.10	0.15	0.29
Actinides						
U ₃ O ₈	2.86	17.86	15.40	15.37	12.54	9.72
NpO ₂	2.12	1.32	1.14	0.20	0.93	1.21
PuO ₂	0.02	0.16	0.14	0.15	0.19	0.14
Am ₂ O ₃	0.44	0.28	0.24	0.17	0.19	0.44
Cm ₂ O ₃	0.10	0.06	0.05	0.01	0.04	0.17
Total	100.01	100.01	100.02	99.99	100.00	100.00

PW-7c is an updated PW-7a waste that reflects changes in criticality control, expected burnup, and mixing ratios of high-level and intermediate-level waste (Ross et al., 1978). The PW-7c composition represents waste from the early years of reactor operation in which fuel burnup, and thus the fission product content, is lower. The shearing operation in the fuel-chop-and-leach process adds the zirconium fines to the waste stream. An increased intermediate-level waste content raises the Na_2O and U_3O_8 concentrations over those in PW-7a and provides the source of MnO_2 .

The PW-8a waste is typical of the high-level waste currently stored at Nuclear Fuel Services, West Valley, New York (McCarthy, 1977a). It is also a dirty or high-sodium waste resulting from combined high-level/intermediate-level waste streams. Excess iron in PW-8a, which was dissolved along with the fuel, results from thin, mild-steel basket liners used in the chopped-fuel transfer process (Mendel et al., 1977).

The PW-9 waste is a relatively clean waste with moderate sodium and uranium concentrations. The PW-9 waste is calculated for a burnup of 40,000 megawatt days per metric ton of heavy metal.

These waste compositions may be expected to vary somewhat from the typical values given in Table 11-1. The fission-product content, which is based on an assumed burnup of 33,000 megawatt days per metric ton of heavy metal, except PW-9, will vary as a function of actual fuel burnup. Start-up and shutdown of reprocessing plants for inspection, maintenance, and material accountability inventories will generate larger volumes of intermediate-level waste. Changes in the types and amounts of reprocessing chemicals will also influence the composition of the waste stream to varying degrees. Waste compositions that account for such changes have been defined by McElroy (1974a; 1974b; 1975; 1976).

A number of other possible waste streams may become important if commercial nuclear fuel reprocessing occurs in the United States. Such wastes could include the THOREX wastes from the reprocessing of uranium-thoria fuels and wastes from UO_2 - PuO_2 fast breeder reactor fuels. The fission-product spectra of such fuels differ somewhat from that of UO_2 light water reactor fuel due both to plutonium or thorium fission products and different burnups of 50,000 megawatt days per metric ton of heavy metal. Comparatively little research has been conducted on waste forms for high-level waste streams from these options.

11.1.1.2 The Chemistry of Waste-Glass Formulations. A large number of glass formulations have been developed and tested for various waste streams both in the United States and abroad. The formulations have included phosphate, borosilicate, and aluminosilicate glasses, as well as partially vitrified glass ceramics. The radioactive waste glasses that have been developed to the point of process application are primarily borosilicate glasses (Mendel, 1978). Borosilicate glass has been chosen as a reference candidate waste form in the United States because of its low dissolution rate in water (at 0.1 megapascal pressure and temperatures less than 100°C) and good physical integrity. Borosilicate glass can accommodate a wide variety of waste elements, is relatively slow to

devitrify under anhydrous conditions, and is stable to radiation effects (McElroy and Burns, 1979). Radioactive waste elements usually constitute 25 to 35 weight percent of the waste glass. At PNL, many glass formulations, including melts containing actual high-level waste, have been prepared and extensively characterized. Several of the borosilicate formulations have been used as reference materials in solid-waste performance tests at PNL, The Pennsylvania State University, and other laboratories across the nation. The chemistries of four PNL-simulated high-level waste glasses are given in Table 11-2, including the designation numbers and compositions of the glass-making frits required by each particular waste stream. These formulations were developed for several of the high-level waste compositions described in Table 11-1. Several hundred grams of fully radioactive waste glass with the compositions listed in Table 11-2 have also been prepared and have undergone testing (Ross et al., 1978; Bradley, 1978; Wald and Westsik, 1979). In addition, two full-size test canisters of radioactive borosilicate waste glass were produced in early 1979 as part of the Nuclear Waste Vitrification Project (McElroy et al., 1979). Borosilicate waste glasses such as these are roughly analogous to waste produced by the Pyrex process in composition (82 percent SiO_2 , 12 percent B_2O_3 , 4 percent Na_2O) and melting temperatures. Boron lowers the melting (and, therefore, the processing) temperature of the glass by lowering its viscosity and increases the solubility of many waste elements in these silica-based glasses.

Ideally, all waste elements should be soluble in waste glasses. In practice, this is not the case. Palladium metal and RuO_2 are usually present in the amorphous matrix as crystalline inclusions and rarely, if ever, dissolve in the glass (Mendel et al., 1977; Turcotte and Wald, 1978). Also present in melts of 72-68 glass were $(\text{Ce}, \text{Zr}, \text{RE}^{+3})\text{O}_{2-x}$ (RE = rare-earth elements) and a trace of spinel structure $(\text{Zr}, \text{Ni})(\text{Fe}, \text{Cr})_2\text{O}_4$.

A glass may partially crystallize (devitrify) under certain conditions. In the devitrification process, atoms in the random, glassy network rearrange themselves, forming an ordered crystalline structure that is more thermodynamically stable than the glass. Usually the remaining glass is more soluble than the glass matrix before devitrification, thereby increasing waste leachability. Devitrification typically occurs only between 500° and 950°C (Mendel, 1978). Above this range, crystals other than those of glass-insoluble materials redissolve in the glass. Below 500°C, crystallization is diffusion-limited because of the high viscosity of the glass matrix and hence is very slow.

A number of crystalline phases have been consistently observed in nuclear waste-glass formulations that have devitrified. Crystallites of these phases are large, compared to those of the phases that are insoluble in glass, and may cause damage (microcracking) in the glass structure. Significant quantities of $(\text{Cs}, \text{Sr}, \text{Ba})\text{MoO}_4$, Zn_2SiO_4 , and $\text{Ca}_2\text{RE}_8(\text{SiO}_4)_6\text{O}_2$ (apatite structure) crystals have been observed in devitrified samples of 72-68 glass (Mendel et al., 1977; Turcotte and Wald, 1978).

TABLE 11-2. Reference Waste Borosilicate Glass Compositions (wt%)* (after Ross et al., 1978).

Glass code	72-68	76-68	77-260	77-107
Waste type	PW-4b	PW-8a	PW-7c	PW-9
Frit code	73-1	76-101	77-269	77-268
SiO ₂	27.3	40.0	36.0	38.0
B ₂ O ₃	11.1	9.5	9.0	13.0
Na ₂ O	4.0	7.5	8.0	2.0
K ₂ O	4.0	--	2.0	4.0
ZnO	21.3	5.0	--	5.0
CaO	1.5	2.0	1.0	2.0
MgO	1.5	--	--	--
SrO	1.5	--	--	--
BaO	1.5	--	--	--
TiO ₂	--	3.0	6.0	3.0
Al ₂ O ₃	--	--	2.0	--
CuO	--	--	3.0	--
Waste	26.3	33.0	33.0	33.0

*Normalized to 100%.

The devitrification phases observed in the other borosilicate-glass formulations varied significantly from those reported for 72-68 glass. These differences may be attributed to both variation of the additives and differences in the waste streams under consideration. For example, in isothermal treatments in the 600° to 900°C range, crystals of the phase NiFeSi₂O₆ slowly grew into the 76-68 glass matrix (Ross and Mendel, 1979). Approximately 30 weight percent (as estimated by X-ray diffraction) of the glass crystallized in this phase during 1 year of annealing at 750°C (McElroy et al., 1979). The devitrification products observed in the four reference glass formulations are summarized in Table 11-3.

TABLE 11-3. Crystalline Phases in Waste-Glass Formulations.^a

Glass	Phase	Maximum wt%	Occurrence
72-68	RuO_2	1.4	Melt insoluble
	$(\text{Ni,Zr})(\text{Fe,Cr})_2\text{O}_4$	trace	Melt insoluble
	Pd	3.0	Melt insoluble
	$(\text{Ce,Zr,RE}^{+3})\text{O}_{2-x}$	5.0	Melt insoluble
	Zn_2SiO_4	14.0	Devitrification product
	$(\text{Ca,Sr,Ba})\text{MoO}_4$	6.0	Devitrification product
	$\text{Ca}_2(\text{RE}^{+3})_8(\text{SiO}_4)_6\text{O}_2$	3.0	Devitrification product
76-68	RuO_2	2.0	Melt insoluble
	NiFe_2O_4	2.0	Melt insoluble
	Pd	trace	Melt insoluble
	$(\text{Ce,U,RE}^{+3})\text{O}_2$	2.0	Devitrification product
	$\text{NaFeSi}_2\text{O}_6$	30.0	Devitrification product
	CaMoO_4	trace	Devitrification product
	$(\text{Ce,RE})\text{PO}_4$	trace	Devitrification product
77-107	RuO_2	NR ^b	Melt insoluble
	NiFe_2O_4	NR	Melt insoluble
	Pd	NR	Melt insoluble
	CeO_2	NR	Devitrification product
	CaMoO_4	NR	Devitrification product
	TiO_2	NR	Devitrification product
	NdBSiO_5	NR	Devitrification product
77-260	RuO_2	NR	Melt insoluble
	NiFe_2O_4	NR	Melt insoluble
	Pd	NR	Melt insoluble
	CeO_2	NR	Devitrification product
	$\text{Gd}_2\text{Ti}_2\text{O}_7$	NR	Devitrification product
	$\text{Ca}_3\text{Gd}_7[\text{SiO}_4]_5(\text{PO}_4)\text{O}_2$	NR	Devitrification product

^aTurcotte and Wald, 1978; Ross et al., 1978; Ross and Mendel, 1979; McElroy et al., 1979; Wald and Westsik, 1979.

^bNot reported.

Measurable anhydrous devitrification occurs in a relatively narrow range of annealing temperatures for these glass formulations. The center of the range, which spans about 300°C, lies at about 750°C for short anneals, and at 650° to 700°C for anneals of several months (Ross and Mendel, 1979). Melt insolubles constitute from 4 to 7 percent of the composition of the four reference waste-glass formulations (see Table 11-2) (Wald and Westsik, 1979). Devitrification on slow cooling or during extended annealings of these glass formulations has yielded a maximum of 45 percent crystalline material in the devitrified specimens (of 72-68 and 77-260), with 76-68 glass being the most devitrification-resistant of the glass specimens studied. No devitrification has been observed in samples annealed at temperatures less than 500°C. However, partial devitrification may occur very slowly in the center of the glass over the waste isolation time period, even though the waste package centerline temperature is expected to be less than 300°C. Fully radioactive analogs of the formulations described above devitrify in a similar manner to the simulated specimens, and contain the same melt-insoluble phases (Wald and Westsik, 1979), although in lesser quantities.

The formation of crystallites within the glass matrix (devitrification) may significantly alter properties such as leach resistance. For instance, the leachability of 72-68 glass was significantly increased by microcracking due to devitrification (Ross et al., 1978). The chances for waste-glass devitrification are greatest during the first 100 years after its production, when the decay heat loads are the largest.

A variety of other waste-glass formulations have been studied by various researchers. The average compositions of various types of waste glasses are presented in Table 11-4. Much interest has focused on the phosphate glasses, although a number of problems have inhibited their development (Mendel, 1978). The phosphorus-based formulations produce low-melting glasses, which eases some processing requirements. However, phosphate solutions exhibit high ruthenium volatilities during denitration, and the melt is extremely corrosive. Phosphate glasses also devitrify rapidly when held at temperatures greater than 500°C, with a 1,000-fold increase in leach rate of the glass occurring as a result.

Aluminosilicate glasses and glass ceramics have also been studied as waste forms. Aluminosilicate glasses have excellent chemical durability, but process considerations (very high melting point) and limited waste loading (less than 10 weight percent) have turned development of waste glasses in other directions (Mendel, 1978). Glass ceramics have also begun to receive modest consideration. A glass ceramic is basically a glass designed to crystallize. The glass is crystallized under controlled conditions, forming very small, uniformly sized crystals embedded in a glass matrix. The crystal phases can be tailored to achieve the desired waste containment properties. Glass ceramics have a higher thermal stability and are tougher than ordinary glasses. However, many questions remain to be answered about the stability of such a waste form under long-term repository storage. For instance, tests with some glass-ceramic waste forms have indicated that only 50 to 60 percent crystallinity may be achieved, with the residual glassy phase exhibiting poorer leach behavior than that of a comparable waste-glass form (Rusin, 1980).

TABLE 11-4. Typical Waste-Glass Compositions (after Mendel, 1978).

Oxides	Glass composition (wt%)			
	Borosilicate	Alumino-silicate	Glass ceramic	Phosphate
SiO ₂	25-50	33-40	32-60	0-6
B ₂ O ₃	9-22	--	1-11	--
P ₂ O ₅	0-2	--	--	30-55
Alkali metal oxides	8-19	18-22	0-13	5-25
Alkaline earth oxides	0-6	13-16	2-33	--
Fe ₂ O ₃ , Cr ₂ O ₃ , NiO	1-20	--	--	0-30
Al ₂ O ₃	0-10	26-30	10-24	0-35
TiO ₂	0-3	--	0-3	--
ZnO	0-22	--	0-13	--
CuO	0-3	--	--	--
PbO	0-50	--	--	0-30
Gd ₂ O ₃	0-12	--	--	--
Fission products	30	5	20	30
Actinides	10	1	7	10

11.1.1.3 Chemical and Physical Properties of Waste Glass. The reference candidate waste form (PNL glass 77-260) for commercial high-level waste is a borosilicate glass containing approximately 31 weight percent of high-level liquid waste oxides from the reprocessing of commercial spent fuel (Slate et al., 1981). Borosilicate glass was chosen because of its resistance to leaching by water and its relatively high compatibility with the nuclides found in the sludge. Additional factors for the choice of a reference defense-waste form were its relatively low melting temperature and the fact that it could be made by means of a well-known technology. The chemical compositions (on a metric-ton-of-uranium basis) of calcined reference commercial high-level waste are given in Tables 11-5 and 11-6. The general chemical and physical properties of reference commercial glass (PNL 77-260) are given in Table 11-7. Although variations in flow sheets for reprocessing and glass formulations are expected to develop as waste-form research and development are continued, the compositions given are representative of what is expected in a final commercial high-level waste form. No accurate measurements of the leachability of these commercial waste glass forms under conditions applicable to a nuclear waste repository in basalt have been made.

TABLE 11-5. Chemical Composition of Reference Combined High-Level and Intermediate-Level Liquid Waste in Calcine Form (Slate et al., 1981).

Composition	Oxides (kg/t U*)
Fission products	34.703
Actinides plus daughters	12.360
Nonradioactive chemicals	
Gd ₂ O ₃ 25.827	39.807
Fe ₂ O ₃ 1.143	
Cr ₂ O ₃ 0.292	
NiO 0.127	
MnO ₂ 0.221	
ZrO ₂ 0.338	
P ₂ O ₅ 5.007	
NaSO ₄ 0.037	
NaCl 0.181	
Na ₂ O 6.634	
Total solids	86.870

*Tonnes of uranium.

TABLE 11-6. Chemical Composition of Fission Products and Actinides
(Plus Daughters) at the Time of Reprocessing of Reference
Commercial High-Level Waste (Slate et al., 1981).

Constituent	Composition (kg/t U)		Constituent	Composition (kg/t U)	
	Element	Oxide*		Element	Oxide*
Fission Products			Fission Products		
SeO ₂	0.055	0.077	La ₂ O ₃	1.200	1.407
Rb ₂ O	0.339	0.371	CeO ₂	2.327	2.859
SrO	0.800	0.946	Pr ₆ O ₁₁	1.100	1.329
Y ₂ O ₃	0.444	0.564	Nd ₂ O ₃	3.968	4.628
ZrO ₂	3.496	4.723	Pm ₂ O ₃	0.037	0.044
MoO ₃	3.292	4.938	Sm ₂ O ₃	0.829	0.961
Tc ₂ O ₇	0.761	1.196	Eu ₂ O ₃	0.143	0.166
RuO ₂	2.180	2.871	Gd ₂ O ₃	<u>0.110</u>	<u>0.127</u>
Rh ₂ O ₃	0.464	0.572		27.759	34.703
PdO	1.402	1.613	Actinides Plus Daughters		
Ag ₂ O	0.078	0.085	U ₃ O ₈	9.566	11.278
CdO	0.112	0.128	NpO ₂	0.438	0.497
SnO ₂	0.091	0.116	PuO ₂	0.087	0.093
TeO ₂	0.479	0.599	Am ₂ O ₃	0.423	0.465
I	0.002	--	Cm ₂ O ₃	<u>0.025</u>	<u>0.027</u>
Cs ₂ O ₃	2.472	2.621		10.539	12.360
BaO	1.578	1.762			

*Converted to oxide form in a calcination process.

TABLE 11-7. General Composition and Physical Properties of Reference Commercial High-Level Waste Glass* (Slate et al., 1981).

Constituents		wt%
SiO ₂		36
B ₂ O ₃		9
P ₂ O ₅		2
Alkali metal oxides		13
Alkaline earth oxides		1
Fe ₂ O ₃ , Cr ₂ O ₃ , NiO		1
Al ₂ O ₃		2
TiO ₂		6
CuO		3
Gd ₂ O ₃		10
Fission product oxides		12
Actinide oxides		5

Property	Value
Waste loading	The oxides from the high-level liquid waste constitute 31 wt% of the glass
Quantity	277 kg/t U; 89 L/t U
Activity	1,616 Ci/kg; 5,029 Ci/L (at 5 yr after reactor discharge)
Decay heat	5.9 W/kg; 18.3 W/L (at 5 yr after reactor discharge)
Density	3.1 g/cm ³
Process melting temperature	1,050° to 1,150°C
Softening temperature	575° to 650°C (viscosity = 4 E+07 poise)
Transition temperature	500° to 550°C (viscosity = 1 E+13 poise)
Temperature limit to prevent devitrification	500°C
Leach rate	1.0 to 2.0 E-06 g/cm ² ·d (25°C water)
Thermal conductivity	0.8 to 1.3 W/m°K from 0° to 500°C
Heat capacity	700 to 800 J/kg°C (estimated)
Thermal expansion	1 E-05/°C
Compressive tensile strength	4 E+07 Pa
Young's modulus	7 E+10 Pa (estimated)

*Normalized for 1 t of reprocessed uranium.

The reference waste form for the defense waste processing facility (Savannah River, South Carolina) is a borosilicate glass, containing approximately 28 weight percent sludge with the remainder a glass frit. The description of defense waste characteristics is given in tabular form by feed composition, glass composition, and mechanical characteristics. The glass composition illustrated here is based on immobilized 5-year or older waste sludge. The chemical and isotopic compositions of defense waste sludge are given in Tables 11-8 and 11-9. The chemical and isotopic content of the borosilicate glass formed from such sludge are shown in Tables 11-10 and 11-11. Physical properties of the reference defense waste processing facility borosilicate have been estimated by laboratory measurement or calculation. These properties are listed in Table 11-12. A number of alternate glass compositions and waste mixtures are being considered as alternatives to the formulation described above, but these variations do not significantly affect the containment and isolation potential of the product. No accurate measurements have been made of the leachability of these defense waste-glass forms under conditions applicable to a nuclear waste repository in basalt.

The temperature of a waste-glass canister at its surface, and the thermal profile through it, will significantly influence any reactions that take place between stored glass and intruding groundwater in the repository system. Such reactions may be particularly severe if they occur early in the thermal history of the canister. The absolute temperature of a waste-glass canister will depend upon factors such as the type of spent fuel, its irradiation history, the age of the waste at vitrification, and the waste loading of the glass (Mendel et al., 1977). The temperature profile across the canister will vary as a function of waste package thermal conductivity, composition, and size. The thermal history during processing is also important. Cracks that are caused by quenching the hot glass/canister combination, which may be inevitable due to gross differences between the conductivity of the glass and its canister (Ross et al., 1978), offer greatly increased surface area for reaction with intruding groundwater in the event of canister breach.

Thermal profiles have been calculated for typical waste-glass/canister systems (see Table 11-13). This glass formulation, when poured into a 30.5-centimeter inner diameter, 3-meter-long canister with 8 internal fins 6.4 millimeters thick (Mendel et al., 1977), produces the center-line thermal profile shown in Figure 11-1, if the waste is 1 year old at vitrification. As illustrated by the figure, the thermal profile of the canister varies in different media, such as air or water, as the waste ages.

11.1.1.4 Packaging of Borosilicate Glass. Borosilicate glass is presently the reference waste form for defense high-level waste (Baxter, 1981) and the reference candidate waste form for commercial high-level waste (Slate et al., 1981). An excellent compilation of data pertaining to early conceptual design work on the packaging of this waste form for defense high-level waste has been prepared by Johanson and Su (1981). See Sections 11.2.3.2.1 and 11.2.3.2.2 for the reference waste package conceptual design for defense and commercial high-level waste- (borosilicate) glass forms, respectively.

TABLE 11-8. Chemical Composition^a of Defense Waste Sludge (Baxter, 1981).

Soluble solids		Insoluble solids			
Species	wt%	Species	wt%	Species	wt%
NaNO ₃	2.892 E+01	Fe(OH) ₃	3.797 E+01	BaSO ₄	3.143 E-01
NaNO ₂	1.171 E+01	Al(OH) ₃	1.571 E+01	PbSO ₄	1.760 E-01
NaAlO ₂	1.608 E+01	MnO ₂	6.414	Cr(OH) ₃	4.778 E-01
NaOH	3.159 E+01	UO ₂ (OH) ₂	4.237	AgOH	2.515 E-02
Na ₂ CO ₃	4.885	Ni(OH) ₂	2.427	Cu(OH) ₂	1.383 E-01
Na ₂ SO ₄	6.550	CaCO ₃	4.992	Co(OH) ₃	7.546 E-02
NaCl	1.980 E-01	Zeolite	4.602	Zn(OH) ₂	3.646 E-01
NaF	1.284 E-02	SiO ₂	7.332	Mg(OH) ₂	6.288 E-01
Na[HgO(OH)]	3.967 E-02	NaOH	4.086	C	1.257 E-01
Group Ab	8.259 E-04	NaNO ₃	3.521	Group Ab	3.416 E-01
Group BC	2.368 E-04	HgO	1.987	Group BC	1.123
Na ₂ PuO ₂ (OH) ₄	1.607 E-06	CaSO ₄	5.911 E-01	PuO ₂	4.557 E-02
UO ₂ (OH) ₂	6.793 E-06	CaC ₂ O ₄	5.030 E-01	SrCO ₃	1.308 E-01
Na ₂ RuO ₄	3.234 E-03	Ca ₃ (PO ₄) ₂	4.652 E-01	Y ₂ (CO ₃) ₃	8.626 E-02
Na ₂ RhO ₄	3.314 E-04	CaF ₂	1.257 E-01	RuO ₂	8.248 E-02
CsNO ₃	6.176 E-03	NaCl	1.257 E-01	RhO ₂	1.748 E-02
BaNO ₃	4.941 E-03	NaI	1.257 E-02	CsNO ₃	1.316 E-02
Sr(NO ₃) ₂	9.284 E-06	ThO ₂	7.168 E-01	Ba(NO ₃) ₂	5.532 E-03
Y(NO ₃) ₃	6.588 E-06				
NaI	1.864 E-05				

^aDry basis.^bTc, Se, Te, Rb, Mo.^cAg, Cd, Cr, Pd, Th, La, Ce, Pr, Pm, Nd, Sm, Tb, Sn, Sb, Co, Zr, Nb, Eu, Np, Am, Cm.

TABLE 11-9. Isotopic Content of Defense Waste Sludge (Ci/gal) (Baxter, 1981).

Isotope	Concentration	Isotope	Concentration	Isotope	Concentration	Isotope	Concentration
^3H	6.35077 E-05	^{126}Sn	2.52141 E-05	^{144}Pr	1.64622 E+01	^{235}U	8.82582 E-08
^{51}Cr	1.48331 E-17	^{124}Sb	1.19509 E-10	^{144}PrM	1.97543 E-01	^{236}U	1.91428 E-06
^{60}Co	2.86177 E-01	^{125}Sb	1.41250 E+00	^{144}Nd	8.02685 E-13	^{238}U	4.86155 E-07
^{79}Se	2.27291 E-04	^{126}Sb	3.52997 E-06	^{147}Nd	2.11823 E-47	^{236}Np	2.89601 E-11
^{87}Rb	1.50827 E-08	^{126}SbM	2.52141 E-05	^{147}Pm	4.03393 E+01	^{237}Np	1.47265 E-05
^{89}Sr	8.48843 E-08	^{125}TeM	3.31008 E-01	^{148}Pm	1.16056 E-13	^{236}Pu	1.04512 E-04
^{90}Sr	5.08585 E+01	^{127}Te	1.44495 E-04	^{148}PmM	1.68276 E-12	^{237}Pu	7.62708 E-15
^{90}Y	5.08717 E+01	^{127}TeM	1.47519 E-04	^{147}Sm	3.18789E -09	^{238}Pu	1.25546 E+00
^{91}Y	1.56656 E-06	^{129}Te	3.65090 E-15	^{148}Sm	9.38640 E-15	^{239}Pu	1.18165 E-02
^{93}Zr	3.03477 E-03	^{129}TeM	5.75014 E-15	^{149}Sm	2.90951 E-15	^{240}Pu	7.46734 E-03
^{95}Zr	1.65653 E-05	^{129}I	1.33014 E-05	^{151}Sm	3.93519 E-01	^{241}Pu	1.40415 E+00
^{95}Nb	3.57166 E-05	^{134}Cs	3.20104 E-03	^{152}Eu	6.34768 E-03	^{242}Pu	9.94960 E-06
^{95}NbM	2.10378 E-07	^{135}Cs	5.52726 E-08	^{154}Eu	1.04271 E+00	^{241}Am	1.80717 E-02
^{99}Tc	4.11355 E-03	^{136}Cs	9.44448 E-45	^{155}Eu	8.25415 E-01	^{242}Am	2.38510 E-05
^{103}Ru	1.90482 E-11	^{137}Cs	2.95309 E-02	^{156}Eu	8.80026 E-35	^{242}AmM	2.39706 E-05
^{106}Ru	2.48778 E+00	^{136}BaM	3.02223 E-45	^{160}Tb	1.86795 E-09	^{243}Am	9.63290 E-06
^{103}RhM	1.90669 E-11	^{137}BaM	2.79362 E-02	^{206}Tl	7.58394 E-21	^{242}Cm	5.85452 E-05
^{106}Rh	2.48779 E+00	^{140}Ba	3.50468 E-43	^{207}Tl	1.12570 E-10	^{243}Cm	9.27861 E-06
^{107}Pd	1.52708 E-05	^{140}La	7.22159 E-40	^{208}Tl	1.75650 E-06	^{244}Cm	2.72091 E-04
^{110}Ag	2.11596 E-02	^{141}Ce	5.99319 E-14	^{209}Tl	7.15550 E-15	^{245}Cm	1.11008 E-08
^{115}CdM	1.53228 E-12	^{142}Ce	1.59243 E-08	^{232}U	8.55505 E-06	^{246}Cm	8.86082 E-10
^{121}SnM	5.46784 E-05	^{144}Ce	1.64616 E+01	^{233}U	1.01380 E-09	^{247}Cm	1.08927 E-15
^{123}Sn	4.43787 E-04	^{143}Pr	1.99844 E-37	^{234}U	2.67192 E-05	^{248}Cm	1.13750 E-15
Total activity decay heat				1.87 E+02 Ci/gal			
Total primary				5.54 E-01 W/gal			
Total gamma				2.50 E-02 W/gal			

TABLE 11-10. Chemical Composition of
Defense Waste Sludge-Based Waste-
Glass Form (Baxter, 1981).

Compound	wt%	Compound	wt%
SiO ₂	45.5	ThO ₂	0.248
Na ₂ O	15.0	Ca ₃ (PO ₄) ₂	0.161
B ₂ O ₃	10.9	Cr ₂ O ₃	0.122
Fe ₂ O ₃	6.57	Ab ^a	0.112
Li ₂ O	4.23	ZnO	0.103
Al ₂ O ₃	3.62	BaO	0.0696
Fe ₃ O ₄	3.13	PbO	0.0448
MnO	1.81	Cu ₂ O	0.0351
MgO	1.64	SrO	0.0318
Zeolite	1.59	RuO ₂	0.0257
UO ₂	1.30	Y ₂ O ₃	0.0188
CaO	1.16	CoO	0.0178
TiO ₂	0.743	PuO ₂	0.0158
NiO	0.677	RhO ₂	0.00544
Ba	0.389	Cs ₂ O	0.00316
La ₂ O ₃	0.371	Total	100.00
ZrO ₂	0.371		

^aAb = Ag, Cd, Cr, Pd, Tl, La, Ce, Pr, Pm, Nd, Sm, Tb, Sn, Sb, Co, Zr, Nb, Eu, Np, Am, Cm.

^bA = Tc, Se, Te, Rb, Mo.

TABLE 11-11. Isotopic Content of Defense Waste Sludge Based on Waste-Glass Form
(Ci/lb) (Baxter, 1981).

Isotope	Concentration	Isotope	Concentration	Isotope	Concentration	Isotope	Concentration
⁵¹ Cr	3.25418 E-20	¹²⁴ Sb	2.62187 E-11	¹⁴⁴ Nd	1.76099 E-13	²³⁶ U	4.19969 E-07
⁶⁰ Co	6.27837 E-02	¹²⁵ Sb	3.09884 E-01	¹⁴⁷ Nd	4.64714 E-48	²³⁸ U	1.06656 E-07
⁷⁹ Se	4.73715 E-05	¹²⁶ Sb	7.74431 E-07	¹⁴⁷ Pm	8.84994 E+00	²³⁶ Np	6.35349 E-12
⁸⁷ Rb	3.14351 E-09	¹²⁶ SbM	5.53166 E-06	¹⁴⁸ Pm	2.54612 E-14	²³⁷ Np	3.23081 E-06
⁸⁹ Sr	1.86225 E-08	¹²⁵ TeM	6.89880 E-02	¹⁴⁸ PmM	3.69177 E-13	²³⁶ Pu	2.29285 E-05
⁹⁰ Sr	1.11577 E+01	¹²⁷ Te	3.01153 E-05	¹⁴⁷ Sm	6.99383 E-10	²³⁷ Pu	1.67329 E-15
⁹⁰ Y	1.11606 E+01	¹²⁷ TeM	3.07456 E-05	¹⁴⁸ Sm	2.05926 E-15	²³⁸ Pu	2.75432 E-01
⁹¹ Y	3.43683 E-07	¹²⁹ Te	7.60915 E-16	¹⁴⁹ Sm	6.38310 E-16	²³⁹ Pu	2.59239 E-03
⁹³ Zr	6.65792 E-04	¹²⁹ TeM	1.19843 E-15	¹⁵¹ Sm	8.63330 E-02	²⁴⁰ Pu	1.63824 E-03
⁹⁵ Zr	3.63421 E-06	¹³⁴ Cs	7.01898 E-04	¹⁵² Eu	1.39260 E-03	²⁴¹ Pu	3.08053 E-01
⁹⁵ Nb	7.83578 E-06	¹³⁵ Cs	1.21197 E-08	¹⁵⁴ Eu	2.28757 E-01	²⁴² Pu	2.18282 E-06
⁹⁵ NbM	4.61544 E-08	¹³⁶ Cs	2.07091 E-45	¹⁵⁵ Eu	1.81086 E-01	²⁴¹ Am	3.96470 E-03
⁹⁹ Tc	8.57338 E-04	¹³⁷ Cs	6.47529 E-03	¹⁵⁶ Eu	1.93067 E-35	²⁴² Am	5.23261 E-06
¹⁰³ Ru	4.17475 E-12	¹³⁶ BaM	6.62690 E-46	¹⁶⁰ Tb	4.09806 E-10	²⁴² AmM	5.25885 E-06
¹⁰⁶ Ru	5.45243 E-01	¹³⁷ BaM	6.12562 E-03	²⁰⁶ Tl	1.66382 E-21	²⁴³ Am	2.11334 E-06
¹⁰³ RhM	4.17886 E-12	¹⁴⁰ Ba	7.68479 E-44	²⁰⁷ Tl	2.46964 E-11	²⁴² Cm	1.28441 E-05
¹⁰⁶ Rh	5.45243 E-01	¹⁴⁰ La	1.58433 E-40	²⁰⁸ Tl	3.85353 E-07	²⁴³ Cm	2.03561 E-06
¹⁰⁷ Pd	3.35023 E-06	¹⁴¹ Ce	1.31483 E-14	²⁰⁹ Tl	1.56983 E-15	²⁴⁴ Cm	5.96933 E-05
¹¹⁰ Ag	4.64215 E-03	¹⁴² Ce	3.49359 E-09	²³² U	1.87687 E-06	²⁴⁵ Cm	2.43538 E-09
¹¹⁵ CdM	3.36163 E-13	¹⁴⁴ Ce	3.61146 E+00	²³³ U	2.22416 E-10	²⁴⁶ Cm	1.94395 E-10
¹²¹ SnM	1.19958 E-05	¹⁴³ Pr	4.38433 E-38	²³⁴ U	5.86186 E-06	²⁴⁷ Cm	2.38971 E-16
¹²³ Sn	9.73614 E-05	¹⁴⁴ Pr	3.61159 E+00	²³⁵ U	1.93628 E-08	²⁴⁸ Cm	2.49552 E-16
¹²⁶ Sn	5.53165 E-06	¹⁴⁴ PrM	4.33383 E-02				
Total activity decay heat				4.11 E+01 Ci/lb			
Total primary				1.22 E-01 W/lb			
Total gamma				5.49 E-03 W/lb			

TABLE 11-12. Physical Properties of Waste-Glass Forms for Defense Waste Sludge (Baxter, 1981).

Property	Value
Thermal conductivity at 100°C	0.952 W/m°C
Heat capacity at 100°C	0.22 cal/g°C
Fractional thermal expansion	1.22 E-05/°C
Young's modulus ^a	62,069 MPa
Tensile strength	62 MPa
Compressive strength	690 MPa
Poisson's ratio ^b	0.2
Density at 100°C	2.75 g/cm ³
Softening point	502°C

^aYoung's modulus, or the modulus of elasticity, measures the stiffness of the material.

^bPoisson's ratio is equivalent to the ratio of equatorial-to-axial strain under an applied axial stress.

TABLE 11-13. Heat-Generation Rates of Simulated PW-4b Waste Glass 72-68 (after Mendel et al., 1977).

kcal/s·m ³	W/L	Approximate age*
66.89	280	150 d
35.84	150	1 yr (ref.)
18.40	77	2 yr
11.47	48	3 yr
8.36	35	4 yr
6.21	26	5 yr
5.26	22	6 yr
4.30	18	7 yr
3.82	16	8 yr
3.66	15.3	9 yr
3.58	15.0	10 yr

*Waste age reflects a reference scale assigned to a particular waste composition and is used strictly for comparative purposes.

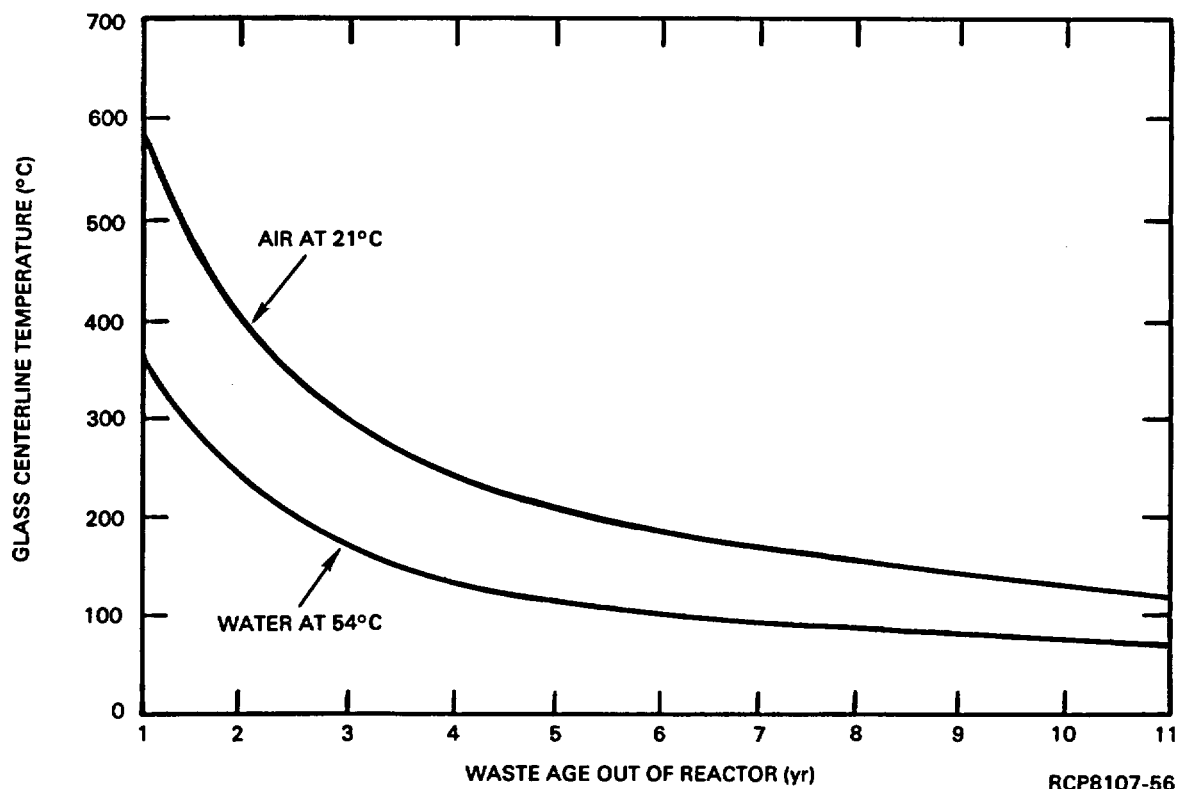


FIGURE 11-1. Centerline Temperatures of a Reference Canister Containing 72-68 Waste Glass (PW-4b type waste), Cooled in Air and Water. Canister: 30.5-centimeter diameter, 3 meters long, with 2.4-millimeter-thick internal fins.

11.1.2 Spent Fuel

Fuel for the pressurized water type power reactors in the United States are manufactured by Westinghouse, Combustion Engineering, Babcock and Wilcox, and Exxon. Fuel assemblies for boiling water type power reactors are manufactured by General Electric and Exxon.

Currently, some 68 light water power reactors (25 boiling water type and 43 pressurized water type) are operating in the United States (DOE, 1980c; Nuclear News, 1981) and numerous others are under construction.

The fuel for both pressurized and boiling water reactors consists of cylindrical pellets of uranium dioxide contained (clad) in sealed metal tubes, called fuel pins or rods. The fuel pins for both of these reactor types are arranged in square arrays within their respective assemblies. For pressurized-water reactors the assemblies range from 14 by 14 and 15 by 15 in older designs to 16 by 16 and 17 by 17 fuel rod arrays in newer designs, with each vendor having their own array design and fixturing systems to form the assembly (Johnson, 1979; Greene, 1980). For boiling water reactors the assemblies (bundles) contain 7 by 7 rod arrays in the older designs and 8 by 8 arrays in the newer designs (Greene, 1980).

Fuel in boiling water reactors operates at lower power ratings than pressurized water reactor fuel and achieves an average assembly burnup of about 27,500 megawatt days per metric ton of heavy metal, during approximately 4 years of service, before discharge from the reactor (AESD, 1980; DOE, 1980c). The average burnup for pressurized water reactor assemblies at discharge, after some 3 years of service, is about 33,000 megawatt days per metric ton of heavy metal (AESD, 1980; DOE 1980c). The actual burnup (i.e., amount of ^{235}U + ^{238}U + ^{239}Pu fissioned) is dependent on a number of design and operational history parameters (ERDA, 1976).

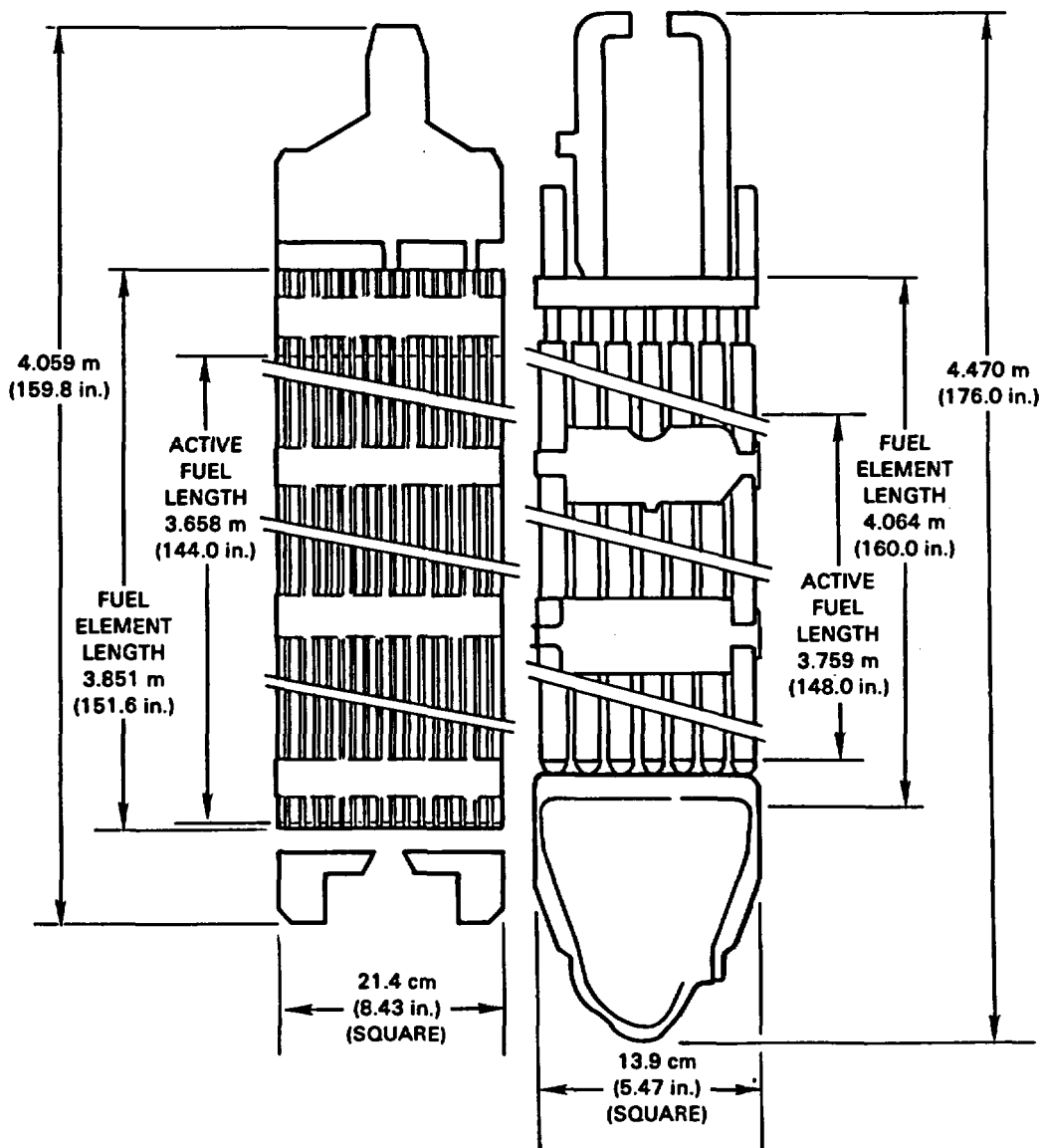
NOTE: The fuel vendors and utilities are currently conducting irradiation tests, under the approval of the NRC, to extend the irradiation of both boiling water and pressurized water reactor fuel assemblies to higher burnups than listed above. See Sections 11.1.2.2 and 11.1.2.3 for discussion of fuel burnup relevant to the BWIP.

11.1.2.1 Physical Properties of Spent Fuel Assemblies and Cladding. The fuel and assembly designs are very different for the two types (pressurized and boiling water) of reactors, and even vary somewhat between reactors of a given type.

Light water reactor fuel systems have been designed and operated using either zirconium alloy or stainless steel alloy cladding. Although a few reactors (3 pressurized water reactors and 1 small boiling water reactor) still contain stainless steel clad fuel, the zirconium alloy (Zircaloy-2/boiling water reactors and Zircaloy-4/pressurized water reactors) clad fuels are the typical systems currently in use and likewise dominate (greater than 90 percent) among the fuel pins currently in basin (water) storage (Johnson, 1977).

The pressurized water reactor fuel pins range from 0.950 to 1.12 centimeters in diameter and from 348 to 410.5 centimeters in length. Boiling-water-reactor fuel pins range from 1.23 to 1.45 centimeters in diameter and from 396.2 to 415.3 centimeters in length. In pressurized water reactors, the cladding thickness ranges from 0.057 to 0.076 centimeter depending on model and manufacturer. In boiling water reactors the thickness is 0.089 centimeter (Greene, 1980). See (Greene, 1980) for a detailed listing of the physical characteristics of fuel pin and assembly designs used in the United States in these two types of light water reactors. Figure 11-2 provides axial profile schematics and values of physical characteristics, for example, fuel assembly designs for the two reactor types.

The general physical integrity of the cladding on spent fuel pins is of some interest to both design and performance considerations for the geologic disposal of spent fuel. Most likely, the primary concern regarding the physical condition of spent fuel cladding will be the planning required to handle and dispose of those pins having broken or breached cladding at the time of canister loading. The following discussion provides a brief summary of the general information available on the basic physical integrity of fuel pin cladding at the end of reactor service and during basin (water) storage.



	<u>PWR</u>		<u>BWR</u>	
FUEL ELEMENT ARRAY	17 x 17		8 x 8	
ASSEMBLY TOTAL WEIGHT	658	1,449.6	283.9	625.3
URANIUM/ASSEMBLY	461.4	1,016.5	188.7	415.7
MO ₂ /ASSEMBLY	523.4	1,153.1	214.1	471.7
ZIRCALOY/ASSEMBLY	108.4	238.8	59.6	131.3
HARDWARE/ASSEMBLY	26.2	57.7	10.2	22.5
TOTAL METAL/ASSEMBLY	134.6	296.5	69.8	153.8
	kg	lb	kg	lb

RCP8107-52A

FIGURE 11-2. Typical Light Water Reactor Fuel Assemblies of Recent Design (after DOE, 1979; 1980c).

The failure rate of the Zircaloy cladding on light water reactor fuel pins during irradiation has been reduced significantly over the last decade by a combination of improved fuel rod design and manufacturing, and conservative reactor operation to limit fuel rod power ramps (rates of change) and fuel maximum temperature (Andrews et al., 1979; Tulenko et al., 1979; von Jan and Hoesl, 1979; Baily et al., 1979; Locke, 1975). Based on data from the preceding references, it is estimated that approximately 1 in 3 boiling water reactor assemblies over 10 years old would likely contain a failed rod, and approximately 1 in 50 recently discharged light water reactor (pressurized water reactor or boiling water reactor) assemblies would contain a failed rod in which the cladding had been breached during its time in the reactor. See also the references by Johnson (1977), Greene (1980), Funk and Jacobson, (1979), Fuhrman et al. (1976), and Courtright (1979) for discussions on the physical condition of spent fuel following irradiation in United States light-water reactors. The reports by Johnson (1977) and Funk and Jacobson, (1979) provide brief summary discussions of the types, approximate numbers, and apparent causes of fuel pin defects observed following irradiation in pressurized and boiling-water-type reactors in the United States through 1976. See Garzarolli et al., 1979; Matta et al., 1979; Cubicciotti et al., 1980; and Cubicciotti and Sanecki, 1978 for more detailed discussions on cladding degradation and failure.

In terms of general characterization, Greene (1980) notes that boiling water reactor fuel pins are usually more thoroughly characterized than their counterparts in pressurized water reactors. This is because essentially all boiling water reactor pins are checked for leaks at the end of each fuel cycle and the fuel pin assemblies used in boiling water reactors can be routinely disassembled (i.e., nondestructively) in the reactor's fuel storage pool, thus allowing detailed visual and nondestructive testing of individual fuel rods. Except for Exxon's assembly design, standard pressurized water reactor fuel assemblies made by the other fuel system manufacturers would require destructive removal of certain assembly hardware before individual pins could be removed or partially withdrawn from the assembly.

Currently, all spent fuel rods from United States light water reactors are stored in water filled basins (pools) constructed as interim storage facilities by reactor owners or service companies in the nuclear industry. Johnson (1977; 1979), Greene (1980), Zima (1979), DOE (1980c), and Bailey et al. (1980) provide summary information on the inventory in the United States of spent light water fuel in storage pools, their general condition, the effect of such storage on the condition of the spent fuel pins, and projections of spent fuel available in the future. Johnson (1977; 1979) has reported that visual inspections and radioactivity monitoring of light water fuel assemblies in basin (water) storage as of 1976 "... suggest that degradation, if present, is occurring very slowly." Johnson (1977) also notes, however, that "... very few detailed fuel examinations have been directed to definition of fuel performance in pool (water) storage." See Funk and Jacobson, (1980) for information on the effect of transportation of the physical integrity of spent fuel.

11.1.2.2 Chemical and Physical Properties of Spent Fuel Pellets. The chemical and physical properties of spent fuel pellets are a key to defining the source term for migration of radionuclides in the postcontainment period of a repository's life cycle. The chemical and physical changes in the fuel that are caused by the thermal and nuclear processes, which occur as a result of controlled fission in the reactor, define the fuel susceptibility to leaching. For example, during reactor operation, steep temperature gradients are generated in the pellets. These gradients reach 650°C between pellet center and edge (Ewart et al., 1976). As a result, the pellets become cracked and certain chemical species redistribute internally along the temperature gradient by diffusion. This evaporation-condensation process occurs along the cracks in the pellet (Cubiciotti, 1978). The microstructure of the UO₂ pellet thus is an important factor in determining the extent to which volatile species migrate radially and are released, should the cladding fail. Although temperature is the primary control on microstructure, the degree of burnup in the reactor exerts an influence (Cubiciotti, 1978).

Cracking in light water reactor fuels has apparently not been assessed quantitatively or at least not reported in the open literature. There appears to be no information available on the fuel fragment-size distribution as a function of irradiation, and thus the increase in the geometric surface area available to a potential leachant as a result of cracking is unknown. On the other hand, the increase in the specific surface area during the irradiation of UO₂ samples of two different grain sizes has been determined (Turnbull and Friskney, 1978). This increase is attributed to the onset of interlinkage of internal porosity, particularly intergranular, with the external surface.

The nuclear processes (neutron capture and nuclear fission) occurring in a reactor have a greater effect on the chemistry of the pellet than on its microstructure. Because the neutron flux is not constant throughout the pellet, chemical inhomogeneities result as a function of fuel pellet radius and axial fuel column position. For example, as a consequence of the resonance capture of thermal neutrons by ²³⁸U, plutonium and other higher actinides will be formed primarily in the peripheral regions of the fuel pellets, where they occur as oxides in solid solution in the remaining urania (Bazin et al., 1974).

Uranium fission yields isotopes of a number of elements (Meek and Rider, 1974), many of which combine with oxygen, released from the fission of uranium atoms in uranium oxide, according to the stability of their oxides at the oxygen chemical potential set by the fuel (Bazin et al., 1974; Davies and Ewart, 1971). Fission-product elements that form oxides include the rare-earth elements, yttrium, zirconium, niobium, barium, strontium, and molybdenum. The rare-earth and zirconium oxides are stable in the uranium oxide crystalline lattice. Niobium oxide is presumably insoluble in UO₂, but is formed in very small amounts and has a negligible influence on bulk chemistry. The alkaline earth oxides, BaO and SrO, have lower solubilities in UO₂ than the other fission-product oxides (Bazin et al., 1974; Davies and Ewart, 1971; Ewart et al., 1976; Bramman and Powell, 1975), particularly in the presence of zirconium (Ewart et al., 1976; Koizumi et al., 1974), and thus may remain as simple oxides or mixed

oxides such as BaUO_3 (Koizumi et al., 1974) or BaZrO_3 (Bazin et al., 1974; Davies and Ewart, 1971; Ewart et al., 1976; Bramman and Powell, 1975; Koizumi et al., 1974). The oxides that are soluble in the UO_2 lattice are probably immobile, remaining where they are produced by the fission process. In the case of those isotopes of barium and strontium whose precursors are the alkali metals cesium and rubidium, respectively, some radial redistribution down the temperature gradient will occur if the alkali metals have access to cracks or voids interlinking toward the fuel surface. Thus barium and, to a lesser extent, strontium are occasionally found near the surface of the fuel pellets, probably in the chemical combinations noted above (Bazin et al., 1974; Bramman and Powell, 1975). Barium has also been found to migrate up the temperature gradient, but the mechanism for this is unknown (Friskney and Simpson, 1975).

Molybdenum is an abundant fission product that, unlike the oxides of the other oxide-forming fission products, exhibits a free energy of formation slightly above the oxygen potential of stoichiometric urania rather than well below it. Consequently, oxygen, in excess of that which is combined in the more stable oxides, reacts with the fuel and, as irradiation proceeds, the average oxygen-to-metal mole ratio (O/M) of the fuel slowly increases (Davies and Ewart, 1971). Near stoichiometry, a small increase in the urania oxygen-to-metal mole ratio causes a relatively large increase in the oxygen chemical potential of the system and the free energy of formation of MoO_2 is soon exceeded. At this point, oxidation of the molybdenum, which resides in noble metal inclusions during the early stages of the irradiation, commences and the oxygen potential of the urania, and hence its oxygen-to-metal mole ratio, are stabilized. Molybdenum can, therefore, be said to act as an oxygen buffer. The urania becomes only slightly hyperstoichiometric and the small oxygen excess tends to move up the temperature gradient, giving the fuel pellets a slightly higher oxygen-to-metal mole ratio along their centerline than on their periphery (Rand and Markin, 1968). If all of the fuel's oxygen excess ($\Delta\text{O/M} \approx 0.010$ at 33,000 megawatt days per metric ton of heavy metal for pressurized water reactor fuel) reacted with molybdenum to yield MoO_2 , approximately 63 percent of the molybdenum would be oxidized. Actually, the fraction oxidized may be somewhat less than this. Molybdenum dioxide exhibits only limited solubility in UO_2 (Giachetti and Sari, 1976). Instead, it may sublime from the high temperature regions of the fuel either as such or perhaps as Cs_2MoO_4 (Johnson and Johnson, 1975) and condense on the cooler surfaces of the fuel and/or Zircaloy cladding. In the presence of BaO (and presumably SrO), MoO_2 may react to form a nonvolatile molybdate and remain in the higher temperature regions of the fuel (Giachetti and Sari, 1976). However, some molybdates are found on the fuels or cladding surface.

The Zircaloy cladding is another sink for oxygen and thus may also tend to stabilize the urania oxygen-to-metal mole ratio. Depending on their relative oxidation rates, the Zircaloy cladding could suppress oxidation of the molybdenum by maintaining the fuel at an oxygen-to-metal mole ratio of 2.00. Cladding oxidation is more extensive at locations where the fuel and cladding are in intimate contact and are sometimes bonded by a cesium-fuel compound (Cubicciotti and Sanecki, 1978).

The remaining fission products are not normally considered oxide formers under the conditions existing in a fuel rod. The noble metals, as well as technetium and silver, display little propensity for migration other than to accumulate in small metallic inclusions (Bazin et al., 1974; Bramman and Powell, 1975; Giachetti and Sari, 1976; Bramman et al., 1968). On the other hand, cesium and rubidium are relatively volatile and are predisposed to move down the temperature gradient (Bramman and Powell, 1975). Cesium, and probably rubidium, occur as halides (CsI and CsBr), tellurides (Cs_2Te), and selenides (Cs_2Se) (Cubicciotti and Sanecki, 1978; Bazin et al., 1974; Bramman and Powell, 1975; Davies et al., 1979; Aitken et al., 1972) in the cooler region of the fuel. There is more than enough cesium in the spent fuel to chemically bind the entire fission production of halogens, tellurium, and selenium. There is some indication, however, that CsI can react with hyperstoichiometric urania, yielding a cesium uranate and elemental iodine (Lorenz et al., 1980). Because of the relatively large cesium-fission yield (Meek and Rider, 1974; Besmann and Lindemer, 1978), the compound Cs_2MoO_4 is also possible (Johnson and Johnson, 1975) although it is apparently less stable than Cs_2UO_4 (Aitken et al., 1972). Another compound that may be formed by cesium reaching the surface of the Zircaloy cladding is Cs_2ZrO_3 . This has been suggested by the close association of cesium and zirconium in certain analytical tests (Bazin et al., 1974; Lorenz et al., 1980).

The inert gases xenon and krypton are the only other elements with significant fission yields (Meek and Rider, 1974). It is probable that the gases diffuse through the urania crystalline matrix to concentrate along grain boundaries (Zimmerman, 1978; Turnbull and Friskney, 1978). Further migration and release from the pellet is primarily dependent on temperature (Zimmerman, 1978; Friskney and Turnbull, 1979) or loss of fuel pin structural integrity (either accidental or intentional). Under normal conditions, more than 90 percent of the fission gases in an intact fuel-rod are retained (Lorenz et al., 1980; Zimmerman, 1978; Meyer et al., 1978). There are data suggesting that the fraction of volatile fission products released is related to the fraction of fission gases released from the fuel (Cubicciotti, 1978; Cubicciotti and Sanecki, 1978). However, the measurement at temperatures above 900°C of diffusion rates for fission products other than fission gases indicates that relations between release fractions are complex (Parker et al., 1967).

Fission product oxide chemistry is complex and may vary not only from fuel to fuel but within individual fuel pellets as well. The discrete fission-product phases that have been reported are listed in Table 11-14.

11.1.2.3 Other Properties of Spent Fuel. Radioactive transmutation within spent fuel results in chemical, phase, and density changes. These changes are most pronounced early after removal from the reactor. For example, as a result of decay of short-lived isotopes, within 1 year after discharge the total activity of the fuel is approximately 1 percent of its activity at discharge (Greene, 1980). See Greene (1980) for ORIGEN (Bell, 1973) code calculations of the elemental composition of reference spent fuel as a function of time after discharge. See DOE (1979) for ORIGEN code calculations of the fission product and actinide inventories in spent fuel.

TABLE 11-14. Reported Fission-Product Phase Chemistry in Spent Fuel.^a

Elements	Phase(s)
Elements in solid solution with UO ₂ ^b	
Rare-earth elements (RE) (Y, La, Ce, Pr, Nd, Pm, Sm, Eu, Gd, Tb, Dy)	REO ₂ or RE ₂ O ₃
Actinides (Pu, Am)	(Pu,Am)O ₂
Zr	ZrO ₂
Sr	SrO
Elements present in metallic inclusions.	
Mo, Tc, Ru, Rh, Pd, Ag, Sn, Cs	Mixed alloys of varying composition.
Elements present in gaseous form.	
Xe, Kr, ³ H, I, Cs, Sb	
Elements present in discrete simple or complex phases.	
Sr, Ba, Zr, Mo	BaZrO ₃ SrZrO ₃ (Sr,Ba)ZrO ₃ (Sr,Ba)(Zr,U,Mo)O ₃ SrO BaO MoO ₂
Cs, Te, I, Br, Mo, Rb	(Cs,Rb)I Cs ₂ Te (Cs,Rb)Br Cs ₂ MoO ₄ Cs ₂ UO ₄ Cs ₂ O
Nb	NbO ₂

^aCubicciotti and Sanecki (1978), Leitnaker (1974), Lindemer (1977), Davies and Ewart (1971), O'Boyle et al. (1969), Jeffrey (1967), Koizumi et al. (1974), Sari et al. (1979), Ewart et al. (1976).

^bA given fission product may be present in more than one phase, depending upon its location in the fuel pellet and the elements present in the locale.

A discussion of the hydrothermal reactions of spent fuel and water, which are the key to the isolation characteristics of spent fuel, is presented in Section 11.3.2.1, where its leachability and dissolution behavior are discussed.

11.1.2.4 Packaging of Spent Fuel. Various packaging arrangements for disposal of spent fuel assemblies are currently being evaluated. Packaging intact assemblies is the simplest approach, though it is relatively space-inefficient from the standpoint of the number of canisters required. Typical canister designs for intact assemblies are sized to hold one pressurized water reactor assembly or three boiling water reactor assemblies. The package design presently baselined for conceptual design of a repository in basalt is based on disassembly of spent fuel assemblies and packaging fuel rods from three pressurized water reactors or seven boiling water reactors into canisters. See Section 11.2.3.1 for the dimension of the conceptual design waste package for spent fuel. Roughly 60 percent of all spent fuel assemblies will be boiling water reactor assemblies, provided the 2-to-1 pressurized water reactor to boiling water reactor ratio of total reactors currently operational, under construction, and on order is maintained. For canisters of disassembled fuel assemblies, this translates to approximately 61 percent of the canisters containing pressurized water reactor spent fuel rods.

The contents of the boiling water reactor and pressurized water reactor canisters described above are similar in heat output, total fuel content, and fission-product content. Spent fuel canisters containing 10-year-old or older boiling water reactor and pressurized water reactor fuel have comparable thermal outputs and probably do not need to be distinguished from one another. The heat-generation values plotted in Figure 11-3 are for burnups of 33,000 megawatt days per metric ton of heavy metal for pressurized-water-reactor fuel and 28,000 megawatt days per metric ton of heavy metal for boiling water reactor fuel. Decay heat in the fuel assemblies is almost directly proportional to burnup or reactor exposure time for cooling periods greater than about 5 years (Greene, 1979).

11.1.3 Strengths and Weaknesses of Reference Waste Forms

The assumption has been made that all waste forms will meet the proposed containment requirements stated in NRC (1981) in the absence of groundwater. In a dry environment, radionuclide transport can only take place via solid-state diffusion. Coefficients of diffusion at low (less than 300°C) temperatures are small fractions of a square centimeter per second (centimeters per year); i.e., waste is contained within a small volume over very long times. Thus, it is the interaction of the canister with intruding groundwater that influences the design of waste packages. After failure containment, the interaction of the waste form with intruding groundwater becomes important because diffusion of radionuclides through static groundwater and/or the flow of radionuclide-bearing groundwater leads to a dispersion of the waste orders of magnitude faster than in a dry repository. The following discussion of the strengths and weaknesses of the principal candidate waste forms is based on studies to date on waste form water interactions.

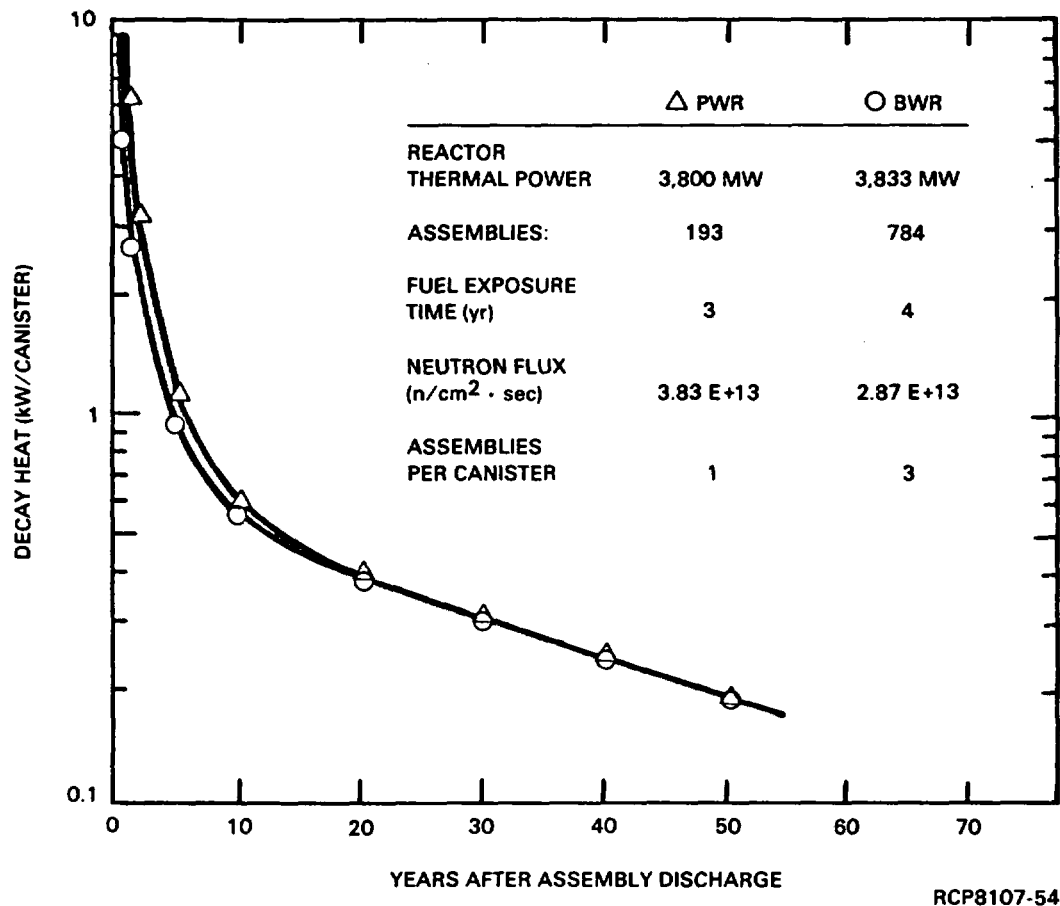


FIGURE 11-3. Decay Heat as a Function of Time for Typical Pressurized-Water-Reactor and Boiling-Water-Reactor Spent-Fuel Canisters Using Intact Assemblies (after NAE/NAS, 1979).

11.1.3.1 Strengths and Weaknesses of Borosilicate Glass. Borosilicate glass, the candidate reference waste form for commercial waste and the reference defense high-level waste, has been studied in a number of formulations including 76-68 (Table 11-1) and 77-260 (Table 11-7). The 76-68 formulation may incorporate a range of waste streams (Table 11-1) into a glass frit made up of the oxides of boron, sodium, silicon, calcium, titanium, and zinc. Some of the strengths of waste-glass forms were discussed previously. In addition, the leachability of 76-68 glass containing the PW-8a waste type is lower for many constituents than for spent fuel, as shown by the preliminary data in Table 11-15. These data were determined in experiments in which distilled water was reacted with the waste forms at 300°C (Smith et al., 1980).

TABLE 11-15. Leachability of Simulated Waste Forms (Smith et al., 1980).

Radionuclide	Percent lost to solution*	
	Simulated spent fuel	Simulated 76-68 borosilicate glass
Rb	100	2
Cs	100	14
Sr	<1	<1
Mo	54	68

*Distilled water at 300°C.

Glass is thermodynamically unstable and will eventually devitrify to a crystalline form. Devitrification times are presently being studied. The products of devitrification of 76-68 glass cannot be predicted accurately, but a conservative estimate would be that most elements would be present as simple oxides or silicates after devitrification. Thus, as in spent fuel, highly soluble phases in the waste form result. There have been efforts to make a glass-ceramic waste form that purposely includes tailored crystals to increase thermal stability. The leach behavior of these forms, however, is poorer than conventional glasses (Rusin, 1980).

The immiscibility of liquid phases in the composition range of candidate borosilicate glasses is another concern. All borosilicate glasses examined have shown microscale separation of two compositionally distinct liquids (Chick et al., 1980). It is likely (though not confirmed) that most of the silicon is contained in one liquid phase and most of the alkali elements (large ionic radii) and highly charged elements (together known as the "incompatible" elements) will enter the other phase unless there are enough tetrahedrally coordinated trivalent ions in the silicon-rich liquid to bind the alkalis through charge-balanced exchange reactions (e.g., $IVSi^{+4} \rightleftharpoons IVA^{+3} + VINa^{+}$).

11.1.3.2 Strengths and Weaknesses of Spent Fuel. The identification of the phases present in spent fuel is imperative to gain an understanding of its stability in the presence of groundwater. As will be discussed in the next section, some of the phases in spent fuel include CsBr, CsI, Cs₂Se, Cs₂Te, SrO, and possibly I₂. Those phases are all soluble in water. Little is known about other phases, such as Cs₂MoO₄ and Cs₂UO₄, but it would appear that much, if not all, of the iodine, bromine, selenium, tellurium, cesium, and strontium will be lost to solution if the waste package fails and the intruding groundwater breaches the fuel cladding.

The oxides of rare-earth elements, as well as uranium and the other actinides, are relatively insoluble when maintained in reduced oxidation states. For example, the solubility of uranium(VI) is approximately four orders of magnitude greater than uranium(IV). Noble metals are not highly soluble, but a study on actual spent fuel has indicated that technetium (which occurs in noble metal inclusions in spent fuel) has a solubility around 10^{-8} to 10^{-9} molality (Johnson et al., 1981). Therefore, complete containment of technetium by the waste package for 1,000 years may be impossible if the canister is breached and the groundwater should encounter the waste during that period. Other experiments have corroborated the earlier speculations showing nearly complete loss of cesium, rubidium, and molybdenum (but no significant strontium loss) from simulated spent fuel powder in contact with distilled water at 300°C (Smith et al., 1980). However, studies with actual spent-fuel monoliths at 150°C (Johnson et al., 1981) displayed much lower fractions of cesium but higher fractions of strontium release per day. It is suggested that the simulated spent fuel incorporated strontium in an inappropriate phase (SrZrO_3 --relatively insoluble) compared to actual fuel, where it is likely to occur as an oxide. Low cesium-release rates are probably related to surface area (monoliths versus powder) and temperature (150° versus 300°C) effects.

11.1.4 Summary of Important Conclusions

In this section the reference candidate waste form for disposal in basalt, borosilicate glass, and the alternate waste form, spent fuel, were discussed. Included were descriptions of their chemical and physical properties. The spent fuel canister packaging concept as baselined by the BWIP for design purposes is a close-packed arrangement of spent fuel rods removed from either three 10-year-old pressurized water reactor fuel assemblies or seven 10-year-old boiling water reactor fuel assemblies. The production and subsequent containerization of borosilicate glass are presently perceived as a two-step process in which the liquid waste stream is first calcined, followed by blending with a glass frit and melting to form a monolithic glass log contained in the process container.

Early leaching studies of simulated spent fuel by distilled water have shown that nearly all solid phases present, except for the uranium dioxide matrix, were soluble in water. By contrast, borosilicate glass, in particular the 76-68 glass containing the PW-8a waste type, appears to be less soluble (leachable). However, the borosilicate glasses are thermodynamically unstable, which leads eventually to devitrification and a possibly a higher eventual leach rate.

The DOE will continue to study these waste forms (NWTS, 1981c) with the objective of establishing performance requirements for waste forms to be disposed of in geologic repositories. The BWIP will continue to evaluate their performance under conditions expected in a repository located in basalt at Hanford. It is important to understand the interaction of the waste form, other components of the waste packages, and the host rock (including groundwater) so that more detailed design criteria for waste form and site-specific waste packages can be developed by the BWIP.

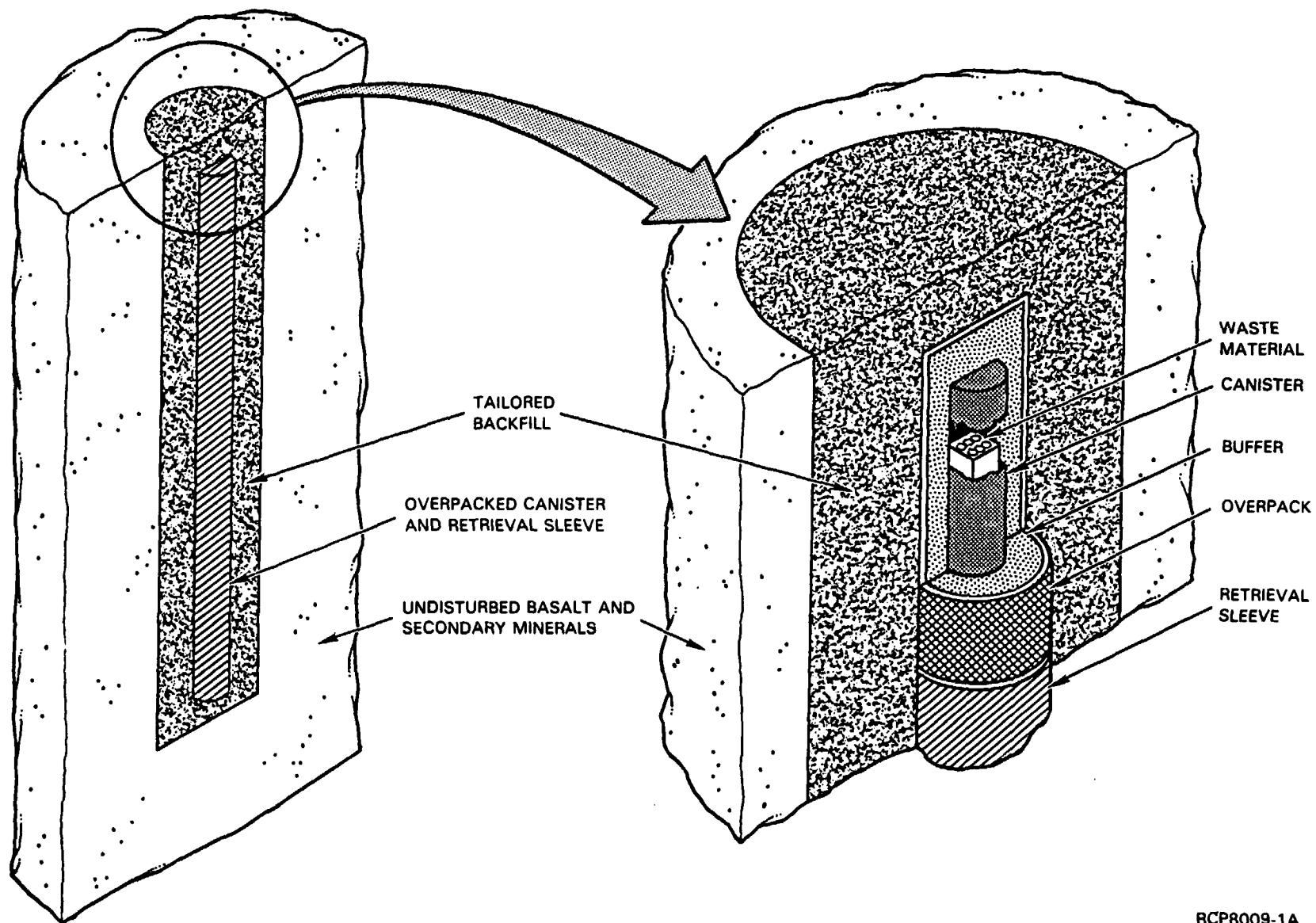
11.2 DESIGN CONCEPTS

Until the end of fiscal year 1982, the BWIP did not have the direct responsibility for the development of waste package designs for basalt. Through the conceptual design phase, which ended in September 1982, the responsibility was given to an engineering firm under contract to the Office of Nuclear Waste Isolation. This approach was felt by the NWTS Program to offer the best potential for achieving optimum commonality of design for waste packages to be emplaced in any candidate host rock. With this approach, the principal product of the BWIP Waste Package Program was only definition of conceptual design requirements for the Office of Nuclear Waste Isolation design contractor to reflect the site-specific nature of the waste package. Beginning with fiscal year 1983, however, each project of the NWTS Program will be responsible for development of its own waste package designs and for working closely with other NWTS Programs projects.

11.2.1 Waste Package Description

Because of the lack of sufficient site-specific data early in the program, the initial waste package concept for basalt was developed to meet the system functional requirements proposed by the NRC without considering the performance capabilities and characteristics of the site. This was accomplished by utilizing a complex system of multiple, functionally redundant barriers. The initial waste package and emplacement concept for basalt is illustrated in Figures 11-4 and 11-5. Five major engineered components were included in the initial waste package design: (1) waste form (spent fuel in this case), (2) canister, (3) buffer, (4) overpack, and (5) backfill. Compacted spent fuel assemblies were to be placed within a carbon-steel canister to meet shipping, handling, and retrievability requirements for the waste form. Because few data were available on the stability of spent fuel in the basalt environment, no credit was given the waste form toward controlling radionuclide release. As a result, a double-containment concept (canister-overpack) was developed to assure containment of the waste for 1,000 years, as proposed by the NRC. The outer container (overpack) consisted of a corrosion-resistant metal such as titanium. A buffer material was placed between the steel canister and the overpack to mitigate canister corrosion, should the overpack fail prematurely. This canister-overpack assemblage was then surrounded by a backfill layer composed of 50 percent crushed basalt and 50 percent bentonite clay, to provide a barrier to groundwater intrusion and radionuclide migration from the waste form and to assure that radionuclide releases after 1,000 years were maintained below 1 part in 100,000. A more detailed discussion of the initial waste package concept for a repository in basalt is presented by Smith et al. (1980) and Coons et al. (1980).

The initial waste package conceptual design was a means of providing long-term performance reliability. This approach was utilized because of a lack of pertinent data on the basalt environment and on materials behavior under site-specific conditions. Because of an extensive research and



RCP8009-1A

FIGURE 11-4. Early Waste Package Emplacement Concept.

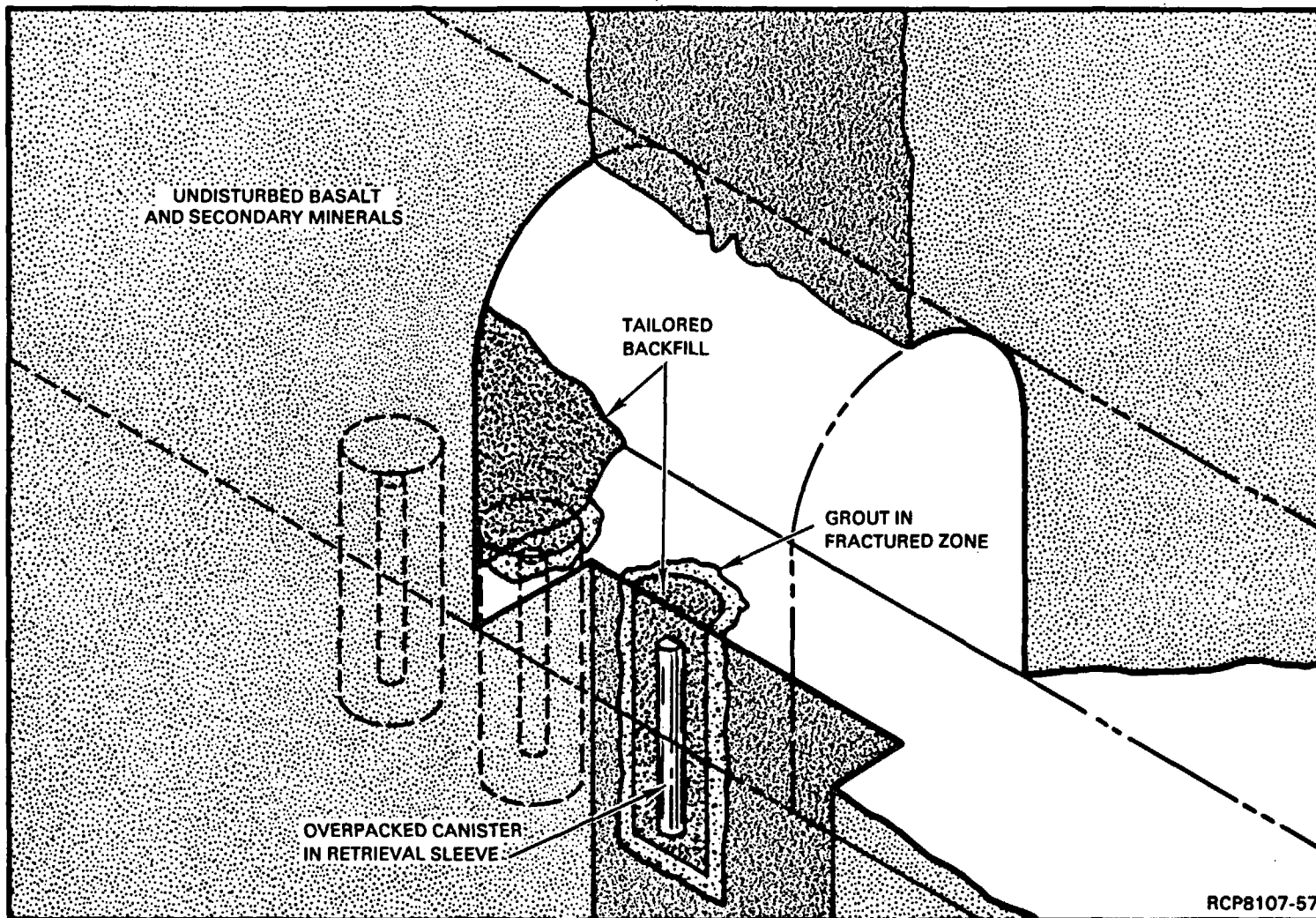


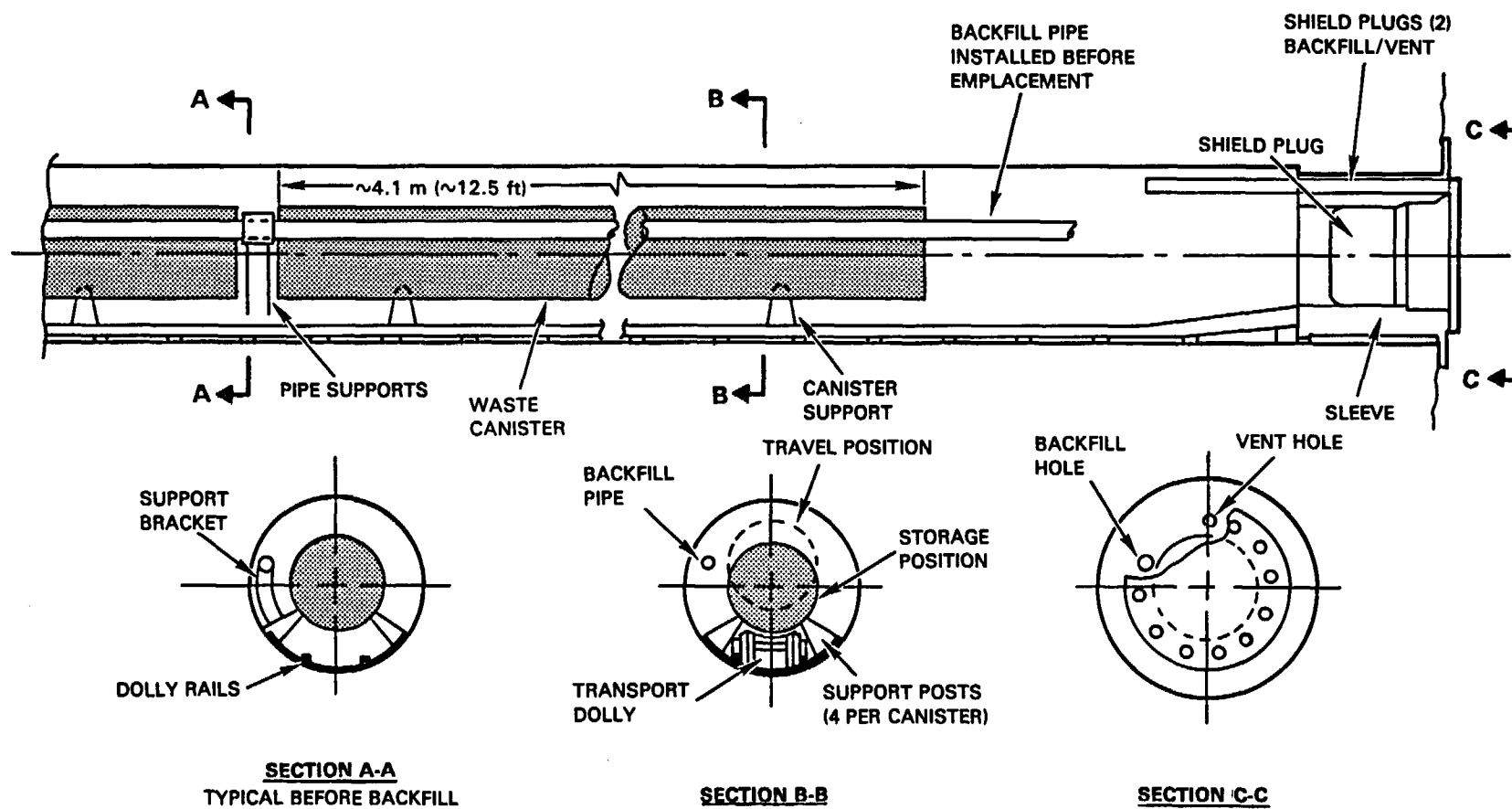
FIGURE 11-5. Typical Waste Package Emplacement Concept for Basalt (early design).

development program conducted by the BWIP to characterize the basalt site, sufficient site-specific data are now available to reevaluate and simplify the initial conceptual waste package design (Anderson, 1982). In addition to a simplified waste package concept, repository conceptual design studies (Chapter 10) propose horizontal borehole emplacement of the waste package as the reference design. The characteristics of the site in terms of radionuclide release and transport were a consideration in this reevaluation.

Important improvements in the definition of environmental conditions and their effects on waste package design were derived from: (1) additional heat-transfer analyses, which provided waste package component temperatures as a function of time after emplacement, (2) scoping analyses of the rate of water migration into the repository near field and through the waste package backfill, and (3) preliminary experimental results from hydrothermal tests, which indicated that a rapid reaction of groundwater with basalt occurs to establish anoxic conditions soon after repository sealing and decommissioning. A detailed discussion of these research effects on the waste package performance requirements is presented by Anderson (1982). A summary of the results is presented here.

Preliminary results of heat-transfer and groundwater-migration analyses and data from high-temperature rock-water interaction experiments indicate that the groundwater will not reach the canister until some time after repository decommissioning (greater than 100 years) and that the repository will have returned to anoxic conditions by that time. Furthermore, preliminary corrosion tests under anoxic conditions indicate that a carbon-steel canister approximately 1.1 centimeters thick can provide containment of the spent fuel or other waste form for 1,000 years. In view of these factors, the highly corrosion-resistant overpack is not needed to assure adequate containment. Due to the benign nature of the basalt groundwater and geochemical environment, the buffer also is not necessary. However, because all radionuclide releases from the waste form may not be solubility controlled below the current proposed limits (EPA, 1981; NRC, 1981) in the basalt environment, the function of the tailored backfill as a diffusion barrier to radionuclide release after canister degradation is retained. While not a required function, the presence of the backfill also provides additional assurance of radionuclide containment by delaying contact of the groundwater with the canister for a significant length of time and by radionuclide sorption-precipitation reactions. As more data are obtained on waste form stability and radionuclide solubilities under basalt environmental conditions, the backfill may decrease in importance or may even be eliminated as a component of the waste package for basalt.

As a consequence of the reevaluation, the initial waste package design and emplacement concepts have been simplified to that shown in Figure 11-6. (For Figure 11-6, spent fuel is the waste form. For a waste package containing borosilicate glass, the glass would be contained in a process container, which would be inserted in the canister.) The present reference waste package design concept for basalt consists of the waste form (spent fuel or borosilicate glass), the canister, and a tailored backfill.



RCP8205-44

FIGURE 11-6. Waste Canister in Horizontal Storage Borehole.

11.2.2 Functions of a Waste Package for Basalt

The operating bases, hence functions, for the waste package can be best described in terms of the repository history, which can be divided into two fundamental periods based on the prevailing conditions at the time.

The early history (e.g., up to 1,000 years) is defined as the containment period and is the period of time during which total containment of all radionuclides is proposed by the NRC (1981). It is also that interval of time during which the ambient geothermal gradient is greatly perturbed by the heat produced by radionuclide decay. This interval includes the portion of time before decommissioning when the repository is under institutional control. The second stage of repository history is the period of geologic control. It is defined as the interval of time after the thermal period when geologic conditions are slowly returning to a static, ambient, thermal condition but prior to decay of long-lived radionuclides to innocuous levels. It is also that period of time for which the proposed criterion (NRC, 1981) for control of any radionuclides that may be released from the engineered system is to be imposed. The different environmental conditions existing during these two time periods give rise to separate problems--different waste package functional requirements and, as a result, different waste package materials requirements.

The function of the waste package during the early repository history is to provide containment for radionuclides in conformance with proposed regulations (NRC, 1981; EPA, 1981) by employing an integrated system of physical and chemical barriers (components) that act in concert with the repository and surrounding geology. The components are not completely redundant to each other; rather, they are mutually supportive, which increases the reliability of performance of the multiple-barrier waste package system.

There are two subsystems within the waste package system. Physical containment of the hazardous material is provided by the impermeable canister. Both chemical and physical containment are provided by a back-fill that is specifically designed for the waste form and that is compatible with the geologic formation surrounding a nuclear repository in basalt. This system will be designed to operate to physically retard water ingress and to chemically restrict release of radionuclides in the event of premature failure of the physical barriers. Because the containment mechanisms of the two systems are different (i.e., physical isolation as opposed to chemical control), it is unlikely that both systems could be rendered inoperative by a single, maximum credible accident during the repository history.

As conceived, the waste package must be designed to meet the needs imposed by waste form leachability (a waste form-specific requirement) while simultaneously maintaining compatibility with the geologic environment (a site-specific requirement). Meeting these requirements is necessary to ensure that the waste package adequately prevents excessive release of hazardous material to the accessible environment in compliance

with the proposed release criteria in NRC (1981). To perform this function, it is required that each waste package be specifically designed around the characteristics of each repository and specific waste form. An important additional design constraint on waste package components is that they should not interact with each other or with the repository so as to diminish performance of the total engineered system.

There are two ways to inhibit dispersal of radionuclides from the waste form: prevent intrusion of water to the waste or remove dissolved waste components from contaminated groundwater by reaction with a backfill material. For redundancy, the operation of both mechanisms is required and will result in the need for a multicomponent waste package, such as the one depicted in Figure 11-6.

The functions of the components of the present reference waste package (Fig. 11-6) are tabulated in Table 11-16 for various periods of the repository history. The waste form has the same function as in the initial waste-package concept (Coons et al., 1980). The canister rather than the overpack, however, now has the function of providing the primary physical barrier to groundwater intrusion and subsequent release of radionuclides during the thermal period. The site conditions have eliminated the need for a buffer and overpack by providing an environment that inhibits canister corrosion (Anderson, 1982). The backfill functions remain the same, although the emphasis has been shifted to providing a physical barrier rather than a chemical barrier to radionuclide migration. At this time, the available data indicate that this simple waste package, acting in conjunction with the basalt system, is sufficient to provide reasonable assurance that adequate isolation can be maintained over a sufficiently long period of time (Anderson, 1982).

TABLE 11-16. Waste Package Component Functions Versus Repository History for Reference Waste Package Conceptual Design.

Barrier	Operating period	Function
Waste form	Preemplacement and repository life	Retard release of radionuclides upon breach of containment
Canister	Preemplacement	Provide physical support and protection of waste form
	Thermal period	Permit retrievability; primary physical barrier to groundwater intrusion and subsequent release of radionuclides
Backfill	Thermal period	Secondary physical barrier (radionuclide diffusion control)
	Geologic control (post-thermal)	Primary physical barrier; secondary chemical barrier (supports geology)

11.2.2.1 Canister Function. The function of the canister is to provide physical support and protection for the waste form during waste loading, handling, and transportation, to permit retrieval if necessary, and to act as a physical barrier to groundwater intrusion during the 1,000-year containment period and for as long as is reasonably achievable into the period of geologic control. Corrosion screening testing of several alloys in low-ionic-strength, anoxic groundwaters typical of a repository in basalt (Section 11.2.5) has provided preliminary verification that several among them could reliably perform to meet the proposed 1,000-year containment criteria. Analysis of the results of the screening testing suggests that either wrought or cast low-carbon steel would be prime candidates for canister design. For waste package conceptual design, wrought low-carbon steel has been selected. Its suitability as a material for continued design will be determined by further testing.

11.2.2.2 Backfill Function. Current data are insufficient to show that the waste form can, by itself, meet the proposed NRC (1981) release rate criterion. Thus, the primary function of the backfill is to aid the waste form in controlling hazardous radionuclide release to the host environment to less than 10^{-5} of the inventory per year after 1,000 years. The slow release criterion currently relates to the entire engineered barrier system (waste package plus repository). Since analyses have not been performed, it is not presently possible to assign partial responsibility for meeting this criterion to each of the parts of the system. It is, therefore, presumed for present waste package design that the slow-release criterion applies solely to the waste package until information becomes available (primarily by reliable modeling of radionuclide transport through the total system) to modify the waste package requirement. Using this assumption, the backfill is required to reduce the release rate of the hazardous radionuclides from the waste form. This can be achieved by (1) minimizing the flux of groundwater to the waste form, thereby limiting the release of radionuclides from the waste form to diffusion through the backfill and (2) maintaining a reducing (e.g., low-Eh) environment to ensure extremely low solubilities of some hazardous radionuclides (e.g., actinides). The question of the role/importance of the backfill as a component of the waste package is at issue and will be explored further.

The backfill must operate on a physical and chemical level to perform this function and it is unlikely that one material can work at both levels satisfactorily. On the one hand, minimization of groundwater and radionuclide transport through the backfill is primarily a physical process that is most easily accomplished by engineering a low-permeability medium that limits mass transport to diffusion. On the other hand, the capability of the backfill to create a reducing environment adjacent to the canister is a chemical process, the results of interaction between groundwater and backfill material.

For a repository in basalt, the tailored backfill material presently recommended by the BWIP is a mixture of approximately 25 percent sodium bentonite and 75 percent crushed basalt, by volume. The purpose of the bentonite is primarily to provide a low-permeability medium, thereby

ensuring diffusional control of mass transport. The purpose of the basalt is to: (1) improve the thermal properties (e.g., increase conductivity) of the backfill, (2) maintain a reducing environment suitable for promoting the low solubility of actinides and other elements with multiple oxidation states, and (3) precipitate certain elements (released from the waste form) as secondary minerals. In addition, the reducing environment also acts to minimize canister corrosion rates.

11.2.3 Reference Horizontal Borehole Emplacement

11.2.3.1 Waste Package Conceptual Design for Spent Fuel. The reference waste package conceptual design for horizontal borehole emplacement is illustrated in Figure 11-6. For spent fuel, rods from spent fuel assemblies are placed in the cylindrical canister in a close-packed array. Pins from seven boiling water reactor (or three pressurized water reactor) disassembled fuel assemblies are placed in a canister. The inside diameter of the canister is 30.5 centimeters (12 inches); the inside length is 3.7 to 4.1 meters (12.2 to 13.4 feet), depending on the length of the fuel pins placed in the canister. The wall thickness of the canister is sized to withstand hydrostatic pressure at the repository without plastic deformation, with an additional 1.1 centimeters (0.45 inch) allowed for loss of material by corrosion. The total thickness of the spent fuel canister is approximately 5.6 centimeters (2.2 inches).

The backfill of the reference waste package conceptual design is in the form of dense pellets of the backfill material. The pellets are blown into a 15-centimeter (6-inch) space surrounding the emplaced canister. The pack density required of the backfill to meet the maximum required permeability is 65 percent of theoretical density (35 percent porosity). If achievement of this pack density with backfill pellets, with the possible use of vibratory compaction, cannot be demonstrated, the alternate concept discussed in Section 11.5.2 can be used.

11.2.3.2 Reference Waste-Package Conceptual Design for Processed High-Level Waste. The components of conceptual designs for defense and commercial high-level waste packages for emplacement in basalt are the same as for spent fuel. The relevant package dimensions are described below. The waste form contained therein, however, is presently assumed to be produced and cast into a waste form container with no assigned containment function after repository emplacement of the waste. The major difference from waste package designs for spent fuel is in the dimensions of the canister.

11.2.3.2.1 Defense High-Level Waste Package. The waste form container for defense high-level waste is 61 centimeters (24 inches) outside diameter by 3 meters (118 inches) long. For the reference waste package conceptual design for borehole emplacement, the canister wall thickness is 8.7 centimeters (3.4 inches). The canister inside diameter of 63.5 centimeters (26 inches) provides sufficient clearance to allow insertion of the waste form container.

11.2.3.2.2 Commercial High-Level Waste Package. The waste form container for commercial high-level waste is 32.5 centimeters (12.75 inches) outside diameter by 3.1 meters (118 inches) long. The canister wall thickness is 5.3 centimeters (2.1 inches), with an inside diameter of 35 centimeters (13.8 inches) used to provide sufficient clearance to allow insertion of the waste form container.

11.2.4 Tunnel Emplacement Alternate

For continuing repository conceptual design studies the horizontal borehole emplacement is the reference, while the tunnel emplacement is an alternate.

11.2.4.1 Reference Waste Package Conceptual Design for Spent Fuel. The reference waste package conceptual design for tunnel emplacement of spent fuel differs from that for the horizontal borehole concept, primarily with respect to canister wall thickness. The wall thickness is increased to about 30 centimeters (12 inches) to provide radiation shielding for repository operations personnel. Because of the increased wall thickness, the canisters would be made of cast steel. The casting process would permit the optimization of the cross-sectional shape to allow a greater ease of handling and emplacement in the repository tunnels. A more detailed discussion of the tunnel emplacement waste packages may be found in AESD (1982).

11.2.4.2 Reference Waste Package Conceptual Design for Commercial and Defense High-Level Waste Borosilicate Glass. The reference candidate borosilicate glass waste packages for tunnel emplacement have not been developed. This is awaiting the completion of repository conceptual design studies.

11.2.5 Waste Package Component Reliability

Estimates of waste package component reliability have not been made to date. In the absence of reliability data, this section summarizes the results of corrosion screening tests, as well as states the limitations of single backfill materials and presents the assurance that a reliable backfill can be developed.

The identification of materials potentially suitable for the fabrication of canisters and overpacks has been made based on the results of early corrosion-screening testing of several alloys conducted by PNL for the BWIP (Anderson, 1981). This testing was conducted at 250°C in simulated Grande Ronde Basalt groundwater at a pH of 9.7 and a partial pressure of oxygen equal to 10^{-51} megapascals (10^{-50} atmospheres). This groundwater, pH, and extremely anoxic condition simulate those conditions expected in a repository in basalt following decommissioning and a return to conditions controlled by the geology. The results of the first phase of testing are tabulated in Table 11-17. Also tabulated are the wall thicknesses required for a 1,000-year canister life. These data were obtained

TABLE 11-17. Results of Screening-Corrosion Tests of Canister/Overpack Materials at 250°C, 5 MPa, and Under Anoxic Conditions.^a

Material	Reference simulated Grande Ronde groundwater (calculated O ₂ <1 mg/L)		Hanford groundwater (measured O ₂ range from 50 mg/L to 2 mg/L) ^b	
	Weight change (mg/dm ² ·yr)	1,000-yr ^c allowance ^d (cm)	Weight change (mg/dm ² ·yr)	1,000-yr ^c allowance ^d (cm)
Inconel 600	-6.3	0.050 - 0.080	-13.2	0.018 - 0.089
Hastelloy G	-22.8, -24.0	0.030 - 0.13	Not tested	--
Inconel 625	25.8	0.030 - 0.15	-3.6	0.016 - 0.081
Titanium, Gr. 2	+27.6, 0.0	0.030 - 0.15	+1.6	0.0099 - 0.048
Titanium, Gr. 12	-9.6, -19.2	0.033 - 0.16	+0.8	0.0041 - 0.020
Ferrallium 25-5	-264, -270	0.36 - 1.7	Not tested	--
Hastelloy C-276	-7.8	0.0089 - 0.043	-7.2	0.012 - 0.058
90-10 Cupronickel	-84.0	0.094	Not tested	--
70-30 Cupronickel	Not tested	--	-356	0.41 - 2.5
Zircaloy-4	+25.8	0.041 - 0.20	Not tested	--
Zircaloy-2	Not tested	--	+9.2	0.69 - 3.3
Inconel 825	-27.6	0.033 - 0.17	Not tested	--
Cast irons, gray and ductile	Not tested	--	-720 to -2,460	0.91 - 2.7
Austenitic stainless steel ^e	Not tested	--	-3.6 to -23.6	0.012 - 0.16
Ferritic stainless steel ^f	Not tested	--	-13.2, -20.4	0.014 - 0.71

^aExposure time was 60 days.

^bAfter Westerman, 1980.

^cDivided by 1,000 to obtain penetration rate.

^dCorrosion rates were obscured by formation of an adherent oxide film for all materials except cupronickel and cast iron. The tabulated allowance ranges are based on observed data for cupronickel and cast iron, and are estimated to range between observed and 5X observed for all others.

^e304, 304L, 316, and 321.

^f405 and 410.

by PNL in a parallel testing effort (Westerman, 1980). The range of the thicknesses shown reflects the uncertainty in the measurements introduced by the formation of an adherent corrosion-product coating during testing. The coating was not completely removed from several of the specimens before reweighing. There was no evidence of preferential attack, such as pitting or stress-corrosion cracking, observed on any of the prestressed specimens. Assuming that general corrosion is the only degradation mechanism operating, this corrosion testing gives preliminary assurance that there are many materials that will lead to canister lives of 1,000 years or more. Indeed, the structural requirements for moving canisters will mandate thicker canister walls than will likely be required to withstand corrosion.

Materials for possible inclusion in backfill have been identified that have the potential for chemically modifying the groundwater that may be found in a decommissioned repository constructed in basalt. It is yet to be determined whether their use will be required and be an effective means of protecting the canister to prevent premature failure by moderating the corrosivity of the intruding groundwater. Such additives to a backfill could also serve to mitigate the result of premature canister failure by retarding the release of waste to the repository. It must be recognized, however, that only a limited thickness of backfill can be contained between the canister and emplacement hole wall because of repository economics. Further, by the very nature of its operation, the backfill additives will be eventually neutralized. Therefore, it is intended only to "buy time" until repository conditions early in the thermal period become less severe with time. It is implicit that a potential backfill additive will be effective only in the case of a minor rupture of the canisters. The consequence of a catastrophic failure cannot be mitigated by a backfill additive.

Candidate backfill materials and additives have been selected for evaluation based on data and information taken from the literature, other NWTs programs, and international waste isolation programs. Since the backfill as a component of the waste package must be designed to function in a dual role, to exclude groundwater and to reduce the rate of release from the waste package, it may become a mixture of several materials. It is felt that, based on current knowledge, a reliable backfill can be developed to work with the other waste package components to successfully contain the nuclear waste form.

11.2.6 Summary of Important Conclusions

In this section, the functional requirements were defined for a waste package to contain nuclear waste to be emplaced in a repository in the deep basalt formations at Hanford. A multicomponent waste package concept and the package emplacement configuration developed by the BWIP for spent fuel and reprocessed high-level waste were described. Reference and alternate package concepts are being evaluated by the BWIP to assess their compatibility with the repository conceptual design and environmental conditions expected to exist at the repository horizon. Preliminary results of waste form and waste package materials testing under the

hydrothermal conditions expected in the repository and on the preliminary modeling of radionuclide behavior in the repository (both described hereafter) have resulted in these simplified package concepts. Continual evaluation of waste package concepts is an important part of the design process. As the design process evolves, determinations of waste package performance will be made and the results factored into the waste package design process. Evaluation is needed to achieve cost-effective waste packages that will meet the NRC proposed containment criteria, radionuclide-release criteria, and other applicable criteria developed by the Federal Government.

11.3 RESEARCH AND DEVELOPMENT

11.3.1 Approach To Research and Development

A policy of technical conservatism for the isolation of nuclear wastes in deep geologic repositories is being pursued by the NWTs Program. This policy calls for the development of a multiple-barrier waste package that will act in concert with natural geologic barriers to successfully isolate nuclear waste. The BWIP Waste Package Program addresses licensing and long-term performance assessment information needs and data required to complete the design process.

The BWIP is cognizant of the proposed NRC (1981) 1,000-year containment criterion and the Waste Package Program fully addresses this criterion by orienting the selection of waste package materials to achieve this goal. It is strongly believed that, in addition to the need for achieving this primary goal, it is necessary to understand how the waste package is required to support the NRC (1981) proposed repository release criterion, the EPA (1981) draft release standard, and the consequence of radionuclide release in the event of premature breach of physical containment during the initial 1,000 years following emplacement. This understanding is to be achieved in the BWIP waste package approach through an assessment of radionuclide behavior (precipitation, dissolution, sorption) in the very near-field environment of the repository in basalt. Preliminary estimates of long-lived radionuclide solubilities indicate that this assessment could reduce the design constraints on the waste package after the 1,000-year containment period and will lead to the development of more cost-effective waste packages than those that would be developed in the absence of such considerations (Wood, 1980b).

The BWIP approach to materials testing focuses on the evaluation of existing waste forms, barrier materials, and the waste package environment expected in basalt, to obtain an understanding of the behavior of these materials under expected repository conditions. The approach proceeds from an initial far-field performance, defining assessment of the maximum allowable release rates of radionuclides to the accessible environment, using a very conservative one-dimensional transport model. This feature recognizes that a waste package must be viewed as a contributor to overall engineered and natural barrier performance. From the far-field performance assessment, key radionuclides (those for which release criteria are most stringent) have been identified (Barney and Wood, 1980). Preliminary performance requirements for waste packages have been established that will limit or retard transport of these key radionuclides from the very near field to meet EPA (1981) draft release criteria to the accessible environment (Section 11.3.2.4). Extensive hydrothermal testing of waste package component materials is being conducted under a range of carefully controlled conditions extending from the normal to the disruptive and reflecting those expected in a repository in basalt. These data will permit the selection of suitable waste package component (canister, over-pack, buffer, backfill) materials and will define thicknesses of the

barrier that will meet the 1,000-year containment requirement. Continued testing of component assemblages and, eventually, full-scale waste packages in the presence of radioactive waste forms (hot cell testing) will be used to: (1) refine package performance requirements, (2) support modeling activities, (3) prepare preliminary and final design requirements, and (4) qualify waste package designs to support repository licensing activities at the Hanford Site. Eventually, they will also be used to validate design and waste package performance.

The BWIP approach also focuses on the development of waste packages that are cost effective in meeting the requirements for safe containment of nuclear wastes in basalt. The program recognizes that in a basalt environment the eventual release of many long-lived radionuclides to the accessible environment will be solubility limited and that these constraints should reduce the complexity, and hence the cost, of packages needed to meet the NRC-proposed long-term, engineered system release criterion (NRC, 1981). Preliminary performance estimates indicate that waste package designs for basalt may not require physical containment of all radionuclides, as presently required by the proposed NRC 1,000-year criterion (Wood, 1980a; 1980b). This feature may greatly reduce waste package complexity for a repository in basalt. Therefore, in addition to using the 1,000-year containment criterion as a basis for canister and overpack materials evaluation, the BWIP approach also addresses the development of an understanding of radionuclide behavior to select buffer and backfill materials for their ability to moderate the corrosivity of the groundwater and limit or retard those radionuclides that are relatively mobile in basalt.

Data and information needed to support preparation of design requirements for site-specific waste packages are being obtained by conducting a sequence of extensive nonradioactive tracer and, eventually, fully radioactive (hot cell) hydrothermal tests of waste forms in host rock with various candidate barrier materials in Grande Ronde Basalt groundwater under controlled Eh and pH conditions. A major emphasis in emplacement environment characterization is to provide a basis for the test conditions used in the hydrothermal tests. Success of waste package development requires a thorough understanding of the surrounding natural (geologic) environment and its capability to limit or retard radionuclide transport from the repository to reduce waste package complexity as much as possible.

The logic governing the conduct of the BWIP Waste Package Program is shown in Chapter 15 (Fig. 15-4), along with summary narratives of each ongoing activity.

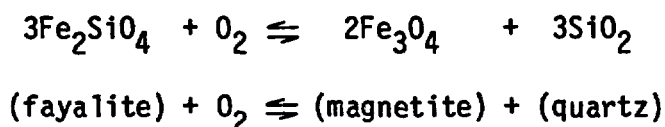
11.3.2 Status of Research and Development

11.3.2.1 Waste Form. The BWIP Waste Package Program is presently scoped to assess the performance of two waste forms, spent fuel and reprocessed high-level waste, under conditions expected in a repository constructed in

basalt. In the past, crystalline ceramic waste forms (supercalcine, Synroc, tailored ceramics, etc.) were considered viable alternates to glass. Crystalline ceramics are still an alternative to glass for defense waste, but are not being considered for commercial waste. Prior to the exclusion of supercalcine as an alternate commercial waste form, the BWIP had conducted limited studies to assess its stability in the repository. The reported data that follow were obtained under conditions that are assumed worst-case conditions for a repository in basalt. The BWIP plans to continue testing under these conditions as well as under expected conditions.

11.3.2.1.1 Hydrothermal Reaction of Spent Fuel and Water. Partial dissolution of the radionuclides present in spent fuel will conceivably occur if the solid fuel comes in contact with groundwater at the high temperature and pressure (hydrothermal) conditions expected in a geologic repository. The extent of any such dissolution will be significantly influenced by the chemical composition of the groundwater, particularly its pH. The oxidizing or reducing capacity of the repository environment will also affect dissolution rates, particularly for elements such as uranium, that can exist in either multiple oxidation states or have differing solubilities. The two most common ways of characterizing the oxidizing power of the environment are in terms of its oxidation-reduction potential (Eh) or its oxygen fugacity (fO₂). These are essentially equivalent; low fO₂ and low Eh are referred to as reducing environments.

As will be discussed in Section 11.4, reducing conditions are expected shortly after closure of a nuclear waste repository in basalt. In basalt, the oxygen fugacity is dictated by iron-bearing phases in the rock. In an oversimplified form the controlling reaction may be written as:

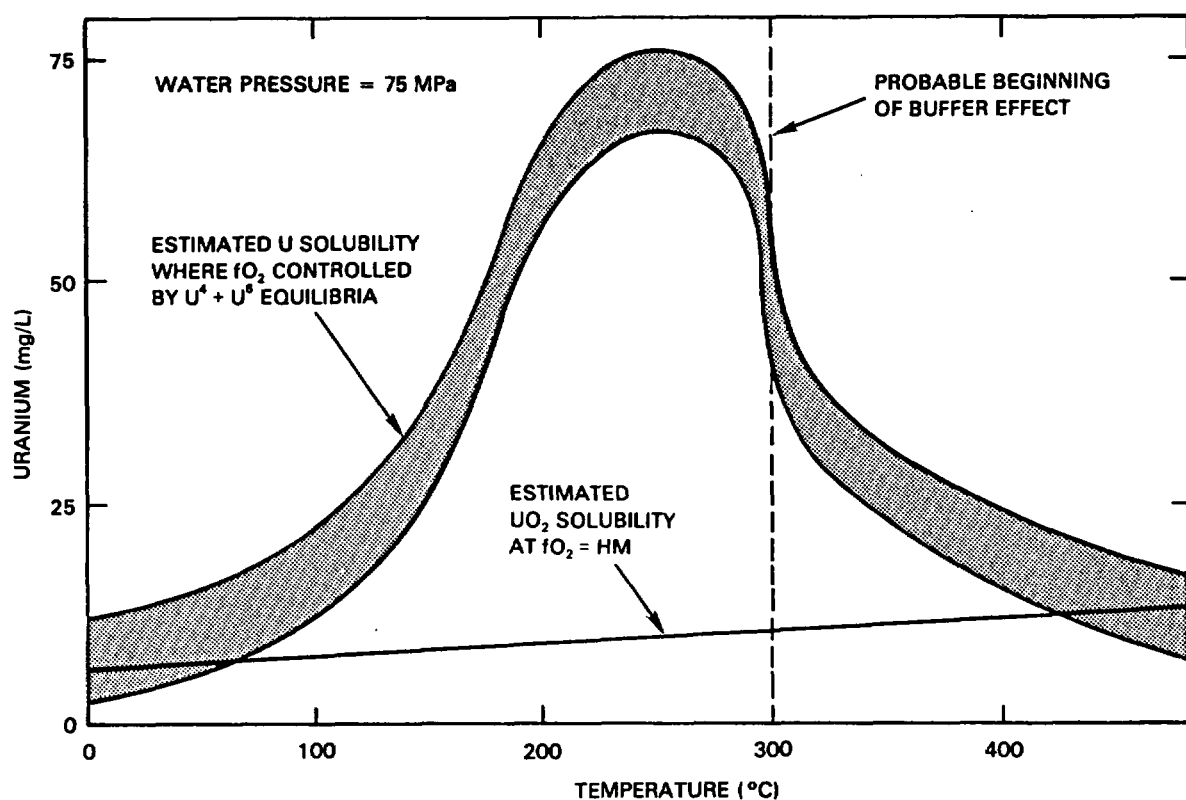


At 650°C (initial estimate of repository temperature), the oxygen fugacity of this buffer is 10⁻⁶⁸ megapascals (10⁻⁶⁷ atmospheres) (Eugster and Wones, 1962). Under such highly reducing conditions, the stable uranium-bearing solid will probably be uraninite (UO₂).

No experiments have been performed with simulated spent fuel, in which direct control of oxidation reduction potential has been attempted. However, data from UO₂ dissolution experiments (Lemoine, 1975; Langmuir, 1978) give an indication of the effects that oxidation reduction have upon potential uranium leachability from spent fuel. Lemoine (1975) obtained the uranium solubility- (in distilled water) versus-temperature curve shown in

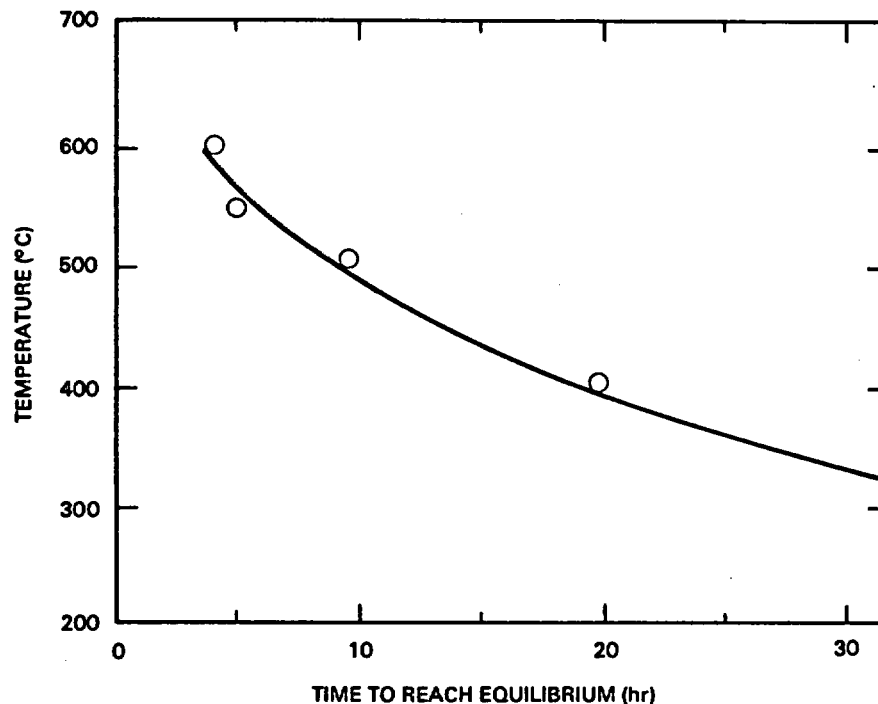
Figure 11-7, using a platinum membrane and a hematite-magnetite solid-state buffer (Eugster and Wones, 1962) to fix the oxygen fugacity. Unfortunately, the solubility curve is not generated at a constant oxygen fugacity, as is apparent for the maximum in the curve. Chou and Eugster (1978) demonstrated that the platinum membrane becomes inoperative below 300°C, as shown in Figure 11-8.

Thus, in Lemoine's experiments, the uranium concentration in the distilled water below 300°C was controlled by oxygen present in the capsule rather than by the solid-state buffer. This portion of the curve may be representative of uranium solubilities in the repository immediately following closure, when the oxidation reduction potential will be near that of atmospheric oxygen. At 300°C and above, the membrane was permeable, allowing the hematite-magnetite buffer to control the oxygen fugacity. The lower oxidation reduction potential stabilized the relatively insoluble UO_2 phase, as reflected by the rapid decrease in the concentration of uranium in solution above 300°C.



RCP8107-84

FIGURE 11-7. Solubility of UO_2 in Water as a Function of Temperature; fO_2 in the Experiments Buffered by the Equilibrium between UO_2 and UO_3 under Oxidizing Conditions (after Lemoine, 1975). Estimated UO_2 solubility at hematite-magnetite (HM) fO_2 plotted as thin line.



RCP8107-85

FIGURE 11-8. The Approach to Equilibrium Using a Hydrogen Diffusion Membrane (after Chou and Eugster, 1978).

Simulated spent fuel has been hydrothermally tested for leach resistance at The Pennsylvania State University (Smith et al., 1980). The composition of this synthetic spent fuel is shown in Table 11-18. It is a fine-grained, generally unconsolidated powder that is a physically poor representation of actual spent fuel, since the latter is heterogeneous and coarse grained. However, the simulated waste is, at present, the only usable material for studies conducted in conventional (cold) laboratories. Results generated using this high-surface-area powder probably represent highly conservative (i.e., worst case) values for spent fuel leaching.

The results of preliminary experiments at 150° to 300°C at 30 megapascals are listed in Table 11-19. Above 100°C, cesium, rubidium, and molybdenum (and by analogy, technetium) were nearly totally leached from the synthetic spent fuel. These data are preliminary in nature and probably are not representative of the repository behavior of actual spent fuel. However, analyses of cooling water (approximately 50°C, oxidizing conditions) from storage pools with failed fuel rods tend to corroborate the observation that cesium is the most soluble element in actual spent fuel. In these pools, which are mildly acidic (pH 4.5 to 5.5), about 72 percent of the total radionuclide activity detected in solution is cesium, while strontium accounts for approximately 27 percent of the activity (Johnson, 1977). A small amount of ¹³¹I has been detected. Iodine-129, while not detected, should also be present. Ambient pressure leach tests of actual light water reactor fuel by the Paige method (Katayama, 1976; 1979) also indicate that cesium, strontium, plutonium,

TABLE 11-18. Simulated Spent Fuel Fission Products Formulation^a
(burnup of 33,000 MWd/thm) (after McCarthy et al., 1978a).

Element	Atomic %	Formulation for a 100-meq batch	Oxide	Oxide (wt%)
Zr	16.51	4.408g $\text{ZrO}(\text{NO}_3)_2 \cdot 2\text{H}_2\text{O}$	ZrO_2	14.3
Mo	14.80	2.131g MoO_3	MoO_3	14.9
Nd (Pm) ^b	11.37	4.980g $\text{Nd}(\text{NO}_3)_3 \cdot 6\text{H}_2\text{O}$	$\text{NdO}_{1.5}$	13.4
Ru	9.19	27.5 mL 10% Ru nitrate solution	RuO_2	8.5
Cs	8.41	1.640g CsNO_3	$\text{CsO}_{0.5}$	8.3
Ce	7.94	3.454g $\text{Ce}(\text{NO}_3)_3 \cdot 6\text{H}_2\text{O}$	CeO_2	9.5
Pd	4.98	5.3 mL 10% Pd nitrate solution	PdO	4.2
Sr	4.21	0.893g $\text{Sr}(\text{NO}_3)_2$	SrO	3.1
Ba	4.21	1.099g $\text{Ba}(\text{NO}_3)_2$	BaO	4.5
La	3.74	1.619g $\text{La}(\text{NO}_3)_3 \cdot 6\text{H}_2\text{O}$	$\text{LaO}_{1.5}$	4.3
Pr	3.58	1.564g $\text{Pr}(\text{NO}_3)_3 \cdot 6\text{H}_2\text{O}$	$\text{PrO}_{1.5}$	4.1
Sm	2.18	0.968g $\text{Sm}(\text{NO}_3)_3 \cdot 6\text{H}_2\text{O}$	$\text{SmO}_{1.5}$	2.6
Y	2.18	0.835g $\text{Y}(\text{NO}_3)_3 \cdot 6\text{H}_2\text{O}$	$\text{YO}_{1.5}$	1.7
Te	1.87	0.299g TeO_2	TeO_2	2.1
Rh	1.56	1.61 mL 10% Rh nitrate solution	$\text{RhO}_{1.5}$	1.4
Rb	1.56	0.231g RbNO_3	$\text{RbO}_{0.5}$	1.0
Gd (Eu, Am, Cm)	1.09	0.492g $\text{Gd}(\text{NO}_3)_3 \cdot 6\text{H}_2\text{O}$	$\text{GdO}_{1.5}$	1.4
Ag	0.31	0.050g AgNO_3	$\text{AgO}_{0.5}$	0.4
Cd	0.31	0.040g CdO	CdO	0.3
				100.0

^aTc, I, Kr, and Xe are not included by the Pennsylvania State University.

^bElements in parentheses indicate that the preceding element is a stand-in for an actual waste element.

TABLE 11-19. Compositions of Residual Solutions from Experiments^a Reacting Simulated Spent Fuel with Distilled Water at 30 Megapascals.

Element	Dissolved concentration (μg/mL)	Relative % dissolved
Temperature = 300°C		
Rb	33	100
Cs	281	100
Sr	ND ^b	--
Mo	190	54
U	3	0.004
Others ^c	ND	--
Temperature = 200°C		
Rb	44	100
Cs	363	100
Sr	1	1
Mo	308	87
U	1	0.003
Others	ND	--
Temperature = 100°C		
Rb	5	16
Cs	51	19
Sr	4	4
Mo	25	7
U	10	0.01
Ba	5	3.5
La	1	0.8
Nd	ND	--
Zr	ND	--
Others	ND	--

^a8 weeks duration; 10:1 water to solid ratio; no oxygen control prior to sealing samples.

^bNone detected by atomic absorption, atomic emission, or fluorometry.

^cBa, La, Nd, and Zr were not detected in solution.

curium, and uranium are leached from spent fuel at significant rates by deionized water. It should be noted that these latter tests were conducted in atmospheric oxygen and, therefore, are not directly extendable to probable repository conditions.

The observed cesium and strontium solubilities in spent fuel correspond well with the phases in irradiated UO_2 . Cesium has been observed as Cs_2O , CsI , Cs_2MoO_4 , and $\text{Cs}_2\text{U}_2\text{O}_7$ (Cubiccioni and Sanecki, 1978). These phases are all highly water soluble, and tend to concentrate in the outer portions of the fuel pellet as a result of volatilization. Strontium oxide, which has a solubility of 0.23 gram per milliliter in water at 100°C , has been observed both in the exterior portions of the fuel pellet and in the interior adjacent to the central void (Koizumi et al., 1974).

11.3.2.1.2 Hydrothermal Reaction of Borosilicate Glass and Water.
Borosilicate glass has been advanced as a leach-resistant waste form that could flexibly accommodate the variations in waste streams arising from the reprocessing of commercial spent fuel. The use of glass as a waste form has created considerable controversy, with some researchers pointing to thermodynamic instability, potential leachability, and reactivity (Roy and Yoder in Carter, 1979; Ringwood, 1978) as disqualifying factors. Others cite low experimental leach rates and persistence of volcanic glass as favorable evidence of the suitability of glass. The debates, plus a long history of waste-glass form research, have resulted in a substantial body of waste-glass performance data, allowing a thorough treatment of borosilicate glass performance.

Various experimenters have subjected borosilicate glass formulations to hydrothermal testing. Most of this experimental work has been done using PNL 76-68 glass. The composition of this glass, which was developed for a PW-7a waste stream (see Table 11-1), was given in Table 11-2. Selected results from long-term hydrothermal leach tests under oxidizing conditions ($f\text{O}_2 = \text{air}$) are shown in Table 11-20. These results cannot be quantitatively applied, because experimental conditions employed in gathering the data were insufficiently controlled.

The data in Table 11-20, however, show that glass tends to release greater quantities of radionuclides at worst-case repository temperatures (300°C). These experiments were conducted by sealing the ground glass and water in gold tubes that were heated in an autoclave. It is also apparent that glass solubility decreases as temperature decreases. The dramatic decrease in dissolved radionuclide concentrations at low temperatures is somewhat misleading, however. The concentrations of dissolved silica, sodium, and boron (all glass network formers) clearly indicate corrosion and degradation of the glass structure. This result implies that the concentrations of dissolved radionuclides will increase if the leach duration is increased even at low temperature. The net result suggests that, given sufficient time, glass may break down even at low temperature and ultimately release greater amounts of contained waste than indicated by the short-term experiments that have been conducted to date. There are insufficient data, however, to quantitatively define the long-term leachability of borosilicate glass versus spent fuel, but glass appears to be a less leachable waste form (McCarthy et al., 1978a).

TABLE 11-20. Compositions of Residual Solutions from Experiments^a Reacting Simulated PNL 76-68 Glass in Distilled Water at 30 Megapascals.

Element	Dissolved concentration (μg/mL)	Relative % dissolved
Temperature = 300°C		
Rb	3	2
Cs	140	14
Sr	ND ^b	--
Mo	1,050	68
U	2.6	0.1
Ba	1	0.1
Si	610	0.3
Na	8,500	9.0
B	15,000	52.0
Others ^c	ND	--
Temperature = 200°C		
Rb	ND	--
Cs	10	1.0
Sr	ND	--
Mo	405	26
U	17	0.4
Ba	ND	--
Si	590	3.1
Na	2,000	21.3
B	1,600	53.8
Others	ND	--
Temperature = 100°C		
Rb	ND	--
Cs	6	0.6
Sr	1	0.01
Mo	40	2.4
U	1.6	0.01
Ba	ND	--
Si	330	1.7
Na	280	2.9
B	90	3.0
Others	ND	--

^a4 months duration; 10:1 water to glass ratio.

^bNone detected by atomic absorption, atomic emission, or fluorometry

^cLa, Nd, and Zr not detected in solution.

To predict the long-term leaching behavior of glass, it is necessary to perform experiments that lead to an understanding of the mechanisms by which glass dissolves. A mechanistic interpretation is a prerequisite for any quantitative extrapolation of experimental results to long geologic times. Various experimental methods are used to enhance reaction rates and gain a definition of steady-state dissolution kinetics. The first method is to use relatively high temperatures (generally around 300°C) and to assume that mechanistic information obtained at such temperatures can be extrapolated down to the milder conditions expected in a repository. The geometry of a glass monolith within a canister can be scaled down by using small-diameter cylinders or spheres, thereby increasing the surface area and accelerating the reaction rates.

Dissolution-rate experiments have been performed on glass spheres (McCarthy et al., 1978a) and cylinders (Westsik and Turcotte, 1978) at temperatures near 300°C in distilled water. In these experiments, a 1.3-centimeter-diameter cylinder hydrated (diffusion of water into the glass) completely after 1 week at 350°C (Westsik and Turcotte, 1978). Extrapolation of these data using standard diffusion equations (Carslaw and Jaeger, 1959) indicates that a full 30.5-centimeter canister of solid glass would completely hydrate in 10 years. Even if this estimate is inaccurate by 1 order of magnitude, 10 to 100 years is a relatively brief span in terms of repository history. It can, therefore, be concluded that an unprotected waste-glass cylinder will rapidly hydrate in contact with groundwater in the event of a canister rupture under worst-case repository conditions. The significance of this result is that inward diffusion of water is the preliminary step to leaching of the mobile constituents of the waste glass. Thus, favorable conditions for leaching of such components could be established rapidly if canisters were to rupture early in the life of a geologic repository in a saturated storage environment. Since hydration is a function of temperature, it would be advantageous to minimize water contact with the glass during the thermal period. To delay mobilization of elements, it would be necessary to provide a relatively impermeable component of the waste package, such as the backfill containing clay, to retard the intrusion of groundwater at least until the maximum temperature has passed.

McCarthy et al. (1978b) performed semiquantitative electron-microprobe analyses of borosilicate glasses that had been leached for 4 weeks at 300°C and 30 megapascals pressure. As can be seen from a scanning electron micrograph (Fig. 11-9), four distinct zones and a rind of encrusted material are clearly visible after leaching under these conditions.

The nature of the zones and the diffusion phenomena that created them can be elucidated by plotting the microprobe analyses as a function of distance across the specimen. The data for each oxide analyzed are shown as the ratio of weight percent divided by the weight percent of SiO₂ in Figure 11-10. It may be seen from this figure that uranium is depleted in the outer zones of the PNL 76-68 glass relative to silicon, indicating that it is leached faster than the latter network-forming element. The



FIGURE 11-9. Scanning Electron Micrograph of a Section through the Product of a 4-Week Hydrothermally Treated Sample of a PNL 76-68 Glass Specimen (after McCarthy et al., 1978b; no scale provided).

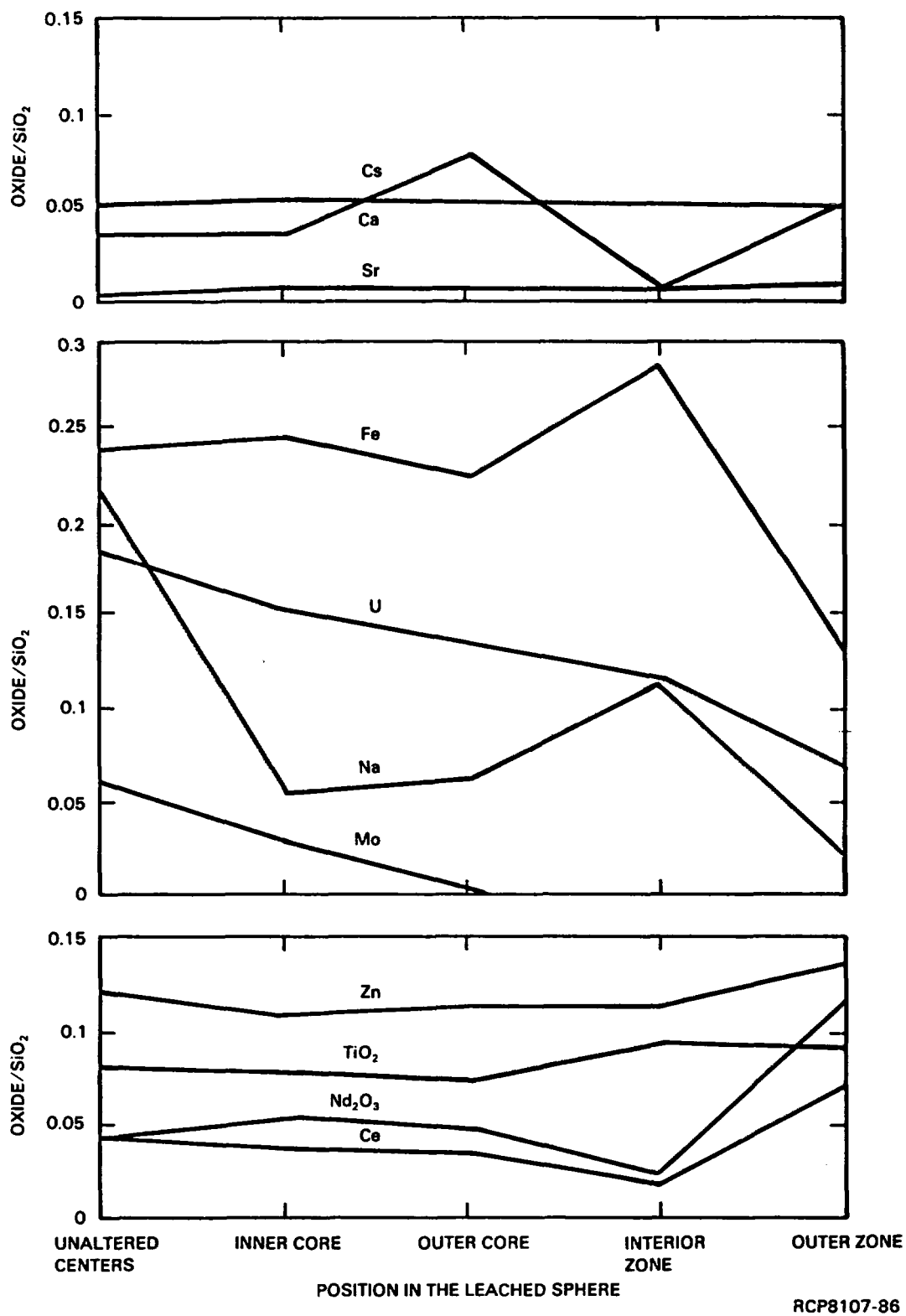


FIGURE 11-10. Composition Distance Profile for Leached PNL 76-68 Glass Sphere Shown in Figure 11-9.

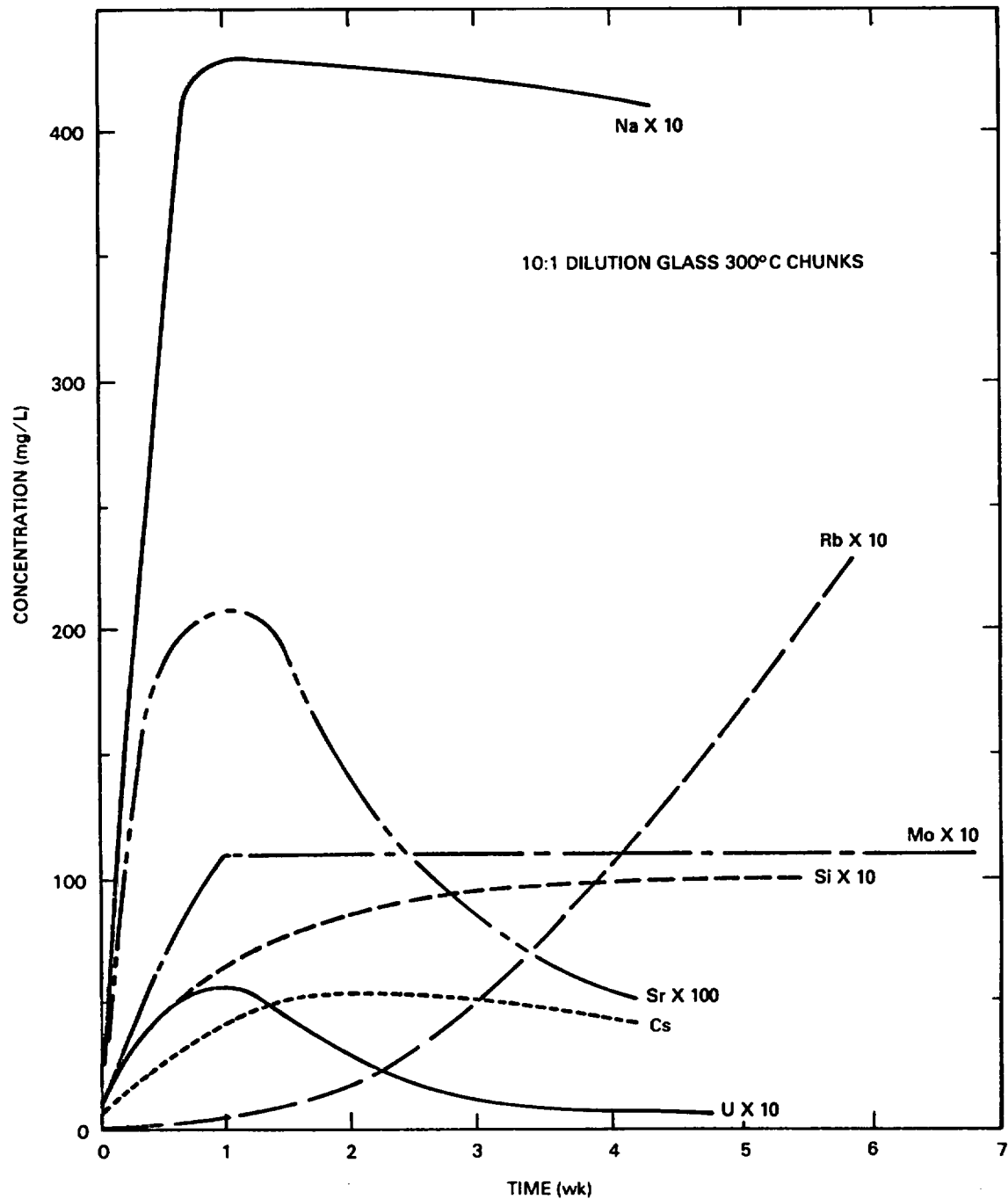
same observation applies to molybdenum and also, by analogy, to technetium, under the oxidizing conditions of the experiment. In contrast, the refractory oxides Nd_2O_3 , CeO_2 , and ZrO_2 show enrichment relative to silicon in the outer zone and depletion in the innermost regions of the sample. This may be explained by the low solubilities of these oxides in hydrothermal solutions; transfer from solid to solution is inhibited and oxide concentration builds up in the solid near its interface with the solution. Iron oxide and Na_2O appear to be leached more rapidly than SiO_2 in the outer zone, but exhibit erratic behavior, with peaks in the interior zone. This latter region of the specimen is largely crystalline, however, containing sodium-iron metasilicates and opaque oxides. Crystallization of the glass matrix leads to dramatic changes in the thermodynamic properties of the specimen. Therefore, the behavior of sodium and iron cannot be quantitatively interpreted at this stage.

To this point, discussion of the hydrothermal leaching of waste glass has focused on the interior alteration zones. In the past, more attention has been directed at the thin, encrusting rind, which is enriched in uranium and strontium (McCarthy et al., 1978b; Westsik and Turcotte, 1978), and in potential actinide hosts (McCarthy et al., 1978a). However, the evidence points to the conclusion that the outermost rind is generated during cooking (quenching) of the sample at the termination of the experiment. The rind is always the same thickness, regardless of the duration of the experiment, and it contains phases and textures that indicate it is a quench phenomenon. Thus, the rind should not be relevant to repository conditions, since it is an artifact of the experimental method rather than a true dissolution reaction zone.

The Group II elements, strontium and calcium, appear to dissolve at the same rate as silica, indicating a direct correspondence between silicon-oxygen and Group II bonds. If this relationship extends to radium, also a Group II element, then radium release will also be directly linked to the dissolution of the silicate network in the glass and will parallel the release of silica.

Figure 11-11 illustrates a compilation of solution-composition data extracted from the literature (Turcotte and Wald, 1978; McCarthy et al., 1978b). Data from experiments conducted under similar conditions at different laboratories are in agreement (Westsik and Turcotte, 1978).

Solution results also suggest early dissolution followed by precipitation and an approach to a steady state. The coincidence of cesium and uranium maxima with silica saturation verifies the contention of McCarthy et al. (1978b) that wecksite $(\text{K,Cs})_2(\text{UO}_2)_2(\text{Si}_2\text{O}_5)_3 \cdot 4\text{H}_2\text{O}$ is a stable product of hydrothermal glass leaching experiments. Similarly, the coincidence of the maximum with molybdenum saturation can be attributed to powellite $(\text{Ca,Sr})\text{MoO}_4$ precipitation. Both of these solids have been identified following hydrothermal reactions of simulated waste glass, but their stability in equilibrium with the solid and solution at temperature and pressure has been uncertain up to now. The solution data presented here confirm these stabilities and imply that uranium, strontium, and perhaps technetium will be at least partially immobilized, even under oxidizing conditions.



RCP8107-87

FIGURE 11-11. Solution Concentrations of Various Ions from PNL 76-68 Glass as a Function of Time at 300°C, 30 Megapascals in Deionized Water.

Solubility behavior of solids is almost always affected by changes in temperature. At this time, accurate estimations of solution composition limits for glass radwaste oxides are not available. However, a qualitative measure of the effect of temperature may be seen in Table 11-20. At this time it is unclear to what extent solution composition is controlled by kinetic and/or quenching phenomena or to what extent the composition differences reflect changes in equilibrium-saturation values. However, it appears that at 100° to 200°C very little hazardous material is leached from glass. (Borehole wall temperature during the thermal period is expected to be 200°C or higher.) It should be noted that the experiments on which this statement is based lasted only 28 days, and while only a small amount of "fission products" were dissolved, the borosilicate network was severely degraded. These accelerated leaching experiments used high temperature, a large glass surface-to-volume ratio, and a high water-to-solids ratio.

11.3.2.2 Design and Development. Until the end of fiscal year 1982, the BWIP waste package design and development activity encompassed only those activities required to develop conceptual design requirements for site-specific waste packages to be emplaced in a repository located in basalt. These requirements were used by an engineering firm accountable to the Office of Nuclear Waste Isolation to develop waste package conceptual designs for basalt. Beginning with fiscal year 1983, the BWIP waste package design effort was expanded to include the responsibility for managing the preliminary and final design of waste packages for a repository in the basalt underlying the Hanford Site. This section discusses the status of research and development on waste package design.

Data have been collected from materials testing and repository conceptual design activities within the BWIP to provide the basis for preparation of conceptual design requirements. The BWIP conceptual waste package for spent fuel and borosilicate glass was discussed in Section 11.2.3.

As part of continuing studies to determine waste package design constraints, preliminary work has been conducted for the early concept of vertically emplaced waste packages, to define the thermal history of a spent fuel waste package emplaced in basalt (Altenhofen, 1981). The conceptualized spent fuel waste package emplaced in basalt was modeled using the heat transfer computer code, HEATING5. This code uses the Crank-Nicholson finite-difference method to evaluate transient temperature behavior. Transient heat transfer analysis is necessary because the heat generated by spent fuel varies with the radioactive decay of fission products. One- and two-dimensional versions of the HEATING5 computer code were first used to determine average rock temperatures at the repository level over the first 10,000 years of repository life. A precise three-dimensional computer model (HEATING5) was then used to determine the very near-field rock and emplacement hole surface temperatures during the first 1,000 years of repository life. Assuming a quasi-steady-state equilibrium condition between the emplacement hole surface and the waste package, steady-state calculations were made to determine temperature histories of various components of the waste package.

For modeling purposes, waste packages, each containing three 10-year-old pressurized water reactor disassembled spent fuel assemblies, were assumed to be emplaced in single rows in long parallel repository rooms separated by basalt pillars. This represents the early design used by the architect-engineer. The individual waste packages were placed in a single row of drilled holes with a center-to-center pitch of 3.66 meters (11.1 feet) in the floor. The separation distance between rows was 36.6 meters (111 feet). The spent fuel rods were placed in a close-packed array inside a carbon-steel canister. A layer of bentonite surrounded the canister, and the canister and bentonite were placed inside a titanium overpack. The canister/overpack assemblage was then surrounded by a backfill layer composed of bentonite clay and a crushed basalt mixture in contact with the emplacement hole surface. Thermal properties of materials in this analysis were based on experimental values and literature data.

The waste package heat transfer analysis was based on assumptions that are necessary in computer-aided modeling of repository conditions and are shown in Table 11-21. It should be noted that these assumptions tend to overestimate the temperatures and hence produce conservative analyses. The results of modeling 10-year-old spent-fuel waste packages are given in Figure 11-12.

TABLE 11-21. Assumptions Used for Thermal Modeling of Spent Fuel Waste Packages in Basalt.^a

-
- Simultaneous emplacement of waste packages each containing 10-yr-old unprocessed spent fuel.
 - Air in rooms above package is stagnant and radiation heat transfer is neglected during retrieval period (first 50 yr).
 - Ambient temperature = 65°C^b at the repository level.
 - Basalt media are semi-infinite.
 - Basalt media are dry.
 - The waste package contents are in quasi-steady-state equilibrium with the basalt.
 - Backfilled regions (waste package and emplacement room) remain unsaturated throughout the analysis.
-

^aSee Altenhofen (Table 2, 1981) for detailed material thermal properties used for modeling.

^bInitial conservative temperature estimate of 65°C used for modeling. Present maximum for the lowermost candidate horizon (Umtanum) is estimated to be 58°C.

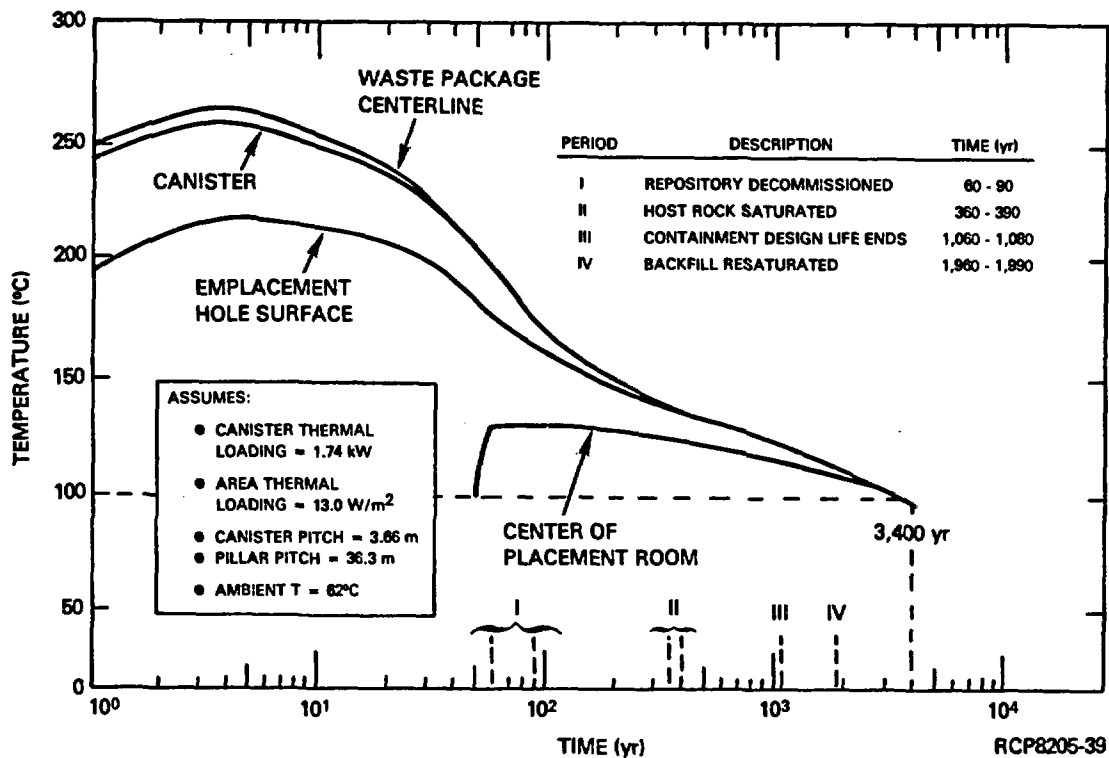
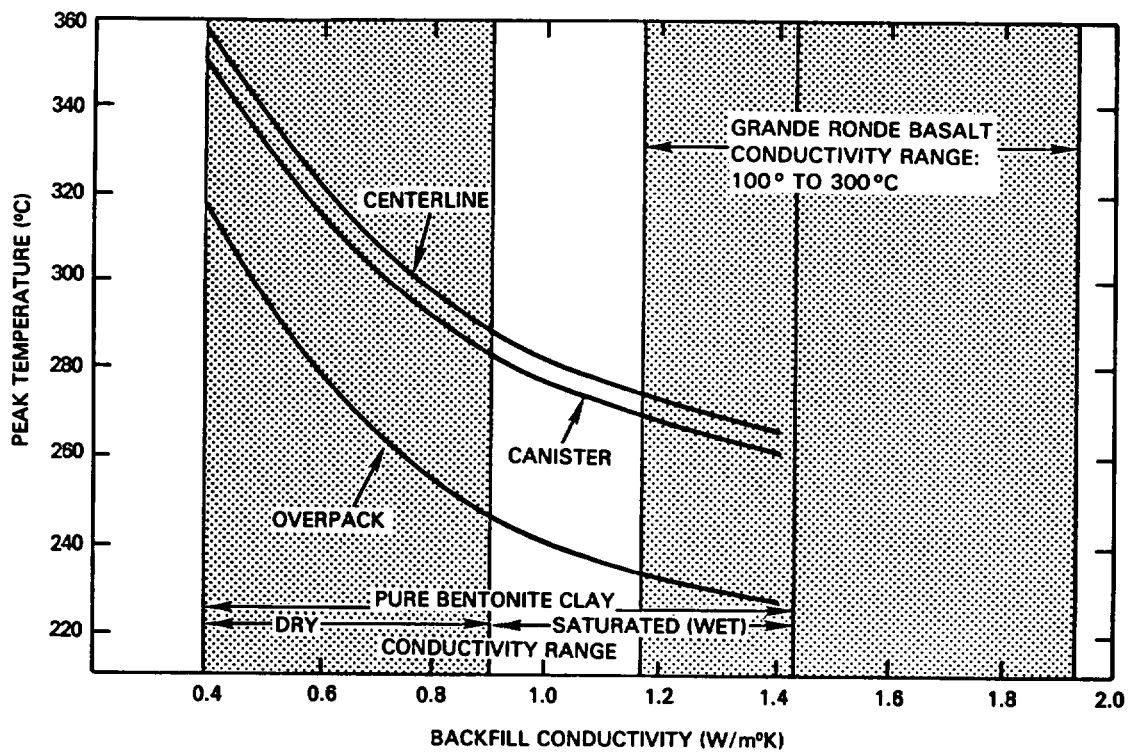


FIGURE 11-12. Temperature-Versus-Time Curves for Different Components of a Vertically Emplaced Spent-Fuel Waste Package in a Repository Located in Basalt.

A major influence on the waste-package temperatures is the thermal conductivity of the backfilled region. The conductivity is influenced by the moisture content and the amount of crushed basalt added to the mixture. The effects on waste-package peak temperatures as a function of a wide range of backfill thermal conductivities are illustrated in Figure 11-13. These results show that the very near-field rock temperatures are independent of the waste-package thermal properties. The emplacement-hole surface temperatures are dependent only on package dimensions, array, and thermal loading. In general, increasing both the moisture content and the basalt content of the backfill will decrease the temperature of the inner components of the waste package. These results show that for the conditions and assumptions made for the thermal modeling, reference 10-year-old pressurized-water-reactor spent fuel can be disposed of in basalt without exceeding present-design temperature limits for the spent-fuel cladding (300°C) (preliminary) and the repository host rock (500°C) (KE/PB, 1980). Comparable temperature-versus-time curves for components of commercial and defense high-level-waste packages are illustrated in Figures 11-14 and 11-15.



RCP8110-33A

FIGURE 11-13. Peak Temperature-Versus-Backfill Conductivity for a Spent Fuel Element Waste Package (buffer conductivity held constant at 0.75 W/m²K).

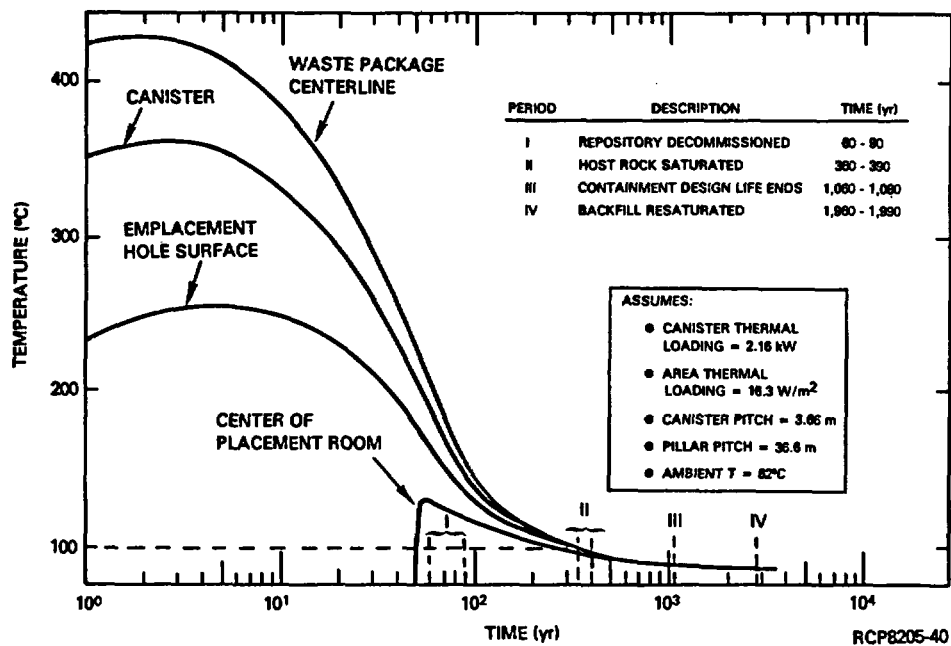


FIGURE 11-14. Temperature-Versus-Time Curves for Different Components of a Vertically Emplaced Commercial High-Level Waste Package in a Repository Located in Basalt.

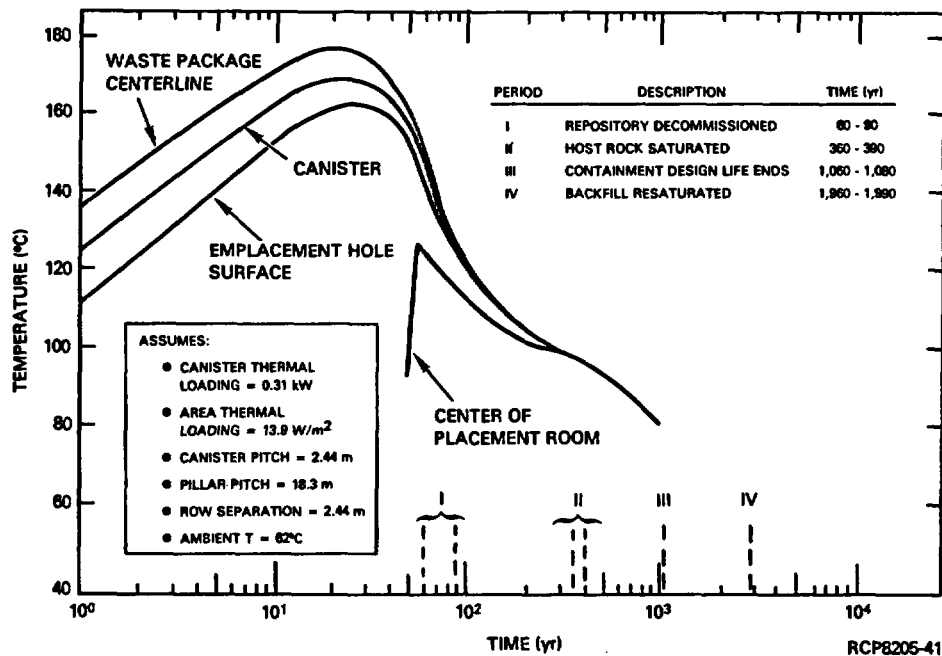


FIGURE 11-15. Temperature-Versus-Time Curves for Different Components of a Vertically Emplaced Defense High-Level Waste Package in a Repository Located in Basalt.

11.3.2.3 Barrier Materials. This activity encompasses the work needed to: (1) characterize the emplacement environment so that parameters can be set for hydrothermal testing and (2) define the potential interactions among waste forms, waste package materials, and the repository host rock. The hydrothermal testing will employ both simulated and radioactive wastes in tests that will increase in complexity as the list of candidate waste-package materials is narrowed to yield qualified reference materials for waste package final design.

Emplacement Environment. The status of the work being conducted to characterize the emplacement environment is described in Section 11.4 of this chapter, together with the reference conditions for a repository in basalt.

Waste-Barrier-Rock Interactions. The BWIP is pursuing a barrier materials testing program that accommodates the approach to waste package development previously discussed.

The specific design-related goals of the testing program include generating the data necessary to establish:

- Which barriers are required for acceptable performance
- Which barriers will operate efficiently
- The composition and required thicknesses of barrier components
- The chemical compatibility of barrier materials.

This information will permit the designer to assemble the most cost-effective system that is appropriately conservative and that still meets the proposed zero-release criterion during the first 1,000 years and the proposed slow-release criterion thereafter (NRC, 1981). The specific model-related goals of the testing program include generating the data necessary to establish:

- Travel times through the package
- Mechanisms for nuclide attenuation within the package
- Source terms at the package-rock boundary.

This information will permit the waste package designer to refine the estimates of barrier element thicknesses and will provide the baseline data necessary to assess whether or not the repository system conforms to the proposed zero-release criterion in the first 1,000 years and the proposed slow-release criterion thereafter.

The strategy for testing barrier materials and resolving these issues is based on sound scientific practices. First, experiments are conducted with site-specific reactants (groundwater) under repository-related conditions. This practice ensures that results are directly applicable to a repository constructed at Hanford. Second, the complex waste-barrier-rock-water system is investigated by evaluating in simpler systems (e.g.,

barrier-water) prior to complex (waste-barrier-water) interaction tests. It should be noted, however, that all experiments are related to the path that water takes to reach the waste or the path waste takes to exit the package. This vectored path is simulated by spiking the water of the simple tests with breakdown products of appropriate barriers. Third, the experimental method concentrates on studies that yield useful results in a cost-effective manner. For example, experiments are conducted primarily with agitated batch containers using powdered samples. This procedure accelerates tests, promotes equilibrium, and makes chemical interaction more visible. In addition, some experiments are conducted with monolithic materials to determine surface-related processes such as corrosion rate and mechanism. Some advanced experiments are conducted in flow-through systems to establish the flow-rate limits at which steady-state results break down and to determine design limits for water flow barriers. Fourth, waste-related experiments are conducted using nonradioactive simulants, tracer-doped simulants, and actual waste forms. Cold simulants are used so that more facilities (e.g., nonradiochemical laboratories) may contribute to the test program. This practice helps to expand the data base rapidly, safely, and at low cost. Tracer-level experiments are conducted to decrease analytical detection limits so that results are more readily compared with proposed NRC (1981) and draft EPA (1981) requirements. Further, tracer-level tests are used to confirm analog behavior observed in the cold experiments and/or to obtain information where no stable analogs exist. This practice provides verification of the cold tests at moderate cost with minimal hazard. Tests are conducted with actual waste to confirm earlier results, to investigate the effects of radiation, and to establish the behavior of the "real" system in general. The number of these tests will be minimized because of their difficulty, cost, and potential hazard.

These tests require monitoring of experimental variables such as temperature, pressure, oxygen fugacity (and perhaps carbon dioxide fugacity), and pH. The procedures for conducting controlled experiments are presently being developed by the BWIP.

Work to define the hydrothermal interactions among simulated waste forms, basalt, and groundwater has been initiated by the BWIP. Studies have been conducted at The Pennsylvania State University for the BWIP in which cesium and strontium compounds known to exist in spent fuel were reacted with simulated Grande Ronde Basalt groundwater with and without basalt being present (Komarneni et al., 1980). The study determined that some cesium and strontium compounds likely to be stable components of spent fuel (i.e., CsOH , Cs_2MoO_4 , $\text{Cs}_2\text{U}_2\text{O}_7$, and SrZrO_3) have significant hydrothermal solubilities. However, these solubilities are greatly reduced in the presence of basalt and/or basalt minerals. Results of experiments with SrZrO_3 showed it to be an unreactive compound.

Prior to the decision to exclude supercalcline (Table 11-22) as an alternate commercial high-level waste form, hydrothermal testing of this waste form was conducted at Arizona State University for the BWIP. (Since a ceramic waste form is still under consideration as an alternate waste

TABLE 11-22. Composition of Supercalcine SP-4
(after McCarthy, 1977b)

Ion	Molarity	Oxide	Grams of Oxide/L of calcined SPC-2 solution	wt% oxide	
From the Modified PW-7 Waste ^a					
RE ^b	0.204	RE ₂ O ₃	34.07	20.4	(16.0) ^c
Gd	0.153	Gd ₂ O ₃	27.69	16.6	(12.9)
Zr	0.106	ZrO ₂	13.04	7.8	(6.1)
Fe	0.100	Fe ₂ O ₃	8.00	4.8	(3.7)
(PO ₄)	0.100	P ₂ O ₅	7.10	4.3	(3.3)
Mo	0.095	MoO ₃	13.68	8.2	(6.4)
Cs	0.054	Cs ₂ O	7.61	4.6	(3.5)
Ba	0.027	BaO	4.13	2.5	(1.9)
Sr	0.027	SrO	2.81	1.7	(1.3)
Cr	0.012	Cr ₂ O ₃	0.91	0.5	(0.4)
Rb	0.010	Rb ₂ O	0.94	0.6	(0.4)
Na	0.010	Na ₂ O	0.31	0.2	(0.1)
Ru ^d	0.006	RuO ₂	0.80	0.5	(0.4)
Ni	0.005	NiO	0.38	0.2	(0.2)
Cd	0.002	CdO	0.26	0.2	(0.1)
Ag	0.002	Ag ₂ O	0.23	0.1	(0.1)
			121.95		
Supercalcine Additives ^a					
Ca	0.062	CaO	3.47	2.1	(1.6)
Sr	0.041	SrO	4.26	2.6	(2.0)
Al	0.148	Al ₂ O ₃	7.55	4.5	(3.5)
Si	0.489	SiO ₂	29.34	17.6	(13.8)
			166.58	100.0	
Other High-Level Waste Constituents ^e					
U(Np,Pu)	0.1195	U ₃ O ₈	38.8		(15.7)
Ru ^d	0.053	RuO ₂	7.1		(3.3)
Pd	0.032	PdO	3.9		(1.8)
Te	0.012	TeO ₂	1.9		(0.9)
Rh	0.010	Rh ₂ O ₃	1.3		(0.6)
			214.38		(100.0%)

^aInitial batch of SPC-4 made up of 73.2% waste and 26.8% additives.

^bRE = 0.133 Nd + 0.051 Ce + 0.014 La + 0.003 Pr + 0.002 Sm + 0.002 others; 0.002 RE is a stand-in for Am + Cm.

^cValue in parentheses is the weight percent of the oxide after addition of the appropriate amounts of U, Ru, Pd, Te, Rh.

^dRu concentration in the spray supercalcine SPC-4 was 10% of the actual PW-7 value of 0.59M. The addition of the remaining 0.053M is made after calcination.

^eThese constituents were not included in the large batch of SPC-4 because of their expense or radioactivity. None require fixation additives. When included, the batch contained 79.2% waste and 20.8% additives. The only PW-7 constituent not included above is Tc.

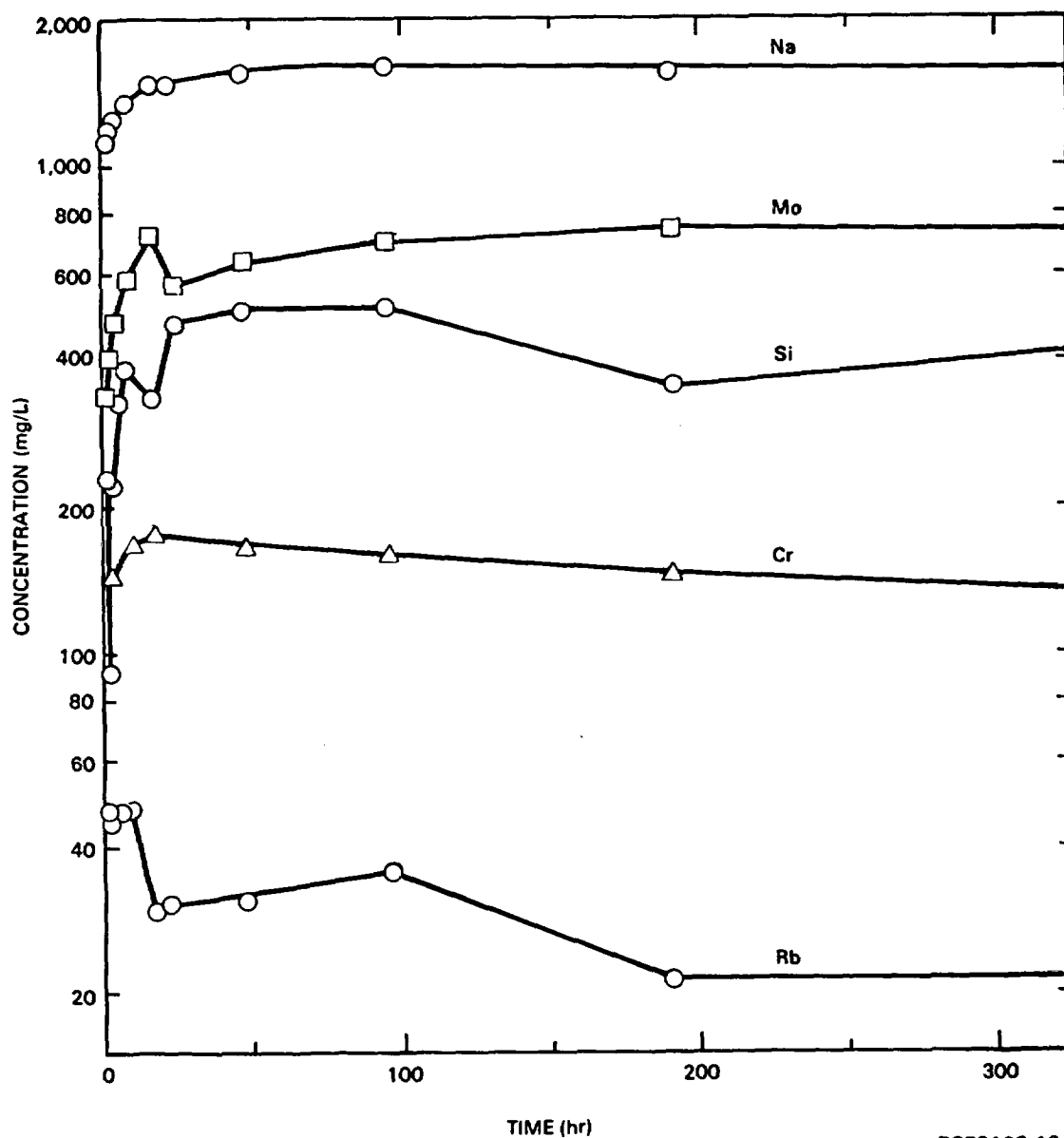
form for defense high-level waste, the discussion of the results of BWIP testing of supercalcine is included for completeness). Two sets of tests were completed. The first was the hydrothermal reaction of supercalcine waste form (SPC-4) with a synthetic Hanford basalt groundwater. The second experiment measured the hydrothermal reaction of supercalcine waste form (SPC-4) with a synthetic groundwater in the presence of Hanford basalt. Solution compositions were profiled for the duration of the experiments. These profiles are presented in Figures 11-16 and 11-17. Comparison of the figures indicates that the presence of basalt decreases the solution concentrations of sodium, rubidium, molybdenum, and chromium while the concentration of silicon increases. The decrease in solution concentration of chromium is the most dramatic and probably results from strong reaction with the basalt component.

Hydrothermal tests to evaluate the interaction among borosilicate glass (PNL 76-68), basalt, and groundwater have also been initiated by Arizona State University for the BWIP. The first test is being performed at 300°C and 30 megapascals pressure. A modified Dixon-type autoclave (Seyfried et al., 1979) is being utilized to permit solution sampling without interruption of the test. The test will evaluate the rate and capacity of basalt to impose reducing conditions within the repository and will determine the basalt hydrothermal alteration products.

As mentioned previously, an important part of the hydrothermal test program will be the testing of candidate waste package materials in the presence of radioactive waste forms to verify material compatibility. Several hot cell facilities are being evaluated.

Quantitative testing will follow the initial scoping experiments. The methodology for experimental control developed earlier will be used. Results of the quantitative tests will determine the performance effectiveness of each candidate waste package component and will permit an estimate to be made of component thicknesses required for the 1,000-year package. Experiments using radioactive waste forms (hot cell testing) will be initiated to improve the materials data base and update the waste package performance requirements for a repository in basalt. Finally, advanced hot cell testing of waste package assemblages and full-scale waste packages will be conducted to validate the performance model and to qualify waste package designs to support the repository licensing process.

The first in a series of corrosion-screening tests of candidate alloys has been completed (Anderson, 1981). The sheet specimens (approximately 10 centimeters long by 2 centimeters wide and containing a weld) were formed in a U-bend configuration and mechanically loaded above yield strength by a bolt across the specimen ends. The specimens were exposed for 60 days to simulated Grande Ronde Basalt groundwater (Table 11-23) at 250°C and a pH of 9.92 (measured at 25°C). Anoxic conditions (10^{-5} megapascals of O_2) were maintained by slowly purging the pressure vessels with an argon-0.19 percent hydrogen-gas mixture. Periodic sampling of the cover gas during the test period confirmed that oxygen control was maintained. Samples of the test solution taken periodically showed that the original composition of the groundwater remained reasonably constant during the test.



RCP8103-19A

FIGURE 11-16. Selected Major Cation Concentrations in Solutions Taken from SPCW 1-1 (SPC-4 + groundwater) Plotted as a Function of Time. Uncertainty is approximately the size of the symbol.

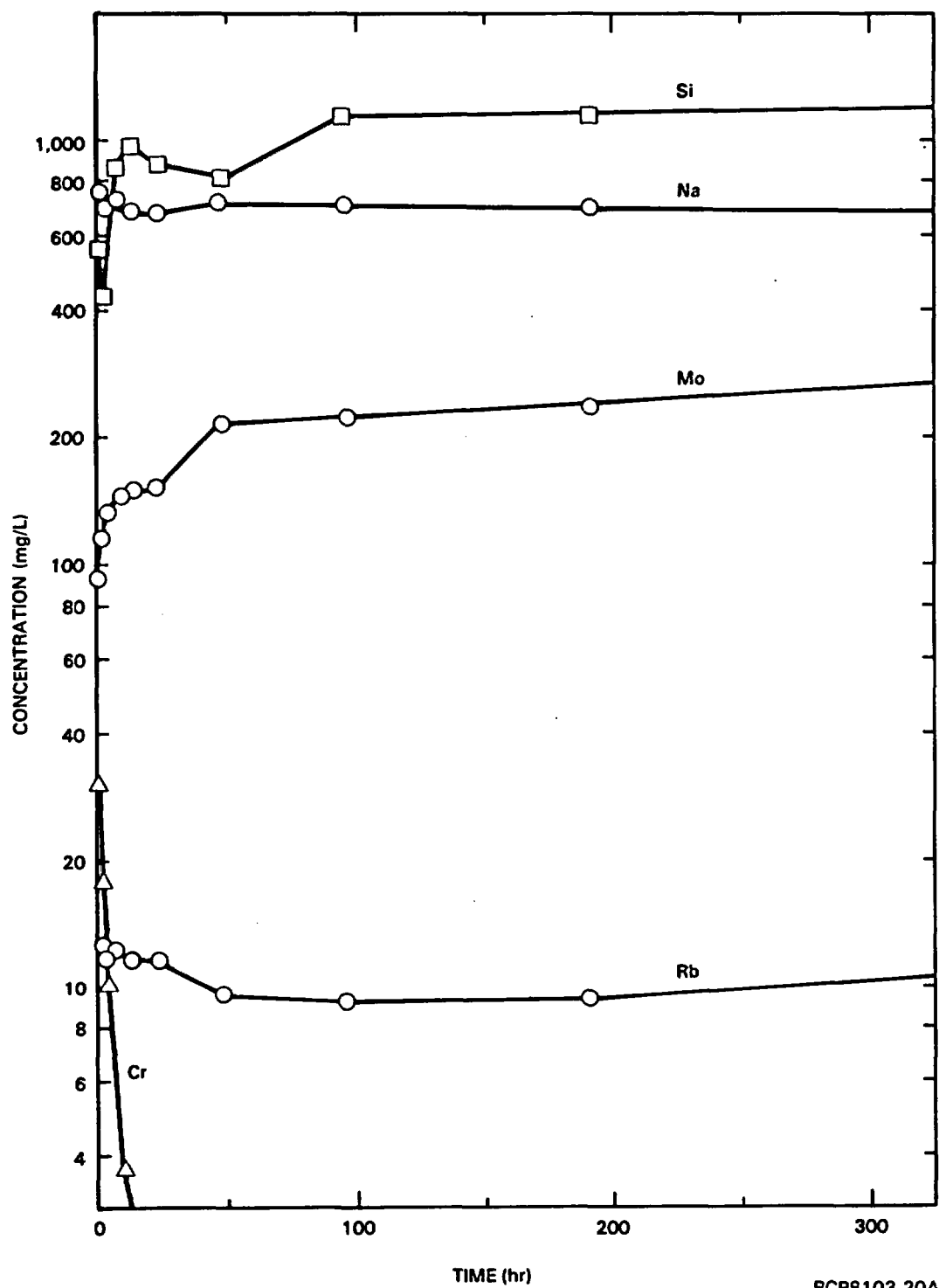


FIGURE 11-17. Selected Major Cation Concentrations in Solutions Taken from BSPW 1-1 (basalt + SPC-4 + groundwater) Plotted as a Function of Time. Uncertainty is approximately the size of the symbol.

TABLE 11-23. Composition of Simulated Grande Ronde Basalt Groundwater.

Compound	Concentration (mg/L)
Na ₂ CO ₃	170
SiO ₂ ·H ₂ O	157
NaCl	235
NaF	82
NaSO ₄	160
CaCl ₂	3,600
MgCl ₂	1,570
KCl	3,650

The corrosion rates exhibited by the materials exposed to the reference simulated Grande Ronde Basalt groundwater were extremely low. None of the materials exhibited evidence of stress corrosion or localized attack of weld metal or heat-affected zones. Results of the corrosion tests were shown in Table 11-17.

For comparison, results of 90-day tests in a simulated groundwater of similar composition, but under less-effective oxygen control, are also shown. The sensitivity of metallic corrosion to oxygen concentration is effectively illustrated by the data for the cupronickel alloys. Cupronickel corrosion was appreciably less in the Grande Ronde Basalt groundwater than in similar water with a higher oxygen concentration. This difference reflects the thermodynamic stability of copper and nickel metal, with respect to oxidation in anoxic groundwater, in chemical equilibrium with Grande Ronde Basalt.

Corrosion allowances (1,000-year canister-overpack design life) for the materials tested, assuming a conservative linear time-dependence of corrosion, were also shown in Table 11-17. These data indicate that less-expensive materials not normally considered to be corrosion resistant in oxygenated aqueous solutions (e.g., carbon steel or cast iron) could be used for canister material for a repository located in basalt. Incorporation of an effective oxygen-getter or reducing agent in the room and waste package backfill may also permit the use of such materials for a canister or overpack.

A continuation of these corrosion screening tests is planned to include other candidate alloys. Candidate materials still under consideration will then be subjected to advanced corrosion testing (see Chapter 15, Work Element W.1.6.A), which will include tests of their compatibility with other waste package component materials. Corrosion tests in this phase of the development will involve increasingly more rigorous determinations of corrosion behavior and will employ more sensitive test techniques to determine the susceptibility of these materials to nonuniform corrosion phenomena. Materials exhibiting acceptable behavior will undergo further screening using cost, availability, and fabricability (weldability) as criteria to identify materials for the BWIP waste package preliminary design activities.

Continued advanced corrosion testing will be directed toward more quantitatively defining the long-term behavior of selected canister and overpack materials. Methods of more precise data extrapolation will be developed to enable reliable extrapolation of short-term data to define long-term materials behavior. Experimental verification of predictive behavior and an assessment of the accuracy of the predictions will be obtained from supporting field testing. The results of advanced corrosion testing and an accurate knowledge of long-term materials behavior will support performance modeling and the BWIP waste package final design activities.

Work leading to the selection of candidate backfill/buffer materials was initiated with a review of the literature, previously reported (Smith et al., 1980); from this review it was concluded that no single material is presently available that can satisfy all the characteristics required for the backfill (Table 11-16). It is unlikely that a satisfactory single-component backfill will be found. In addition to meeting the requirements listed in Table 11-16, two general constraints must be imposed when selecting candidate materials. First, since backfill will be in direct contact with the geologic environment, (basalt, secondary minerals, groundwater), it must remain stable as ambient conditions change during the repository history. Preference is given to those natural materials presently found in the basalt environment. Second, potential major-component materials must be readily available in quantities sufficient to satisfy the needs of waste packages and to fill the bulk of the repository volume.

Three potential major component candidates satisfy these two criteria and are presently being evaluated. They include: (1) bentonite, (2) crushed basalt, and (3) zeolites. Bentonite has been studied in depth, primarily by Swedish scientists (Pusch, 1979), and has been shown to have a variety of useful properties. In particular, the low permeability and swelling capacity of this clay make it an attractive material for minimizing contact between the groundwater and the overpack or canister metal. In addition to its water-excluding potential, bentonite has a very high sorption capacity for radionuclides, relative to other clays and

geologic materials. Crushed basalt is an obvious candidate in a repository located in basalt, because of its availability following the excavation of the repository and the need to dispose of this material. Preliminary hydrothermal and sorption tests conducted under oxidizing conditions indicate that altered basalt is highly reactive with uranium, plutonium, americium, cesium, and strontium (Smith et al., 1980). Zeolites are considered as potential backfill components because of their high cation-exchange capacity. Also, minor amounts of zeolites are found in the fracture mineralization in the Columbia Plateau basalts.

There is also a need for a minor backfill component that is specifically tailored for transport retardation (either by sorption or reaction) of key long-lived radionuclides (e.g., ^{129}I , ^{99}Tc , and possibly ^{79}Se) that are potentially mobile in the repository host rock. Attention is focused on single phases but the minor backfill component may be composed of several phases needed to control specific troublesome radionuclides.

Using estimates from transport models, preliminary backfill performance requirements were developed (Wood, 1980b) following the literature review. The use of a one-dimensional transport model enabled the calculation of the maximum permissible release rates to the accessible environment. These release rates were then translated into permissible concentrations at the inner and outer surfaces of the backfill under low- and high-water flow conditions to establish performance requirements for the backfill component of the waste package.

A series of experiments has also been completed to determine the dehydration temperatures of the minerals in fractures found in Hanford basalts as a function of pressure. The purpose of the experimental study was to determine the extent of dehydration and subsequent mineral alteration that is likely to occur in basalt, through the increase in rock temperature, as a result of waste emplacement. The minerals in fractures were chosen for study because they are the only hydrous phase in the basalt phase assemblage and are the phases that will undergo dehydration. Thus, the overall effects of dehydration on basalt can be extrapolated with the data collected from these experiments. These data are being used to draw conclusions concerning the effect of dehydration reactions on the suitability of basalt as a backfill material and as a host medium for the disposal of nuclear waste.

Differential thermal analysis was carried out on 50- to 100-milligram samples of the minerals in fractures in an internally heated pressure vessel. Dehydration temperatures of the smectite clay (nontronite) at pressures of 0.1 and 30 megapascals are shown in Figures 11-18 and 11-19, respectively. In each figure, two episodes of water loss are represented by two large endothermic peaks. At 0.1 megapascal of pressure, water loss occurred at 126° to 134° and 780°C. At 30 megapascals, water loss occurred at approximately 430° and 788°C. Dehydration by loss of interlayer water occurred at the lower temperatures and dehydration by loss of structural water occurred at the higher temperatures. These figures illustrate the large increase in the temperature of interlayer water loss (from

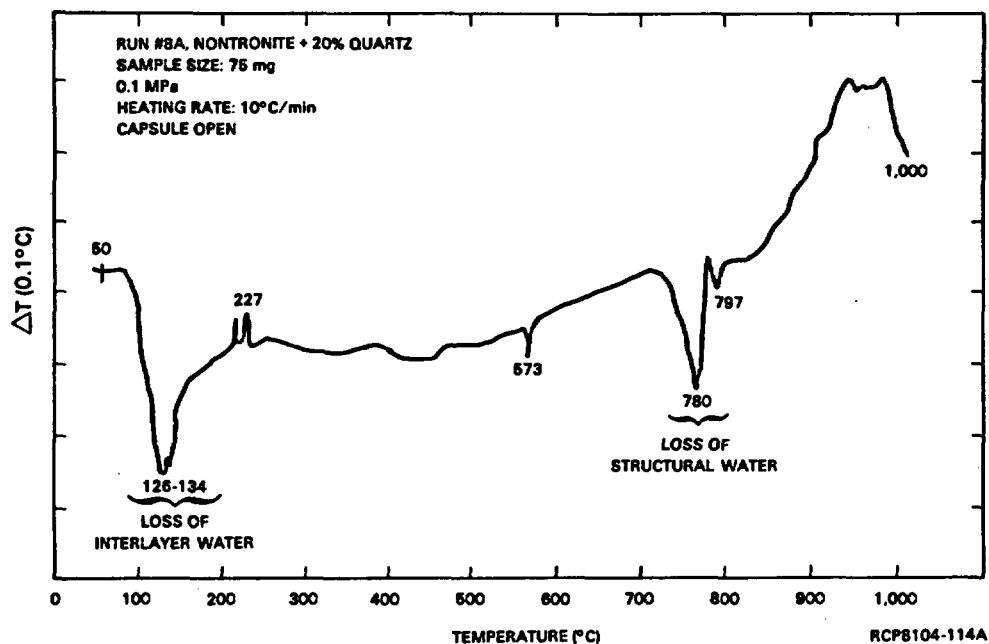


FIGURE 11-18. Dehydration of Fracture Mineralization at 0.1 Megapascal.

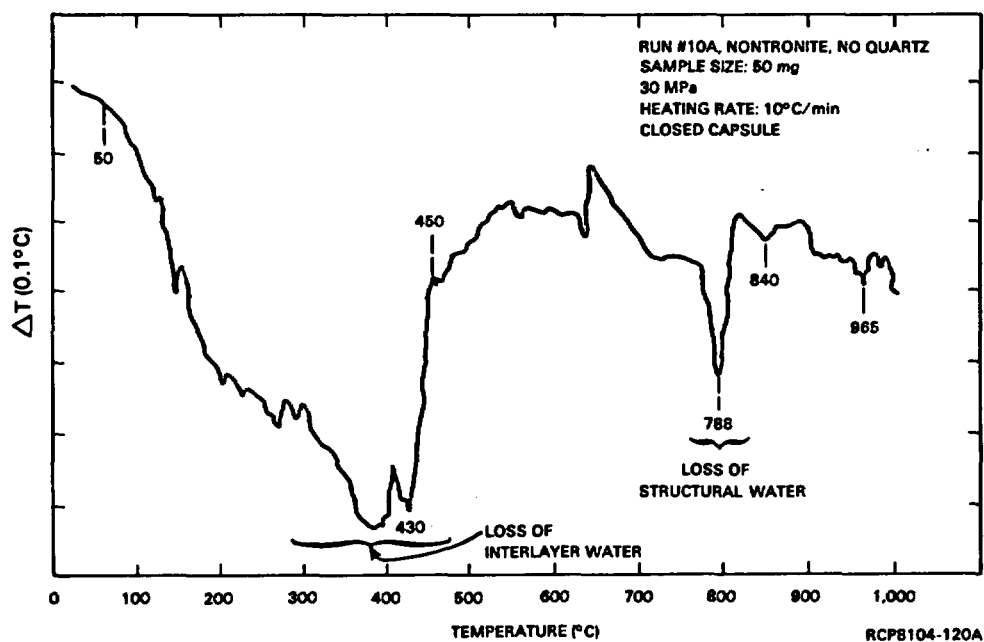


FIGURE 11-19. Dehydration of Fracture Mineralization at 30 Megapascals.

approximately 135° to 430°C) with the increase of pressure. This suggests that interlayer water-loss temperatures are slightly above the boiling point of water at any given pressure. Analysis of dehydrated samples by X-ray diffraction indicates that chemical alteration begins at 300°C. A minor amount of nontronite (approximately 5 to 10 percent) appears to have altered to a mica phase. These data are insufficient at this time to accurately assess the extent of this alteration process. For conceptual design purposes, however, a waste package design temperature limit of 300°C will be used to avoid potential backfill alteration.

The following conclusions were drawn concerning the usefulness of crushed basalt as a backfill material, from the results of the aforementioned experiments:

- The expected temperature and pressure history of the repository indicates that dehydration of basalt-backfill will only occur during the early stages of the repository life when temperature is at a maximum and pressure at a minimum. Loss of interlayer water should be largely reversible unless chemical alteration of the smectite to a mica phase is extensive. These preliminary data suggest that only minor alteration of the basalt will occur if temperatures are kept at or below 300°C. Thus crushed basalt should not be significantly affected by the dehydration process.
- The minerals in fractures outside of the disturbed zone created by excavation of the repository will not dehydrate following emplacement of the waste. These phases exist under a confining pressure of 30 megapascals (the lithostatic load), and with a maximum expected basalt temperature of 300°C, dehydration should not occur. Consequently, an increase in groundwater pathways, due to dehydration and reduction of the volume in fractures filled with secondary minerals, should not occur outside the disturbed zone of the repository site.

Because the backfill component is also to function as a retardant to radionuclide migration from the waste package, and because crushed basalt will probably be a major component, the discussion in Section 6.4 on radionuclide retardation by the repository host rock is applicable. Extensive studies of basalt and other candidate backfill materials, however, are planned to obtain quantitative data on their sorptive capacity for radionuclides. In this manner, their capability for assisting the waste package to meet the proposed 1,000-year containment criteria (NRC, 1981) can be assessed. Reference materials and component thicknesses can then be selected to support the preparation of design requirements for site-specific waste packages. Studies are also planned that will evaluate and eventually select reference buffer materials.

11.3.2.4 Performance Evaluation. This activity encompasses the subactivities required to evaluate the performance of candidate waste packages under the environmental conditions expected in a repository located in basalt. Performance modeling and natural analogs of backfills, canisters, and overpacks will be used along with accelerated field tests to verify

waste package designs prior to repository operations. The waste package performance model will consist of two major submodels, a degradation model that will describe the potential processes operating to degrade the waste package and a geochemical model that will describe the behavior of radionuclides within the waste package and in close proximity (very near field).

Preliminary performance requirements for a waste package emplaced in a repository in basalt have been defined using a one-dimensional transport model. Two release and transport scenarios were modeled to determine the most hazardous radionuclides in the waste inventory and to estimate the maximum permissible release rate the waste package must meet for various nuclides. The criterion used to define these release rates is that the cumulative release of nuclides must meet draft requirements as stated in 40 CFR 191 (EPA, 1981). The two scenarios and assumptions used in the model are as follows:

Case I: (nondisruptive case) Horizontal transport through 10 kilometers of basalt to the accessible environment

- 0.32-meter-per-year water velocity
- 0.01 effective porosity in basalt flow top
- Zero transport time to the flow top (water-bearing zone) from the repository.

Case II: (disruptive case) Horizontal transport through 10 kilometers of interbed zone (confined aquifer)

- 7.9-meter-per-year water velocity
- 0.2 effective porosity in interbed zone
- Zero travel time to interflow zone (aquifer) from repository horizon.

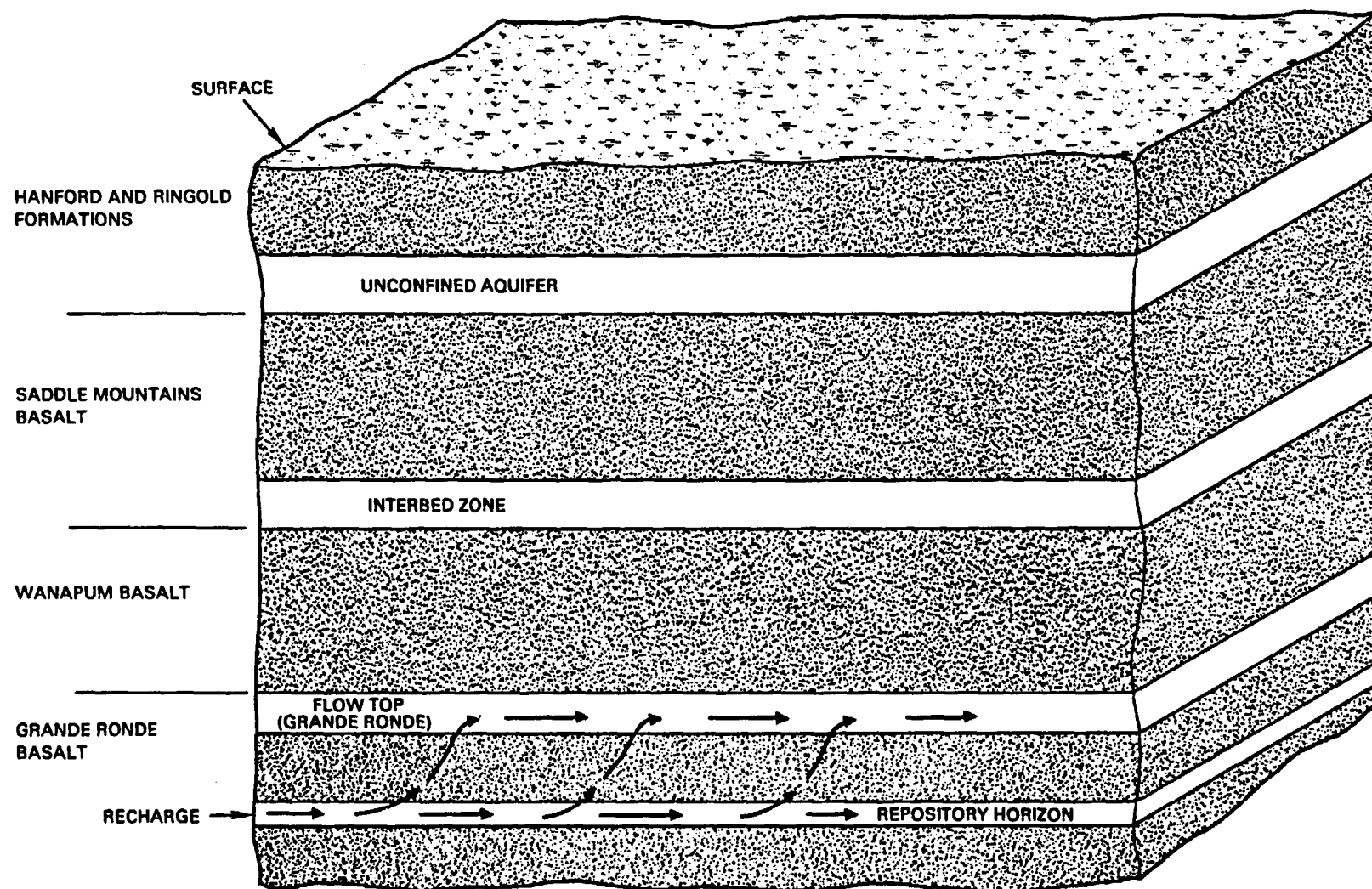
Assumptions common to Cases I and II:

- One-dimensional transport model (Wood, 1980a)
- All waste packages fail simultaneously after 1,000 years of containment
- 1,000-year release time for all nuclides after package failure
- No thermal effects considered
- Repository inventory equivalent to 46,500 metric tons of heavy metal
- Minimal nuclide retardation by basalt.

Schematic representations of the two scenarios considered are shown in Figures 11-20 and 11-21. It is important to note that both scenarios considered represent conservative analyses of repository performance since containment for all waste packages was assumed to fail simultaneously in a water-saturated repository 1,000 years after closure. Furthermore, radionuclide solubilities rather than leach rates are used to limit radionuclide release because they are relatively time independent and represent the maximum amount of a given radionuclide that can be in solution at any one time. In addition, by assuming zero travel time to the water-bearing zone, the model essentially places the repository in a water-bearing zone (Case I) and a confined aquifer (Case II).

Preliminary analyses (Table 11-24) were first conducted to establish potential problem (mobile) radionuclides for a repository in basalt using no solubility constraints on radionuclide release. Table 11-25 lists, for Cases I and II, those radionuclides requiring a release rate less than 10^{-3} per year of their inventory to meet EPA draft limits and are considered to be potential problem radionuclides. Results of these analyses indicate that, for Case I, only ^{14}C , ^{99}Tc , ^{237}Np , and the uranium isotopes and their daughter products require release rates less than 10^{-3} per year to meet EPA draft limits. For Case II, preliminary analyses indicate that ^{135}Cs , ^{126}Sn , ^{107}Pd , ^{243}Am , ^{242}Pu , ^{93}Zr , in addition to those radionuclides listed for Case I, will require release rates less than 10^{-3} per year to meet EPA draft limits. Other radionuclides either are too short-lived, are well sorbed, or have too small an inventory to constitute a problem.

Analyses were then conducted to evaluate the potential release rates of radionuclides from a repository in basalt using solubility constraints. The results of these analyses for uranium, neptunium, plutonium, and americium are summarized in Table 11-25 and are compared with calculated release rates required to meet EPA draft release limits for Cases I and II. The actinide solubilities are estimates of the expected solubilities in the basalt environment and are based on available thermodynamic and laboratory data. (Sufficient geochemical data are not available at this time to adequately evaluate the release of other potentially hazardous radionuclides from a repository in basalt.) These results indicate that actinide release rates from a repository in basalt are well below those required to meet EPA draft limits for both Case I and Case II. In addition, the predicted actinide release rates are well below the one part in 100,000 proposed release rate required by the NRC. The basalt site, therefore, appears to be capable of adequately controlling the release of the actinides to the accessible environment. Consequently, in terms of meeting the EPA draft and NRC proposed release criteria, the required engineered system performance for these radionuclides is zero. The waste package, although possibly necessary for other radionuclides, would function simply as a secondary barrier to the release of the long-lived actinides to the accessible environment. However, the waste package would still be necessary to meet the NRC's proposed 1,000-year containment criterion, but a much simpler waste package design would now be adequate for the repository.



RCP8109-284

FIGURE 11-20. Schematic Representation of Groundwater Flow Path for Case I.

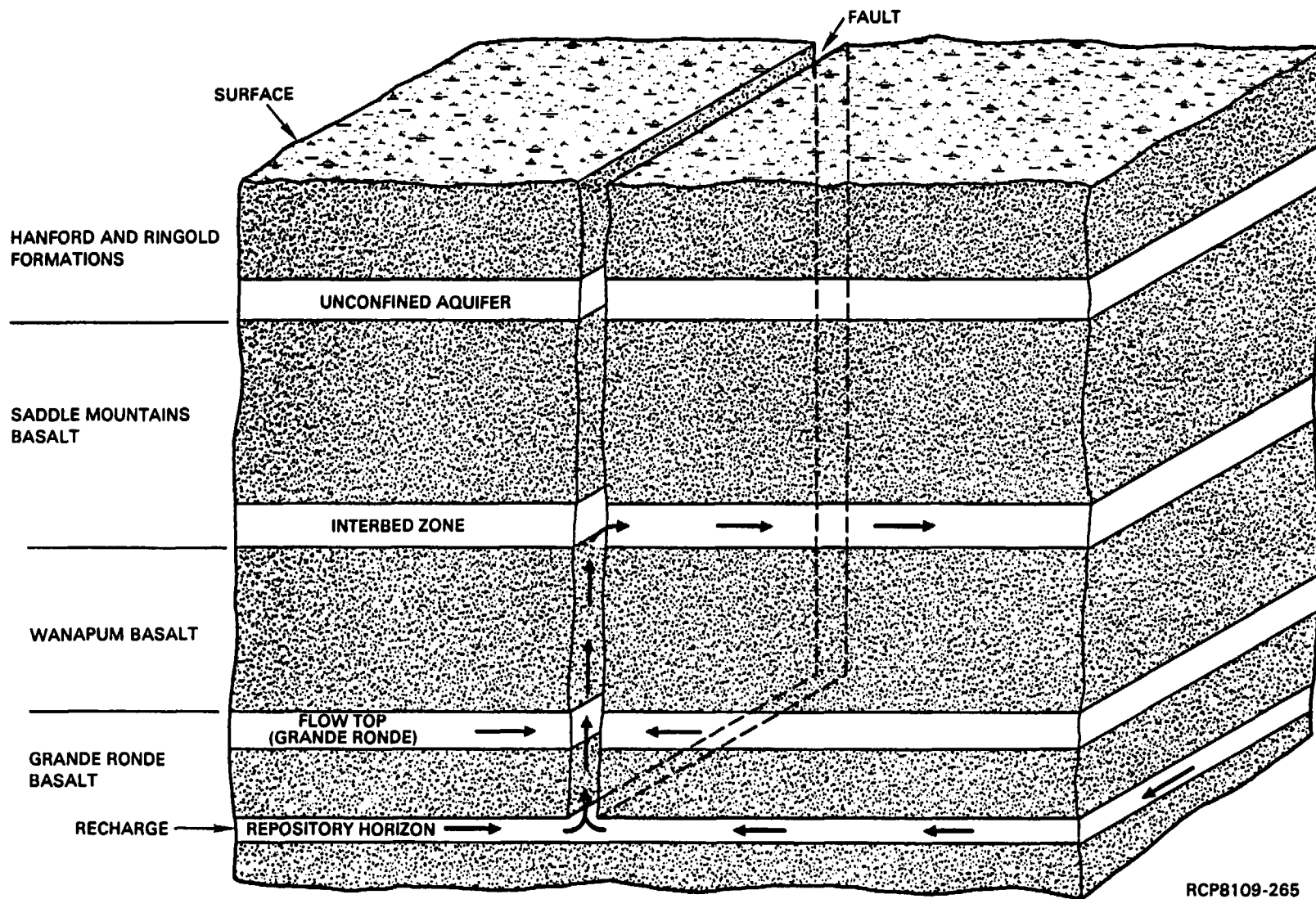


FIGURE 11-21. Schematic Representation of Groundwater Flow Path for Case II.

TABLE 11-24. Nuclides Whose Release Rates Must Be Less Than 10^{-3} per Year to Meet U.S. Environmental Protection Agency Release Draft Limits.

Nuclide	Case I release rate (parts/yr) required to meet EPA draft limits	Case II release rate (parts/yr) required to meet EPA draft limits
^{233}U	1 E-03	1 E-03
^{234}U	4 E-06	4 E-06
^{235}U	2 E-04	2 E-04
^{236}U	1 E-05	1 E-05
^{238}U	1 E-05	1 E-05
^{237}Np	7 E-05	7 E-06
^{239}Pu	*	1 E-03
^{242}Pu	*	4 E-04
^{243}Am	*	4 E-04
^{230}Th	4 E-05	4 E-05
^{226}Ra	2 E-05	2 E-05
^{135}Cs	*	3 E-03
^{126}Sn	*	7 E-05
^{107}Pd	*	2 E-03
^{99}Tc	1 E-05	1 E-05
^{93}Zr	*	1 E-04
^{14}C	3 E-04	1 E-04

*Release rate can be $>1 \text{ E-03}$ and still meet EPA draft release limits.

TABLE 11-25. Comparison of Estimated Actinide Release Rates from a Repository in Basalt with Release Rates Required to Meet Current U.S. Environmental Protection Agency Draft Limits.

Nuclide	Total solubility (mol/L)	Case I release rate required to keep below EPA draft limits (yr ⁻¹)	Case II release rate required to keep below EPA draft limits (yr ⁻¹)	Case I solubility-controlled release rate (yr ⁻¹)	Case II solubility-controlled release rate (yr ⁻¹)
²³³ U	1 E-08	1 E-03	1 E-03	4 E-12	2 E-09
²³⁴ U	1 E-08	4 E-06	4 E-06	4 E-12	1 E-09
²³⁵ U	1 E-08	2 E-04	2 E-04	4 E-12	2 E-09
²³⁶ U	1 E-08	1 E-05	1 E-05	5 E-12	2 E-09
²³⁸ U	1 E-08	1 E-05	1 E-05	4 E-12	2 E-09
²³⁷ Np	1 E-15	7 E-05	7 E-06	4 E-16	2 E-13
²³⁹ Pu	1 E-09	1 E-03	1 E-03	1 E-10	5 E-08
²⁴² Pu	1 E-09	1 E-03	4 E-04	1 E-10	5 E-08
²⁴³ Am	1 E-12	1 E-03	4 E-04	1 E-12	7 E-10

For the important nuclides identified in Cases I and II, there is little advantage to be gained by producing a 1,000-year as opposed to a 100-year waste package. Waste package lifetime only has a significant effect on the maximum permissible release rate of a nuclide if the lifetime is several times the half-life of the nuclide (Wood, 1980a). A 1,000-year waste package is only important for short-lived nuclides such as ^{90}Sr ($t_{1/2} = 28$ years), and only then if the nuclide travel time to the biosphere is ignored (i.e., assumed to be zero). None of the short-lived fission products such as ^{90}Sr appeared as hazards because their travel times to the accessible environment are all much longer than their half-lives. Thus, even if they escape the waste package instantaneously, they are unlikely to constitute a hazard because they decay before reaching the environment.

The following conclusions may be summarized from the above discussion of release and transport modeling:

- (1) Modeling of release and transport scenarios can yield useful preliminary waste package performance criteria (see Tables 11-24 and 11-25).
- (2) Solubility constraints on isotopes of uranium, plutonium, neptunium, and americium result in cumulative releases below EPA draft limits for both disruptive and nondisruptive cases (see Table 11-25).

The continued application of geochemical modeling techniques to a repository in basalt will require the extension of existing data on key radionuclides by determining their solubilities and kinetic behavior in a basalt environment. These data plus those resulting from hydrothermal testing of waste-barrier-rock interactions will continually upgrade the geochemical model. This model will then be combined with the NWTS waste-package degradation model, presently being modified for use by the BWIP, to yield a waste package performance model. The performance model will then be experimentally verified with hot cell hydrothermal testing and in situ and field testing data to support the preparation of site-specific waste package final designs.

11.3.3 Summary of Important Conclusions

In this section, the BWIP approach to research and development of waste packages for emplacement in a repository in basalt has been discussed. The materials test program, as part of the research and development activity, focuses on the evaluation of existing waste forms, waste package (barrier) materials, and the emplacement environment in basalt. This effort has been undertaken to obtain an understanding of the behavior of these materials under the expected repository conditions. For example, the results of early hydrothermal testing show that cesium and strontium compounds likely to exist in spent fuel have significant hydrothermal solubilities. The solubility, however, exhibits a marked decrease in the presence of basalt. Even so, it can be concluded that spent fuel may still require protection by waste packages of suitable complexity. While

borosilicate glass appears to be less leachable, there is insufficient data to compare quantitatively the long-term stability of borosilicate glass versus spent fuel in the basalt environment. The results of preliminary corrosion studies and estimates of radionuclide behavior in the near-field of the repository indicate, however, that the complexity of the initial early spent fuel waste package developed by the BWIP may be simplified. This has been accomplished by eliminating the corrosion-resistant titanium overpack and the buffer, and by designing the backfill component to limit or retard only those key radionuclides found to be mobile in the basalt environment. The results of thermal modeling of the BWIP reference pressurized water reactor spent fuel waste packages emplaced in the repository show that the cladding temperature limit (300°C) and the basalt temperature limit (500°C) will not be exceeded as the result of waste emplacement. These limits are considered preliminary; thus, a final temperature limit for the waste form, waste package components, and repository host rock must be defined to allow completion of the waste package design process. Important conclusions drawn from the measurement of the rate of dehydration of minerals in fractures found within the basalts at the Hanford Site are:

- At the maximum temperature (300°C) and minimum pressure (0.10 megapascal) expected during the early stage of the repository history, dehydration of crushed basalt used as a component of the backfill will be minor.
- An increase in groundwater pathways, due to dehydration and volume reduction of fracture-filling secondary mineralization, should not occur outside the disturbed zone of the repository site.

Preliminary radionuclide release and transport modeling has yielded useful preliminary waste package performance criteria.

11.4 EMPLACEMENT CONDITIONS

The design of effective waste packages requires an understanding of the physical, chemical, and radiologic conditions that will exist in and around a repository in basalt throughout its lifetime. Physicochemical parameters such as the host rock temperature, pressure, Eh, pH, and water chemistry will control package material stability, chemical reactions, and radionuclide transport in and around the repository. Therefore, knowledge of such parameters as a function of time is necessary for the proper design of experiments to be used as a basis for waste package component materials, the design selection, the design of waste packages, and computer modeling to qualify package designs to support repository licensing. This section brings together existing data relevant to physical, chemical, and radiologic conditions that would exist in a nuclear waste repository to be constructed in the basalt beneath the Columbia Plateau. Of the several basalt flows within the Grande Ronde Basalt, as noted earlier, both the middle Sentinel Bluffs and the Umtanum flows are considered candidate repository horizons. In this section, the physicochemical environment of the Umtanum flow is discussed. A separate paper (Long et al., 1982) compares the middle Sentinel Bluffs and Umtanum emplacement environment. In general, available data suggest that, except for temperature and pressure, a close similarity in environmental conditions exists for these two horizons. When a choice is made between the candidate repository horizons (May 1983), comparable data bases for each will be available.

11.4.1 Physicochemical Conditions

11.4.1.1 Water Chemistry. The groundwater chemistry of water-bearing zones beneath the Hanford Site was discussed in detail earlier (see Section 6.2). The chemistry of groundwater in the Grande Ronde Basalt will be briefly discussed here, since the Grande Ronde Basalt contains the candidate repository horizons and its water chemistry will have the greatest effect on the design and selection of materials for the waste package. The chemistry of the groundwater within the Grande Ronde Basalt is summarized in Figure 11-22. The composition of the Grande Ronde Basalt groundwater is unique, in that it is saturated with respect to silica and has relatively large concentrations of F^- , SO_4^{2-} , and Cl^- compared to the concentrations of CO_3^{2-} and HCO_3^- . The significance of these concentrations is discussed in the following sections.

11.4.1.2 Temperature. Temperature is an important parameter that must be considered when defining the repository environment, because thermal energy is a primary driving force for chemical reactions. Temperature also exerts a strong influence on aqueous transport rates. Repository temperature can be estimated by knowing the age, nature, and emplacement configuration of the nuclear waste. The presence of water, voids, or compositional heterogeneity in the rock will also affect repository temperature. The heating, resulting from burial of nuclear waste, is a consequence of the power generated by radioactive decay, and since the nuclides are continually decaying, the power output changes with time. Thus, the prevailing repository temperature will decrease as a function of time, leading to more benign repository conditions.

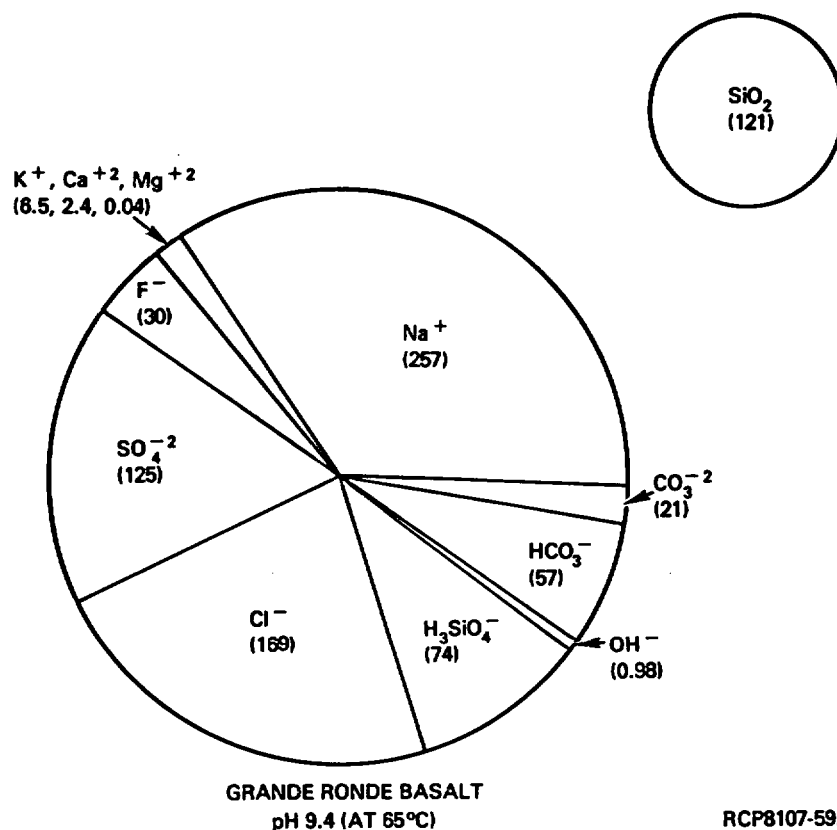


FIGURE 11-22. Summary of Grande Ronde Groundwater Composition. Values in parentheses are in milligrams per liter (after Chapter 5 and Gephart et al., 1979).

The Earth in some respects is a natural analog for a radioactive waste repository. The Earth's interior is comprised of rock containing small amounts of naturally occurring radioisotopes (e.g., ⁴⁰K, ⁸⁷Rb, ²³⁵U, ²³⁸U). Decay of these isotopes results in a release of energy in the form of heat. Because heat tends to migrate toward cooler areas, heat flow occurs from the Earth's interior toward the surface. However, rock is not an efficient thermal conductor, so much of the heat is retained in the interior, resulting in a geothermal gradient. The actual value of the gradient varies, depending on the thermal properties of the rock and the geologic environment. For areas without active igneous activity, this gradient commonly ranges from 20° to 50°C per kilometer of depth (Miyashiro, 1973; Winkler, 1974).

The temperatures existing at depth have been measured directly in drill holes on the Hanford Site. An estimated geothermal gradient of approximately 45°C per kilometer as an upper limit can be obtained from

the borehole data in Chapters 5 and 6. This result is within the range of normal crustal gradients. Such data enable estimation of the baseline (i.e., unperturbed) repository temperature for any candidate horizon. At a depth of 1 kilometer, the anticipated depth of a repository at Hanford, the calculation is simple, involving only the multiplication of the gradient times the depth in kilometers and adding the result to the average surface temperature of 12°C (Blackwell, 1978). The present estimate for the maximum ambient temperature within the middle Sentinel Bluffs flow is 51°C, whereas that for the Umtanum flow is approximately 58°C. This temperature represents the reference temperature for a repository at Hanford. It will be applied in two ways: (1) as a starting reference point for temperature estimates during the thermal period and (2) the long-term, "steady-state" repository conditions that will prevail during the period of geologic control after the 1,000-year thermal period.

Repository temperature estimates for the thermal period are calculated by adding the baseline temperature to the change in the rock temperature produced by radiogenic heating. The radiogenic heating is a function of the power output of waste per unit volume of repository and the thermal conductivity of the rock. This is necessarily a complex function, because the power output of the waste changes as the nuclides decay and the efficiency of heat dissipation decreases as thermal resistance is accumulated.

To estimate the temperature in the very near field of the repository as a function of time for vertical emplacement, the reference waste package conceptual design for spent fuel and borosilicate glass for a repository in basalt has been modeled using the heat-transfer computer code, HEATING5 (see Section 11.3.2.2). Preliminary results of the modeling (see Fig. 11-9, 11-11, and 11-12) predict peak temperatures and the approximate times at which they occur for the canister, overpack, and emplacement hole surface.

11.4.1.3 Pressure. Two types of pressure, lithostatic and hydrostatic, are important to discussions of pressure within the Earth. Lithostatic pressure at a point within the Earth is simply the pressure resulting from the weight of the overlying column of rock. Hydrostatic pressure at a point within the Earth is the pressure that would exist at the bottom of a body of water with a depth equal to the thickness of the overlying rock column. The difference between lithostatic and hydrostatic pressure is a result of the different densities of rock (2.8 grams per cubic centimeter for basalt) and water (1.0 gram per cubic centimeter). The pressure transmitted from grain to grain within a rock is generally equal to the lithostatic pressure.

Hydrostatic and lithostatic pressures within a repository can be calculated from the equation:

$$P = \rho gh \quad (11-1)$$

where

P is pressure

ρ is density

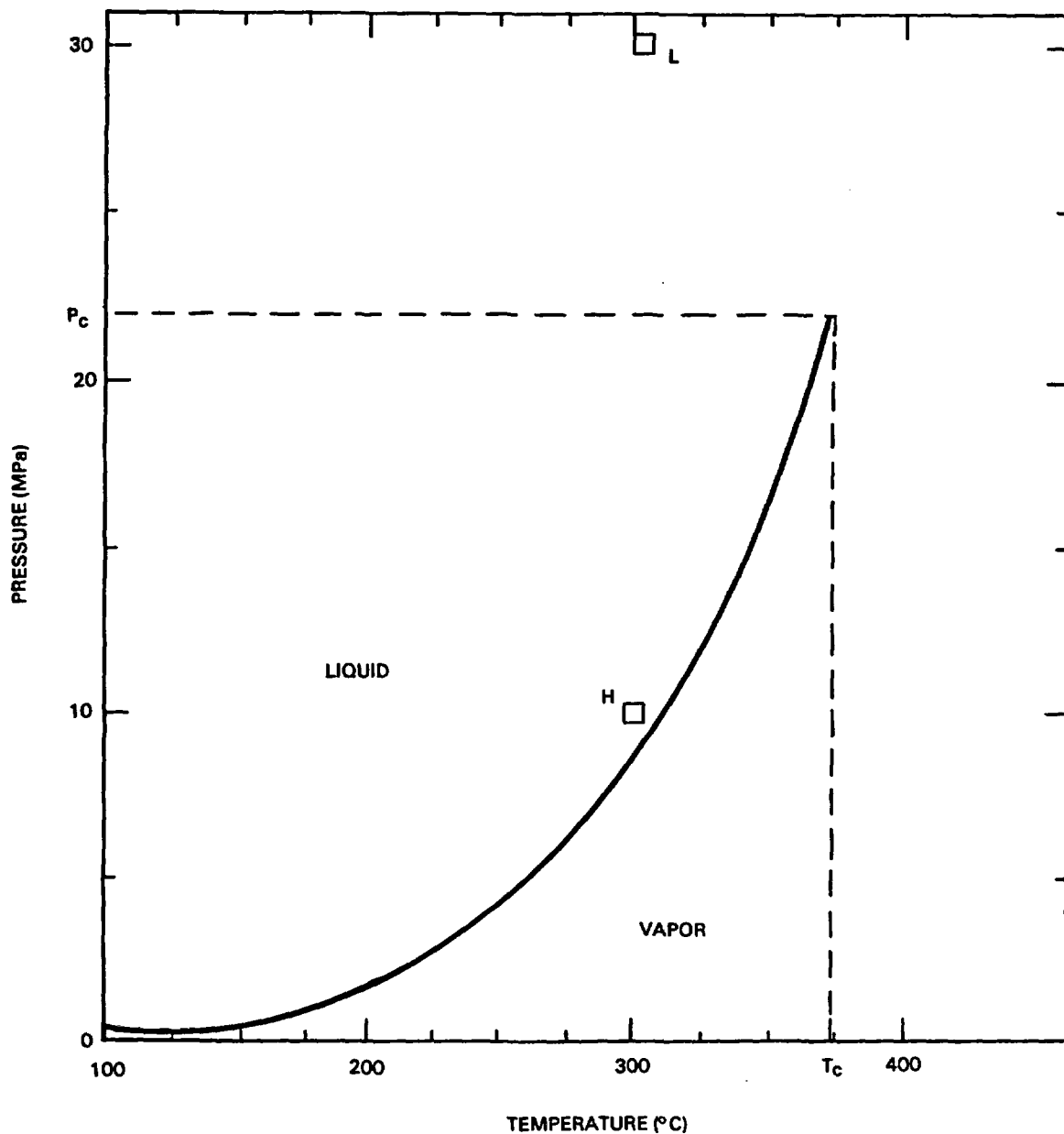
g is acceleration due to gravity

h is depth.

Assuming a density of 2.8 grams per cubic centimeter for basalt, the lithostatic pressure in the middle Sentinel Bluffs flow (945 meters deep) would be approximately 26 megapascals and approximately 31 megapascals for the Umtanum flow (1,128 meters deep). The hydrostatic pressures for the same flows would be approximately 9.3 and 11.1 megapascals, respectively (see Chapter 6, Fig. 6-12). This calculation for hydrostatic pressure assumes that the pressure is exerted by a column of water extending to the surface.

The pressure within the repository prior to backfilling and closure will be 0.1 megapascal plus the weight of the column of air between sea level and repository depth, a result insignificantly different from 0.1 megapascal. After backfilling and sealing of the repository, two different pressure scenarios must be considered, one with nonexpanding backfill and the other with expanding backfill. The pressure on solids and any fluid (water or air) trapped in voids or pore spaces immediately after backfilling will be essentially 0.1 megapascal in either case. In the first case, where the repository is backfilled with nonexpanding material, pressure buildup within the repository will be controlled principally by movement of water into the repository from the surrounding rock. Water entering the repository would fill intergranular voids and eventually raise repository fluid pressure to the fluid pressure that exists in the surrounding rock.

This scenario could be complicated if water were to come in contact with hot canisters or heated material adjacent to canisters and form steam before the pressure has risen sufficiently to block its formation. At temperatures below 300°C the vapor pressure of water is only 8.6 megapascals (Fig. 11-23), somewhat less than the hydrostatic pressure; thus, steam should not be capable of displacing water from the surrounding rock and escaping from the repository. In the event of steam formation within a sealed repository, pressure would rise rapidly to the liquid-vapor divariant curve and remain on that divariant curve until the continued influx of water into the repository raised the pressure into the liquid field. The pressure buildup should also be aided somewhat by the expansive alteration of crushed basalt within the backfill. The hydrothermal alteration of basalt will produce clays that occupy a volume considerably greater than the original basalt. However, reaction kinetics for the alteration of basalt are not yet well known. Also, the rate of reaction will depend to a large degree on the percentage of glass in the basalt used for backfill, since this is the reactive phase. Thus, the degree to which basalt-backfill alteration will contribute to the overall pressure cannot be quantitatively evaluated at this time. Two other effects that



RCP8107-62

FIGURE 11-23. Divariant Curve (liquid-vapor) for Water (H_2O). P_c and T_c are the critical pressure and the critical temperature. The small squares indicate the relative positions of hydrostatic pressure (H) and lithostatic pressure (L) at a repository temperature of 300°C.

may be important are the hydrothermal alteration and thermal expansion of basalt adjacent to the repository. Both effects should produce expansion of wall rock into the repository volume and thus work to increase pressure within the repository toward the lithostatic value.

In the second case, where the repository is backfilled with a mixture in which expanding clay (e.g., bentonite) is a major component, the pressure history within the repository will be influenced by the expansion of the clays. Expansive clays (those belonging to the smectite- or montmorillonite-clay group, which includes bentonite) are characterized by their ability to reversibly gain or lose water, resulting in expansion or shrinkage. Water gain or loss at temperatures below 100°C involves water loosely bound to the surfaces of the clay particles. Water gain or loss at temperatures between 100° and 200°C involves water loosely bound between the silicate sheets of the clay structure. Irreversible loss of water from smectite clays does not occur at temperatures below 300°C (Deer et al., 1967).

If expanding clay within the backfill has been partly or completely dehydrated (reversible water only) prior to emplacement, it will react with any water entering the repository. The resultant expansion will result in a rapid pressure increase within the repository. However, the low density of the clay portion of the backfilled repository will prevent a large pressure increase. It is apparent from Figure 11-23, the phase diagram for water in the region of interest, that hydrostatic pressure (10 megapascals) at 1,000 meters is sufficient to keep water in the liquid state at temperatures as high as 300°C. Therefore, hydrostatic pressure imposed by saturation of the repository backfill will dominate the repository pressure history.

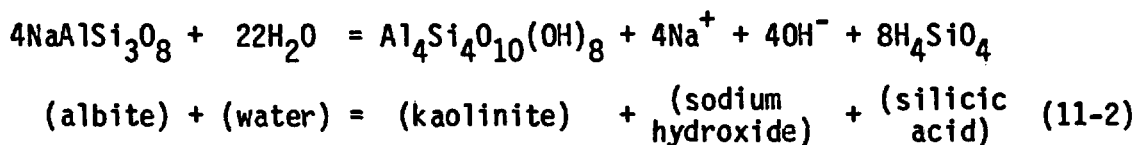
In addition to the hydrostatic and lithostatic pressure, the stress field within the basalt is an important consideration. A stress field results when the horizontal stress in a rock is either less than or greater than the vertical stress (usually the lithostatic pressure). The ratio of the horizontal to vertical stress is a parameter to consider because the waste package must have sufficient mechanical strength to withstand any directed stress during the entire life of the repository. The lithostatic load at a 1,000-meter depth (approximately 30 megapascals) corresponds to an engineering stress of just over 4,000 pounds per square inch. The differential stress at depth is probably less. Most alloys considered as waste canister materials can probably withstand such compressive stresses quite well.

11.4.1.4 Eh and pH. Eh and pH are the two dominant intensive variables in aqueous solutions. They control the stability and solubility of solid species and the form taken by aqueous species in solution. They are not completely independent, however, and in considering aqueous solutions they must be evaluated together. In this section, pH is considered first because it can be measured directly with reasonable accuracy. Eh is considered next because its value must be inferred from a model that is pH dependent.

The pH is a measure of the activity of hydrogen ions in solution and is defined as the negative logarithm of the hydrogen-ion activity, which in dilute solutions is essentially equal to the hydrogen-ion concentration. Low values of pH correspond to acidic solutions and high values correspond to alkaline solutions. At room temperature (25°C) a pH of 7 corresponds to neutrality; however, at higher temperatures the neutral point shifts to lower values because of shifts in the ionization constant of water. At 200°C, for instance, neutrality corresponds to a pH of approximately 6.5.

Measurements of the pH of groundwaters sampled from the Grande Ronde Basalt (Gephart et al., 1979) indicate that the pH of these waters at 450°C is approximately 10.0. Extrapolation of the pH to temperatures approximating ambient in the middle Sentinel Bluffs (51°C) and Umtanum (58°C) flows yields values ranging between 9.4 and 9.9. The high pH values found in the Grande Ronde Basalt groundwaters are consistent with groundwater isolated from the atmosphere and in contact with silicates and/or carbonates where hydrolysis reactions result in a high pH (Krauskopf, 1979).

Consider, for instance, a simplified scheme for hydrolysis of the albite component of plagioclase, a mineral contained in basalt. Albite plus water generates the clay (kaolinite, sodium hydroxide, and silicic acid).



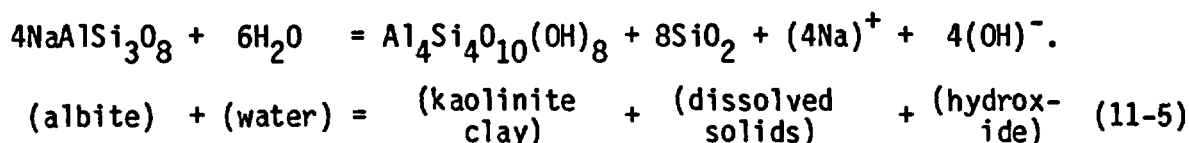
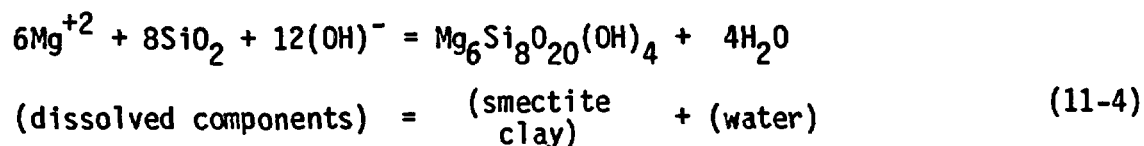
The product silicic acid dissociates, forming hydrogen ions, and yields a solution pH that is about 9.4 at 65°C (Smith and Martell, 1976).



The Hanford groundwater is saturated with respect to silica (Gephart et al., 1979) and is depleted in other dissolved solids. This suggests that the groundwater pH is largely controlled (i.e., buffered) by the dissociation of silicic acid.

The pH range appropriate to tests simulating ambient repository conditions is 9.4 to 9.9. However, this pH range will shift downward when the natural geotherm is perturbed by burial of nuclear waste. At elevated temperatures, two processes affect pH: precipitation of clay from solution and hydrolysis of silicates. Precipitation of clay occurs as the groundwater is heated and results in a decrease in pH because of consumption of OH^- and generation of H^+ . On the other hand, hydrolysis of

silicates involves the production of clay by solid-liquid reaction. In contrast to precipitation, the hydrolysis reaction causes a rise in pH (Krauskopf, 1979). To gain a clearer understanding of the difference between these two processes, consider the reactions given below:

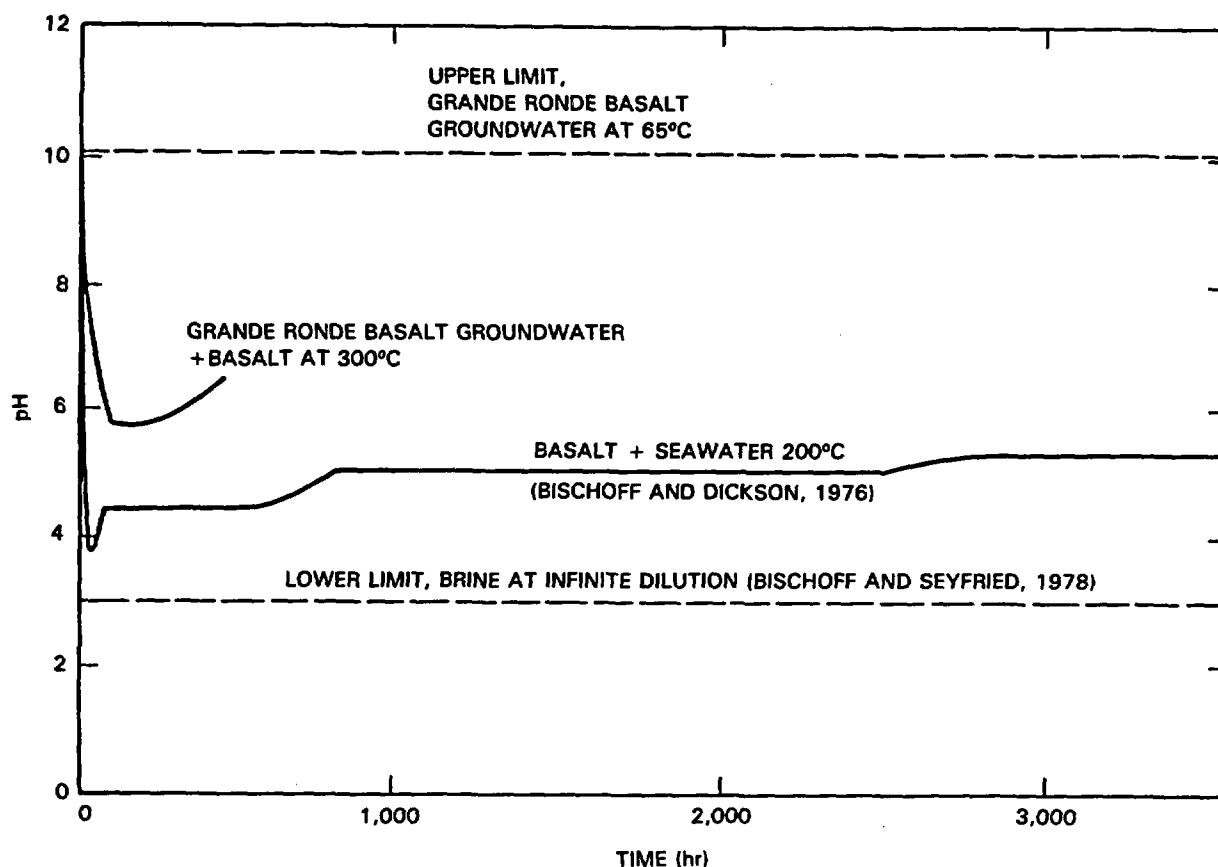


Equation 11-4 involves the formation and direct precipitation of clay from groundwater as a result of the alteration of magnesium silicate. This reaction consumes hydroxide, leaving an excess of hydrogen ion and resulting in a decrease in pH.

Equation 11-5 is another form of Equation 11-2 and describes the hydrolysis of silicates such as albite. In natural basalt, glass is the most reactive phase and would likely contribute most to the elevation of pH. However, glass is noncrystalline with a variable stoichiometry; therefore, any illustrative example using glass as a reactant is unnecessarily confusing. For increased clarity, Equation 11-5 is written as the hydrolysis of albite. The equation shows that the reaction of water and silicates to yield clay will produce OH^- ions (equivalent to consuming H^+ ions). The result is a decrease in hydrogen-ion activity and consequent rise in groundwater pH.

Precipitation and hydrolysis may occur simultaneously. The two reactions occur at different rates and have opposite effects. Therefore, the combined result is a complex variation of groundwater pH as a function of time. The trend commonly observed during hydrothermal experiments reacting "natural" waters with basalt at elevated temperatures is shown in Figure 11-24. An early pH depression results from the precipitation of clay from the heated water. This reaction is favored kinetically and precedes reaction of the silicate and groundwater (Eq. 11-5). Later, the dominant effect is produced by the hydrolysis reaction. The characteristic result is a rise in groundwater pH with an asymptotic approach to a steady-state value.

It is important to note that the extent of pH depression is dependent on temperature, water composition, and the water-to-solid ratio. Some of these relations are depicted in Figure 11-24. Note that minimum pH is produced when the water-to-solid ratio is infinite (lower dashed curve). In addition, waters with abundant dissolved salts (e.g., seawater) produce



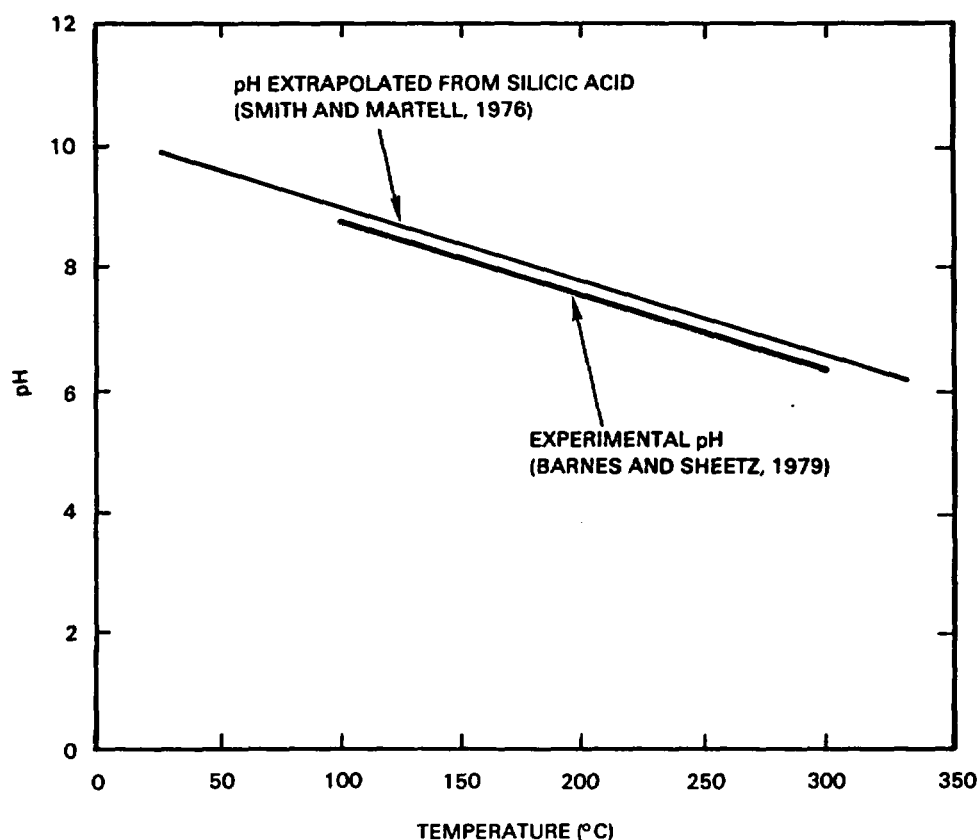
RCP8107-64

FIGURE 11-24. Variation Trend of Solution pH as a Function of Time.

greater pH depression than solutions of low ionic strength (e.g., simulated Grande Ronde Basalt groundwater). This effect is great enough to overwhelm the results of increased temperature. For instance, pH depressions observed using Grande Ronde Basalt groundwater are less extreme at 300°C than those produced in similar experiments at 200°C using seawater.

Increased temperature and water-to-solid ratios also decrease pH. At elevated temperatures precipitation of clay is enhanced and pH depression is increased. Similarly, at high water-to-rock ratios, processes that occur predominantly in the liquid phase prevail over processes requiring both solid and liquid. Thus, at high water-to-rock ratios, pH depression is increased. At low water-to-rock ratios, solid-liquid reactions control pH. In these cases, pH depression is minimized (or not observed) and steady-state conditions are rapidly approached.

Barnes and Scheetz (1979) have performed experiments in which simulated Grande Ronde Basalt groundwater was reacted with Hanford basalt (low water-to-rock ratio) to steady-state conditions at temperatures of 100°, 200°, and 300°C. Experimental pH values as a function of temperature are illustrated in Figure 11-25.



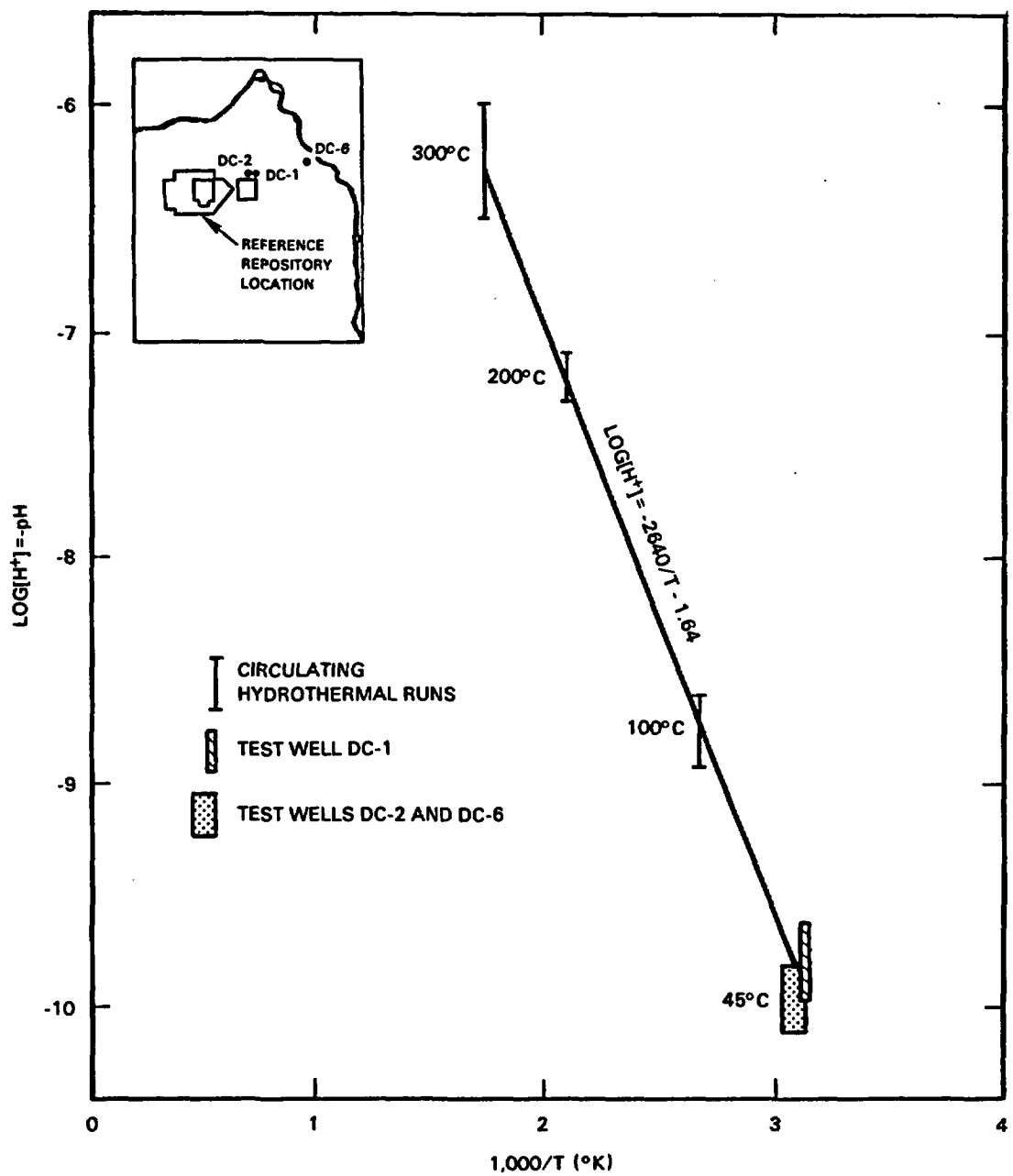
RCP8107-65

FIGURE 11-25. Relationship Between Estimated pH Resulting from the Dissociation of Silicic Acid and pH Measured in the Hanford Basalt/Groundwater System Between 100° and 300°C.

The experimental pH values have been fit to an inverse temperature relationship as follows:

$$\text{pH} = \frac{2,640}{T(^{\circ}\text{K})} + 1.64. \quad (11-6)$$

As seen in Figure 11-26, extrapolation of Equation 11-6 to lower temperatures results in close agreement with the in situ pH and measurements of simulated Grande Ronde Basalt groundwater at 45°C (Gephart et al., 1979). In addition, the empirical results of Barnes and Scheetz (1979) are in close agreement to the trend for the dissociation of silicic acid calculated by extrapolating low-temperature data (Smith and Martell, 1976) to elevated temperatures (see Fig. 11-25). The two relationships above



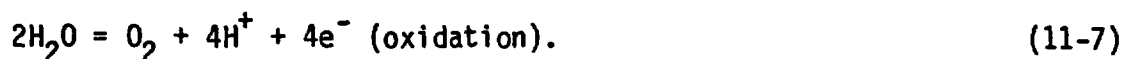
RCP8107-66

FIGURE 11-26. Plot of pH Versus $1/T$ for Groundwater in Equilibrium with Umtanum Basalt.

(Fig. 11-25 and 11-26), coupled with the silica-saturated nature of the groundwater, lend support to the belief that groundwater pH at repository depths is largely controlled by the dissociation of silicic acid, provided groundwater flow rates and water-to-rock ratios are low.

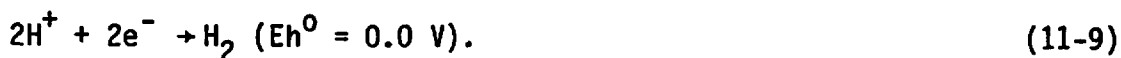
Eh is a measure of the electrical potential (volts) necessary to cause oxidation or reduction of a material. Consequently, the prevailing Eh of a system can be used to determine the stable oxidation state of polyvalent elements.

Eh is generally applied to aqueous systems and is therefore constrained by the oxidation reduction relations for water:

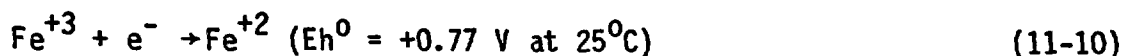


(e^- refers to an electron in aqueous solution).

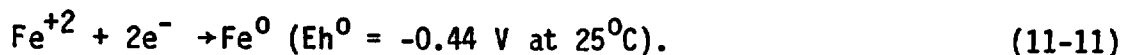
As mentioned previously, Eh is measured in volts (V). For convenience, the hydrogen half-cell reaction is defined as having a value of zero at all temperatures.



This reference is then used as a basis for measurement of any half-cell of interest. For example:



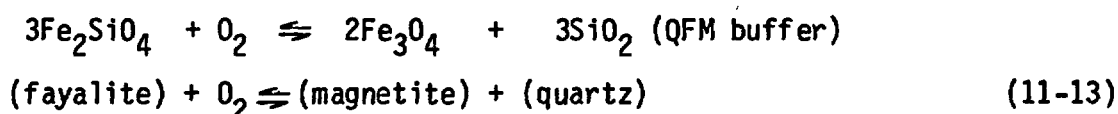
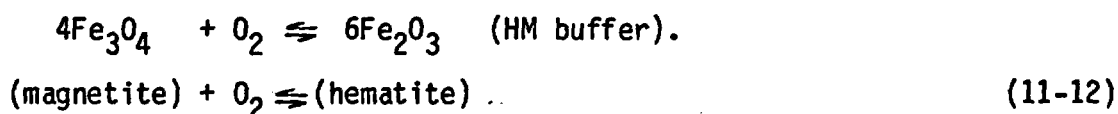
or



A positive value results from a half-cell with a potential that is more oxidizing than the hydrogen half-cell and a negative value results from one that is more reducing.

In the laboratory, Eh can be measured directly under carefully controlled conditions. However, field measurements of natural Eh are imprecise (Morris and Stumm, 1967). Therefore, natural Eh conditions are often inferred indirectly.

A common method of estimating Eh indirectly involves thermodynamic calculations. The key assumption necessary for the calculation of Eh is that the iron-bearing minerals in the host rock control the oxygen fugacity. Because the compositions of minerals change from rock to rock, there is no unique oxygen fugacity associated with a given rock type. Instead, there are generally recognized ranges. For basalt, two appropriate oxygen fugacity buffers, hematite-magnetite (Eugster, 1959) and quartz-fayalite-magnetite (Eugster and Wones, 1962) may be defined by iron oxide and iron silicate chemistry (Carmichael et al., 1974):



For simplicity, it is usually assumed that the solids are present as the pure phase (i.e., activity = 1). Then the equilibrium constant for each reaction can be written as follows:

$$K_{\text{MH}} = \frac{(\text{Fe}_2\text{O}_3)^6}{(\text{Fe}_3\text{O}_4)^4 (\text{O}_2)} = \frac{1}{f\text{O}_2} \quad K_{\text{QFM}} = \frac{(\text{Fe}_3\text{O}_4)^2 (\text{SiO}_2)^3}{(\text{Fe}_2\text{SiO}_4)^3 (\text{O}_2)} = \frac{1}{f\text{O}_2}. \quad (11-14)$$

A numerical result for each equilibrium constant (K) can be obtained using tabulated thermodynamic data (Robie et al., 1978) and the relationship:

$$\Delta G_r^0 = -RT(^0\text{K}) \ln K \quad (11-15)$$

where

ΔG_r^0 is the change in Gibbs free energy for the reaction at equilibrium

R is the universal gas constant

T is the temperature in °K

K is the equilibrium constant.

The equations for determining oxygen fugacity at any temperature for the two buffers are (Robie et al., 1978):

$$+ \log f_{O_2} \text{ (Pa)} = 13.96 - 25,323/T(^{\circ}\text{K}) \text{ for the HM buffer} \quad (11-16)$$

$$+ \log f_{O_2} \text{ (Pa)} = 9.0 - 25,680/T(^{\circ}\text{K}) \text{ for the QFM buffer.} \quad (11-17)$$

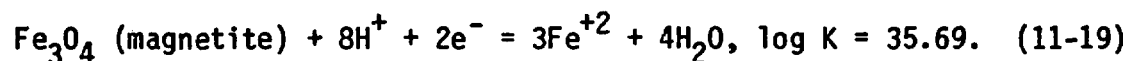
The oxygen fugacity is related to Eh through the reaction describing oxidation of water (see Eq. 11-7). To complete the Eh calculation, it is also necessary to know pH at the desired temperature. For a repository at Hanford, pH can be calculated from Equation 11-6.

The results of the above calculations may be fed into the expression below to determine Eh at any temperature and oxygen fugacity.

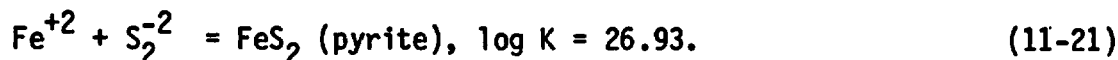
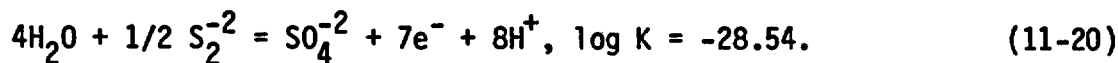
$$\begin{aligned} \text{Eh(volts)} = & 1.23 + 4.96 \times 10^{-5} T(^{\circ}\text{K}) \log f_{O_2} \\ & - 1.984 \times 10^{-4} T(^{\circ}\text{K}) \text{ pH} - [T(^{\circ}\text{K}) - 298] 1.7 \times 10^{-4}. * \end{aligned} \quad (11-18)$$

The total range of Eh values for the middle Sentinel Bluffs and Umtanum flows using the HM and QFM buffers from 51° to 300°C (calculated with Equations 11-16 through 11-18) is -0.54 to -0.37 volt, respectively.

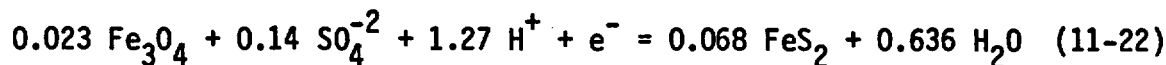
Another possible and perhaps more relevant Eh buffer for the Hanford basalt groundwater system is the equilibrium between magnetite, groundwater, and pyrite:



*The last term of this expression is required in order to ensure that the hydrogen reference electrode remains 0.00 volts at all temperatures. Application of this expression to determining ΔG or ΔK from half-cell potentials requires deletion of the last term.



Combining and simplifying the above equations yields:



where

$$\log K = 6.54; \Delta G_r^0 = -8,917 \text{ cal}; E^0 = +0.39 \text{ V}; \Delta S_r^0 = +10.02 \text{ cal/K}.$$

Assuming that the activities of all solids are unity, substitution into the following equation (Krauskopf, 1979)

$$E_h = E^0 + \frac{2.303 RT}{nF} \log K - \frac{(T-298)}{nF} \Delta S_r^0 \quad (11-23)$$

where

E^0 is standard potential

K is ratio of the product of activity (raised to stoichiometric coefficient powers) for products and reactants.

yields:

$$E_h = +0.39 - 1.98 \times 10^{-4} T \log K + (T-298) 4.34 \times 10^{-4} \quad (11-24)$$

$$E_h = +0.39 - 2.5 \times 10^{-4} T \text{ pH} + 2.77 \times 10^{-5} T \log (\text{SO}_4^{-2}) + (T-298) 4.34 \times 10^{-4} \quad (11-25)$$

where

T is given in $^{\circ}\text{K}$

ΔS_r^0 is the change in entropy for the reaction

E^0 is the half-cell potential for the reaction

n is the number of electrons

F is the Faraday constant.

Substitution of the concentration of SO_4^{2-} in Grande Ronde Basalt groundwater (1.25×10^{-1} gram per liter) into Equation 11-25 with the temperature and pH of interest will yield equilibrium Eh values. The range of Eh values for the magnetite-pyrite buffer from 51° to 300°C (calculated with Equation 11-25) is -0.41 to -0.43 volt, which is within the range calculated with the HM and QFM buffer.

The reducing conditions imposed by the basalt are conducive to metal (i.e., canister and overpack) stabilities and favor formation of insoluble transuranic oxides. In addition, Eh is so low that the hydrogen pressure in equilibrium with liquid water at 30 megapascals total pressure is in the range 0.25 to 0.90 megapascal. This is significant because it may inhibit the radiolysis of water.

Radiolysis results from radiation-induced dissociation of water. The species produced (e.g., H_2O_2 , HO_2^{\cdot} , OH^{\cdot}) are generally short lived but strongly oxidizing. For this reason, radiolysis is a major concern when predicting canister (or overpack) life. However, the presence of hydrogen may cause the radicals to recombine quickly, thus mitigating corrosion and perhaps negating the effects of radiolysis altogether (Stobbs and Swallow, 1962).

The previous discussion has dealt exclusively with estimations of equilibrium Eh. More oxidizing conditions are certain to result from repository excavation and subsequent backfilling. These conditions will be temporary, lasting only until the air trapped between particles of backfill is exhausted by reaction with the basalt. The exact rate of oxygen consumption by basalt (or backfill) will be directly dependent on the surface area of the solid and the temperature prevailing at the air-particle interface. Detailed knowledge of the specific reaction kinetics is lacking and this prevents making a confident estimate of how long Eh will be outside of geologic control.

11.4.1.5 Summary of Conditions. A summary of estimated repository conditions as a function of repository history is given in Table 11-26.

TABLE 11-26. Summary of Repository Equilibrium Conditions.^a

Period	Temperature (°C) ^b	Equilibrium pH	Log oxygen fugacity (MPa)	Eh(V)
Geologic control	51, 58	9.5	-62 to -68	-0.43 to -0.53
Thermal	100	8.7	-55 to -61	-0.42 to -0.54
	150	7.9	-47 to -53	-0.42 to -0.54
	200	7.2	-41 to -46	-0.41 to -0.53
	250	6.7	-35 to -41	-0.39 to -0.54
	300	6.2	-31 to -37	-0.37 to -0.54
Operating	51, 58	9.4	-1.7	+0.54

^aThe pressure in the repository is estimated to range between 0.1 and 30 megapascals over the life of the repository. With the exception of ambient temperature and pressure, differences in environmental parameters between the middle Sentinel Bluffs and Umtanum flows probably are not significant.

^bThe temperature in the waste package and very near field of the repository is expected to range between 51°C for the middle Sentinel Bluffs and 58°C for the Umtanum as lower temperature estimates and 300°C during the containment period.

11.4.2 Radiological Conditions

Characterization of the radiation environment within and around the waste package is important for evaluating package performance. The effects of radiolysis on solution chemistry, radiation damage to solids, and potential criticality hazards are of importance in this regard and are discussed below.

Interactions between radiation and crystalline solids can result in the creation of lattice imperfections: (1) by the introduction of chemical impurities through (n,γ) and (n,α) reactions and atomic transmutations and (2) by displacement of atoms from their equilibrium positions. The effects of these interactions on the physical and mechanical properties of metallic materials have been important to the development of nuclear technology, hence they have been extensively studied. The results have been reported in reviews by Dienes and Vineyard (1957) and Billington and Crawford (1961). Radiation effects on the potential backfill minerals are not well understood, but should not affect the important functional characteristics of the backfill (e.g., a chemical-physical barrier to water and radionuclide transport (Friedlander et al., 1964)).

Metallic materials exhibit measurable radiation effects only when exposed to high neutron doses (10^{24} neutrons per square centimeter), as in a reactor (Sutton and Leaser, 1954). Much lower neutron flux levels (10^3 neutrons per square centimeter per second) associated with a typical 3-year-old pressurized water reactor spent fuel assembly (Davis, 1979) would not yield dose levels (during the period of geologic isolation) where radiation effects would be measurable. Hence, the major concern in evaluation of nuclear waste isolation materials is the effect of the intense gamma radiation on the corrosion resistance of canister/overpack materials.

Incident radiation can affect the corrosion resistance of metallic materials by affecting changes in: (1) the metal itself, (2) the protective layer, and/or (3) the corrodant. Researchers have concluded that gamma radiation principally affects the corrodant and does so by producing chemical changes (radiolysis) through excitation and ionization (Stobbs and Swallow, 1962; Byalobzhetskii, 1970; Wu, 1978). The primary radiolysis process in aqueous solutions is the decomposition of water to form short-lived radicals, e_{aq}^- , H^\cdot , OH^\cdot , and HO_2^\cdot , and the long-lived molecular products, H_2 and H_2O_2 . If in some manner the radiolytic H_2 is continuously removed from the system, the oxidation potential of the solution will be increased. Conversely, in a closed system such as a sealed repository located in basalt, where the hydrogen fugacity remains high (see Section 11.4.1.4), the radiolysis reaction will be suppressed and the oxidation potential will remain essentially unchanged. Under such conditions, radiation should have little effect on corrosion.

Under conditions where radiolysis can easily occur, however, the solution will generally exhibit oxidizing properties and the general corrosion rate of metallic materials exposed to these solutions may increase, decrease, or remain essentially unchanged, depending on the nature of the metal. Alloys such as stainless steel, and those of aluminum, titanium, and zirconium that are rendered passive by the presence of an adherent surface-oxide film, should be little affected by oxidizing radiolysis products in aqueous solutions. The experimental study of the effect of gamma radiation on the corrosion of stainless steel in 3 percent NaCl solution (Byalobzhetskii, 1970) showed that the general corrosion rate was essentially unaffected after 1,200 hours of exposure. Similarly, studies cited by Stobbs and Swallow (1962) in their review showed that stainless steels in high-purity aqueous systems at temperatures up to 300°C and pH values around 10 are affected little by neutron irradiation.

Incident gamma radiation can be beneficial in reducing crevice corrosion in stainless steels and other alloys that exhibit susceptibility to this form of attack (Wu, 1978). Crevice corrosion is initiated as a result of differential aeration. Oxygen within a crevice is consumed by reaction with the metal, thus becoming depleted relative to the surrounding metal, and corrosion proceeds within the crevice. Under irradiation, the radiolysis reaction promotes oxidizing conditions within the crevice and the differential aeration cell is removed, thus preventing further corrosion.

Byalobzheskii (1970) has reported in his review that radiation can slightly reduce or have no effect on the corrosion rate of aluminum exposed to aqueous solutions. Radiation slightly reduced the corrosion rate of aluminum alloys with nickel (up to 2 percent), iron (about 0.5 percent), and silicon (0.90 to 0.21 percent), as revealed by 700-hour tests in a water-cooled reactor at 260°C. In a 1,000-hour test where aluminum was exposed at room temperature to a 3 percent NaCl solution under gamma radiation of 4×10^{15} electronvolts per square centimeter per second, the corrosion rate was unchanged.

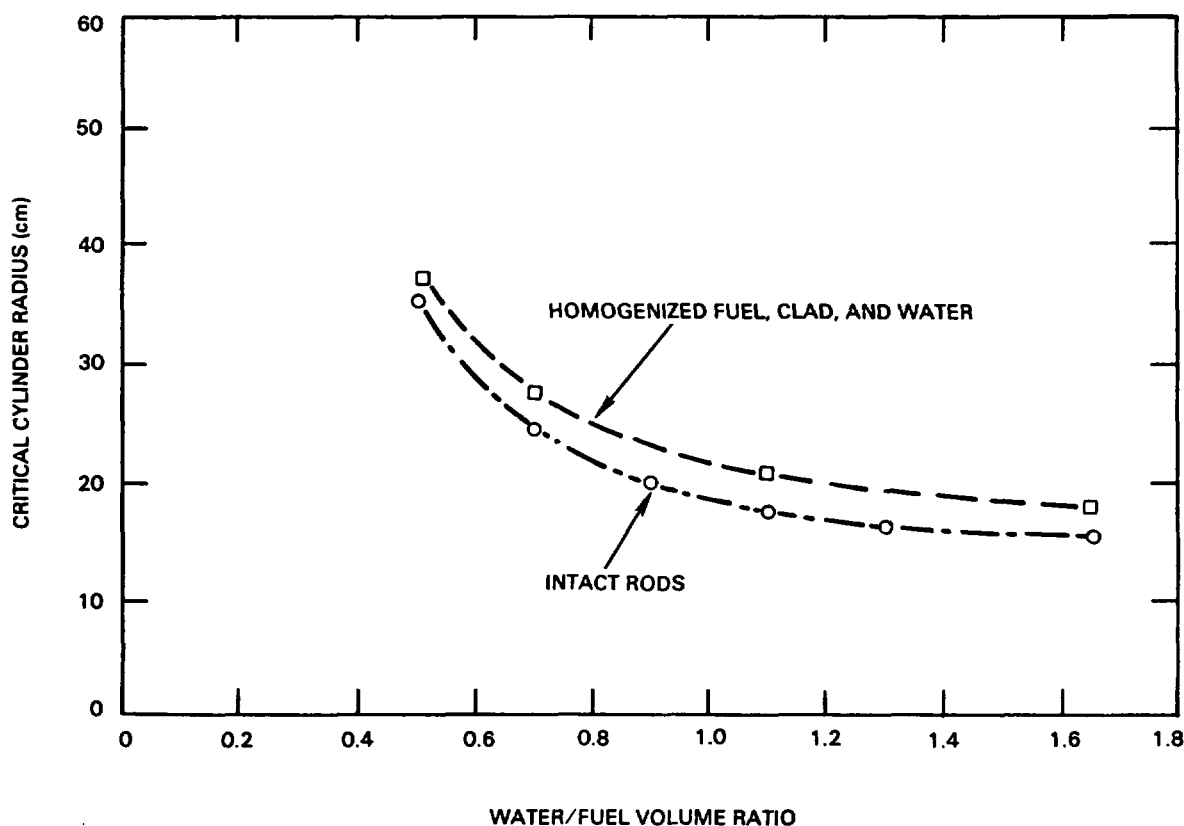
The corrosion resistance of zirconium and titanium, like aluminum, is determined by the tendency of these elements to passivate as a result of the formation of a dense oxide film on their surface. However, in reactor environments at higher temperatures, the film on unalloyed zirconium starts to disintegrate, leading to rapid corrosion. As a result, zirconium alloys such as the Zircalloys, which are covered with oxide films of greater stability, are used instead. According to Byalobzheskii (1970) the corrosion resistance of these alloys should not be affected by gamma radiation. A study was conducted by Braithwaite et al. (1980), in which titanium alloys were exposed to brine solutions and seawater at 90°C in a gamma field of 10^7 rads. In this study, the general corrosion rate of TiCode-12 in seawater was unaffected by radiation and the rate only doubled in the brine solution.

Because of the absence of a protective oxide surface layer and the facilitation of the cathodic reaction by the oxidizing radiolysis products, the corrosion rate of carbon steel exposed to aqueous solutions should increase. This behavior was observed by Byalobzheskii (1970). The corrosion rate of carbon steel increased 60 percent in distilled water, 80 percent in 0.5 nNaCl solution, and 400 percent in 0.01N H₂SO₄ under gamma irradiation (4.0×10^{15} electronvolts per square centimeter per second) after 1,000 hours at 20°C. In other studies conducted by Byalobzheski (1970), copper exhibited a marked increase in corrosion rate when exposed to HCl under gamma irradiation, which was also due to cathodic depolarization by the oxidizing radiolysis products. Samples of electrolytic copper were exposed to X-rays in a 1 nNaCl solution. The corrosion rate increased by a factor of 4.5 for a 10-hour exposure where the total energy absorbed by the solution was equal to 0.37×10^{16} electronvolts per cubic centimeter.

Concerns over potential criticality problems in the waste package are of importance and have been summarized recently (Gore et al., 1980). Criticality hazards will be dependent on the type of waste to be disposed of, the age of the waste, and the amount and configuration of the waste in the package. Presently, the NWTS Program assumes spent fuel with an age of 10 years out of the reactor to be the reference waste form. The packaging configuration now being used as a reference by the BWIP consists of either three disassembled pressurized water reactor spent fuel assemblies or seven boiling water reactor spent fuel assemblies in a close-packed array in a canister. For the analysis, a burnup of 33,000 megawatt days per metric ton of heavy metal and an initial enrichment of 3 percent were assumed. The results of Gore et al. (1980) for spent fuel in close-packed arrays are summarized in Figure 11-27. The curves represent the maximum

cylinder (canister) radius as a function of the water-to-fuel ratio in the cylinder before critical conditions are approached (K_{eff} equal to or less than 0.95). The curve for homogenized fuel, clad, and water reflects the lower neutron activity that results if the intact fuel rods are breached and the fuel and cladding disintegrate and mix homogeneously. The proposed canister radius and water-to-fuel ratio presently being considered for the waste package are 15 centimeters and approximately 0.3, respectively. As is shown in Figure 11-27, this waste package arrangement is well below the critical curve, suggesting that the BWIP reference spent fuel waste package should be critically safe.

A criticality hazards analysis of waste packages containing the defense and commercial high-level glass waste forms has not been made. However, since the fissile materials remaining in the waste stream incorporated in the glass would be a small fraction of that contained in spent fuel because of reprocessing, waste packages containing the borosilicate glass waste form should also be critically safe. Indeed, a critical mass in any configuration should not be possible because of the low volume of fissile material in such wastes.



RCP8107-67

FIGURE 11-27. Cylinder (Canister) Radius Versus Water-to-Fuel Ratio for the Onset of Critical Conditions in Spent-Fuel Waste Packages.

11.4.3 Summary of Important Conclusions

In this section the physicochemical and radiologic conditions expected to exist at the repository horizons in basalt at Hanford are described. These conditions are concluded from several preliminary investigations and may change as more data become available. In general, however, the geochemical characteristics of the host rock and groundwater in the preemplacement, as well as the project postemplacement environment support waste containment and isolation. The mildly alkaline pH and the reducing conditions work to minimize corrosion, limit the solubility of key radionuclides, and retard the migration of radionuclides from the very near- and near-field repository environment. The reference groundwater chemistry is that associated with the Grande Ronde Basalt. This groundwater is saturated with respect to silica and contains relatively large concentrations of F^- , SO_4^{2-} , and Cl^- . Based on measurements made in deep-drilled boreholes and preliminary results of thermal modeling of emplaced waste packages, a conservative estimate for the temperature rise in the repository near field is from an ambient of about 51°C for the middle Sentinel Bluffs and 58°C for the Umtanum to a maximum of 300°C throughout the repository history. Two important intensive variables in aqueous solutions are Eh and pH, as they control the stability and solubility of solids and the form taken by aqueous species in solution. During the operating phase of the repository, the Eh is expected to be high (+0.54 volt) because of the availability of oxygen. Sometime after repository sealing, reducing conditions will be imposed by the basalt, and by calculation the Eh will range from -0.43 to -0.54 during the remainder of the geologic history for both the middle Sentinel Bluffs and Umtanum flows. These reducing conditions are conducive to canister materials stability (low corrosion rate). In addition, at this Eh and the pressures expected at repository depths, the hydrogen pressure will be significant and may inhibit the radiolysis of groundwater. Thus, radiation is not expected to affect the corrosivity of groundwater under these conditions. This must be experimentally verified, however. The pH of the groundwater sampled from the Grande Ronde Basalt and extrapolated to the ambient temperature of the middle Sentinel Bluffs (51°C) and Umtanum (58°C) flows is between 9.4 and 9.9. Assuming that at elevated temperatures the pH of Grande Ronde Basalt groundwater is controlled by the dissociation of silicic acid (verified experimentally), calculations yield values ranging from 8.7 to 6.2 as the temperature increases from 100° to 300°C.

Further experimental verification of the expected environmental conditions that will exist at the repository horizons are vital to allow accurate waste package design and performance modeling. This work is planned and is part of the site characterization program being managed by the BWIP.

11.5 ALTERNATE WASTE PACKAGE

An alternate conceptualized design for horizontal borehole emplacement is shown in Figure 11-28. This design concept differs from that shown in Figure 11-6 in the physical arrangement of the components. For the alternate concept, preformed high-density backfill surrounds the waste form container (containing either spent fuel or reprocessed high-level waste) and both are sealed in the canister. This concept allows the handling and horizontal emplacement of the waste package as an integral unit. The clearance space required around the waste package in the borehole for emplacement operations is then filled with a crushed basalt-bentonite backfill mixture. Later swelling of the backfill as water moves into the borehole will eliminate voids and the smear density will reach the required 65 percent of theoretical density.

The canister for spent fuel and commercial high-level-waste measures 68.6 centimeters (27.0 inches) inside diameter with a wall thickness of 9.9 centimeters (3.9 inches). For defense high-level-waste borosilicate glass, the canister measures 96.5 centimeters (38.0 inches) and 13.0 centimeters (5.1 inches), respectively.

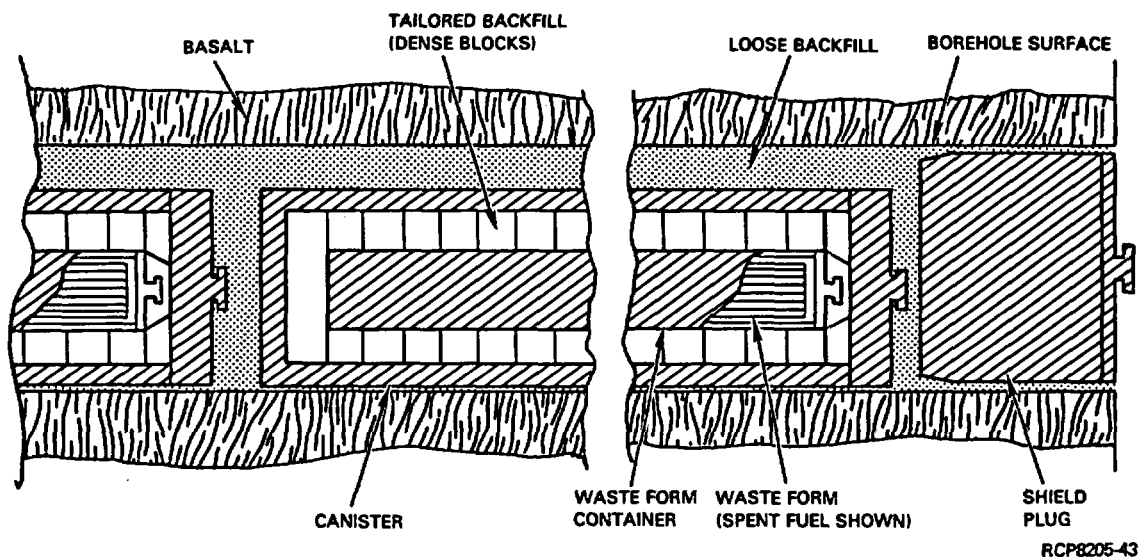


FIGURE 11-28. An Alternate Waste-Package Borehole-Emplacement Concept.

11.6 SUMMARY

The purpose of this chapter was to describe the current understanding of the performance of the reference commercial high-level-waste form and spent fuel. The adequacy of the current waste package conceptual design to meet the required performance for a repository constructed in basalt was also described. The physical and chemical properties of these waste forms and their performance under conditions relevant to a repository at Hanford were discussed. The current BWIP waste package conceptual design for spent fuel and reprocessed high-level waste was reviewed together with the functional requirements for each package component. The BWIP waste package program plan and the status of the program were reviewed, as were the emplacement conditions expected in the repository.

Calcination of high-level waste solutions is now perceived as a possible first step in the production of solid reprocessed waste forms. Several calcine compositions exist; each is based on a particular fuel-reprocessing waste stream. From these, a large number of glass formulations have been developed and tested; however, those that have been brought closest to the point of process application are the borosilicate glasses. These glasses can accommodate a wide variety of waste elements, are relatively slow to devitrify under anhydrous conditions (no devitrification has been observed in samples annealed at temperatures below 500°C), and are relatively unaffected by radiation. A number of crystalline phases form in the 76-68 borosilicate glasses above 500°C as a consequence of devitrification, which leads to microcracking and a resultant increase in leachability. The products of devitrification of 76-68 glass are impossible to predict accurately, but a conservative estimate would be that most elements would be present as simple oxides after devitrification. Thus, as in spent fuel, the same problem results (i.e., having highly soluble phases in the waste form). However, the leachability of 76-68 glass, for example, is generally lower than that of spent fuel. The absolute temperature of a canister containing glass waste will depend on factors such as the irradiation history of the spent fuel, its type, the age of the waste at vitrification, and the waste loading of the glass.

The BWIP reference waste package for spent fuel consists of close-packed spent fuel rods sealed in carbon steel canisters that are emplaced in a horizontal borehole. The BWIP reference waste package for commercial high-level waste and defense high-level waste consists of borosilicate glass sealed in a stainless steel container and then sealed in a carbon steel canister which serves to provide containment. Alternate designs for waste packages for both borehole and tunnel emplacement were discussed. This design concept is predicated on the perceived need for a system of engineered components or barriers that must act in concert with the repository engineered system to provide containment for nuclear waste to meet existing federal regulations. The functions of the conceptual waste package are keyed to two time periods in repository history: the thermal period or first 1,000 years and the period of time following, called isolation or the period of geologic control (post-thermal period). During the two periods the waste package components function either physically or chemically to provide containment or controlled release of the waste form. Thus, over the long time spans during which a repository must

function, the repository environment will cycle from its initial (preemplacement) unperturbed state, through a thermally perturbed period and, after most of the significant heat-producing isotopes in the waste have decayed, reapproach the conditions originally found in the host rock. This cycle is summarized in Table 11-27. Conceptual designs of waste packages for commercial and defense high-level waste (borosilicate glass) have been completed for basalt by Westinghouse-Advanced Energy Systems Division and are being evaluated by the BWIP.

The NWTS approach to waste package research and development has focused on an evaluation of recognized waste forms, candidate waste package materials, and the environment expected in basalt, to obtain an understanding of the behavior of these materials under expected repository conditions (NWTS, 1981c). The approach proceeds from an initial far-field assessment of maximum allowable rates of release of radionuclides to the accessible environment (biosphere). From this assessment, key radionuclides (those for which the criteria governing the maximum permissible release rate to the biosphere are the most stringent) are identified and preliminary performance requirements for a waste package in basalt are established to meet existing regulations for the containment of radionuclides. An extensive program of hydrothermal testing of reference waste forms and candidate waste-package materials under site-specific repository conditions is conducted to identify suitable waste package materials. This, together with waste package degradation and near-field radionuclide-behavior modeling, is used to prepare design requirements for the design of waste packages. Field and in situ testing methods are then used to qualify the waste package designs to meet licensing requirements for a repository to be constructed in basalt.

The BWIP waste package research and development program encompasses four activities: (1) waste form, (2) design and development, (3) barrier materials, and (4) performance evaluation. Work has been initiated and is progressing within each activity. The waste form activity is directed toward assembling data and information on the stability of reference and alternate waste forms in a basalt environment and obtaining simulated and radioactive waste forms for hydrothermal testing. In relevant studies taken from the literature, it has been learned that the most leachable elements contained in spent fuel appear to be cesium, rubidium, molybdenum (and by analogy technetium), and strontium. Cesium and strontium should readily sorb on the basalt and secondary minerals. Molybdenum and technetium solubilities should be significantly smaller under the highly reducing conditions expected in the basalt environment than if the conditions were oxidizing. If such is not the case, technetium release from spent fuel will present a significant problem throughout the repository's history. The release of long-lived uranium and its toxic daughters will also be significantly influenced by the redox conditions in the repository. Under reducing conditions they will be extremely insoluble and thus immobile.

TABLE 11-27. Expected Repository Conditions at the Emplacement Location.

Period	Condition/operation	Time (yr)	General characteristics (reference horizon)
Preemplace-ment	Natural undisturbed host rock	0	Low-permeability basalt saturated with alkaline, anoxic water (0.1% by volume) at 60C at lithostatic pressure.
Thermal	Construction of waste emplacement panels	1 to 20	Host rock exposed to atmosphere provided by repository ventilation system.
	Waste emplacement initiated, filled panels isolated from main ventilation system	10 to 80	Basalt heated by the waste package dries the rock in the vicinity of the waste packages. Maximum temperatures reached in emplacement environment.
	Panels, tunnels, and shafts are backfilled and sealed and the repository is decommissioned	80 to 90	Decreased heat-generation rates, as a result of continued radioactive decay, cause lower emplacement environment temperature, trapped oxygen being consumed by emplacement media.
	Wastes are contained by the canister	90 to 1,000	Waste package backfill slowly resaturated, emplacement temperature drops, hydrostatic repository pressure established, and anoxic/alkaline conditions reestablished.
Geologic	Wastes isolated by action of waste form, tailored backfill, repository backfill, and host rock characteristics	1,000 and beyond	Repository conditions approach those of original undisturbed host rock.

Borosilicate glass appears to be more leach resistant than spent fuel. Sodium, silicon, molybdenum (technetium), uranium, and cesium appear to be the most leachable elements in the glass waste under oxidizing conditions. Strontium and calcium are also leachable, but to a much lesser extent. Changes in oxidation potential, particularly to the extremely reducing conditions likely in a sealed repository in basalt, may significantly alter the results presented here. Although dissolution of borosilicate glass appears to be slow at temperatures less than 150°C, some key radionuclides will be steadily released as a function of silicate network breakup. Unless fixed by specific tailoring agents added to the backfill, these radionuclides may be concentrated at a migration front and could represent a possible hazard. Static- or low-flow conditions will allow some precipitation to occur and thus will reduce the solution concentrations of cesium, uranium, and perhaps technetium. The concentrations of radionuclides that remain in solution after precipitation are governed by temperature and equilibrium constants for these phases. Further investigation of these phenomena are necessary to quantify waste species solubility for final hazards determination and waste package design.

The design and development activity encompasses the conduct of studies that will, with data and information developed by the barrier-materials and performance evaluations activities, provide the basis for preparation of design requirements for waste packages to be emplaced in basalt. Until the beginning of fiscal year 1983, the BWIP did not have the responsibility for the conceptual design of waste packages (this is being done by a single contractor responsible to ONWI). Reference and alternate waste packages have been conceptualized by Westinghouse-Advanced Energy Systems Division and Kaiser Engineers, Inc./Parsons Brinckerhoff Quade & Douglas, Inc. to support conceptual design studies for a repository in basalt. The conceptual design incorporates the canister and backfill, presently envisioned as needed for the successful isolation of spent fuel and borosilicate glass in basalt.

The barrier materials activity encompasses the development of data and information on the waste emplacement environment of the repository, and on waste-barrier-rock interactions that may occur within the emplacement environment. It is also focused on the selection of reference waste package component materials and support of the preparation of design requirements for site-specific waste packages. Waste package emplacement conditions will be affected by the temperature of the waste package, which may range from the ambient of about 58°C at the Umtanum (51°C at the middle Sentinel Bluffs) to a high of 300°C throughout the history of the repository. Recent calculations have shown that the spent fuel waste package centerline temperature will rise to a maximum of approximately 270°C 4 years after waste emplacement, while the emplacement hole surface will reach approximately 220°C 6 years after emplacement. Temperatures throughout the waste package will converge 2,000 years after emplacement, at which time they will be approximately 125°C. After 3,400 years, the waste package temperature will have dropped to less than 100°C. Pressure will vary from 0.1 to 30 megapascals. Pressure of 0.1 megapascal will prevail while the repository is open during the operating period. Upon closure, the pressure will begin to build and will ultimately return to that exerted by

the rock load (30 megapascals). The equilibrium pH of the groundwater associated with the repository will probably be controlled by the dissociation of silicic acid and will vary with temperature. The pH values for the Grande Ronde Basalt have been calculated and lie in the range of 6.2 to 9.9, corresponding to temperatures of 300° and 510°C, respectively. In the sealed repository in Grande Ronde Basalt, the equilibrium oxidation potential (Eh) is controlled by oxygen exchange with the repository host rock. Under geologic control, Eh will lie in the range of -0.37 to -0.54 volt, varying with temperature. During the operating phase while the repository is open, the Eh will be that determined by groundwater equilibrated with atmospheric oxygen and will be +0.54 volt. The neutron flux levels associated with the spent fuel waste packages are not expected to yield integrated dose levels where radiation effects in metallic materials would be measureable. Consequently, a major concern in evaluating candidate waste package materials will be the effect of intense gamma radiation. Researchers have concluded that gamma radiation principally affects the corrodant and does so by producing changes (radiolysis) through excitation and ionization. The primary radiolysis process in aqueous solutions is the decomposition of water to permit oxidizing conditions. However, in a closed system such as a sealed repository located in basalt, where the hydrogen fugacity remains high, the radiolysis reaction will be suppressed and reducing conditions will be preserved. Radiation effects in candidate backfill materials are not well understood, but should not degrade the ability of the backfill to function as a barrier to water intrusion and radionuclide transport.

Two sets of hydrothermal experiments were conducted at 300°C to determine the interactions among simulated supercalcine, basalt, and simulated Grande Ronde Basalt groundwater. Analysis of test solutions, sampled periodically during the hydrothermal experiments, showed that the presence of basalt decreased sodium, rubidium, molybdenum, and chromium concentrations while silicon concentration increased. The decrease in chromium concentration was the most dramatic, which probably resulted from a strong reaction with basalt. Hydrothermal testing of simulated 76-68 borosilicate glass in the presence of basalt has been initiated. Preliminary corrosion screening tests of several candidate canister/overpack materials at 250°C, 30 megapascals pressure, pH of 9.93, and under anoxic conditions (less than 1 part per billion of O₂) have been completed. Based on the results of these tests and assuming a linear time dependence for general corrosion, the calculated wall thicknesses needed for a 1,000-year design life varied from a low of 0.043 centimeter for the nickel-base alloy (Hastelloy C-276) to a high of 0.16 centimeter for grade 12 titanium (TiCode 12). From a review of the literature it has been concluded that no single material is available that can satisfy the performance requirements for the backfill; thus, to be effective, the backfill must be a multicomponent material. Candidates for the major components include bentonite, crushed basalt, and zeolites. There may also be a need for a minor component specifically tailored for retardation of some radionuclides that may be potentially mobile in the repository host rock. In tests conducted to determine the dehydration of fracture mineralization found in basalt, preliminary conclusions are that:

- (1) only minor alterations of basalt are expected to occur below 300°C

and (2) below this temperature an increase in groundwater pathways, due to dehydration and volume reduction of fracture-filling secondary mineralization, should not occur outside the disturbed zone of the repository site.

The performance evaluation activity encompasses evaluation of the performance of waste package designs under the environmental conditions expected in a repository in basalt. Preliminary waste package performance requirements have been defined using a simple one-dimensional transport model.

Two release and transport scenarios were modeled to determine the most hazardous radionuclides in the waste inventory and to estimate the maximum permissible release rate for various nuclides that the waste package must meet.

11.7 SUMMARY OF UNRESOLVED ISSUES

During the development of the BWIP Waste Package Program plan, and as a result of past research and development, several issues have been identified, the resolutions of which are necessary to achieve the design of waste packages for emplacement in a repository in basalt. These issues are identified and discussed in Chapter 15, together with the plans for their resolution. The extent to which previous investigations have addressed these issues is also discussed in Chapter 15 as well as the approach for obtaining the additional information needed to resolve them.

11.8 REFERENCES

AESD, 1980, Engineered Waste Package Design Specification, AESD-TME-3055, Advanced Energy Systems Division, Westinghouse Electric Corporation, Pittsburgh, Pennsylvania, October 1980.

AESD, 1982, Waste Package Conceptual Designs for a Nuclear Waste Repository in Basalt, RHO-BW-CR-136/AESD-TME-3142, Advanced Energy Systems Division, Westinghouse Electric Corporation for Rockwell Hanford Operations, Richland, Washington, September 1982.

Aitken, E. A., Evans, S. K., Rubin, B. F., and Ludlow, T. E., 1972, Transport and Reaction of Cs, Te, I, and Mo with Fast Reactor Fuel and Stainless Steel Cladding: I, GEAP-12268, General Electric Company, Pleasanton, California.

Altenhofen, M. K., 1981, Waste Package Heat-Transfer Analysis: Model Development and Temperature Estimates for Waste Packages in a Repository Located in Basalt, RHO-BWI-ST-18, Rockwell Hanford Operations, Richland, Washington, October 1981.

Anderson, W. J., 1981, Corrosion Tests of Canister and Overpack Materials in Simulated Basalt Groundwater, RHO-BWI-ST-15, Rockwell Hanford Operations, Richland, Washington, May 1981.

Anderson, W. J., 1982, Conceptual Design Requirements for Spent Fuel, High-Level Waste, and Transuranic Waste Packages, RHO-BW-ST-25 P, Rockwell Hanford Operations, Richland, Washington.

Andrews, M. G., Freeburn, H. R., and Wenisen, W. D., 1979, "The Performance of Combustion Engineering Fuel in Operating PWRs," in Proceedings of the ANS Topical Meeting on LWR Fuel Performance, April 29 to May 3, 1979, American Nuclear Society, Portland, Oregon.

Baily, W. E., Armijo, J. S., Jacobson, J., and Proebstle, R. A., 1979, "BWR Fuel Performance," in Proceedings of the ANS Topical Meeting on LWR Fuel Performance, American Nuclear Society, Chicago, Illinois.

Bailey, W. E., Morris, C. J., Reich, F. R., and Swinth, K. L., 1980, Assessment of Current Onsite Inspection Techniques for Light Water Reactor Fuel Systems - Executive Summary, NUREG/CR-1380, PNL-3325 Vol. 1, Pacific Northwest Laboratory, Richland, Washington, July 1980.

Barnes, M. W. and Scheetz, B. E., 1979, "Laboratory Alteration of a Columbia River Basalt by Hot Groundwater: An Application to Deep Geologic Disposal of Nuclear Waste," Geological Society of America Bulletin, Abstracts, No. 11, p. 384.

Barney, G. S. and Wood, B. J., 1980, Identification of Key Radionuclides in a Nuclear Waste Repository in Basalt, RHO-BWI-ST-9, Rockwell Hanford Operations, Richland, Washington, May 1980.

Baxter, R. G., 1981, Description of DWPF Reference Waste Form and Canister, DP-1606, E. I. du Pont de Nemours & Company, Savannah River Laboratory, Aiken, South Carolina.

Bazin, J., Jouan, J., and Vignesoult, N., 1974, "Comportement et État Physico-Chimique des Produits de Fission dans les Éléments Combustibles pour Réacteur à Eau Pressurisée," Bulletin d' Information Scientifique et Technique, Vol. 196, No. 55.

Bell, M. G., 1973, ORIGEN - The ORNL Isotope Generation and Depletion Code, ORNL 4628, Oak Ridge National Laboratory, Oak Ridge, Tennessee.

Besmann, T. M. and Lindemer, T. B., 1978, "Chemical Thermodynamics of the System Cs-U-Zr-H-I-O in the Light Water Reactor Fuel-Cladding Gap," Nuclear Technology, Vol. 40, p. 297.

Billington, D. S. and Crawford, J. H., 1961, Radiation Damage in Solids, University Press, Princeton, New Jersey.

Bischoff, J. L. and Dickson, F. W., 1976, "Seawater-Basalt Interactions at 200°C, 500 Bars, Implication for Origin of Sea-Floor Heavy Metal Deposits and Regulation of Seawater Chemistry," Earth and Planetary Science Letter, Vol. 25, pp. 385-397.

Bischoff, J. L. and Seyfried, W. E., 1978, "Hydrothermal Chemistry of Seawater from 25°C to 350°C," American Journal of Science, Vol. 278, pp. 838-860.

Blackwell, D. D., 1978, "Heat Flow and Energy Loss in the Western United States," in Cenozoic Tectonics and Regional Geophysics of the Western Cordillera, Smith, R. B. and Eaton, G. P., eds., Memoir 152, Geological Society of America, Boulder, Colorado.

Bradley, D. J., 1978, Leaching of Fully Radioactive High-Level Waste Glass, PNL-2664, Pacific Northwest Laboratory, Richland, Washington.

Braithwaite, J. W., Magnani, N. J., and Munford, J. W., 1980, "Titanium Alloy Corrosion in Nuclear Waste Environments," Paper No. 213 in Proceedings, Corrosion 80, Chicago, Illinois.

Bramman, J. I. and Powell, H. J., 1975, "Redistribution of Fuel and Fission Products in Irradiated Oxide Fuel Pins," Journal of the British Nuclear Energy Society, Vol. 14, p. 63.

Bramman, J. I., Sharpe, R. M., Thom, D., and Yates, G., 1968, "Metallic Fission-Product Inclusions in Irradiated Oxide Fuels," Journal of Nuclear Materials, Vol. 25, p. 201.

Byalobzhetskii, A. V., 1970, Radiation Corrosion, AEC-TR-7096, U.S. Atomic Energy Commission, Washington, D.C.

Carmichael, I. S. E., Turner, F. J., and Verhoogen, J., 1974, Igneous Petrology, McGraw Hill, New York, New York.

Carslaw, H. S. and Jaeger, J. C., 1959, Conduction of Heat in Solids, Oxford University Press, London, England.

Carter, L. J., 1979, "Academy Squabbles over Radwaste Report," Science, Vol. 205, pp. 287-289.

Chick, L. A., McVay, G. L., Mellinger, G. B., and Roberts, F. P., 1980, Annual Report on the Development and Characterization of Solidified Forms for Nuclear Waste, PNL-3465, Pacific Northwest Laboratory, Richland, Washington.

Chou, I. and Eugster, H. P., 1978, "Diffusion of Hydrogen Through Platinum Membranes at High Pressures and Temperatures," Geochimica et Cosmochimica Acta, Vol. 42, pp. 281-288.

Clark, R. G. and Reynolds, A. W., 1979, "Uranium Market Forecasts," in Proceedings, Uranium Industry Seminar, October 12, 1979, Grand Junction, Colorado.

Cleveland, J. M., 1970, The Chemistry of Plutonium, Gordon and Breach Science Publishers, New York, New York.

Coons, W. E., Moore, E. L., Smith, M. J., and Kaser, J. D., 1980, The Functions of an Engineered Barrier System for a Nuclear Waste Repository in Basalt, RHO-BWI-LD-23, Rockwell Hanford Operations, Richland, Washington, January 1980.

Courtright, E. L., 1979, A Survey of Potential Light-Water Reactor Fuel Rod Failure Mechanism and Damage Limits, NUREG/CR-1132, PNL-2787, Pacific Northwest Laboratory, Richland, Washington, July 1979.

Cubicciotti, D. D., 1978, State-of-the-Art Model for Release of Volatile Fission Products from UO₂ Fuel, SRI Project 7453, Stanford Research Institute, Stanford, California.

Cubicciotti, D. D. and Sanecki, J. E., 1978, "Characterization of Deposits on Inside Surfaces of LWR Cladding," Journal of Nuclear Materials, Vol. 78, pp. 96-111.

Cubicciotti, D. D., Jones, R. L., and Syrett, B. C., 1980, Stress Corrosion Cracking of Zircalloys, EPRI-NP-1329, Electric Power Research Institute, Palo Alto, California.

Davies, J. H. and Ewart, F. T., 1971, "The Chemical Effects of Composition Changes in Irradiated Oxide Fuel Materials," Journal of Nuclear Materials, Vol. 41, pp. 143-155.

Davies, J. H., Frydenbo, F. T., and Adamson, M. G., 1979, "Determination of the Chemical Activity of Fission Product Iodine in Zircaloy Clad UO₂ Fuel Rods," Journal of Nuclear Materials, Vol. 80, p. 366.

Davis, R. B., 1979, Data Report for the Nondestructive Examination of Turkey Point Spent Fuel Assemblies B02, B03, B17, B41, and B43, TC-1284, Hanford Engineering Development Laboratory, Richland, Washington.

Deer, W. A., Howie, R. A., and Zussman, J., 1967, Rock-Forming Minerals, Longmans, Green and Co., London, England, Vol. 1-5.

Dienes, G. J. and Vineyard, G. H., 1957, "Radiation Effects in Solids," Interscience Publishers, New York, New York and London, England.

DOE, 1979, Technology for Commercial Radioactive Waste Management, DOE/ET-0028, U.S. Department of Energy, Washington, D.C., Vol. 1.

DOE, 1980a Final Environmental Impact Statement, Management of Commercially Generated Radioactive Waste, DOE/EIS-0046F, U.S. Department of Energy, Washington, D.C., Vol. 1.

DOE, 1980b, Final Environmental Impact Statement, Management of Commercially Generated Radioactive Waste, DOE/EIS-0046F, U.S. Department of Energy, Washington, D.C., Vol. 2.

DOE, 1980c, Spent Fuel Storage Fact Book, DOE/NE-0005, U.S. Department of Energy, Washington, D.C.

DOE, 1980d, United States of America Nuclear Regulatory Commission, In the Matter of Proposed Rulemaking on the Storage and Disposal of Nuclear Waste (Waste Confidence Rulemaking), Statement of Position of the United States Department of Energy, DOE/NE-0007, U.S. Department of Energy, Washington, D.C., April 15, 1980.

DOE/USGS, 1980, Earth Science Technical Plan for Disposal of Radioactive Waste in a Mined Repository, DOE/TIC-11033 (Draft), U.S. Department of Energy and the U.S. Geological Survey, Washington, D.C.

EPA, 1981, Working Draft No. 20, Environmental Protection Agency, 40 CFR 191, Environmental Standards and Federal Radiation Protection Guidance for Management and Disposal of Spent Nuclear Fuel, High-Level and Transuranic Radioactive Wastes, U.S. Environmental Protection Agency, Washington, D.C.

ERDA, 1976, Alternatives for Managing Wastes from Reactors and Post-Fission Operations in the LWR Fuel Cycle, ERDA-76-43, U.S. Energy Research and Development Administration, Washington, D.C., Vol. 1.

Eugster, H. P., 1959, "Reduction and Oxidation in Metamorphism," in Researches in Geochemistry, P. H. Nelson, ed., John Wiley & Sons, Inc., New York, New York.

Eugster, H. P. and Wones, D. R., 1962, "Stability Relations of Ferruginous Biotite, Annite," Journal of Petrology, Vol. 3, pp. 82-125.

Ewart, F. T., Taylor, R. G., Horspool, J. M., and James, G., 1976, "The Chemical Effects of Composition Changes in Irradiated Oxide Fuel Materials II - Fission Product Segregation and Chemical Equilibria," Journal of Nuclear Materials, Vol. 61, pp. 254-270.

Friedlander, G., Kennedy, J. W., and Miller, J. M., 1964, Nuclear and Radiochemistry, John Wiley & Sons, Inc., New York, New York.

Friskney, C. A. and Simpson, K. A., 1975, "The Behavior of Fission-Product Barium and Strontium in Irradiated UO₂," Journal of Nuclear Materials, Vol. 57, p. 121.

Friskney, C. A. and Turnbull, J. A., 1979, "The Characteristics of Fission Gas Release from Uranium Dioxide During Irradiation," Journal of Nuclear Materials, Vol. 79, p. 184.

Fuhrman, N., Pasupathi, B., Scott, D. B., Temple, S. M., Pati, S. R., and Hallowell, T. E., Combustion Engineering, 1976, Evaluation of Fuel Rod Performance in Maine Yankee Core 1, Task C, EPRI NP-218, Project 586-1, Final Report, Electric Power Research Institute, Palo Alto, California, November 1976.

Funk, C. W. and Jacobson, L. D., 1979, Inventory and Characterization of Spent LWR Fuel, HEDL-TME 77-82, Hanford Engineering Development Laboratory, Richland, Washington, April 1979.

Funk, C. W. and Jacobson, L. D., 1980, Spent Fuel Integrity During Transportation, HEDL-TME 78-58, Hanford Engineering Development Laboratory, Richland, Washington, January 1980.

Garzarolli, F., Manzell, R., and Stehle, H., 1979, "KWU Fuel Performance with Emphasis on High Burnup," Proceedings of ANS Topical Meeting on LWR Fuel Performance, April 29 to May 3, 1979, American Nuclear Society, Portland, Oregon.

Gephart, R. E., Arnett, R. C., Baca, R. G., Leonhart, L. S., and Spane, F. A., Jr., 1979, Hydrologic Studies Within the Columbia Plateau, Washington: An Integration of Current Knowledge, RHO-BWI-ST-5, Rockwell Hanford Operations, Richland, Washington, October 1979.

Giachetti, G. and Sari, C., 1976, "Behavior of Molybdenum in Mixed-Oxide Fuel," Nuclear Technology, Vol. 31, p. 62.

Gore, B. F., McNair, G. W., and Heaberlin, S. W., 1980, Criticality Safety Considerations in the Geologic Disposal of Spent Nuclear Fuel Assemblies, PNL-3268, Pacific Northwest Laboratory, Richland, Washington.

Greene, E. M., 1979, Spent Fuel for Waste Storage Programs, HEDL-TC-1374, Hanford Engineering Development Laboratory, Richland, Washington.

Greene, E. M., 1980, Spent Fuel Data for Waste Storage Programs, HEDL-TME 79-20, Hanford Engineering Development Laboratory, Richland, Washington.

IRG, 1979, Report to the President by the Interagency Review Group on Nuclear Waste Management, TID-29442, U.S. Department of Energy, Washington, D.C.

Jeffrey, B. M., 1967, "Microanalysis of Inclusions in Irradiated UO₂," Journal of Nuclear Materials, Vol. 22, pp. 33-40.

Johanson, N. and Su, S., 1981, Consolidated High-Level Defense Waste (HLDW) Description, General Atomic Company, San Diego, California.

Johnson, A. B., Jr., 1977, Behavior of Spent Nuclear Fuel in Water Pool Storage, BNWL-2256, Battelle, Pacific Northwest Laboratories, Richland, Washington.

Johnson, A. B., Jr., 1979, "Spent Fuel Storage Experience," Nuclear Technology, Vol. 43, pp. 165-173.

Johnson, I. and Johnson, C. E., 1975, "Migration of Cesium and Molybdenum in Irradiated Oxide Fuels," Thermodynamics of Nuclear Materials-1974, International Atomic Energy Agency, Vienna, Austria, pp. 99-107.

Johnson, L. H., Burns, K. I., Joling, H., and Moore, C. J., 1981, The Dissolution of Irradiated UO₂ Fuel Under Hydrothermal Oxidizing Conditions, AECL-TR-128, White Shell Nuclear Research Establishment, Atomic Energy of Canada Limited, Pinawa, Manitoba, April 1981.

Katayama, Y. B., 1976, Leaching of Irradiated LWR Fuel in Deionized and Typical Groundwater, BNWL-2057, Battelle, Pacific Northwest Laboratories, Richland, Washington.

Katayama, Y. B., 1979, Spent LWR Fuel Leach Tests, PNL-2982, Pacific Northwest Laboratory, Richland, Washington.

KE/PB, 1980, Nuclear Waste Repository in Basalt, Project B-301, Functional Design Criteria, RHO-BWI-CD-38 REV 3, KE/PB, A Joint Venture of Kaiser Engineers, Inc./Parsons Brinkerhoff Quade & Douglas, Inc. for Rockwell Hanford Operations, Richland, Washington, November 1980.

Koizumi, M., Satoh, M., and Noro, K., 1974, "Phase Study on Solid Fission Products, Ba, Sr, and Zr in Oxide Fuel," Journal of Nuclear Materials, Vol. 51, pp. 90-94.

Komarneni, S., Scheetz, B. E., McCarthy, G. J., and Coons, W. E., 1980, Hydrothermal Interactions of Cesium and Strontium Phases from Spent Unreprocessed Fuel With Basalt Phases and Basalts, RHO-BWI-C-70, The Pennsylvania State University for Rockwell Hanford Operations, Richland, Washington, March 1980.

Krauskopf, K. B., 1979, Introduction to Geochemistry, McGraw-Hill, New York, New York.

Kupfer, M. J. and Palmer, R. A., 1980, Physical and Chemical Characterization of Borosilicate Glasses Containing Hanford High-Level Wastes, RHO-SA-189, Rockwell Hanford Operations, Richland, Washington.

Langmuir, D., 1978, "Uranium Solution-Mineral Equilibria at Low Temperatures with Applications to Sedimentary Ore Deposits," Geochimica et Cosmochimica Acta, Vol. 42, pp. 547-569.

Leitnaker, J. M., 1974, "Applications of Thermodynamics for Predicting and Understanding the Performance of Fast Breeder Reactor Oxide Fuels," Journal of Nuclear Materials, Vol. 51, pp. 95-105.

Lemoine, A., 1975, Contribution à L' Étude du Comportement de UO₂ en Milieu Aquex à Haute Température et Haute Pression, Ph. D. Thesis, Université de Nancy 1, Nancy, France.

Lindemer, T. B., 1977, "Measurement and Interpretation of CO and Kr + Xe in Irradiated ThO₂-Containing HTGR Fuel Particles," Journal of American Ceramics Society, Vol. 60, pp. 409-416.

Locke, D. H., 1975, "Review of Experience with Water Reactor Fuels 1968 to 1973," Nuclear Engineering and Design, 33.

Long, P. E., Apted, M. J., Spane, F. A. Jr., and Kim, K., 1982, Geologic, Geochemical, Rock Mechanics, and Hydrologic Characteristics of Candidate Repository Horizons, RHO-BW-SA-252 P, Rockwell Hanford Operations, Richland, Washington, September 1982.

Lorenz, R. A., Collins, J. L., Malinauskas, A. P., Kirkland, O. L., and Towns, R. L., 1980, Fission Product Release from Highly Irradiated LWR Fuel, NUREG/CR-0722, Oak Ridge National Laboratory, Oak Ridge, Tennessee.

Matta, R. F., Yaggee, F. L., and Neimark, L. A., 1979, "Iodine Stress-Corrosion Cracking in Irradiated Zircaloy Cladding," Proceedings of the ANS Topical Meeting on LWR Fuel Performance, April 29 to May 3, 1979, American Nuclear Society, Portland, Oregon.

McCarthy, G. J., 1977a, "High-Level Waste Ceramics: Materials Considerations, Process Simulation, and Product Characterization," Nuclear Technology, Vol. 32, pp. 92-105.

McCarthy, G. J., 1977b, Advanced Waste Forms Research and Development, Comprehensive Progress Report, C00-2510-12, The Pennsylvania State University, University Park, Pennsylvania, pp. 14-17.

McCarthy, G. J., Scheetz, B. E., Komarneni, S., Barnes, M., Smith, C. A., Lewis, J. F., and Smith, D. K., 1978a, Simulated High-Level Waste/Basalt Interaction Experiments. First Interim Progress Report, RHO-BWI-C-12, The Pennsylvania State University for Rockwell Hanford Operations, Richland, Washington, March 1978.

McCarthy, G. J., Scheetz, B. E., Komarneni, S., and Smith, D. K., 1978b, Reaction of Water with a Simulated High-Level Nuclear Waste Glass at 300°C, 300 Bars, RHO-BWI-C-35, The Pennsylvania State University for Rockwell Hanford Operations, Richland, Washington, October 20, 1978.

McElroy, J. L., 1974a, Quarterly Progress Report, Research and Development Activities, Waste Fixation Program, BNWL-1841, Battelle, Pacific Northwest Laboratories, Richland, Washington, pp. 28-29.

McElroy, J. L., 1974b, Quarterly Progress Report, Research and Development Activities, Waste Fixation Program, BNWL-1871, Battelle, Pacific Northwest Laboratories, Richland, Washington, p. 23.

McElroy, J. L., 1975, Quarterly Progress Report, Research and Development Activities, Waste Fixation Program, January through March 1975, BNWL-1908, Battelle, Pacific Northwest Laboratories, Richland, Washington, p. 34.

McElroy, J. L., 1976, Quarterly Progress Report, Research and Development Activities, Waste Fixation Program, BNWL-1994, Battelle, Pacific Northwest Laboratories, Richland, Washington, p. 2.10.

McElroy, J. L. and Burns, R. E., 1979, Nuclear Waste Management Status and Recent Accomplishments, EPRI NP-1087, Electric Power Research Institute, Palo Alto, California.

McElroy, J. L., Mendel, J. E., Bonner, W. F., and Henry, M. H., 1979, Quarterly Progress Report, Research and Development Activities, High-Level Waste Immobilization Program: January through December 1978, PNL-2999, 1, 2, 3, 4, Pacific Northwest Laboratory, Richland, Washington.

Meek, M. E. and Rider, B. F., 1974, Compilation of Fission Product Yields, Vallecitos Nuclear Center - 1974, NEDO-12154-1, General Electric Company, Pleasanton, California.

Mendel, J. E., 1978, The Storage and Disposal of Radioactive Waste as Glass in Canisters, PNL-2764, Pacific Northwest Laboratory, Richland, Washington.

Mendel, J. E., Ross, W. A., Roberts, F. P., Katayama, Y. B., Westsik, J. H., Jr., Turcotte, R. P., Wald, J. W., and Bradley, D. J., 1977, Annual Report on the Characteristics of High-Level Waste Glasses, BNWL-2252, Battelle, Pacific Northwest Laboratories, Richland, Washington.

Meyer, R. O., Beyer, C. E., and Voglewede, J. C., 1978, Fission Gas Release from Fuel at High Burnup, NUREG-0418, Rensselaer Polytechnic Institute, Troy, New York.

Miyashiro, A., 1973, Metamorphism and Metamorphic Belts, Halsted Press, John Wiley & Sons, New York, New York.

Morris, J. C. and Stumm, W. L., 1967, "Redox Equilibria and Measurement of Potentials in the Aquatic Environment," in Equilibrium Concept in Natural Water Systems: Advances in Chemistry Series No. 67, American Chemical Society, Washington, D.C.

NAE/NAS, 1979, Solidification of High-Level Radioactive Wastes, NUREG/CR-0895, National Academy of Engineering and National Academy of Sciences, Washington, D.C.

NAS, 1979, Implementation of Long-Term Environmental Standards: The Issue of Verification, Committee on Radioactive Waste Management, National Academy of Sciences, Washington, D.C.

NRC, 1981, "Nuclear Regulatory Commission, 10 CFR 60, Disposal of High-Level Radioactive Wastes in Geologic Repositories," Federal Register, Vol. 46, No. 130, July 8, 1981, Proposed Rules.

Nuclear News, 1981, World List of Reactor Power Plants, pp. 85-104, August 1981.

NWTS, 1981a, NWTS Program Criteria for Mined Geologic Disposal of Nuclear Waste, Program Objectives, Functional Requirements, and System Performance Criteria, DOE/NWTS-33(1), National Waste Terminal Storage Program, U.S. Department of Energy, Washington, D.C.

NWTS, 1981b, NWTS Program Criteria for Mined Geologic Disposal of Nuclear Waste, Waste Package Performance Criteria, DOE/NWTS-33(4), National Waste Terminal Storage Program, U.S. Department of Energy, Washington, D.C.

NWTS, 1981c, NWTS Waste Package Program Plan, Vol. 1 and 2, DOE/NWTS-96, National Waste Terminal Storage Program, U.S. Department of Energy, Washington, D.C.

O'Boyle, D. R., Brown, F. L., and Sanecki, J. E., 1969, "Solid Fission Product Behavior in Uranium-Plutonium Oxide Fuel Irradiated in a Fast Neutron Flux," Journal of Nuclear Materials, Vol. 29, pp. 27-42.

Parker, G. W., Creek, G. E., Burton, C. J., Martin, W. J., and Lorenz, R. A., 1967, Out-of-Pile Studies of Fission Product Release from Overheated Reactor Fuels at ORNL, 1955-1965, ORNL-3981, Oak Ridge National Laboratory, Oak Ridge, Tennessee.

Pusch, R., 1979, "Highly Compacted Sodium Bentonite for Isolating Rock-Deposited Radioactive Waste Products," Nuclear Technology, Vol. 45, pp. 153-157.

Rand, M. H. and Markin, T. L., 1968, "Some Thermodynamics Aspects of (U, Pu)O₂ Solid Solutions and Their Use as Nuclear Fuels," Thermodynamics of Nuclear Materials, 1967 Meeting of the International Atomic Energy Agency, Vienna, Austria, pp. 637-650.

Ringwood, A. E., 1978, Safe Disposal of High-Level Nuclear Reactor Wastes: A New Strategy, Australian National University Press, Canberra, Australia.

Robie, R. A., Hemingway, B. S., and Fisher, J. R., 1978, "Thermodynamic Properties of Minerals and Related Substances at 298.15°K and 1 Bar and at Higher Temperatures," Geological Society of America Bulletin, No. 1452.

Ross, W. A., Bradley, D. J., Bunnel, L. R., Gray, W. J., Katayama, Y. B., Mellinger, G. B., Mendel, J. E., Roberts, F. P., Turcotte, R. P., Wald, J. W., Weber, W. E., and Westsik, J. H., Jr., 1978, Annual Report on the Characterization of High-Level Waste Glasses, PNL-2625, Pacific Northwest Laboratory, Richland, Washington.

Ross, W. A. and Mendel, J. E., 1979, Annual Report on the Development and Characterization of Solidified Forms for High-Level Wastes, PNL-3060, Pacific Northwest Laboratory, Richland, Washington.

Rusin, J. M., 1980, "A Review of Glass-Ceramic Waste Forms," in Proceedings, Alternate Nuclear Waste Forms and Interactions in Geologic Media--a Workshop, May 13-15, Gatlinberg, Tennessee.

Sari, C., Walker, C. T., and Schumacher, G., 1979, "Solubility and Migration of Ba in Oxide Fuel," Journal of Nuclear Materials, Vol. 79, pp. 244-259.

Seyfried, W. E., Jr., Gordon, P. C., and Dickson, F. W., 1979, "A New Reaction Cell for Hydrothermal Solution Equipment," American Mineralogist, Vol. 64, pp. 646-649.

Slate, S. C., Ross, W. A., and Partain, W. L., 1981, Reference Commercial High-Level Waste Glass and Canister Definition, PNL-3838, Pacific Northwest Laboratory, Richland, Washington.

Smedes, H. W., 1980, Rationale for Geologic Isolation of High-Level Radioactive Wastes and Assessment of the Suitability of Crystalline Rocks, Open File Report 80-1065, U.S. Department of Interior, Washington, D.C.

Smith, M. J., Anttonen, G. J., Barney, G. S., Coons, W. E., Hodges, F. N., Johnston, R. G., Kaser, J. D., Manabe, R. M., McCarel, S. C., Moore, E. L., Noonan, A. F., O'Rourke, J. E., Schulz, W. W., Taylor, C. L., Wood, B. J., and Wood, M. I., 1980, Engineered Barrier Development for a Nuclear Waste Repository in Basalt: An Integration of Current Knowledge, RHO-BWI-ST-7, Rockwell Hanford Operations, Richland, Washington, May 1980.

Smith, R. M. and Martell, A. E., 1976, Critical Stability Constants, Vol. 4, Inorganic Complexes, Plenum Press, New York, New York.

Stobbs, J. J. and Swallow, A. J., 1962, "Effects of Radiation on Metallic Corrosion," Metallurgic Reviews, Vol. 7, No. 25.

Sutton, C. R. and Leeser, D. O., 1954, "Radiation Effects in Reactor Materials," Nucleonics, Vol. 12, No. 9.

Tulenko, J. S., Wilson, H. W., and Montgomery, M. H., 1979, "Extended Burnup-Fuel Development and Performance," in Proceedings of ANS Topical Meeting on LWR Fuel Performance, American Nuclear Society, Chicago, Illinois.

Turcotte, R. P. and Wald, J. W., 1978, Devitrification Behavior in a Zinc Borosilicate Nuclear Waste Glass, PNL-2247, Pacific Northwest Laboratory, Richland, Washington.

Turnbull, J. A. and Friskney, C. A., 1978, "The Relation Between Microstructure and the Release of Unstable Fission Products During High-Temperature Irradiation of Uranium Dioxide," Journal of Nuclear Materials, Vol. 71, p. 238.

von Jan, R. and Hoesl, S., 1979, "Load Follow Capability of LWR Fuel-KWU Experience," Proceedings of ANS Topical Meeting on LWR Fuel Performance, April 29 to May 3, 1979, American Nuclear Society, Portland, Oregon.

Wald, J. W. and Westsik, J. H., 1979, "Devitrification and Leaching Effects in HLW Glass - Comparison of Simulated and Fully Radioactive Waste Glass," in Proceedings of an International Symposium on Ceramics in Nuclear Waste Management, Chikalla, T. D. and Mendel, J. E., eds., CONF-790420, U.S. Department of Energy, Washington, D.C.

Westerman, R. E., 1980, Investigation of Metallic, Ceramic, and Polymeric Materials for Engineered Barrier Applications in Nuclear-Waste Packages, PNL-3484, Pacific Northwest Laboratory, Richland, Washington.

Westsik, J. H. and Turcotte, R. P., 1978, Hydrothermal Reactions of Nuclear Waste Solids - a Preliminary Report, PNL-2759, Pacific Northwest Laboratory, Richland, Washington.

Winkler, H. G. F., 1974, Petrogenesis of Metamorphic Rocks, Springer-Verlag, New York, New York.

Wood, B. J., 1980a, Estimation of Waste Package Performance Requirements for a Nuclear Waste Repository in Basalt, RHO-BWI-ST-10, Rockwell Hanford Operations, Richland, Washington, July 1980.

Wood, B. J., 1980b, Backfill Performance Requirements Estimates from Transport Models, RHO-BWI-SA-58, Rockwell Hanford Operations, Richland, Washington, October 1980.

Wu, C. S., 1978, Sensitization, Intergranular Attack, Stress Corrosion Cracking, and Irradiation Effects on the Corrosion of Iron-Chromium-Nickel Alloys, ORNL/TM-6311, Oak Ridge National Laboratory, Oak Ridge, Tennessee.

Zima, G. E., 1979, An Evaluation of Potential Chemical/Mechanical Degradation Processes Affecting Fuel and Structural Materials Under Long Term Water Storage, NUREG/CR-0668, PNL-2379, Pacific Northwest Laboratory, Richland, Washington, May 1979.

Zimmerman, H., 1978, "Investigations on Swelling and Fission Gas Behavior in Uranium Dioxide," Journal of Nuclear Materials, Vol. 75, p. 154.

12. PERFORMANCE ASSESSMENT

Repository performance assessment is the process of evaluating component and system behavior, relative to containment and isolation of radioactive wastes, to assure conformance with regulatory standards. The application of performance assessment in support of site selection for a repository will require predictive analyses using a formalized methodology. As shown in Chapter 2, the decision process used to identify a reference repository location at the Hanford Site was based on numerous criteria, but did not include results from a formal performance assessment. Nevertheless, a number of independent hydrologic analyses of the candidate siting area have been performed with available data and models, to provide an indication of the expected performance of a repository in basalt. The results of these analyses are supportive of the reference repository location identified.

In this chapter, the information presented focuses on four major aspects of the repository-system performance assessment:

- Identification of the major performance issues
- Description of the methodology developed for assessing repository-system performance
- Review of results of previous performance analyses for a repository in the Columbia River basalts
- Presentation of results for performance analyses conducted specifically for this document.

The scope of this chapter is limited to repository-system performance assessment related to the postclosure phase. It does not address aspects or issues of repository-system performance for the preclosure or operating phase. These aspects will be addressed upon completion of the repository conceptual design.

12.1 LONG-TERM REPOSITORY PERFORMANCE ISSUES

In general, the principal objectives of long-term repository performance assessment are to quantify the degree of waste isolation achieved by the repository system (i.e., engineered systems and geologic medium). A basic set of performance measures will be used to quantify system performance; they consist of: (1) groundwater flow paths and travel times from the repository to the accessible environment, (2) rate of radionuclide release from the repository, and (3) total activity (of individual radionuclides) leaving the boundaries of a specified control or buffer zone around the repository. The long-term repository performance issues center on these measures with specific regard to the numerical limits required for compliance with the proposed technical criteria (NWTS, 1981; NRC, 1981) and the regulations for deep geologic repositories that will eventually be developed by the U.S. Environmental Protection Agency (EPA).

12.1.1 Groundwater Flow Paths and Travel Times

It is generally recognized that the most probable mode by which radionuclides could be released from a repository facility is through the groundwater system. Thus, the first and perhaps most fundamental objective of the long-term repository performance assessment is to determine the potential flow paths from the proposed repository and to estimate the travel times along these paths to the accessible environment.

Hydrologic conditions considered favorable for waste isolation are long flow paths to the accessible environment, which are confined to the deep formations, and travel times ranging from several thousands to hundreds of thousands of years. A minimum groundwater transit time of 1,000 years to the accessible environment is the current technical criterion proposed by the U.S. Nuclear Regulatory Commission (NRC). With these aspects in mind, the first performance issue simply stated is:

Are the pre-waste-emplacement groundwater travel times near the repository sufficient to assure compliance with U.S. Nuclear Regulatory Commission technical criteria?

Resolution of this issue will be achieved using predictive models that are specifically applicable to the hydrologic system of the Columbia River Basalt Group beneath the Hanford Site. Bounding estimates for the flow paths and travel times will be obtained by using a systematic and conservative long-term performance-assessment approach that considers the anticipated geologic conditions and postulated disruptive conditions (Arnett et al., 1980).

12.1.2 Repository Release Rates

Although many factors determine the degree of long-term waste isolation achieved by the repository system, the basic factors are (1) the containment period provided by the engineered system, including the waste package and the underground facility and (2) the rate of radionuclide release from the emplacement horizon. The initial containment period (i.e., time period during which the nuclear wastes are confined to the engineered system) following repository closure is important because it mitigates any processes or events induced by the repository environment that adversely affect long-term waste isolation. After the containment period, it is assumed that any potential release will be controlled by the engineered barriers in the underground facility and the primary geologic barrier (i.e., emplacement horizon). Technical criteria proposed by the NRC require a minimum containment period of 1,000 years and a maximum annual release rate of 1 part in 100,000 for any radionuclide from the engineered system, assuming anticipated processes and events.

The long-term radionuclide release rate will be affected by the hydrologic and geochemical characteristics of the emplacement horizon; however, the period of containment depends on the engineered barriers and waste package designs. The next performance issue may be expressed in general terms as:

Does the very near-field interaction between the waste package and its components, the underground facility, and the geologic setting compromise waste package or engineered system performance? (i.e., What is the maximum expected release rate from the engineered system?)

To address this issue, predictive models for radionuclide transport, which take into account waste package degradation, waste form leaching, groundwater flow, and thermal conditions in the fractured-porous rock, will be applied to estimate the release rates and mass fluxes for a set of key radionuclides (Barney and Wood, 1980). Predictions of these quantities and their variations over the waste isolation period will be obtained for both expected natural and postulated geologic conditions.

12.1.3 Releases to the Accessible Environment

To set numerical limits on the quantity of radionuclides potentially released to the biosphere, the NRC has proposed a 10-kilometer control zone for the repository site (NRC, 1982). Beyond this 10-kilometer boundary, the groundwater system is considered part of the accessible environment. This proposed definition establishes a site-specific boundary across which controlled releases (i.e., limited by the geologic barriers) shall be quantified and compared to numerical limits to be set by the EPA.

The regulations under consideration by the EPA would limit the total quantity of radionuclides released over a 10,000-year period. It follows, then, that the third performance issue is:

What is the total amount (activity) of radionuclides potentially releasable to the accessible environment in a 10,000-year period, and is this amount in compliance with appropriate U.S. Environmental Protection Agency regulations?

Since the amount of radionuclides leaving the designated buffer zone will depend on the repository release rates, groundwater flow paths, and travel times, the resolution of this important issue hinges on the degree to which the first two issues are resolved.

As indicated in the latest available EPA draft regulations (EPA, 1981), a satisfactory resolution of this issue will require a comprehensive long-term risk assessment that: (1) identifies the plausible release modes, (2) estimates the probabilities of each release mode, and (3) conservatively bounds the consequences of releases. As part of the planned performance assessment, a large number of hydrologic simulations, considering a broad range of conditions, will be carried out to provide sufficient assurance that the model predictions compensate for uncertainties and thereby give a reasonable expectation of compliance with the EPA draft regulations (EPA, 1981).

12.1.4 Related Issues

While the three aforementioned long-term performance issues are relatively clear, straightforward, and definitive, their resolution is strongly tied to many work elements that, in themselves, may constitute important performance assessment subissues and are discussed in Chapters 13 and 16. Many of these work elements are related to the fact that proof of compliance with the technical criteria and regulations depends on the reliability of numerical models to predict system performance.

In addition, Basalt Waste Isolation Project (BWIP) studies will also evaluate repository performance during the operating time frame of a repository, to assure safe operations and compliance with criteria under normal and abnormal conditions. These operating performance studies will serve to refine the repository design and will input to the license application.

12.2 APPROACH TO LONG-TERM REPOSITORY PERFORMANCE ANALYSIS

A long-term performance analysis of a nuclear waste repository is a systematic evaluation process that quantifies how well the system achieves its basic design objective, which is the long-term isolation of the nuclear waste from the accessible environment. Principal applications of such long-term performance analysis are twofold: to assist in the design of the engineered facility so that compliance with technical criteria is assured and to predict the long-term behavior of the repository system under anticipated and postulated geologic conditions. In this section, the basic elements of the BWIP long-term performance analysis approach are discussed.

12.2.1 Long-Term Repository Performance Analysis Framework

To evaluate the long-term performance of a repository system, a specific time frame that represents the critical period of waste isolation must be adopted. Beyond this time period, it is presumed that the radiologic risk of the nuclear waste is at an acceptable level because of the reduction of toxicity by decay and/or dilution. A period of 10,000 years is currently considered a reasonable time frame for evaluation of post-closure performance by the federal regulatory agencies (EPA, 1981; NRC, 1981). Primary focus of the performance analysis is thus placed on the first 10,000 years after closure. Longer time frames may be considered, however, for selected cases.

The major stages of the long-term performance analysis approach consist of:

- Identification and specification of plausible release modes for anticipated and postulated geologic conditions
- Prediction of release consequences using numerical models for hydrologic, thermomechanical, and transport processes.

These stages should lead to a clear quantification of expected compliance with the numerical limits set in technical criteria and federal regulations.

In the first stage of long-term repository performance analysis, the objective is to identify the geotechnical factors and physical processes that have the most significant impact on containment and degree of isolation. Moreover, a quantitative understanding of the cause-and-effect relationships is developed between the potential release initiating events/processes and the rate of release. With this information, the consequences of radionuclide release and movement through the groundwater can be predicted to quantify long-term performance of the repository system. Because of the inherent uncertainties in such predictions, a

conservative consequence analysis is required that is based on the use of both deterministic and probabilistic models. These consequence analyses should provide the information needed to quantify the likelihood of compliance with applicable criteria and regulations. Applying this approach to the set of release scenarios quantifies the radiologic risk of the repository system.

12.2.1.1 Repository Release Modes. Several generic lists have been constructed of possible release inducing phenomena that may have application to basalts (Lee et al., 1978; Stottlemire et al., 1981). These lists include a wide variety of failure modes and disruptive events and establish a comprehensive information base from which relevant and site-specific release scenarios can be selected. These generic phenomena can be divided into the following categories:

- Natural phenomena or processes
- Man-induced phenomena
- Repository-induced effects.

The basic approach of the BWIP in release scenario analysis is discussed in Arnett et al. (1980). The starting list of generic release-inducing phenomena is presented in Table 12-1.

A brief examination of Table 12-1 indicates a wide diversity in the type and nature of the release-inducing phenomena. They vary from celestial events, such as meteorite impact, to undetected natural features and from weapons testing to resource development. In developing the initial scenario list, only a limited attempt was made to consider the specifics of either the host medium (basalt) or the particular setting of a potential repository system as they might influence any given scenario. Thus, it is a rather general list, which can be reduced by considering site-specific information.

Site-specific release scenarios are generally selected by means of an objective and consistent methodology that is documented in a step-by-step fashion. As a first step, it is advantageous to eliminate certain release-inducing phenomena by considering the credibility or plausibility of individual scenarios in a basalt setting. Selection of the most meaningful scenarios from those remaining is influenced by perceived as well as real risk. Also, certain cases can be justified on the basis of the bounding conditions they represent. The basic selection criteria used consider the following aspects:

- Credibility of the event or process
- Probability of a significant release
- Consistency with site-specific data and knowledge.

TABLE 12-1. Potential Release Inducing Phenomena.

Natural Phenomena	
Celestial bodies Meteorites Asteroids Comets Surface phenomena Hurricanes Landslides Seiches Tornados Tsunamis Water erosion Weathering Sea-level changes Glacial erosion Flooding Earth tides Glaciation Climatic changes Water pathways Aquifers Other water-bearing zones	Tectonic processes Orogenic faulting Epeirogenic deformation Fracturing Surficial fissuring Impact fracturing Hydraulic fracturing Microearthquake-induced fracturing Magmatic activity Extrusive Intrusive Undetected features Faults Lava tubes Gas pockets Shear zones
Man-Induced Phenomena	
Inadvertent future intrusion Archaeological exhumation Weapons testing Resource recovery (drilling) Waste disposal Undetected past intrusion Boreholes Mine shafts	Hydrologic perturbations Irrigation Reservoirs Artificial recharge New groundwater withdrawals Improper design/operation Shaft seal failure Improper waste emplacement
Repository-Induced Effects	
Mining-related fracturing Thermally induced groundwater buoyancy	Thermally induced rock stress/fracturing

It is apparent that the most credible release scenarios should be considered first and the least credible scenarios last.

The list presented in Table 12-1 can be considerably reduced by considering the nature and extent of the effects. For example, most of the surface phenomena listed are generally recognized as having no significant effect on a repository located several hundred meters below land surface. Only glaciation and climatic changes might influence a deep repository in basalt by affecting the hydrologic regime; these events, however, possess very small likelihoods of occurrence within a 10,000-year time frame.

A preliminary list has been compiled of disruptive event scenarios that warrant further consideration for a repository in basalt (Arnett et al., 1980). The list consists of the following scenarios, ranked in order of decreasing significance:

- Interconnecting fault
- Shaft seal degradation or failure
- Borehole intrusion
- Fracturing due to microearthquake swarm
- Magmatic dike or sill intrusion.

While the above list is considered useful, it is not complete. Further work to identify other significant scenarios is under way. A technical evaluation (Arnett et al., 1980) of each of these scenarios, except borehole intrusion, indicated the following:

- (1) An interconnecting fault, depending on its hydrologic properties, could impact waste isolation; therefore, a consequence analysis should be included in the performance assessment.
- (2) Shaft seal degradation, like the fault, could create a short hydraulic pathway, and thus a consequence analysis is needed.
- (3) Fracturing due to a microearthquake swarm appears to have a very marginal significance even under worst case conditions; however, a consequence analysis would be useful for confirmation.
- (4) A significant magmatic dike or sill intrusion is not a plausible scenario for the Pasco Basin because it is inconsistent with the nature of the existing geologic conditions.

A technical evaluation of the borehole intrusion scenario is planned. It appears to be a subset of the shaft seal failure scenario.

12.2.1.2 Consequence Analysis Approach. A long-term performance analysis of a repository site requires the evaluation of the consequences of potential releases. The problem centers on predicting repository system performance over large-space scales and very long time frames (i.e., tens of

kilometers and 10,000 years). The nature of the space and time scales virtually precludes the use of physical models or field experiments to predict the long-term performance of the repository system (underground facility and geologic medium). Mathematical models based on the principles of physics provide an efficient and versatile way to predict the long-term changes of the physical system. From such simulations, long-term performance measures are compared with the criteria proposed by the regulatory agencies.

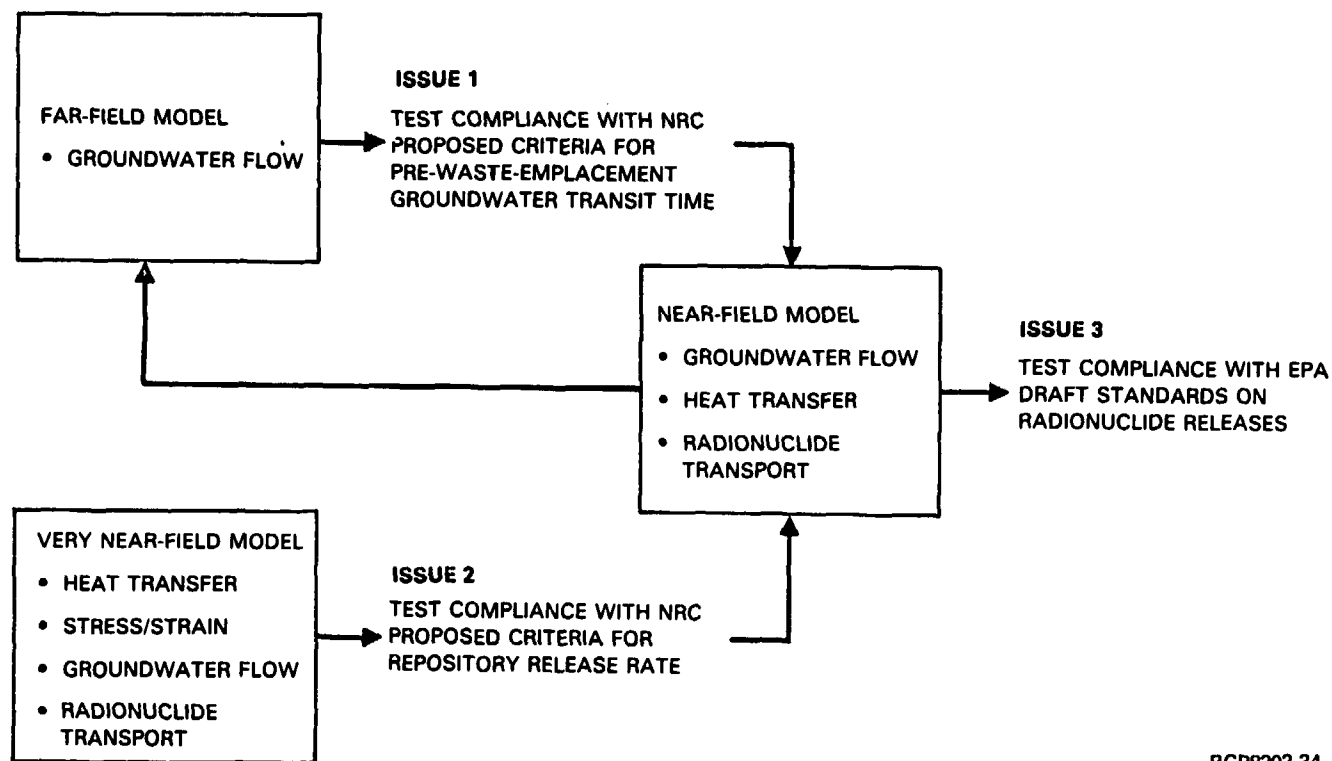
Because of the complexity of the processes, the overall long-term performance analysis problem must be broken down to one of analyzing the hydrologic processes in three subregions. These are very near field (canister to room scale), near field (repository scale), and far field (basin-wide scale). By this approach, mathematical models for each subregion can be developed that realistically portray the dominant physical processes, while accounting for less important processes in an approximate manner.

The consequence analysis approach that will be used to address the long-term performance analysis issues is presented in Figure 12-1. The individual modeling approaches are designed to analyze the set of processes relevant to specific performance analysis issues. The very near-field and far-field models provide information needed for the near-field model, such as boundary conditions and source terms, whereas the near-field model provides flow path starting locations for the far-field model. More detailed descriptions of the modeling approaches are presented in the next section.

Recognizing that the future decisions regarding the repository site will place much reliance on model predictions, consideration of uncertain elements in the consequence analysis is of fundamental and key importance. For the most part, the uncertainty in model predictions can be attributed to four major sources:

- Limitations in the mathematical models, including the computer codes that describe hydrologic and transport processes
- Random and systematic errors in field measurements of hydrologic properties
- Errors arising from subjective interpretations of the spatial variations of hydrologic parameters from discrete data points
- Incompleteness of geohydrologic characterization.

The first source, which may be termed model uncertainty, can be addressed by code benchmarking and verification and by comparing model simulations with experimental data; these results, in turn, can be analyzed to determine the degree of correlation between measurement and calculation (i.e., model validation (Shannon, 1975)). The other three sources, which represent data uncertainty, can be evaluated using a number of approaches. Various statistical techniques (McLaughlin, 1979) are



RCP8202-34

FIGURE 12-1. Relationship Between Individual Models and Outstanding Long-Term Performance-Assessment Issues.

available that estimate the impact of uncertain elements, given a probabilistic description of the model input (i.e., a probability density function for each hydrologic parameter). The last two elements can also be grouped into a descriptive uncertainty category, which is perhaps the most difficult to analyze in a rigorous fashion. Kriging techniques (Delhomme, 1976; Doctor, 1979), used in combination with a systematic scenario analysis, will provide a pragmatic approach to developing continuous representations of hydrologic data with uncertainty bounds and evaluating hydrologic significance of possible undetected geologic features.

The large quantity of measured data required for a rigorous uncertainty analysis appears to be a major obstacle in applying this technique to diverse geohydrologic systems. This indication is further reinforced by the simple fact that characterization of a candidate site may be limited to assure that natural barriers are not disturbed or compromised. An alternate approach to the problem of addressing predictive uncertainty is to adopt a systematic and conservative methodology that compensates for uncertain elements in the consequence analysis without assuming conditions that are not credible. Such a methodology should provide a framework for guiding the system simulations so that bounding estimates of radionuclide migration are obtained.

A methodology based on these concepts is currently being used in the BWIP long-term performance analysis. The principal components of this analysis approach include:

- Simulation models for coupled heat, groundwater flow, and radionuclide transport in fractured-porous media
- Parametric and sensitivity analysis of postulated release scenarios
- Decision- or logic-tree strategy to guide parametric studies.

The decision-tree approach (Raiffa, 1968) involves the development of a sequence network that gives a pictorial representation of parameter variations. When a decision tree is properly constructed, the sequence of parametric studies bounds the results of the consequence analysis, which can then be compared to long-term performance criteria.

12.3 PREDICTIVE MODELS

Four major processes and their interplay generally determine the degree of waste isolation achieved by the repository system. These processes are rock stress/strain, heat transfer, groundwater flow, and solute transport. The relationships between them are illustrated in Figure 12-2. As indicated in the figure, the state of the repository system is characterized in terms of four basic state variables: (1) stress, σ_{ij} , and strain, ϵ_{ij} ; (2) temperature, T ; (3) hydraulic head, h (flow rate, q_i , and buoyancy, δ_b); and (4) radionuclide concentrations, C_i .

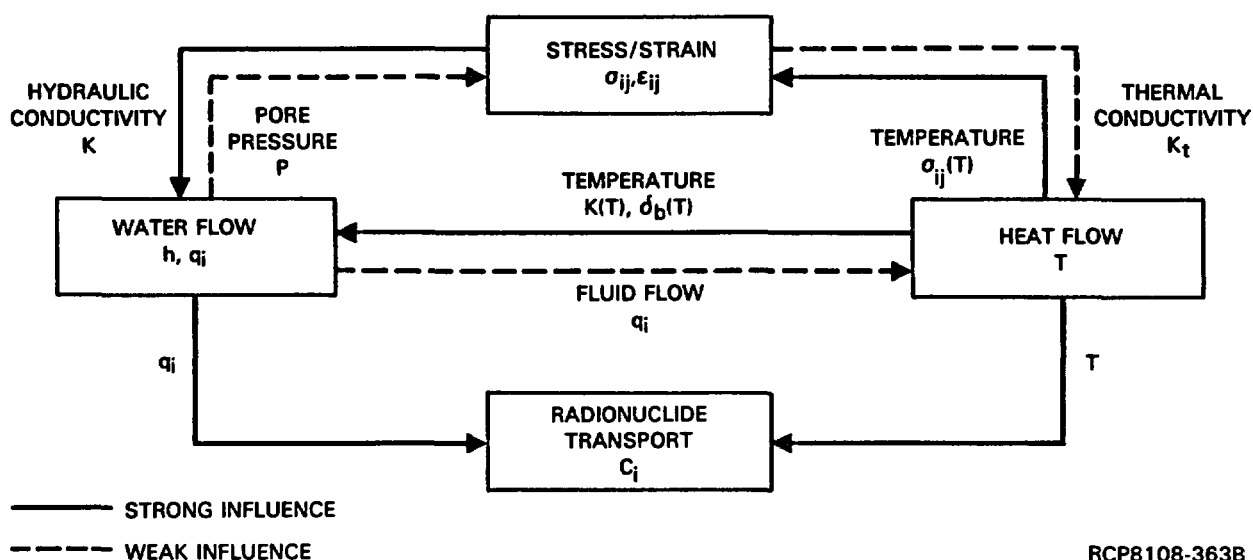


FIGURE 12-2. Relationship of Important Processes Occurring in the Vicinity of a Repository.

A set of mathematical models have been formulated for use in detailed performance analyses of a repository in basalt at the three space scales. This section outlines the theoretical framework of the mathematical models, describes the specific numerical models that have been developed, and outlines the capabilities and limitations of the models.

12.3.1 Mathematical Models

Mathematical models of the important hydrologic processes have been developed from the basic principles of mass and energy conservation and are presented herein.

12.3.1.1 Stress/Strain Model. The mechanical behavior of the rock strata in the vicinity of the repository will change over the postclosure period, primarily in response to heat transfer from the waste form. These thermal stresses in the rock will generally have an effect on the hydraulic properties (e.g., fracture permeabilities and porosities) (Iwai, 1976), because of small-scale rock displacements.

The mathematical models of rock stress and strain are formulated on the basis of Newton's second law (Malvern, 1969) and Hooke's law (Timoshenko and Goodier, 1970). The actual governing equations may be found in Hardy et al. (1978) and Baca et al. (1980). The applicability of these mathematical models to basalt rock is based on the following assumptions:

- The jointed rock behaves mechanically as a continuous medium.
- The thermal properties of the rock mass (e.g., thermal expansion coefficient, thermal conductivity, and specific heat) are homogeneous and isotropic.
- The constitutive relations (stress/strain relations) are linear.

With regard to the last assumption, some recently developed stress/strain models can accommodate nonlinear behavior. However, the usefulness of such detailed models to performance analysis studies, in general, may be limited by the availability of required data.

It is expected that the principal application of the stress/strain models will be to examine the repository performance at the canister to room scale (i.e., very near field). Example applications of the available stress/strain models may be found in Hardy and Hocking (1978a; 1978b).

12.3.1.2 Groundwater Flow Model. Groundwater flow in a nonisothermal regime is dependent on the temperature of the water-rock system. This coupling is particularly important in the near-field zone because variations in fluid density and hydraulic conductivity occur with temperature changes. Dependence of these properties on the thermal regime is made clear by considering the nonisothermal form of Darcy's law (Bear, 1972).

By combining Darcy's law and the equation for fluid continuity, one obtains the governing equation for groundwater flow in a changing thermal environment. The specific governing equations may be found in Baca and Arnett (1981) and Baca et al. (1980). Over the temperature range expected in the vicinity of the repository, the fluid density changes by only a few percent; however, the fluid viscosity decreases by 20 to 30 times. Consequently, the hydraulic conductivity can change by a significant amount.

This particular formulation is based on the following set of basic assumptions:

- (1) The fluid and rock together form a continuous system (i.e., an equivalent porous continuum), see Bear (1972).

- (2) The groundwater flow regime is laminar and gradually varying (Freeze and Cherry, 1979; Bear, 1972).
- (3) The fluid density variations are important only as they induce buoyancy effects (i.e., Boussinesq approximation, see Cheng (1978)).
- (4) The smallest spatial unit of analysis (i.e., representative elementary volume) is of such size that it possesses uniform hydraulic properties (Bear, 1972).

While the first three assumptions are well justified, the validity of the last assumption is limited to the near-field and far-field scales, where the representative elementary volume is relatively large. At the very near-field scale, however, the groundwater flow is determined by the "discrete" properties of the fractures and not by the "average" properties of the rock mass. For this more complex case, mathematical models have been developed and may be found in Baca et al. (1981b).

The issue of deciding which type of groundwater flow model (continuous or discrete) applies to a particular space scale can be resolved on the basis of the so-called "scale effect" criterion (Snow, 1965; Maini, 1971; Roegiers et al., 1979). In essence, this criterion provides a means of estimating the representative rock-mass size at which flow through discrete fractures can be represented by an equivalent continuum (i.e., Darcian flow) model. Typically, if the smallest characteristic rock size is 50 times (or more) greater than the fracture spacing, then the rock volume will generally have a high enough fracture density so as to behave like a porous continuum. A more rigorous criterion is currently being developed by Witherspoon et al. (1981).

12.3.1.3 Heat Transport Model. Transfer of thermal energy from the repository to the surrounding geohydrologic system will occur by advection and dispersion in the groundwater and by simple conduction through the rock mass. To describe these heat transport processes, the first law of thermodynamics (Malvern, 1969) is invoked and used with Fourier's law of conduction (Holman, 1980) to formulate the general mathematical model. The governing equation for heat transport in the water-rock system may be found in Baca et al. (1981a; 1981b).

Basic assumptions made in this mathematical formulation are as follows:

- The temperature of the fluid and rock mass is the same at any point; i.e., thermal equilibrium exists between fluid and solid phases (Cheng, 1978).
- The thermal properties of the rock mass are isotropic.

- The hydrothermal regime is single phase.
- The heat generation rate in the repository is a known function of time.

These assumptions are well justified and apply to postclosure performance at all space scales.

In the case of a relatively low-porosity rock, such as basalt, the principal mode of heat transport is by conduction through the rock mass. This fact may be confirmed by examining the Peclet number (Ozisik, 1977; Combarrous and Bories, 1975) characteristic of repository conditions.

12.3.1.4 Radionuclide Transport Model. Movement of radionuclides in groundwater is determined by the combined effects of various processes. To predict the rate and direction of potential radionuclide migration from the repository, the radionuclide transport model must describe the processes of advection, dispersion/diffusion, sorption, radioactive decay, and mass release. A mathematical model can be formulated from the principle of mass conservation (Malvern, 1969) and Fick's law (Bird et al., 1960) for mass diffusion. The system of governing equations describing multicomponent radionuclide transport may be found in Gephart et al. (1979) and King et al. (1981).

Applicability of the mathematical model is constrained by certain basic assumptions:

- Radionuclide (and groundwater) movement occurs slowly relative to the rate of chemical interaction (i.e., sorption).
- Sorption of the dissolved radionuclide is described by a linear isotherm.
- Transport properties are independent of fluid temperature.
- Hydrodynamic dispersion is described by a Fickian-type law.
- The smallest spatial unit of analysis is of such a size that it possesses average transport properties.

It is important to point out that the formulation of the transport model is generalized so as to apply to all types of radionuclides (activation and fission products) and to actinide elements that possess decay-chain couplings. In addition, the last assumption restricts the applicability of the formulation to near-field and far-field scales.

A more complex mathematical model has been developed for the very near-field scale. This model describes transport of any radionuclide in fractured-porous media. The model considers transport through both continuum and discontinuum portions of the rock mass. The governing equations for this very near-field transport model may be found in Baca et al. (1981a).

12.3.2 Numerical Models

A numerical model or computer code represents the implementation of the mathematical model in the form of a computational algorithm that is generalized to use an arbitrary set of data to compute the changes in a set of state variables. The major computer codes developed for performance analysis of a repository in basalt are described herein. The computer codes are grouped into very near-field, near-field, and far-field categories.

A large suite of computer codes have been developed and/or applied as part of the BWIP studies. These computer codes span the areas of waste package/engineered barrier design, rock mechanics, and hydrology. The primary computer codes currently being adapted to long-term repository performance analysis are listed in Table 12-2.

12.3.2.1 Very Near-Field Models.

12.3.2.1.1 BETA. The BETA finite-element code is a modified version of a code developed by the University of Minnesota. The BETA code is designed to simulate the thermomechanical response of a continuous rock mass in two dimensions (i.e., cartesian- or cylindrical-coordinate systems). Stresses and strains in the rock mass surrounding the repository are computed as functions of stress boundary conditions, gravity loads, and transient thermal conditions. Heat transport through the rock mass is assumed to occur by conduction only; advection of the groundwater and convective boundary conditions are not considered.

The specific governing equations, which may be found in most stress-analysis (Timoshenko and Goodier, 1970) and finite-element texts (Cook, 1981), deal with linear elastic behavior. Some of the basic features of the BETA code are:

- The continuous rock mass is represented by quadrilateral isoparametric elements.
- The model formulation accommodates plane stress and plane strain analysis.
- The computer code provides an option for isothermal stress, coupled stress, and temperature calculations.
- The transient heat transfer calculations accommodate arbitrary heat source loading.
- The computer code is easy and inexpensive to use.

A draft user's guide and manual has been prepared.

TABLE 12-2. Summary of Codes for Repository Performance Analysis.

Computer code	Approach		Stress/strain		Ground-water flow		Heat		Radionuclide transport			Computational method			
	CO	DC	LI	NL	IS	NI	AD	DS	S	MC	DE	FE	FD	AL	DI
Very Near Field															
BETA	X		X		X	X		X				X			2
DAMSWEL	X		X	X	X	X		X				X			2
ANSYS	X	X	X	X	X	X		X				X			3
HEATING5	X					X		X					X		3
MAGNUM 2D	X	X			X	X	X	X				X			2
CHAINT	X	X							X	X	X	X			2
BARRIER ^a	X					X			X				X		1
WAPPA ^a	X					X			X				X		1
Near Field															
PORFLO	X				X	X	X	X	X				X		2
PATH ^b	X	X			X	X	X	X				X			2
MAGNUM 2D	X	X			X	X	X	X				X			2
CHAINT	X	X							X	X	X	X			2
SWIFT	X				X	X	X	X	X	X	X		X		3
Far Field															
MAGNUM 3D	X				X							X			3
PATH 3D ^b	X				X							X			3
FECTRA	X								X			X			3
SWIFT	X				X	X	X	X	X	X	X		X		3
FE3DGW	X				X							X			3
WOOD/SALTER	X				X				X	X				X	1
NUTRAN	X								X	X				X	1
AD-Advection		DE-Decay Chains				FE-Finite Element				NI-Nonisothermal					
AL-Analytical		DI-Dimensionality				IS-Isothermal				NL-Nonlinear Properties					
CO-Continuum		DS-Diffusion				LI-Linear Properties				S-Single Component					
DC-Discontinuum		FD-Finite Difference				MC-Multicomponent									

^aCodes currently under development.

^bComputes pathlines, streamlines, and travel times.

12.3.2.1.2 DAMSWEL. The DAMSWEL computer model was developed by the Advanced Technology Group of Dames & Moore for thermomechanical analysis. Similar in application to the BETA code, DAMSWEL is a two-dimensional finite-element code. DAMSWEL, however, has the following major differences and advantages:

- The model formulation accommodates linear and nonlinear rock properties.
- The computer code calculates rock temperatures by solving the nonlinear heat equation.
- The computational algorithms used in the code are more advanced and sophisticated than those in the BETA code.
- The code has been verified using problems with known analytical solutions.

A technical report prepared for the DAMSWEL code includes sample input and output for various test cases (Boonlualohr et al., 1980).

12.3.2.1.3 ANSYS. The ANSYS computer code is a generalized stress-analysis code widely used in the nuclear industry. This proprietary computer code, developed by Swanson Analysis Systems, has a broad capability to analyze the thermomechanical response of the basalt rock. Some of the special capabilities of this computer code are:

- The model formulation is generalized to simulate coupled heat and stress transients.
- The model may be used to analyze stresses and strains in two or three dimensions.
- The model can consider linear and nonlinear rock properties.
- The code accommodates a continuous rock mass. Jointing may be modeled by means of gap elements.

The ANSYS computer code is very well documented with regard to theoretical basis, input instructions, and model use (DeSalvo, 1976; Kohnke, 1977; DeSalvo and Swanson, 1981).

12.3.2.1.4 HEATING5. This code is designed to solve steady-state and/or transient heat conduction in one, two, or three dimensions using one of several finite-difference techniques. The principal application of HEATING5 in performance analysis studies has been to model the thermal environment of the waste package. The discussion of the governing equations, input and output description, and model use may be found in the report by Turner et al. (1977). Some of the general features and capabilities of this code are:

- The formulation is generalized to accommodate cartesian-, cylindrical-, or spherical-coordinate systems.

- The code accommodates temperature-dependent thermal properties.
- The code can handle a wide variety of boundary conditions.

This code has been applied to Near-Surface Test Facility and waste package studies. Verification and benchmarking are planned.

12.3.2.1.5 MAGNUM 2D. The MAGNUM 2D code is a two-dimensional (2D) finite-element code designed to simulate transient groundwater flow and heat transport in fractured-porous rock systems. The theoretical framework of the model is based on concepts for a porous continuum and for discrete conduits. In particular, a dual-porosity approach is used to represent the continuous rock mass, where flow through planar conduits is described by Poiseuille's equation. The governing equations and finite-element solution techniques are presented by Baca et al. (1981b). The principal features of the MAGNUM 2D code are as follows:

- Continuous rock mass is represented with isoparametric finite elements; line elements are embedded along the sides of two-dimensional elements to represent discrete fractures.
- Model accommodates complex stratigraphic features with variable media properties.
- Computer code provides options for coupled or uncoupled solutions of heat and flow equations.
- Flow-field calculations are provided for input to pathline and transport models.

Formal documentation on the MAGNUM 2D code will include a discussion of model theory, numerical techniques, verification, and validation test cases. This code is interfaced with the codes PATH and CHAINT.

12.3.2.1.6 CHAINT. The CHAINT code simulates multicomponent radionuclide transport in a fractured-porous medium. The processes modeled include advection, dispersion/diffusion, sorption, chain-decay coupling, and mass release. The computational method is based on a finite-element solution of the system of equations. Continuum portions of the medium are modeled as a single-porosity system, using two-dimensional isoparametric elements. Discrete features are modeled using isoparametric line elements that are embedded along the sides of the two-dimensional elements. Principal input to this code is the groundwater flow calculations obtained with the MAGNUM 2D code (or a comparable nonisothermal flow model). The CHAINT code has the following major features:

- Model formulation is generalized to handle any combination of nuclides (actinides, fission, or activation products) with contrasting half-lives.

- Computational algorithm accommodates subzone calculations in which the region of active nodes, within the finite-element mesh, is varied with time as the problem progresses.
- Numerical algorithms are second-order accurate and fully implicit.

The CHAINT code has been verified with boundary value problems and successfully compared with the PORFLO code. Additional work is proceeding to reduce computational times and to compare the model predictions with experimental data.

12.3.2.1.7 BARRIER. This code is specifically designed for use in performance analyses of the engineered barriers around a canister. The BARRIER code takes into account material properties, geometry, corrosion, thermal expansion, internal pressure, creep strain, compaction, and temperature variations. This code, in conjunction with waste form codes, will provide a basis for estimating waste package release rates. Some of the advantages of the BARRIER code are:

- The formulation considers various processes that determine waste package performance.
- The code is relatively simple and inexpensive to use.

This code, developed for the Office of Nuclear Waste Isolation (Lester et al., 1979), is currently being evaluated for use by the BWIP.

12.3.2.1.8 WAPPA. The WAPPA code, currently under development for the Office of Nuclear Waste Isolation, is a generalized waste package performance model. The WAPPA code is an extended version of BARRIER, with greater capabilities to describe the corrosion process, radiation effects, thermomechanical response of the canister, and leaching of the waste form. Some assumptions of the model are:

- The repository temperature is constant.
- The repository is completely resaturated.
- The initial radionuclide concentration in water outside of the waste package is zero. (This implies a large volume of water and/or high near-field water turnover rate.)
- The corrosion rates are dependent on temperature ranges and radiation level (i.e., linear corrosion).
- The stress field around the package is uniform.
- The backfill is intact at all times.

Although the WAPPA code will provide a very general predictive capability, some modifications will be necessary to tailor the code to basalt conditions. For example, modifications to the code may include: (1) capability to handle temperature history at the waste package-basalt interface, (2) consideration of desaturation/resaturation phenomena, (3) laboratory bulk corrosion data, and (4) solubility limitation of waste form dissolution.

12.3.2.2 Near-Field Models.

12.3.2.2.1 PORFLO. PORFLO is a finite-difference code with options for modeling the coupled processes of groundwater flow, heat transfer, and radionuclide transport. The model is applicable to porous media or highly jointed rock systems that may be represented as an equivalent porous continuum. The finite-difference method is based on a nodal point integration technique used in conjunction with an alternating direction implicit method. Additional description of this model is contained in Baca et al. (1981a). Major features of the PORFLO computer code are as follows:

- The computer code is easy and inexpensive to use.
- The numerical method ensures energy and mass conservation at the grid-block level (Patankar, 1980).
- A donor-cell method is used to accommodate advection-dominated flow regimes (Runchal, 1972).
- The computer code computes the total activity crossing specified boundaries for the simulation period.

12.3.2.2.2 PATH. Using the numerical results from a two-dimensional groundwater model, the PATH code computes the pathlines or streamlines for an arbitrary set of starting points in the study region. In addition to computing the particle trajectories, the model computes the cumulative time of travel along each trajectory (i.e., travel times). The program solves the pathline equations on a finite-element grid network, thereby tracing the particle trajectory from element to element. Major features of the PATH code are as follows:

- The pathline equations are solved using a predictor-corrector algorithm and finite-element shape functions.
- The computational algorithm accommodates two-dimensional isoparametric elements with one-dimensional line elements.
- The computer output is in graphic form with options provided for superimposing the finite-element mesh, rock-type boundaries, etc., as well as generating plots for subzone grids.

The PATH computer code is designed for interactive use on a standard graphics terminal. Versions of this program are currently interfaced with the MAGNUM 2D and PORFLO computer codes.

Some very near-field and far-field category codes, such as MAGNUM 2D, CHAINT, and SWIFT, may also be useful in the near field.

12.3.2.3 Far-Field Models.

12.3.2.3.1 MAGNUM 3D. A code has been developed to solve the three-dimensional (3D) form of the groundwater flow equation, using the same fundamental numerical procedures as the MAGNUM 2D code. The MAGNUM 3D code is limited to isothermal conditions; future versions may consider three-dimensional nonisothermal effects as needed. The model is based on the continuum theory of porous media and is designed for analysis of flow patterns in large-scale groundwater basins. Some of the important features of MAGNUM 3D are:

- The code accommodates complex three-dimensional geometry through the use of various three-dimensional isoparametric finite elements (e.g., tetrahedrons and parallelepipeds).
- The code can consider different types of boundary conditions (e.g., specified heads and/or fluxes).
- The code provides a three-dimensional flow field for input to pathline and transport codes.

Formal documentation for MAGNUM 3D is in preparation. The code has been successfully compared with other codes and known analytic solutions.

12.3.2.3.2 PATH 3D. The PATH 3D code is similar to PATH except that it calculates three-dimensional pathlines or streamlines. It is interfaced with the MAGNUM 3D code.

12.3.2.3.3 FECTRA. The FECTRA code analyzes radionuclide transport in porous media. This transport model is based on the dual-porosity approach that considers the interaction of radionuclides in the mobile and immobile phases. The mobile component is the dissolved radionuclide moving through the primary pores, whereas the immobile phase is contained in the secondary or dead-end pores (Coats and Smith, 1964). The theoretical framework considers the basic processes of advection, dispersion/diffusion, sorption, decay, and mass release of a single species. The computer code was originally developed for application to the partially saturated flow regime. Basic features of FECTRA are:

- Two versions are available (two-dimensional and three-dimensional), using various isoparametric finite elements.
- Numerical techniques are second-order accurate and fully implicit.
- The code has been successfully compared to other transport codes and verified with analytic solutions.

The FECTRA code is designed to be interfaced with a three-dimensional fluid-flow model such as MAGNUM 3D. It is being considered for simulation of the natural groundwater hydrochemical stratification (see Chapter 5), as well as for far-field radionuclide transport.

12.3.2.3.4 SWIFT. This computer code is one of the more general simulation codes for repository performance analysis. The SWIFT code is capable of simulating the coupled processes of heat transport, groundwater flow, and radionuclide transport. The general governing equations (Dillon et al., 1979) are solved using finite-difference techniques. Some of the essential features of the SWIFT code are:

- The code can consider a variety of hydrologic regimes and boundary conditions.
- The code can simulate the transport of a variety of radionuclides (i.e., fission products, activation products, and actinide elements).
- The computer code has numerous options for solving the governing equations.

12.3.2.3.5 FE3DGW. As part of the Assessment of Effectiveness of Geologic Isolation Systems (AEGIS) Program, Pacific Northwest Laboratory (PNL) has developed a generalized code for groundwater flow analysis. The model, referred to as FE3DGW, solves the governing equations for three-dimensional flow in an isothermal-porous media. Salient features of this code are:

- The code can accommodate geohydrologic systems with complete geometries.
- The code uses a variety of types of finite elements.
- The computer code is highly modularized.

This code has been used in groundwater modeling studies of the Pasco Basin (Dove et al., 1981). The available documentation on FE3DGW provides a good discussion of model theory and application approach (Gupta et al., 1979).

12.3.2.3.6 NUTRAN. The NUTRAN code is a generalized systems model for nuclear-waste-disposal consequence analysis (Berman et al., 1978). One of the components of this code is designed to model radionuclide transport from the repository to the accessible environment. The model assumes steady flow and uses a streamtube analysis approach. The governing equations for radionuclide transport are solved using a Green's function approach. General features and capabilities of the NUTRAN code (Ross et al., 1979) are:

- The code is easy and inexpensive to use.

- The code can be used in a Monte Carlo mode (i.e., probabilistic descriptions of input parameters).
- The code is interfaced with various submodels having the capability to complete dose-to-man.

This code has been recently applied in performance analysis studies for a repository site at Hanford. A detailed user's manual (TASC, 1980) is currently available for the NUTRAN code.

12.3.2.3.7 WOOD/SALTER. This radionuclide transport model has been primarily used to evaluate waste package performance requirements (Wood, 1980). The model is based on the closed-form analytic solution to the one-dimensional radionuclide transport equation developed by Haderman (1980). Basic features of the computer code are:

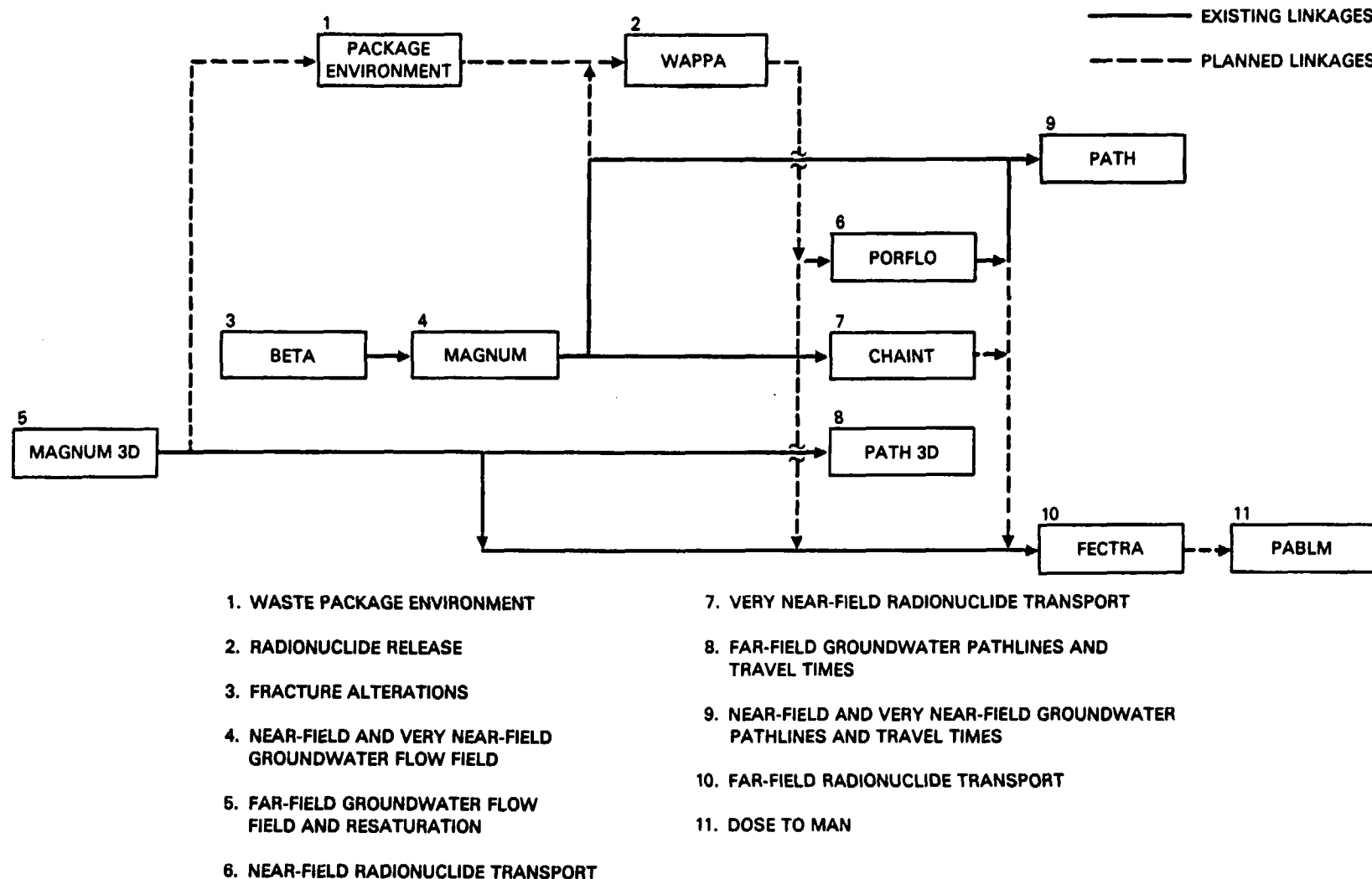
- The theoretical framework assumes a band radionuclide release rate.
- The code is applicable to a variety of sorbing and nonsorbing radionuclides.
- The computer code is simple and inexpensive to use.

The governing equations, basic assumptions, and analytic solution are documented in Haderman (1980).

12.3.2.4 Summary. Selected codes from the aforementioned set can be integrated to produce a system model capable of modeling the processes that take place from the waste package environment through groundwater transport leading to possible dose-to-man.

The relationships of the subsystem models in such an overall system model are presented in Figure 12-3. The final selection of subsystem models is not fixed; substitution or supplementation by other models may occur as need dictates.

The codes presented in the typical system model represent an integrated set of models specifically applicable to a repository system in basaltic rock. The complete set of codes provides a predictive capability for use in evaluating compliance with the criteria and regulatory requirements. Documentation is currently being prepared for the predictive models to be used by the BWIP.



RCP8209-122

FIGURE 12-3. Typical System Model.

12.3.3 Code Verification and Benchmarking

Code verification and benchmarking are an important phase of the code-development effort, because considerable reliance will ultimately be placed on model predictions. The basic objective of the testing process is to verify the correctness and veracity of the computer code. The result and benefit of code verification and benchmarking is, quite simply, the confidence that the predictive model correctly performs the calculations of the underlying mathematics, given specific input.

The basic procedure of verifying and benchmarking, as adopted by the BWIP, consists of two levels of computational experiments or tests. These are:

- (1) Analytical Test Cases: Testing the numerical model using idealized boundary-value problems with known analytic solutions.
- (2) Simulation Test Cases: Testing the numerical model against other computer codes using realistic simulation problems.

Within each level of the code testing process, the set of test cases are formulated so as to represent physical situations relevant to, or characteristic of, a repository setting in a geologic system.

The set of numerical models developed for very near-field, near-field, and far-field scales are in various stages of development, refinement, verification, and benchmarking. In addition to code verification and benchmarking, efforts are under way to compare the model results to data from field or laboratory experiments. The process of demonstrating that a computer model adequately represents physical reality is termed model validation.

12.4 PRELIMINARY LONG-TERM REPOSITORY PERFORMANCE ANALYSIS

12.4.1 Far-Field Studies to Assess Compliance with U.S. Nuclear Regulatory Commission Proposed Technical Criteria for Ground- water Transit Time

Over the past several years, several far-field hydrologic analyses have been performed within the Columbia River basalts that are in the category of performance assessment precursors. These studies basically take the form of steady-state groundwater flow modeling and streamline/travel time predictions. The discussion herein focuses on the results and methodologies as they apply to the pre-waste-emplacement groundwater flow path and travel time performance issue. Some of the studies have the benefit of more recent deep basalt information than others, but all were performed using a hypothetical repository location near borehole DC-3 (Fig. 12-4). Substantial interpolation and subjective judgment were required to prepare the model inputs. This is because models require quantitative definition of geometry, material properties, and boundary conditions, whether this information is well known or not.

There are differences in the orientation of the streamlines and in the travel times of these studies. The important reasons for these differences are, for the most part, related to different input data sets and varying interpretations of conditions where insufficient data existed. In spite of the differences, each study concluded that the predicted groundwater travel time from the hypothetical repository location under pre-waste-emplacement conditions to the discharge point exceeded 10,000 years.

12.4.1.1 Preliminary Studies.

12.4.1.1.1 LATA/Intera Analysis.

12.4.1.1.1.1 Scope. In 1978, a preliminary risk assessment study was initiated for the BWIP by Los Alamos Technical Associates, Inc. (LATA) with assistance from Intera Environmental Consultants, Inc. (Intera) in the area of groundwater transport modeling analysis.

As part of a preliminary risk assessment, groundwater transport analysis was provided by a groundwater transport model developed by Intera under contracts with the U.S. Geological Survey and Sandia National Laboratories. It has been referred to as the SWIFT model and was briefly reviewed in Section 12.3.2.3.4.

The purpose of the Intera effort was to simulate groundwater conditions in the Pasco Basin and to estimate groundwater and radionuclide transport away from the vicinity of a hypothetical repository in basalt, using information and data available at the time. The discussion presented here is a summary of the groundwater transport analysis.

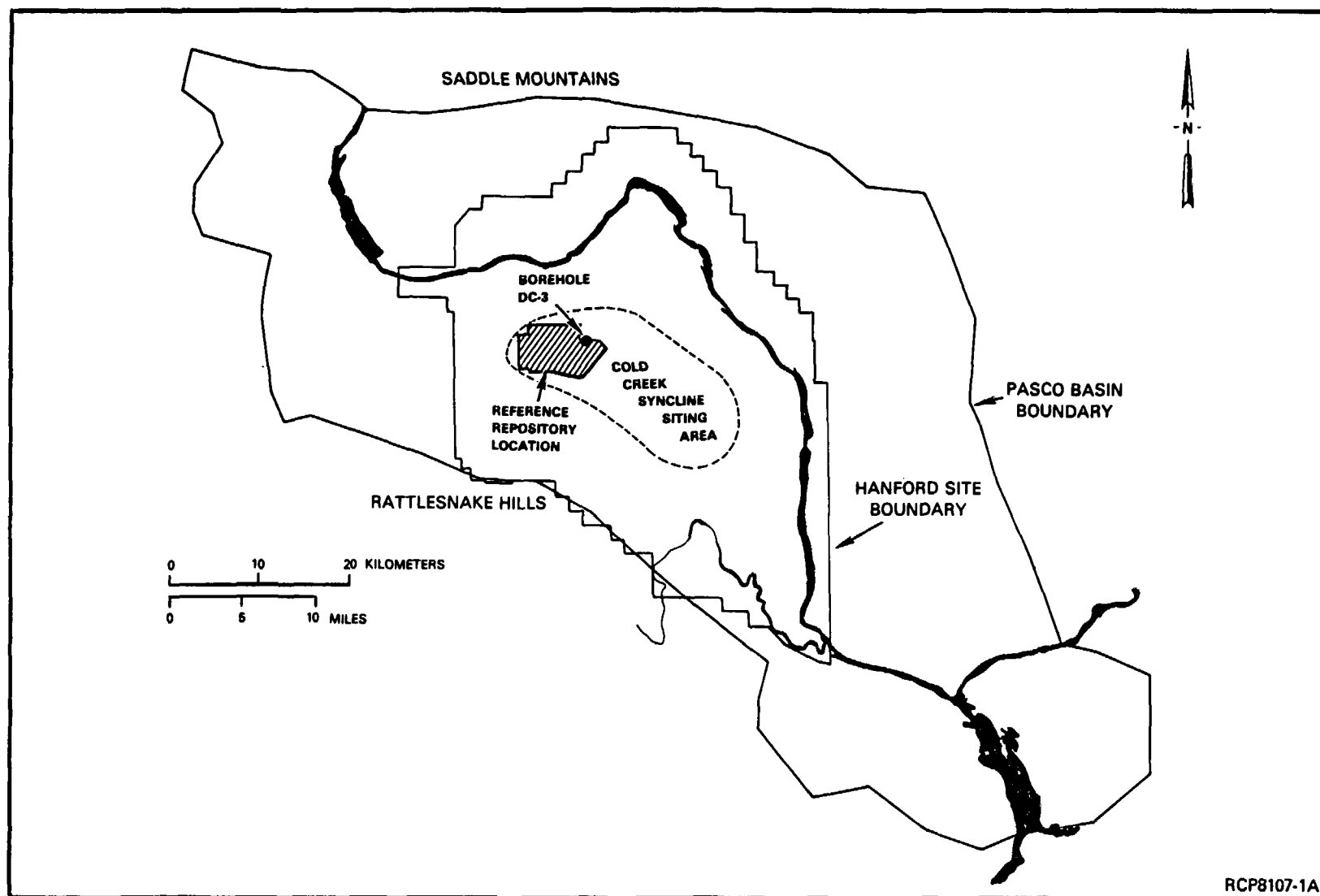


FIGURE 12-4. Location of Cold Creek Syncline Siting Area, Showing the Reference Repository Location and Borehole DC-3.

12.4.1.1.1.2 Scenarios. Three scenarios were considered in the LATA/Intera study: (1) natural conditions or base case, (2) the case of a hypothetical fault connecting the repository with upper aquifers, and (3) a situation in which borehole seal degradation or failure occurred. Though the latter two scenarios are not applicable to pre-waste-emplacement conditions, the results are summarized here for completeness.

The natural release scenario defined the basic waste isolation capability of the repository geohydrologic system under no-disruption conditions and was used as the base case for reference conditions.

12.4.1.1.1.3 Conditions and Assumptions. The primary source of hydrologic data for the hydrology and groundwater transport calculations performed by Intera was Gephart et al. (1979).

Five horizontal layers defined for study with the Intera three-dimensional code corresponded to (1) the upper confined and unconfined layers, (2) a composite of the Saddle Mountains Basalt interbeds (except the Mabton), called Layer 2, (3) the Mabton interbed, (4) the Vantage interbed, and (5) the Umtanum flow top. The last three layers were separated by aquitards. The vertical hydraulic conductivity of Layer 2 also included the intervening basalt layers.

Constant head boundary conditions were established for each layer in the model, using head trend maps in Gephart et al. (1979). Values for hydraulic conductivities were then obtained through available field measurements (including reanalysis of one pressure response test using the Intera code) and calibration of the model with available information so as to estimate spatial distribution of hydraulic conductivity.

Model calibration resulted in assigning a vertical conductivity to each layer and intervening aquitard a value of one-tenth that of the corresponding horizontal hydraulic conductivity. As part of the calibration process, the vertical hydraulic conductivity for all layers directly beneath the Columbia River was assumed to be a factor of 1,000 larger than in the other regions. Hydraulic conductivities used for the base case are summarized in Table 12-3. The thickness and porosity of each model layer are given in Table 12-4.

It was assumed that the repository was located within the Umtanum flow at a site directly beneath the Hanford Meteorological Station (within a few meters of borehole DC-3). The pathline for a particle starting in the center of the Umtanum flow was close to horizontal and northward within the Umtanum until reaching the vicinity of the Columbia River, whereupon the flow was upward to the river. The total travel time from repository to river was calculated to be 33,000 years.

12.4.1.1.1.4 Interconnecting Fault Scenario. The base case involved calculation of performance of the repository geohydrologic system, assuming there were no disruptive events to alter conditions. A fault occurring either through or close to the repository could provide a near-vertical pathway having a greater conductivity than the competent basalt.

TABLE 12-3. Hydraulic Conductivities Assumed by Los Alamos Technical Associates, Inc./Intera Environmental Consultants, Inc.

Layer	Hydraulic conductivity (m/s)		
	Horizontal	Vertical	Vertical near river
1. Upper confined and unconfined aquifers	1.18 E-03	1.18 E-04	1.18 E-01
2. Layer 2 aquifers	1.41 E-05	1.41 E-06	1.41 E-03
3. Mabton interbed	7.1 E-05	7.1 E-06	7.1 E-03
4. Vantage interbed	3.5 E-07	3.5 E-08	3.5 E-05
5. Umtanum flow top	7.1 E-08	7.1 E-09	7.1 E-06
Aquitards	7.1 E-10	7.1 E-10	7.1 E-07

TABLE 12-4. Thickness and Porosity of Each Model Layer Assumed by Los Alamos Technical Associates, Inc./Intera Environmental Consultants, Inc.

Layer	Thickness (m)	Effective porosity (%)
1. Upper confined and unconfined aquifer	90	10
2. Layer 2 aquifers	215	2
3. Mabton interbed	29	4
Aquitard	158	2
4. Vantage interbed	9	4
Aquitard	244	2
5. Umtanum flow top*	61	2

*The Umtanum flow top layer was assigned a thickness corresponding to the total thickness of the Umtanum flow.

12.4.1.1.1.5 Additional Assumptions.

- The repository inventory and release rates were unchanged from the base case.
- The fault connected all layers from the lower Umtanum to the Mabton interbed.
- The fault width was 1.0 meter.
- The gouge material in the fault consisted of uniform 1.0-centimeter spherical particles.
- The porosity of the fault was 10 percent.
- The radionuclide sorption coefficients were the same in the fault zone as in the undisturbed rock.
- The longitudinal and transverse dispersivities for radionuclide transport were assumed to be 90 and 9 meters, respectively.

Harleman's equation (Bear, 1972, p. 168) was used to calculate a fault hydraulic conductivity of 0.60 meter per second.

A model block 4,000 by 4,000 meters in the planar dimension was used in the vicinity of the repository containing the 2,400- by 3,000-meter repository, and the length of the fault was assumed to extend across one entire block. The composite or average vertical hydraulic conductivities for the model grid blocks that included the fault were calculated using a formula in Bear (1972, p. 152) to be 1.5 to 1.6×10^{-4} meter per second. This composite vertical hydraulic conductivity was used in the calculation of the groundwater travel time.

Hydrologic flow calculations with the altered vertical hydraulic conductivities (1.6×10^{-4} meter per second) in the vicinity of the repository changed the pathline and travel time from the base-case results. The pathline for a particle, starting in the repository, was upward along the fault zone pathway to the Mabton interbed, then northward within the Mabton to the vicinity of the river, followed by upward travel to the river. The travel time was calculated by the SWIFT model to be 16,700 years, approximately one-half that for the base case. More than 70 percent of the total travel time was for the vertical travel in the fault zone to the Mabton. Accordingly, these calculations showed contaminated groundwater appearing in the Mabton approximately 12,700 years after repository closure.

12.4.1.1.1.6 Shaft Seal Failure. The shaft seal failure scenario was added to the base case and the interconnecting fault case to ensure comprehensiveness of the preliminary safety assessment. Hydrologic calculations of the type used for the base case and the interconnecting fault

case were not available, so approximate methods were used to estimate the hydrologic conditions. This level of treatment was judged to be adequate for the preliminary risk assessment.

12.4.1.1.1.7 Additional Assumptions.

- Five circular shafts are used during construction and operations.
- Shaft seal degradation may occur through fracture of the seal structure (an extreme of this is fragmentation), deterioration of the bond between the seal and surrounding rock, and/or fracturing in the surrounding rock.
- Clay/sand segments are somehow channeled to the hydraulic equivalent of crushed basalt.
- Concrete seal material experiences complete degradation to the equivalent of crushed basalt.
- Material in the shafts after degradation is similar to the gouge material in the fault (i.e., vertical hydraulic conductivity is 0.60 meter per second).
- Disturbed rock zone extends out to a diameter 1.5 times the bore diameter.

A composite vertical hydraulic conductivity was calculated using undisturbed rock properties, the aggregate cross-sectional areas of the five shafts, the vertical hydraulic conductivity of the degraded shaft material, and the area of a 4,000- by 4,000-meter grid block (planar dimension). The composite vertical conductivity was calculated from Bear (1972, p. 152) to be 5×10^{-6} meter per second. This value was lower than the composite vertical conductivity for the fault scenario by a factor of 30, but was greater than the undisturbed base case conditions.

The shaft seal failure conditions were analyzed using a simpler modeling technique rather than the SWIFT code. This approach was felt to be adequate since the value of the vertical composite hydraulic conductivity was intermediate between the base case and the fault case.

The travel time was estimated to be between 18,000 and 45,500 years. A value of 33,600 years was used for comparison purposes.

12.4.1.1.2 Early Rockwell Hanford Operations Analysis.

12.4.1.1.2.1 Scope. Early Rockwell Hanford Operations (Rockwell) modeling of the Pasco Basin was primarily aimed at understanding the groundwater flow systems and in identifying data and conceptual model limitations. Preliminary travel-time calculations were also performed. The results are partially documented by Arnett (1980).

12.4.1.1.2.2 Assumptions and Conditions.

- Three layers were assigned to the model, corresponding to the Saddle Mountains, Wanapum, and Grande Ronde Basalts.
- A set of boundary conditions were synthesized from available data, using hydrologic judgment. It was felt that the regional head trend maps in Gephart et al. (1979) were quite uncertain, due to the limited data for the Pasco Basin vicinity used in their construction. Consequently, heaviest reliance for boundary conditions was placed upon the Pasco Basin-scale head map for the Mabton interbed (Gephart et al., 1979). The Wanapum and Grande Ronde Basalt boundary conditions were extrapolated from the Mabton map and limited available data for those basalts.
- Each of the model layers was assumed to be homogeneous (but anisotropic) throughout the Pasco Basin.
- The initial ratios of horizontal-to-vertical hydraulic conductivities were determined for each layer by compositing the estimated conductivities of dense basalt, interflow, and interbed materials.
- For the purposes of travel time calculations, groundwater was assumed to travel vertically from the repository level (Umtanum flow depth) to the Mabton. (A pathline model was not used.)
- A version of the FE3DGW model was used to simulate heads for this analysis.

12.4.1.1.2.3 Results. Only the natural or base case conditions were examined in the early Rockwell groundwater modeling. The ratio of horizontal-to-vertical hydraulic conductivities was varied over a range of several orders of magnitude and the head patterns at the interface between the Saddle Mountains and Wanapum Basalt layers were compared to the Mabton interbed head map in Gephart et al. (1979). With the given boundary conditions, the ratio that gave the best relative comparison was in the range of 10^4 to 10^5 (horizontal over vertical).

The model computed absolute heads that were larger than measured values in the deep basalts underlying Hanford. This was attributed in part to the existence of some structural features that were not well defined and were, therefore, not included in the model.

Preliminary estimates of travel time were determined by assuming vertical movement from the repository to the Mabton interbed and horizontal movement within the Mabton to the model predicted discharge area just below the Priest Rapids dam. A planar view of the model predicted head distribution at the Mabton depth is presented in Arnett (1980, Fig. 6). The travel time was estimated to be in the range of 20,000 to 100,000 years.

12.4.1.1.3 Pacific Northwest Laboratory Demonstration of Assessment of Effectiveness of Geologic Isolation Systems Methodology.

12.4.1.1.3.1 Scope. One component of the National Waste Terminal Storage Program was the AEGIS Program conducted by PNL and coordinated by the Office of Nuclear Waste Isolation. In fiscal year 1979, the Office of Nuclear Waste Isolation directed the AEGIS Program to perform a reference site initial assessment of a hypothetical nuclear waste repository in the Columbia Plateau as a demonstration of capabilities and to assist in methodology development. The results are documented in Dove et al. (1981).

Similar to the early Rockwell and LATA/Intera efforts, the AEGIS study used input from a variety of sources, but relied heavily on the information in Gephart et al. (1979) for definition of the groundwater flow system. The approach used by PNL was to model the hydraulic head in the Washington State portion of the Columbia Plateau, an area of approximately 54,000 square kilometers. Attempts were made to quantify the groundwater recharge to the model area to obtain an approximate groundwater flow budget.

12.4.1.1.3.2 Assumptions. The AEGIS assumptions are summarized in Table 12-5, taken from Dove et al. (1981, pp. IV-VI).

The Columbia Plateau regional model was calibrated using available data and the head boundary conditions of the northern and eastern boundaries of the Pasco Basin interpolated from the output of the regional model. The eastern and southern boundaries of the Pasco Basin coincided with portions of the regional model boundary. These boundaries were assigned no-flow conditions throughout the vertical sequence. Using those boundary conditions and estimated values for hydrologic properties of the basalt, a separate, more detailed model was developed for the Pasco Basin, and flow paths and travel times were calculated. The FE3DGW code was used to model the Pasco Basin.

12.4.1.1.3.3 Results. The streamline orientations are shown in Figures 12-5, 12-6, and 12-7. For a set of streamlines within the envelope of the two streamlines shown in Figures 12-5 through 12-7, the travel time varied from 13,000 to 17,000 years; the travel distance varied from 12,000 to 15,500 meters. The average calculated travel time and travel distance for that set of streamlines were 15,000 years and 13,700 meters, respectively.

The PNL effort was conducted with pre-1980 data. The most recent information used was the hydraulic head profile of borehole DC-14 from the water table to the Mabton interbed (the Wanapum and Grande Ronde Basalt portions of the borehole had yet to be drilled at that time). A substantial upward head gradient was measured in the upper portion of borehole DC-14. Examination of the PNL model results reveals a significant upward hydraulic head gradient in the deep basalts (Wanapum and Grande Ronde) in the center of the Hanford Site.

TABLE 12-5. Major Assumptions in the Assessment of Effectiveness of Geologic Isolation Systems (AEGIS) Basalt Demonstration (after Dove et al., (1981).

Assumption	Class*	Comments
Conceptual Model		
Composite transmissive zones for equivalent porous flow	Reasonable	Integrates limited point-source data into continuous lumped parameters (nonhomogeneous in areal extent)
Composite confining layers for equivalent porous flow	Reasonable	Integrates limited point-source data into continuous lumped parameters (nonhomogeneous in areal extent)
Grande Ronde Basalt is hydrologically similar to Wanapum Basalt	Conservative	Limits groundwater flow to recharge/discharge within model boundaries
Hydrologic Simulation		
No flow boundary in Horse Heaven Hills and Blue Mountains	Conservative	Based on groundwater divide in Wanapum Basalt and anticlinal structure
Pasco Basin is regional discharge area	Conservative	Topographic low in regional elevations, potentiometric low in Wanapum Basalt
Vertical and horizontal groundwater flow in Pasco Basin	Conservative	Based on well hydrographs and hydraulic conductivities of basalt formations
Hydraulic conductivity increases in vertical direction and decreases in horizontal direction at anticlinal structures	Conservative	Based on interpretations of field data (Apps et al., 1979)
Basalt formations generally discharge groundwater to Columbia, Snake, and Yakima Rivers	Nonconservative	Fixed potential boundaries (elevation head)

*Reasonable-Best estimate of actual conditions.

Conservative-Such that results will be "worse" from a waste-isolation standpoint (shorter travel time, higher radionuclide fluxes, etc.) than if reasonable values were used.

Nonconservative-Such that results will be "better" from a waste-isolation standpoint (longer travel time, lower radionuclide fluxes, etc.) than if reasonable values were used.

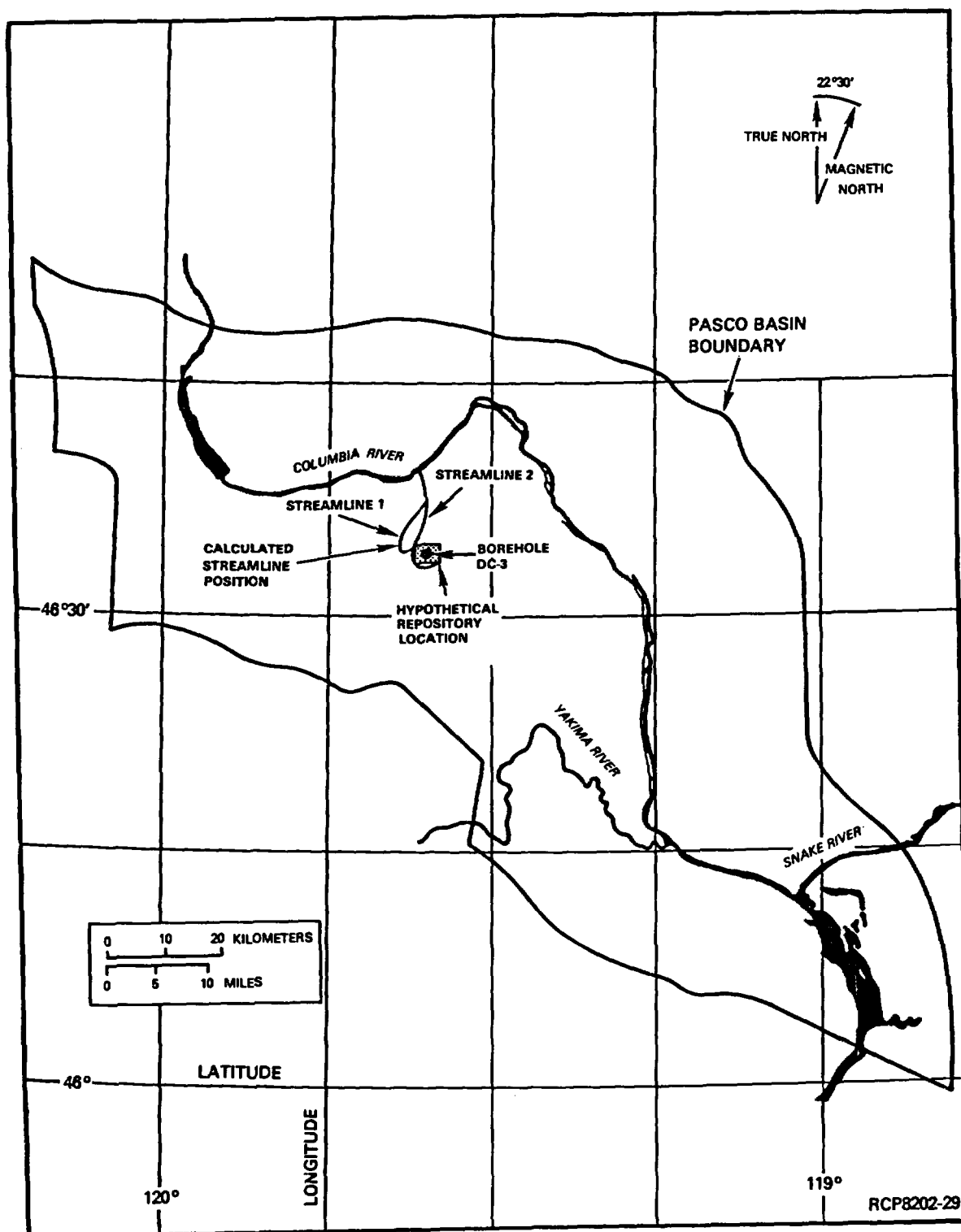


FIGURE 12-5. Plan View (X-Y) of Two Streamlines Originating at the Repository, Assessment of Effectiveness of Geologic Isolation Systems (AEGIS) Model.

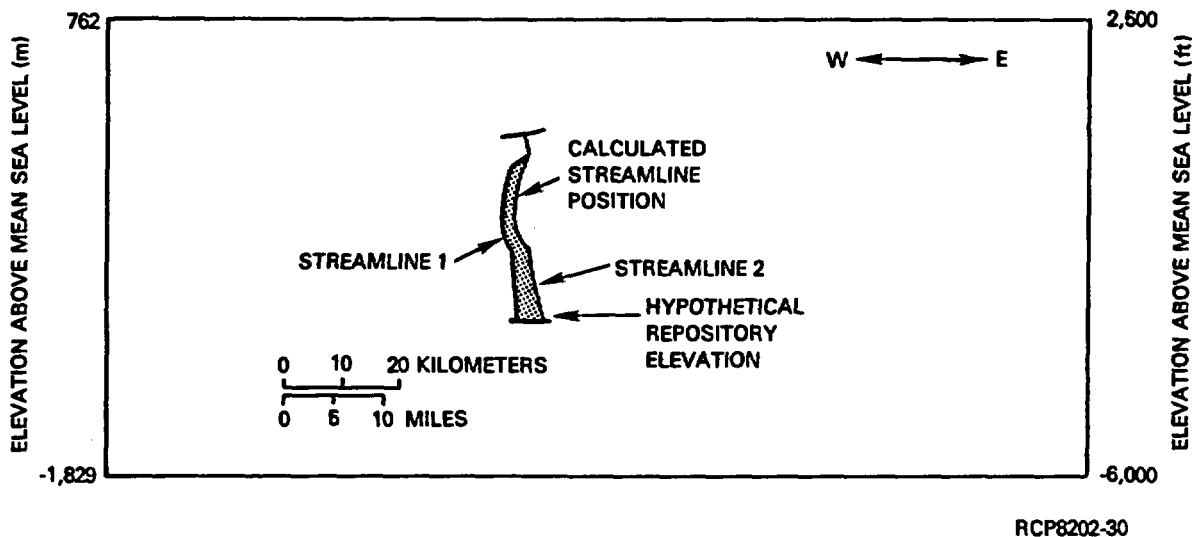


FIGURE 12-6. East-West Cross-Sectional View (X-Z) of Two Streamlines Originating at the Repository, Assessment of Effectiveness of Geologic Isolation System (AEGIS) Model.

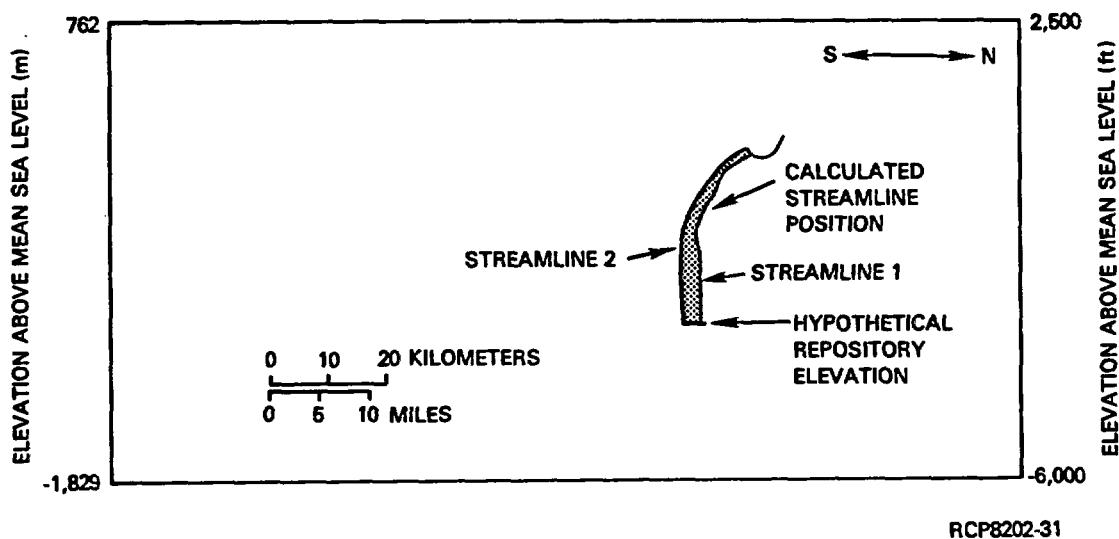


FIGURE 12-7. North-South Cross-Sectional View (X-Z) of Two Streamlines Originating at the Repository, Assessment of Effectiveness of Geologic Isolation System (AEGIS) Model.

12.4.1.2 Recent Studies.

12.4.1.2.1 Rockwell Analysis.

12.4.1.2.1.1 Scope. A more recent Rockwell analysis (Arnett et al., 1981) was conducted using post-1979 data and an updated conceptual model. While both three-dimensional (three-layer) and two-dimensional cross-sectional (nine-layer) analyses were performed, the two-dimensional analysis was basically an instructional exercise and the results are considered nonconservative. Hence, only the three-dimensional analysis is summarized here.

12.4.1.2.1.2 Assumptions and Methods.

- The top of the system coincides with the top of basalt.
- The heads for the upper boundary nodes lying below the Columbia, Yakima, and Snake Rivers were assumed to be equal to the average river stages. By implication, the head in the unconfined region between the rivers and the basalt-groundwater system was assumed to be hydrostatic. The average river stages were obtained from Gephart et al. (1979, Plate III-4).
- The heads for the upper boundary nodes lying below the unconfined sedimentary aquifer were assumed to be equal to the unconfined heads. The unconfined heads were assumed to be hydrostatic and were obtained from Gephart et al. (1979, Plate III-4).

Pacific Northwest Laboratory established a separate layer for the overlying sediments, but fixed the heads along the upper surface of this layer to match the unconfined aquifer. The PNL approach was similar to Rockwell's, except that transport could (and did) occur in the PNL sedimentary layer, whereas no transport beyond the basalts was simulated with the Rockwell model. An examination of the head at the top and bottom of the PNL sedimentary layer indicated hydrostatic conditions almost uniformly throughout the layer. Use of an unconfined aquifer layer was not attempted at this point because of the extra effort involved. The value of using the unconfined aquifer as a calibration surface is limited by several factors:

- The piezometric surface of the currently well-characterized unconfined aquifer is dominated by Hanford Site activities (largely process cooling water discharges); the natural piezometric surface is much less well known.
- A portion of the unconfined aquifer sediments are glaciofluvial material of very high conductivity relative to basalt, hence rather extreme variances in groundwater exchanges between the basalts and the unconfined aquifer in those areas would likely be required to be useful in a calibration process.

- Other portions of the overlying sediments have clay layers that have been used as no-flow surfaces in Hanford unconfined aquifer modeling.

Modeling of the unconfined aquifer is being considered in future BWIP modeling.

- The lower (bottom of Grande Ronde Basalt) boundary is assumed to be a no-flux boundary. This boundary was intentionally located sufficiently far below the surface (approximately 1,000 meters below the top of the Grande Ronde Basalt) to be beyond the influence of recharge and pumpage. At this depth, the vertical head profile should be hydrostatic and vertical flow should be negligible.
- The surface fluxes for the upper boundary elements lying below recharge areas were assumed to be proportional to annual rainfall. One-fifth of the long-term average annual rainfall (3.7 centimeters per year) was assumed to reach the basalt groundwater system. The recharge areas were defined in Gephart et al. (1979, Plate III-12).
- The horizontal hydraulic conductivities were assumed to be uniform throughout each layer, since there was limited information on horizontal hydraulic conductivity variations.
- The hydraulic conductivity was isotropic in the horizontal plane, but anisotropic in the vertical plane.
- The hydraulic conductivities for the model layers can be represented for purposes of flow rate by compositing the hydraulic conductivities of the individual interbeds, interflows, and dense basalt units.
- The regional head information and results of regional modeling are insufficient to obtain a firm estimate of boundary conditions along the edge of the Pasco Basin.
- The hydraulic conductivity values in the Cold Creek syncline siting area (see Fig. 12-3) are representative of the Pasco Basin as a whole.
- The effective porosity of the Grande Ronde Basalt was assumed to be 1 percent.

The MAGNUM 3D code was used to model the groundwater heads, while the PATH 3D code was used to calculate the streamlines and travel times.

The model composite hydraulic conductivities were derived from Table 3 of Spane in BWIP (1980), together with a value for the dense basalts of less than 10^{-12} meter per second. Using the composite formula (Freeze and Cherry, 1979, p. 34), a ratio of horizontal-to-vertical conductivity of 10^6 was calculated. Because the value of the dense basalt hydraulic conductivity used in the compositing calculation was a measure of the

horizontal conductivity, and the fractures in the dense basalt appear to be oriented more frequently in the vertical than in the horizontal direction, the vertical hydraulic conductivity in the dense basalt was believed to be higher than the horizontal conductivity. The vertical conductivity in the dense basalts was assumed to be 100 times higher than the dense basalt horizontal hydraulic conductivity. The anisotropy ratio for the composite layers was thereby reduced to 10^4 . During the preliminary calibration, the ratio was further reduced to 10^3 .

During the modeling process, the results of some transmissivity tests in the Grande Ronde Basalt became available. These tests measured the effective transmissivity over an interval of 400 meters for borehole DC-4 and 40 meters for DC-7. When the transmissivity results were converted to hydraulic conductivity (dividing transmissivity by the depth interval), the effective DC-4 value was 2.7×10^{-9} meter per second and the effective DC-7 value was 1.16×10^{-10} meter per second. Since the DC-4 value represented a longer interval and aggregated more individual flows, it was probably more typical of the Grande Ronde Basalt as a whole. It was also the more conservative choice from a waste transport point of view, since it is larger and more conducive to the migration of radionuclides away from the repository. Some of the borehole test results presented in Chapter 5 were not available at the time modeling was performed. Composite conductivities higher than 10^{-9} meter per second have recently been measured and will be taken into consideration in future modeling.

The composite Grande Ronde Basalt layer was assigned a horizontal-conductivity value of 1×10^{-9} meter per second. The horizontal-to-vertical conductivity ratio of 10^3 caused a value of 10^{-12} meter per second to be assigned to the vertical conductivity of the composite Grande Ronde Basalt. The anisotropy in the model composite layers resulted from the relatively more permeable flow contacts alternating with less permeable dense basalts. Even though the vertical conductivity is believed to be higher than the horizontal conductivity in the dense basalts themselves, the contrast between the vertical conductivity in dense basalts and the horizontal conductivity in the flow contacts causes the ratio of horizontal-to-vertical conductivity in the composite layer to be 10^3 . The final set of hydraulic conductivity values used in the three-dimensional modeling studies are presented in Table 12-6.

TABLE 12-6. Effective Hydraulic-Conductivity Values Used in the Initial MAGNUM 3D Pasco Basin Simulation.

Basalt layer	Conductivity (m/s)	
	Horizontal	Vertical
Saddle Mountains	1.0 E-08	1.0 E-11
Wanapum	3.0 E-09	3.0 E-12
Grande Ronde	1.0 E-09	1.0 E-12

The initial boundary conditions along the edge of the Pasco Basin were developed from Pasco Basin maps of the Mabton interbed (Spane, 1980), geologic arguments (e.g., no-flow conditions along the upper portions of mountain ridges), and other available data. Reasonable adjustments in the values of the boundary conditions were made to obtain a match with the head data within the model boundaries. For the Wanapum and Grande Ronde Basalts, emphasis was placed on adjusting boundary conditions to approximate the head measurements in boreholes DC-12, -14, and -15. These boreholes showed a very low vertical head gradient in the Wanapum and Grande Ronde Basalts. For pathway and travel time calculations, the repository horizon was assumed to be the Umtanum flow.

12.4.1.2.1.3 Results. Although many uncertainties still exist in the revised conceptual model, a pattern of near horizontal movement away from the siting area emerged. This was due to little or no upward head gradient, as measured in the field, together with the concept of a layered system of more permeable flow contacts alternating with less permeable dense basalts. The groundwater was calculated to move away from the siting area in a southeasterly direction, beneath the Columbia River, toward the area around Lake Wallula (Fig. 12-8).

The compositing process assures that volumetric flow in the composite layer is the same as in the actual set of discrete layers. However, the groundwater velocity in the narrow, more permeable flow contacts that dominate the horizontal flow will be much higher than the velocity in the composite layer. For the purpose of calculating travel time, it was assumed that all flow was through a layer that represented only 1 percent of the thickness of the Grande Ronde Basalt. This assumption is equivalent to assuming a horizontal hydraulic conductivity of 10^{-7} meter per second for travel time calculations. This procedure maintained the correct volumetric flow through the composite layers, yet adjusted for the fact that most of the flow is likely to occur at higher velocities through only a fraction of the layer. After reduction by a factor of 100, the final travel time was reported as greater than 100,000 years.

The principal limitation of this study is considered to be the assumption of uniform hydraulic conductivity for the composite layers throughout the entire Pasco Basin. The adjustments in travel time needed to compensate for too-few layers are closely related.

Both the streamline orientation and the travel time estimates are expected to be refined as further information is gathered and the conceptual model is improved. A parametric and sensitivity analysis is under way to evaluate the waste isolation significance of ranges in model parameters and inputs.

12.4.1.2.2 WOOD/SALTER. A preliminary performance assessment of the basalt site was also performed by Salter et al. (1982) to determine the most hazardous radionuclides in the waste inventory and to estimate the maximum permissible release rates for various radionuclides from the

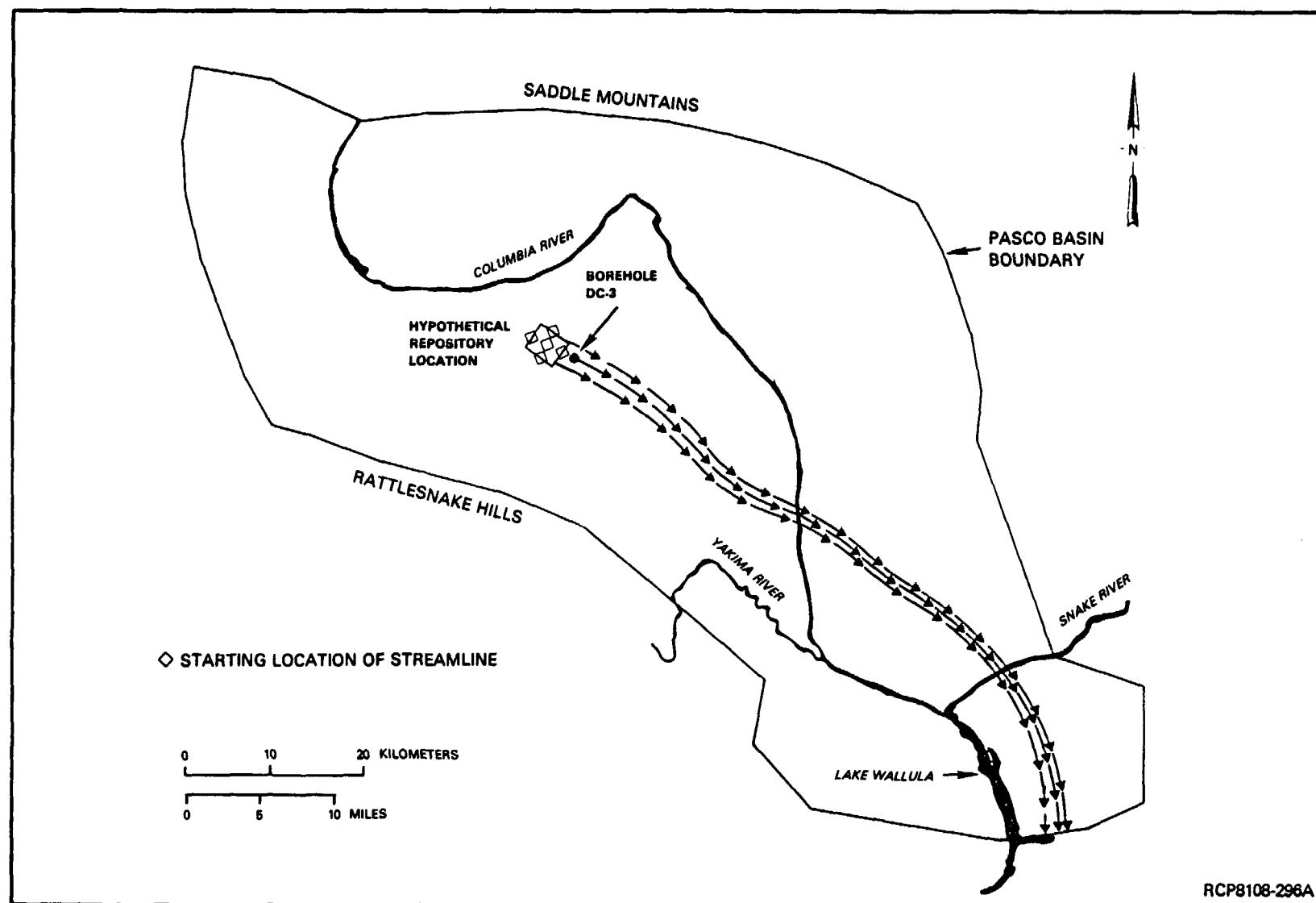


FIGURE 12-8. Planar View of Streamlines from Hypothetical Repository to Boundary.

engineered system to the accessible environment. The results are presented primarily in terms of the release rate required to maintain radionuclide fluxes below current EPA draft regulations (EPA, 1981). For that reason, a complete summary is presented in Section 12.4.2.

The travel time for the base case (no-disruption conditions and repository located in Umtanum flow) is calculated to be approximately 30,000 years for a 10-kilometer travel distance.

12.4.1.2.3 The Analytic Sciences Corporation.

12.4.1.2.3.1 Scope. A study to assess the need for additional data from small-diameter boreholes has recently been completed by The Analytic Sciences Corporation. Part of this study involved analyzing the performance of a repository located in the Umtanum flow within the Pasco Basin. This performance analysis provides an independent assessment of the BWIP borehole needs.

12.4.1.2.3.2 Scenarios. Three scenarios describing groundwater flow paths between the repository and the accessible environment were analyzed:

- (1) Vertical migration from the repository to the flow top of the Umtanum flow, followed by horizontal migration to the accessible environment
- (2) Vertical migration from the repository to the Mabton interbed, followed by horizontal migration to the accessible environment
- (3) Vertical migration along a presumed fault that connects the repository and the Mabton interbed, followed by horizontal migration to the accessible environment.

12.4.1.2.3.3 Assumptions and Methodology. All three scenarios assumed:

- Elevated temperatures due to decaying nuclear waste provided the driving force for vertical groundwater migration for the initial period after the repository was closed.
- The accessible environment was the Columbia River at Wallula Gap, 60 kilometers southeast of the repository.

Essentially, two steps were involved in analyzing the above scenarios:

- (1) Statistically analyze the available horizontal hydraulic conductivity data from the Umtanum flow and the Mabton interbed. This was accomplished with the geostatistical interpolation technique of kriging, which allowed estimates of hydraulic conductivity and their uncertainties to be determined at key locations.
- (2) Evaluate the repository performance for each scenario. This was accomplished with the computer code NUTRAN, which was developed by The Analytic Sciences Corporation (Ross et al., 1979).

The locations and values of the hydraulic conductivity data used in the kriging analysis are seen in Figure 12-9 and Table 12-7, respectively. Logarithms of these data were taken prior to kriging, because it was found that this transformation produced a variable that had a smaller range and was statistically easier to interpret. Linear and isotopic semivariogram models that were estimated from these data provided the correlation functions necessary for the kriging analysis. An appropriate kriging algorithm was then used to assign point estimates of log hydraulic conductivity and their associated kriging errors at the location of borehole RRL-2 (Fig. 12-9). In addition to estimating the mean log hydraulic conductivity at RRL-2, the 90 and 97.5 percent confidence limit log hydraulic conductivities were also estimated from the kriging values and their kriging errors. These estimates of log hydraulic conductivities were transformed back to hydraulic conductivities before being input to the scenarios. An additional assumption used in analyzing the scenarios was that the kriging values of hydraulic conductivity at RRL-2 were representative of the mean hydraulic conductivities along the pathways between the repository and Wallula Gap.

The NUTRAN computer code used to model the groundwater flow in these scenarios solves the one-dimensional form of the transport equation, assuming steady groundwater flow. Thus, each scenario had to be defined by a series of streamtubes leading from the repository to the accessible environment. Unique hydrogeologic and geometric parameters were then assigned to each streamtube. To assess the impact that uncertainty in horizontal hydraulic conductivity had on groundwater travel times, each scenario was run with the 90 and 97.5 percent confidence limit hydraulic conductivities determined in the kriging analysis. This gave some indication of the lower bound on travel time between the repository and the accessible environment. The parameters assigned to the horizontal and vertical streamtubes in the scenarios are listed in Tables 12-8 and 12-9, respectively.

12.4.1.2.3.4 Results. The groundwater velocities, volumetric flow rates, and travel times in each of the horizontal and vertical streamtubes that composed the scenarios are listed in Tables 12-10 and 12-11, respectively. The travel times between the repository and the accessible environment for the three scenarios analyzed are listed in Table 12-12. Groundwater moving vertically through the basalts to the Mabton interbed and then to the accessible environment takes the longest time. Groundwater travel time is the shortest in Scenario (3), which involves the vertical fault. The effect of the increased vertical driving force caused by the elevated temperatures in the repository is evident when comparing pre-waste- and post-waste-emplacement travel times.

In all cases, the estimates of groundwater travel time to the accessible environment under pre-waste-emplacement conditions exceed the 1,000-year minimum requirement.

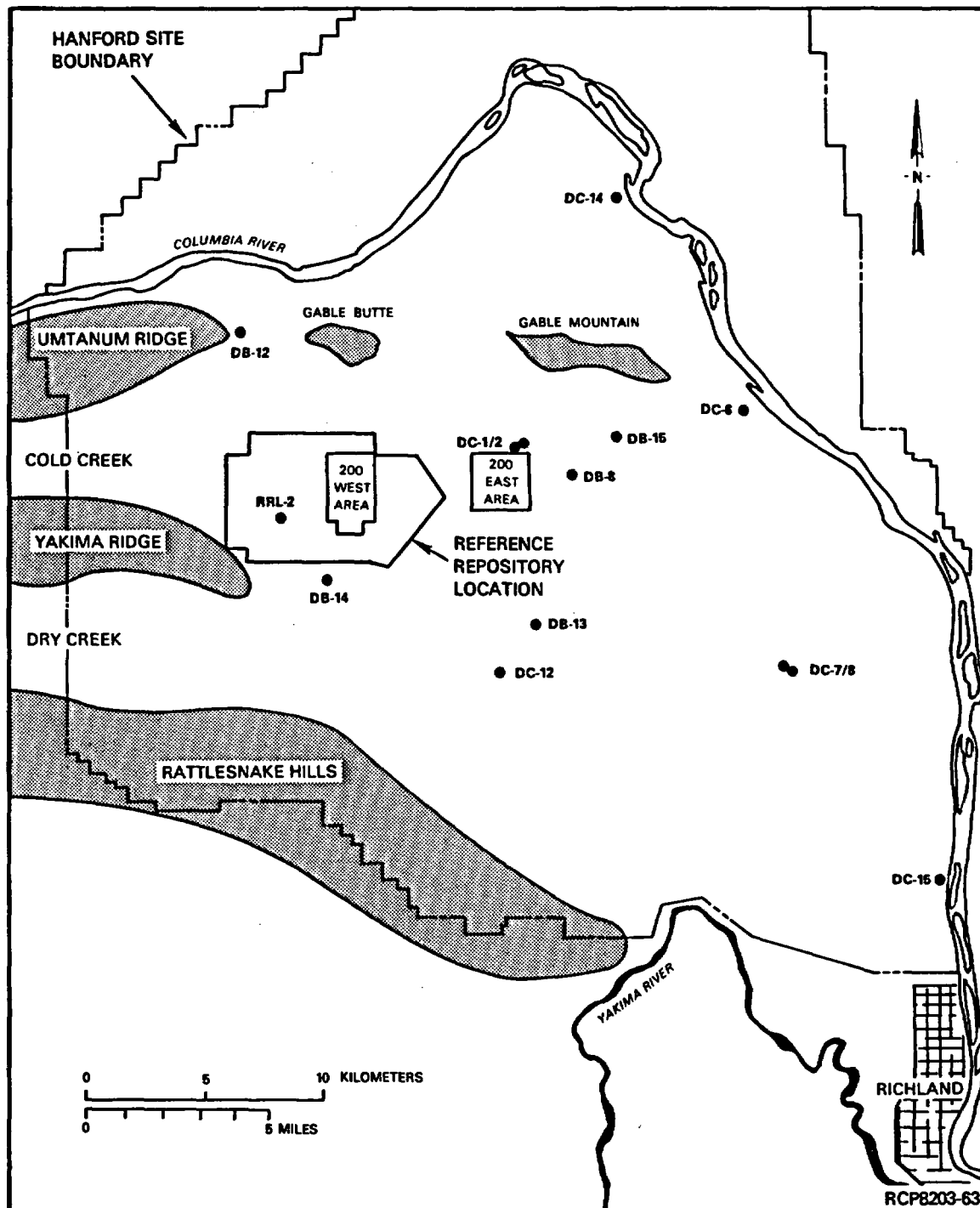


FIGURE 12-9. Location of Boreholes Used in the Kriging Analysis.

TABLE 12-7. Hydraulic Conductivity Data Used in the Kriging Analysis.

Borehole	Hydraulic conductivity (m/s)	
	Umtanum flow top	Mabton interbed
DC-1/2	1.05 E-07	1.31 E-05
DC-7/8	3.53 E-10	
DC-12	2.12 E-09	
DC-15	1.06 E-06	4.94 E-07
DC-6	7.06 E-10	
DC-14	3.53 E-07	2.96 E-06
DB-12		4.16 E-05
DB-13		7.06 E-05
DB-14		4.94 E-06
DB-8		4.41 E-04
DB-15		3.88 E-05

TABLE 12-8. Parameters for Horizontal Streamtubes.

Streamtube	Length (m)	Cross section area (m ²)	Hydraulic gradient	Hydraulic conductivity (m/s)	Effective porosity
Flow top of Umtanum flow	6.0 E+04	8.2 E+04	3.0 E-04	4.0 E-05 ^a 2.0 E-06 ^b	0.06
Mabton interbed	6.0 E+04	8.4 E+04	3.0 E-04	2.0 E-04 ^a 7.0 E-05 ^b	0.1

^a97.5% confidence limit value.

^b90% confidence limit value.

TABLE 12-9. Parameters for Vertical Streamtubes.

Streamtube	Length (m)	Cross section area (m ²)	Hydraulic gradient		Hydraulic conductivity (m/s)	Effective porosity
			Natural	Thermal		
Repository to flow top of Umtanum flow	30	7.2 E+06	2.0 E-03	0.16 ^a	1 E-11	1 E-03
Repository to Mabton interbed	650	7.2 E+06	2.0 E-03	0.03 ^b	3.0 E-11	0.02
Repository to Mabton interbed through fault zone	650	173	2.0 E-03	0.03 ^b	9.0 E-05	0.1

^aReverts to natural gradient at 10,000 years after waste emplacement.

^bReverts to natural gradient at 30,000 years after waste emplacement.

TABLE 12-10. Groundwater Velocities, Flow Rates, and Travel Times for Horizontal Streamtubes.

Streamtube	Confidence limit on hydraulic conductivity (%)	Velocity (m/yr)	Volumetric flow rate (m ³ /yr)	Travel time (yr)
Flow top of Umtanum flow	97.5	5.0	2.5 E+04	1.2 E+04
	90	0.3	1.6 E+03	1.9 E+05
Mabton interbed	97.5	19.0	1.6 E+05	3.2 E+03
	90	6.3	5.3 E+04	9.5 E+03

TABLE 12-11. Groundwater Velocities, Flow Rates, and Travel Times for Vertical Streamtubes.

Streamtube	Waste status in repository	Velocity (m/yr)	Volumetric flow rate (m ³ /yr)	Travel time (yr)
Repository to flow top of Umtanum flow	Preemplacement	6.3 E-04	4.5	4.8 E+04
	Postemplacement	0.05	360	590
Repository to Mabton interbed	Preemplacement	9.5 E-05	14	6.9 E+06
	Postemplacement	1.4 E-03	360	6.4 E+06
Repository to Mabton interbed through fault zone	Preemplacement	57	980	11
	Postemplacement	850	1.5 E+04	0.8

TABLE 12-12. Groundwater Travel Times for Each Scenario.

Scenario	Waste status in repository	Travel time (yr)	
		90% confidence	97.5% confidence
(1) Repository to flow top of Umtanum, then to Wallula Gap	Preemplacement	2.4 E+05	6.0 E+04
	Postemplacement	1.9 E+05	1.2 E+04
(2) Repository to Mabton, then to Wallula Gap	Preemplacement	6.9 E+06	6.9 E+06
	Postemplacement	6.4 E+06	6.4 E+06
(3) Repository to Mabton through fault zone, then to Wallula Gap	Preemplacement*	9,500	3,200
	Postemplacement	9,500	3,200

*Preemplacement and postemplacement refer to isothermal and nonisothermal conditions, respectively. The existence of a significant preemplacement fault would likely cause relocation of the repository.

12.4.1.3 Conclusions of Studies to Date Regarding Groundwater Transit Time. Far-field hydrologic modeling studies of the groundwater system in the basalts have been performed over the past several years by a number of independent organizations, using the hydrologic data sets available at the time each study was performed. The emphasis of some of these studies was to simulate the three-dimensional groundwater head patterns and to estimate flow paths and travel times from a hypothetical repository location to the biosphere. The major basalt formations were generally represented as multilayer confined aquifer systems extending across the Pasco Basin. Two of these studies were one-dimensional analyses using assumed flow paths and head gradients. The results of these studies are briefly summarized in Table 12-13. There is a variety of streamline orientations and travel times. These variations result from somewhat different data sets and different assumptions used in the modeling process. Particularly important in terms of the difference are the estimates of boundary conditions and hydraulic conductivity values and ratios. Additional hydrologic data are needed to demonstrate a satisfactory understanding of the flow path orientations and transit times.

TABLE 12-13. Summary of Pre-Waste-Emplacement Travel Time Estimates.

Study	Year	Distance traveled* (km)	Travel times (yr)
Early Rockwell	1979	15	20,000 - 100,000
LATA/Intera	1979	10	34,000
PNL (AEGIS)	1979	8	13,000 - 17,000
Rockwell/RMA	1981	65	>100,000
WOOD/SALTER	1980-1982	10	~30,000
TASC	1982	60	60,000 - 7,000,000

AEGIS -Assessment of Effectiveness of Geologic Isolation System Program

Intera -Intera Environmental Consultants

LATA -Los Alamos Technical Associates

PNL -Pacific Northwest Laboratory

RMA -Resource Management Associates

Rockwell-Rockwell Hanford Operations

TASC -The Analytic Sciences Corporation

*Distance from reference repository location to Columbia River, except for WOOD/SALTER, which is the distance to the accessible environment boundary.

Recently, a modeling task force has been organized to understand the differences and resolve them to the degree possible. The differences in the preliminary models have served as useful catalysts in focusing upon important areas of uncertainty and in greatly improving the understanding of the groundwater flow patterns in the deep basalts.

Even with the different assumptions used and in light of different organizations performing these analyses, the pre-waste-emplacement travel times calculated to date are significantly longer than the NRC proposed technical criteria (NRC, 1981) of 1,000 years minimum travel time from the repository to the accessible environment.

The uncertainty of the far-field groundwater transit time calculations is briefly discussed in Section 12.4.5.

Although a PATH 3D model run was not performed using the middle Sentinel Bluffs flow as the repository horizon, it is expected that the pathway would be in the same general direction and the travel time would be in the same range (greater than 10^5 years) as with the Umtanum flow as the repository horizon. This expectation is based primarily upon the non-vertical head profiles (small gradients) existing in the Grande Ronde and Wanapum Basalts throughout much of the Cold Creek syncline area. A comparison between the Umtanum and middle Sentinel Bluffs flows will be performed as part of the next series of far-field model analyses using the latest data and conceptual models.

12.4.2 Very Near-Field Studies to Assess Compliance with U.S. Nuclear Regulatory Commission Proposed Technical Criteria for Repository Releases

12.4.2.1 Scope. A preliminary performance assessment of the basalt site was performed by Salter et al. (1982) to determine the hazardous radionuclides that could be released from a repository in basalt and to estimate the maximum permissible release rates for various radionuclides from the engineered system to the accessible environment. These releases can then be compared to current draft regulatory criteria; required radionuclide releases that the site cannot meet will define the required engineered system performance of the repository. The criterion used to define these release rates is that the cumulative release of radionuclides must meet appropriate EPA (1981) regulations.

12.4.2.2 Scenarios and Methodology. A simple, one-dimensional transport model (Haderman, 1980) was used to evaluate the release of radionuclides from the repository. Both expected (normal) condition and disruptive condition scenarios were considered in estimating the maximum radionuclide release rates. The two scenarios and assumptions used in the analyses are as follows:

Case I: Nondisruptive Phenomenon: Transport through a basalt flow top to the accessible environment.

Assumptions:

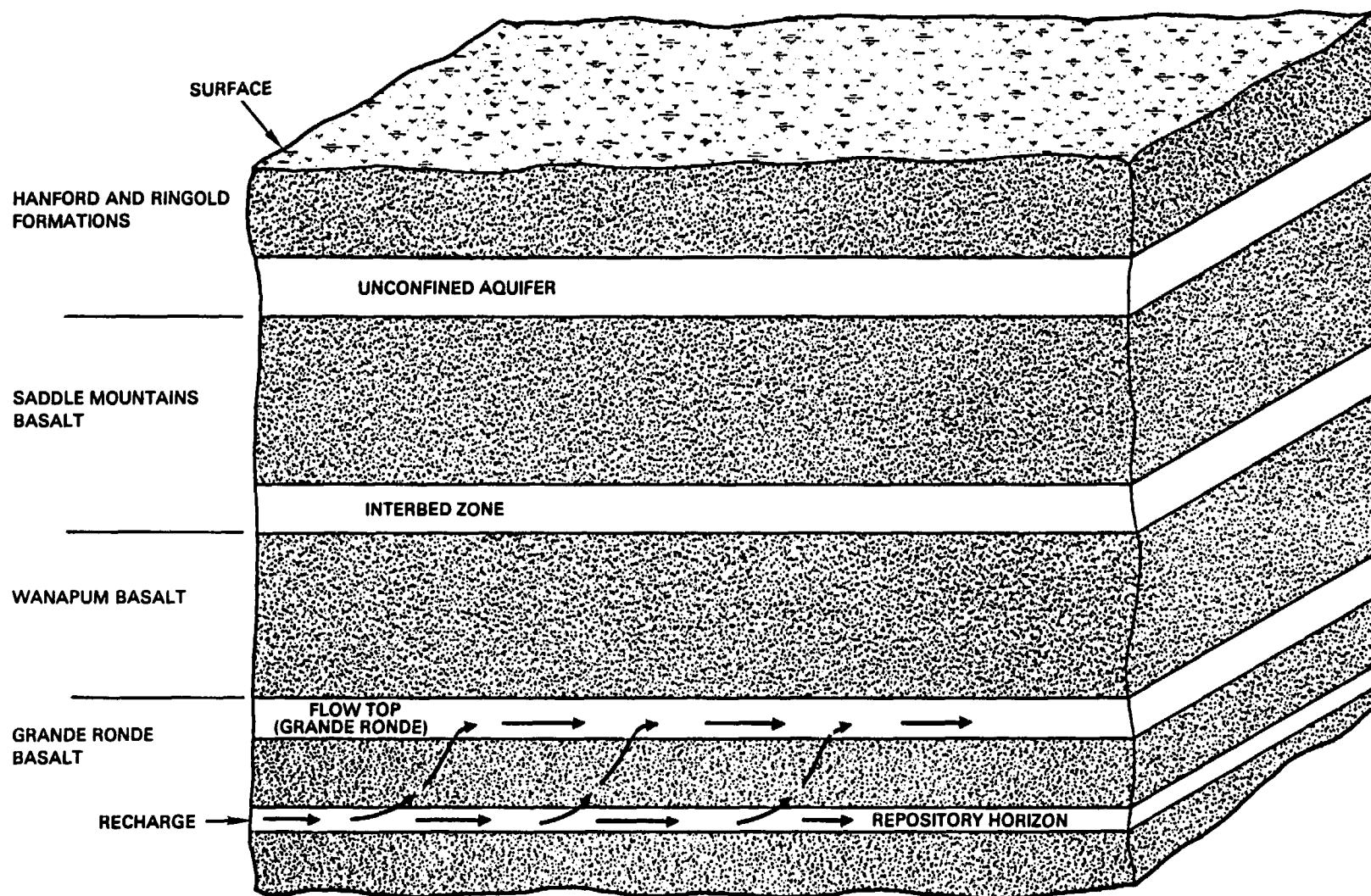
- A 10-kilometer distance was used as a reference flow path.
- A groundwater velocity of 0.32 meter per year was assumed.
- An effective porosity of 0.01 was assumed for the basalt.
- Zero transport time to the water-bearing zone (flow top) from the Umtanum candidate repository horizon was assumed.
- Waste form containment for all waste packages was assumed to cease after 1,000 years, and subsequent release of radionuclides would be solubility limited (see Sections 11.3.2.4 and 6.4.1).
- No thermal effects were considered.
- A waste inventory equivalent to 46,500 metric tons of heavy metal was assumed.
- Minimal radionuclide retardation (sorption) by basalt (see Section 6.4.2) was assumed.

Case II: Disruptive Phenomenon: Transport through an interbed zone (confined aquifer) to the accessible environment.

Assumptions:

- A 10-kilometer flow path to the reference boundary was assumed.
- A groundwater velocity of 7.9 meters per year was assumed.
- An effective porosity of 0.2 was assigned to the interbed zone.
- Zero travel time to the interbed zone from the Umtanum candidate repository horizon was assumed.
- All other assumptions were the same as in Case I.

Schematic representations of Cases I and II are presented in Figures 12-10 and 12-11, respectively. Case II is essentially a model of a vertical fault intersecting the repository horizon. It is important to note that both the scenarios considered represent very conservative analyses of repository performance, since containment for all waste packages



RCP8109-264

FIGURE 12-10. Schematic Representation of Groundwater Flow Path for Case I.

12.4-27

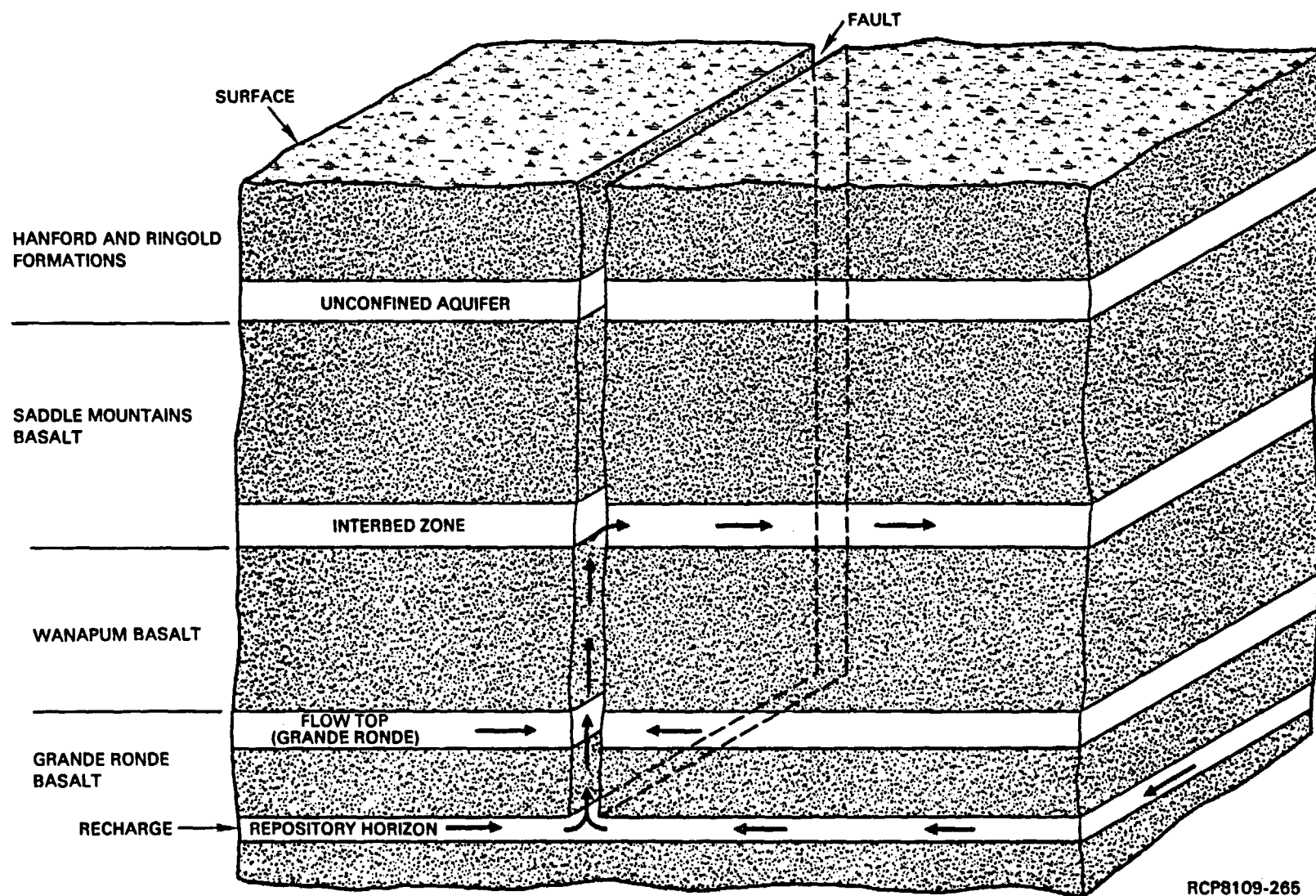


FIGURE 12-11. Schematic Representation of Groundwater Flow Path for Case II.

was assumed to fail simultaneously in a water-saturated repository 1,000 years after closure. Furthermore, radionuclide solubilities rather than leach rates are used to limit radionuclide release because they are relatively time independent and represent the maximum amount of a given radionuclide that can be in solution at any one time (see Section 6.4.1). In addition, by assuming zero travel time to the water-bearing zone, the model essentially places the repository in a water-bearing zone (Case I) and in a confined aquifer (Case II).

12.4.2.3 Results. The results of these preliminary analyses are discussed in detail in Section 11.3.2.4 and only a summary is presented here. Potential problem (mobile) radionuclides for a repository in basalt initially were determined by assuming no solubility constraints on radionuclide release. Those radionuclides requiring a release rate of less than 10^{-3} per year of their inventory to meet EPA draft regulations (EPA, 1981) are considered to be potential problem radionuclides. A release rate of 10^{-3} per year is 100 times larger than the maximum annual release of 10^{-5} in the NRC proposed regulations (NRC, 1981).

From this very conservative analysis, the following basic results were obtained for the case of no-solubility limitation (see Chapter 11, Tables 11-25 and 11-26):

- For the no-disruption scenario, a release rate of 10^{-3} per year or less was required for: ^{14}C , ^{99}Tc , ^{237}Np , and uranium isotopes and their daughter products.
- For the fault zone scenario, a release rate of 10^{-3} per year or less was required for ^{135}Cs , ^{126}Sn , ^{107}Pd , ^{234}Am , ^{242}Pu , and ^{93}Zr , in addition to the radionuclides listed for the no-disruption scenario.
- Other radionuclides in the inventory do not appear to constitute a problem of compliance with the proposed criteria and regulations, because of high sorption characteristics, short half-lives, and/or small inventory.

Under solubility-limited conditions, the transport analyses for uranium, neptunium, plutonium, and americium indicate that the release rate would be well below the NRC proposed criterion (NRC, 1981) of 10^{-5} per year (see Chapter 11, Table 11-26). Additional geochemical data for the basalt environment are needed to evaluate the release rates of other radionuclides under solubility-limited conditions.

12.4.3 Near-Field Studies to Assess Compliance with U.S. Environmental Protection Agency Draft Regulations

A preliminary long-term performance analysis for the reference repository location was conducted for the specific purposes of this document. The data used in this analysis are presented and discussed in a subsequent section. For the purposes of comparison, the long-term performance of the

repository location is examined for expected natural conditions and for a postulated disruptive event condition. Basic hydrologic state variables, such as groundwater flow paths and travel times, radionuclide concentrations, and total radionuclide activity crossing a specified boundary, are calculated for comparison with the draft regulations (EPA, 1981). The scope of the performance analysis is limited to consideration of the deep basalt in the candidate siting area within the Cold Creek syncline, and thereby does not consider the entire groundwater system beneath the Hanford Site.

Two candidate repository horizons are evaluated in this performance analysis: the Umtanum and the middle Sentinel Bluffs flows within the Grande Ronde Basalt. At the reference repository location, the middle Sentinel Bluffs flow is located about 93 meters below the Vantage interbed and 105 meters above the Umtanum flow. The purpose of considering both candidate horizons is twofold. First, it is important to determine if the candidate horizons could, in fact, meet the long-term performance requirements. Second, if both horizons indeed meet these requirements, it is beneficial to know if the hydrostratigraphic differences (flow thickness, depth from ground surface, vertical gradients, sequence of and distance to adjacent flow contacts) alone make a significant difference to waste isolation. In other words, it is important to know if one candidate horizon is much more favorable than the other.

For this near-field performance analysis, the numerical model PORFLO, described in Section 12.3.2, was applied to simulate the coupled flow and transport processes. The near field or disturbed zone is defined as the region surrounding the emplacement horizon that is affected by the presence of, and conditions in, the repository facility. The release scenarios evaluated assume the release of radionuclides during the significant thermal period. The rate and extent of waste migration are estimated for a 10,000-year period after closure.

12.4.3.1 Selection of Scenarios. The methodology for identifying and screening hypothetical release scenarios for the basalt geology has been addressed in a number of independent studies (Lee et al., 1978; Stottlemire et al., 1981; Arnett et al., 1980). The selection of primary scenarios and supporting technical rationale is described in Arnett et al. (1980). As discussed in Section 12.2.1.1, two primary scenarios were initially selected for further consequence analysis, consisting of: (1) fault near or through the repository facility and (2) shaft seal degradation or failure. Occurrence of a microearthquake swarm near the repository is also considered a potentially significant scenario. Subsequent to the work of Arnett et al. (1980), a new scenario was added to the list which assumes a permeable water-bearing zone below the repository horizon; this scenario is based on the idea that the permeable zone might act as a more direct pathway to the accessible environment.

The following bounding scenarios were selected for this performance analysis:

- (1) A no-disruption event base case
- (2) An interconnecting fault zone.

The shaft seal failure scenario is not considered here, primarily because radionuclide transport for this case is expected to be less significant than that for the fault zone case. Thus, the consequences for the shaft seal failure are conservatively bounded by those for the interconnecting fault zone scenario. In addition, the analysis of a permeable zone below the repository horizon and possibly swarm zone scenario will be addressed in future documents.

12.4.3.2 Reference Data for Near-Field Performance Analysis. Performance analyses conducted to date for a repository in basalt have been primarily limited to generic hydrologic modeling of the Cold Creek syncline siting area (Fig. 12-4). A reference data set has been compiled for the model study area using (1) available hydrologic data for deep boreholes in the Hanford Site (Chapter 5), (2) estimates of the regional head gradient developed from far-field hydrologic modeling of the Pasco Basin (Arnett et al., 1981), and (3) transport parameters reported in the technical literature (Isherwood, 1981; Guzowski et al., 1982) for similar geologies.

12.4.3.2.1 Geologic Data. The major basalt formations (Saddle Mountains, Wanapum, and Grande Ronde Basalts) comprise a stratiform or tabular geology. This geologic system is characterized by sequences of individual basalt flows that, in certain locations, are separated by pervious water-bearing horizons. A simplified stratigraphic section through these basalt formations in the model study area is shown in Figure 12-12. The stratigraphic section lists the major rock sequences and hydrologic units, which are designated as layers in the geologic conceptual model. The prefixes on the model layer numbers indicate the particular formation; e.g., GR 1 means the first layer of the Grande Ronde Basalt. The characteristics and dimensions of the rock layers in this geologic model are summarized in Table 12-14. The nominal layer thicknesses were estimated from data for boreholes RRL-4, DC-4, and -12.

The layer thicknesses assigned to the two candidate repository horizons are based on borehole RRL-2 data. In the case of the Umtanum, the thickness of the flow top and dense interior exhibit considerable spatial variability within the candidate siting area. On the basis of observations from various boreholes in the Cold Creek syncline, the average thickness for the flow top and dense interior are 17 and 42 meters, respectively. These values are more representative over the region of interest (10 kilometers); however, the data from RRL-2 are assumed to introduce conservatism in the performance analysis. The variability of layer thickness is of lesser importance for the middle Sentinel Bluffs flow; however, the dense interior of this flow exhibits a laterally extensive vesicular zone.

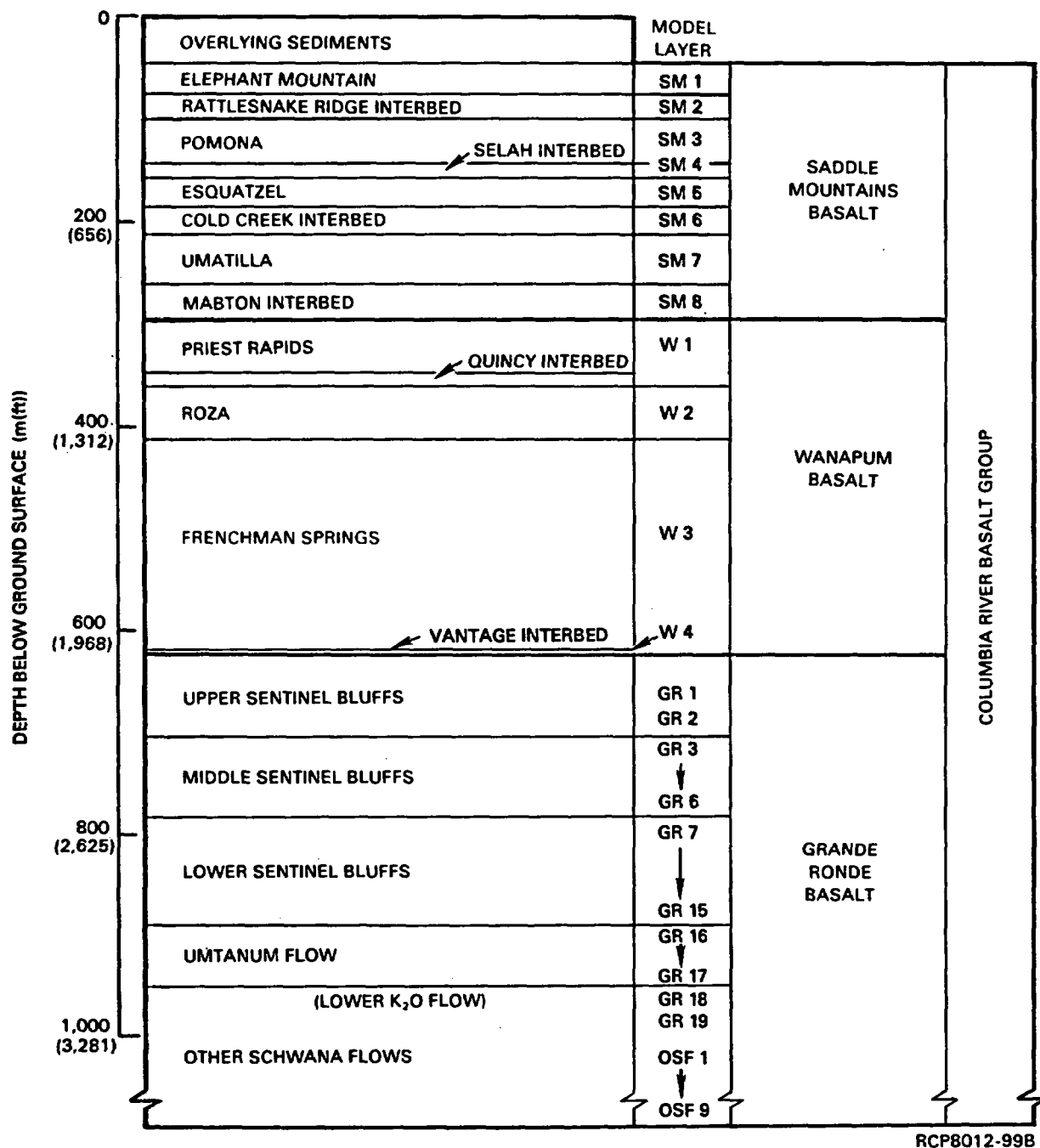


FIGURE 12-12. Simplified Stratigraphic Section for Columbia River Basalt.

TABLE 12-14. Description and Dimensions of Rock Layers for the Geologic Conceptual Model.

Formation					
Grande Ronde Basalt			Wanapum Basalt		
Member or sequence	Layer	Thickness (m) ^a	Member or sequence	Layer	Thickness (m) ^a
Sentinel Bluffs	GR-1	10.1	Priest Rapids	PR-1	50.6
Sentinel Bluffs	GR-2 FT	6.1	Priest Rapids	PR-2 FT	7.9
Sentinel Bluffs	GR-2	25.3	Priest Rapids	PR-2	10.4
Sentinel Bluffs	GR-3 FT	5.2	Roza	Roza-1 FT	3.4
Sentinel Bluffs	GR-3	46.6	Roza	Roza-1	5.4
Sentinel Bluffs	GR-4FT	4.6	Roza	Roza-2 FT ^b	3
Sentinel Bluffs	GR-4	23.5	Roza	Roza-2	40.9
Sentinel Bluffs	Vesicular ^c	8.5	Frenchman Springs	FS-1 FT	7
Sentinel Bluffs	GR-4	43.3	Frenchman Springs	FS-1	48.5
Sentinel Bluffs	GR-5 FT	10.7	Frenchman Springs	FS-2 FT ^b	3
Sentinel Bluffs	GR-5	29.8	Frenchman Springs	FS-2	31.5
Sentinel Bluffs	GR-6 FT	3.7	Frenchman Springs	FS-3 FT	3.4
Sentinel Bluffs	GR-6	5.3	Frenchman Springs	FS-3	13.1
Sentinel Bluffs	GR-7 FT	4.7	Frenchman Springs	FS-4 FT ^b	3
Sentinel Bluffs	GR-7	12.8	Frenchman Springs	FS-4	30.5
Sentinel Bluffs	GR-8 FT	5.8	Frenchman Springs	FS-5 FT	8.2
Sentinel Bluffs	GR-8	32	Frenchman Springs	FS-5	24.7
Schwana	Umtanum FT ^d	47.6	Frenchman Springs	FS-6 FT	3.4
Schwana	Umtanum	25.6	Frenchman Springs	FS-6	35.6
Schwana	GR-10 FT	7	Frenchman Springs	FS-7 FT ^b	3
Schwana	GR-10	8.9	Frenchman Springs	FS-7	17.1
Schwana	GR-11 FT	11.9			

FS-Frenchman Springs

FT-Flow top

GR-Grande Ronde

PR-Priest Rapids

^aLayer thicknesses are based on stratigraphy from borehole RRL-2 unless otherwise noted.^bMinimal layer thickness is 3 m due to consideration of the grid aspect ratio during preparations of input for numerical simulations.^cVesicular zone in middle Sentinel Bluffs though-runner is based on stratigraphy from borehole DC-4.^dUmtanum flow-top thickness is not laterally extensive (c.f., stratigraphy from boreholes DC-3 and -12).

Field testing of this unique feature indicates that it may be of little or no hydrologic significance. However, for conservatism, the vesicular zone is modeled as a relatively transmissive feature.

A number of basic assumptions were made in developing the geologic model for the reference repository location. The fundamental assumptions were:

- (1) Within the model study region, the rock layers are laterally extensive and homogeneous.
- (2) Each rock layer is horizontal and has uniform thickness.
- (3) The hydraulic properties assigned to each rock layer are representative of the average or most probable values.
- (4) No undetected geologic features exist that would alter the pattern of regional groundwater flow.

Some of these assumptions were made to simplify the computer modeling problem, but they are also considered compatible with the amount of site-specific information currently available to describe the hydrologic system at the scale of interest.

12.4.3.2.2 Hydrologic Data. To analyze the performance of a repository in this type of system, a basic set of hydrologic parameters are required. These consist of: (1) hydraulic conductivities, (2) hydraulic heads and gradients, (3) specific storage coefficients, (4) porosities, (5) sorption coefficients, (6) mass dispersivities, and (7) groundwater temperatures. The model parameters and coefficients assigned for the reference repository location are presented in this section.

12.4.3.2.2.1 Hydraulic Conductivity. More than 100 measurements of hydraulic conductivity have been made to date from some 30 shallow and deep boreholes on the Hanford Site (Chapter 5). The representative or mean values for horizontal hydraulic conductivity are estimated to be 10^{-7} meter per second for flow contacts and 10^{-11} meter per second for the dense columnar portion of basalt flows. The horizontal hydraulic conductivity assigned to the flow contacts was obtained by characterizing the statistical properties of the field data for the Grande Ronde Basalt. The 50-plus data values were found to closely follow a log-normal distribution. The mode of the distribution, which is the "most probable" value, is slightly less than 10^{-7} meter per second. With regard to the hydraulic conductivity of the dense interiors, the measured data for the Grande Ronde Basalt indicate a range from 5×10^{-12} to 5×10^{-14} meter per second. Thus, the adopted value of 10^{-11} meter per second is a conservative assumption. The vesicular zone in the middle Sentinel Bluffs flow is assigned a hydraulic conductivity of 10^{-8} meter per second. This is done for conservatism, although recent measurements of the hydraulic conductivity of the vesicular zone in borehole RRL-2 result in much smaller values.

In assigning hydraulic conductivities to the rock strata in the geologic model, the following general assumptions are made:

- (1) The hydraulic conductivity of the flow contacts is isotropic with a uniform value of 10^{-7} meter per second.
- (2) The horizontal hydraulic conductivity in the dense basalt flows is 10^{-11} meter per second; vertical hydraulic conductivity is 10^{-10} meter per second.

With regard to the first assumption, it is important to note that there is some evidence that basalt flow contacts may be anisotropic. Rocha and Franciss (1977), for example, found the anisotropy ratio (ratio of vertical-to-horizontal hydraulic conductivity) in a basalt breccia to be less than 0.1. If this degree of anisotropy is typically the case, then the assumption of isotropy is on the conservative side. Concerning the second assumption, the anisotropy ratio for the dense interiors was assigned a value of 10. Recent statistical modeling (Sagar and Runchal, 1982) of fracture sets characteristic of basalt suggests a maximum anisotropy ratio of 3.5.

No attempt is made here to assign distinct values to individual rock layers except for the Vantage interbed and the vesicular zone in the middle Sentinel Bluffs flow; these values are 3×10^{-7} and 10^{-8} meter per second, respectively.

12.4.3.2.2 Hydraulic Heads and Gradients. The available data (Chapter 5) indicate that the regional (horizontal) hydraulic gradient ranges between 10^{-3} and 10^{-4} , and vertical hydraulic gradients across the three formations fall in the same range. Vertical (upward) head gradients across the Umtanum flow range between 10^0 and 10^{-2} . Although most of the head profiles indicate a slight upward vertical gradient, localized downward gradients are also observed. Borehole DC-15, for example, indicates a downward vertical gradient across the Umtanum flow of about 10^{-1} . A large downward head gradient is a favorable condition, since it inhibits the potential upward movement of radionuclides from the repository.

The following basic assumptions are made to provide initial and boundary conditions for the groundwater flow system in the geologic model:

- (1) The regional (horizontal) head gradient across the model study region is a constant value of 10^{-3} .
- (2) The vertical head profile measured at borehole RRL-2 is representative across the model study area.

With regard to the first assumption, recent modeling of the three-dimensional groundwater flow in the Pasco Basin (Arnett et al., 1981) provides supporting information on the magnitude of the regional gradient in the reference repository location. The vertical head profile is shown in Chapter 5 (Fig. 5-41).

12.4.3.2.2.3 Specific Storage Coefficients. At the present time, only a few reliable values for storage coefficients are available for the Columbia River basalts. These values, as explained in Chapter 5, clearly reflect the characteristics of a confined aquifer system. The specific storage coefficient value assumed for the flow contacts is 10^{-4} . For the dense basalt flows, specific storage coefficient values of about 10^{-7} are assumed; this particular value was computed using the fluid (water) and rock compressibility data.

12.4.3.2.2.4 Porosities. As indicated in Chapter 5, only one in situ measurement of effective porosity is available for the deep basalt in the candidate siting area. The effective porosities are assumed to be 0.01 for the flow contacts and 0.001 for the dense basalt flows which is consistent with values reported in the technical literature (Isherwood, 1981; Guzowski et al., 1982). These values are believed to be representative of, if not smaller than, the values expected for the Columbia River Basalt Group; see Chapter 5, especially Section 5.2.1.2. By assigning low porosity values, groundwater and radionuclide travel times can be conservatively estimated.

12.4.3.2.2.5 Sorption Coefficients. In the performance analysis conducted for this document, the long-term predictions of waste migration considered one key radionuclide, ^{14}C . This radionuclide was selected because of its relatively long half-life, high specific activity, radiological significance, and mobility in groundwater (no sorption in basalt). Data on sorption coefficients for this and other radionuclides are presented in Chapter 6.

12.4.3.2.2.6 Mass Dispersivities. Mass dispersivities reflect the characteristic scale of mixing in a hydrogeologic system produced by the process of hydrodynamic dispersion (Neuman et al., 1979). The available literature on dispersion in fractured rocks (Isherwood, 1981) is very limited and, moreover, indicates a divergence of opinion on the magnitude of dispersivities. For the purposes of this analysis, the values assumed are: (1) $\alpha_L = 50$ meters and $\alpha_T = 2$ meters for the flow contacts and (2) $\alpha_L = 2$ meters and $\alpha_T = 0.2$ meter for the dense basalt flows.

12.4.3.2.2.7 Groundwater Temperatures. The groundwater temperature measurements for various shallow and deep wells on the Hanford Site are presented in Chapter 5. From these data the average geothermal gradient has been estimated to be about 40°C per kilometer. A linear variation of groundwater temperature with depth is assumed, so as to provide initial and boundary conditions for the thermal regime of the model study region.

12.4.3.2.3 Thermomechanical Data. A basic set of parameters is needed to model the coupling or interdependence between hydrologic, thermal, and mechanical (stress/strain) processes. The specific parameters applicable to this performance analysis are presented and discussed in Chapter 4.

12.4.3.2.4 Repository Data. The proposed repository is assumed to be located in the dense central portion of the candidate horizon. The current conceptual design of the repository facility consists of two sections separated by a horizontal distance of 830 meters. The rooms of the repository would be 3 meters high and 6 meters wide with the canisters placed horizontally (see Chapter 10) in the walls. The room backfill in the repository is assumed to be a mixture of crushed basalt and bentonite clay.

With regard to the hydraulic and thermal properties of the backfill material, the following values are assumed: (1) hydraulic conductivity is 10⁻¹⁰ meter per second; (2) effective porosity is 0.01; (3) density is 2,780 kilograms per cubic meter; (4) specific heat capacity is 920 joules per kilogram °C; (5) thermal conductivity is 2.2 joules per meter second °C; (6) longitudinal and transverse dispersivities are 2.0 and 0.2 meters, respectively; and (7) sorption is zero.

The spent fuel inventory is assumed to be one-half of the year 2000 projection for the United States' commercial nuclear industry, which is approximately 47,000 metric tons of heavy metal. This inventory would be contained in some 24,000 canisters. Each canister would have a peak power output of about 1.7 kilowatts, producing a maximum areal thermal loading of 14 watts per square meter of panel (see Chapter 10).

12.4.3.3 No-Disruption Base Case. It is recognized that the final selection of a specific repository site in basalt (or in any other geologic medium) will be based on rigid performance criteria that will ensure the safe and long-term isolation of the waste inventory. One intuitively expects, however, that tens of thousands of years after closure the process of groundwater ingress to the repository will eventually produce some degradation of the waste package, gradual leaching of the waste form, and the migration of dissolved radionuclides through the engineered barriers. The degree of waste isolation achieved by the repository system will depend upon the rate of leaching and the rate of migration from the repository to the accessible environment.

12.4.3.3.1 Scenario Basis. The no-disruption base case scenario, simply stated, represents the expected performance of the repository system under unperturbed geologic conditions. In defining the base case scenario, the following assumptions are made regarding the nature of the release sequence and the properties of the reference repository:

- (1) The repository contains 10-year-old spent fuel.
- (2) The repository system is completely backfilled and shafts are plugged and sealed.
- (3) The waste package and engineered barriers retain integrity for 1,000 years after closure, after which the waste release is initiated; i.e. all canisters fail simultaneously after 10,000 years.

- (4) The radionuclides are released to the groundwater in the repository at a constant fractional rate of 10^{-5} per year.

The last two scenario assumptions are consistent with the technical criteria proposed by the NRC (1981).

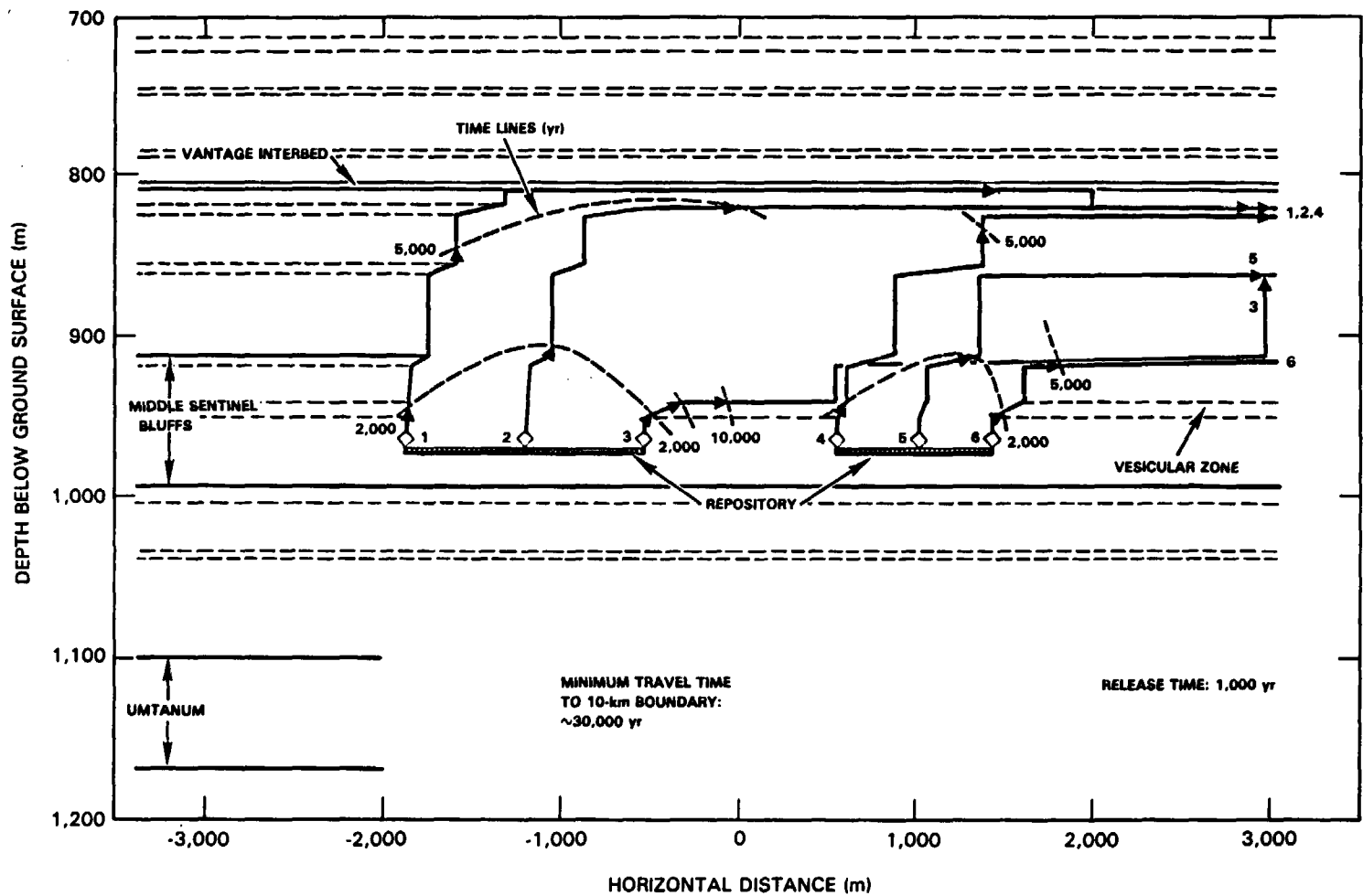
12.4.3.3.2 Groundwater Pathline and Travel Times. Pathlines, which are the trajectories of particles moving with the groundwater, provide a detailed representation of the principal pathways of potential waste movement. The cumulative time of travel along any pathline is simply the associated groundwater travel time. By connecting points of equal time along a set of pathlines, a visualization of the flow field or flow fronts between the bounding pathlines is also obtained.

12.4.3.3.2.1 Repository in Middle Sentinel Bluffs Flow. The pathline patterns predicted for this candidate repository horizon generally show an upward flow direction in the zone of thermal influence (see Fig. 12-13). The dominant upward flow velocity component producing this effect is buoyancy driven; i.e., the fluid density changes by virtue of the temperature field creating an upward driving force. As the pathlines traverse a flow contact, they exhibit a "stair-step" pattern; this refraction of the pathlines is an expected feature (Freeze and Cherry, 1979) and is the result of the large permeability contrasts (3 orders of magnitude) between the flow contacts and dense basalt flows.

Outside the zone of thermal influence, the pathline patterns are controlled by the natural head gradients. In this region, the pathline directions are predominantly horizontal and, as a result, remain in the flow contacts for some distance. Over a 10-kilometer distance or greater, the pathlines would be expected to move upward as the vertical head gradient becomes greater than the regional head gradient.

The time lines above the repository sections (see Fig. 12-13) show a relatively well-developed flow front. The travel times along the pathlines are determined by the spatial and temporal variations in groundwater velocities. The maximum and minimum travel times to the 10-kilometer boundary are estimated to be 40,000 and 30,000 years, respectively. Since these travel times are significantly longer than the waste isolation period of interest, they basically assure compliance with the EPA draft regulations (EPA, 1981); i.e., the total activity crossing the 10-kilometer boundary in 10,000 years would be zero for all radionuclides.

12.4.3.3.2.2 Repository in Umtanum Flow. The series of pathlines computed for this candidate repository horizon depict flow patterns quite distinct from the previous case. As can be seen in Figure 12-14, the large flow contact (assumed for conservatism) of the Umtanum flow is the controlling feature. All but two pathlines are effectively "trapped" in the flow contact where they would remain for very long distances (e.g., 10 kilometers or more). The significance of this large flow top is that it minimizes the effects of buoyancy. More importantly, the flow contact becomes the path of least resistance for groundwater movement.



RCP8209-166

FIGURE 12-13. Groundwater Pathlines and Travel Times for Middle Sentinel Bluffs Flow: No-Disruption Base Case.

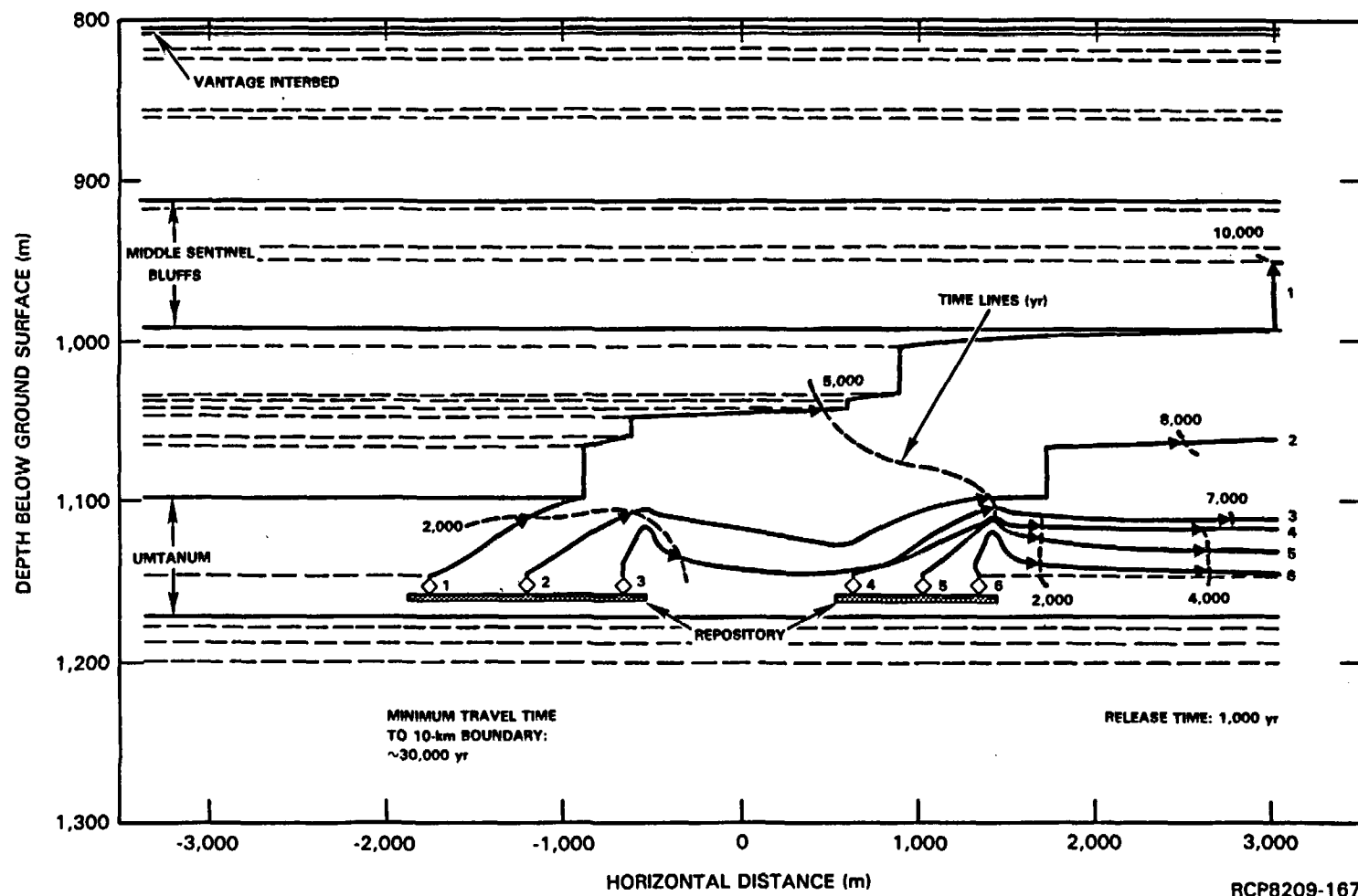


FIGURE 12-14. Groundwater Pathlines and Travel Times for Umtanum Flow; No-Disruption Base Case.

One other unique feature of these flow patterns is that there is the ascending then descending trajectories of the outermost pathlines. This basically indicates that the flow field is very near to setting up a recirculating flow system. The combined effects of buoyancy driving force, pore pressure buildup, and low hydraulic gradients below the Umtanum create a condition where the flow through the smaller repository section is virtually supply limited.

Time lines for this case show a rapid transition to horizontal flow. Whereas the results in Figure 12-14 assume a release time of 1,000 years after closure, releases at later times would show nearly co-flowing pathlines with a uniform flow front in the Umtanum flow contact. The groundwater travel times to the 10-kilometer boundary, for 1,000 years containment, are estimated to be in the range of 30,000 to 37,000 years. As in the previous case, these travel times are sufficiently long to assure compliance with the EPA draft regulations (EPA, 1981), since no activity would cross the 10-kilometer boundary in a 10,000-year time frame.

12.4.3.3.3 Radionuclide Movement. The patterns of radionuclide movement are strongly dependent on the groundwater flow paths and travel times from the repository horizon. Even though radionuclide movement is attenuated along these paths by the hydrodynamic dispersion process (microscopic mixing due to variations in flow velocities and directions), there generally exists an observable correlation between the position of the pathlines and the distribution of the radionuclide plume. Results from transport calculations for each candidate repository horizon are presented in the following set of contour plots; the plots consist of concentration contours for ^{14}C .

12.4.3.3.3.1 Repository in Middle Sentinel Bluffs Flow. Radionuclide migration from this candidate repository horizon is predominantly controlled by dispersion in the low-permeability rock layers and by convection in the pervious flow contacts. The net effects of these processes are clearly reflected in the ^{14}C concentration contours shown in Figure 12-15. At 10,000 years, the plume extends about 200 meters above the repository and about 3 kilometers from the downstream end. An elongation of the plume occurs along the flow contact where the groundwater velocities are the greatest.

The concentration levels of ^{14}C in the groundwater are relatively low because of the small initial inventory of ^{14}C and the cumulative effect of radioactive decay. The model predictions indicate that the concentrations of ^{14}C fall below the conservative maximum permissible concentration level within a few tens of meters from the repository. In the period of concern (i.e., 10,000 years after closure) radionuclide plumes are only about a third of the distance to the 10-kilometer boundary. Consequently, the time integrated mass flux would be zero. For the purpose of comparing the two candidate repository horizons, the mass flux was calculated for the near-field boundary at 1.6 kilometers; the total

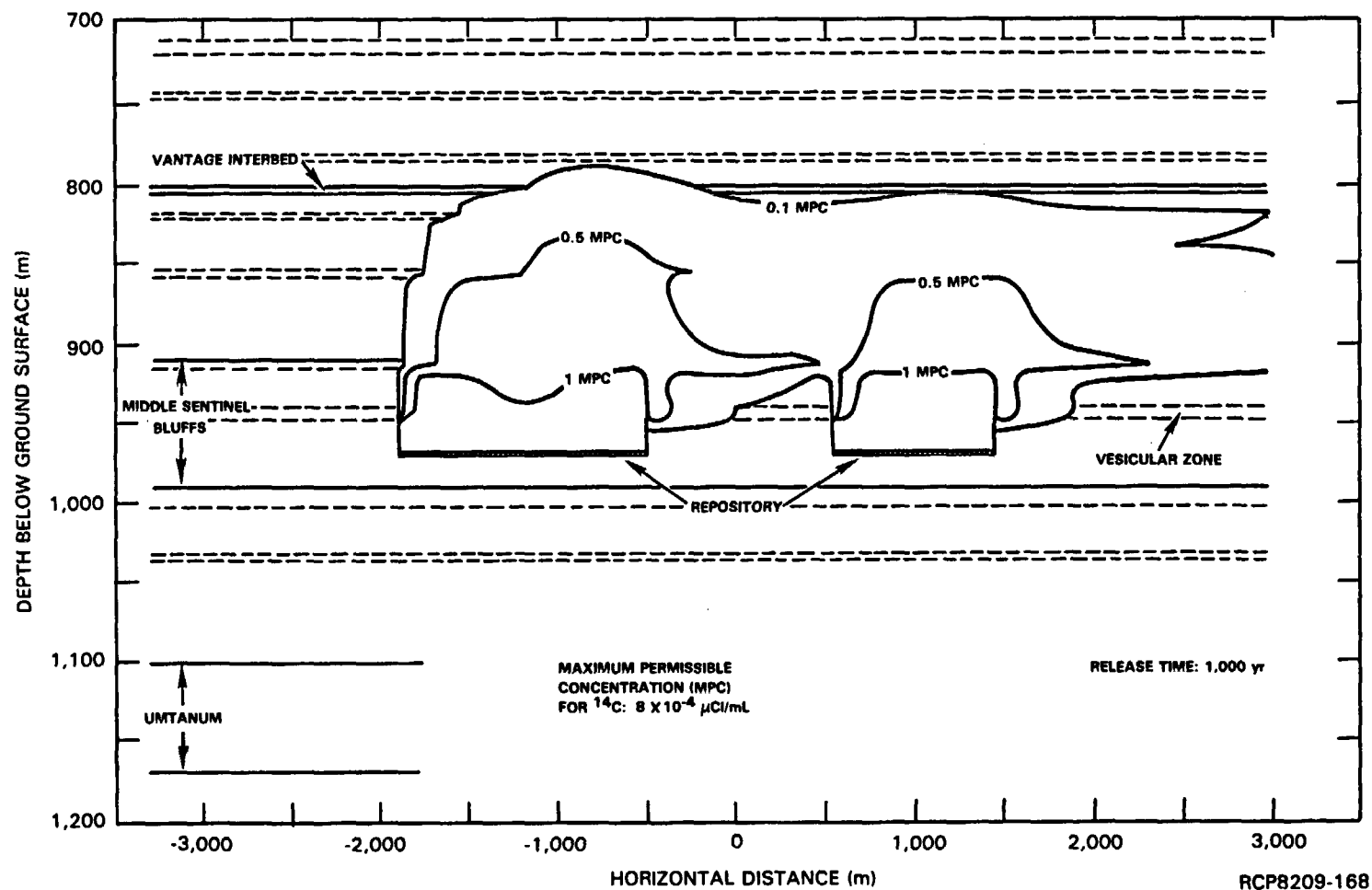


FIGURE 12-15. Carbon-14 Concentration Contours at 10,000 Years for Middle Sentinel Bluffs Flow: No-Disruption Base Case.

activity of ^{14}C crossing this boundary is less than 4.0 curies per 1,000 metric tons of heavy metal. As discussed previously, the total activity crossing the 10-kilometer boundary in 10,000 years is zero. The EPA draft regulations (EPA, 1981) set a maximum release for ^{14}C of 200 curies per 1,000 metric tons of heavy metal.

12.4.3.3.2 Repository in the Umtanum Flow. The radionuclide migration patterns for this candidate repository horizon are shown in Figure 12-16. Consistent with the calculated groundwater pathlines, the movement of the plume is controlled by the Umtanum flow top. At 10,000 years, the ^{14}C plume extends about 150 meters above the repository and approximately 3 kilometers from the downstream end.

Concentration levels of ^{14}C are below the maximum permissible concentration for the major portion of the plume. These low concentrations are due to the enhanced dilution in the Umtanum flow top, as well as the effects of decay and the low initial inventory. Since the plume extends only a few kilometers along the flow contact, the time integrated mass flux at 10,000 years would be zero. At the 1.6-kilometer boundary, the mass flux of ^{14}C is estimated to be less than 7.0 curies per 1,000 metric tons of heavy metal. This amount is only slightly larger than the mass flux estimated for the other candidate repository horizon.

The effective thicknesses assigned to the Umtanum flow top and dense interior (based on borehole RRL-2 data) were initially chosen to introduce conservatism. However, these calculations suggest that the mass flux is relatively insensitive to these values. This is probably due to the conservative assumption of a 10-to-1 anisotropy ratio for the dense interiors.

12.4.3.4 Interconnecting Fault Scenario.

12.4.3.4.1 Scenario Basis. The occurrence of a vertically extensive fault in the siting area could potentially create a hydraulic interconnection between the repository horizon and any pervious water-bearing zones (i.e., flow contacts or interbeds). Under such conditions, the vertical movement of radionuclides would be expected to be faster than in the unperturbed case. The impact on the overall waste isolation system, however, depends on the actual size and extent of the discontinuity, its specific location in relation to the repository, and the hydraulic properties of the infilling gouge material. Location of the fault is of particular importance, since a discontinuity through the repository rooms would have relatively greater impact than the case where it would be located at some nominal distance from the repository.

Within the context of a near-field disruptive event scenario, a plausible situation is to consider a macroscale discontinuity of limited extent. The specific hypothetical conditions assumed for this scenario are:

- (1) A fault develops immediately after closure and is located at 0.8 kilometer (0.5 mile) from the downstream end of the repository.

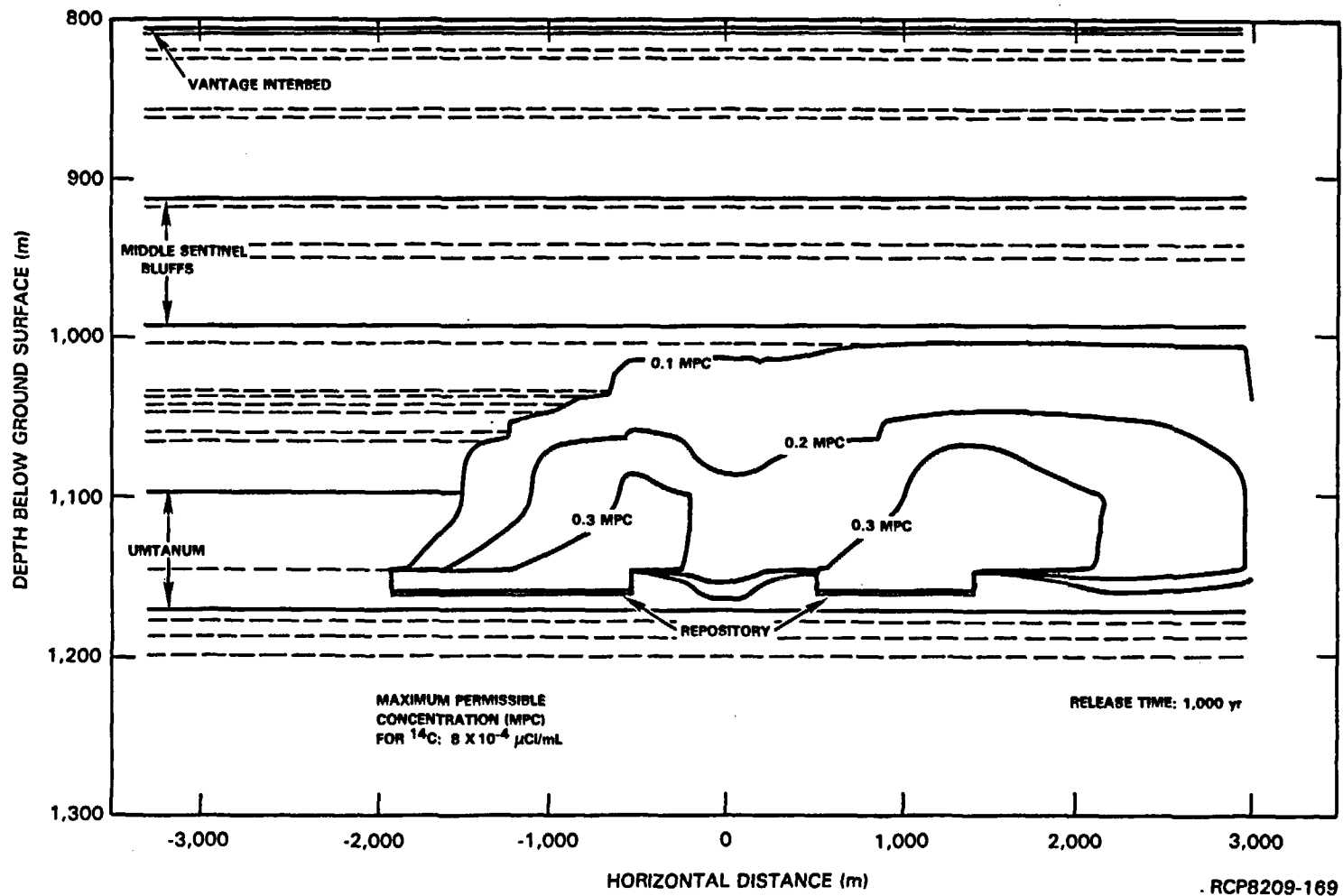


FIGURE 12-16. Carbon-14 Concentration Contours at 10,000 Years for Umtanum Flow: No-Disruption Base Case.

- (2) The fault creates a hydraulic interconnection between the candidate repository horizon and the Vantage interbed.
- (3) The fault is vertical with a gouge zone 20 meters wide filled with porous material.
- (4) The properties of the fault zone consist of a hydraulic conductivity of 10^{-7} meter per second and an effective porosity of 10^{-3} .

12.4.3.4.2 Groundwater Pathlines and Travel Times

12.4.3.4.2.1 Repository in Middle Sentinel Bluffs Flow. As seen in Figure 12-17 the pathline orientations and travel times are fundamentally insensitive to the presence of the fault. This may be explained by the low natural vertical head gradient, which may be further reduced or even reversed by certain portions of the thermally induced groundwater circulation pattern (convective cell) near the ends of the repository. Pathline 6 is seen to actually move downward after reaching the fault as a result of the increased vertical conductivity and the fact that it enters the downward leg of the thermally induced circulation pattern. Outside the zone of thermal influence, the fault acts as a partial barrier to horizontal flow (pathline 3). The travel times of the pathlines to the 10-kilometer accessible environment boundary were calculated to range from approximately 30,000 to 41,000 years.

12.4.3.4.2.2 Repository in Umtanum Flow. The fault has produced a slightly more discernible effect in the case of the Umtanum flow repository location (Fig. 12-18). Upon reaching the fault, two pathlines follow the fault upward for several tens of meters before exiting and continuing in a horizontal direction. Several others show a slight upward deflection in their essentially horizontal orientations as they cross the fault. The differences between the Umtanum flow fault case and the middle Sentinel Bluffs flow fault case can be explained in part by the existence of the large flow top above the Umtanum that modifies the thermally induced groundwater circulation pattern such that the interaction with the fault is weakened and interference with the natural upward head gradient is reduced.

The differences between the Umtanum and middle Sentinel Bluffs fault cases do not appear to be significant from a performance assessment point of view and are expected to be primarily a function of the relative locations of the repository and fault and also the extent of the thermally induced groundwater circulation. The existence of the fault does little to accelerate the groundwater moving from the repository toward the accessible environment and may even retard movement to the lateral boundary. As in the case of the middle Sentinel Bluffs flow repository location, the travel times of the pathlines to the 10-kilometer accessible environment boundary are calculated to be in the range of 30,000 to 36,000 years.

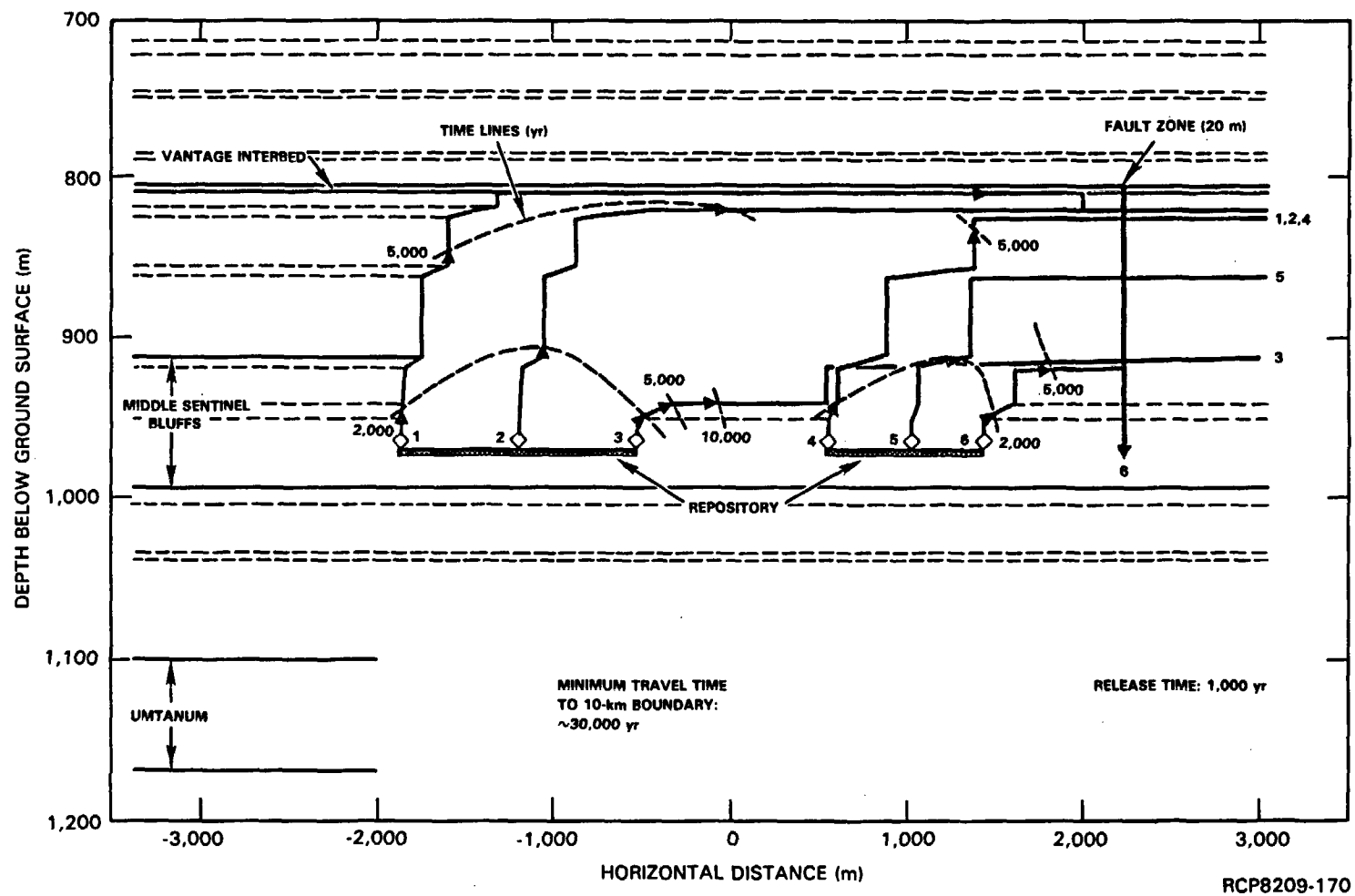


FIGURE 12-17. Groundwater Flow Pathlines for Middle Sentinel Bluffs Flow: Fault Scenario.

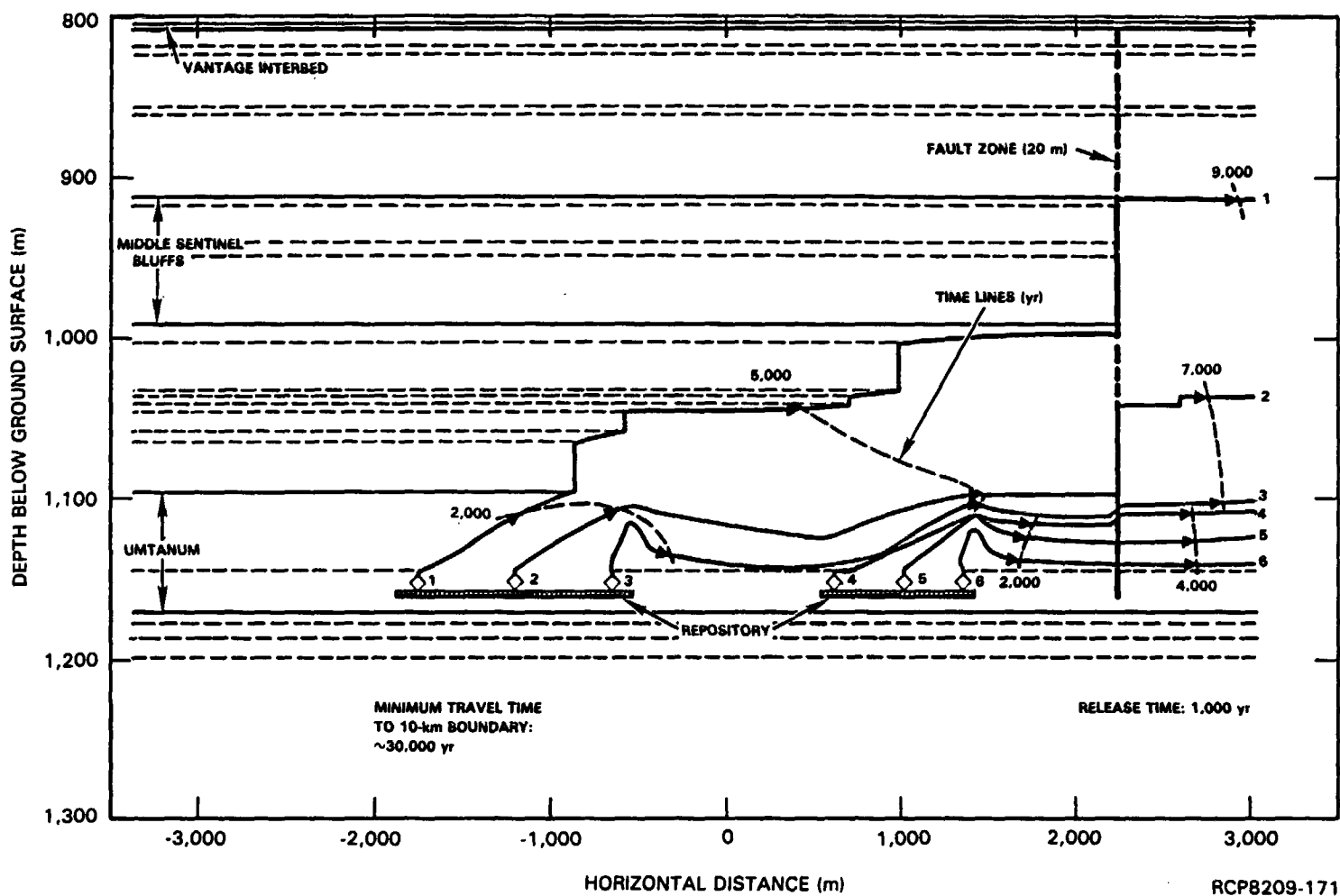


FIGURE 12-18. Groundwater Flow Pathlines for Umtanum Flow: Fault Scenario.

12.4.3.4.3 Radionuclide Movement. The existence of a fault down-gradient of the repository could be expected, in general, to redistribute a radionuclide concentration pattern over a larger vertical extent while possibly providing some mild delay in horizontal movement.

12.4.3.4.3.1 Middle Sentinel Bluffs Flow. As seen in Figure 12-19, some mild perturbations in the radioactive ^{14}C concentration patterns can be seen near the fault. Most noticeable are the downward deflections in the contour lines near the bottom of the fault. This is consistent with the orientation of pathline 6 of Figure 12-17, and is the result of the interaction of the thermally induced recirculation pattern and the higher hydraulic conductivity of the fault. As might be expected, the radionuclide flux toward the accessible environment is not significantly different from the base case. Calculations of cumulative fluxes of ^{14}C at intermediate boundaries show only small differences between the fault and base cases. As in the base case and as expected from the travel times, there is no ^{14}C cumulative mass flux at the 10-kilometer accessible environment boundary through 10,000 years.

12.4.3.4.3.2 Umtanum Flow. For the Umtanum flow, the impact of the fault is somewhat more pronounced (see Fig. 12-20) than for the middle Sentinel Bluffs case. This is explainable for the reasons given in the discussion on pathlines and travel times (Section 12.4.3.4.2) and also because the fault is longer than in the middle Sentinel Bluffs case. There are upward displacements of several of the ^{14}C concentration contours by several tens of meters, but the overall impact upon radionuclide flux toward the accessible environment is minor. As in the case of the middle Sentinel Bluffs case, there is no cumulative flux of ^{14}C at the 10-kilometer accessible environment after 10,000 years.

12.4.3.4.3.3 Evaluation. It is evident that the 20-meter fault zone does not appear to be particularly effective in moving significant amounts of radionuclides upward in the basalt sequence. This result is explained in part by the low natural vertical head gradient, which may be further reduced or even reversed in certain parts of the thermally induced groundwater circulation pattern. It is useful to note that some preliminary analyses of a fault passing directly through or at the edge of the repository have been performed. The discovery of a 20-meter fault zone during excavation of the repository would probably prompt remedial action such as reorientation of the repository panels. For this reason the presence of a preexisting fault through the repository is not considered likely. Even under such conditions, however, a fault is not effective in transferring significant amounts of radionuclides upward in the basalt sequence. In that situation, the thermal buoyancy would induce an additional component upward flow in the area around the fault. For that very reason, however, flow is parallel to the fault and a very small portion of the radionuclide released enters the fault.

Further analyses of a variety of credible conditions and parameter values are planned for both base case and disruptive scenarios.

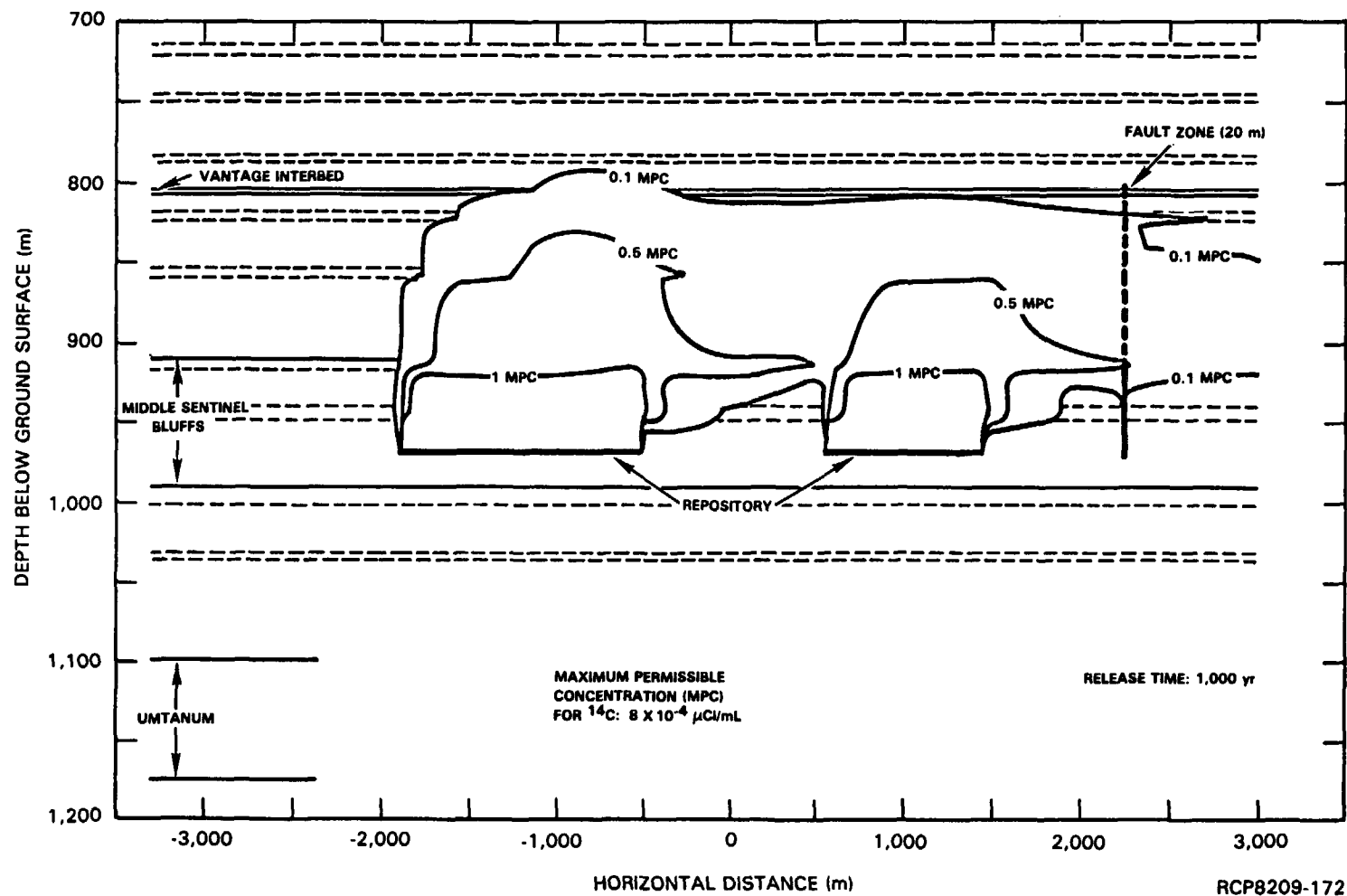


FIGURE 12-19. Carbon-14 Concentration Contours for Middle Sentinel Bluffs Flow: Fault Scenario.

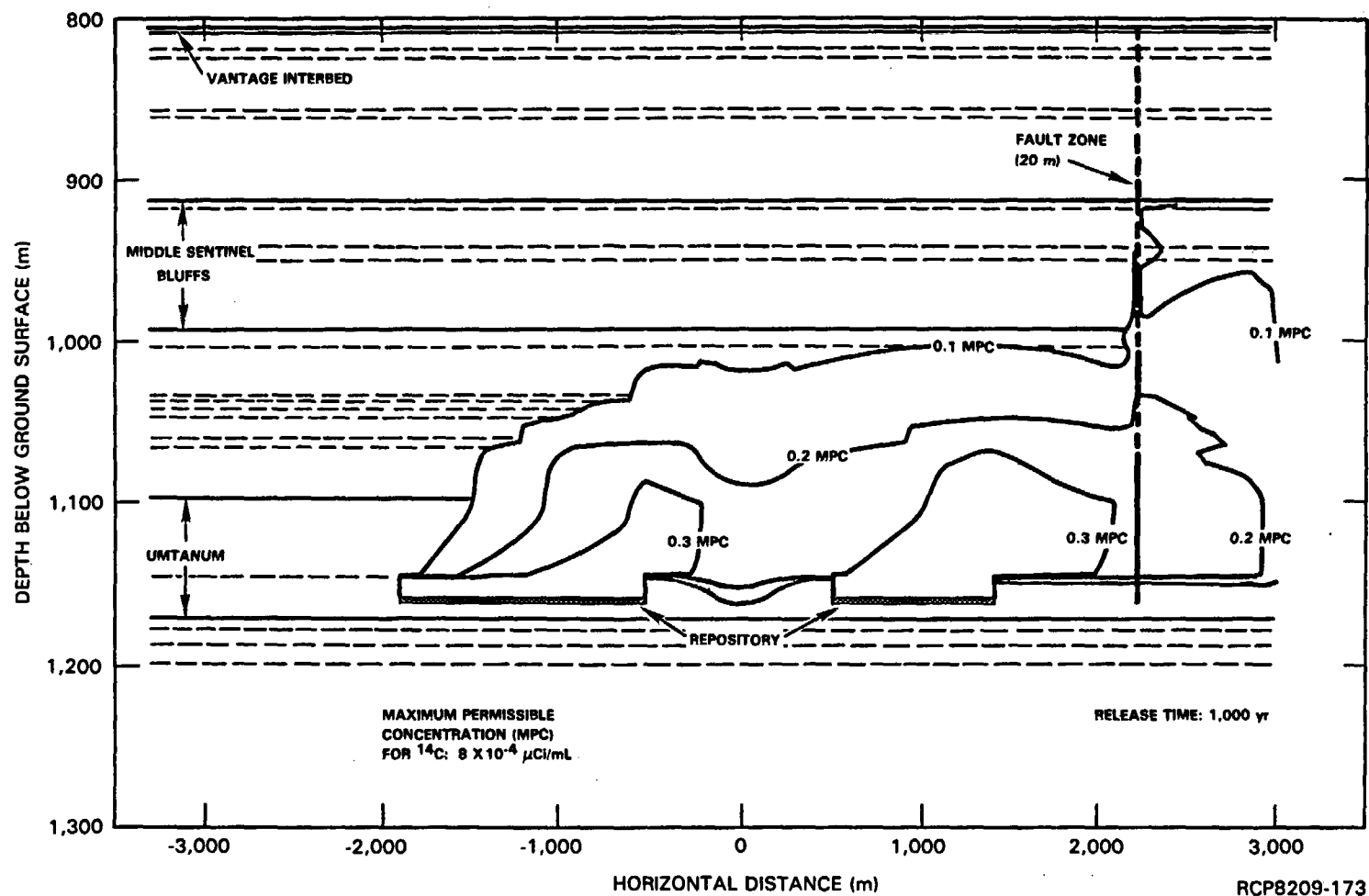


FIGURE 12-20. Carbon-14 Concentration Contours for Umtanum Flow: Fault Scenario.

12.4.3.5 Conclusions. In judging the performance of the repository system, two basic measures of performance are generally considered: (1) radionuclide releases (i.e., total activity per 1,000 metric tons of heavy metal leaving a 10-kilometer boundary) over a 10,000-year period and (2) the minimum travel time to the accessible environment. The results and findings described in the previous sections provide a basis for developing a perspective on the waste isolation capability of the basalts beneath the Hanford Site.

First, if one compares the predicted consequences for the two release scenarios, it becomes evident that the overall performance of the repository system under adverse conditions is not significantly altered or different from that predicted using anticipated geologic conditions. This fact is clearly shown by the estimates that no ^{14}C would be released to the accessible environment after 10,000 years.

Second, a comparison of the minimum groundwater travel times to the reference boundary, 10 kilometers from the repository, leads to a similar conclusion. The minimum groundwater travel times for the no-disruption base case for the fault zone are comparable and in excess of 10,000 years. These estimates are considered conservative, in that they do not include the travel time through the repository backfill, which could contribute significantly to the total travel time.

Third, in view of the fact that the two release scenarios are of a bounding nature, a natural and logical conclusion is that the overall performance of the repository system does not appear to hinge on a single hydrogeologic factor or condition. Moreover, the interdependence of the controlling physical processes can, in certain cases, offset adverse conditions. The tabular or stratiform geology of the basalts also appears to be a beneficial attribute to the long-term confinement capability of the system.

The analysis results described here represent the current technical bases, which give a quantitative indication that the repository system will perform as prescribed in the applicable technical criteria and regulations. The fact that the predicted results indicate that compliance with the criteria and regulations would be achieved with a considerable margin gives confidence to the suitability of the site selected.

12.4.4 Summary of Conclusions from Preliminary Long-Term Repository Performance Analysis

12.4.4.1 Far-Field Modeling Studies. Far-field hydrologic modeling studies of the groundwater system in the basalts have been performed over the past several years by a number of independent organizations using the hydrologic-data sets available at the time each study was performed. These studies provide an analysis of the three-dimensional groundwater head patterns and estimate flow paths and travel times from a hypothetical repository location to the Columbia River.

Even with the different assumptions used, and in light of different organizations performing these analyses, the pre-waste-emplacement travel times calculated to date significantly exceed the 1,000-year travel time from the repository to the accessible environment in the NRC proposed regulations (NRC, 1981). The uncertainty of the far-field groundwater transit time calculations is discussed in Section 12.4.5.

12.4.4.2 Very Near-Field Modeling Studies. The modeling studies completed to date have emphasized the estimation of waste package performance requirements. Simulation studies of the very near field clearly reflect the favorable geochemical environment of the basalt. In particular, the reducing (anoxic) environment of the deep basalt increases the stability of the canisters and significantly decreases the solubility of many key radionuclides.

The primary conclusions developed from the available modeling studies (Wood, 1980; Salter et al., 1982) are as follows:

- Solubility of radionuclides limits the repository release rates to levels well below the NRC proposed criteria (NRC, 1981), particularly for such radionuclides as technetium, americium, neptunium, and plutonium.
- There is no incentive for a complex waste package with an extended containment capability.
- High sorptive properties of basalt will retard the movement of radionuclides such as cesium, strontium, radium, and americium.

12.4.4.3 Near-Field Modeling Studies. Modeling studies for the reference repository location have been performed that predict groundwater and radionuclide pathways and travel times. Performance analysis models that describe the coupled processes of heat transfer, fluid flow, and radionuclide transport have been applied using representative hydrologic data obtained from field testing. These near-field simulations generally indicate that the groundwater flow paths are controlled by the occurrence and hydraulic characteristics of the basalt flow contacts above the candidate repository horizon. This trend is expected because groundwater will follow the path of least resistance, which is primarily along the pervious flow contacts.

With regard to waste isolation effectiveness, the results of the near-field performance analysis support the following conclusions:

- The post-waste-emplacement groundwater travel times from the repository to the reference boundary (10 kilometers from the edge of the repository) are estimated to be greater than 10,000 years, ignoring the travel time through the engineered barriers.
- The groundwater flow paths from both candidate repository horizons are predominantly horizontal and are restricted to the Grande Ronde Basalt.

- The transport of mobile long-lived radionuclides, such as ^{14}C , is limited to about 200 vertical meters and less than a few kilometers horizontally after 10,000 years.
- The radionuclide release across a reference boundary (at 10 kilometers) appears to remain well below the EPA draft regulations (EPA, 1981) for both no-disruption and postulated fault zone conditions.

12.4.5 Assessment of Uncertainty in Performance Assessment Results

To develop a general perspective on the meaning and significance of the performance assessment results obtained to date, it is important to identify and discuss those aspects that contribute to predictive uncertainty. In this section, we review the three basic performance assessment issues and discuss those factors that constrain the expectations of compliance with the criteria and regulations.

12.4.5.1 Groundwater Travel Time. The various hydrologic modeling studies, described in the previous sections, indicate different flow paths and a range of travel times from the repository site to the accessible environment. The differences in predicted results can, for the most part, be explained and justified in terms of the specific data used and assumptions made in the analyses. Nevertheless, the lack of a general consensus in these predictions clearly reflects the uncertainty in the existing hydrologic conceptual model. In essence, this means that the hydrologic data base is not, as yet, sufficient to provide a single (and widely accepted) interpretation of the basic hydrologic relationships in the Pasco Basin. To reduce this uncertainty, a more complete hydrologic characterization of the basalts will be needed, with particular focus on hydrologic factors that represent the dominant sources of uncertainty.

Among the various factors that contribute to the uncertainty in the predicted flow paths and travel times, some of the more important are:

- Limited amount of hydraulic head profiles along the boundaries of the Pasco Basin (i.e., boundary conditions)
- Lack of areal distribution maps of hydraulic conductivity, particularly in the Grande Ronde Basalt
- Lack of effective porosity data for the deep basalt flows and flow contacts
- Lack of firm estimates of vertical hydraulic conductivity, at least in and near the reference repository location
- Limited understanding of the role of certain geologic structures in determining groundwater flow patterns and in establishing actual boundaries around the reference repository location.

The planned geologic and hydrologic studies as described in this document will fill many of the gaps in the existing hydrologic data base and thereby reduce significantly the uncertainty in the hydrologic conceptual model. As a result, future predictions of groundwater flow paths and travel times obtained by independent organizations should reach greater degrees of consensus. Achievement of this technical consensus will not only develop confidence in the hydrologic predictions, but will also be useful in deciding how much additional data will be needed for the final performance assessment.

In noting the uncertainties in the hydrologic predictions, it is also important to place them in perspective in terms of the NRC proposed regulations (NRC, 1981) for groundwater travel time. Studies conducted to date by Rockwell and other independent organizations unanimously agree that the minimum travel time from the repository to the accessible environment under natural, pre-waste-emplacement conditions is likely to be on the order of 10,000 years or longer. As a result, considerable confidence exists that compliance with the 1,000-year minimum travel time to the accessible environment specified in NRC proposed technical criteria will be demonstrated for the reference repository location.

12.4.5.2 Repository Release Rates. The very near-field performance analyses conducted to date have been carried out using a methodology (Wood, 1980) consisting of: (1) a simple and conservative radionuclide transport model, (2) baseline and potential worst case release scenarios, and (3) the EPA draft regulations (EPA, 1981) for releases to the accessible environment. This approach has been used to back-calculate the repository release rates needed to comply with the EPA draft regulations (EPA, 1981).

As indicated in Section 12.4.2, the basic finding of these analyses is that compliance with the NRC proposed technical criterion (NRC, 1981) of a 1-part-in-100,000-per-year maximum fractional release rate would be achieved with considerable margin for many radionuclides. The conservative analysis indicates that the combination of solubility properties of the waste form and the reducing conditions of the basalt groundwater contribute greatly to the low release rates that are calculated to be substantially below the NRC proposed technical criteria (NRC, 1981) for many radionuclides. Since solubility limitations on the release rate are such a dominant factor, it follows that the uncertainty in these predictions should be minimized by developing a reliable data base on solubility and related thermodynamic properties of the key radionuclides.

12.4.5.3 Radionuclides Releases to the Accessible Environment. The issue of the radionuclide releases was addressed to a limited extent in the near-field performance analysis presented in Section 12.4.3. The principal results of this preliminary analysis provide a reasonable idea of the possible performance of the reference repository location. Overall, the findings suggest that, for the release scenarios considered, the radionuclide plumes would be contained in the deep basalt flows. The predicted releases of ^{14}C (a key radionuclide) at 10 kilometers comply with EPA draft regulations (EPA, 1981).

Since this preliminary analysis is based on a combination of generic and measured hydrologic data and an idealized representation of the rock strata, a high degree of confidence in the numerical predictions cannot be asserted at this time. On the other hand, the qualitative argument can be made that certain conservative assumptions, which have been incorporated in the analysis, may compensate for data uncertainty and, therefore, the predictions may be in fact bounding estimates. Some idea of the degree of uncertainty will be gained in the near term as other independent predictions of releases are completed and compared to the present results and as additional data for the candidate siting area are obtained.

12.5 SUMMARY OF UNRESOLVED ISSUES

As explained in earlier sections, the basic objectives of a long-term performance analysis are twofold: (1) to assist in planning the site-characterization effort and designing the engineered facility and (2) to perform predictions of postclosure performance of the repository system. The major long-term performance issues, however, primarily relate to the second objective, with specific regard to the question of compliance with the applicable technical criteria and regulations. The major issues were discussed in Section 12.1. Plans for their resolution are addressed in Chapters 13 and 16.

12.6 REFERENCES

Apps, J., Doe, T., Doty, B., Doty, S., Galbraith, R., Kearns, A., Kohrt, B., Lons, J., Monroe, A., Narsimhan, T. N., Nelson, P., Wilson, C. R., and Witherspoon, P. A., 1979, Geohydrologic Studies for Nuclear Waste Isolation at the Hanford Reservation, LBL-8764, Vol. 2, Lawrence Berkeley Laboratory, Berkeley, California.

Arnett, R. C., 1980, "Far-Field Modeling: Simulation of the Natural Groundwater System in the Pasco Basin," in Basalt Waste Isolation Project Annual Report - Fiscal Year 1980, RHO-BWI-80-100, Rockwell Hanford Operations, Richland, Washington, November 1980.

Arnett, R. C., Baca, R. G., Caggiano, J. A., Price, S. M., Gephart, R. E., and Logan, S. E., 1980, Preliminary Hydrologic Release Scenarios for a Candidate Repository Site in the Columbia River Basalts, RHO-BWI-ST-12, Rockwell Hanford Operations, Richland, Washington, November 1980.

Arnett, R. C., Mudd, R. D., Baca, R. G., Martin, M. D., Norton, W. R., and McLaughlin, D. B., 1981, Pasco Basin Hydrologic Modeling and Far-Field Radionuclide Migration Potential, RHO-BWI-LD-44, Rockwell Hanford Operations, Richland, Washington, June 1981.

Baca, R. G., Case, J. B., and Patricio, J. G., 1980, "Coupled Geomechanical/Hydrological Modeling, An Overview of Basalt Waste Isolation Project Studies," Proceedings of the Second Workshop on Thermomechanical and Hydrochemical Modeling for a Hardrock Waste Repository, Berkeley, California, July 27-29, 1980; also RHO-BWI-SA-82, Rockwell Hanford Operations, Richland, Washington, July 1980.

Baca, R. G. and Arnett, R. C., 1981, "Analysis of Fracture Flow and Transport in the Near-Field of a Nuclear Waste Repository," Proceedings of the Symposium on Uncertainties Associated with the Regulation of the Geologic Disposal of High-Level Radioactive Waste, Gatlinberg, Tennessee; also RHO-BWI-SA-81, Rockwell Hanford Operations, Richland, Washington, March 1981.

Baca, R. G., Langford, D. W., and England, R. L., 1981a, "Analysis of Host Rock Performance for a Nuclear Waste Repository Using Coupled Flow and Transport Models," Proceedings of the Workshop on Near-field Phenomena in Geologic Repositories for Radioactive Wastes, OECD Workshop, Seattle, Washington; also RHO-BWI-SA-140, Rockwell Hanford Operations, Richland, Washington, August 1981.

Baca, R. G., Arnett, R. C., and King, I. P., 1981b, "Numerical Modeling of Flow and Transport Processes in a Fractured-Porous Rock System," Proceedings of the 22nd Annual Symposium on Rock Mechanics, Massachusetts Institute of Technology, Cambridge, Massachusetts, June 19-July 2, 1981; also RHO-BWI-SA-113, Rockwell Hanford Operations, Richland, Washington, June 1981.

Barney, G. S. and Wood, B. J., 1980, Identification of Key Radionuclides in a Nuclear Waste Repository in Basalt, RHO-BWI-ST-9, Rockwell Hanford Operations, Richland, Washington, May 1980.

Bear, J., 1972, Dynamics of Fluids in Porous Media, American Elsevier Publishing Company, New York, New York.

Berman, L. E., Ensminger, D. A., Giuffre, M. S., Koplik, C. M., Oston, S. G., Pollak, G. D., and Ross, B. I., 1978, Analysis of Some Nuclear Waste Management Options, Volume 1: Analysis and Interpretation, TR-1103-1-1, The Analytic Sciences Corporation, Reading, Massachusetts.

Bird, R. B., Stewart, W. E., and Lightfoot, E. N., 1960, Transport Phenomena, John Wiley & Sons, New York, New York.

Boonlualohr, P., Mustoe, G., and Williams, J. R., 1980, Program DAMSWEL Programming Manual, Code Verification, Program Listing, RHO-BWI-C-74, Dames & Moore for Rockwell Hanford Operations, Richland, Washington, July 1980.

Cheng, P., 1978, "Heat Transfer in Geothermal Systems," in Advances in Heat Transfer, Vol. 14, Academic Press, New York, New York, pp. 1-105.

Coats, K. H. and Smith, B. D., 1964, "Dead-End Pore Volume and Dispersion in Porous Media," Society of Petroleum Engineers Journal, pp. 73-84, March 1964.

Combarnous, M. A. and Bories, S. A., 1975, "Hydrothermal Convection in Saturated Porous Media," in Advances in Hydroscience, Vol. 10, Academic Press, New York, New York, pp. 231-307.

Cook, R. D., 1981, Concepts and Applications of Finite Element Analysis, 2nd ed., John Wiley & Sons, New York, New York.

Delhomme, J. P., 1976, Kriging in Hydroscience, Ph.D. Thesis, Centre D'Information Géologique, École Nationale Supérieure Des Mines de Paris (University of Paris), Paris, France.

DeSalvo, G. J., 1976, ANSYS - Verification Manual, Swanson Analysis Systems, Inc., Houston, Pennsylvania.

DeSalvo, G. J. and Swanson, J. A., 1981, ANSYS - User's Manual, Swanson Analysis Systems, Inc., Houston, Pennsylvania.

Dillon, R. T., Lantz, R. B., and Pahwa, S. B., 1979, A Model for Calculating Radioactive Waste Migration, the Sandia Waste Isolation Flow and Temperature (SWIFT) Model, SAND 78-L1267, Sandia Laboratories, Albuquerque, New Mexico.

Doctor, P. G., 1979, An Evaluation of Kriging Techniques for High Level Radioactive Waste Repository Site Characterization, PNL-2903, Pacific Northwest Laboratory, Richland, Washington.

Dove, F. H., Cole, C. R., Foley, M. G., Bond, F. W., Brown, R. E., Deutsch, W. J., Freshley, M. D., Gupta, S. K., Gutknecht, P. J., Kuhn, W. L., Lindberg, J. W., Rice, W. A., Schalla, R., Washburn, J. F., and Zellmer, J. T., 1981, Assessment of Effectiveness of Geologic Isolation Systems: AEGIS Technology Demonstration for a Nuclear Waste Repository in Basalt, PNL-3632, Pacific Northwest Laboratory, Richland, Washington.

EPA, 1981, Working Draft No. 20, Environmental Protection Agency, 40 CFR 191, Environmental Standards and Federal Radiation Protection Guidance for Management and Disposal of Spent Nuclear Fuel, High-Level and Transuranic Radioactive Wastes, U.S. Environmental Protection Agency, Washington, D.C.

Freeze, R. A. and Cherry, J. A., 1979, Groundwater, Prentice-Hall, Inc., Englewood Cliffs, New Jersey.

Gephart, R. E., Arnett, R. C., Baca, R. G., Leonhart, L. S., and Spane, F. A., Jr., 1979, Hydrologic Studies Within the Columbia Plateau, Washington: An Integration of Current Knowledge, RHO-BWI-ST-5, Rockwell Hanford Operations, Richland, Washington, October 1979.

Gupta, S. K., Cole, C. R., and Bond, F. W., 1979, Finite-Element Three-Dimensional Groundwater (FE3DGW) Flow Model - Formulation, Program Listings and Users Manual, PNL-2939, Pacific Northwest Laboratory, Richland, Washington.

Guzowski, R. V., Nimick, F. B., and Muller, A. B., 1982, Repository Site Definition in Basalt: Pasco Basin, Washington, NUREG/CR-2352, SAND-81-2088, Sandia National Laboratories, Albuquerque, New Mexico.

Haderman, J., 1980, "Radionuclide Transport Through Heterogeneous Media," Nuclear Technology, Vol. 47, pp. 312-323.

Hardy, M. P., St. John, C. M., and Hocking, G., 1978, Numerical Modeling of Rock Stresses Within a Basaltic Nuclear Waste Repository, Phase I- Problem Definition, RHO-BWI-C-24, University of Minnesota and Dames & Moore for Rockwell Hanford Operations, Richland, Washington, April 1978.

Hardy, M. P. and Hocking, G., 1978a, Numerical Modeling of Rock Stresses within a Basaltic Nuclear Waste Repository, Phase II, Parametric Design Studies, RHO-BWI-C-23, University of Minnesota and Dames & Moore for Rockwell Hanford Operations, Richland, Washington, July 1978.

Hardy, M. P. and Hocking, G., 1978b, Numerical Modeling of Rock Stress within a Basaltic Nuclear Waste Repository, Final Report, RHO-BWI-C-32, University of Minnesota and Dames & Moore for Rockwell Hanford Operations, Richland, Washington, October 1978.

Holman, W. P., 1980, Heat Transfer, McGraw-Hill Book Company, New York, New York.

Isherwood, D., 1981, Geoscience Data Base Handbook for Modeling a Nuclear Waste Repository, NUREG/CR-0912, Vol. 1 and 2, Lawrence Livermore Laboratory, Livermore, California.

Iwai, K., 1976, Fundamental Studies of Fluid Flow Through a Single Fracture, Ph.D. Thesis, University of California, Berkeley, California.

King, I. P., McLaughlin, D. B., Norton, W. R., Baca, R. G., and Arnett, R. C., 1981, Parametric and Sensitivity Analysis of Waste Isolation in a Basalt Medium, RHO-BWI-C-94, Resource Management Associates for Rockwell Hanford Operations, Richland, Washington, February 1981.

Kohnke, P. C., 1977, ANSYS - Theoretical Manual, Swanson Analysis Systems, Inc., Houston, Pennsylvania.

Lee, W. W. L., Nair, J., and Smith, G., 1978, Basalt Waste Isolation Disruptive Events Analysis, RHO-BWI-C-43, Woodward-Clyde Consultants for Rockwell Hanford Operations, Richland, Washington, December 1978.

Lester, D. H., Stula, R. T., and Kirstein, B. E., 1979, System Study in Engineered Barriers-Task 3-Barrier Performance Analysis, ONWI/Sub/79/E515-02000-1, Office of Nuclear Waste Isolation, Battelle Memorial Institute, Columbus, Ohio.

Logan, S. E. and Berbano, M. C., 1978, Development and Application of Risk Assessment Method for Radioactive Waste Management, EPA 520/6-78-005, U.S. Environmental Protection Agency, Washington, D.C.

Maini, R. Y. N., 1971, In Situ Hydraulic Parameters in Jointed Rock-Their Measurement and Interpretations, Ph.D. Thesis, Imperial College, London, England.

Malvern, L. E., 1969, Introduction to the Mechanics of a Continuous Medium, Prentice-Hall Inc., Englewood Cliffs, New Jersey.

McLaughlin, D. B., 1979, Hanford Groundwater Modeling: Statistical Methods for Evaluating Uncertainty and Assessing Sampling Effectiveness, RHO-C-18, Resource Management Associates for Rockwell Hanford Operations, Richland, Washington.

Neuman, S. P., Sagar, B., deMarsity, G., and Simpson, E. S., 1979, Progress and Problems in the Analysis and Prediction of Subsurface Mass Transport, Department of Hydrology and Water Resources, University of Arizona, Tucson, Arizona.

NRC, 1981, "Nuclear Regulatory Commission, 10 CFR 60, Disposal of High-Level Radioactive Wastes in Geologic Repositories," Federal Register, Vol. 46, No. 130, July 8, 1981, Proposed Rules.

NWTS, 1981, NWTS Program Criteria for Mined Geologic Disposal of Nuclear Waste, Site Performance Criteria, DOE/NWTS-33(2), National Waste Terminal Storage Program Office, U.S. Department of Energy, Washington, D.C.

- Ozisik, M. N., 1977, Basic Heat Transfer, McGraw-Hill Book Company, New York, New York.
- Patankar, S. V., 1980, Numerical Heat Transfer and Fluid Flow, Hemisphere Publishing Corporation, McGraw-Hill Book Company, New York, New York.
- Raiffa, H., 1968, Decision Analysis: Introductory Lectures on Choices Under Uncertainty, Addison-Wesley, New York, New York.
- Rocha, M. and Franciss, F., 1977, "Determination of Permeability in Anisotropic Rock Masses from Integral Samples," Rock Mechanics, Vol. 9, No. 2-3, pp. 67-84.
- Roegiers, J. L., Curran, J. H., and Bawden, W. F., 1979, Numerical Modeling of Flow in Fractured Rock Masses, ISSN 0316-798b, Publication 79-02, University of Toronto, Toronto, Ontario.
- Ross, B., Koplik, C. M., Giuffre, M. S., Hodgins, S. P., and Duffy, J. J., 1979, NUTRAN: A Computer Model of Long-Term Hazards from Waste Repositories, TR-1797-7, The Analytic Sciences Corporation, Reading, Massachusetts.
- Runchal, A. K., 1972, "Convergence and Accuracy of Three Finite Difference Schemes for a Two-Dimensional Conduction and Convection Problem," International Journal of Numerical Methods in Engineering, Vol. 4, p. 541.
- Sagar, B. and Runchal, A. K., 1982, "Permeability of Fractured Rock: Effect of Fracture Size and Data Uncertainties," Water Resources Research, Vol. 18, No. 2, pp. 266-274.
- Salter, P. F., Anderson, W. J., and Deju, R. A., 1982, Application of Systems Analysis to Develop Engineered Systems Performance Requirements for a Hard Rock Nuclear Waste Repository, RHO-BW-SA-210 P, Rockwell Hanford Operations, Richland, Washington, March 1982.
- Shannon, R. E., 1975, Systems Simulation - The Art and Science, Prentice-Hall, Inc., Englewood Cliffs, New Jersey.
- Snow, D. T., 1965, A Parallel Plate Model of Fractured Permeable Media, Ph.D. Thesis, University of California, Berkeley, California.
- Spane, F. A., Jr., 1980, "Groundwater Hydrology of the Columbia River Basalts Beneath the Hanford Site," in Basalt Waste Isolation Project Annual Report - Fiscal Year 1980, RHO-BWI-80-100, Rockwell Hanford Operations, Richland, Washington, November 1980.
- Stottlemire, J. A., Petrie, G. M., Benson, G. L., and Zellmer, J. T., 1981, A Conceptual Model for Release Scenario Analysis of a Hypothetical Site in Columbia Plateau Basalts, PNL-2892, Pacific Northwest Laboratory, Richland, Washington.

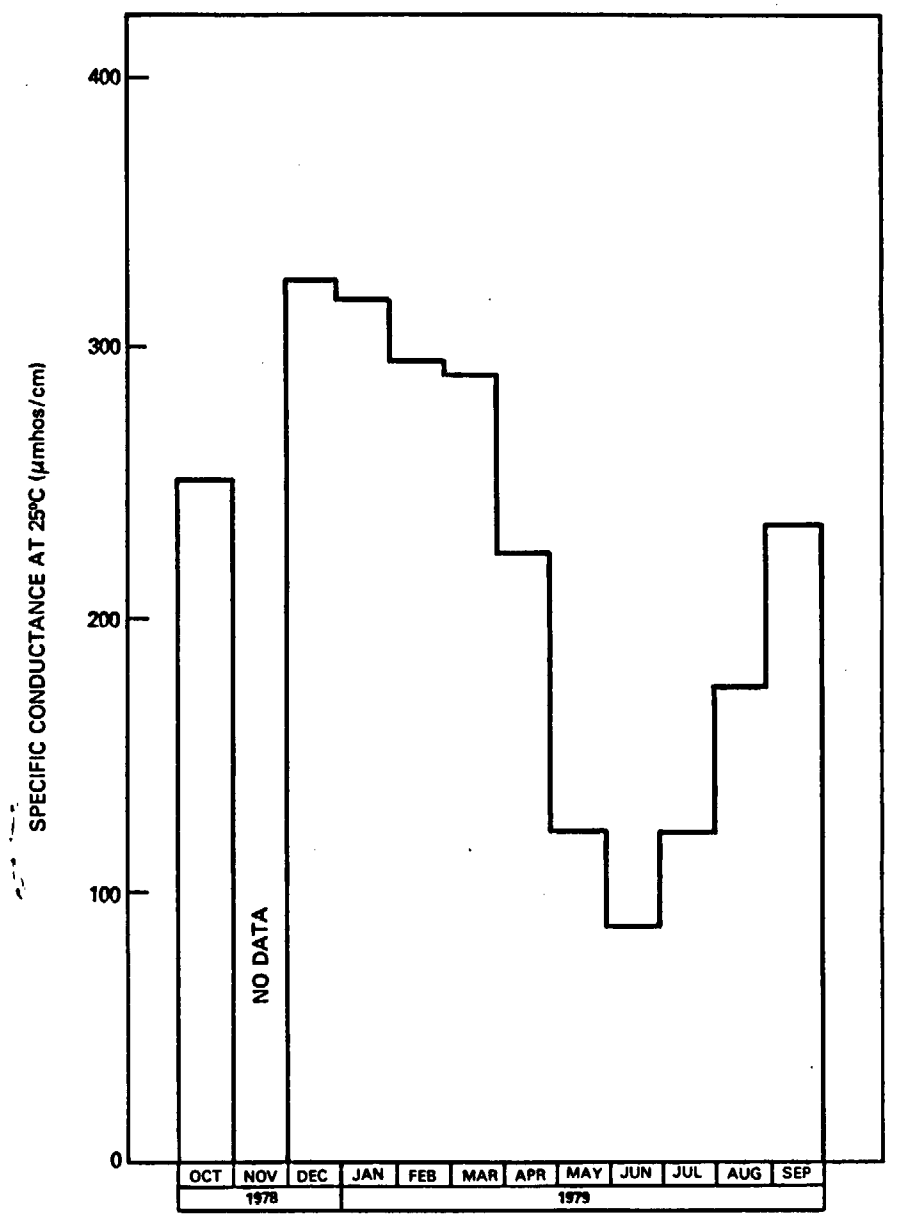
TASC, 1980, User's Guide to NUTRAN: A Computer Analysis System for Long-Term Repository Safety, The Analytic Sciences Corporation, Reading, Massachusetts.

Timoshenko, S. and Goodier, J., 1970, Theory of Elasticity, 3rd ed., McGraw-Hill Book Company, New York, New York.

Turner, W. D., Elrod, D. C., and Siman-Tov, I. I., 1977, HEATING5-An IBM 360 Heat Conduction Program, ORNL/CSD/TM-15, Oak Ridge National Laboratory, Oak Ridge, Tennessee.

Witherspoon, P. A., Tsang, Y. W., Long, J. C. S., and Noorishad, J., 1981, "New Approaches to Problems of Fluid Flow in Fractured Rock Masses," Proceedings of the 22nd U.S. Symposium on Rock Mechanics, Massachusetts Institute of Technology, Cambridge, Massachusetts.

Wood, B. J., 1980, Estimation of Waste Package Performance Requirements for a Nuclear Waste Repository in Basalt, RHO-BWI-ST-10, Rockwell Hanford Operations, Richland, Washington, July 1980.



RCP8112-149

FIGURE 7-29. Monthly Mean Specific Conductance in 1979 of the Snake River near Burbank, Washington.

TABLE 7-19. Summary of U.S. Geological Survey Surface Water Quality Data for Stations on the Columbia River Within the Pasco Basin. (Sheet 1 of 4)

Quality parameter/group	Units	Vernita Bridge				Richland				Umatilla			
		No. of samples	Highest	Lowest	Mean	No. of samples	Highest	Lowest	Mean	No. of samples	Highest	Lowest	Mean
Physical													
Discharge, daily	m ³ /s (ft ³ /s)	Continuous	4,300 (152,000)	1,430 (50,500)	2,900 (102,700)	--	--	--	--	Continuous	8,300 (293,000)	1,650 (58,100)	4,180 (147,700)
Turbidity	NTU	12	4.3	0.4	1.8	4	3.6	0.60	1.8	--	--	--	--
Temperature	°C	Continuous	20.0	0.0	11.0	Continuous	21.0	0.5	11.0	Continuous	21.5	0.0	11.5
Specific conductance	µmhos/cm at 25°C	12	156	109	135	4	150	123	134	11	244	107	175
pH	Units	8	8.8	7.5	8.2	4	8.6	7.7	8.3	10	8.5	7.6	8.1
Gross alpha, dissolved	µg/L as U-Nat	--	--	--	--	--	--	--	--	--	--	--	--
Gross alpha, suspended total	µg/L as U-Nat	--	--	--	--	--	--	--	--	--	--	--	--
Gross alpha, dissolved	pCi/L as U-Nat	--	--	--	--	--	--	--	--	--	--	--	--
Gross beta, dissolved	pCi/L as Cs-137	--	--	--	--	--	--	--	--	--	--	--	--
Gross beta, suspended total	pCi/L as Cs-137	--	--	--	--	--	--	--	--	--	--	--	--
Gross beta, dissolved	pCi/L as Sr/Yt-90	--	--	--	--	--	--	--	--	--	--	--	--
Gross beta, suspended total	pCi/L as Sr/Yt-90	--	--	--	--	--	--	--	--	--	--	--	--
Radium-226, dissolved radon method	pCi/L	--	--	--	--	--	--	--	--	--	--	--	--
Uranium, dissolved, extraction	µg/L	--	--	--	--	--	--	--	--	--	--	--	--
Chemical													
Major Constituents													
Oxygen, dissolved	mg/L	12	15.8	9.2	12.2	4	15.0	9.5	12.3	11	13.8	8.5	11.0
Carbon dioxide, dissolved	mg/L	--	--	--	--	--	--	--	--	2	1.2	0.5	0.9
Solids, residue at 180°C, dissolved	mg/L	12	93	70	80	4	89	70	80	11	139	72	101
Solids, sum of constituents, dissolved	mg/L	12	90	67	78	4	86	67	77	--	--	--	--
Solids, dissolved	tons/acre-ft	12	0.13	0.10	0.11	4	0.12	0.10	0.11	11	0.19	0.10	0.14
Solids, dissolved	tonnes/day (tons/day)	12	29,200 (32,200)	7,530 (8,300)	18,960 (20,900)	--	--	--	--	11	58,600 (64,600)	23,405 (25,800)	37,285 (41,100)
Solids, residue at 105°C, suspended	mg/L	12	9	0	3	4	8	0	4.5	11	80	0	16.9
Hardness	mg/L as CaCO ₃	12	76	59	66	4	76	59	66	--	--	--	--
Hardness, non-carbonate	mg/L as CaCO ₃	12	22	3	13	4	16	7	12	--	--	--	--
Alkalinity	mg/L as CaCO ₃	12	62	43	54	4	60	45	54	3	68	47	59
Silica, dissolved	mg/L as SiO ₂	12	5.2	3.2	4.4	4	4.9	3.0	4.4	11	13	4.0	8
Carbon, organic total	mg/L as C	8	8.6	0.0	2.8	2	3.6	2.4	3.0	10	4.5	1.7	2.7
Carbon, organic dissolved	mg/L as C	4	3.8	1.7	2.9	2	4.4	2.1	3.3	--	--	--	--
Carbon, organic suspended total	mg/L as C	4	0.8	0.1	0.3	2	0.6	0.2	0.4	--	--	--	--
Phosphorus, total	mg/L as P	12	0.050	0.010	0.030	4	0.040	0.010	0.023	11	0.170	0.000	0.044
Phosphorus, dissolved	mg/L as P	12	0.050	0.000	0.020	--	--	--	--	--	--	--	--

TABLE 7-19. Summary of U.S. Geological Survey Surface Water Quality Data for Stations on the Columbia River Within the Pasco Basin. (Sheet 2 of 4)

Quality parameter/group	Units	Vernita Bridge				Richland				Umatilla			
		No. of samples	Highest	Lowest	Mean	No. of samples	Highest	Lowest	Mean	No. of samples	Highest	Lowest	Mean
Major Constituents													
Phosphorus, ortho, dissolved	mg/L as P	4	0.01	0.00	0.01	4	0.01	0.00	0.01	--	--	--	--
Phosphate, ortho, dissolved	mg/L as PO ₄	4	0.03	0.00	0.02	4	0.03	0.00	0.02	--	--	--	--
Nitrogen, nitrate, total	mg/L as N	4	0.12	0.00	0.08	4	0.15	0.01	0.07	--	--	--	--
Nitrogen, nitrite, total	mg/L as N	4	0.02	0.00	0.01	4	0.02	0.00	0.01	--	--	--	--
Nitrogen, NO ₂ + NO ₃ , total	mg/L as N	12	0.28	0.00	0.10	4	0.15	0.03	0.08	11	0.84	0.02	0.24
Nitrogen, ammonia, total	mg/L as N	12	0.02	0.00	0.01	4	0.01	0.00	0.01	10	0.08	0.01	0.04
Nitrogen, organic, total	mg/L as N	12	0.61	0.08	0.23	4	0.61	0.08	0.27	10	0.59	0.13	0.33
Nitrogen, ammonia + organic, total	mg/L as N	12	0.62	0.08	0.24	4	0.61	0.09	0.28	--	--	--	--
Nitrogen, ammonia + organic, suspended, total	mg/L as N	12	0.42	0.02	0.11	--	--	--	--	--	--	--	--
Nitrogen, ammonia + organic, dissolved, total	mg/L as N	12	0.37	0.00	0.13	--	--	--	--	--	--	--	--
Nitrogen, total	mg/L as N	12	0.90	0.10	0.33	4	0.64	0.21	0.36	10	1.3	0.23	0.63
Nitrogen, total	mg/L as NO ₃	12	4.0	0.44	1.47	4	2.8	0.93	1.61	10	5.6	1.0	2.77
Sulfate, dissolved	mg/L as SO ₄	12	16	8.3	13	4	13	10	12	3	15	12	14
Chloride, dissolved	mg/L as Cl	12	2.1	0.9	1.3	4	2.5	1.1	1.8	3	3.9	2.1	3.0
Fluoride, dissolved	mg/L as F	12	0.2	0.1	0.1	4	0.2	0.1	0.1	--	--	--	--
Sodium, dissolved	mg/L as Na	12	2.7	1.8	2.0	4	2.3	2.0	2.2	--	--	--	--
Sodium	Percent	12	10	6	7	4	8	6	7	--	--	--	--
Sodium adsorption ratio	Units	12	0.1	0.1	0.1	4	0.1	0.1	0.1	--	--	--	--
Potassium, dissolved	mg/L as K	12	1.1	0.6	0.8	4	0.9	0.6	0.7	--	--	--	--
Calcium, dissolved	mg/L as Ca	12	23	17	20	4	22	17	19	--	--	--	--
Magnesium, dissolved	mg/L as Mg	12	5.2	1.3	4.1	4	5.2	3.7	4.4	--	--	--	--
Trace Constituents													
Chromium, suspended recoverable	ug/L as Cr	4	0	0	0	--	--	--	--	--	--	--	--
Chromium, dissolved	ug/L as Cr	4	0	0	0	--	--	--	--	--	--	--	--
Chromium, total recoverable	ug/L as Cr	4	0	0	0	4	20	0	5	11	20	0	7
Cobalt, total recoverable	ug/L as Co	4	1	0	0	4	2	0	1	--	--	--	--
Cobalt, suspended recoverable	ug/L as Co	4	0	0	0	--	--	--	--	--	--	--	--
Cobalt, dissolved	ug/L as Co	4	<3	0	--	--	--	--	--	--	--	--	--
Copper, total recoverable	ug/L as Cu	4	12	4	7	4	19	2	10	11	50	1	18
Copper, suspended recoverable	ug/L as Cu	4	12	3	6	--	--	--	--	--	--	--	--
Copper, dissolved	ug/L as Cu	4	1	0	0	--	--	--	--	--	--	--	--
Iron, total recoverable	ug/L as Fe	4	130	80	98	4	180	90	133	10	4,200	140	377
Iron, suspended recoverable	ug/L as Fe	4	100	0	63	--	--	--	--	--	--	--	--
Iron, dissolved	ug/L as Fe	4	100	10	40	--	--	--	--	--	--	--	--
Arsenic, total	ug/L as As	4	1	1	1	4	1	1	1	10	3	1	2
Arsenic, dissolved	ug/L as As	4	1	0	1	4	1	0	1	--	--	--	--
Barium, total recoverable	ug/L as Ba	4	0	0	0	--	--	--	--	--	--	--	--
Barium, suspended recoverable	ug/L as Ba	4	0	0	0	--	--	--	--	--	--	--	--
Barium, dissolved	ug/L as Ba	4	40	0	28	--	--	--	--	--	--	--	--
Cadmium, total recoverable	ug/L as Cd	3	3	1	2	4	7	0	3	10	9	0	3

TABLE 7-19. Summary of U.S. Geological Survey Surface Water Quality Data for Stations on the Columbia River Within the Pasco Basin. (Sheet 3 of 4)

Quality parameter/group	Units	Vernita Bridge				Richland				Umatilla			
		No. of samples	Highest	Lowest	Mean	No. of samples	Highest	Lowest	Mean	No. of samples	Highest	Lowest	Mean
Trace Constituents													
Cadmium, suspended recoverable	ug/L as Cd	3	2	0	1	--	--	--	--	--	--	--	--
Cadmium, dissolved	ug/L as Cd	3	2	<1	--	--	--	--	--	--	--	--	--
Lead, total recoverable	ug/L as Pb	3	73	8	33	4	130	27	75	10	42	3	15
Lead, suspended recoverable	ug/L as Pb	3	61	8	29	--	--	--	--	--	--	--	--
Lead, dissolved	ug/L as Pb	3	12	2	5	--	--	--	--	--	--	--	--
Manganese, total recoverable	ug/L as Mn	4	20	0	13	4	20	10	18	--	--	--	--
Manganese, suspended recoverable	ug/L as Mn	4	20	0	12	--	--	--	--	--	--	--	--
Manganese, dissolved	ug/L as Mn	4	5	0	3	--	--	--	--	--	--	--	--
Mercury, total recoverable	ug/L as Hg	4	0.1	0.0	0.1	4	0.3	0.0	0.1	10	0.5	0.0	0.1
Mercury, suspended recoverable	ug/L as Hg	4	0.1	0.0	0.1	--	--	--	--	--	--	--	--
Mercury, dissolved	ug/L as Hg	4	0.0	0.0	0.0	--	--	--	--	--	--	--	--
Selenium, total	ug/L as Se	4	0	0	0	4	0	0	0	10	0	0	0
Selenium, suspended total	ug/L as Se	4	0	0	0	--	--	--	--	--	--	--	--
Selenium, dissolved	ug/L as Se	4	0	0	0	--	--	--	--	--	--	--	--
Silver, total recoverable	ug/L as Ag	4	0	0	0	--	--	--	--	--	--	--	--
Silver, suspended recoverable	ug/L as Ag	4	0	0	0	--	--	--	--	--	--	--	--
Silver, dissolved	ug/L as Ag	4	0	0	0	--	--	--	--	--	--	--	--
Zinc, total recoverable	ug/L as Zn	4	70	10	38	4	40	20	33	11	170	0	45
Zinc, suspended recoverable	ug/L as Zn	4	50	0	23	--	--	--	--	--	--	--	--
Zinc, dissolved	ug/L as Zn	4	30	4	15	--	--	--	--	--	--	--	--
Organic Compounds													
PCB, total	ug/L	--	--	--	--	--	--	--	--	--	--	--	--
Aldrin, total	ug/L	--	--	--	--	--	--	--	--	--	--	--	--
Chlordane, total	ug/L	--	--	--	--	--	--	--	--	--	--	--	--
DDD, total	ug/L	--	--	--	--	--	--	--	--	--	--	--	--
DDE, total	ug/L	--	--	--	--	--	--	--	--	--	--	--	--
DDT, total	ug/L	--	--	--	--	--	--	--	--	--	--	--	--
Diazinon, total	ug/L	--	--	--	--	--	--	--	--	--	--	--	--
Dieldrin, total	ug/L	--	--	--	--	--	--	--	--	--	--	--	--
Endrin, total	ug/L	--	--	--	--	--	--	--	--	--	--	--	--
Ethion, total	ug/L	--	--	--	--	--	--	--	--	--	--	--	--
Heptachlor, total	ug/L	--	--	--	--	--	--	--	--	--	--	--	--
Heptachlor epoxide, total	ug/L	--	--	--	--	--	--	--	--	--	--	--	--
Lindane, total	ug/L	--	--	--	--	--	--	--	--	--	--	--	--
Malathion, total	ug/L	--	--	--	--	--	--	--	--	--	--	--	--
Methoxychlor, total	ug/L	--	--	--	--	--	--	--	--	--	--	--	--
Methylparathion, total	ug/L	--	--	--	--	--	--	--	--	--	--	--	--
Methyltrithion, total	ug/L	--	--	--	--	--	--	--	--	--	--	--	--
Parathion, total	ug/L	--	--	--	--	--	--	--	--	--	--	--	--
Toxaphene, total	ug/L	--	--	--	--	--	--	--	--	--	--	--	--
Total trithion	ug/L	--	--	--	--	--	--	--	--	--	--	--	--

TABLE 7-19. Summary of U.S. Geological Survey Surface Water Quality Data for Stations on the Columbia River Within the Pasco Basin. (Sheet 4 of 4)

Quality parameter/group	Units	Vernita Bridge				Richland				Umatilla			
		No. of samples	Highest	Lowest	Mean	No. of samples	Highest	Lowest	Mean	No. of samples	Highest	Lowest	Mean
Biological													
Biomass													
Periphyton biomass ash weight	g/m ²	4	8.90	0.000	2.97	--	--	--	--	--	--	--	--
Periphyton biomass total dry weight	g/m ²	4	13.5	0.000	4.24	--	--	--	--	--	--	--	--
Chlor-A periphyton chromographic fluorom	mg/m ²	4	24.5	0.000	6.26	--	--	--	--	--	--	--	--
Chlor-B periphyton chromographic fluorom	mg/m ²	4	7.92	0.000	1.98	--	--	--	--	--	--	--	--
Length of exposure	Days	4	28	21	24	--	--	--	--	--	--	--	--
Phytoplankton													
Total count	cells/mL	4	19,000	1,900	10,000	--	--	--	--	--	--	--	--
Division, diversity	index (d̄)	4	0.6	0.1	0.3	--	--	--	--	--	--	--	--
Class, diversity	index (d̄)	4	0.6	0.1	0.3	--	--	--	--	--	--	--	--
Order, diversity	index (d̄)	4	1.1	0.3	0.8	--	--	--	--	--	--	--	--
Family, diversity	index (d̄)	4	1.2	0.3	0.9	--	--	--	--	--	--	--	--
Genus, diversity	index (d̄)	4	1.9	0.3	1.4	--	--	--	--	--	--	--	--
Bacteria													
Coliform, fecal 0.7 UM-MF	colonies/100 mL	12	13	<1	~2	4	10	<1	~3	11	K*19	K2	K6
Streptococci, fecal KF AGAR	colonies/100 mL	12	71	<1	~8	4	16	<1	~9	11	1,100	K1	K112
Sediment													
Sediment, suspended	mg/L	12	7	1	4	4	8	2	5	--	--	--	--
Sediment, discharge suspended	tons/day	12	2,420 (2,670)	187 (206)	907 (1,000)	--	--	--	--	--	--	--	--
Sediment, suspended (fall diameter <0.002 mm)	Percent	↑	↑	↑	↑	--	--	--	--	--	--	--	--
Sediment, suspended (fall diameter <0.004 mm)	Percent	↑	↑	↑	↑	--	--	--	--	--	--	--	--
Sediment, suspended (fall diameter <0.008 mm)	Percent	↑	↑	↑	↑	--	--	--	--	--	--	--	--
Sediment, suspended (fall diameter <0.016 mm)	Percent	↑	↑	↑	↑	--	--	--	--	--	--	--	--
Sediment, suspended (fall diameter <0.031 mm)	Percent	↑	↑	↑	↑	--	--	--	--	--	--	--	--
Sediment, suspended (fall diameter <0.062 mm)	Percent	8	100	49	99	--	--	--	--	--	--	--	--
Sediment, suspended (fall diameter <0.125 mm)	Percent	↑	↑	↑	↑	--	--	--	--	--	--	--	--
Sediment, suspended (fall diameter <0.250 mm)	Percent	↑	↑	↑	↑	--	--	--	--	--	--	--	--
Sediment, suspended (fall diameter <0.500 mm)	Percent	↑	↑	↑	↑	--	--	--	--	--	--	--	--
Sediment, suspended (fall diameter <1.00 mm)	Percent	↑	↑	↑	↑	--	--	--	--	--	--	--	--

*Results based upon colony counts outside the ideal range.

TABLE 7-20. Summary of U.S. Geological Survey 1979 Surface Water Quality Data for Columbia River Tributaries. (Sheet 1 of 4)

Quality parameter/group	Units	Yakima River at Kiona				Snake River at Burbank				Walla Walla River Near Touchet			
		No. of samples	Highest	Lowest	Mean	No. of samples	Highest	Lowest	Mean	No. of samples	Highest	Lowest	Mean
Physical													
Discharge, daily average	m ³ /s (ft ³ /s)	Continuous	125 (4,400)	14 (497)	47 (1,675)	Continuous	4,050 (143,000)	76 (2,700)	1,200 (42,510)	Continuous	220 (7,900)	0.02 (0.82)	15 (543)
Turbidity	NTU	12	15	0.60	6.4	12	54	0.7	10.1	11	40	10	24
Temperature	°C	Continuous	28	0.0	14.5	Continuous	23.5	0.0	11.5	11	26.7	2.2	14.0
Specific conductance	µmhos/cm at 25°C	12	362	190	291	Continuous	476	63	215	11	775	180	329
pH	Units	12	8.9	7.8	8.2	9	8.4	7.6	7.9	11	8.5	7.4	7.9
Gross alpha, dissolved	µg/L as U-Nat	--	--	--	--	2	3.6	3.0	3.3	--	--	--	--
Gross alpha, suspended total	µg/L as U-Nat	--	--	--	--	2	<0.4	<0.4	<0.4	--	--	--	--
Gross alpha, dissolved	pCi/L as U-Nat	--	--	--	--	1	2.0	2.0	2.0	--	--	--	--
Gross beta, dissolved	pCi/L as Cs-137	--	--	--	--	1	<0.3	<0.3	<0.3	--	--	--	--
Gross beta, suspended total	pCi/L as Cs-137	--	--	--	--	2	<0.4	<0.4	<0.4	--	--	--	--
Gross beta, dissolved	pCi/L as Sr/Yt-90	--	--	--	--	2	3.3	2.4	2.9	--	--	--	--
Gross beta, suspended total	pCi/L as Sr/Yt-90	--	--	--	--	2	<0.4	<0.4	<0.4	--	--	--	--
Radium-226, dissolved radon method	pCi/L	--	--	--	--	2	0.06	0.03	0.05	--	--	--	--
Uranium, dissolved, extraction	µg/L	--	--	--	--	2	2.1	1.9	2.0	--	--	--	--
Chemical													
Major Constituents													
Oxygen, dissolved	mg/L	12	16.8	8.9	12.18	12	14.2	7.0	10.7	11	13.0	7.0	9.5
Carbon dioxide, dissolved	mg/L	--	--	--	--	--	--	--	--	--	--	--	--
Solids, residue at 180°C, dissolved	mg/L	12	234	119	180	11	211	69	148	--	--	--	--
Solids, sum of constituents, dissolved	mg/L	12	235	120	178	12	213	59	145	--	--	--	--
Solids, dissolved	tons/acre-ft	12	0.32	0.16	0.25	12	0.29	0.09	0.20	--	--	--	--
Solids, dissolved	tonnes/day (tons/day)	12	1,107 (1,220)	435 (480)	797 (878)	12	33,384 (36,800)	2,658 (2,930)	17,835 (19,660)	--	--	--	--
Solids, residue at 105°C, suspended	mg/L	12	57	1	27	12	50	0	13	--	--	--	--
Hardness	mg/L as CaCO ₃	12	160	73	113	12	140	36	82	--	--	--	--
Hardness, non-carbonate	mg/L as CaCO ₃	12	6	0	2	12	25	0	9	--	--	--	--
Alkalinity	mg/L as CaCO ₃	12	150	78	114	12	110	29	74	--	--	--	--
Silica, dissolved	mg/L as SiO ₂	12	29	19	24	12	24	11	16	--	--	--	--
Carbon, organic total	mg/L as C	8	7.1	2.0	3.6	7	5.5	1.9	3	--	--	--	--
Carbon, organic dissolved	mg/L as C	4	7.3	1.8	4.3	4	7.1	2.9	4.8	--	--	--	--
Carbon, organic suspended total	mg/L as C	4	4.3	0.4	1.7	3	0.9	0.2	0.4	--	--	--	--
Phosphorus, total	mg/L as P	12	0.210	0.070	0.119	12	0.130	0.020	0.053	11	0.290	0.070	0.150
Phosphorus, dissolved	mg/L as P	12	0.160	0.030	0.084	12	0.100	0.000	0.037	--	--	--	--
Phosphorus, ortho, dissolved	mg/L as P	--	--	--	--	--	--	--	--	11	0.25	0.01	0.08

TABLE 7-20. Summary of U.S. Geological Survey 1979 Surface Water Quality Data for Columbia River Tributaries. (Sheet 2 of 4)

Quality parameter/group	Units	Yakima River at Kiona				Snake River at Burbank					Walla Walla River Near Touchet			
		No. of samples	Highest	Lowest	Mean	No. of samples	Highest	Lowest		Mean	No. of samples	Highest	Lowest	Mean
Major Constituents														
Phosphate, ortho, dissolved	mg/L as PO ₄	--	--	--	--	--	--	--		--	11	0.77	0.03	0.25
Nitrogen, nitrate, total	mg/L as N	--	--	--	--	--	--	--		--	11	1.8	0.00	0.69
Nitrogen, nitrate, total	mg/L as N	--	--	--	--	--	--	--		--	11	0.04		0.02
Nitrogen, NO ₂ + NO ₃ , total	mg/L as N	12	1.5	0.42	0.89	12	1.5	0.08		0.48	11	1.8	0.02	0.70
Nitrogen, ammonia, total	mg/L as N	12	0.13	0.00	0.03	12	0.19	0.01		0.04	11	0.16	0.00	0.05
Nitrogen, organic, total	mg/L as N	12	0.67	0.09	0.40	12	0.70	0.01		0.32	11	1.7	0.17	0.60
Nitrogen, ammonia + organic, total	mg/L as N	12	0.67	0.10	0.43	12	0.71	0.13		0.36	11	1.7	0.19	0.65
Nitrogen, ammonia + organic, suspended total	mg/L as N	11	0.45	0.00	0.14	11	0.63	0.00		0.18	--	--	--	--
Nitrogen, ammonia + organic, dissolved, total	mg/L as N	11	0.54	0.08	0.31	11	0.32	0.00		0.18	--	--	--	--
Nitrogen, total	mg/L as N	12	2.2	0.85	1.3	12	1.8	0.23		0.84	11	2.2	0.57	1.4
Nitrogen, total	mg/L as NO ₃	12	9.6	3.8	5.9	12	8.1	1.0		3.7	11	9.9	2.5	6.0
Sulfate, dissolved	mg/L as SO ₄	12	29	8.9	19	12	40	7.6		25	--	--	--	--
Chloride, dissolved	mg/L as Cl	12	8.8	4.6	7.2	12	21	3.4		11	--	--	--	--
Fluoride, dissolved	mg/L as F	12	0.3	0.1	0.2	12	0.4	0.2		0.3	--	--	--	--
Sodium, dissolved	mg/L as Na	12	25	11	18	12	24	5.8		17	--	--	--	--
Sodium	Percent	12	26	23	25	12	45	26		31	--	--	--	--
Sodium adsorption ratio	Units	12	0.9	0.5	0.7	12	1.0	0.4		0.8	--	--	--	--
Potassium, dissolved	mg/L as K	12	4.3	2.0	3.2	12	3.6	0.7		2.5	--	--	--	--
Calcium, dissolved	mg/L as Ca	12	40	18	28	12	36	9.6		21	--	--	--	--
Magnesium, dissolved	mg/L as Mg	12	14	6.8	10.3	12	11	2.8		7.3	--	--	--	--
Trace Constituents														
Chromium, suspended recoverable	µg/L as Cr	4	10	0	8	4	10	0		5	--	--	--	--
Chromium, dissolved	µg/L as Cr	4	0	0	0	4	0	0		0	--	--	--	--
Chromium, total recoverable	µg/L as Cr	4	10	0	8	4	10	0		5	--	--	--	--
Cobalt, total recoverable	µg/L as Co	4	3	0	1	4	2	0		1	--	--	--	--
Cobalt, suspended recoverable	µg/L as Co	4	0	0	0	4	0	0		0	--	--	--	--
Cobalt, dissolved	µg/L as Co	4	<3	0	<3	4	<3	0		<3	--	--	--	--
Copper, total recoverable	µg/L as Cu	4	14	5	10	4	47	1		16	--	--	--	--
Copper, suspended recoverable	µg/L as Cu	4	13	4	7	4	26	0		9	--	--	--	--
Copper, dissolved	µg/L as Cu	4	6	1	3	4	21	1		7	--	--	--	--
Iron, total recoverable	µg/L as Fe	4	1,300	270	783	4	1,200	50		495	--	--	--	--
Iron, suspended recoverable	µg/L as Fe	4	1,200	110	683	4	1,100	20		430	--	--	--	--
Iron, dissolved	µg/L as Fe	4	200	40	113	4	90	30		58	--	--	--	--
Arsenic, total	µg/L as As	4	2	2	2	4	3	1		2	--	--	--	--
Arsenic, dissolved	µg/L as As	4	2	2	2	4	4	2		2	--	--	--	--
Barium, total recoverable	µg/L as Ba	4	100	0	50	4	100	0		25	--	--	--	--
Barium, suspended recoverable	µg/L as Ba	4	80	0	35	4	70	0		18	--	--	--	--
Barium, dissolved	µg/L as Ba	4	40	0	20	4	30	0		20	--	--	--	--

TABLE 7-20. Summary of U.S. Geological Survey 1979 Surface Water Quality Data for Columbia River Tributaries. (Sheet 3 of 4)

Quality parameter/group	Units	Yakima River at Kiona				Snake River at Burbank				Walla Walla River Near Touchet			
		No. of samples	Highest	Lowest	Mean	No. of samples	Highest	Lowest	Mean	No. of samples	Highest	Lowest	Mean
Trace Constituents													
Cadmium, total recoverable	µg/L as Cd	3	1	0	1	3	280	0	94	--	--	--	--
Cadmium, suspended recoverable	µg/L as Cd	3	0	0	0	3	0	0	0	--	--	--	--
Cadmium, dissolved	µg/L as Cd	3	<1	<1	<1	3	300	<1	100	--	--	--	--
Lead, total recoverable	µg/L as Pb	3	22	9	13	3	310	14	134	--	--	--	--
Lead, suspended recoverable	µg/L as Pb	3	22	7	13	3	220	11	102	--	--	--	--
Lead, dissolved	µg/L as Pb	3	2	0	1	3	95	3	34	--	--	--	--
Manganese, total recoverable	µg/L as Mn	4	130	50	78	4	60	20	33	--	--	--	--
Manganese, suspended recoverable	µg/L as Mn	4	120	20	58	4	30	10	23	--	--	--	--
Manganese, dissolved	µg/L as Mn	4	30	9	20	4	30	0	10	--	--	--	--
Mercury, total recoverable	µg/L as Hg	4	0.1	0.0	0.1	4	0.1	0.0	0.1	--	--	--	--
Mercury, suspended recoverable	µg/L as Hg	4	0.1	0.0	0.0	4	0.1	0.0	0.1	--	--	--	--
Mercury, dissolved	µg/L as Hg	4	0.1	0.0	0.0	4	0	0	0	--	--	--	--
Selenium, total	µg/L as Se	4	0	0	0	4	1	0	0	--	--	--	--
Selenium, suspended total	µg/L as Se	4	0	0	0	4	0	0	0	--	--	--	--
Selenium, dissolved	µg/L as Se	4	0	0	0	4	1	0	0	--	--	--	--
Silver, total recoverable	µg/L as Ag	4	0	0	0	4	0	0	0	--	--	--	--
Silver, suspended recoverable	µg/L as Ag	4	0	0	0	4	0	0	0	--	--	--	--
Silver, dissolved	µg/L as Ag	4	0	0	0	4	0	0	0	--	--	--	--
Zinc, total recoverable	µg/L as Zn	4	50	20	28	4	60	10	33	--	--	--	--
Zinc, suspended recoverable	µg/L as Zn	4	50	0	23	4	30	0	15	--	--	--	--
Zinc, dissolved	µg/L as Zn	4	20	<3	~7	4	50	<3	<17	--	--	--	--
Organic Compounds													
PCB, total	µg/L	4	ND	ND	ND	--	--	--	--	--	--	--	--
Aldrin, total	µg/L	4	ND	ND	ND	--	--	--	--	--	--	--	--
Chlordane, total	µg/L	4	ND	ND	ND	--	--	--	--	--	--	--	--
DDD, total	µg/L	4	ND	ND	ND	--	--	--	--	--	--	--	--
DDE, total	µg/L	4	ND	ND	ND	--	--	--	--	--	--	--	--
DDT, total	µg/L	4	ND	ND	ND	--	--	--	--	--	--	--	--
Diazinon, total	µg/L	4	ND	ND	ND	--	--	--	--	--	--	--	--
Dieldrin, total	µg/L	4	ND	ND	ND	--	--	--	--	--	--	--	--
Endrin, total	µg/L	4	ND	ND	ND	--	--	--	--	--	--	--	--
Ethion, total	µg/L	4	ND	ND	ND	--	--	--	--	--	--	--	--
Heptachlor, total	µg/L	4	ND	ND	ND	--	--	--	--	--	--	--	--
Heptachlor epoxide, total	µg/L	4	ND	ND	ND	--	--	--	--	--	--	--	--
Lindane, total	µg/L	4	ND	ND	ND	--	--	--	--	--	--	--	--
Malathion, total	µg/L	4	ND	ND	ND	--	--	--	--	--	--	--	--
Methoxychlor, total	µg/L	4	ND	ND	ND	--	--	--	--	--	--	--	--
Methylparathion, total	µg/L	4	ND	ND	ND	--	--	--	--	--	--	--	--
Methyltrithion, total	µg/L	4	ND	ND	ND	--	--	--	--	--	--	--	--

TABLE 7-20. Summary of U.S. Geological Survey 1979 Surface Water Quality Data for Columbia River Tributaries. (Sheet 4 of 4)

Quality parameter/group	Units	Yakima River at Kiona				Snake River at Burbank					Walla Walla River Near Touchet			
		No. of samples	Highest	Lowest	Mean	No. of samples	Highest	Lowest		Mean	No. of samples	Highest	Lowest	Mean
Organic Compounds														
Parathion, total	ug/L	4	ND	ND	ND	--	--	--		--	--	--	--	--
Toxaphene, total	ug/L	4	ND	ND	ND	--	--	--		--	--	--	--	--
Total trithion	ug/L	4	ND	ND	ND	--	--	--		--	--	--	--	--
Biological														
Biomass														
Periphyton biomass ash weight	g/m ²	3	3.54	0.080	1.81	4	12.1	0.000		3.13	--	--	--	--
Periphyton biomass total dry weight	g/m ²	3	5.04	0.160	2.57	4	19.7	0.000		5.06	--	--	--	--
Chlor-A periphyton chromographic fluorom	mg/m ²	3	10.8	0.140	5.32	4	96.5	0.000		24.15	--	--	--	--
Chlor-B periphyton chromographic fluorom	mg/m ²	3	3.39	0.000	1.65	4	37.8	0.000		9.45	--	--	--	--
Length of exposure	Days	3	38	24	31	4	36	19		26	--	--	--	--
Phytoplankton														
Total count	cells/mL	8	57,000	1,900	13,850	6	1,800	15		504	--	--	--	--
Division, diversity	index (d̄)	8	1.6	0.1	1.1	6	1.6	0.0		0.6	--	--	--	--
Class, diversity	index (d̄)	8	1.6	0.1	1.1	6	1.6	0.0		0.6	--	--	--	--
Order, diversity	index (d̄)	8	1.8	0.0	1.4	6	2.4	0.0		1.0	--	--	--	--
Family, diversity	index (d̄)	8	2.5	0.0	1.7	6	3.0	0.0		1.4	--	--	--	--
Genus, diversity	index (d̄)	8	2.7	0.0	2.1	6	2.6	0.0		1.9	--	--	--	--
Bacteria														
Coliform, fecal 0.7 UM-MF	colonies/100 mL	12	220	17	61	11	K*1,200	<1		K112	--	--	--	--
Streptococci, fecal KE AGAR	colonies/100 mL	12	1,900	3	440	12	79	<1		15	--	--	--	--
Sediment														
Sediment, suspended (instantaneous discharge)	mg/L (ft ³ /s)	2	240 (3,780)	66 (3,660)	153 (3,720)	11	60 (51,800)	2 (71,600)		1,318 (49,200)	--	--	--	--
Sediment, discharge suspended (instantaneous discharge)	tonnes/day (m ³ /s) tons/day (ft ³ /s)	2	2,222 (107) 2,450 (3,780)	591 (104) 652 (3,660)	1,407 (105) 1,551 (3,720)	11	7,611 (46,990) 8,390 (51,800)	41 (238) 45 (8,400)		1,722 (1,393) 1,899 (49,200)	--	--	--	--
Sediment, suspended (fall diameter <0.002 mm)	Percent	2	29	29	29	--	--	--		--	--	--	--	--
Sediment, suspended (fall diameter <0.004 mm)	Percent	2	52	35	44	--	--	--		--	--	--	--	--
Sediment, suspended (fall diameter <0.008 mm)	Percent	2	69	48	59	--	--	--		--	--	--	--	--
Sediment, suspended (fall diameter <0.016 mm)	Percent	2	80	66	73	--	--	--		--	--	--	--	--
Sediment, suspended (fall diameter <0.031 mm)	Percent	2	87	83	85	--	--	--		--	--	--	--	--
Sediment, suspended (fall diameter <0.062 mm)	Percent	2	90	85	88	--	--	--		--	--	--	--	--
Sediment, suspended (fall diameter <0.125 mm)	Percent	2	94	90	92	--	--	--		--	--	--	--	--
Sediment, suspended (fall diameter <0.250 mm)	Percent	2	99	95	97	--	--	--		--	--	--	--	--
Sediment, suspended (fall diameter <0.500 mm)	Percent	2	100	99	100	--	--	--		--	--	--	--	--
Sediment, suspended (fall diameter <1.00 mm)	Percent	2	100	--	100	--	--	--		--	--	--	--	--

*Results based upon colony counts outside the ideal range.

In the years following the deposition of insoluble radioactive material on river sediments, periodic increases in river flow rate, caused by operation of large hydroelectric plants upstream and downstream of the Hanford reach, annual freshets, and occasional floods, have resulted in the resuspension and subsequent deposition of some of the material on river shoreline areas above the current normal river water levels. Following the closure in 1971 of the last once-through cooled reactor, the discharge of radioactive materials into the river from Hanford operations decreased to relatively insignificant levels. Since 1971, the radionuclide burden of the sediments and exposed shoreline areas downstream of the reactor sites has been decreasing, as the radioactive materials deposited in these areas decay.

A recent, extensive radiological survey documents the magnitude and distribution of contamination on the riverbank, broad floodplains, low-lying peninsulas, sloughs, and islands along the Hanford reach and downstream to the confluence of the Columbia and Snake Rivers (Sula, 1980). Contamination on these exposed areas was found to be present in three different distributions:

- A fairly constant, uniformly distributed layer of contamination was observed over the entire study area. The average exposure rate over the area measured 11 ± 3 microrentgens per hour compared to a background exposure rate measured along the shoreline upstream of the Hanford Site of 7 ± 1 microrentgens per hour.
- Ninety-two areas were located in which exposure rate readings exceeded 25 microrentgens per hour. These areas of increased radiation levels are attributed to contaminated sediments that have been concentrated in some places by river action and are referred to as "contamination deposits." The areas ranged in size from a few square meters to several thousand square meters and were usually located in areas of dense vegetation. Areas found to contain the highest levels of river deposited contamination were the White Bluffs slough area, where exposure rates reached 40 microrentgens per hour; the Hanford townsite peninsula, in which an area reading of 45 microrentgens per hour was identified; and Island-344 near the 300 Area, which read 38 microrentgens per hour. The remaining "contamination deposits" were in the 25 to 30 microrentgen-per-hour range and appeared to be evenly distributed over the survey area. Samples of soil and vegetation taken at several sites along the river showed the "contamination deposits" to consist of a mixture of ^{60}Co , ^{137}Cs and ^{152}Eu in approximately equal proportions.
- Discrete particles of contamination containing ^{60}Co were found along the river, usually in flat, rocky areas with little or no vegetation. The particles were observed to be metallic flakes, possibly fragments from cooling system components of the production reactors. Fourteen of the particles were recovered. These particles were found at depths from 0 to 13 centimeters (0 to 5 inches) below the surface and contained from 1.7 to 24 microcuries of ^{60}Co activity.

has facilities for commuter and private air traffic, while the Kennewick Airport is limited to serving private aircraft. Commercial rail service is centered in Pasco, including a passenger train station and a major switching yard for freight traffic. Rail service within the Hanford Site is controlled and maintained by the DOE. Port facilities for barge traffic on the Columbia River are available at each of the three cities. Primary roads in the area include Routes 12, 395, 260, and 17 and Interstate-82, which is presently under construction. Routes 240 and 24, which traverse the Hanford Site, are maintained by the state of Washington while other secondary roads within the site are maintained by the DOE. Bridges across the Columbia River currently exist at Vernita in the northwest corner of the Hanford Site and at two locations connecting Kennewick and Pasco. Currently, a new bridge is being constructed across the Columbia River which will connect Richland to West Pasco.

Major transportation facilities in areas within and surrounding the Hanford Site are shown in Figure 9-1.

9.2.1.12 Utility Transportation Lines. Existing utility lines on the Hanford Site are shown in Figure 9-6.

9.2.1.13 Communication Facilities. Communication facilities on the Hanford Site are shown in Figure 9-6.

9.2.1.14 Community Service Facilities. See Section 9.3.3.

9.2.2 Land-Use Change

Growth in the population of the Tri-Cities metropolitan area is resulting in increasing urban land uses. Between 1970 and 1980, population in Benton and Franklin Counties grew by 62 and 36 percent, respectively, as compared to the state-wide average of 21 percent. Continued population growth and attendant urbanization are largely dependent on the future of the DOE energy-related projects at Hanford and the continued diversification of the local economy.

Irrigated agriculture in areas adjacent to the Hanford Site has also undergone substantial growth. Between 1975 and 1979, irrigated cropland acreage in the Columbia Plateau region increased by 20 percent (Wukelic et al., 1981, Fig. 4). Agricultural growth will likely continue in the Pasco Basin. However, continued demand and competition for increasingly scarce water resources, particularly on Yakima Basin project lands, may tend to constrain potential agricultural growth.

Potential land-use changes on the Hanford Site, other than the construction of a repository, include possible expansion of existing facilities and new construction projects. Preliminary feasibility studies sponsored by the Puget Sound Power and Light Company are currently under way at several locations to evaluate potential sites for a nuclear power reactor.

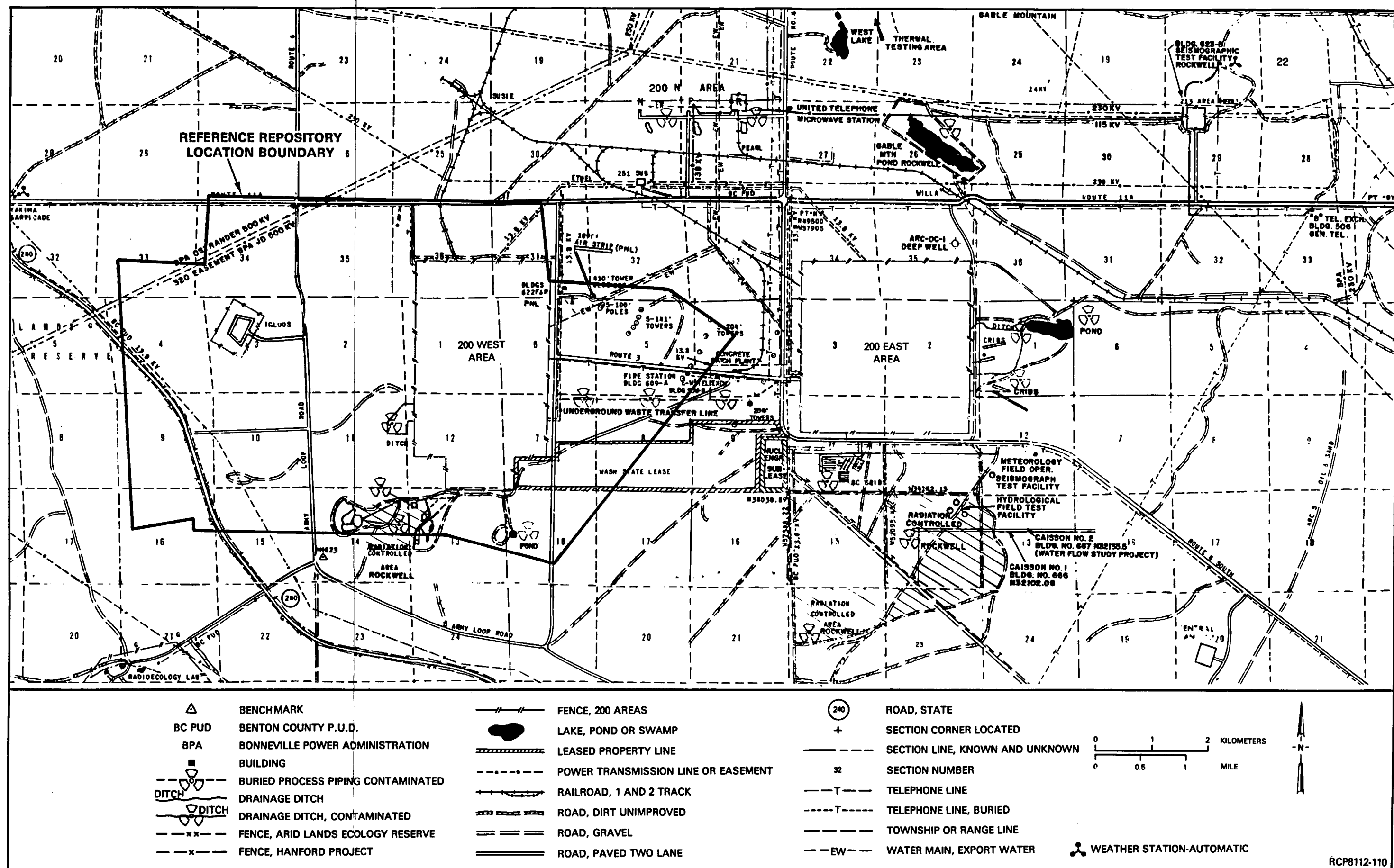


FIGURE 9-6. Utilities and Communications.